

Development of a genetic model for targeting gold mineralisation in the Dalradian Supergroup, Scotland

Thesis submitted for the degree of
Doctor of Philosophy
at the University of Leicester

Nyree Joanna Hill MSci (Dunelm)

Department of Geology
University of Leicester

July 2014

Development of a genetic model for targeting gold mineralisation in the Dalradian Supergroup, Scotland

Nyree Joanna Hill

The mid-Neoproterozoic to mid-Cambrian Dalradian Supergroup metasedimentary rocks of Scotland and Ireland contain vein-hosted gold mineralisation, including the Cononish deposit, Tyndrum, with a resource of 163,200 oz Au. Through identifying new mineralised occurrences and understanding the genesis of these and the Cononish deposit, the characteristic features of the hydrothermal system are identified. This study aims to improve exploration strategy by defining a specific genetic model.

Newly identified veins, in the Tyndrum area, are classified into three types: early molybdenite-bordered fractures, later gold-bearing poly-metallic veins and quartz-only veins. High-grade (>10 ppm) gold mineralisation at the Cononish deposit has distinct high Te (104 ppm) and Ag (119 ppm) with low Au/Ag (0.25). Other gold-bearing poly-metallic veins exhibit lower Te (8 ppm), higher As (234 ppm) and Au/Ag (1.3) at high grade (>10 ppm Au).

Gold occurs with sulphides and $\delta^{34}\text{S}$ data (average $+6.7\pm 2.8$ ‰) indicate a significant portion of the sulphur is sourced from the metasedimentary succession (≥ 32 -100%) with a small, but genetically significant, magmatic-sourced component ($\leq 68\%$). The source of sedimentary sulphur is not the immediate host rock and is inferred to be stratigraphically overlying, but structurally underlying, Easdale Subgroup lithologies.

$^{40}\text{Ar}/^{39}\text{Ar}$, Re-Os and U-Pb geochronology on muscovite, K-feldspar, molybdenite and rutile from veins and altered wall rock records two metallogenic events; metamorphic molybdenite at 477-439 Ma and post-metamorphic gold at 408-407 Ma. All gold-bearing veins are coeval with the gold-bearing Rhynie Chert (*c.* 407 Ma), suggesting a regional system of hydrothermal fluid flow. This is coincident with the last stage of emplacement of the post-orogenic granite suite (*c.* 430-408 Ma) and fault movement on the Great Glen and subsidiary faults (*c.* 430-390 Ma) interpreted to be as a result of the change of the stress field to sinistral transtension (*c.* 420-400 Ma).

Acknowledgements

This project was funded by the Natural Environmental Research Council with additional funding from Scotgold Resources Ltd, the Institute of Materials, Minerals and Mining, the Society of Geology Applied to Mineral Deposits and the Northern Mine Research Society, who are all thanked for their contribution. The Society for Economic Geology and the Society of Geology Applied to Mineral Deposits are thanked for funding my attendance on two international field trips during my studentship.

Thank you to my Leicester supervisors, Gawen Jenkin, for all his support and suggestions throughout the last 4 years and Dave Holwell, for discussion of ideas. Thank you to the department administrative & technical staff, in particular Jenna Booth, Colin Cunningham and Rob Wilson, for their assistance.

Chris Sangster, Dave Catterall and Jeff Smith were actively involved in the project from the beginning and Scotgold provided a huge amount of financial and logistical support and access to company datasets, without which this project wouldn't have been possible. Thank you to all of the Scotgold staff but I am particularly grateful to Ian 'Yeti' McPherson for putting up with my endless falling over and for generally being a great field assistant. Thank you to Charlotte, Heather and the late Greg Bryce for making me feel so welcome. Greg went above and beyond to look after me and always welcomed me back to Crianlarich with such a big smile, he will be greatly missed.

At SUERC, Adrian Boyce was a font of knowledge for all things stable isotope related and I cannot thank him enough for all his help. Darren Mark is thanked for his invaluable assistance with Ar/Ar dating and isotope applications. Thank you to all the technical staff, with particular thanks to Alison MacDonald, Terry Donnelly and Jim Imlach for their assistance during my time at SUERC.

Clive Rice is thanked for his on-going support and collaborative efforts, without his contributions to the improvement of age constraints on gold mineralisation in the Dalradian Supergroup this work would not have reached the conclusion it did. Thank you to Jon Naden and Gus Gunn (BGS) for useful discussion and for help with papers. Thank you to Nick Roberts (NIGL) for all your help with U-Pb dating and answering my multitude of last minute questions. Dave Selby (Durham) is thanked for his assistance with Re-Os dating. I would also like to thank Geoff Tanner, Rob Willan, Rob Chapman, Norman Moles and Graham Leslie, whose useful discussion greatly improved this thesis.

To Ade Band, thank you for your on-going encouragement, for making sure I ate more than pasta and cheese in the last few weeks and for persevering with drawing tectonic models until I finally understood.

Finally I would like to thank my family, Mum, Dad, Richard, Dayna and Grandad for trying to understand what I have been doing for the last four years, for not worrying too much when you didn't know where I was and for the unending supply of support in all the random things I have taken it upon myself to try and do.

Nyree Joanna Hill

16th July 2014

Table of Contents

List of figures	xi
List of tables	xvi
List of abbreviations.....	xvii

Chapter 1

Introduction

1.1. Background and rationale	2
1.2. Aim and objectives	3
1.3. Outline.....	4

Chapter 2

Nature and genesis of mineralisation at the Cononish deposit: Orogenic vs. Intrusion-related

<i>Abstract:</i>	8
2.1 Introduction.....	8
2.2 History of the Cononish deposit	9
2.3 Gold occurrences in the Scottish Dalradian Supergroup	10
2.3.1 Cononish Deposit.....	10
2.3.1.1 Geological setting.....	11
2.3.1.2 Structural controls	14
2.3.1.3 Deposit Mineralogy.....	14
2.3.2 Other gold occurrences in the Tyndrum area.....	15
2.3.2.1 Halliday's Veins	15
2.3.2.2 Mother Vein.....	15
2.3.2.3 Beinn Udlaidh Main Vein.....	16
2.3.3 Other gold occurrences in the Scottish Dalradian Supergroup	16
2.3.3.1 Rhynie Chert	16
2.3.3.2 Calliachar-Urlar.....	16
2.3.3.3 Tombuie.....	17
2.3.3.4 Lagalochoan.....	17
2.3.4 Constraints on mineralisation in the Scottish Dalradian.....	17
2.3.4.1 Oxygen isotopes and ore fluids	17
2.3.4.2 Sulphur isotopes	19
2.3.4.3 Geochronology	19
2.4 Gold occurrences in the Irish Dalradian Supergroup	21
2.4.1 Cavanacaw and Curraghinalt.....	21
2.4.1.1 Variation at the Cavanacaw deposit.....	21
2.4.1.2 Variation at the Curraghinalt deposit	22
2.4.2 Bohaun deposit	22
2.4.3 Constraints on mineralisation in the Irish Dalradian.....	23

2.4.3.1 Oxygen isotopes and ore fluids	23
2.4.3.2 Sulphur isotopes	24
2.4.3.3 Geochronology	24
2.5 Global deposit models	25
2.5.1 Orogenic gold deposits	25
2.5.1.1 Definition	25
2.5.1.2 Interpretation of deposit type.....	25
2.5.1.3 Relevance to the Cononish deposit	26
2.5.2 Epithermal gold deposits	28
2.5.2.1 Definition	28
2.5.2.2 Interpretation of deposit type.....	28
2.5.2.3 Relevance to the Cononish deposit	30
2.5.3 Reduced intrusion-related gold systems	30
2.5.3.1 Definition	30
2.5.3.2 Interpretation of deposit type.....	30
2.5.3.3 Relevance to the Cononish deposit	31
2.6 Characterisation of gold occurrences.....	32
2.6.1 Mineralogy and sulphide assemblage	32
2.6.2 Structural setting	32
2.6.3 Geochronology.....	33
2.6.4 Summary.....	33
2.7 A working model for the Cononish deposit.....	35
2.8 Research aims	37

Chapter 3

The geological setting of the Grampian Highlands and the Tyndrum area

<i>Abstract</i>	41
3.1 Introduction.....	41
3.2 General setting	42
3.3 Basement geology	43
3.4 Lithostratigraphy of the Dalradian Supergroup	45
3.4.1 Grampian Group	45
3.4.2 Appin Group	46
3.4.2.1 Lochaber Subgroup.....	46
3.4.2.2 Ballachulish Subgroup	46
3.4.2.3 Blair Atholl Subgroup.....	49
3.4.3 Argyll Group.....	49
3.4.3.1 Islay Subgroup	50
3.4.3.2 Easdale Subgroup.....	50
3.4.3.3 Crinan Subgroup.....	50
3.4.3.4 Tayvallich Subgroup.....	51
3.4.4 Southern Highland Group.....	51
3.4.5 Variation in the Tyndrum area.....	51

3.4.5.1 Lochaber Subgroup	51
3.4.5.2 Missing stratigraphy.....	51
3.4.5.3 Argyll Group variation	52
3.5 Overlying stratigraphy.....	52
3.6 Dating the Dalradian.....	53
3.7 Caledonian Orogenesis	55
3.7.1 Deformation during the Grampian Event.....	56
3.7.2 Age of Metamorphism	57
3.8 Lineaments.....	58
3.9 Brittle Fault movement.....	60
3.9.1 Great Glen Fault.....	60
3.9.2 Highland Boundary Fault	61
3.9.3 The Tyndrum fault.....	61
3.10 Igneous Activity.....	61
3.10.1 Syn-depositional intrusions	61
3.10.2 Grampian Event granites.....	62
3.10.3 Decompression granites.....	63
3.10.4 Post-orogenic granites.....	63
3.10.5 Siluro-Devonian Lamprophyre and Appinite suite	64
3.10.6 Permo-Carboniferous dykes.....	64
3.11 Regional fluid flow in the Dalradian Supergroup, Scotland.....	64
3.12 Conclusions	66

Chapter 4

Hydrothermal occurrences in the Tyndrum area; constraints on genesis from field relations and petrography

<i>Abstract</i>	69
4.1 Introduction.....	69
4.2 Methods	70
4.3 Vein Classification	72
4.4 Field relations	73
4.4.1 Glen Cononish.....	73
4.4.1.1 Eas Anie.....	73
4.4.1.2 Mother Vein.....	75
4.4.1.3 Coire Nan Sionnach.....	76
4.4.1.4 Kilbridge	76
4.4.1.5 Alt an Rund	76
4.4.2 Beinn Udlaidh.....	79
4.4.2.1 Breccia bodies	79
4.4.2.2 Beinn Udlaidh Main Vein.....	83
4.4.2.3 Coire Daimh Vein	86
4.4.3 Glen Orchy	88
4.4.3.1 Molybdenite-bordered fracture	91

4.4.3.2 Quartz-pyrite \pm K-feldspar veins.....	92
4.4.3.3 Lamprophyre sills	93
4.4.3.4 Pyrite-bearing veins	93
4.4.3.5 Poly-metallic quartz veins	94
4.4.3.6 Quartz-only veins	94
4.4.3.7 Carboniferous dykes	95
4.4.3.8 Constraints on timing relationships.....	95
4.4.4 Alt Ghamhain.....	97
4.4.5 Auch Estate.....	100
4.4.6 Auchtertyre	101
4.4.7 Sron Garbh	101
4.4.7.1 Igneous intrusions	101
4.4.7.2 Quartz veins	103
4.5 Petrography	106
4.5.1 Host metasedimentary rocks	106
4.5.1.1 Meall Garbh Psammite Formation	106
4.5.1.2 Other metasedimentary units	106
4.5.2 Igneous intrusions.....	111
4.5.2.1 Siluro-Devonian intrusions	111
4.5.2.2 Permo-Carboniferous intrusions.....	112
4.5.3 Molybdenite-bordered fractures	113
4.5.4 Pyrite-bearing veins	115
4.5.5 Poly-metallic quartz veins	116
4.5.5.1 Cononish set	117
4.5.5.2 River Vein set.....	119
4.5.5.3 Kilbridge set.....	119
4.6 Discussion.....	122
4.6.1 Constraints on relative timing of hydrothermal activity.....	122
4.6.2 Implications	124
4.7 Conclusions	124

Chapter 5

Geochemical characterisation of gold mineralisation in the Tyndrum area

<i>Abstract:</i>	127
5.1 Introduction.....	127
5.2 Analytical methods	128
5.2.1 Sampling methods.....	128
5.2.2 Whole rock geochemistry	129
5.2.3 Microprobe analysis.....	133
5.2.4 Stream sediment sampling	133
5.3 Comparison between whole rock geochemical methods.....	133
5.3.1 Implications for geochemical trends of vein sets.....	138
5.4 Geochemical variation by location in gold-bearing quartz veins.....	139

5.4.1 Field and petrographic classifications	139
5.4.2 Whole rock geochemistry	140
5.4.2.1 Molybdenite-bordered fractures.....	140
5.4.2.2 Pyrite-bearing and quartz-only veins.....	142
5.4.2.3 Poly-metallic veins.....	143
5.4.2.4 Tyndrum Lead Mine-style.....	146
5.4.3 Whole rock gold/silver ratios.....	147
5.4.3.1 Gold/silver ratios in electrum	149
5.4.4 Summary.....	150
5.5 Discussion.....	153
5.5.1 Regional geochemical anomalies.....	153
5.5.1.1 Literature data	153
5.5.1.2 This study – stream sediment data.....	153
5.5.1.3 Implications of results	158
5.5.2 Gold/silver ratios in poly-metallic veins	159
5.5.2.1 Gold/silver ratios of other gold deposit types.....	160
5.5.3 Comparison to gold deposit models	162
5.5.4 Potential geochemical criteria for exploration.....	163
5.6 Conclusions	165

Chapter 6

How the Neoproterozoic S-isotope record illuminates the genesis of vein gold systems: an example from the Dalradian Supergroup in Scotland

<i>Abstract</i>	168
6.1 Introduction.....	168
6.2 Geological setting of the Scottish Dalradian sequence	170
6.2.1 Global context.....	170
6.2.2 Deposition and tectonic setting.....	171
6.2.3 Chronostratigraphic and biostratigraphic constraints	171
6.2.4 Deformation and metamorphism.....	172
6.2.5 Post-tectonic magmatic activity	172
6.3 Isotope stratigraphy of the Dalradian Supergroup	175
6.3.1 Global Context.....	175
6.3.2 Carbon isotopes	175
6.3.3 Strontium isotopes.....	176
6.4 Mineralisation in the Tyndrum area.....	176
6.4.1 Previous S-isotope data.....	177
6.5 Analytical methods	179
6.6 Field relations of newly identified mineralisation	179
6.7 Ore petrography.....	181
6.8 S-isotope results	184
6.8.1 Relationship between veins and host rock alteration	185
6.8.2 S-isotope fractionations between mineral pairs.....	197

6.9 Discussion.....	201
6.9.1 Magmatic S-sources	201
6.9.2 Sedimentary S-sources.....	201
6.9.3 Input of sedimentary vs. magmatic sulphur into mineralised veins and breccia bodies.....	206
6.9.4 Implications of structure.....	208
6.9.5 Metal source rocks	209
6.10 Conclusions	212

Chapter 7

Geochronology and geochemistry of the River Vein prospect, Tyndrum and its relationship to the Cononish deposit

<i>Abstract</i>	215
7.1 Introduction.....	215
7.2 Regional setting	216
7.2.1 Caledonian Orogenesis.....	216
7.2.2 Fault movement	219
7.2.3 Magmatic intrusions	219
7.2.4 Existing age constraints on gold mineralisation	221
7.3 The Glen Orchy area.....	223
7.3.1 Cross-cutting relationships in the Glen Orchy area.....	224
7.3.1.1 Molybdenite-bordered fractures.....	225
7.3.1.2 Poly-metallic quartz veins	225
7.3.2 Relationship to the Cononish deposit.....	227
7.4 Analytical methods	229
7.4.1 Sample preparation	229
7.4.2 $^{40}\text{Ar}/^{39}\text{Ar}$ geochronology	229
7.4.3 U-Pb geochronology	231
7.4.4 Re-Os geochronology.....	232
7.5 Petrographic constraints on dated phases.....	233
7.5.1 Zircon U-Pb.....	233
7.5.2 Molybdenite Re-Os.....	233
7.5.3 K-feldspar $^{40}\text{Ar}/^{39}\text{Ar}$	233
7.5.4 Rutile U-Pb	233
7.5.5 Muscovite $^{40}\text{Ar}/^{39}\text{Ar}$	235
7.6 Results.....	236
7.6.1 $^{40}\text{Ar}/^{39}\text{Ar}$ geochronology.....	236
7.6.1.1 K-feldspar syn-molybdenite.....	236
7.6.1.2 Metamorphic muscovite	236
7.6.1.3 Sericite pre- and post-gold mineralisation	238
7.6.2 U-Pb geochronology.....	241
7.6.2.1 Detrital zircon.....	241
7.6.2.2 Rutile.....	241

7.6.3 Re-Os geochronology.....	244
7.7 Discussion.....	245
7.7.1 Constraints on the age of gold-bearing poly-metallic quartz veins.....	245
7.7.1.1 Glen Orchy	245
7.7.1.2 Tyndrum area.....	245
7.7.1.3 Implications of metamorphic muscovite age	247
7.7.2 Constraints on the age of molybdenite-bordered fractures	247
7.8 Synthesis	250
7.8.1 Molybdenum-bearing hydrothermal event.....	250
7.8.2 Gold-bearing hydrothermal event in Scottish Dalradian Supergroup	252
7.8.2.1 Comparison to the orogenic gold model.....	253
7.8.2.2 Tectonic events at 407-408 Ma.....	253
7.8.2.3 Model for gold mineralisation at 407-408 Ma	256
7.9 Conclusions.....	257

Chapter 8

Synthesis and Conclusions

8.1 Introduction.....	259
8.2 Possible Analogues	259
8.3 Synthesis and ore deposit formation.....	262
8.4 Regional exploration implications	266
8.5 Unresolved problems and future work.....	267
8.6 Conclusion	268

Appendices

Appendix 4.1 - Large-scale topography, geology and sample maps	269
Appendix 7.3 - U-Pb methodology.....	272

References

Reference list.....	276
---------------------	-----

Digital Appendices

Appendix 4.2 - Sample list.....	Digital
Appendix 4.3 - Photo location list	Digital
Appendix 5.1 - Detection limits in Scotgold Resources Ltd assay database.....	Digital
Appendix 5.2 - Four-acid digestion whole-rock geochemistry	Digital
Appendix 5.3 - Stream sediment data.....	Digital
Appendix 6.1 - Sulphide isotope standards	Digital
Appendix 6.2 - Sulphur isotope full dataset	Digital
Appendix 6.3 - Oxygen isotope standards.....	Digital
Appendix 6.4 - Oxygen isotope database from this study.....	Digital
Appendix 6.5 - Oxygen isotope database from Plewes (2012)	Digital

Appendix 7.1 - $^{40}\text{Ar}/^{39}\text{Ar}$ results data table.....	Digital
Appendix 7.2 - $^{40}\text{Ar}/^{39}\text{Ar}$ results with full uncertainties	Digital
Appendix 7.4 - U-Pb zircon data table.....	Digital
Appendix 7.5 - U-Pb rutile data table.....	Digital
Appendix 8.1 - Published version of Hill <i>et al.</i> (2013)	Digital

List of figures

Chapter 2

Figure 2.1 - Map showing major gold occurrences in the Dalradian Supergroup.....	9
Figure 2.2 - Development of the Cononish deposit since its discovery in 1984.....	10
Figure 2.3 - Cononish deposit and other previously identified mineralisation in the Tyndrum area	12
Figure 2.4 - Oxygen and hydrogen isotope results for fluids	19
Figure 2.5 - Paragenesis for main Irish gold deposits at Curraghinalt and Cavanacaw.....	22
Figure 2.6 - Model of formation of intrusion-related gold deposits and orogenic and shows variation observed in orogenic and epithermal gold deposit formation	28
Figure 2.7 - Model for reduced intrusion-related gold deposits.	32
Figure 2.8 - Schematic cross-section showing hypothetical model for mineralisation at Cononish	37

Chapter 3

Figure 3.1 - Terrane map of the UK and Ireland showing the Grampian Terrane, host to the Dalradian Supergroup.....	43
Figure 3.2 - Schematic cross section through the crust and upper-most mantle in northern Britain	44
Figure 3.3 - Map to show key locations discussed in the text and the rift basins controlling deposition of the Grampian Group	45
Figure 3.4 - Simplified geology of the Grampian Terrane in Scotland.....	47
Figure 3.5 - Composite lithostratigraphic section for the southwestern Dalradian Supergroup	48
Figure 3.6 - Schematic cross-section showing development of the Laurentian margin in Scotland during deposition of the Dalradian Supergroup.	49
Figure 3.7 - Schematic cross section for the Great Glen to Loch Etive area	52
Figure 3.8 - Composite lithostratigraphic section showing known age constraints for the deposition of the Dalradian Supergroup	54
Figure 3.9 - Tectonic evolution of the Dalradian Supergroup from pre- to end-Caledonian Orogenesis	55
Figure 3.10 - Simplified distribution of metamorphic facies in the Dalradian Supergroup in Scotland.....	59
Figure 3.11 - Distribution of igneous rocks in the Dalradian Supergroup.	62
Figure 3.12 - Existing age constraints for the Dalradian Supergroup	67

Chapter 4

Figure 4.1 - Simplified geology of the local area showing key structural features and the extent of the study area	71
---	----

Figure 4.2 - Detailed geology of Glen Cononish showing location of key veins and structural features	73
Figure 4.3 - 3D representation of the geology draped over the topography in the Cononish area.....	74
Figure 4.4 - Photo plate of Mother Vein and Alt an Rund	77
Figure 4.5 - Photo plate of the Coire Nan Sionnach and Kilbridge.....	78
Figure 4.6 - Detailed geology of the Beinn Udlaidh area showing location of key veins and breccia bodies	79
Figure 4.7 - 3D representation of the geology draped over the topographic variation in the Beinn Udlaidh and Glen Orchy areas.....	80
Figure 4.8 - Schematic representation of the quartz- and lamprophyre-dominated matrix end-members within the breccia bodies at Beinn Udlaidh	81
Figure 4.9 - Photo plate of Beinn Udlaidh Main Vein.	84
Figure 4.10 - Map and cross-section showing variation in the Beinn Udlaidh Main Vein from drill core evidence.	85
Figure 4.11 - Photo plate of the Coire Daimh Vein.....	87
Figure 4.12 - Glen Orchy area geology showing extent of detailed re-mapping of the area.....	88
Figure 4.13 - Detailed map of the NE-extent of mapping in Glen Orchy.....	89
Figure 4.14 - Detailed map of the SW-extent of mapping in Glen Orchy.....	90
Figure 4.15 - Detailed map of the River Vein area of Glen Orchy showing key cross cutting relationships.	91
Figure 4.16 - Photo plate of Glen Orchy area.	92
Figure 4.17 - Photo plate of Glen Orchy area	93
Figure 4.18 - Cross-cutting relationships of quartz-only veins in the Glen Orchy River.....	94
Figure 4.19 - Schematic representation of the cross cutting relationships in the Glen Orchy area.....	96
Figure 4.20 - Cross-cutting relationship between molybdenite-bearing and gold-bearing quartz veins in the Glen Orchy area.....	97
Figure 4.21 - Map of Alt Ghamhain	99
Figure 4.22 - Detailed geology of Sron Garbh, Auch Estate and Auchtertyre showing locations of key intrusions and veins.	100
Figure 4.23 - 3D representation of the geology draped over the topography in the Auch, Auchtertyre and Sron Garbh areas.....	102
Figure 4.24 - Photo plate of Auch Estate and Auchtertyre area.....	104
Figure 4.25 - Photo plate of Sron Garbh area	105
Figure 4.26 - Photo plate of Meall Garbh Psammite Formation.....	108
Figure 4.27 - Photo plate of Dalradian metasediments in the Tyndrum area.....	109
Figure 4.28 - Photo plate of Dalradian metasediments in the Tyndrum area.....	110
Figure 4.29 - Photo plate of Siluro-Devonian dyke-sill swarm.....	111
Figure 4.30 - Photo plate of Carboniferous dyke swarm.....	112
Figure 4.31 - Schematic representation of molybdenite-bearing fracture development with subsequent quartz-pyrite \pm K-feldspar vein emplacement.....	113
Figure 4.32 - Paragenesis and photo plate of molybdenite-bearing fractures.....	114

Figure 4.33 - Paragenesis and photo plate of pyrite-bearing veins	115
Figure 4.34 - Sub-sets of poly-metallic veins defined in this study based on orientation and mineralogy.....	116
Figure 4.35 - Paragenesis and photomicrographs for the Cononish vein set	118
Figure 4.36 - Paragenesis and photo plate for the River Vein set	120
Figure 4.37 - Paragenesis and photo plate for the Kilbridge set.....	121
Figure 4.38 - Simplified schematic constraints on the timing of hydrothermal events in the Tyndrum area.	123

Chapter 5

Figure 5.1 - Accuracy and precision of gold pathfinder elements by four acid digestion methods.....	131
Figure 5.2 - Accuracy and precision of elements of importance in the Tyndrum area mineralisation by four acid digestion methods.....	132
Figure 5.3 - Variation in data obtained for sulphur from four acid digestion, aqua regia and LECO analytical methods..	134
Figure 5.4 - Comparison of four-acid and aqua-regia digestion geochemical methods for key gold pathfinder elements.....	137
Figure 5.5 - Comparison of geochemical methods for base metals	138
Figure 5.6 - Geochemical trends for key gold pathfinder elements in molybdenite-bearing veins in the study area.....	141
Figure 5.7 - Mo vs. Sb for selected vein sets.....	142
Figure 5.8 - General trend in pyrite-bearing and barren veins in the Tyndrum area.....	142
Figure 5.9 - Geochemical trends for Cononish set poly-metallic quartz veins.....	144
Figure 5.10 - Geochemical trends for River Vein (green) and Kilbridge (red) poly-metallic vein sets	145
Figure 5.11 - As vs. Te plot to show de-coupled nature of arsenic and tellurium at high and low grade within each poly-metallic vein set.....	146
Figure 5.12 - Geochemical trends for the Tyndrum Lead Mine and Tyndrum Lead mine style mineralisation at Cononish.....	147
Figure 5.13 - Whole rock gold/silver ratios for each vein set as defined by the field and petrographic constraints.....	148
Figure 5.14 - Gold/silver ratios for electrum at Glen Orchy, River Vein and Kilbridge.	149
Figure 5.15 - Whole rock vs. Microprobe Au/Ag ratios for key samples from each vein set.....	152
Figure 5.16 - Au, Ag, As and Bi stream sediment results for the Tyndrum area.....	156
Figure 5.17 - Te, Se, Sb and Zn stream sediment results for the Tyndrum area	157
Figure 5.18 - Pb and W stream sediment results for the Tyndrum area	158
Figure 5.19 - Whole rock Gold/silver ratios vs. depth of formation for major gold deposit types compared to data from the Cononish deposit and River Vein set	160
Figure 5.20 - Geochemical trends for the three major deposit types comparabled to the Cononish deposit.	164

Chapter 6

Figure 6.1 - Simplified geological map of the Dalradian Supergroup in Scotland and Northern Ireland.....	170
Figure 6.2 - Simplified composite stratigraphic column of the lower three Groups of the Dalradian Supergroup showing missing stratigraphy in the Tyndrum area due to the Boundary Slide.....	173
Figure 6.3 - Simplified geology of the study area.....	174
Figure 6.4 - Previous sulphide and sulphate $\delta^{34}\text{S}$ data for sedimentary, magmatic bodies and mineralisation in the Dalradian Supergroup.....	178
Figure 6.5 - Schematic illustration of orientations and cross-cutting relationships of the veins and breccia pipes in Glen Orchy.....	181
Figure 6.6 - Petrographic constraints photo plate	183
Figure 6.7 - New S-isotope data for different mineralisation types, intrusions and host rocks in the Tyndrum area.....	186
Figure 6.8 - Variation in host rock $\delta^{34}\text{S}$ and S% with distance away from gold-bearing quartz veins.....	197
Figure 6.9 - The global composite sulphide S-isotope curve of Halverson <i>et al.</i> (2010) superimposed onto the Dalradian stratigraphy.....	205
Figure 6.10 - Mixing diagram showing percentage of sulphur from a magmatic and various possible sedimentary components.	207
Figure 6.11 - Cross-section through the Tyndrum area.....	211

Chapter 7

Figure 7.1 - Map to show local geology and area mapped as part of this work.....	217
Figure 7.2 - Tectonic evolution of the Dalradian Supergroup from pre-Caledonian Orogenesis through the orogenic cycle.....	218
Figure 7.3 - Late Caledonian granites and appinites with ages given for key intrusions.....	220
Figure 7.4 - Existing age constraints for the Dalradian Supergroup and orogenic and magmatic processes affecting the sequence from literature data.....	222
Figure 7.5 - Simplified geology of the study area.....	223
Figure 7.6 - Detailed map of Glen Orchy showing River Vein area and location of sample GO02	225
Figure 7.7 - Detailed map of the River Vein area of Glen Orchy	226
Figure 7.8 - Schematic representation of cross-cutting relationships in the Glen Orchy area.....	227
Figure 7.9 - Key field relationships in the Glen Orchy and River Vein area	228
Figure 7.10 - Paragenesis for mineralisation in the Glen Orchy area.....	235
Figure 7.11 - Step-heating spectra and isochron for $^{40}\text{Ar}/^{39}\text{Ar}$ on muscovite (A) and K-feldspar (B) from RV10	239
Figure 7.12 - Step-heating spectra and isochron for $^{40}\text{Ar}/^{39}\text{Ar}$ on K-feldspar (A) from RV16 and sericite (B) from RV18.....	240

Figure 7.13 - Age probability spectra and isochron for $^{40}\text{Ar}/^{39}\text{Ar}$ on muscovite from GO02b using in situ laser analysis.	241
Figure 7.14 - U-Pb LA-ICPMS detrital zircon results from RV10 and RV16	242
Figure 7.15 - U-Pb LA-ICPMS hydrothermal rutile results for RV10 and RV16	243
Figure 7.16 - New data from this study for molybdenite-bordered fractures (red) and gold-bearing poly-metallic quartz veins (yellow) compared to existing constraints on the age of the Dalradian Supergroup a.....	246
Figure 7.17 - Cooling profile of the Grampian Orogen from closure temperatures and ages obtained in this study.....	249
Figure 7.18 - Two proposed models for heat and fluid fluxing event at c. 410 Ma.....	255

Chapter 8

Figure 8.1 - Schematic synthesis model through time showing key depositional, tectonic and magmatic events and the hydrothermal systems developed in the Tyndrum area.	263
--	-----

Appendices

Figure A4.1 - Map to show topography of the study area and location of places named in the main text.	270
Figure A4.2 - Sample map detailing location of all samples in the main text.	271
Figure A7.1 - Concordia plot for all zircon reference material 91500 run	274
Figure A7.2 - Concordia plot for all zircon reference material GJ-1 run.	274
Figure A7.3 - Concordia plot for all zircon reference material Plešovice run.	275

List of tables

Chapter 2

Table 2.1 - A comparison of the characteristics of Cononish deposit and Rhynie Chert, Scotland and the Curraghinalt deposit, Northern Ireland.....	13
Table 2.2 - Characteristics of key gold deposit types compared to Cononish.....	27
Table 2.3 - Characterisation of the gold deposits in the Dalradian Supergroup.....	34
Table 2.4 - Characteristics of intrusion-related gold deposits in the Lachlan belt, Australia compared to the Cononish deposit.....	36

Chapter 3

Table 3.1 - Summary of existing age constraints for Grampian Event Orogenesis	58
Table 3.2 - Post-metamorphic quartz veins stages.....	65

Chapter 4

Table 4.1 - Classification of veins based on field and petrographic constraints	72
Table 4.2 - Characteristics of clast and matrix in breccia pipes at Beinn Udlaigh.....	82

Chapter 5

Table 5.1 - Four acid digestion and aqua-regia digestion methods comparison.....	136
Table 5.2 - Classification of veins based on field criteria and mineralogy.....	140
Table 5.3 - Electrum data from microprobe analysis from this study	151

Chapter 6

Table 6.1 - S-isotope results from mineralisation, sedimentary and magmatic sulphide showings in the Tyndrum area.....	187
Table 6.2 - Geochemistry and S-isotope data of host lithology and key magmatic bodies and associated cross-cutting veins in the Tyndrum area.....	195
Table 6.3 - S-isotope fractionation data and calculated apparent equilibrium temperatures for mineral pairs in the Tyndrum area.....	199

Chapter 7

Table 7.1 - Sample type and phases dated with methods.....	234
Table 7.2 - Geochronology results for all samples from this study.....	237
Table 7.3 - Closure temperatures of minerals dated in this study.....	238
Table 7.4 - Re-Os results.....	244

List of abbreviations

4AD	Four acid digestion
A	Auch Estate
Apy	Arsenopyrite
AR	Aqua Regia
Ba	Barite
Bb	Breccia bodies
BCq	Ben Challum Quartzite
Bio	Biotite
BLa	Ben Lawers Schist
BM	Blackmount
BU	Beinn Udlaidh
BUq	Beinn Udlaidh Quartzite
Bv	Barren veins
C	Cononish
Cal	Calcite
Chl	Chlorite
CMq	Carn Maing Quartzite
CNS	Coire Nan Sionnach
Cp	Chalcopyrite
DC	Drill core sample
El	Electrum
Ga	Galena
GGF	Great Glen Fault
GO	Glen Orchy
GO-L	Lamprophyre from Glen Orchy
HBF	Highland Boundary Fault
Hes	Hessite
HS	Hand sample from <i>in situ</i> sampling
KIL	Kilbridge
Ksp	K-feldspar
Lamp	Lamprophyre

LC	Late Caledonian intrusions
LS	Leven Schist
Lst	Limestone
M/Moly	Molybdenite
MGp	Meall Garbh Psammite
Mo	Molybdenite-related samples
Musc	Muscovite
OC	Surface outcrop <i>in situ</i> sample
Po	Pyrrhotite
Py	Pyrite
PPL	Plain polarised light
Qtzite	Quartzite
Qtz	Quartz
Ru	Rutile
RL	Reflected light
SEM	Scanning Electron Microscope
S	Sulphides
SG	Sron Garbh
Ser	Sericite
Sph	Sphalerite
Tet	Tetrahedrite
UG	Underground <i>in situ</i> sample
T_h	Homogenisation temperature
XPL	Cross polarised light

Chapter 1

Introduction

1.1. Background and rationale

Gold deposits have formed throughout the last 3 billion years of Earth's evolution (Goldfarb 2001) and gold has underpinned the global financial market over the last 120 years. Today, gold is a key source of wealth creation with £46.5 billion generated directly from gold mining in 2012 (Pricewaterhouse Coopers 2013). Gold mining was one of the largest economic contributors in Papua New Guinea (15% gross domestic product [GDP]), Ghana (8% GDP) and Tanzania (6% GDP) in 2012 (Pricewaterhouse Coopers 2013). However, gold deposit discovery peaked in 1988 and the number and size of the deposits discovered has since declined (McKeith *et al.* 2010). The cost of discovering gold resources has also increased significantly in the last 40 years from £2 in 1960 to £28 per oz gold since 2000 (McKeith *et al.* 2010). In addition, the average grade of global gold discoveries and mined gold is decreasing (1.1 g/t average; McKeith *et al.* 2010). Global demand for gold in 2013 was 3756 tonnes (World Gold Council 2014) whereas global mine production was 2770 tonnes (USGS Gold 2014), with the deficit met by recycled gold. Demand is predicted to continue to increase (World Gold Council 2014) while the supply of newly mined gold is anticipated to decrease in line with the lower grade and size of new discoveries (McKeith *et al.* 2010). In recent years the increasing challenges of discovering large gold deposits in traditional mining districts has resulted in areas previously not considered as potential mineral provinces beginning to be explored for gold (McKeith *et al.* 2010). Exploration companies are looking for new gold deposits, small and large, in both green- and brownfield settings. While the price of gold has also increased, the increasing cost of discovery has implications for the way exploration companies explore for new deposits. New and innovative exploration methods need to be developed and collaborative work between industrial and academic partners on mineral occurrences may provide additional detail to improve exploration efficiency.

Occurrences of vein-hosted gold have been recorded in the Dalradian Supergroup of the Scottish Highlands since at least 1962 (Halliday 1962), and the definition of a gold resource near Tyndrum by Scotgold Resources in 2008 (Scotgold Resources Ltd 2008) was the impetus for this study. The Dalradian Supergroup is host to the UK's only operating gold mine at Cavanacaw, Northern Ireland (326, 300 oz Au; Galantas Gold Corporation 2013) and the largest gold resource at Curraghinalt, Northern Ireland (2.7 Moz Au; Dalradian Resources 2012). The genesis of the vein-hosted gold occurrences is poorly understood and the relationship between deposits is unclear. For example, it is not yet clear whether the gold occurrences in the Dalradian Supergroup represent single or multiple gold

mineralisation events and thus there is little geological understanding on which to base effective exploration.

The Cononish deposit, host to a JORC (Australasian Joint Ore Reserves Committee) compliant resource of 163, 200 oz gold and 631, 300 oz silver (Scotgold Resources 2012a), was first discovered in the early-1980's by Ennex International PLC. In 2007, in response to an increasing gold price, Scotgold Resources Ltd sought to bring the deposit into production and planning permission was granted in October 2011. Around the Cononish deposit further gold occurrences have been identified by previous workers (Halliday 1962; Patrick *et al.* 1988; Curtis *et al.* 1993) and by new exploration work, carried out since 2007 by Scotgold Resources Ltd, led by consulting geologist Mr David Catterall. These occurrences are poorly understood and limited work has been undertaken on them. In addition, the Tyndrum-Glen Orchy license area has large areas where little or no exploration has been carried out.

The Cononish mine is expected to create 50 jobs for the local community and input some £50 million directly into the Scottish economy. The creation of year-round jobs for the local community will help support economic development in an area largely dependent on seasonal work. This economic impact does not take into account potential tertiary industries expected to develop, such as the development of a mining visitors centre in Tyndrum. Some 25% of the mined gold will be processed on site at Cononish and therefore will be traceable Scottish gold. There is potential for this gold to achieve a premium price through the development of a Scottish gold jewellery industry, using gold that has never left Scotland. The identification of further deposits in the area is a key part of Scotgold's strategy to sustain the positive economic impact beyond the projected ten-year lifetime of the Cononish deposit. In this project the mineralisation will be understood in detail to develop a genetic model for gold mineralisation in the Tyndrum area. In turn, this will be used to make exploration more efficient, both in locating new deposits, and by minimising the need for drilling and its associated environmental impact. In addition, understanding the processes that have controlled the formation of the mineralisation has the potential to provide new insight into the post-orogenic geology of an otherwise relatively well-understood part of the Earth's crust.

1.2. Aim and objectives

The overall aim of this work is to investigate the genesis of the Cononish deposit, other known mineralised occurrences, and barren veins, and to try to identify new occurrences in the Tyndrum area. Through constraining the geometry and characteristic features of the hydrothermal system the aim is to improve exploration strategy by defining a series of exploration criteria to maximise efficiency. The research objectives of this thesis are to:

- Characterise mineralised and un-mineralised vein types in the Tyndrum area based on the field relations, petrography and geochemical signatures.
- Assess whether anomalies in the stream sediment data can be tied to trends in vein mineralogy and geochemistry and to establish if variation in lithogeochemistry and stream sediment anomalies can be used as exploration criteria in the Tyndrum area.
- Describe the sulphur isotope ratio variation in different mineralisation types across the study area in order to model the potential proportions of magmatic and sedimentary sources and to constrain the origin of sulphur in the mineralisation, which may be a proxy for the origin of the gold, and will constrain possible fluid pathways.
- Establish if all gold mineralisation in the Tyndrum area is coeval and deposited from the same mineralising event or whether multiple gold mineralisation events have occurred
- Place observed mineralisation into the context of the evolution of the Dalradian Supergroup to create a model to increased efficiency of exploration for gold and associated mineralisation.

1.3. Outline

This thesis describes and discusses the nature of gold veins and associated hydrothermal occurrences in the Dalradian Supergroup in the Tyndrum area, Scotland.

The genesis of the previously identified Cononish deposit remains in question and previous workers have advocated differing models for genesis (Curtis *et al.* 1993; Goldfarb *et al.* 2005). *Chapter 2* gives a detailed background of the discovery of the Cononish deposit and reviews the existing data regarding it to provide the starting point for this research. The deposit characteristics are compared to existing models for classic gold deposits to

highlight the atypical nature of Cononish gold mineralisation. This chapter details the reasoning behind the research questions.

Gold mineralised veins are contained in the Dalradian Supergroup and the depositional, metamorphic, structural and post-orogenic evolution of the sequence place a range of controls on mineralisation in the Tyndrum area. Thus, *Chapter 3* details the geological history of the Dalradian Supergroup.

The identification of new mineral occurrences and re-examination of those previously known is detailed in *Chapter 4*. This provides a comprehensive description of the field relations and petrographic characterisation of the various hydrothermal occurrences in the Tyndrum area. A classification of the different vein types is erected that provides a framework for subsequent chapters to build on. New mineralised occurrences identified in this chapter include molybdenite-bearing veins and additional gold-bearing quartz veins.

To establish if there are clear chemical distinctions between the vein sets identified in *Chapter 4* the lithogeochemical trends are discussed in *Chapter 5*. The lithogeochemistry is compared to stream sediment geochemistry across the study area to establish if enrichment in veins is reflected by anomalies in the stream sediment data. Geochemical data from the Cononish deposit and other gold mineralisation styles in the Tyndrum area are compared to classic global gold deposit models to attempt to classify the deposit.

Gold in hydrothermal veins in the Tyndrum area is closely associated with sulphides. Sulphur isotope analysis enables investigation of the origin of sulphur within sulphides since different sources of sulphur have distinct signatures. The origin of sulphur may be a proxy for the origin of the gold. Variation in the S-isotope ratios in different mineralisation types from different locations within the Tyndrum area is discussed in *Chapter 6* and the utility of the Neoproterozoic S-isotope record on understanding mineralised occurrences in Neoproterozoic rocks is investigated. A version of this chapter was published as a paper in a Geological Society of London Special Publication; Ore Deposits in an Evolving Earth (Hill *et al.* 2013). All associated field work, sample preparation and sulphur isotope analysis (with supervision from Adrian Boyce) was completed by Nyree Hill. Christopher Sangster and Dave Catterall assisted with collection of field data and access to company data (lithogeochemical data undertaken at ALS Laboratories, Ireland). The paper was written by Nyree Hill and benefited from editorial assistance from Gawen Jenkin, Dave Holwell, Adrian Boyce, Clive Rice and Jon Naden.

A key research question of this study is to establish if all mineralised veins are of the same age. Using $^{40}\text{Ar}/^{39}\text{Ar}$, U-Pb and Re-Os techniques on vein minerals and altered wall rocks the age of hydrothermal events can be constrained. *Chapter 7* presents new age data for both gold- and molybdenite-mineralising hydrothermal events in the Glen Orchy area. The new ages are compared with published data in the Dalradian Supergroup to establish if all gold mineralisation is of the same age and emplaced in the same tectonic setting. These data are used to determine the likely processes driving hydrothermal fluid flow leading to mineralisation.

Chapters 4-7 are written as independent data sections; *Chapter 8* concludes the thesis with a discussion on the genesis of gold and associated mineralisation in the Tyndrum area and places it in the context of the evolution of the Dalradian Supergroup as a whole. This chapter will also address the potential for further work, the implications for local and regional exploration and the implications for this research on gold occurrences beyond the Dalradian Supergroup and Scotland.

Chapter 2

Nature and genesis of mineralisation at the Cononish deposit: Orogenic vs. Intrusion- related

Abstract: The Dalradian metamorphic belt of Scotland and Northern Ireland is host to widespread vein-hosted gold deposits and occurrences, including the UK's only producing gold mine, Cavanacaw and the largest resource at Curraghinalt, both in Northern Ireland. Whilst the Cavanacaw and Curraghinalt deposits are relatively well constrained, the conditions and formation mechanisms of the Cononish deposit are poorly understood, with the deposit previously being classified as both orogenic and intrusion-related. Here, characteristics of the Cononish deposit are compared to defining criteria for existing gold deposit models. While the Cononish deposit has some characteristics of orogenic, epithermal and intrusion-related gold deposits it does not fit enough of the defining criteria of any of these established deposit types to be easily classified as one of them. It appears that gold deposits in the Dalradian Supergroup do not represent a single gold mineralising hydrothermal event. A working model is proposed, relating emplacement of gold-bearing quartz veins in the Tyndrum area to the intrusion of batholith scale granites at *c.* 410 Ma based on existing age and stable isotope data; this thesis aims to test and improve this working model.

2.1 Introduction

Globally a wide variety of gold deposit types have been identified and the differences in the genesis of these deposits types have implications for the exploration and extraction strategies used. Distinct deposit types are often described by a deposit model. It is commonly accepted that each deposit type model is just that, a model, and while many characteristics of a model will fit an individual deposit, not all are required to. Deposit models should be adapted locally based on the data available for the individual deposits and occurrences considered.

Throughout the Dalradian Supergroup there are a number of mineralised occurrences of varying types, of particular note for this study are the numerous vein-hosted gold occurrences in the Scottish and Irish Dalradian Supergroup. Some are of clearer origin than others – Curraghinalt and Cavanacaw appear to be orogenic in origin but other Irish gold occurrences and the Scottish vein-hosted gold deposits are of uncertain origin. In this chapter, the existing data for the Cononish deposit, and other known gold occurrences across the Scottish and Irish Dalradian Supergroup, are reviewed and compared to existing deposit models to highlight the atypical nature of the Cononish deposit. This is important as the previous work in the area frames the questions that need to be addressed in this study; this chapter develops the reasoning behind the research aims of the thesis.

2.2 History of the Cononish deposit

The Cononish deposit was discovered as a result of exploration in the Tyndrum area, Scotland, by Ennex International PLC (Ennex henceforth) following their discovery of economic gold mineralisation in the Dalradian Supergroup of Northern Ireland (Fig. 2.1). Ennex commenced regional exploration in 1985, with trenching and diamond drilling conducted at Cononish based on anomalies in the stream sediment geochemistry (Fig. 2.2; Dominy & Platten 2008). A 1280 m adit was driven between 1988 and 1990 (Dominy & Platten 2008) and a resource of 211, 200 oz at 7.99 g/t Au and 1.137 Moz at 42.99 g/t Ag was defined (Earls *et al.* 1992).

In 1995, Caledonia Mining Corporation took control of the Cononish deposit and under the operation of Fynegold Exploration Limited, mine design and regional exploration was continued (Fig. 2.2). The project was put under care and maintenance in 1997 due to the low gold price (Dominy & Platten 2008).

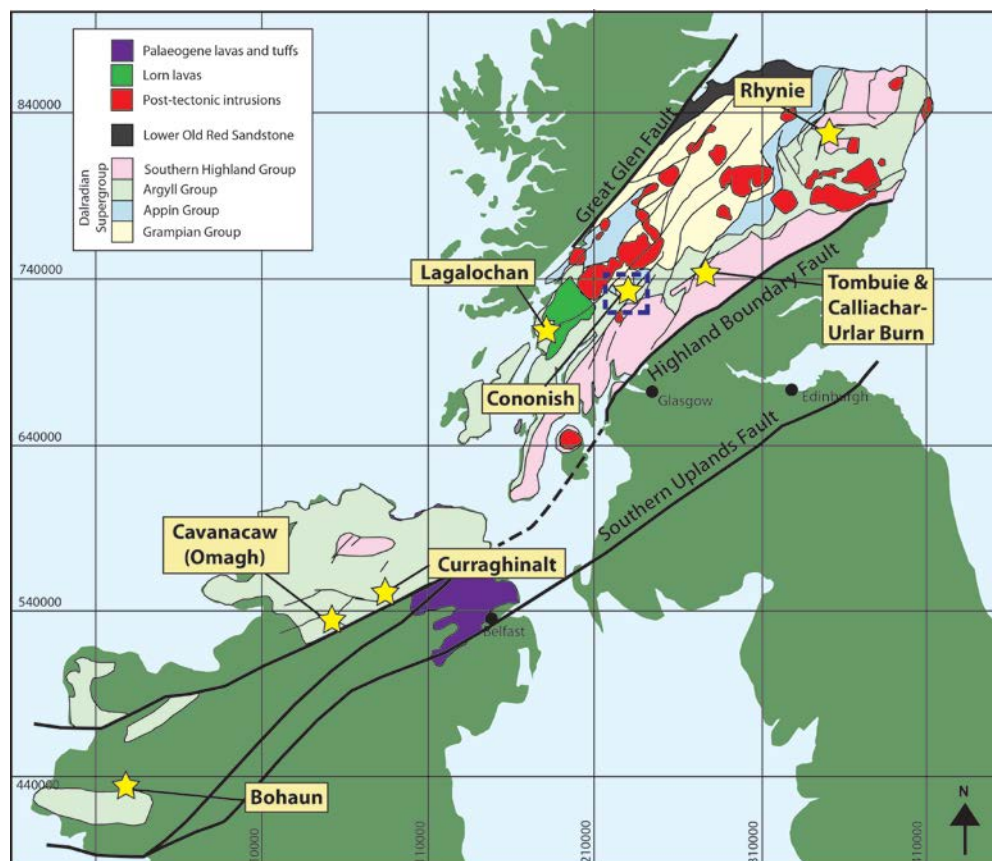


Figure 2.1: Map showing major gold occurrences in the Dalradian Supergroup. Blue dashed square shows Tyndrum area as shown in Figure 2.3.

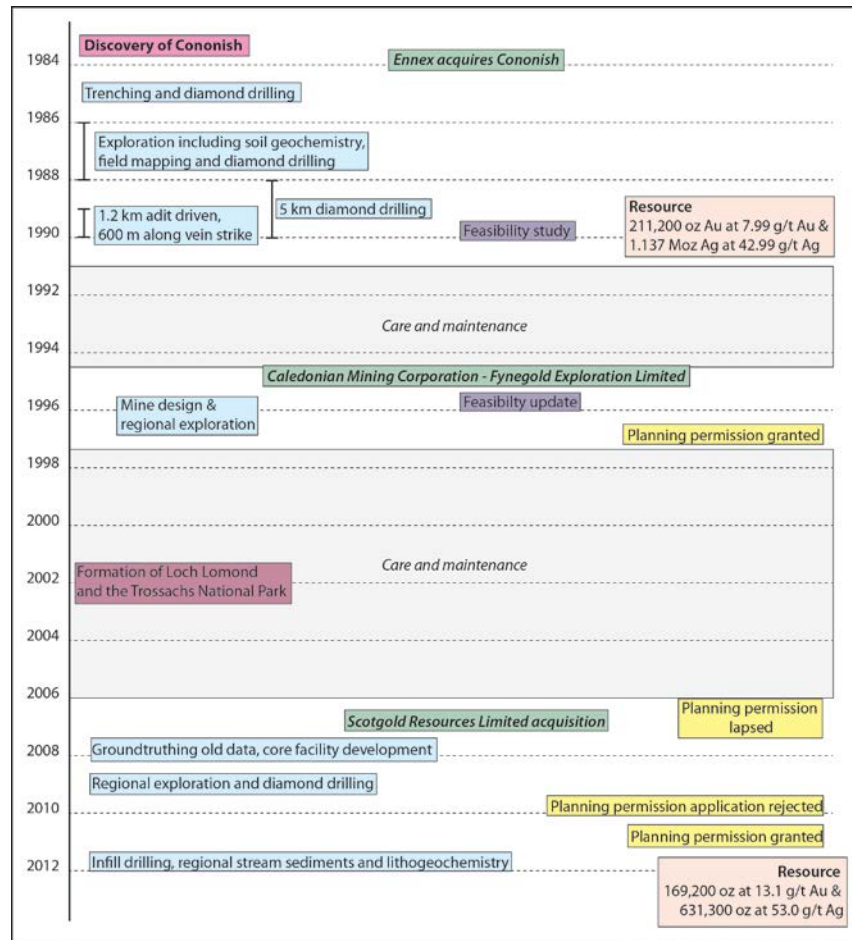


Figure 2.2: Development of the Cononish deposit since its discovery in 1984. Details from Earls *et al.* (1992); Dominy & Platten (2008) and Scotgold Resources Ltd (2012a).

In 2007, in response to an increasing gold price, Scotgold Resources Ltd gained control of the Cononish project and began moving forward to bring the deposit into production (Fig. 2.2). In October 2011, planning permission was granted by the Loch Lomond and the Trossachs National Park.

2.3 Gold occurrences in the Scottish Dalradian Supergroup

2.3.1 Cononish Deposit

A number of previous workers (Patrick *et al.* 1988; Earls *et al.* 1992; Curtis 1990; Curtis *et al.* 1993; Treagus *et al.* 1999; Dominy & Platten 2008; Tanner 2012), both independent of and in conjunction with the operating companies, have undertaken small studies to characterise the nature of mineralisation at the Cononish deposit (Table 2.1) and in the surrounding Tyndrum area.

The Eas Anie vein, host to the Cononish deposit, is a quartz-breccia vein reaching up to 6 m in width (Earls *et al.* 1992). The width of the vein varies along a 1 km proven length, reaching a minimum width of 1.5 m (Scotgold pers. comm.). The vein trends on average

050° and has a variable dip between 70°SE and 70°NW moving through the vertical (Fig. 2.1; Earls *et al.* 1992; Tanner 2012).

2.3.1.1 Geological setting

The Cononish deposit is hosted in the lower- to mid-Dalradian Supergroup Meall Garbh Psammite, Beinn Udlaidh Quartzite and Leven Schist Formations (Fig. 2.3). There are significant sections of the Lochaber Group (lower-middle Dalradian) stratigraphy missing, represented by the Boundary Slide (formerly the Iltay Boundary Slide; Bailey 1922; Roberts & Treagus 1979; Tanner & Thomas 2009; Chapter 3). Previous workers suggested the vein cross-cut mid- to upper-Dalradian Formations and therefore the Eas Anie structure cross-cut the Boundary Slide (Earls *et al.* 1992). Recent mapping by Tanner (2012) shows the Boundary Slide is not cross-cut by the Eas Anie structure (Fig. 2.3) and therefore stratigraphy above the Leven Schist Formation is not present in the adit (Chapter 3). Observations from this study suggest the vein dies out before it reaches the Boundary Slide.

Igneous intrusions around the Cononish deposit are limited to small-scale dykes. A Permo-Carboniferous dyke cross-cuts the Eas Anie Vein (Earls *et al.* 1992; Tanner 2012) and two microdiorite dykes have been mapped at Beinn Chuirn. There is no outcrop of post-orogenic Late-Caledonian granite within 10 km of the Cononish deposit; however, a gravity low extends from the Etive Complex, a multiphase granite intrusion, into the Tyndrum area (Fig. 2.3; Hussein & Hipkin 1981). Pattick *et al.* (1988) interpreted the gravity low to represent a concealed granite at depth. The lack of clear relationship with an igneous intrusion has been argued to preclude the deposit from being igneous-related (Dominy & Platten 2008), in contrast to the intrusion-related model proposed by Curtis *et al.* (1993) based on stable isotope data that indicated a mixed magmatic and meteoric fluid source.

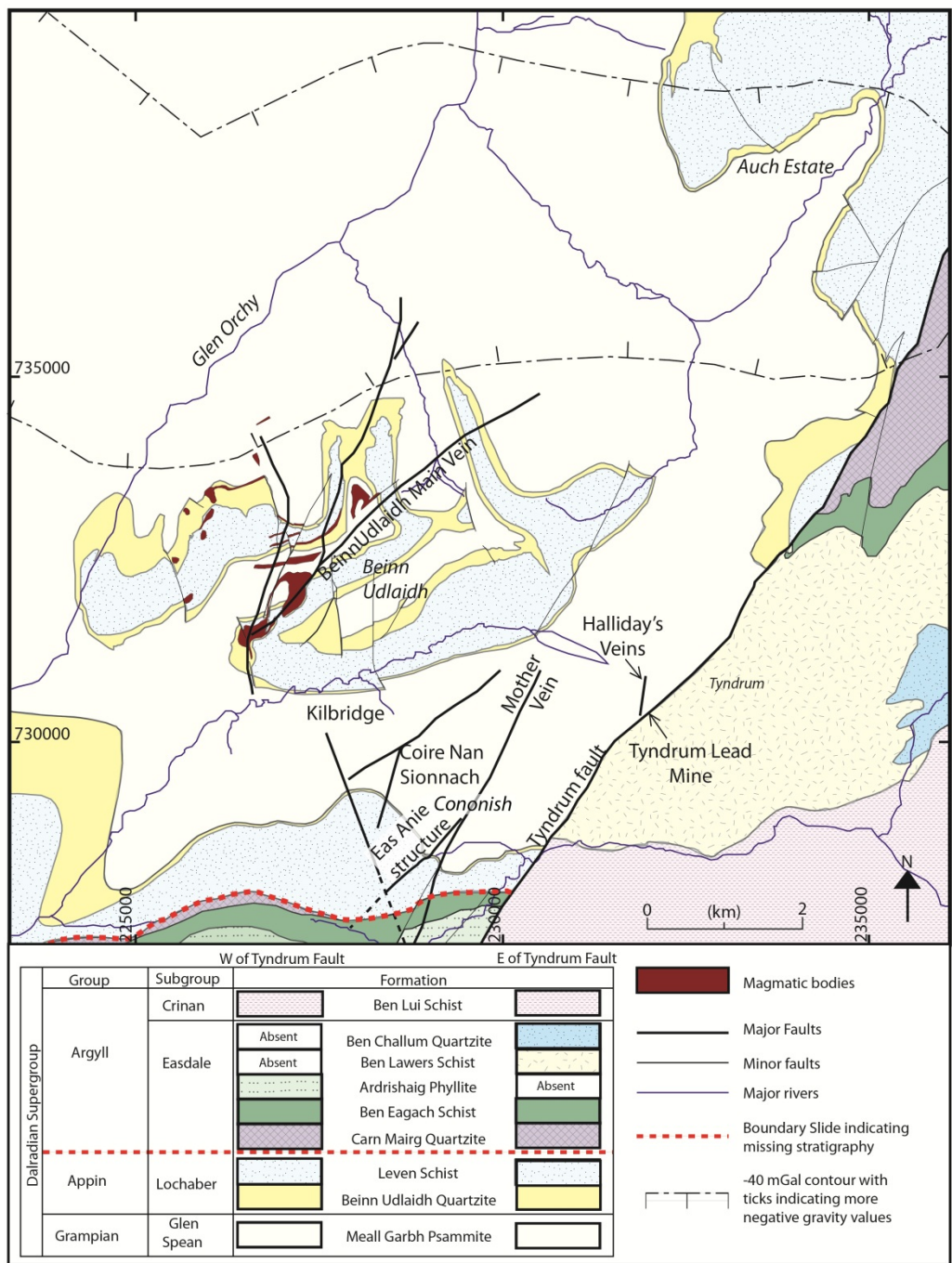


Figure 2.3: Cononish deposit and other previously identified mineralisation in the Tyndrum area with simplified geology modified from the BGS Crianlarich bedrock geology sheet and mapping by Tanner & Thomas (2009).

Table 2.1 *A comparison of the characteristics of Cononish deposit and Rhynie Chert, Scotland and the Curraghinalt deposit, Northern Ireland*

Characteristic	Cononish deposit	Rhynie Chert	Curraghinalt deposit
Tectonic setting of host rocks	Late-tectonic within an orogenic belt ¹	Late-tectonic within an orogenic belt ³	Syn-tectonic within an orogenic belt, thrusting component ⁴
Structural setting	Hosted in splay off the NE-SW trending Tyndrum Fault ¹	Pull apart basin above NE-SW transcurrent fault ³	NW-trending structures in E-W-trending shear zones ⁴
Depth of emplacement	4 km ¹	Surface ³	<10 km ⁵
Genetically related rocks	None ¹	Andesites ³	None ⁵
Host rocks	Dalradian metasedimentary rocks ¹	Devonian sediments ³	Dalradian metasedimentary rocks ⁴
Metamorphism of host rocks	Lower-amphibolite ¹	Un-metamorphosed ³	Upper-greenschist ⁵
Deposit form	Steeply-dipping vein ²	Hot spring sinters ³	Steeply-dipping veins ⁵
Gangue	Quartz ² Calcite ² K-feldspar	Chalcedony ³ Barite ³ Calcite ³	Quartz ⁴ Carbonate ⁴ Barite ⁵
Sulphides	Pyrite ² Chalcopyrite ² Galena ² Sphalerite ²	Pyrite ³	Pyrite ⁴ Arsenopyrite ⁴ Chalcopyrite ⁴ Sphalerite ⁴
Other Minerals	Electrum ² Tellurides ²	Native gold ³	Tellurides, Tennantite ⁴ Electrum ⁴
Vein textures	Brecciation, euhedral quartz ²	Chert breccia ³	Euhedral quartz, fracturing ⁴
Alteration	Sericite ² Quartz ² Carbonate ²	K-feldspar ³ Quartz ³ Illite ³ Chlorite ³ Calcite ³	Quartz ⁴ Fe-carbonate ⁴
Ore fluids	H ₂ O-dominated 29-45% CO ₂ ¹ CO ₂ dominated 92-95% CO ₂ ¹ 6-7 equiv. wt. % NaCl ¹ at 290-350°C ¹	Boiling ³ at 150-225°C ⁶ Low salinity ³ Meteoric water component ³	High temp. brine (300-420°C) with 10 wt. % NaCl + KCl equiv. and 15 wt. % CO ₂ ⁴ Mixing with low temp (120°C). and low salinity fluid (<5 wt. % NaCl + KCl equiv.) ⁴ Late low temp (124-174°C) basinal brine causes remobilisation of the gold ⁴

¹ Curtis *et al.* (1993); ² Dominy & Platten (2008); ³ Rice *et al.* (1995); ⁴ Wilkinson *et al.* (1999); ⁵ Parnell *et al.* (2000); ⁶ Baron *et al.* (2004).

2.3.1.2 Structural controls

The Eas Anie structure is spatially associated with a splay off the Tyndrum Fault (Fig. 2.3; Dominy & Platten 2008), one of the NE-SW-trending Caledonian faults, which include the Dalradian Supergroup-bounding Great Glen and Highland Boundary Faults (Fig. 2.1).

There is an apparent <5 m vertical displacement across the Eas Anie vein, downthrown to the SE (Parker *et al.* 1989). Dominy & Platten (2008) report the same stratigraphy present on the NW and SE adit walls in most places but, occasionally, pelite is juxtaposed against psammite. This is interpreted to suggest that while there is some displacement, it is small and likely to be <5 m (Dominy & Platten 2008).

Northerly trending faults are inferred to displace the Eas Anie vein and downthrow the metasedimentary succession to the west (Earls *et al.* 1992). The displacement is up to 9 m (Earls *et al.* 1992) but is not consistent throughout the vein (Dominy & Platten 2008).

There is little consistency in the amount of movement and nature of the faults reported in Eas Anie and therefore it is difficult to establish the true nature of the faults.

2.3.1.3 Deposit Mineralogy

The vein has two distinct generations of mineralisation (Earls *et al.* 1992); primary gold-bearing mineralisation is termed ‘A-min’ by Earls *et al.* (1992) while late galena-sphalerite mineralisation is termed ‘B-min’.

‘A-min’ is characterised by four stages of quartz-sulphide mineralisation, early white quartz, grey pyritic quartz, mottled quartz and late white quartz (Earls *et al.* 1992). Early white quartz is the main gold-bearing phase, with gold correlated with overall abundance of sulphides comprising pyrite, galena, chalcopyrite and sphalerite (Earls *et al.* 1992). Grey pyritic quartz is fracture filling and quartz is microgranular, due to cataclasis and recrystallization (Earls *et al.* 1992). The mottled quartz is characterised by brecciation of early white quartz and cementation by grey pyritic quartz (Earls *et al.* 1992). Apart from quartz, non-sulphide gangue minerals are rare; there is some K-feldspar (syn-Au) and calcite (post-Au).

Dominy & Platten (2008) group the four ‘A-min’ quartz stages into event 1, early white quartz of Earls *et al.* (1992) and event 2, grey pyritic quartz and mottled quartz (Earls *et al.* 1992). The classification of Dominy & Platten (2008) does not reflect the subtlety in the vein but is appropriate for resource estimation. This study believes Earls *et al.* (1992) is a better representation of the mineralogy of the vein.

Traditionally electrum is used to describe Au-Ag alloys with 20-80 wt. % Au (*c.f.* Boyle 1979), in this study this division is ignored and electrum is used to describe all Au-Ag alloys. Gold occurs as electrum and minor native gold, with silver as hessite (Dominy & Platten 2008). Dominy & Platten (2008) report electrum between <10 µm and 550 µm in size with 10% greater than 100 µm. The base metal sulphide assemblage consists of chalcopyrite, galena and sphalerite; some of these carry electrum and silver-tellurides. There is a spatial association between pyrite-galena and electrum. Galena occurs in fractures within pyrite and is a useful field observation to track gold mineralisation in the adit (Dominy & Platten 2008).

‘B-min’, as defined in Earls *et al.* (1992), does not host gold and cross-cuts the main Eas Anie vein and therefore the ‘A-min’. Vuggy quartz with galena, sphalerite, barite and carbonate characterises ‘B-min’. The quartz shows crustiform textures and is differentiated from ‘A-min’ by an absence of pyrite and presence of coarse galena and sphalerite (Dominy & Platten 2008). Brecciated clasts of psammite and gold-bearing ‘A-min’ are hosted within the ‘B-min’ vein (Dominy & Platten 2008). ‘B-min’ is interpreted to be equivalent to Pb-Zn mineralisation at the Tyndrum Lead Mine (Earls *et al.* 1992) and this study concurs with this interpretation.

2.3.2 Other gold occurrences in the Tyndrum area

2.3.2.1 Halliday's Veins

Halliday's Veins were first reported by Halliday (1962), with further work by Pattrick *et al.* (1988; Fig. 2.3). N-trending veins contain chalcopyrite, pyrite, electrum and hessite (Ag_2Te) with minor sylvanite (AuAgTe_4) and petzite (Au_3AgTe_2) (Pattrick *et al.* 1988). Electrum is found as inclusions in galena and infilling fractures in pyrite (Pattrick *et al.* 1988). The veins are not reactivated by later fault movement and there is a lack of evidence of any offset of the stratigraphy (Curtis 1990). The veins are interpreted to have formed early in the mineralisation history at the Tyndrum Lead Mine and it is suggested the veins formed in response to sinistral movement (Curtis 1990). The veins were not observed in this study due to extensive mature Forestry Commission tree growth.

2.3.2.2 Mother Vein

The Mother Vein, formerly Mother Reef (Curtis *et al.* 1993; Treagus *et al.* 1999), is sub-parallel to the Tyndrum Fault. The vein can be traced for 2 km and is interpreted to represent a series of segments at an oblique trend to the main structure. The vein is largely

barren except where the projected line of the Eas Anie vein would meet the Mother Vein (Fig. 2.3; Tanner 2012). Tanner (2012) interpret the Mother Vein to be later than the Eas Anie vein in contradiction to cross-cutting relationships reported by Treagus *et al.* (1999) who state the Eas Anie Vein is observed to cross-cut the Mother Vein. Tanner (2012) is interpreted to have reported the correct field relations.

Treagus *et al.* (1999) proposed the Mother Vein consists of five segments within dilational R fractures, parallel to Tyndrum Fault with fractures moving in response to left-lateral transtension (Treagus *et al.* 1999). Tanner (2012) does not support the interpretation of Treagus *et al.* (1999); Tanner (2012) reports the vein has an overall trend of 028° and is a single structure. The reported drag folds on both side of the vein (Treagus *et al.* 1999) could not be found by Tanner (2012) and were not noted in this study.

2.3.2.3 Beinn Udlaidh Main Vein

The NE-trending Beinn Udlaidh Main Vein is hosted in the Meall Garbh Psammite, Beinn Udlaidh Quartzite and Leven Schist Formations, dips sub-vertically and averages 4 m in width (Fig. 2.3; Tanner 2012). The Main Vein contains gold, as electrum, hosted in pyrite; galena and sphalerite are noted (Plewes 2012).

2.3.3 Other gold occurrences in the Scottish Dalradian Supergroup

2.3.3.1 Rhynie Chert

The Rhynie outlier, Aberdeenshire, is an area of Old Red Sandstone, 21 km long and <3 km wide (Rice *et al.* 1995) and is host to the gold-bearing Rhynie Chert (Fig. 2.1; Table 2.1). Andesitic lavas are observed 40-60 m beneath the Rhynie Chert and around the northern margin of the Rhynie outlier (Rice *et al.* 1995). Mark *et al.* (2013) report an unclear relationship between the Rhynie Chert and andesitic lavas.

The Rhynie Chert is enriched in gold, arsenic and antimony (Rice & Trewin 1988) with a high concentration of tin, molybdenum and mercury and moderate enrichment of chromium and vanadium (Rice *et al.* 1995). There is arsenic enrichment in altered sediments next to the cherts and a close correlation between arsenic and gold (Rice *et al.* 1995). No arsenic minerals were noted but pyrite in the chert-breccia is arsenian in nature (Rice *et al.* 1995).

2.3.3.2 Calliachar-Urlar

The Calliachar-Urlar deposit is hosted in a NW-trending joint set within the Pitlochry Schist Formation (Fig. 2.1; Ixer *et al.* 1997). The mineralogy is characterised by mercurian

electrum with silver-, bismuth- and lead-tellurides in late galena (Ixer *et al.* 1997; Mason *et al.* 1991). Two mineralisation stages are observed; the high-grade assemblage is quartz-galena-pyrite with base metals and electrum. The low-grade assemblage is galena-chalcopyrite with base metals (Ixer *et al.* 1997). Gold is found in pyrite and arsenopyrite as small (<20 μm) electrum inclusions but mainly as inter-growths with galena.

2.3.3.3 Tombuie

Mineralisation at Tombuie, first identified by Colby Gold Plc., is within a NW-trending joint set in the Pitlochry Schist Formation (Fig. 2.1; Mason *et al.* 1991). The NNE-trending Tombuie Fault cuts the area and mineralisation is hosted in a series of near vertical joints (Corkhill *et al.* 2010). The deposit mineralogy is base-metal sulphide-rich with gold-, silver-, bismuth- and tellurium-bearing minerals in a late galena stage (Corkhill *et al.* 2010). Tetrahedrite and tennantite inclusions, within galena, are particularly enriched in silver (>17 wt. % silver) (Corkhill *et al.* 2010). The Tombuie veins are comparable to Calliachar-Ullar and the mineralisation across the area is defined by a bismuth anomaly in stream sediment geochemistry (Corkhill *et al.* 2010).

2.3.3.4 Lagalochoan

The Lagalochoan occurrence is a copper-gold mineralised epithermal-porphyry style deposit hosted in a hydrothermally altered Caledonian-age granodiorite intrusion within the Lorne Lavas (Fig. 2.1; Harris *et al.* 1988). Mineralisation occurs with the last emplacement phase of the Kilmelford calc-alkaline granodiorite intrusion. Three phases of mineralisation are recorded; early Cu-Mo-Au hosted in veinlets, followed by shear-related Pb-Zn-Ag-Au-As-Sb mineralisation with a component of near-surface hydrothermal circulation (Harris *et al.* 1988). The final mineralisation is Pb-Zn-Ag in carbonate veins.

2.3.4 Constraints on mineralisation in the Scottish Dalradian

2.3.4.1 Oxygen isotopes and ore fluids

Curtis *et al.* (1993) used oxygen isotope analyses and fluid inclusion microthermometry to constrain the temperature and salinity of ore fluids at the Cononish deposit. Two fluid inclusion types were identified; both are CO₂-bearing, with varying H₂O and CO₂. Fluid one is characterised by H₂O-dominated inclusions containing 29-48 vol. % CO₂. Fluid two is CO₂-dominated with 92-95 vol. % CO₂ in inclusions. Both inclusion types have 6-7 equivalent wt. % NaCl (Curtis *et al.* 1993). These fluid inclusions constrain measured T_h at the Cononish deposit to between 293 ± 17 and $340\pm 29^\circ\text{C}$ (Curtis *et al.* 1993). Fluid

inclusions were not tied to the quartz stages defined by Earls *et al.* (1992) but Curtis *et al.* (1993) assume that the measured fluid compositions represent the gold-bearing fluids.

Fluid inclusion work by Pattick (1985) concluded Halliday's Veins to have 6-8 equivalent wt. % NaCl in inclusions, comparable with Cononish, but with 7 mol. % CO₂ and a homogenisation temperature in the range 295 to 325°C. Halliday's veins have low CO₂; however, this may be a function of the small sample set and may not reflect the full range of fluids in the vein.

A limited fluid inclusion dataset for the Calliachar-Ural occurrence suggests the deposit formed from CO₂-bearing fluids with 2-13 equivalent wt. % NaCl at 320-340°C (Ixer *et al.* 1997).

The fluid inclusion data for the three vein-hosted gold occurrences is generally comparable; fluids record temperatures between 290-340°C with NaCl and CO₂ components. Pattick (1985) interpreted Halliday's Veins to have formed at 4 km depth and Curtis *et al.* (1993) interpret the veins to be coeval to the Cononish deposit. This interpretation seems reasonable given the comparable nature of fluid inclusion data, but due to the small sample set, the full range of fluids in both veins may not be recorded.

Oxygen and hydrogen isotopic data on vein quartz from Cononish were used to establish the origin of the mineralising fluids (Curtis *et al.* 1993). Curtis *et al.* (1993) show that Cononish ore fluids in two samples plot outside of the magmatic water box on an O (fluid) vs. δD plot (Fig. 2.4) and suggest the fluids originate from magmatic/metamorphic water mixed with a meteoric water component. Bruce (1996) reports no apparent variation between Q1-3 white quartz with $\delta^{18}O_{\text{quartz}}$ in the range 10-13.4‰. Grey quartz from the pyritic shears has slightly lighter $\delta^{18}O_{\text{quartz}}$ data (9-11.3‰; Bruce 1996). A mixed deep-crustal and surface-derived mineralising fluid is suggested for deposition of all quartz generations at 300-340°C (Bruce 1996) comparable to data reported in Curtis *et al.* (1993).

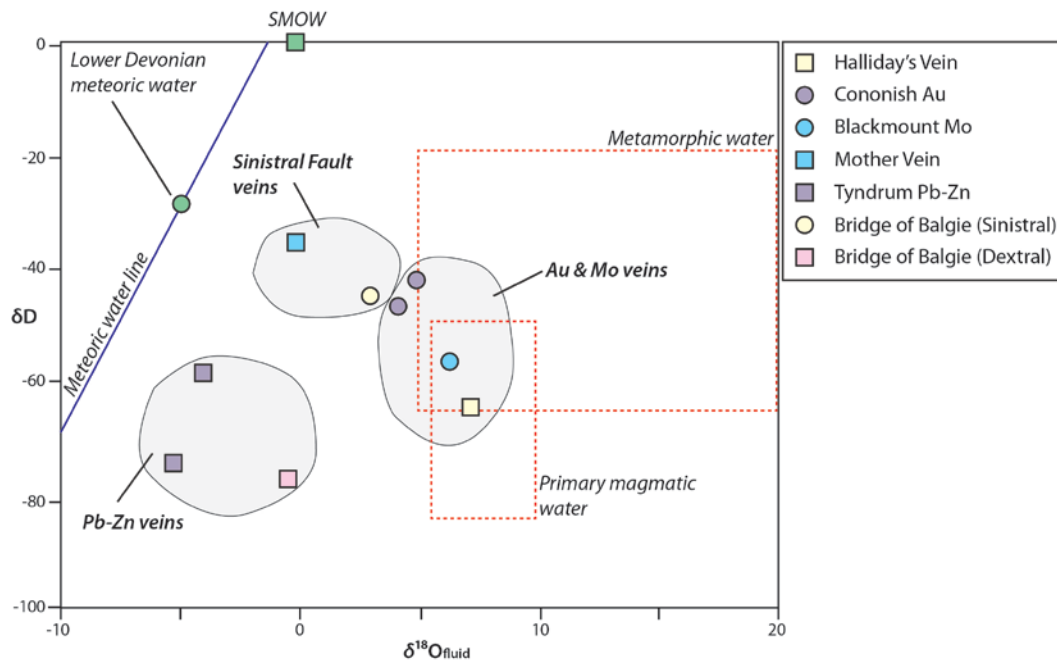


Figure 2.4: Oxygen and hydrogen isotope results for fluids depositing the mineralisation. Modified from Curtis *et al.* (1993).

2.3.4.2 Sulphur isotopes

A number of previous workers have obtained small S-isotope datasets on gold mineralisation across the Scottish Dalradian Supergroup. Curtis *et al.* (1993) measured a range of $\delta^{34}\text{S}$ of 6.0-8.4‰ (n=9) on samples from the Cononish deposit. Pattick *et al.* (1988) and Curtis *et al.* (1993) presented a small dataset of sulphur isotope results from the gold-bearing Halliday's Veins (pyrite $\delta^{34}\text{S}$ = -0.6 to +8.8‰; galena $\delta^{34}\text{S}$ = +1.5 to +2.0‰; n = 6). Pattick *et al.* (1983, 1988) and Curtis *et al.* (1993) undertook a small sulphur isotope study on the Mother Vein with pyrite $\delta^{34}\text{S}$ between +8.0 and +9.8‰ and galena $\delta^{34}\text{S}$ between +7.2 and +11.2‰ (n = 7).

The mineral S-isotope values at Cononish were interpreted to indicate a mixed source of sulphur in the mineralisation (Curtis *et al.* 1993). The sulphide phases sampled were not tied to the complex paragenesis of the gold-bearing quartz veins in the Pattick *et al.* (1983, 1988), Earls *et al.* (1992) and Curtis *et al.* (1993) studies.

The existing sulphur isotope data suggest all of the gold mineralisation in the Tyndrum area has a comparable sulphur source, although lower $\delta^{34}\text{S}$ values are seen at Halliday's Vein. The small number of samples in all veins may not reflect the true variation in $\delta^{34}\text{S}$ values.

2.3.4.3 Geochronology

Previous $^{40}\text{Ar}/^{39}\text{Ar}$ and K-Ar K-feldspar dating at the Cononish deposit suggests mineralisation occurred at 410 ± 14 Ma (Treagus *et al.* 1999), recent geochronological work

($^{40}\text{Ar}/^{39}\text{Ar}$ K-feldspar; Rice *et al.* 2012) supports a formation age close to 410 Ma (Rice *et al.* 2012). The Treagus *et al.* (1999) K-feldspar date was not tied to the paragenesis but work by Spence-Jones (2013) suggests K-feldspar forms syn-gold. The sample dated was not an *in situ* sample with the sample taken from the spoil tip during drilling of the adit. The step-heating profiles for the Treagus *et al.* (1999) date are not flat, and better step-heating profiles are recorded for the Rice *et al.* (2012) date (Rice pers. comm.).

Improvements in $^{40}\text{Ar}/^{39}\text{Ar}$ dating methods have reduced the error on the age for Cononish to a few million years (Rice pers. comm.) compared to the 14 Ma error on the existing date (Treagus *et al.* 1999). The Rice *et al.* (2012) age is tied to the existing paragenesis through gold inclusions, within the K-feldspar, indicating K-feldspar was coeval with gold mineralisation (Rice *et al.* 2012).

Dating work on adularia at the gold-bearing Rhynie Chert, Aberdeenshire by Mark *et al.* (2011a) has constrained mineralisation to 407.6 ± 2.2 Ma by $^{40}\text{Ar}/^{39}\text{Ar}$ (reported in Mark *et al.* 2013). A U-Pb zircon age by Parry *et al.* (2011) has dated the Milton of Noth andesite, in the base of the stratigraphic sequence, to be 411.5 ± 1.1 Ma. While Parry *et al.* (2011) interpreted this age to represent the age of mineralisation at Rhynie, Mark *et al.* (2013) attribute this age to only date emplacement of the slightly earlier andesite. The relationship between the gold-bearing chert and the andesite is poorly constrained (Mark *et al.* 2013).

While the dates for gold mineralisation in the Scottish Dalradian are very similar, two dates are not a large enough dataset to establish if all gold mineralisation is coeval. In addition, all dating work has utilised $^{40}\text{Ar}/^{39}\text{Ar}$ K-feldspar dating. While this method is robust in well characterised homogenous samples it is a technique that is viewed with some scepticism due to the potential for re-setting at low temperatures by later fluids (Lee 1995; Parsons & Lee 2000; Mark *et al.* 2008).

2.4 Gold occurrences in the Irish Dalradian Supergroup

All gold occurrences in the Irish Dalradian Supergroup are gold-bearing vein-hosted occurrences that post-date ductile deformation associated with Grampian Event orogenesis. Across the region quartz veins are generally poorly mineralised, whereas the Curraghinalt and Cavanacaw deposits have economic gold and have been interpreted to be structural fluid traps maximising gold deposition (Parnell *et al.* 2000).

2.4.1 Cavanacaw and Curraghinalt

The Cavanacaw deposit is the only operating gold mine in the Dalradian Supergroup and contains a resource of 438, 000 oz Au (Fig. 2.1; Galantas Gold Corporation 2013). The largest gold resource in the Dalradian Supergroup is at Curraghinalt (Fig. 2.1; 2.7 Moz Au; Dalradian Resources Inc. 2012)

Curraghinalt and Cavanacaw are hosted in the graphitic semipelitic to pelitic Glengawna Formation (Argyll to Southern Highland Subgroup; Table 2.1; Arthurs 1976; Parnell *et al.* 2000). The mineralised vein systems at Curraghinalt and Cavanacaw were emplaced during Caledonian thrusting and are structurally controlled by variation in the geometry of the Omagh thrust and pre-existing structures in underlying pre-Caledonian rocks (Parnell *et al.* 2000). The quartz textures, in both deposits indicate a shallow deposition depth (<10 km; Groves & Foster 1993).

2.4.1.1 Variation at the Cavanacaw deposit

The Cavanacaw deposit is characterised by tellurides within pyrite with some tetrahedrite (Fig. 2.5; Parnell *et al.* 2000). The veins at Cavanacaw are arsenic-rich (up to 3.5% As) and there is a strong correlation between gold and silver, as electrum, and copper-iron sulphides (Parnell *et al.* 2000).

A late brittle tectonic overprint of the vein coincided with introduction of a high-salinity low-temperature fluid that mixed with a low-salinity higher-temperature fluid, precipitating carbonates, base-metal sulphides and electrum (Parnell *et al.* 2000).

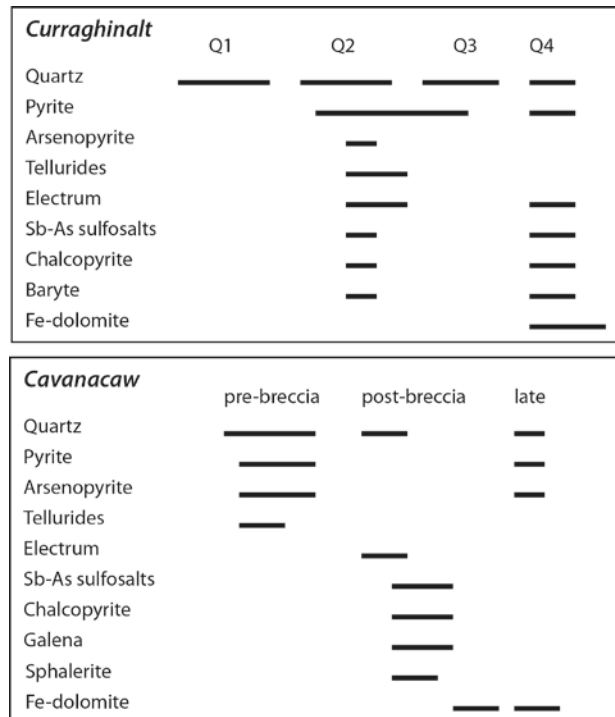


Figure 2.5: Paragenesis for main Irish gold deposits at Curraghinalt and Cavanacaw. After Wilkinson *et al.* (1999).

2.4.1.2 Variation at the Curraghinalt deposit

The veins are hosted in NW-trending NE-dipping structures associated with E-W trending shear zones (Table 2.1; McCaffery & Johnston 1996); the main movement on the faults was dextral with a late component of sinistral movement (Parnell *et al.* 2000). The veins vary from mm scale to 2.75 m in width and thicken towards the E-W trending shear zones (Parnell *et al.* 2000); the largest veins formed as a result of reopening and brecciation of existing veins (McCaffery & Johnston 1996).

An arsenic soil anomaly resulted in initial exploration at Curraghinalt (Parnell *et al.* 2000) but it has since been noted gold mineralisation is arsenic poor (max. 0.013%; Parnell *et al.* 2000). The veins contain abundant quartz, carbonate, barite, sulphide and gold, as electrum. The sulphide assemblage is dominated by pyrite, arsenopyrite, chalcopyrite with tennantite/tetrahedrite and tellurides (of Bi, Au-Ag, Hg, Pb; Earls *et al.* 1996). Late electrum is Ag-rich compared to early Au-rich electrum (Parnell *et al.* 2000). Curraghinalt veins have higher bismuth and copper and lower lead and antimony concentrations than at Cavanacaw (Parnell *et al.* 2000).

2.4.2 Bohau deposit

The Bohau deposit, County Galway, western Ireland, is hosted within an extensional fault, proximal to a major accretionary boundary, in Silurian sediments unconformably overlying

Dalradian metasediments (Fig. 2.1; Lusty *et al.* 2011). The mineralogy is dominated by quartz-sericite-chlorite and minor sulphides with high silver contents (up to 41 wt. %) and some native gold (Lusty *et al.* 2011). Lusty *et al.* (2011) discounted an orogenic origin (after Groves *et al.* 2003) for the Bohaun veins based on the nature of the mineralising fluids involved in mineralisation. The veins have atypical characteristics for orogenic gold and although the veins do not seem orogenic (after Groves *et al.* 2003) in nature, there is no clear magmatic association (Lusty *et al.* 2011). A model for precipitation of the veins is proposed by Lusty *et al.* (2011) involving transportation and deposition of gold from basinal brines, rather than remobilisation of orogenic gold by basinal brines as seen at Curraghinalt (Wilkinson *et al.* 1999).

2.4.3 Constraints on mineralisation in the Irish Dalradian

2.4.3.1 Oxygen isotopes and ore fluids

The ore fluids at Curraghinalt and Cavanacaw have been well documented (Wilkinson *et al.* 1999; Parnell *et al.* 2000) and early fluids are characterised by mixing between a fluid with a significant magmatic component and a low-temperature formation water (Parnell *et al.* 2000). A late low-temperature, high-salinity brine is recorded and this fluid remobilises early gold mineralisation (Wilkinson *et al.* 1999). Cavanacaw ore fluids salinities vary from 1.1 to 16.3 wt. % NaCl equiv. and have low homogenisation temperatures (T_h 124-174°C; Parnell *et al.* 2000). A very extensive study into the nature of fluids at the Curraghinalt and Cavanacaw deposits is reported in Parnell *et al.* (2000) with both oxygen isotopes and fluid inclusions tied to the quartz generations. This suggests the oxygen isotopes and fluid inclusion data is robust and represents the full variation in fluids at Curraghinalt and Cavanacaw.

Four quartz stages are identified at Curraghinalt; Q1 is an early barren phase followed by the abundant Q2 and primary electrum precipitation (Wilkinson *et al.* 1999). Q3 is distinct vuggy quartz, Q4 is only present in larger veins at the centre of the deposit. Q4 is associated with base metal and remobilised gold mineralisation (Wilkinson *et al.* 1999).

Oxygen isotope data from Curraghinalt constrain Q2 quartz to be precipitated from a fluid with $\delta^{18}O$ of +4.6 to +9.6‰. Fluid inclusions show gold mineralising fluids precipitating Q2 are low to moderate salinity (3.3-13.4 wt. % NaCl equiv.) at 125-500°C (average 330°C) and contain CO₂ (15 wt. %; Wilkinson *et al.* 1999).

Fluid inclusions in Q3 are a low- to moderate-salinity (0.1-15.4 wt. % NaCl equiv.) at <280°C (Wilkinson *et al.* 1999). The late brine (Q4 quartz) is characterised by a high salinity

fluid (12-21 wt. % NaCl equiv.) at 120°C with no CO₂ (Wilkinson *et al.* 1999). It is suggested Q3 and Q4 fluids were partially contemporaneous based on mixing trends and textural relationships between Q3 and Q4 quartz (Wilkinson *et al.* 1999).

Late brine (Q4) $\delta^{18}\text{O}$ is close to zero (Wilkinson *et al.* 1999) and the source of the high-salinity is interpreted to be either pre-existing evaporites or contemporaneous evaporated seawater (Wilkinson *et al.* 1999). The timing of brine fluid movement, associated with upgrading of the electrum content, is controlled by the reactivation of the host structures. Brine fluid emplacement is the only significant event of post-Caledonian tectonism and is thought to be of Variscan age (Earls *et al.* 1996; Wilkinson *et al.* 1999).

Bohaun vein deposition is associated with two fluids; moderate to high salinity (8.0-23.6 wt. % NaCl equivalent) and low to moderate salinity (0-7.8 wt. % NaCl equivalent), both with low CO₂ (<3.5 wt. %) at 175-245°C. (Lusty *et al.* 2011). Lusty *et al.* (2011) favour basinal fluids as the source of mineralising fluids. The fluid inclusions in this study were tied to the gold-hosting stage but no clear relationship between the fluids and quartz stages is reported (Lusty *et al.* 2011).

2.4.3.2 Sulphur isotopes

A limited sulphur isotope study at Curraghinalt reports pyrite $\delta^{34}\text{S}$ values with an average of $+8.9 \pm 4.1\text{‰}$ (1 σ ; n = 16) and variable barite $\delta^{34}\text{S}$ values between +20.8‰ and +30.4‰ (Parnell *et al.* 2000). At Cavanacaw pyrite $\delta^{34}\text{S}$ is $7.1 \pm 2.1\text{‰}$ (1 σ ; n=8; Parnell *et al.* 2000) within the range at Curraghinalt. Pyrite $\delta^{34}\text{S}$ at Cavanacaw and Curraghinalt is largely comparable with data reported for the quartz vein-hosted gold in the Scottish Dalradian (section 2.3.4.2).

2.4.3.3 Geochronology

At the Curraghinalt deposit, Rice *et al.* (2012) dated muscovite ($^{40}\text{Ar}/^{39}\text{Ar}$) and molybdenite (Re-Os) from the vein and wall rock. Gold mineralisation is bracketed between 458 (Re-Os molybdenite) and 453 Ma ($^{40}\text{Ar}/^{39}\text{Ar}$ on vein muscovite) with metamorphic muscovite in the wall rock dated at 459 Ma ($^{40}\text{Ar}/^{39}\text{Ar}$; Rice *et al.* 2012). The ages are well constrained and obtained using dating methods considered to be robust. Rice *et al.* (2012) suggest the wall rock muscovite date records metamorphic cooling and the 453 Ma muscovite reflects a fluid event at temperatures <350°C. The age relationship between wall rock and vein muscovite suggests the veins are orogenic in nature as they formed within a few 10's of millions of years of peak metamorphism (*c.* 475-470 Ma; Chew & Strachan 2014; Chapter 3).

2.5 Global deposit models

Globally metamorphic rocks are known to host gold deposits. The deposits are variably classified with three main classes considered here, orogenic (Groves *et al.* 1998); epithermal (Hedenquist *et al.* 2000) and reduced intrusion-related (Thompson *et al.* 1999; Lang & Baker 2001; Hart & Goldfarb 2005). Classification of gold systems in or around intrusions is complicated as many deposit types have some spatial or temporal relationship with intrusions but are not genetically tied to the magmatism (Lang & Baker 2001). For example some orogenic gold deposits are hosted in intrusions but are emplaced much later than the host rocks (Goldfarb *et al.* 2001). Many epithermal gold deposits are also related to intrusions with mineralising fluids interpreted be of magmatic origin (Hedenquist *et al.* 2000). Reduced intrusion-related gold systems specifically refer to deposits hosted in, or genetically related to, reduced granite and gabbro intrusions (defined as reduced based on an absence of magnetite in the assemblage; Hart & Goldfarb 2005).

In this study, the definition of Groves *et al.* (1998) is used for orogenic gold, epithermal gold deposits are defined by Hedenquist *et al.* (2000) and reduced intrusion-related gold by Thompson *et al.* (1999). Here, the Cononish deposit characteristics are compared to the existing deposit models for orogenic, epithermal and reduced intrusion-related gold systems to develop a testable model for vein-hosted gold mineralisation in the Scottish Dalradian Supergroup.

2.5.1 Orogenic gold deposits

2.5.1.1 Definition

Orogenic gold deposits have been characterised and studied by a number of workers (e.g. Groves *et al.* 1998; Goldfarb *et al.* 2001, 2005; Bierlein *et al.* 2004; Table 2.2). This study uses the definition of Groves *et al.* (1998), which states that deposits are post-orogenic with respect to the tectonism of the immediate host rocks but are syn-orogenic with respect to on-going deep crustal, subduction-related, thermal processes. Orogenic gold deposits are hosted in variably metamorphosed rocks with mineralisation at syn- to post-peak metamorphic conditions (Groves *et al.* 1998).

2.5.1.2 Interpretation of deposit type

Orogenic gold mineralisation is temporally associated with the exhumation of an orogen and addition of heat to a thickened crust (Fig. 2.6; Goldfarb *et al.* 1993). The deposits are recognised in deformed metamorphic terranes of all ages and a strong association between

gold and greenschist to lower-amphibolite facies rocks is recorded (Groves *et al.* 1998). Orogenic gold deposits occur in higher and lower grade rocks (e.g. McCuaig *et al.* 1993) but with less frequency. Bierlein *et al.* (2004) report that with increasing metamorphic grade the time of mineralisation gets closer to the time of peak metamorphism.

Structurally, veins are commonly found sub-parallel to major steeply-dipping transcrustal faults and are hosted in lower-order structures off the main faults (Groves *et al.* 1998). There is no clear relationship with regional granitic intrusions, however, there is often an apparent spatial relationship between gold mineralisation and the presence of lamprophyre sills but this is not a definitive characteristic (Groves *et al.* 2003).

Orogenic deposits are commonly associated with a broad alteration zone that is larger than the dimensions of the ore body (Bierlein *et al.* 2004). The mineralogy of the deposit is dominated by a pyrite-arsenopyrite assemblage with variable concentrations of Fe, Pb, Cu, Zn, Mo, Sb and As (Bierlein & Crowe 2000). The Au/Ag ratio varies significantly from 10-1 (by mass) with lower values less commonly observed (Groves *et al.* 1998). Ore fluids typically have 3-10 wt. % NaCl and <5 mol% CO₂, precipitated at 200-600°C (Groves *et al.* 1998; Tomkins & Grundy 2009). Bierlein *et al.* (2004) report P-T conditions of 1-3 kbar and 180-350°C, a narrower range than reported by other workers.

2.5.1.3 Relevance to the Cononish deposit

The Cononish deposit has characteristics in common with the orogenic gold model as defined by Groves *et al.* (1998). The deposit is hosted in a splay off the major first-order Tyndrum Fault within the Dalradian orogenic belt. The host rocks have undergone amphibolite facies metamorphism, which should indicate gold mineralisation occurred close to peak-metamorphism, if the Cononish deposit is orogenic in origin (Groves *et al.* 1998; Bierlein *et al.* 2004). There is no clear association with granite batholiths, unless the gravity low extending from the Etive Complex represents a concealed granite (Patrick *et al.* 1988). Fluid inclusion microthermometry and oxygen isotope data at the Cononish deposit suggests ore fluids were at a comparable temperature with similar NaCl contents to the Groves *et al.* (1998) orogenic gold model but that the Cononish deposit has a much higher CO₂ content. The CO₂ content may be comparable given Groves *et al.* (1998) report a bulk value and the Cononish deposit is likely to have undergone un-mixing of the fluid producing CO₂-rich and CO₂-poor fluids. The Au/Ag ratio at the Cononish deposit (0.25) is not comparable to orogenic gold deposits (1-10; Groves *et al.* 1998).

Table 2.2 Characteristics of key gold deposit types and whether they are present at Cononish. Orogenic gold after Groves *et al.* (1998), low-sulphidation epithermal after Hedenquist *et al.* (2000), reduced intrusion-related after Thompson *et al.* (1999) and Hart & Goldfarb (2005).

Characteristic	Orogenic gold deposits	<i>Cononish</i>	Low-sulphidation epithermal	<i>Cononish</i>	Reduced Intrusion-related	<i>Cononish</i>
Tectonic setting of host rocks	Deformed continental margin	<i>Present</i>	Extension to transtensional settings	<i>Present</i>	Accretionary to collisional subduction related setting	<i>Present</i>
Structural setting of host rocks	Lower-order structures adjacent to first order transcrustal structures	<i>Present</i>	Lower-order splays from first order structures, domes, diatremes	<i>Present</i>	Proximal to distal from an intrusive body, fracture controlled	<i>Possible</i>
Depth of emplacement	2-20 km	<i>Present</i>	<1 km	<i>Absent</i>	1-6 km	<i>Present</i>
Genetically related rocks	Immediate host rocks do not control mineralisation	<i>Present</i>	Andesite-rhyolites, alkali rocks	<i>Absent</i>	Multiphase intermediate-felsic subalkalic intrusives	<i>Absent</i>
Host rocks	Variable, normally metasedimentary rocks	<i>Present</i>	Pyroclastic and sedimentary rocks	<i>Absent</i>	Metasedimentary rocks	<i>Present</i>
Metamorphism of host rocks	Normally greenschist but observed in amphibolite facies	<i>Present</i>	Essentially un-metamorphosed	<i>Absent</i>	Proximal - within the thermal metamorphic areole	<i>Possible</i>
Deposit form	Large veins, vein array, saddle reef	<i>Present</i>	Veins, veins swarms, breccias	<i>Present</i>	Veins, hydrothermal breccia	<i>Present</i>
Gangue	Quartz	<i>Present</i>	Quartz, chalcedony	<i>Present</i>	Quartz	<i>Present</i>
	Sericite	<i>Present</i>	Sericite	<i>Present</i>	Sericite	<i>Present</i>
	Chlorite	<i>Present</i>	Chlorite	<i>Present</i>		
	Alkali feldspar	<i>Present</i>	Adularia	<i>Present</i>		
	Minor Fe-Mg \pm Ca carbonate	<i>Present</i>	Rhodochrosite, barite, anhydrite	<i>Absent</i>		
Sulphides	Pyrite	<i>Present</i>	Pyrite (Au-Ag) sulphides	<i>Present</i>	Pyrite	<i>Present</i>
	Arsenopyrite	<i>Minor</i>	Arsenopyrite	<i>Minor</i>	Arsenopyrite	<i>Minor</i>
			Pyrrhotite	<i>Absent</i>	Pyrrhotite	<i>Absent</i>
	Variable Fe, Pb, Cu, Zn, Mo, Sb and As sulphides	<i>Present</i>	Variable sphalerite, galena, chalcopryrite, tetrahedrite/tennantite in intermediate sulphidation	<i>Present</i>	Low concentration of base metals. Elevated Bi, W, As, Mo, Te and Sb	<i>Absent</i> <i>Low As, Sb & W; no Bi; High Te, Mo</i>
Vein textures	Banded margins, anhedral quartz, veinlets, breccias	<i>Present</i>	Crustiform-colloform banding, coarse bands	<i>Absent</i>	Steep veins, breccias	<i>Present</i>
Alteration	Quartz	<i>Present</i>	Quartz	<i>Present</i>	Quartz	<i>Present</i>
	Carbonate	<i>Present</i>	Rhodochrosite	<i>Absent</i>	Sericite	<i>Present</i>
	Sericite/muscovite	<i>Present</i>	Sericite	<i>Present</i>	Chlorite	<i>Present</i>
	Chlorite	<i>Present</i>	Chlorite	<i>Present</i>	Feldspar	<i>Present</i>
	Albite	<i>Present</i>	Adularia	<i>Present</i>		
Ore fluids	150-450°C (typically 275-350°C),	<i>Present</i>	<220 to 280°C	<i>Present</i>	>200 to <600°C	<i>Lower end of range only</i>
	<6 wt % NaCl equiv.	<i>Present</i>	<10 wt % NaCl	<i>NaCl present</i>	CO ₂ rich fluids	<i>Present</i>
	C-O-H \pm N, near neutral to low-pH	<i>Possible</i>	Intermediate has 3 to 10 wt. % NaCl	<i>Present</i>	NaCl in fluids from shallow depths (<1.5 km)	<i>NaCl present</i>

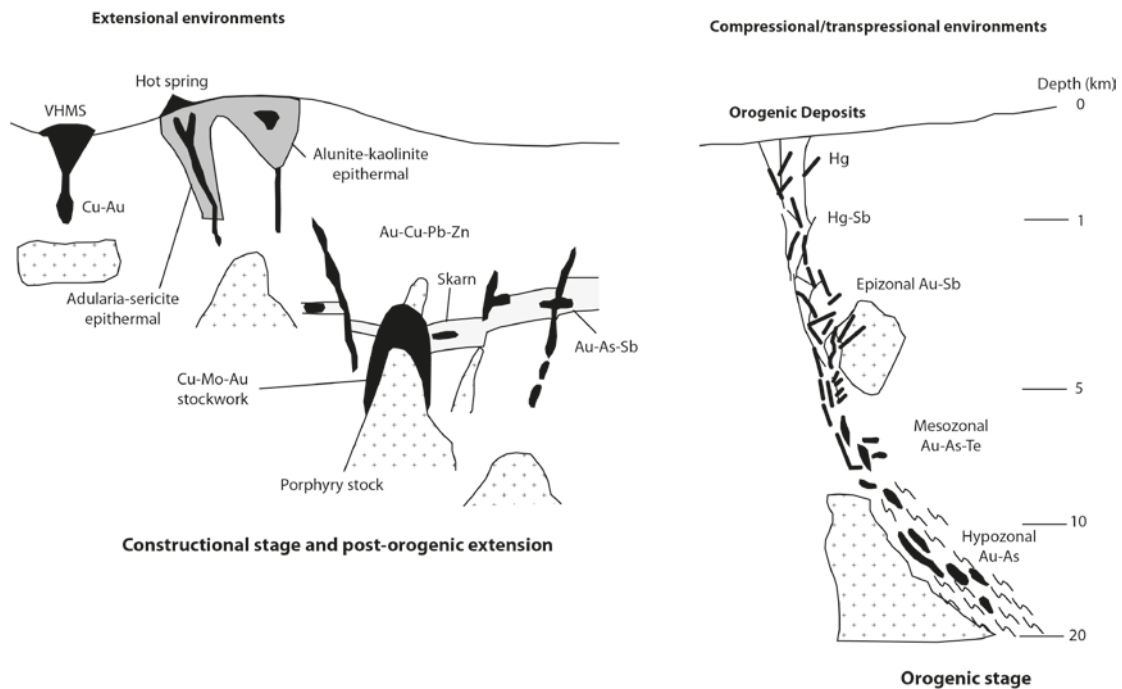


Figure 2.6: Model of formation of intrusion-related gold deposits and orogenic and shows variation observed in orogenic and epithermal gold deposit formation. Figure after Groves *et al.* (1998).

2.5.2 Epithermal gold deposits

Epithermal describes gold deposits formed at shallow depths (<1 km; Hedenquist *et al.* 2000). Three subgroups of epithermal gold deposits are defined, high, low and intermediate sulphidation by Hedenquist *et al.* (2000) based on the sulphidation state of the sulphide assemblage. These deposits form in a variety of tectonic settings but commonly have magmatic fluids genetically associated with the deposit (Fig. 2.6; Hedenquist *et al.* 2000; Simmons *et al.* 2005). High sulphidation deposits are characterised by pyrite-enargite-luzonite-covellite assemblage, this deposit type is not considered here due to the lack of enargite-luzonite-covellite in the Cononish assemblage.

2.5.2.1 Definition

Low sulphidation deposits contain pyrite-pyrrhotite-arsenopyrite and high Fe-sphalerite (Hedenquist *et al.* 2000). Hedenquist *et al.* (2000) define an intermediate-sulphidation subset to low-sulphidation epithermal deposits, characterised by pyrite-tetrahedrite/tennantite-chalcopyrite and low Fe-sphalerite with high Ag and base-metals compared to Au-rich low sulphidation deposits.

2.5.2.2 Interpretation of deposit type

Low sulphidation epithermal deposits occur in extensional to transtensional settings forming in lower-order structures off the major first-order structures in the area (Table

2.2). There is a strong structural control and deposits have a highly variable form, due to varying permeability of the host rocks. The deposits take the form of veins, vein swarms, brecciation and dissemination of mineralisation into the wall rock. The largest tonnage deposits are disseminated ores with the highest grade forming in veins in fractures (Hedenquist *et al.* 2000). Typically epithermal gold deposits are hosted in rocks only a few Ma older than the mineralisation itself (Hedenquist *et al.* 2000). However, epithermal ore bodies can be hosted in much older rocks, e.g. at the Mesquite mining district Oligocene epithermal deposits are hosted in Jurassic gneisses (age of metamorphism) intruded by Cretaceous granite, pegmatite and aplite (Tosdal *et al.* 1985; Willis & Tosdal 1992). The Mesquite epithermal gold deposits are thought to have been formed from fluids, driven by Oligocene age intrusions outside of the mining district, utilising high-angle faults to flow into the mining district (Willis & Tosdal 1992).

Vein mineralogy is dominated by adularia-sericite-quartz with the sulphide mineralogy characterised by pyrite with Au-Ag. The veins have metal enrichments in Zn, Pb, Cu, As, Sb and Hg in sulphides with some sulphosalts (Hedenquist *et al.* 2000). There is also often well-developed pyrrhotite and arsenopyrite in low-sulphidation epithermal deposits. Shallow low sulphidation deposits (0-300 m) have an Au-Ag-As-Sb-Se-Hg-Tl metal assemblage with <0.1-1 % base metals and high Au/Ag ratios (>1; Hedenquist *et al.* 2000). Intermediate sulphidation deposits are a subset of low sulphidation epithermal gold deposits and form at deeper depths (300-800 m; Hedenquist *et al.* 2000). Intermediate sulphidation have Ag-Au-Pb-Zn, Ba, Mn and Se (with andesite-rhyolite) and 2-10 % base metals with a low Au/Ag ratio (Hedenquist *et al.* 2000).

Hedenquist *et al.* (2000) report low sulphidation deposits to be low salinity and low temperature (<1 wt. % NaCl equiv. and <220°C) with deeper deposits more saline and formed at higher temperatures (3-10 wt. % NaCl equiv., 220-280°C). Later workers suggest fluids are not as saline but can be higher temperature (<5 wt. % NaCl equiv. and 150-300°C; Simmons *et al.* 2005). Simmons *et al.* (2005) do not report a difference between fluids forming shallow and deep deposits. The higher fluid salinity suggested by Hedenquist *et al.* (2000) accounts for higher Ag and base metal content in intermediate sulphidation deposits (Henley 1990; Simmons 1995), the later study by Simmons *et al.* (2005) cannot account for this with the lower reported salinities.

2.5.2.3 Relevance to the Cononish deposit

Cononish is hosted in a transtensional structural regime in a lower order structure. The deposit is postulated to be formed at depths of *c.* 4 km (Curtis *et al.* 1993) greater than generally accepted for epithermal gold deposits. Adularia is recorded in the paragenesis at Cononish comparable to epithermal gold deposits. The Cononish deposit has low Au/Ag ratios (0.25) which are not comparable to low sulphidation epithermal deposits (>1 ; Hedenquist *et al.* 2000). The fluid inclusions data at the Cononish deposit suggests ore fluids are higher temperature and salinity than typical epithermal deposits. Intermediate sulphidation epithermal deposits are the most comparable to the Cononish deposit, with a pyrite, chalcopyrite and low Fe sphalerite assemblage, and are silver and base metal-rich. While, there is some evidence for epithermal textures in mineralisation at the Cononish deposit and the higher salinity at Cononish could be invoked to account for the high base metal content, the higher temperature of fluids compared to the epithermal deposit model of Hedenquist *et al.* (2000) cannot be accounted for.

2.5.3 Reduced intrusion-related gold systems

2.5.3.1 Definition

Reduced intrusion-related gold systems (RIGS) are characterised by a spatial association with reduced granites and a dominance of carbonic hydrothermal fluids (Fig. 2.7; Table 2.2; Thompson *et al.* 1999; Hart & Goldfarb 2005). RIGS commonly occur in regions with intrusion-related tin and tungsten deposits (Thompson *et al.* 1999).

2.5.3.2 Interpretation of deposit type

The tectonic setting of the deposits is poorly understood and deposits have been recorded in back-arc, collisional, post-collisional and arc settings (Lang & Baker 2001). These deposits are noted in rocks of varied metamorphic facies, from unmetamorphosed to amphibolite facies. The intrusions themselves are undeformed and are emplaced post-regional deformation. The intrusions are metaluminous, subalkalic and intermediate to felsic in composition (Lang & Baker 2001), comprising batholiths, plutons, dome complexes and dykes or sills (Thompson *et al.* 1999; Lang *et al.* 2000). The intrusions are defined as reduced by the absence of magnetite, which places the intrusions into the ilmenite series (Hart & Goldfarb 2005). The depth of formation ranges from >1 to <8 km, with most gold deposits forming between 4 and 6 km (Hart & Goldfarb 2005). RIGS differ from the traditional porphyry deposit model because there is a lack of multi-directional veining in the igneous complex (Thompson *et al.* 1999).

RIGS show variation from early high-temperature magmatic mineralisation to late low-temperature hydrothermal mineralisation, metal assemblages are zoned away from the central pluton (Fig. 2.7) with silver and base metal-rich veins forming distally from the main intrusion. Intrusion-related gold deposits exhibit a low sulphide content ($<5\%$) with gold and anomalous Bi, W, Mo, Te and Sb (Lang & Baker 2001); a higher sulphide content is observed in deposits distal to the intrusive centre (Lang & Baker 2001).

Fluid inclusion data indicate pressures of formation vary greatly (0.3-3.5 kbar; Lang & Baker 2001; Mair 2004; Hart & Goldfarb 2005). The composition of the mineralising fluids is highly variable and the temperature of formation varies from >200 to $<600^{\circ}\text{C}$ with ore fluids having a significant carbonic component (Lang & Baker 2001).

2.5.3.3 Relevance to the Cononish deposit

The data from the Cononish deposit suggest that while the deposit may be related to a concealed granitic intrusion at depth and reduced intrusion-related gold systems are commonly associated with I-type granite intrusions (based on a lack of magnetite; Hart & Goldfarb 2005), the Cononish deposit is not a reduced intrusion-related gold system. The Etive Complex, the nearest exposed granite to Cononish, is an oxidised I-type granite, based on the presence of abundant magnetite and minor ilmenite (Haslam *et al.* 1985) and the postulated Lochaber batholith is expected to be comparable to the Etive Complex. The characteristic Bi and W enrichment associated with reduced intrusion-related gold systems is not seen in the Tyndrum area (Chapter 5) and while the abundant lamprophyre sills may be indicative of a reduced-intrusion related gold system, they equally may be un-related to gold emplacement and may be utilising the same structural traps as hydrothermal fluids (Rock & Groves 1988).

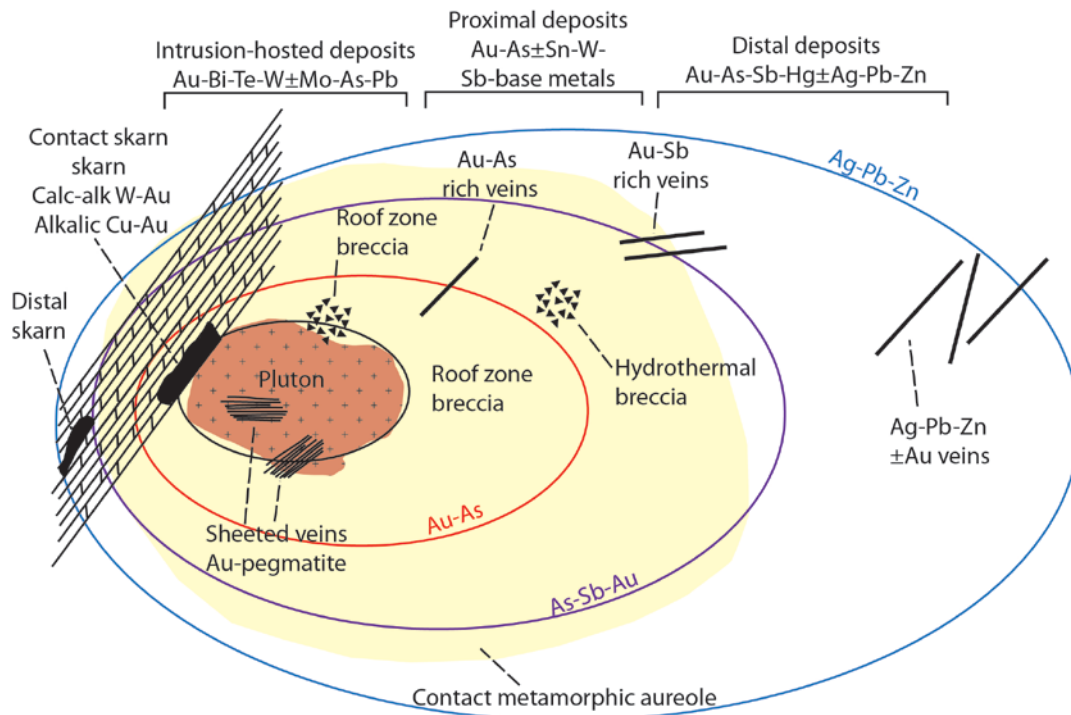


Figure 2.7: Model for reduced intrusion-related gold deposits. Modified from Lang & Baker (2001) and Hart *et al.* (2002).

2.6 Characterisation of gold occurrences

The Cononish deposit does not fit any of the classic deposit models and this also seems likely for a number of the other gold occurrences in the Dalradian Supergroup. In the following sections classifications based on mineralogy, structural setting and geochronology using data from this study and previous workers (Rice *et al.* 2012; Tanner 2012; Mark *et al.* 2013) are reviewed.

2.6.1 Mineralogy and sulphide assemblage

Tanner (pers. comm.) characterises gold-bearing quartz veins in the Dalradian Supergroup based on mineralogy and sulphide assemblage, and defines two groups. Group A is characterised by a poly-metallic assemblage with pyrite, chalcopyrite, arsenopyrite, galena and sphalerite. In addition, gold, as electrum, with native gold and hessite, tetrahedrite and bismuth minerals are noted. Group A includes the majority of gold occurrences in the Dalradian Supergroup (Table 2.3). Group B is defined by a simpler assemblage of quartz, pyrite, native gold and minor sulphides and includes Rhynie and Bohaun.

2.6.2 Structural setting

Structural observations of the gold-bearing quartz veins are considered as a method of classification. Tanner (2012) applied a modified Coulomb model to the vein-hosted gold occurrences in the Tyndrum area and concluded the veins formed in response to simple

shear whilst the Tyndrum and Ericht-Laidon Faults moved as a shear couple. The majority of the previously identified gold showings in the Tyndrum area fit this model (Table 2.3). The veins at Calliachar-Urlar Burn and Tombuie also fit this model with the occurrences hosted parallel to major faults in splays off the major structures or along the trace of calculated Riedel fractures (Tanner pers. comm.). The Bohaun deposit does not occur on the trace of either σ_1 or along the Riedel fracture and as a result does not fit the Tanner (2012) model. In addition, the Curraghinalt and Cavanacaw deposits do not fit the structural model proposed by Tanner (2012).

2.6.3 Geochronology

Geochronology is only available for the larger gold occurrences; recent work at Curraghinalt by Rice *et al.* (2012) has constrained the age of gold mineralisation to 458-453 Ma. The ages place gold mineralisation after but closely following peak metamorphism (*c.* 475-470 Ma; Stephenson *et al.* 2013; Chew & Strachan 2014) suggesting an orogenic origin for the deposit. The Rhynie Chert is dated at 407.6 ± 2.2 Ma (2σ ; $^{40}\text{Ar}/^{39}\text{Ar}$ K-feldspar; Mark *et al.* 2013). This age is comparable to existing data (410 ± 14 Ma; Treagus *et al.* 1999) and new data for the Cononish deposit (407-408 Ma; $^{40}\text{Ar}/^{39}\text{Ar}$ K-feldspar; Rice *et al.* 2012). The geochronology for Rhynie and Cononish suggests emplacement of the deposits occurred significantly post-peak metamorphism and that they could be related to the emplacement of large granite intrusions across the Scottish Dalradian (433 ± 1.8 Ma to 408 ± 0.4 Ma; Re-Os molybdenite & U-Pb zircon respectively; Neilson *et al.* 2009). At Rhynie there is not a clear link to igneous rocks with andesites in the base of the host stratigraphic sequence argued to be earlier and unrelated to mineralisation (Mark *et al.* 2013). A relationship to intrusive activity is not observed at Cononish with no outcrop of Caledonian granite within 10 km of the deposit (Patrick *et al.* 1988; Hill *et al.* 2011).

2.6.4 Summary

The gold deposits in the Dalradian Supergroup cannot be easily classified. When considering the mineralogy Group A is comparable with the assemblage expected in orogenic gold deposits but has anomalously high base metal sulphide, while Group B may be comparable to the low-sulphidation epithermal hot spring type. The characterisation of the Cononish deposit is challenging and while the location of the deposit in a metamorphic belt suggests it may be orogenic, the late-tectonic timing of mineralisation precludes the deposit from being an orogenic gold deposit (Groves *et al.* 1998).

The characterisation of the Curraghinalt deposit suggests the deposit is likely to be orogenic but the structural setting is not typical of the Groves *et al.* (1998) orogenic gold model. The geochronology suggests mineralisation at Curraghinalt (458-453 Ma; Rice *et al.* 2012) occurs close to peak metamorphism (*c.* 475-470 Ma; Chew & Strachan 2014). This is a defining characteristic of the orogenic gold model (Groves *et al.* 1998) and suggests the Curraghinalt deposit is an orogenic gold deposit.

Table 2.3 Characterisation of the gold deposits observed in the Dalradian Supergroup.

Mineralogy and sulphide assemblage	<i>Group A</i> ¹	<i>Group B</i> ¹
	<i>Complex sulphide assemblage with pyrite, chalcopyrite, arsenopyrite, galena and sphalerite. Gold as electrum with minor native gold and tellurides</i> ¹	<i>Quartz, pyrite, native gold and minor sulphides</i> ¹
	Cononish ¹	Rhynie ¹
	Curraghinalt ¹	Bohaun ¹
	Cavanacaw ¹	
	Calliachar-Urilar Burn ¹	
	Kilmelford-Lagalochoan ¹	
Structural controls	<i>Group 1</i> ¹	<i>Group 2</i> ¹
	<i>Development along Riedel shears associated with Caledonian-trending faults</i> ²	<i>Structural setting does not match with Tyndrum area</i> ²
	Cononish ¹	Curraghinalt ¹
	Calliachar-Urilar Burn ¹	Cavanacaw ¹
		Bohaun ¹
Geochronology	<i>~410 Ma</i> ²	<i>458-453 Ma</i> ²
	Cononish ²	Curraghinalt ²
	Rhynie ³	

¹Tanner pers. com., ²Rice *et al.* (2012), ³Mark *et al.* (2011)

Current data suggest a variety of gold deposit types are present in the Dalradian Supergroup. Gold occurrences can be classified as intrusion-hosted (Lagalochoan), orogenic (Curraghinalt and Cavanacaw) and low-sulphidation epithermal (Rhynie). The Bohaun deposit does not easily fit any of the deposit types as it is hosted in a terrane comparable to orogenic gold but has vein textures comparable to quartz-adularia epithermal deposits and the nature of fluids suggest the deposit was emplaced from Carboniferous basinal brines (Lusty *et al.* 2011).

2.7 A working model for the Cononish deposit

This chapter demonstrates the current level of understanding of the characteristics of the Cononish and other gold occurrences in the Tyndrum area. Additional work is required to understand the mineralising system of quartz vein-hosted gold mineralisation in the Tyndrum area and wider Dalradian Supergroup in Scotland. This study needs to identify the potential source rocks for metals and sulphur, fluid sources and pathways, deposition mechanisms and sources of heat in order to assess their respective roles in gold-bearing quartz vein emplacement.

Some of the gold deposits in the Caledonides, Curraghinalt and Cavanacaw, appear to fit well to the orogenic gold model as defined by Groves *et al.* (1998), however, the model does not fit the mineralisation in the Tyndrum area. In addition, while aspects of the low- to intermediate-sulphidation epithermal model (Hedenquist *et al.* 2000), and the proximal to distal RIGS model (Lang & Baker 2001), fit some aspects of the mineralisation in the Tyndrum area it is difficult to attribute all of the characteristics of the Cononish deposit to either deposit type. While RIGS are the commonly seen gold deposits at moderate depths (4-6 km depth), gold deposits are also seen associated with other intrusion types.

Poly-metallic gold mineralisation in the Lachlan Orogenic belt, Australia has elevated Sb, W, Mo and Cu and is associated with emplacement of early-Devonian and middle- to late-Devonian intrusions (Table 2.4; Bierlein *et al.* 2002). The poly-metallic gold mineralisation is geochemically distinct from gold-only orogenic gold in the orogenic belt and is intrusion-related in origin (Groves *et al.* 1998; Bierlein *et al.* 2001). Plutons in Central Victoria, Australia, post-date peak metamorphism and orogenic gold mineralisation by up to 80 Ma (Table 2.4; Arne *et al.* 1998; Foster *et al.* 1998; Bierlein *et al.* 2001) comparable with the >50 Ma time gap between peak metamorphism and I-type post-orogenic granite emplacement seen in the Dalradian Supergroup. The Cononish deposit fits the characteristics of the post-orogenic poly-metallic intrusion-related deposits in the Lachlan Orogenic belt (Bierlein *et al.* 2002) in terms of the geochronological relations, tectonic and structural settings – perhaps representing a possible analogue (Table 2.4).

Table 2.4 Characteristics of intrusion-related gold deposits in the Lachlan belt, Australia compared to the Cononish deposit. Data for the Lachlan intrusion-related gold from Bierlein *et al.* (2002). Cononish as in Table 2.3 except where stated

Characteristic	Lachlan intrusion-related gold	Cononish deposit
Tectonic setting of host rocks	Deformed fore arc setting, possible accretionary prism	<i>Deformed continental margin</i>
Structural setting of host rocks	West-dipping thrust faults on limb of regional anticline	<i>Lower order structure off major regional transcrustal fault</i>
Depth of emplacement	<10 km	<i>4 km</i>
Host rocks	Metamorphosed turbidites and volcanogenic sediments	<i>Metasediments</i>
Metamorphism of host rocks	Lower-greenschist	<i>Upper-greenschist to lower-amphibolite</i>
Timing of metamorphism	455 to 440 Ma	<i>c. 470 Ma (Chew & Strachan 2014)</i>
Genetically related rocks	Granites such as the Stawell and Bute granites	<i>None, Etive intrusive complex 10 km NW</i>
Timing of emplacement of genetically related rocks	Bute granite – 370±4 Ma (Arne <i>et al.</i> 1998)	<i>408±0.5 Ma (Neilson <i>et al.</i> 2009)</i>
Time between peak metamorphism and gold vein emplacement	~70 Ma	<i>~60 Ma</i>
Deposit form	Veins, veinlets, some breccia	<i>Brecciated quartz vein</i>
Gangue	Quartz	<i>Present</i>
	Carbonate	<i>Present</i>
	Chlorite	<i>Present</i>
Sulphides	Pyrite	<i>Present</i>
	Pyrrhotite	<i>Absent</i>
	Arsenopyrite	<i>Minor</i>
Elevated metals	Sb	<i>Absent</i>
	W	<i>Minor</i>
	Mo	<i>Elsewhere in area</i>
	Cu	<i>Present</i>
Vein textures	Fault breccia	<i>Breccia within vein</i>
Alteration	Some potassic within granite contact metamorphism halo	<i>Some K-feldspar</i>
	Phyllic	<i>Some sericite</i>
	Carbonate	<i>Present</i>

It is proposed here, on the basis of the currently available data, gold mineralisation at the Cononish deposit and in the Tyndrum area is an intrusion-related gold system focussed around the post-orogenic late-Caledonian granites found in Dalradian Supergroup (Fig. 2.8). The model involves emplacement of the granite plutons providing a source of heat to drive hydrothermal fluid flow. The granites will cause contact metamorphism, which may release sulphur and metals from the metasedimentary sequence (as suggested for the Cornubian granite, Cornwall; Wilkinson *et al.* 1995). The role of the local host metasedimentary rocks is unconstrained but there is a suggestion the local sequence contributes sulphur to mineralisation as demonstrated by the mixed magmatic-sedimentary $\delta^{34}\text{S}$ signatures reported by Curtis *et al.* (1993).

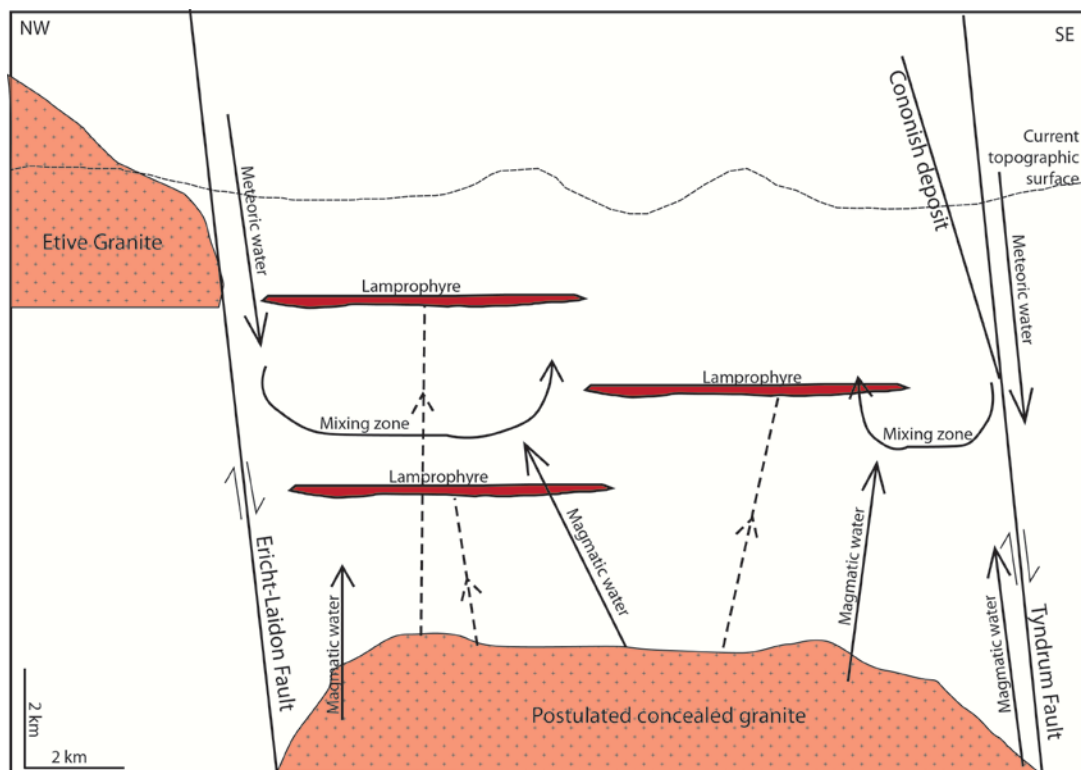


Figure 2.8: Schematic cross-section showing hypothetical model for mineralisation at Cononish. A postulated granite at depth drives mineralisation through mixing of a magmatic water with a meteoric component. Adapted from Tanner (2012).

2.8 Research aims

The aim of this work is to investigate the genesis of the Cononish deposit and other mineralised and barren veins and to identify new mineral occurrences in the Tyndrum area.

This study will test the hypothetical model for the Cononish deposit by addressing research aims identified through review of the existing data. The following hypothesis will be tested; vein-hosted gold mineralisation in the Scottish Dalradian Supergroup is precipitated from

hydrothermal fluids driven by heat from granite batholiths. The key testable criteria are as follows:

1. Establish if all gold mineralisation in the Tyndrum area is coeval and deposited from the same mineralising event or whether multiple gold mineralisation events can be identified in the study area.

At current understanding it is unclear whether all gold-bearing quartz vein mineralisation in the Tyndrum area is coeval with the Cononish deposit (410 ± 14 Ma; Treagus *et al.* 1999; Rice *et al.* 2012). While Curtis *et al.* (1993) proposed Halliday's Veins were coeval with the Cononish deposit, the relationship between Cononish and other occurrences in the area has not been considered. This work will investigate the nature and genesis of the Cononish deposit and other known mineralised and barren veins in the Tyndrum area and classify their relationships based on their field relations, petrographic and geochemical signatures.

Geochronology will determine the age of gold mineralisation in the Tyndrum area and compare it to existing data for major events, including peak metamorphism and late orogenic pluton emplacement. If gold mineralisation is dated close to 470 Ma, this will disprove the hypothesis. Whereas, if gold mineralisation is constrained to between 430 and 400 Ma this will support the hypothesis that, gold mineralisation is contemporaneous with post-orogenic granite emplacement.

2. Assess whether geochemical trends in stream sediment samples can be tied to the observed vein mineralogy and geochemistry.

A large dataset of existing company data is available and this study aims to assess the potential use of regional anomalies for tracing potential gold occurrences, as illustrated by a bismuth anomaly in stream sediments at Calliachar-Urlar (Corkhill *et al.* 2010). The anomalies and geochemical trends will be considered for their potential as exploration criteria in the Tyndrum area.

If the Cononish deposit is related to hydrothermal fluids driven by the emplacement of late-orogenic granitic intrusions across the Dalradian Supergroup, the stream sediment geochemical signatures are expected to reflect the complex mineralogy within poly-metallic veins with likely elevated Cu, Mo, Pb and Te in the stream sediment data.

3. Describe the sulphur isotope ratio variation in different mineralisation types from differing locations in the study area and model the potential input of magmatic and sedimentary sources to constrain the origin of sulphur in mineralisation.

Previous workers have established variation by mineralisation type and location in the Tyndrum area on limited datasets (Pattrick *et al.* 1983; Curtis *et al.* 1993). Sulphur isotope data provide a direct tracer of igneous vs. metasedimentary input into the hydrothermal system and sulphides are directly related to gold. The origin of sulphur in most of the mineralisation is poorly constrained; Curtis *et al.* (1993) suggested the sulphur originated from the Dalradian metasedimentary succession but had a magmatic component.

Determining the sulphur isotope composition and its variation in the gold-bearing and associated hydrothermal systems through space and time will allow for comparison with measurements from the local metasedimentary succession and literature data for other sulphur sources. This will indicate the proportions of sulphur from different sources in different parts of the mineralising system. The presence of a magmatic sulphur component in sulphides within gold-bearing mineralising will support the overall hypothesis.

4. Place observed mineralisation into the context of the evolving Dalradian Supergroup to create a model to assist in the exploration of gold and associated mineralised occurrences.

The final outcome of this work is to develop a refined version of the hypothetical working model for gold mineralisation in the Tyndrum area, which can be applied to the wider Dalradian Supergroup, utilising field relations, petrographic and geochemical relationships, stable isotope work and geochronology. The model aims to create a set of criteria for gold exploration in the Tyndrum and wider regional area.

Chapter 3

The geological setting of the Grampian Highlands and the Tyndrum area

Abstract: The mid-Neoproterozoic (Cryogenian) to mid-Cambrian Dalradian Supergroup is a deformed meta-sedimentary sequence that constitutes the Grampian terrane in Scotland and Ireland. Vein-hosted gold occurrences are found in the Dalradian Supergroup and understanding the evolution of the sequence is crucial for placing controls how veins formed, e.g. times when fluid may have been generated from this volume of rock. The Supergroup was deposited on the developing Laurentian margin before a period of Supercontinent rifting and ocean development from *c.* 600 Ma. The beginning of subsequent closure of the Iapetus Ocean *c.* 470 Ma caused regional deformation and metamorphism in the terrane. Continued subduction of the Iapetus oceanic plate, beneath the Grampian terrane, drove increased heat flow causing intrusion of granite batholiths across the region. The final stages of the Caledonian Orogenic cycle, *c.* 430 Ma, are expressed by movement along the major trans-Caledonide faults, including the terrane bounding Great Glen and Highland Boundary Faults, bringing the Northern Highland and Grampian terranes together in the current configuration. The lithostratigraphic succession may have been redistributed through regional overturned folds during regional deformation and has the potential to contribute metals, released during orogenesis or late fluid flow, to mineralisation. Changes in the metamorphic condition in the Supergroup and emplacement of post-orogenic intrusions may contribute heat, fluids and metals to mineralisation. Post-orogenic fault movement may provide a potential route for regional hydrothermal and meteoric fluid flow through the Dalradian Supergroup.

3.1 Introduction

The Dalradian Supergroup is host to widespread gold mineralisation of uncertain origin (Chapter 2). The evolution of the Dalradian Supergroup has implications for the genesis of vein-hosted gold mineralisation in the Supergroup.

- The Dalradian Supergroup lithostratigraphic succession has the potential to be a source of metals and sulphur, released during orogenesis (Stüwe 1998) or late fluid flow (Curtis *et al.* 1993). In particular, it is known that the Supergroup contains horizons that were mineralised during sedimentation such as the stratabound exhalative barite mineralisation in the Easdale Subgroup (Moles *et al.* 2014).
- Metamorphism is known to produce metamorphic fluids. Metamorphism, during the Caledonian Orogenic cycle could provide a source of fluids from the breakdown of minerals (Stüwe 1998) and these fluids could source metals from the metasediments themselves (Pitcairn *et al.* 2006).

- Deformation forms regional overturned folds (Tanner & Thomas 2009) that modify the distribution of potential metal source rocks and mineralised horizons.
- Post-orogenic intrusions throughout the Dalradian Supergroup (Oliver *et al.* 2008; Neilson *et al.* 2009) had the potential to provide heat and fluids to hydrothermal circulation and may have contributed metals and sulphur to mineralisation. In addition, the Supergroup contains unusual igneous types including appinites and lamprophyre sills (Stephenson *et al.* 2013) that have often been linked with gold mineralisation (Rock & Groves 1988).
- The Supergroup contains deep-seated structures in NW-SE-trending lineaments that have persisted through orogenesis and post-orogenic igneous emplacement (Fettes *et al.* 1886a; Stephenson & Gould 1995). These may have been important in controlling the distribution of sedimentation, intrusions and hydrothermal fluid flow.
- The Supergroup is cut by a series of NE-SW-trending faults, including the terrane bounding Great Glen and Southern Highland Faults which underwent significant movement post-orogenesis (Stephenson *et al.* 2013). The structures could represent high permeability pathways for regional hydrothermal and meteoric fluid flow through the Supergroup (Mark *et al.* 2007).

This chapter reviews the Dalradian Supergroup lithostratigraphic succession, associated basement geology, deformation and metamorphism related to the Caledonian Orogenic cycle, post-orogenic magmatism and fault movement. Throughout, an emphasis is placed on those features that may have particular bearing on vein gold mineralisation.

3.2 General setting

The Dalradian Supergroup (Fig. 3.1) was deposited along the developing east Laurentian passive margin between the mid-Neoproterozoic Era (Cryogenian) and the mid-Cambrian Period (Tanner & Sutherland 2007; Stephenson *et al.* 2013). The Supergroup is bounded by the Great Glen Fault to the north and Highland Boundary Fault to the south (Anderton 1985). The formation of the Rodinia supercontinent (1100-1000 Ma; Kennedy *et al.* 2006), and subsequent break-up due to rifting developing the Iapetus Ocean, dominates the tectonic setting of the early- to mid-Neoproterozoic Era. The northwards drift of Laurentia relative to Gondwana, at *c.* 600 Ma, began to open the Iapetus Ocean (Cawood *et al.* 2001). The beginning of the subsequent closure of the Iapetus Ocean is recorded by regional deformation and metamorphism in the Dalradian Supergroup (Soper & Hutton 1984;

Pickering *et al.* 1988; Soper *et al.* 1992) at *c.* 470 Ma (Stephenson *et al.* 2013). Post-orogenesis, the Dalradian sequence was intruded by a series of granite and gabbros, and significant movement along the Caledonian-trend faults is recorded in the late-Silurian to early-Devonian (Treagus *et al.* 1999; Stewart *et al.* 2001).

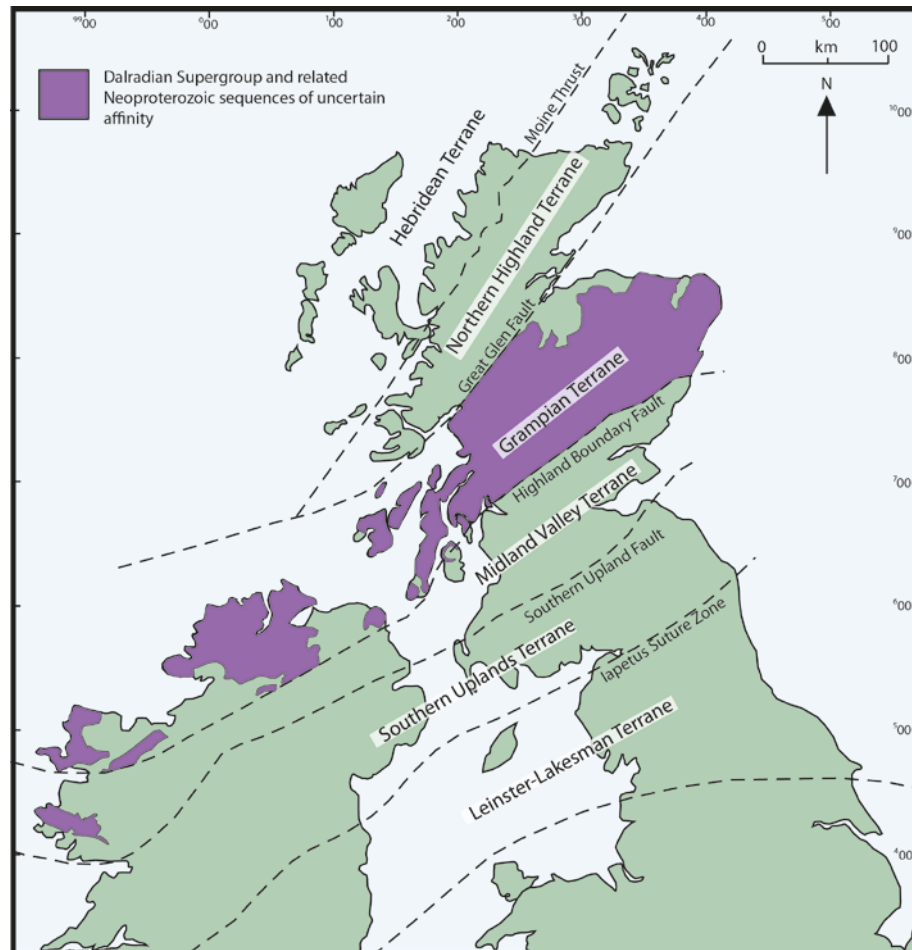


Figure 3.1: Terrane map of the UK and Ireland showing the Grampian Terrane, host to the Dalradian Supergroup, in purple. After Stephenson *et al.* (2013) and BGS 1:50000 scale Tectonic map of Britain Ireland and adjacent areas.

3.3 Basement geology

The crust beneath the Dalradian Supergroup averages ~ 30 km in thickness (Fig. 3.2) with a significant change in the seismic record across the Great Glen and Highland Boundary Faults (Bamford *et al.* 1977; Bamford 1979). There is limited knowledge of the basement geology beneath the Dalradian Supergroup. Exposure is limited to outcrop of the Rhinns Complex on Islay and Colonsay, SW Scotland and on Inishtrahull, off the northern coast of Ireland (Figs. 3.3; 3.4) and outcrops of the Badenoch Group in the NE Scotland. The relationship between the Rhinns Complex to the south and Badenoch Group to the north is not constrained.

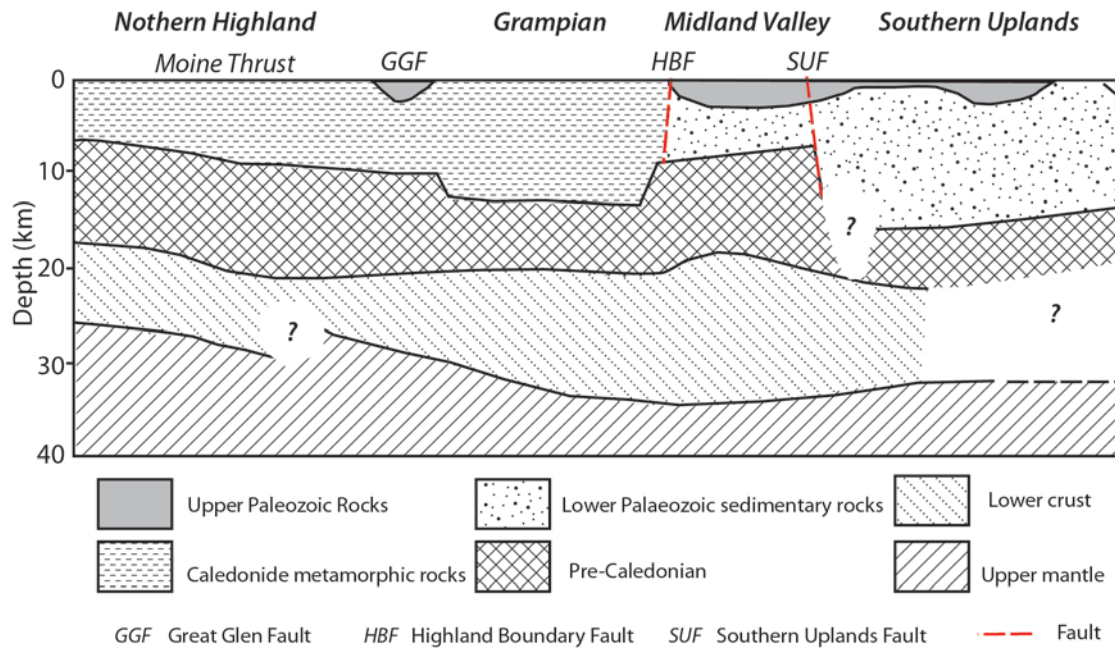


Figure 3.2: Schematic cross section through the crust and upper-most mantle in northern Britain. After Bamford (1979) and Stephenson & Gould (1995).

The Rhinns Complex is a series of granitic and syenitic gneisses deformed and metamorphosed, up to amphibolite facies, before emplacement of further gabbro sheets and additional deformation (Wilkinson 1907). Metasyenite U-Pb zircon ages from the Rhinns Complex on Islay are interpreted to represent the age of the protolith (1782 ± 5 Ma; Marcantonio *et al.* 1988). The Complex is interpreted to be continuously present between Scotland and Ireland (Stephenson *et al.* 2013).

The Colonsay Group unconformably overlies the Rhinns Complex (Fig. 3.5; Muir *et al.* 1995). The Colonsay Group is a sequence of deformed meta-sandstones and phyllites, with the lower succession exposed on Islay and the upper sequence on Colonsay (Stewart & Hackman 1973; Bentley 1988). The relationship between the Colonsay Group and Dalradian Supergroup is poorly constrained as the Colonsay Group remains of uncertain affinity (Fig. 3.5; Muir *et al.* 1992).

The Badenoch Group is dominated by psammites and semipelites (Leslie *et al.* 2013) and has been interpreted to be broadly equivalent to the Moine Supergroup of the Northern Highland terrane (Chew & Strachan 2014). The presence of Knoydartian tectonothermal events within the Badenoch Group (*c.* 840 Ma; Highton *et al.* 1999; Robertson & Smith 1999) is taken to indicate an unconformable relationship between the Badenoch Group and the overlying Dalradian Grampian Group, as an undisturbed contact has not been observed (Leslie *et al.* 2013).

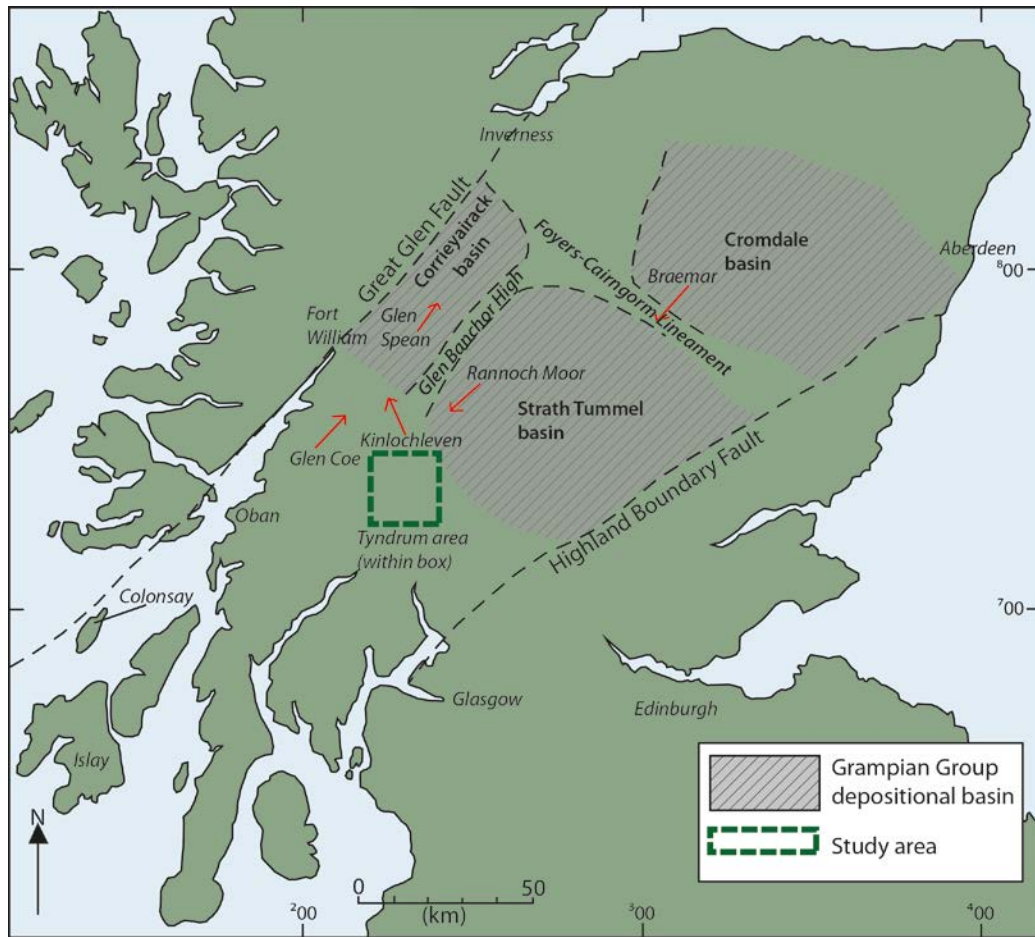


Figure 3.3: Map to show key locations discussed in the text and the rift basins controlling deposition of the Grampian Group after Smith *et al.* (1999). The basin locations are based on correlation of the Foyers-Cairngorm lineament and Glen Bancher High. Basins are defined in Smith *et al.* (1999) who report location of the basins after structural restoration and removal of major fault movement.

3.4 Lithostratigraphy of the Dalradian Supergroup

The Dalradian Supergroup has a complex and varied lithostratigraphic succession (Figs. 3.4, 3.5). Four Groups are defined in the Supergroup, Grampian, Appin, Argyll and Southern Highland Groups. The upper-Appin and lower-Argyll Group stratigraphy is absent in the Tyndrum area; the missing stratigraphy is represented by the Iltay Boundary slide (Bailey 1922; Hutton 1979; Roberts & Treagus 1979; Tanner 2012) discussed in section 3.4.5.2. Here, the lithostratigraphy for the southwestern Dalradian Supergroup is described (Fig. 3.5).

3.4.1 Grampian Group

The Grampian Group is dominated by psammites and semipelites with occasional quartzite beds (Stephenson *et al.* 2013). Deposition is interpreted to have occurred in three basins, Corrieairack, Strath Tummel and Cromdale, bounded by syn-depositional faults and lineaments (location of basins prior to deformation and fault movement shown in Fig. 3.3).

The facies variation within the basins makes correlation between basins difficult (Leslie *et al.* 2013) with the full succession only recorded in the Corrieyairack basin. Detrital zircons within the Grampian Group suggest a source area dominated by Palaeoproterozoic rock; there is a marked absence of Archaean detritus in the Grampian Group (Cawood *et al.* 2003). Three subgroups are defined in the Grampian Group; Glenshirra, Corrieyairack and Glen Spean (Fig. 3.5; Glover *et al.* 1995). The Glenshirra Subgroup records basin flooding with rapid deposition. The Corrieyairack Subgroup is interpreted to record basin filling due to subsidence associated with rift-related extension (Banks 2005). The Glen Spean Subgroup is conformable with the underlying Corrieyairack Subgroup and records a shallow marine shelf sequence dominated by semipelite and psammite (Stephenson *et al.* 2013).

3.4.2 Appin Group

The Appin Group comprises highly varied shelf sediment sequences with rapid lateral facies variation (Anderton 1985; Wright 1988). The sequence was deposited in a shallow-marine setting on a tidal shelf (Anderton 1985; Wright 1988). Three Subgroups are defined within the Appin Group; Lochaber, Ballachulish and Blair Atholl (Fig. 3.5).

3.4.2.1 Lochaber Subgroup

The Lochaber Subgroup is a sequence of pelites and semipelites with some quartzite horizons (Fig. 3.5; Stephenson *et al.* 2013) and is broadly conformable with the underlying Grampian Group, however, local stratigraphic omissions suggests local unconformities (Stephenson *et al.* 2013). The Subgroup exhibits lateral variation in the lower stratigraphy; e.g. three quartzites noted in the Glen Coe and Kinlochleven areas thin to the NE and are absent in the Glen Spean area (Fig. 3.3; Key *et al.* 1997). The lower quartzites are interpreted to be near shore tidal sand bodies (Hickman 1975; Wright 1988) and this supports interpretation of deposition of the Subgroup in a shallow marine environment (Stephenson *et al.* 2013).

3.4.2.2 Ballachulish Subgroup

The Ballachulish Subgroup is conformable with the underlying Lochaber Subgroup and records a change to graphitic pelites, with the first deposition of significant limestone in the Supergroup (Fig. 3.5; Stephenson *et al.* 2013). The lateral continuity of units in the Subgroup suggests stability during deposition (Stephenson *et al.* 2013). The lowest stratigraphic units record marine transgression on a stable shelf (Anderton 1985; Wright 1988) with the Ballachulish Slate interpreted to be a pro-delta deposit and the Appin

Phyllite and Limestone Formations recording renewed transgression. In addition, the Subgroup records the first known occurrence of Archaean age detritus in the Dalradian Supergroup (Cawood *et al.* 2003).

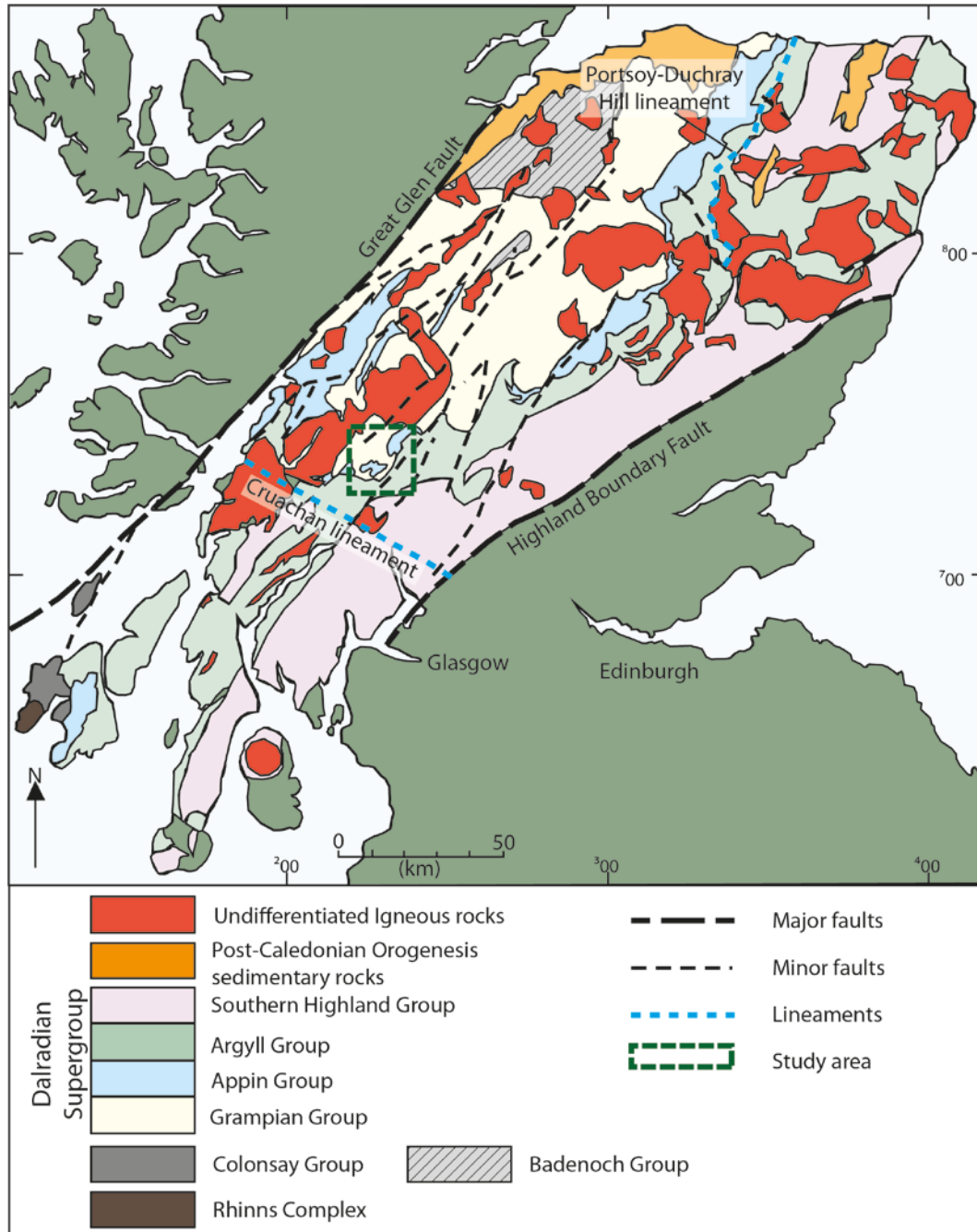


Figure 3.4: Simplified geology of the Grampian Terrane in Scotland. Adapted from Stephenson & Gould (1995) and BGS 1:652000 Bedrock Geology.

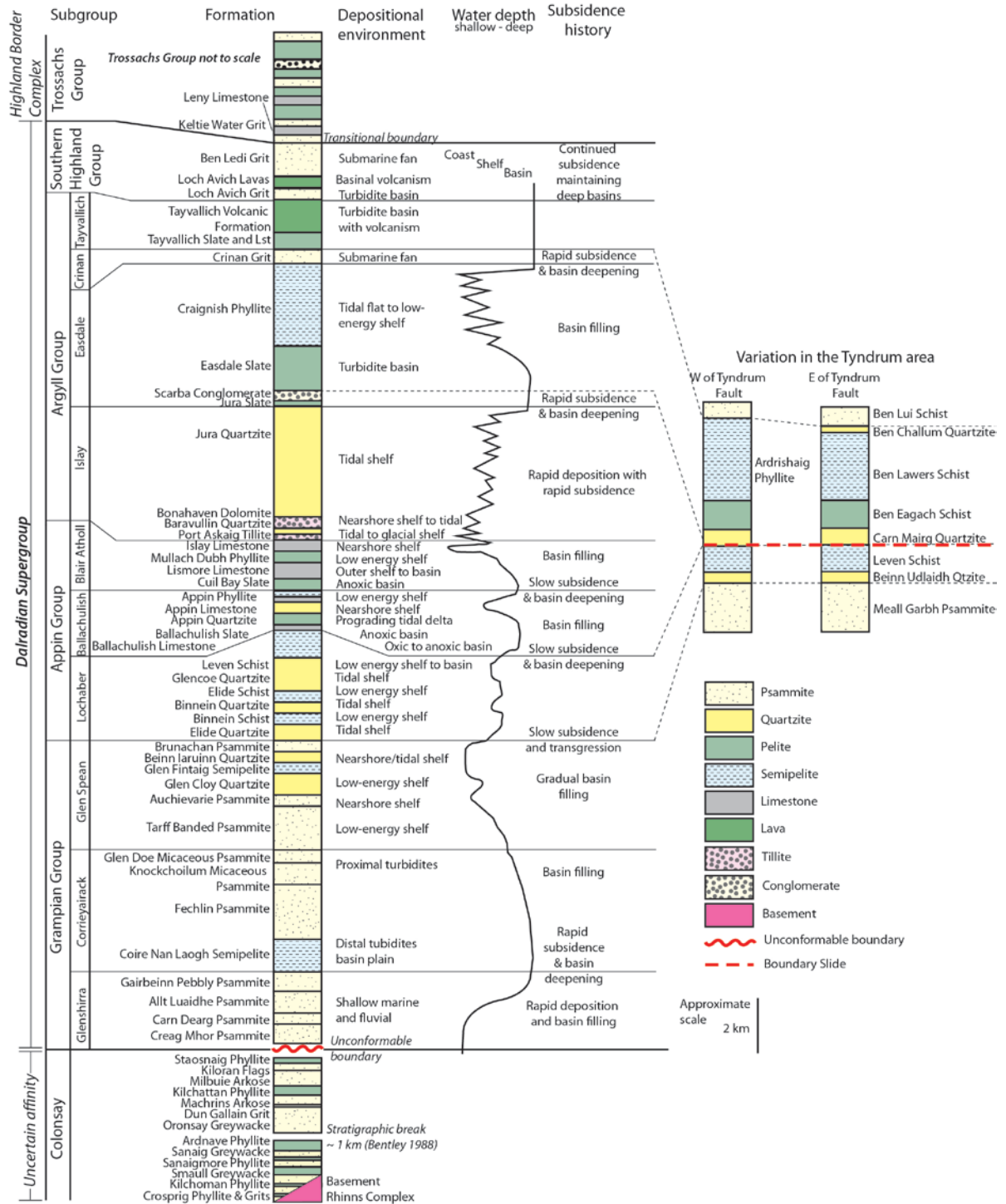


Figure 3.5: Composite lithostratigraphic section for the southwestern Dalradian Supergroup and over- and underlying units, with variation in the Tyndrum area shown. Depositional environment, water depth and subsidence history from Stephenson *et al.* (2013). Colonsay Group stratigraphy after Stephenson & Gould (1995). Glenshirra and Corrieairack Subgroup stratigraphy after Haselock & Whittles (1982), Glen Spean after Stephenson *et al.* (2013). Appin and Argyll Group stratigraphy from the composite lithostratigraphic sections for Lochaber and Islay (Stephenson & Gould 1995). Southern Highlands Group stratigraphy is a composite from Lochaber and Southern Highland lithostratigraphic sections (Stephenson & Gould 1995). Trossachs Group stratigraphy after Tanner & Sutherland (2007).

3.4.2.3 Blair Atholl Subgroup

The Blair Atholl Subgroup is dominated by pelites and limestones (Stephenson *et al.* 2013) with significant lateral facies variation. Variation is attributed to deposition in small basins (Fig. 3.6; Stephenson *et al.* 2013) with slump folds and syn-depositional breccias interpreted to represent sediment instability along basin margins (Stephenson *et al.* 2013).

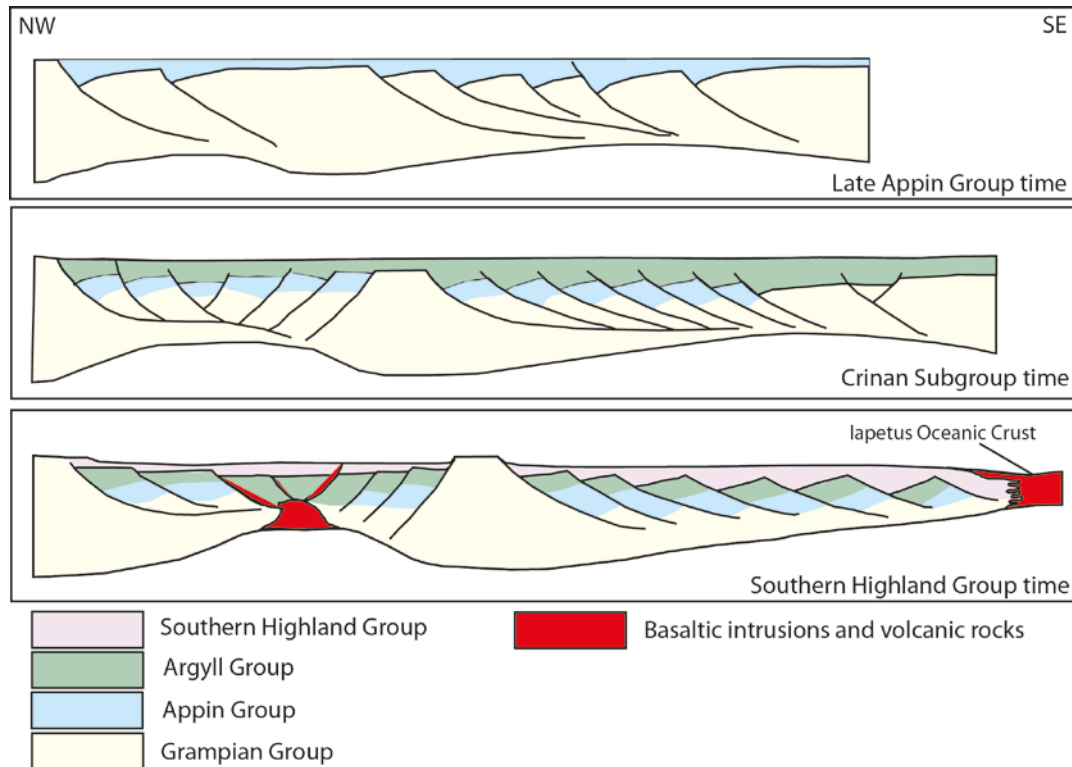


Figure 3.6: Schematic cross-section showing development of the Laurentian margin in Scotland during deposition of the Dalradian Supergroup. After Anderton (1985).

3.4.3 Argyll Group

The base of the Argyll group is defined by the presence of the Port Askaig Tillite; which is generally interpreted as a sequence of glacial deposits (Fig. 3.5; Stephenson *et al.* 2013). The mid to upper-Argyll Group records a change to basin deposits including turbidites and slump deposits. Correlations in the Easdale and Crinan Subgroups are difficult due to significant lateral and vertical facies variation (Stephenson *et al.* 2013). The late-Argyll Group marks a change to tidal shallow-water environments as a result of uplift and tectonically induced marine transgression (Stephenson *et al.* 2013). Four Subgroups are defined in the Argyll Group; Islay, Easdale, Crinan and Tayvallich.

3.4.3.1 Islay Subgroup

The Islay Subgroup is dominated by diamictites and a thick quartzite formation. The Port Askaig Tillite, base of the Subgroup, is recognised across the Dalradian sequence (Stephenson *et al.* 2013) and consists of 47 separate tillites (Spencer 1971, 1981). Basal tillites are dominated by clasts of the underlying Appin Group whereas upper tillites are dominated by clasts of granite and gneiss from outside of the basin (Fitches *et al.* 1990). The Port Askaig Tillite marks a dramatic change in climatic conditions and is correlated with either Marinoan or Sturtian glacial episodes (Thomas *et al.* 2004; Prave *et al.* 2009; Stephenson *et al.* 2013). The Bonahaven Dolomite Formation (Fig. 3.5) has microbial lamination and desecration cracks indicating deposition in a very shallow water environment (Spencer & Spencer 1972; Fairchild 1980). Previous workers have postulated the Bonahaven Dolomite to be the cap carbonate to the Port Askaig Tillites (Brasier & Shields 2000; McCay *et al.* 2006). Prave *et al.* (2009) disagree and point out that the Bonahaven Dolomite is tens of meters above the tillites and thus is unlikely to represent the cap carbonate of the Port Askaig Tillite.

3.4.3.2 Easdale Subgroup

The Easdale Subgroup records a change to deep water sedimentation with some turbidite deposition (Fig. 3.5; Stephenson *et al.* 2013). The Easdale Subgroup shows lateral and vertical variation in lithology across the Dalradian Supergroup (Stephenson & Gould 1995). The Subgroup is interpreted to be deposited during early rifting of the Iapetus Ocean, demonstrated by the first occurrence of basalts, now amphibolites, in the sequence (Fettes *et al.* 2011). The Easdale Subgroup is host to stratabound mineralisation, and most of the mineralisation within the Argyll Group is found in the Ben Eagach Schist Formation, a lateral equivalent of the Easdale Slates. The most notable stratabound mineralisation is a 50 m thick bed of barite and celsian, with sulphides, at the Aberfeldy deposit (Stephenson *et al.* 2013; Moles *et al.* 2014). The SEDEX barium and base-metal mineralisation is interpreted to have developed as a result of ponding of exhalative brines in basins adjacent to active faults (Willan & Coleman 1983; Coats *et al.* 1984). The Ben Lawers Schist Formation has a zone of stratabound sulphide at the top of the formation, the Ben Challum Quartzite Formation, and has chloritic beds of volcanoclastic origin (Stephenson *et al.* 2013).

3.4.3.3 Crinan Subgroup

The Crinan Subgroup has simple stratigraphy represented by a single formation, the Crinan Grits and its finer grained correlative the Ben Lui Schists (Fig. 3.5). The Crinan Grits are a

turbidite sequence deposited in a rapidly subsiding NE-trending basin, generally fining from SW to NE suggesting sediment input from the SW (Fig. 3.6; Stephenson *et al.* 2013).

3.4.3.4 Tayvallich Subgroup

The Tayvallich Subgroup is characterised by the Tayvallich Limestone and extensive Tayvallich Lava (Stephenson *et al.* 2013). The volcanism is extensive in the southwestern Highlands but absent in the rest of the Dalradian Supergroup. Fettes *et al.* (2011) interpreted the volcanism to reflect local pull apart basins on the rifted Laurentian margin.

3.4.4 Southern Highland Group

The Southern Highland Group is dominated by poorly sorted greywacke turbidites with some volcanics (Figs. 3.4, 3.5; Stephenson *et al.* 2013). Detailed stratigraphic correlations are challenging due to rapid lateral facies variation and across-strike changes in metamorphic grade (Stephenson *et al.* 2013). The Group is chloritic, interpreted to reflect a lower regional metamorphic grade and an increased volcanoclastic component (Fig. 3.6; Stephenson *et al.* 2013); volcanoclastic green beds are widespread in the Southern Highland Group. The Loch Avich Lavas represent the last magmatic phase in Dalradian basin (Stephenson *et al.* 2013).

3.4.5 Variation in the Tyndrum area

3.4.5.1 Lochaber Subgroup

Between Glen Orchy and Braemar (Fig. 3.3), the full Lochaber Subgroup succession is not seen and therefore a reduced lithological succession occurs in the Tyndrum area (Fig. 3.5; Treagus & King 1978; Roberts & Treagus 1979; Upton 1986; Treagus 1987, 2000; Stephenson *et al.* 2013). In the Glen Orchy area, the sequence of quartzites and schists is represented by a single quartzite, locally the Beinn Udlaidh Quartzite, beneath the Leven Schists (Fig. 3.5).

3.4.5.2 Missing stratigraphy

The stratigraphy between the base of the Ballachulish Subgroup and the Easdale Slate (mid-Argyll Subgroup; Fig. 3.5) is absent in the Tyndrum area due to the Boundary Slide (formerly Iltay Boundary Slide; Bailey 1922; Roberts & Treagus 1979; Tanner & Thomas 2009). Two interpretations have been proposed for the Boundary Slide. Bailey (1922) interpreted the Slide to be a tectonic slide that formed syn- to post-D2 (Roberts & Treagus 1979) with stratigraphy removed by extensional movement along the slide. Alternatively, Tanner & Thomas (2009) propose the Boundary Slide to be a pre-tectonic disconformity

with missing units not deposited due to either, a topographic high or, a change in sediment supply (Fig. 3.7).

3.4.5.3 Argyll Group variation

The Argyll Group stratigraphy in the Tyndrum area shows lateral variation from the generalised lithostratigraphic succession for the southwestern Dalradian Supergroup (Fig. 3.5). The Easdale Slate is represented by the Carn Mairg Quartzite and Ben Eagach Schist in the Tyndrum area. Within the Ben Eagach Schists syn-sedimentary mineralised hydrothermal SEDEX horizons occur in the Tyndrum area (Willan & Coleman 1983).

The Cragnish Phyllite is represented by the Ardrishaig Phyllite to the W of the Tyndrum Fault (Fig. 3.5). To the SE of the Tyndrum Fault, the Cragnish Phyllite is the Ben Lawers Schist. The top of the Ben Lawers Schist is marked by the Ben Challum Quartzite, a 500 m unit of quartzite and semipelite with at least two horizons of stratabound mineralisation (Willan & Coleman 1983; Stephenson *et al.* 2013). Elsewhere in the Dalradian Supergroup the Cragnish Phyllite transitions into the Crinan Grits, locally Ben Lui Schist, without the quartzite present.

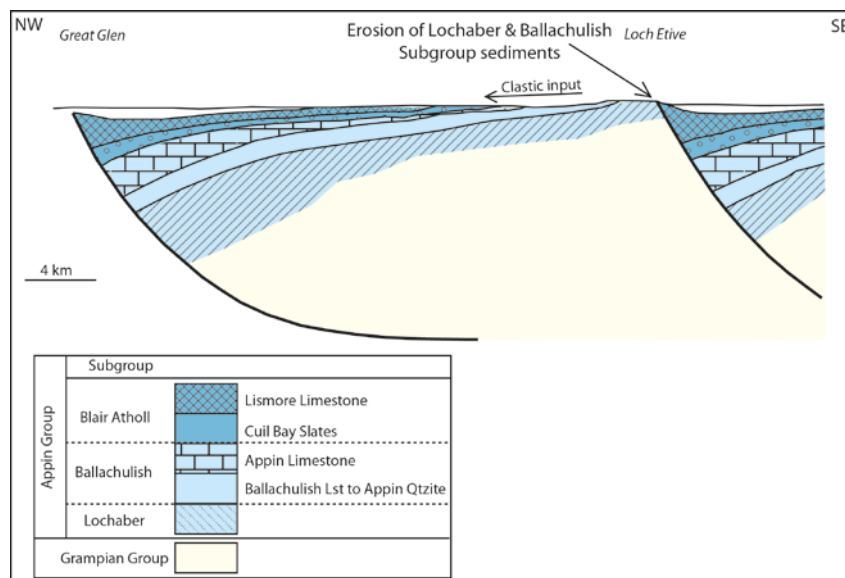


Figure 3.7: Schematic cross section for the Great Glen to Loch Etive area to illustrate possible explanation for the absence of Lochaber Subgroup lithology in the Tyndrum area. After Anderton (1985).

3.5 Overlying stratigraphy

The Dalradian Supergroup is overlain by the Trossachs Group, part of the Highland Border Complex (Fig. 3.5). The Ben Ledi Grits (Southern Highland Group) transition into the Keltie Water Grit Formation, host to the Leny Limestone. The Dalradian Supergroup

is interpreted to be in stratigraphical continuity with the Trossachs Group (Tanner 1995; Tanner & Sutherland 2007).

3.6 Dating the Dalradian

The age of deposition of the Dalradian Supergroup is poorly constrained with limited chronostratigraphic constraints available (Rooney *et al.* 2011; Prave *et al.* 2009). There are two radiometric dates for sedimentation within the Dalradian sequence (Fig. 3.8); U-Pb zircon age has constrained the emplacement of the Tayvallich Volcanics to 601 ± 4 Ma (Dempster *et al.* 2002), and a Re-Os whole rock age on the Ballachulish Slate at 659 ± 9.6 Ma is interpreted to represent deposition (Rooney *et al.* 2011).

The base of the Dalradian sequence is younger than *c.* 800 Ma based on 840 Ma pegmatites and Knoydartian deformation in the Badenoch Group and an absence of pre-Caledonian mineral ages in the Dalradian Supergroup (Noble *et al.* 1996). It is likely that sedimentation in the Grampian Group began between 800–700 Ma based on $^{87}\text{Sr}/^{86}\text{Sr}$ isotope signatures of limestones (Thomas *et al.* 2004), the current best estimate is 730–700 Ma (Stephenson *et al.* 2013).

The basal Argyll Group tillites have been correlated to global glaciation events as a method of constraining the age of Mid-Dalradian sedimentation (Fig. 3.8). The Port Askaig Tillite has been correlated with the 746 to 663 Ma (Condon & Bowring 2011) Sturtian glacial episodes by a number of workers (Prave 1999; Brasier & Shields 2000; Condon & Prave 2000; McCay *et al.* 2006). However, if sedimentation of the Grampian Group is not initiated until between 730 and 700 Ma there is a limited amount of time to deposit the Grampian and Appin Group stratigraphy. Furthermore a Sturtian age for the Port Askaig Tillite would be inconsistent with the 659 ± 9.6 Ma date for the Ballachulish Slate (Rooney *et al.* 2011). Alternatively Leslie *et al.* (2008) proposed Argyll Group basal tillites could be correlated with the Marinoan glaciation *c.* 653 Ma (Condon & Bowring 2011), allowing for Dalradian sedimentation to begin at *c.* 700 Ma and Ballachulish Slate deposition at 659 ± 9.6 Ma (Rooney *et al.* 2011).

The Leny Limestone within the Highland Border Complex is dated at 510–515 Ma (Fig. 3.8; Cowie *et al.* 1972) based on the presence of the rare *Pagetides* trilobite (Pringle 1940, Cowie *et al.* 1972, Rushton *et al.* 1999).

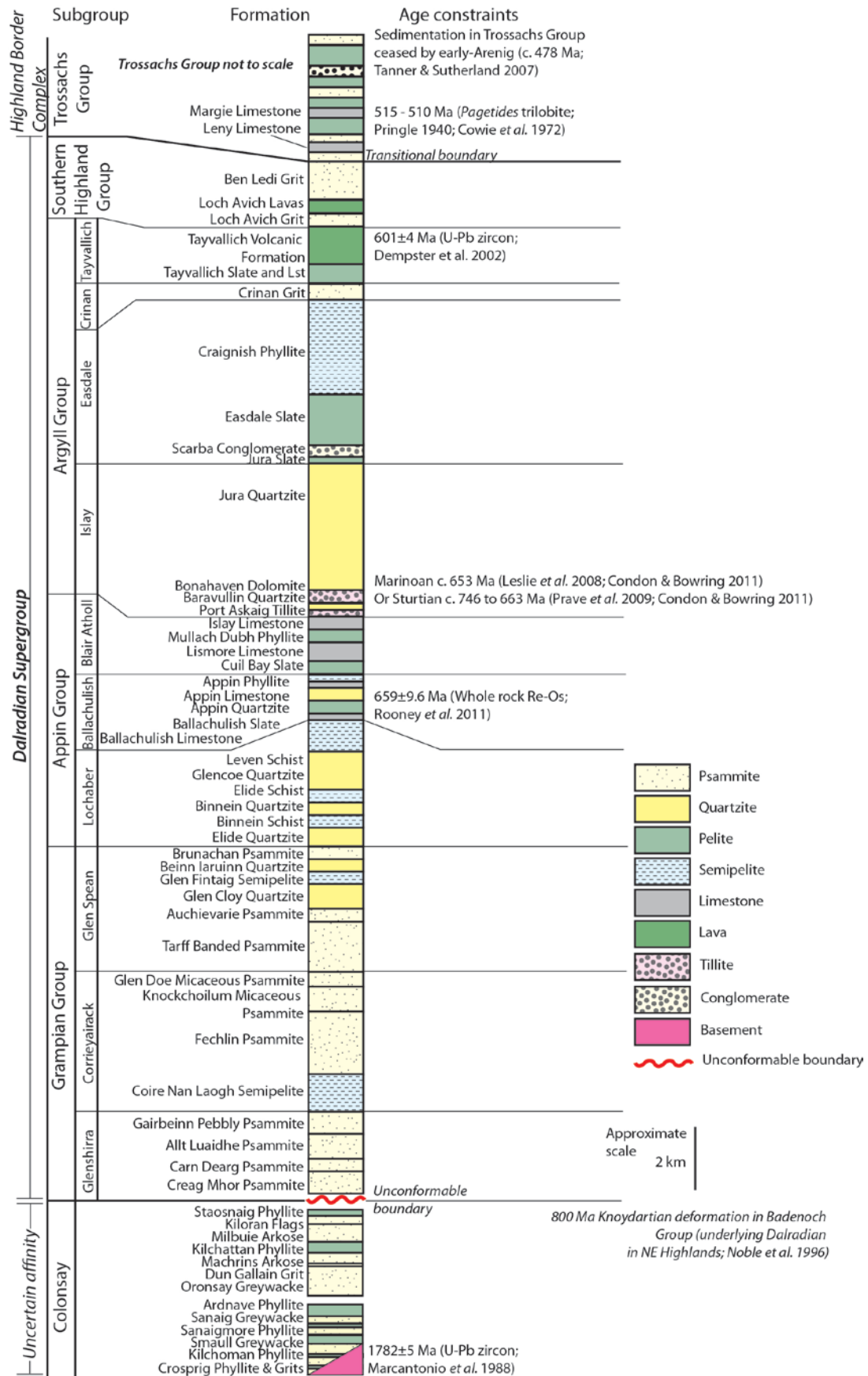


Figure 3.8: Composite lithostratigraphic section showing known age constraints for the deposition of the Dalradian Supergroup. References as in Figure 3.4.

3.7 Caledonian Orogenesis

The Dalradian sequence underwent polyphase deformation, part of the Caledonian Orogenic cycle, as a result of the collision of Laurentia with a series of oceanic arcs (*c.* 490 to 465 Ma; Oliver 2001; Baxter *et al.* 2002; Stephenson *et al.* 2013). The Grampian Event, records the collision of the Midland Valley Arc with the Scottish sector of the Dalradian Supergroup (Fig. 3.9). The Irish sector collided with the Lough-Nafooe and Tyrone arcs. Oceanic arc collision caused the emplacement of ophiolites across the region, emplacement of these pre-dates the main deformation stage and began as early as *c.* 490 Ma based on recent dating work in the soles of the ophiolites (Chew *et al.* 2010; Tanner 2013).

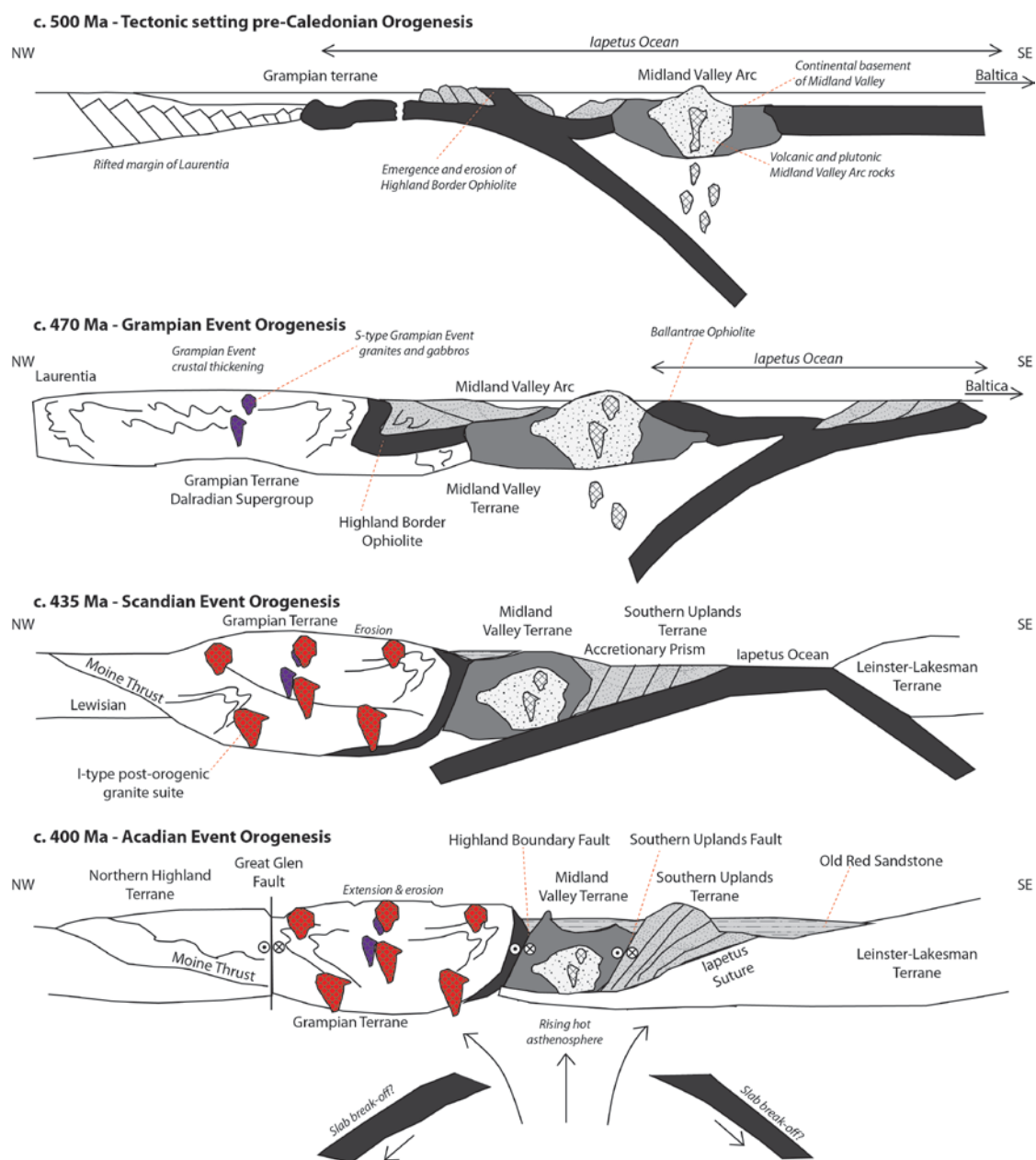


Figure 3.9: Tectonic evolution of the Dalradian Supergroup from pre- to end-Caledonian Orogenesis. Diagram after Dewey & Ryan (1990); Strachan (2000); Oliver *et al.* (2008) and Tanner (2013)

The Grampian Event was completed by 455 Ma and a hiatus in orogenic activity in the Supergroup is recorded between 455–435 Ma, with the exception of emplacement of decompression granites related to erosion of the metamorphic pile (Oliver *et al.* 2008).

The Scandian (Fig. 3.9; 435–425 Ma; Chew & Strachan 2014) and Acadian (Fig. 3.9; *c.* 400–390 Ma; Mendum & Noble 2010) events of the Caledonian Orogenic cycle are not thought to be represented in the Dalradian Supergroup. During the Scandian Event, emplacement of subduction-related granites occurs in the Grampian terrane, during on-going subduction of the Iapetus oceanic plate beneath the margin of Laurentia. The absence of Scandian Event age deformation in the Grampian terrane, whilst being present in the Northern Highland terrane, suggests the two terranes were not docked at this time. The Northern Highland terrane is postulated to be located to the north and underwent a harder docking between Laurentia and Baltica than the Grampian terrane due to the oblique nature of the collision (Chew & Strachan 2014).

The Acadian Event is not thought to be recorded in the Grampian or Northern Highland terranes and represents the final oblique collision within the Caledonian Orogenic process. There is no deformation associated with this event in the Dalradian Supergroup; however, coincident with this event is a period of significant movement on the Great Glen Fault and subsidiary Caledonian trend faults (section 3.9).

3.7.1 Deformation during the Grampian Event

The structural development of the Dalradian Supergroup during the Grampian Event is interpreted as a single evolving event though the whole terrane (e.g. Coward 1983; Fettes *et al.* 1986a, b). Earliest deformation, D1, is characterised by greenschist facies metamorphism and dominantly NE-SW trending folds and ductile shears associated with over-thrusting on the Laurentian margin (Strachan *et al.* 2002). The folds are affected by later deformation and do not record the primary attitude of F1 folds (Stephenson *et al.* 2013). During D2, peak metamorphism and maximum deformation occurred (Shackleton 1958; Krabbendam *et al.* 1997; Crane *et al.* 2002). D2 is characterised by rotation and stacking of existing close to isoclinal, asymmetrical fold nappes (Strachan *et al.* 2002). D3 is dominated by NE-trending steeply-dipping structures, recording decreasing intensity of deformation (Strachan *et al.* 2002). The final stage of deformation within the Grampian Event, D4, records less intense deformation forming open near upright structures trending ENE to NE. D4 has gently plunging, NE-SW trending upright folds, late crenulation and brittle structures and is

generally geographically restricted to the Highland Border Downbend (Stephenson *et al.* 2013).

3.7.2 Age of Metamorphism

Metamorphism in the Dalradian Supergroup exhibits significant variation with a general increase from greenschist facies in the SW to upper amphibolite in the NE (Fig. 3.10; Fettes *et al.* 1985; Harte 1988). Graham (1983) estimated pressures of 8-10 kbar in epidote-amphibolite facies rocks in SW Highlands; it is known to be lower elsewhere in the Grampian Terrane. In the Tyndrum area, garnet-grade amphibolite-facies metamorphism was reached (Fig. 3.10; Harte 1988; Tanner 2013). The Buchan metamorphic zone, NE Scotland, is an area that underwent high-temperature and low-pressure metamorphism contemporaneous with Barrovian metamorphism (Stephenson *et al.* 2013). Metamorphism was broadly coeval with deformation (Elles & Tilley 1930), peak porphyroblast growth occurred after the main nappe-forming phase but before late uplift (syn-D2 to late-D3; Strachan *et al.* 2002). The maximum age of metamorphism is constrained by the youngest rocks affected, the Trossachs Group in South Perthshire, deposited between *c.* 520 and *c.* 478 Ma (Fig. 3.8; Tanner & Sutherland 2007).

Peak metamorphism is contemporaneous across the Supergroup constrained to between *c.* 475-470 Ma supported by the age range of broadly syn-metamorphic intrusions (Table 3.1; Chew & Strachan 2014). The Dalradian underwent rapid cooling post-Grampian Event and had undergone erosion exposing the metamorphic root by *c.* 460 Ma (Dempster 1985; Dempster *et al.* 1995; Soper & Evans 1997; Soper *et al.* 1999; Oliver 2001; Oliver *et al.* 2000). Work by Dempster (1985) to constrain the cooling rate of the metamorphic pile suggests the sequence cooled to 350°C by 440 Ma with a further 50°C of cooling by 430 Ma.

Table 3.1 *Summary of existing age constraints for Grampian Event Orogenesis*

Location	Technique	Mineral	Age (Ma)	Comments	Reference
<i>Scotland ages</i>					
Leven Schist, Glen Spean	Lu-Hf	Garnet	470.8±3.2	Garnet growth during prograde metamorphism	Bird <i>et al.</i> (2013)
Auchlee Granite	U-Pb	Zircon	475±12	Syn-D2	Dempster <i>et al.</i> (2002)
Portsoy Gabbro	U-Pb	Zircon	471.3±0.6	Syn-D2	Carty <i>et al.</i> (2012)
Metapelite, Glen Clova	Sm-Nd	Garnet	472.9±2.9	Garnet growth, Syn-D2	Baxter <i>et al.</i> (2002)
Insch Gabbro	U-Pb	Zircon	470±9	Post-D2, Pre-D3	Dempster <i>et al.</i> (2002)
Garnet-mica schist, Pitlochry	Sm-Nd	Garnet	467±2.5	End of garnet growth	Oliver <i>et al.</i> (2001)
Kennethmont granite	U-Pb	Zircon	457±1	Post-D4, undeformed	Oliver <i>et al.</i> (2000)
<i>Ireland ages: Connemara</i>					
Currywongaun Gabbro	U-Pb	Zircon	474.5±1	Syn-D2	Friedrich <i>et al.</i> (1999a)
Cashel Gabbro	U-Pb	Zircon	470±1.4	Syn-D2	Friedrich <i>et al.</i> (1999a)
Late D3 granite	U-Pb	Zircon	463±4	Late-D3	Cliff <i>et al.</i> (1996)
	U-Pb	Zircon	467±2	Late-D3	Friedrich <i>et al.</i> (1999b)
Oughterard granite	U-Pb	Xenotime	462.5±1.2	Post-D4	Friedrich <i>et al.</i> (1999a)

3.8 Lineaments

NW-SE-trending lineaments have been identified in the Dalradian Supergroup and are interpreted to represent deep-seated crustal fractures that have persisted through episodes of orogenic compression and post-orogenic igneous emplacement (Fettes *et al.* 1986a; Stephenson & Gould 1995). The lineaments focus structural activity and mark variations in the stratigraphic succession caused by syn-depositional movement (Soper & Anderton 1984). The Caledonian granite plutons are commonly emplaced at the point Caledonian NE-SW shear zones meet NW-SE lineaments (Jacques & Reavy 1994); the lineaments have been interpreted to be important in controlling Caledonian magmatism (Trewin 2002).

The Cruachan-Loch Lomond (Cruachan) lineament runs in a NW-SE orientation from Oban to the Highland Boundary Fault (Fig. 3.3, 3.4). The Cruachan lineament cuts the Etive granite (Trewin 2002) and passes close to the Tyndrum area (Fig. 3.4; Fettes *et al.*

1986a). Geophysical and lithological changes are observed across the Cruachan lineament (Plant *et al.* 1984; Fettes *et al.* 1986a); to the NE of the Cruachan lineament the proportion of syn-sedimentary basaltic rocks within the Dalradian succession is greatly reduced (Graham 1986). A steep NW-SE gradient in the Bouguer gravity anomaly map is recorded across the lineament and is interpreted by Graham (1986) to represent a change in the Dalradian basement.

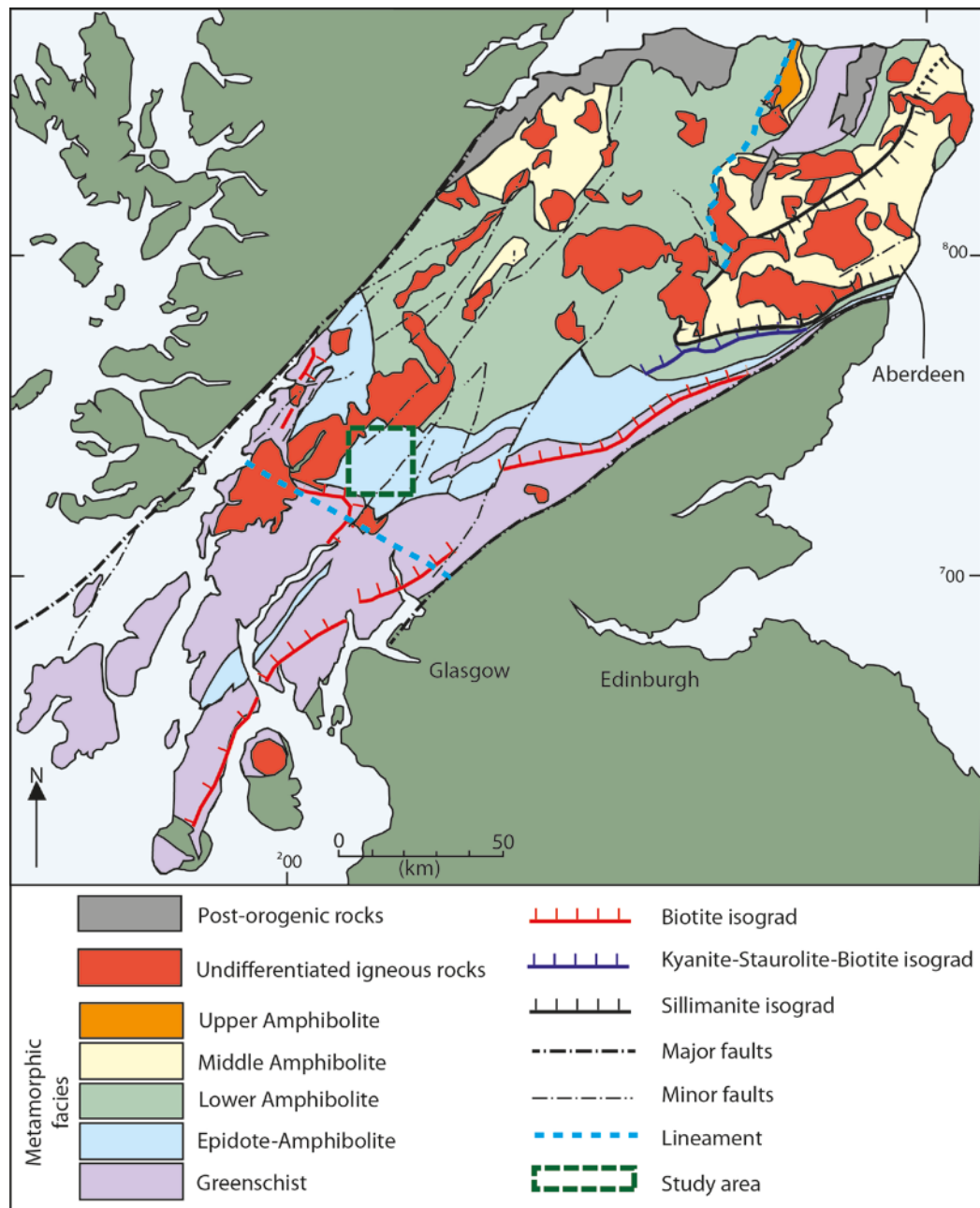


Figure 3.10: Simplified distribution of metamorphic facies in the Dalradian Supergroup in Scotland. Adapted from Fettes *et al.* (1985) by Stephenson & Gould (1995) and Stephenson *et al.* (2013).

3.9 Brittle Fault movement

There are numerous faults sub-parallel to the NE-SW structural trend of the Dalradian Supergroup. The faults have undergone largely sinistral strike-slip movement with a component of normal movement during transtension (Treagus *et al.* 1999). The change to a transpressional regime is recorded by D4 and features a component of dextral strike-slip movement on the major Caledonian faults (Strachan *et al.* 2002). Other faults in the Great Glen set (i.e. Tyndrum Fault; section 3.9.3) show an early phase of dip-slip movement followed by sinistral strike-slip (Treagus *et al.* 1999) with movement in the late Silurian to early Devonian (Trewin 2002).

3.9.1 Great Glen Fault

The Great Glen Fault (GGF) extends to 40 km depth and underwent significant movement after the Ordovician supported by the absence of definite Dalradian Supergroup rocks to the north and Lewisian rocks to the south of the GGF (Harte 1988). In addition, there is a distinct step in the basement in the Lithospheric Seismic Profile in Britain (LISPB) associated with the GGF (Fig. 3.2; Bamford *et al.* 1977). This is interpreted to indicate separate terranes to the north and south of the GGF (Northern Highland and Grampian terranes; Fig. 3.1), that were juxtaposed by major strike-slip movement on the GGF (Harte 1988). The presence of mantle-derived lamprophyres suggests an expression of the GGF, and possibly others Caledonian-trend faults, in the mantle (Trewin 2002).

The GGF underwent significant movement between *c.* 428-390 Ma (Stewart *et al.* 2001). Within the microstructures of the Clunes Tonalite there is evidence it was emplaced during early sinistral movement on the GGF (Stewart *et al.* 2001). The Tonalite has yielded a U-Pb zircon age of 428 ± 2 Ma (Stewart *et al.* 2001). The minimum age of movement on the faults is constrained by the Old Red Sandstone, of probable Devonian age, which unconformably overlies the sinistrally sheared rocks within the fault zone (Stewart *et al.* 2001).

The subsidiary faults within the Grampian terrane, forming the Caledonian fault suite, exhibit variable movement, largely constrained by work by Treagus (1991). Fault movement was constrained to up to 8 km of left lateral strike slip and 2 km of dip slip movement (Treagus 1991). Movement on the faults was further constrained by detailed work undertaken on the Tyndrum Fault (see section 3.8.3).

3.9.2 Highland Boundary Fault

The movement and structure of the Highland Boundary Fault (HBF) is poorly constrained at the time of movement on the GGF. The nature of movement on the fault during Caledonian Orogenesis is unclear; it has been postulated the fault is a graben-bounding normal fault (George 1960), a sinistral strike-slip fault (Ryan *et al.* 1995; Woodcock & Strachan 2000), or a NW-dipping reverse fault (Allan 1928, 1940; Ramsey 1964). Tanner (2008) postulates if major sinistral strike-slip movement occurred on the fault, it was between 460 and 420 Ma along the present fault line, and there was minimal post-early Devonian displacement. The HBF's present structural setting is a steep NW-dipping reverse fault (Tanner 2008).

3.9.3 The Tyndrum fault

The Tyndrum Fault can be traced over a 60 km strike length and is a single dipping fracture plane with fractures and splays in a zone 1.5 km wide on the NW side of the fault plane (Treagus *et al.* 1999). The fault is steeply dipping and in the Tyndrum Lead mine dips 80°E (Wilson & Flett 1921). Initial extension in a WSW-ESE orientation opened a series of 040-trending fractures and the fault underwent 1.8 km of dip-slip movement, down to the east (Treagus 1991) at *c.* 430 Ma. Late movement on the Tyndrum fault was under a transtensional regime dominated by at least 4 km of sinistral strike-slip movement (Treagus *et al.* 1999) between 429-412 Ma (Clayburn *et al.* 1983; Rogers & Dunning 1991; Treagus *et al.* 1999).

3.10 Igneous Activity

The Dalradian Supergroup has a number of large-scale intrusive suites emplaced throughout the tectonic evolution of the sequence (Fig. 3.11). Oliver *et al.* (2008) identified four major granite types based on the intrusion age and geochemical signatures; syn-depositional intrusions (A-type), Grampian Event granites (S-type), decompression granites (S-type) and post-orogenic granites (I-type). In addition, small-scale lamprophyre and appinites occur throughout the Dalradian Supergroup (Stephenson *et al.* 2013).

3.10.1 Syn-depositional intrusions

A-type granites, characterised by Tanner *et al.* (2006), are typical of granites with a crustal source formed during continental rifting (Fig. 3.11; 600-590 Ma; Loiselle & Wones 1979; Eby 1992). The Tayvallich basaltic lavas are contemporaneous with the granites (Graham

1986). The granites and basalts were metamorphosed by the *c.* 470 Ma Grampian Event in the Grampian Terrane (Dalziel 1997; Dalziel & Soper 2001; Oliver *et al.* 2008).

3.10.2 Grampian Event granites

Grampian Event granites (Fig. 3.11; Oliver *et al.* 2008) were emplaced syn-regional metamorphism at *c.* 470 Ma and are characterised as S-type with high $^{87}\text{Sr}/^{86}\text{Sr}$ initial ratios (Oliver *et al.* 2008). Grampian Event granites are foliated and contain a muscovite-biotite

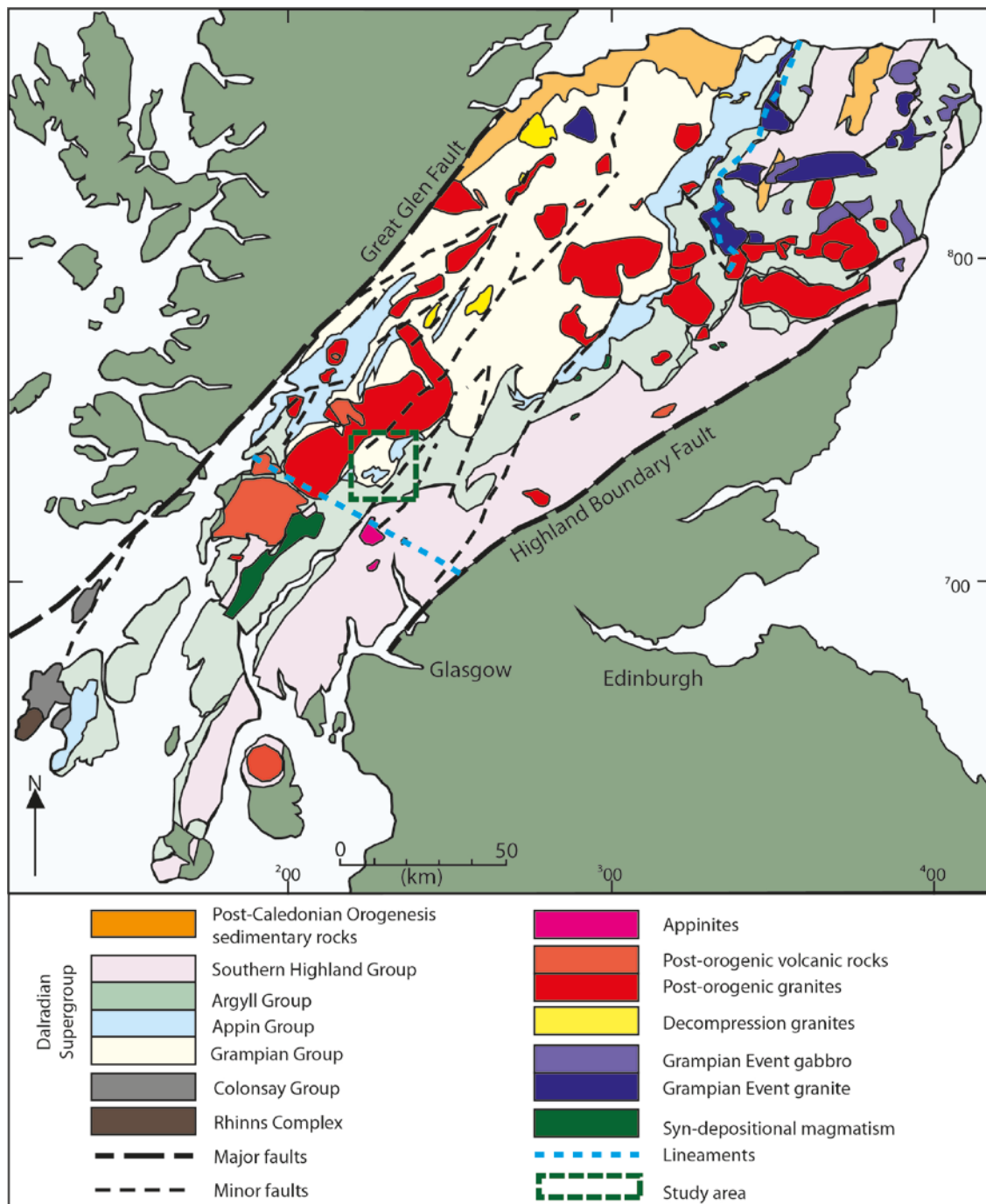


Figure 3.11: Distribution of igneous rocks in the Dalradian Supergroup. After Stephenson & Gould (1995) and Oliver *et al.* (2008).

dominated assemblage with minor tourmaline. Gabbros intruded syn-Grampian Event orogenesis occur in areas of intense D3 deformation and are commonly associated with Buchan metamorphic conditions (Oliver *et al.* 2008; Stephenson *et al.* 2013).

3.10.3 Decompression granites

Later S-type granites (Fig. 3.11; Oliver *et al.* 2008) were intruded between *c.* 460-435 Ma (Oliver *et al.* 2008). The late S-type granites formed as a result of decompression melting of continental crust during exhumation and erosion (Oliver *et al.* 2002). There is no evidence of subduction zone I-type granites forming at the same time as decompression-related S-type granites (Oliver *et al.* 2008).

3.10.4 Post-orogenic granites

The post-orogenic Caledonian Granite suite was emplaced over a period of *c.* 25 Ma from 433 Ma (Fig. 3.11; Conliffe *et al.* 2010, Neilson *et al.* 2009). The Ballachulish igneous complex is the oldest (433 ± 1.8 Ma, Re-Os molybdenite; Conliffe *et al.* 2010) and the Inner Starav intrusion of the Etive Complex, the youngest (408 ± 0.4 Ma, U-Pb zircon; Neilson *et al.* 2009) with mineralisation reported in some intrusions (e.g. molybdenite at Etive Complex; Porter & Selby 2010). Oliver *et al.* (2008) report younger ages for the Rannoch Moor pluton (411 ± 7 Ma; U-Pb zircon) than Neilson *et al.* (2009; 422.5 ± 0.5 Ma; U-Pb zircon). Neilson *et al.* (2009) argue the Rannoch Moor pluton is cut by Etive dykes which predate the Outer Starav Complex dated by Oliver *et al.* (2008) at 415 ± 6 Ma. In addition, Neilson *et al.* (2009) highlight issues with Fraser *et al.* (2004) ages (398 ± 2 Ma; U-Pb zircon) for the Glencoe andesite. The ID-TIMS data from Fraser *et al.* (2004) is based on unabraded multigrain zircon fractions and are difficult to reconcile with the field relations and Neilson *et al.* (2009) date (419.6 ± 5.4 ; U-Pb zircon). The range of emplacement ages reported in Neilson *et al.* (2009) is considered to be the most robust age constraint and henceforth the post-orogenic granites are reported to be emplaced from *c.* 433-408 Ma.

The I-type granites are non-foliated and dominated by a calc-alkaline hornblende and biotite assemblage (Oliver *et al.* 2008). The suite is interpreted to record the beginning of mantle wedge melting under the Grampian terrane (Dewey 1971; Soper 1986; Thirlwall 1988; Oliver *et al.* 2002). An apparent delay between initiation of subduction and emplacement of subduction-related granites of *c.* 30 Ma is recorded (Oliver 2001). The bulk of the volume of the granites across Scotland was emplaced during this time period (*c.* 410 Ma; Oliver *et al.* 2008) with two hypotheses postulated for this; either the Iapetus subduction zone did not reach below the Grampian Terrane until *c.* 430 Ma or it was too

shallow dipping to initiate granite formation (Oliver 2001). Granite emplacement beginning at *c.* 430 Ma also coincides with a change from orthogonal under-thrusting to sinistrally oblique under-thrusting in the Southern Uplands Terrane (Tanner 2013).

3.10.5 Siluro-Devonian Lamprophyre and Appinite suite

In the Grampian Terrane, lamprophyres are found as sheets and dykes. Appinites are commonly found as plugs and are often located along Caledonian faults and pre-Caledonian lineaments (Rogers & Dunning 1991; Neilson *et al.* 2009). There is a spacial and temporal relationship with the Caledonian granite suite, where they pre-date or are closely contemporaneous with the granitic magmas (Strachan *et al.* 2002).

The Garabal Hill-Glen Fyne, Arrochar and Rubha Mor appinites, 40 km south of Tyndrum, have been dated at 426 ± 4.2 to 428 ± 9.8 Ma (U–Pb titanite and zircon; Rogers & Dunning 1991). These appinitic units are interpreted to be related to melting of basalt-andesite melts in the lower crust in a zone of mixing, fractionation, partial melting, assimilation and hybridisation (Oliver *et al.* 2008). The close relationship between the appinite suite and lamprophyres is evident from their spacial proximity and comparable petrography and geochemistry (Rogers & Dunning 1991).

3.10.6 Permo-Carboniferous dykes

A suite of E-W trending quartz-dolerite dykes, observed in the Tyndrum area and found throughout the Midland Valley terrane, form part of the Permo-Carboniferous dyke swarm intruded between *c.* 290–270 Ma (Francis 1991; Treagus *et al.* 1999). The dykes post-date the latest dextral fault movement in the Tyndrum area and are not significantly hydrothermally altered (Treagus *et al.* 1999).

3.11 Regional fluid flow in the Dalradian Supergroup, Scotland

The Dalradian Supergroup has undergone regional fluid flow during the evolution of the terrane. The regional fluid flow in the Dalradian Supergroup may contribute to hydrothermal systems controlling gold-bearing veins emplacement (Craw 1990) and therefore needs to be considered when assessing the nature and genesis of gold-bearing quartz veins in the Tyndrum area. Craw (1990) postulate post-Caledonian fluid flow to have a significant impact on the development of gold and other metal occurrences throughout the Dalradian Supergroup.

In most metamorphic belts the formation of veins occurs throughout the metamorphic and uplift history of the terrane (Craw 1990). In the Dalradian Supergroup, most vein

formation is concentrated within a short period in the uplift history, with minor vein development early and late in the uplift history. Vein development is synchronous with late uplift and folding related to D4 deformation (*c.* 460-440 Ma; Craw 1990) causing peak-dewatering conditions. Early vein formation (10-30 Ma; Anderson *et al.* 2004) after peak metamorphism; is associated with the transition from ductile to brittle conditions at greenschist facies conditions with veins precipitated from fluids derived from syn-metamorphic dehydration at depth (Anderson *et al.* 2004). Craw (1990) suggests there may be some variation in the timing of peak de-watering due to variation in the metamorphic grade with garnet-grade rocks reaching the brittle-ductile transition and peak de-watering conditions later (*c.* 400 Ma; Dempster 1985) than lower grade rocks (*c.* 460-440 Ma; Craw 1990). Later de-watering is interpreted to explain the source of fluids for gold mineralisation (Craw 1990) in the garnet-grade rocks in the Tyndrum area (410 ± 14 Ma; Treagus *et al.* 1999).

Three main post-metamorphic quartz vein events occur in the rocks of the Dalradian Supergroup (Table 3.2; Craw 1990). Craw (1990) inferred stage 2 veins to form from low salinity (1-5 wt. % NaCl and KCl), CO₂-bearing (3-16 wt. % CO₂) metamorphic waters.

Table 3.2 *Post-metamorphic quartz veins stages. Details after Craw (1990).*

Vein stage	Stage 1	Stage 2	Stage 3
Gangue	Quartz	Quartz, muscovite, calcite, chlorite	Ankerite
Sulphides	None	Minor pyrite	Pyrite
Other information	Schistosity parallel, contain metamorphic minerals comparable to host rock	Most abundant vein type	Not volumetrically significant
Timing	Formed close to peak metamorphism	Cross-cuts stage 1 and cross-cut by stage 3	Cross-cuts both stage 1 and 2

Craw (1990) suggests gold mineralisation in Scotland and Northern Ireland is interpreted to be controlled by fluid movement along shear zones in the latter stages of the Caledonian Orogeny during strike-slip movement along major faults (*c.f.* Thompson *et al.* 1992). Curtis *et al.* (1993) attribute gold mineralisation at Cononish, Tyndrum, to deposition by a magmatic fluid mixed with a component of Palaeozoic meteoric water. In contrast to both Craw (1990) and Curtis *et al.* (1993), Craw & Chamberlain (1996) proposed gold mineralisation could be attributed to an evolved meteoric fluid with contribution from basement formation water but with no magmatic component to the mineralising fluid, this does not preclude fluid movement from being controlled by fault movement.

Parnell *et al.* (2000) examined gold mineralisation in the Sperrin Mountains, Northern Ireland, and suggest gold was deposited from a moderate to high temperature H₂O-CO₂-NaCl-KCl fluid mixing with lower temperature formation water, different to the model for gold-bearing fluids proposed by Craw (1990), Curtis *et al.* (1993) and Craw & Chamberlain (1996).

Throughout the Dalradian Supergroup post-gold base metal mineralisation is observed; Curtis *et al.* (1993) concluded at the Tyndrum Lead Mine the parent fluid was highly saline, supported by Parnell *et al.* (2000)'s work in Northern Ireland. Carboniferous mineralising activity is significant in the Dalradian Supergroup (Parnell *et al.* 2000) with fluids mobile over a large area suggesting remobilisation of earlier mineralising events may be significant as suggested for gold mineralisation at the Curraghinalt deposit (Wilkinson *et al.* 1999). Late carbonate mineralisation in the Scottish Dalradian Supergroup has comparable oxygen, carbon isotope and fluid inclusion characteristics to unmineralised dolomite veins in the Southern Highlands and Antrim, Northern Ireland (Anderson *et al.* 2004). These fluids are interpreted to have originated from overpressured overlying Permo-Carboniferous sedimentary basins with fluids utilising existing fracture networks (Anderson *et al.* 2004).

3.12 Conclusions

Understanding the evolution of the Dalradian Supergroup (summarised in Fig. 3.12) is important for the understanding of the genesis of gold mineralisation in the sequence. The lithostratigraphic succession (*c.* 730 Ma to at least 510 Ma) has the potential to contribute metals to mineralisation from stratabound mineralised horizons (Moles *et al.* 2014), possibly released with fluids during metamorphism (Stüwe 1998). In the Tyndrum area, large D2 folds have overturned stratigraphy (Tanner & Thomas 2009) and there the stratigraphy may have been re-distributed. While there is no surface exposure of post-orogenic granite in the study area, a gravity anomaly extends across the study area from the Etive Complex (408 ± 0.4 Ma; Neilson *et al.* 2009). The anomaly has been postulated to represent a concealed granite (Pattrick *et al.* 1988). This, in addition to extensive lamprophyre sills and an appinite intrusion (*c.* 430 Ma) in the study area suggests there is potential for a magmatic component to mineralisation. The study area is crossed by the NW-SE-trending Cruachan lineament that may reflect a change in the basement and which may have focussed magmatism and hydrothermal fluids. The area is cut by the Tyndrum Fault, part of the Caledonian NE-SW-trending fault suite. The fault underwent significant movement (*c.* 430-

410 Ma) creating a high permeability conduit that could have provided a pathway and focussed fluids from depth.

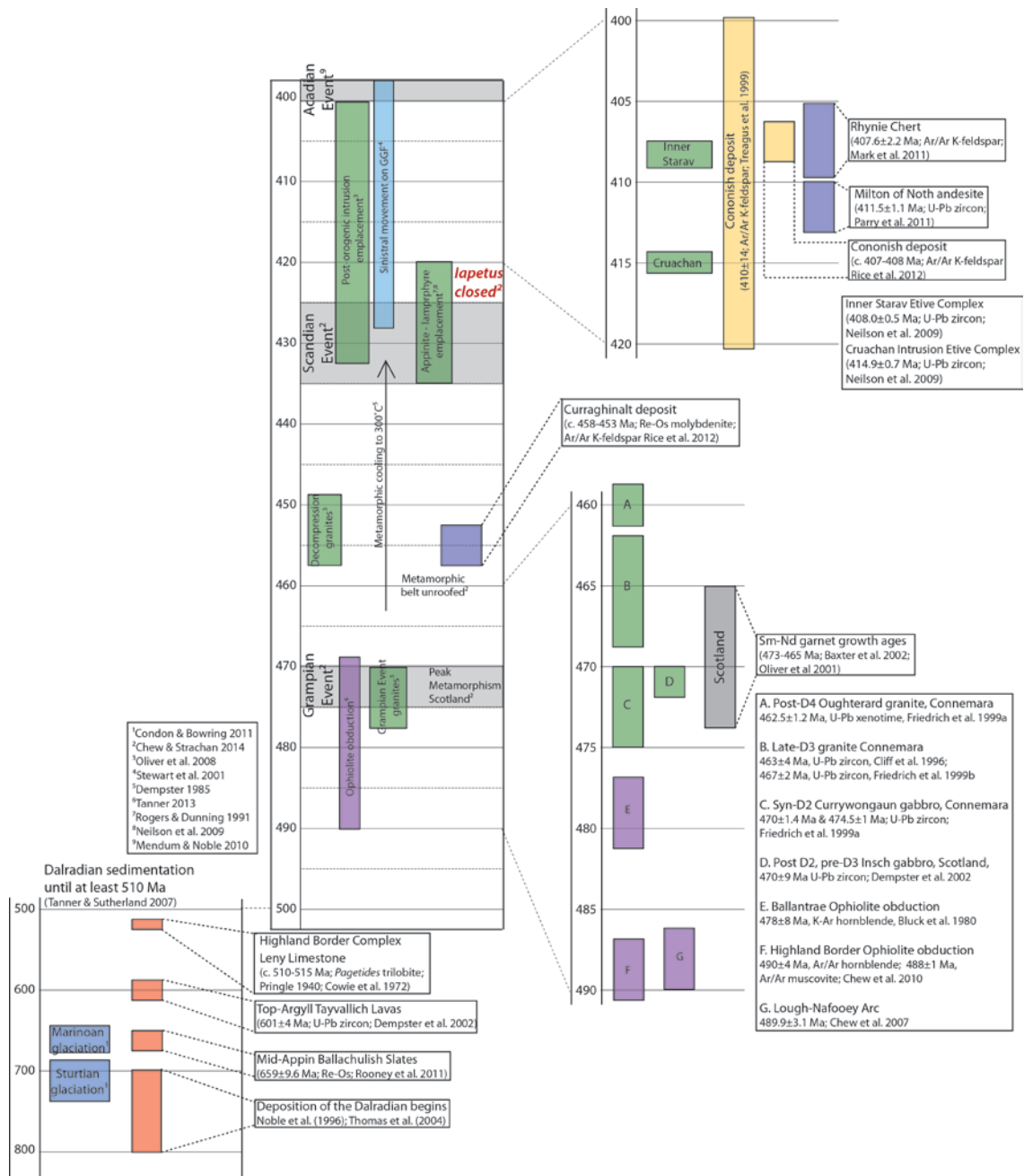


Figure 3.12: Existing age constraints for the Dalradian Supergroup showing key events in the evolution of the sequence through Grampian Event orogenesis and post-orogenic igneous intrusion and fault movement.

Chapter 4

Hydrothermal veins in the Tyndrum area; constraints on genesis from field relations and petrography

Abstract: Gold-bearing quartz veins occur throughout the Tyndrum area and include Scotland's largest gold resource at the Cononish deposit. The genesis of these veins remains controversial and few attempts have been made to relate the veins to each other or to place them into the context of the temporal evolution of the area. Detailed mapping of key localities in the Tyndrum area was carried out with the aim of re-examining known gold-bearing quartz veins, identifying further gold-bearing and other hydrothermal occurrences, and determining the temporal and structural relationships between different hydrothermal events. Together with detailed petrographic characterisation of all hydrothermal mineralisation types these observations enable a classification of different vein types. Early hydrothermal activity is recorded by molybdenite-bearing fractures, quartz-pyrite \pm K-feldspar and pyrite-bearing veins. Lamprophyre sills are intruded syn- to post-emplacement of gold-bearing breccia bodies. The major gold-bearing hydrothermal event is represented by poly-metallic quartz veins. These veins are cross-cut by quartz-only veins, Tyndrum Lead Mine-style veins and Permo-Carboniferous dykes.

4.1 Introduction

The Tyndrum-Glen Orchy license area is host to the largest known gold deposit in the SW Scottish Dalradian, the Cononish deposit (Fig. 4.1), and has a number of other gold occurrences noted by previous workers (Patrick *et al.* 1988; Curtis *et al.* 1993; Treagus *et al.* 1999; Tanner & Thomas 2009). The Cononish deposit was discovered in the early 1980's by Ennex (Chapter 2) and is host to a resource of 163, 200 oz Au and 631, 300 oz Ag (Scotgold Resources Ltd. 2012a). As discussed in Chapter 2, the genesis of the Cononish deposit is poorly understood and the deposit cannot be easily classified at the current level of understanding. During the course of this research new occurrences and styles of hydrothermal processes are identified in the study area.

Detailed field mapping and petrographic characterisation of a range of mineralisation styles aims to further the understanding of the hydrothermal events in the Tyndrum area through measuring vein trends and constraining cross-cutting relationships. The understanding of the hydrothermal evolution in the Tyndrum area is key to the continuation of mining beyond the life of the current prospect at Cononish. This research will provide criteria for exploration to enable companies to streamline efforts by highlighting key vein types, vein trends and petrographic relationships to maximise deposit discovery.

This chapter presents field relations and petrographic constraints on re-examined and newly identified gold and other occurrences, the background host metasedimentary rocks and igneous intrusions in the study area (Fig. 4.1). Field mapping and petrographic classification has clarified the relationship between deformation of the host Dalradian metasedimentary rocks, lamprophyre sill intrusion and gold mineralisation events. This developed a framework upon which work undertaken in the following chapters is applied to in order to assess the nature and genesis of the hydrothermal system in the Tyndrum area. The detailed field and petrographic classification will be used in the subsequent chapters to place geochemistry (Chapter 5), sulphur isotopes (Chapter 6) and geochronology (Chapter 7) work into a detailed context.

4.2 Methods

Mapping was undertaken over three field seasons between July 2010 and August 2012, in conjunction with Scotgold Resources Ltd's on-going exploration program and with assistance from Scotgold field assistants and Masters students from the University of Leicester (Matthews 2011; Moore 2011; Plewes 2012; Graham 2013; Spence-Jones 2013). Samples were obtained from *in situ* surface and underground outcrop and from quarter NQ drill core from Scotgold's on-going drill program. Petrographic reflected and transmitted light microscopy was carried out at the University of Leicester. Detailed mineralogical analysis employed a Hitachi S-3600N Environmental Scanning Electron Microscope, coupled with an Oxford Instruments INCA 350 energy dispersive X-ray analysis system. Sample details are given in Appendix 4.2 with large topography and geology reference maps showing sample locations in Appendix 4.1. Grid references for all photographs are in Appendix 4.3 and are given relative to the British National Grid.

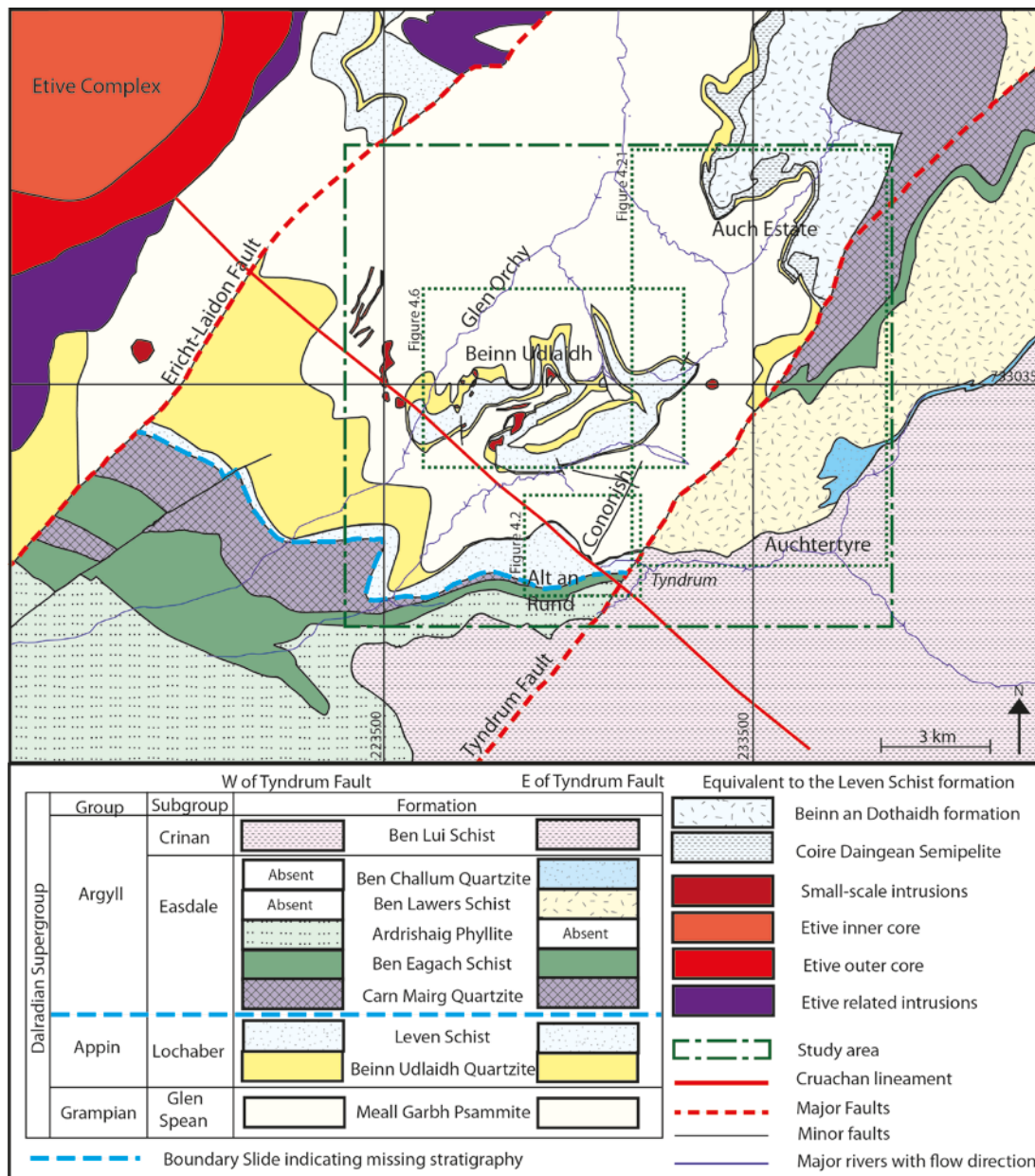


Figure 4.1: Simplified geology of the local area showing key structural features and the extent of the study area. Geology adapted from the British Geological Survey 1:50 000 scale Bedrock Geology Crianlarich and Dalmally sheets with additional detail from Tanner & Thomas (2009) and mapping in conjunction with Scotgold Resources Ltd.

4.3 Vein Classification

Vein types throughout the study area have been classified based on field relations with complex vein types sub-classified by variation in the trend and petrography (Table 4.1). Gold mineralisation within the breccia bodies is hosted in quartz veins cross-cutting the breccia bodies (further details in section 4.4.2.1)

In this work, open-space filling quartz is defined by the presence of euhedral termination of crystals growing into open space, which has been subsequently filled by late quartz or calcite. Vuggy texture is defined as quartz with unfilled vugs.

Table 4.1 *Classification of veins based on field and petrographic constraints from this study*

Vein type	Field classification	Subset	Number of veins	Trend	Key characteristics
Molybdenite-bordered fracture	Molybdenite in K-feldspar altered host rock		20	010-025°	Extensive K-feldspar alteration of host rock, molybdenite in alteration halo
Quartz-pyrite \pm K-feldspar	N-S trending veins with quartz \pm K-feldspar and pyrite		50	N-032°	White quartz and pyrite in vein with some K-feldspar alteration to host rock and as clasts in vein
Pyrite-bearing	Pyrite-bearing quartz vein		5	065-070°	Pyrite only sulphide present in quartz vein. Brecciated host rock clasts in vein
Breccia body quartz veins	Breccia body quartz vein		20	Within breccia bodies	Hosted with breccia bodies, clear to white quartz, some Au-Ag tellurides and pyrite
Poly-metallic	Complex veins with multiple sulphide phases dominantly pyrite and galena. Multiple quartz generations with brecciated host rock	Cononish set	15	040-060°	Gold-bearing, pyrite and galena with chalcopyrite, multiple quartz generations
		River Vein set	17	108-138°	Inclusions of K-feldspar altered host rock, gold-bearing, pyrite-galena dominated assemblage
		Kilbridge set	5	090-125°	Pyrite with arsenopyrite, gold-bearing,
Tyndrum Lead Mine-style	Galena and sphalerite bearing quartz vein		4	035-045°	Friable quartz, absence of pyrite, abundant galena and pale brown sphalerite
Quartz-only	Quartz-only		53	Various	Quartz brecciation by later quartz. Absence of sulphides

4.4 Field relations

4.4.1 Glen Cononish

4.4.1.1 Eas Anie

The Eas Anie Vein is host to the Cononish deposit, Scotgold's main prospect in the Tyndrum area (Fig. 4.2; 4.3). Previous work on the deposit is discussed in Chapter 2 with some new observations presented here to clarify the relations noted by previous workers (Patrick *et al.* 1988; Earls *et al.* 1992; Curtis *et al.* 1993; Treagus *et al.* 1999).

Treagus *et al.* (1999) mapped a galena-sphalerite-bearing quartz vein cross-cutting the main Eas Anie structure. This was interpreted to be early-Carboniferous in age and to represent a Tyndrum Lead Mine-style mineralising event (Treagus *et al.* 1999). This study concurs that the vein is in the adit and is comparable to mineralisation at the Tyndrum Lead Mine, based on a notable absence of pyrite and the presence of large blebs of galena and brown sphalerite, together with friable and vuggy quartz.

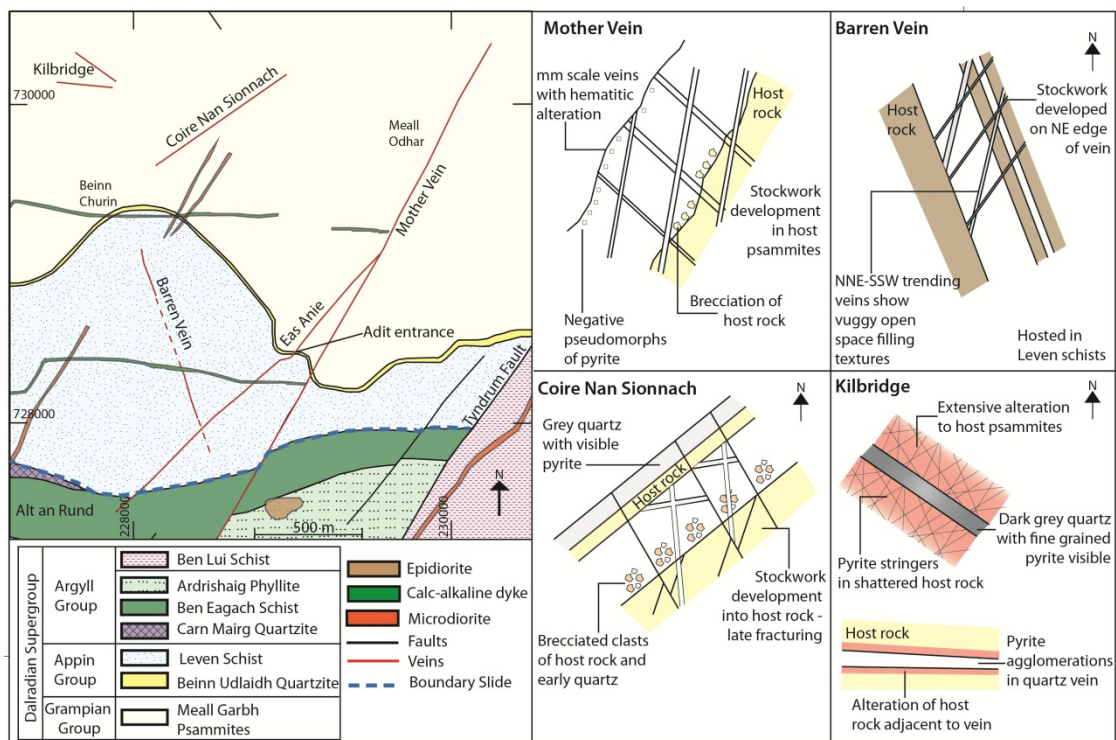


Figure 4.2: Detailed geology of Glen Cononish showing location of key veins and structural features. Panels to right show schematic representations of main veins in Glen Cononish in addition to the Eas Anie vein. Geology adapted from the British Geological Survey 1:50,000 scale Bedrock Geology Crianlarich sheet with additional detail from this study.

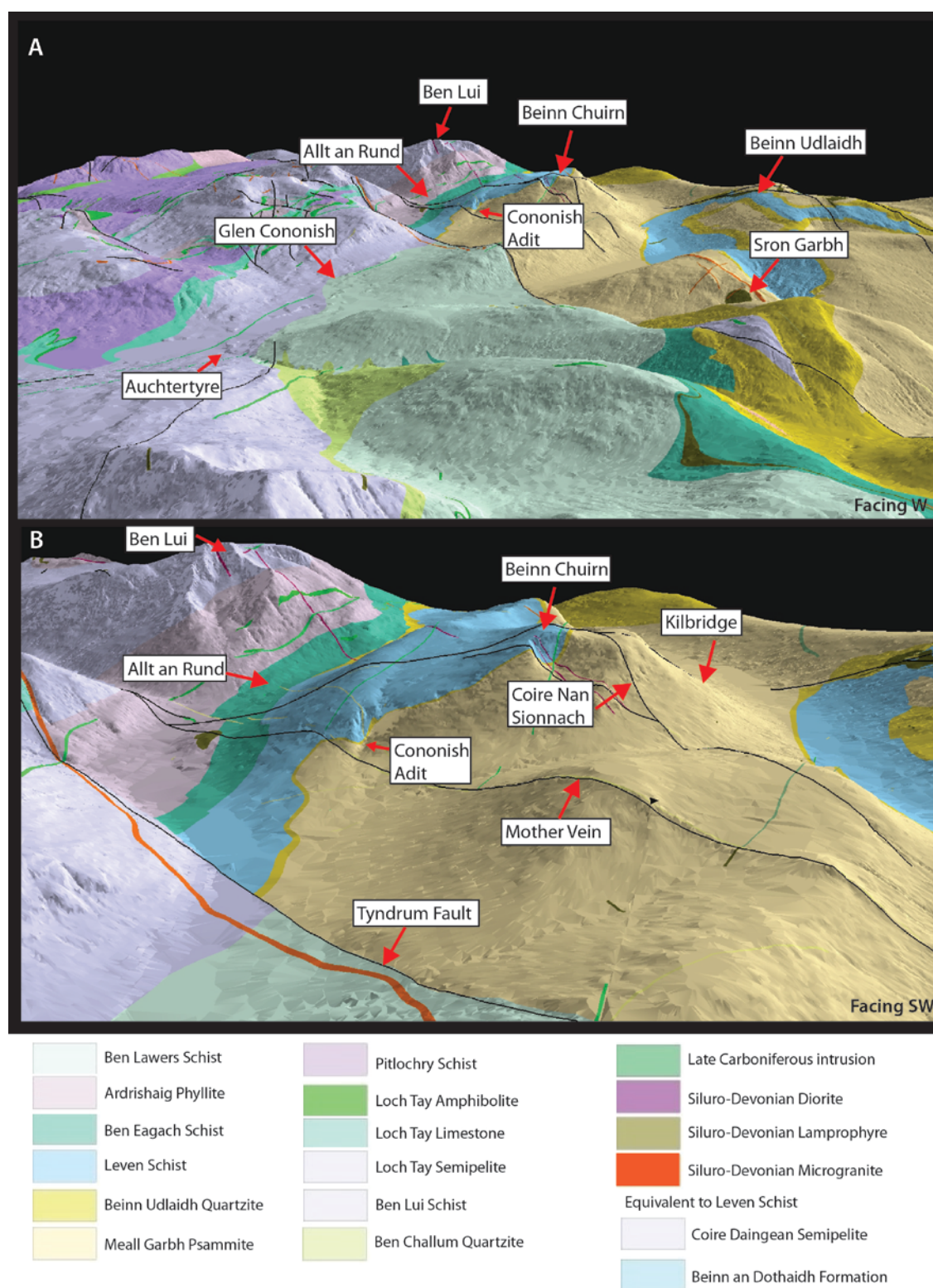


Figure 4.3: 3D representation of the geology draped over the topography in the Cononish area. A is viewed from Beinn Chullum, B is viewed from close to Tyndrum. Topographic surface was created in ArcScene by the author and the geology was draped over the surface. Geology (Crainlarich sheet) and topographic contours (British National Grid squares NN 22, 23, 32, 33) from EDINA. No vertical exaggeration. The colour scheme for geology on all 3D representations is the BGS Lexicon of Named Rock Units colour scheme, on other maps the colour scheme has been adapted for this work to improve the clarity between the units.

Earls *et al.* (1992) and Treagus *et al.* (1999) mapped a quartz-dolerite dyke on surface and in the adit. This study has re-examined this structure and concludes that underground the 090-102°-striking dyke cuts Eas Anie at an oblique angle (040-050° to the strike of vein) with chilled margins visible (Spence-Jones 2013). The dyke is a significant structure and can be traced on surface for >400 m, with breaks in exposure. The relationship between the Tyndrum Lead Mine-style mineralisation and quartz-dolerite dyke, both of which cross-cut Eas Anie, is complicated. Dominy & Platten (2008) report Tyndrum Lead Mine-style mineralisation, host to clasts of altered basalt, to be cross-cut by fresh basalt. The fresh basalt is host to clasts of both Tyndrum Lead Mine-style mineralisation and altered basalt (Dominy & Platten 2008). This complicated relationship was not recorded in this study and here Tyndrum Lead Mine mineralisation is cross-cut by a Permo-Carboniferous dyke, both of which cross-cut the Eas Anie vein. Calcite veinlets, the youngest veins in the area, cross-cut mineralisation at the Tyndrum Lead Mine (Patrick *et al.* 1983) and the Cononish deposit (Dominy & Platten 2008; Spence-Jones 2013).

A 1 m wide 147°-trending quartz-only vein is mapped on surface at Beinn Chuirn (Fig. 4.2); this was also noted by Earls *et al.* (1992). This vein is projected to cross-cut Eas Anie but previous workers and this study have been unable to establish a relationship between the veins either at the surface or underground.

4.4.1.2 Mother Vein

The Mother Vein is a steeply-dipping multi-phase quartz vein, reaching up to 10 m wide, first noted 500 m NE of the adit entrance (Fig. 4.2; 4.3; 4.4A). The vein pinches and swells along a lateral extent of >5 km, with breaks in continuity, reaching a minimum width of 1.5 m. The western edge of the vein is defined by a river cut and previous mine workings for base metals have been noted in the cut (Treagus *et al.* 1999). Patrick *et al.* (1988) identified electrum in the Mother Vein; this study has not identified any potential precious metal mineralisation, however, cubic negative pseudomorphs are interpreted to represent weathered out pyrite.

Multiple generations of quartz are recorded; many of these are dilational, with open-space filling quartz noted. Clasts of psammite have acted as nuclei for the formation of quartz and banded quartz growth occurs perpendicular to the surface of the clasts (Fig. 4.4B). No alteration of the host psammite occurs within the vein stockwork and clasts within the main vein have not been significantly altered (Fig. 4.4C). Late hematite alteration affects all earlier quartz generations.

4.4.1.3 Coire Nan Sionnach

A significant poly-metallic steeply-dipping 5 m wide vein, Coire Nan Sionnach, is mapped 1.4 km NW of the adit entrance (Fig. 4.2). The vein plunges steeply, down with topography, for 150 m before dipping beneath cover, with a small (<2 m) outcrop of stockwork interpreted to be the vein in the valley base (Fig. 4.3; 4.5C). Stockwork is also developed at the edge of the vein and both the vein and stockwork have late fracturing (152°-trending) followed by 2 cm of post-emplacement sinistral dip-slip movement. Quartz in the stockwork has an open-filling texture.

Early white quartz and psammite host rock are found as sub-angular brecciated clasts within the SE side of the vein (Fig. 4.2). Moving towards the NW side of the vein, brecciation decreases and is replaced by extensive chlorite and iron oxide alteration (Fig. 4.5A). At the NW side of the vein, the highly altered zone transitions into clean white quartz followed by a zone of host rock. A small vein on the NW side of the main structure contains grey quartz with abundant fine-grained pyrite, at heights above 670 m pyrite cubes (up to 1 cm diameter) occur in the grey quartz zone (Fig. 4.5B).

4.4.1.4 Kilbridge

At Kilbridge, 2 km NW of the adit entrance, a series of poly-metallic quartz veins with a distinct salmon-pink alteration are mapped (Fig. 4.2). The quartz veins vary in size from 20 cm to mm scale and are dominated by fine grained pyrite, concentrated in a zone up to 3 cm wide at the centre of the veins (Fig. 4.5D & E). Small pyrite cubes are visible in altered host rock. There is no evidence of open-space filling quartz at Kilbridge suggesting differing mineralising conditions to Eas Anie and Coire Nan Sionnach.

4.4.1.5 Alt an Rund

Mapping was undertaken in Alt an Rund to sample the host metasedimentary sequence and to attempt identify the Eas Anie Vein in river cuts (Fig. 4.3). At the point the Eas Anie vein would cross the Alt an Rund River if projected, the vein is not seen. A highly weathered coarse grained microdiorite dyke (Fig. 4.4D) was identified at the western extent of the mapping area and a lamprophyre sill was noted within the Leven Schist. Pyrite is identified within the Ben Eagach Schist, the pyrite occurs throughout the unit but is concentrated into horizons within the bedding (Fig. 4.4E). Pyrite comprises around 5% of the schist comparable to observations in the Ben Eagach Schist in other areas (average 5% reaching a maximum of 20%; Smith *et al.* 1977).

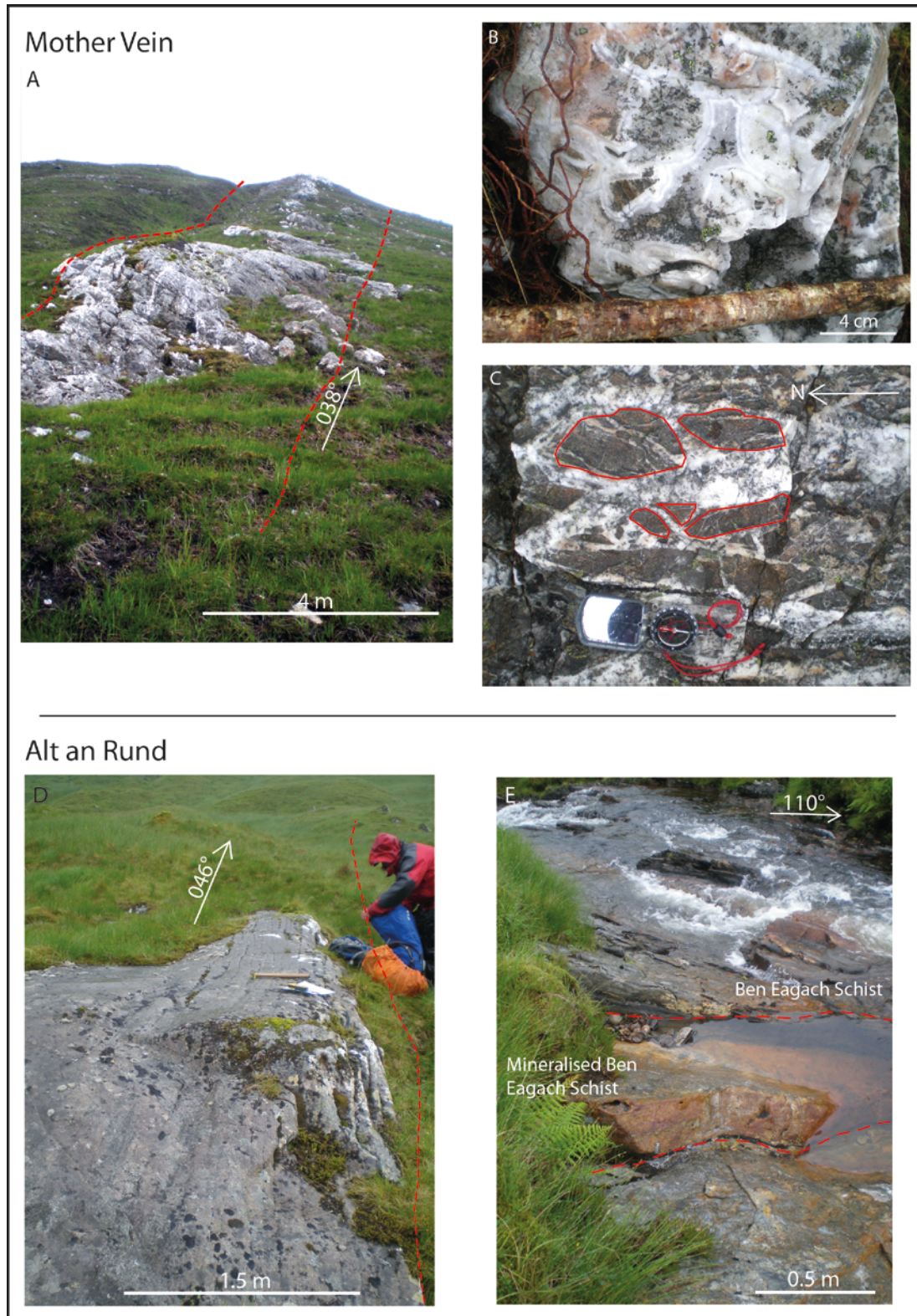


Figure 4.4: Photo plate of Mother Vein and Alt an Rund. A. Extent of Mother Vein. B. Crustiform quartz growth around clasts of host rock within Mother Vein. C. Brecciated clasts of schist host rock within Mother Vein quartz. D. Microdiorite dyke in Alt an Rund. E. Mineralised Ben Eagach Schist.

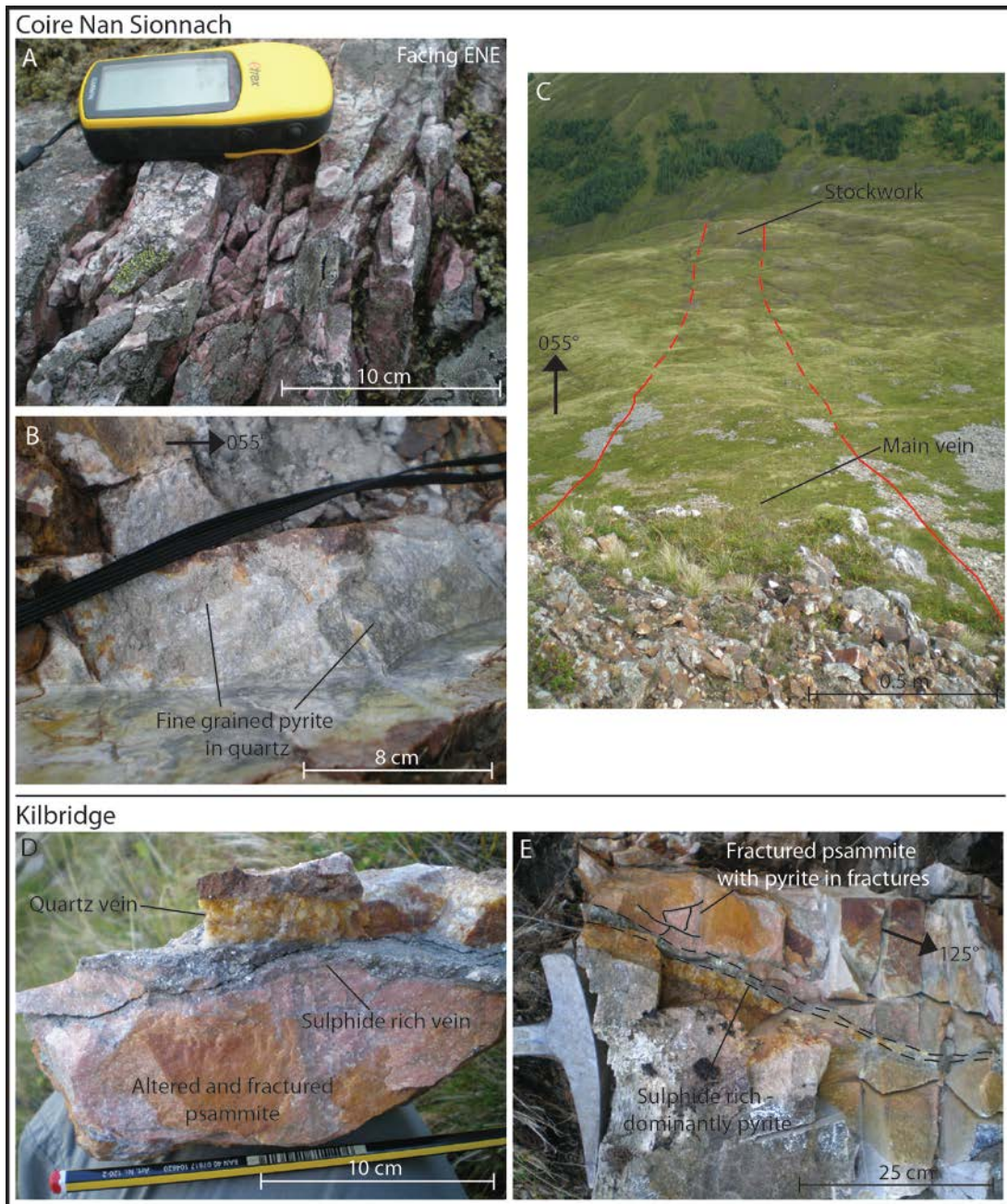


Figure 4.5: Photo plate of the Coire Nan Sionnach and Kilbridge. A. Distinct red-purple alteration to quartz seen at Coire Nan Sionnach. B. Fine grained pyrite in grey quartz. C. Extent of Coire Nan Sionnach vein and stockwork visible after un-exposed portion. D. Hand sample of Kilbridge mineralisation. E. In situ vein at Kilbridge.

4.4.2 Beinn Udlaidh

4.4.2.1 Breccia bodies

Breccia bodies, on the Glen Orchy side of Beinn Udlaidh (Fig. 4.6), show significant variation in size and clast composition. The surface area of the breccia bodies varies from 15 m² to 150 x 70 m (Moore 2011). The breccia bodies are dominated by angular clasts (up to 50 cm in diameter) of the Meall Garbh Psammite, Beinn Udlaidh Quartzite and Leven Schist Formations (Fig. 4.8; Table 4.2). The type of clast varies but appears to be controlled by the immediate host rock of the breccia body, demonstrated by the absence of Beinn Udlaidh Quartzite in pipes below 380 m ASL, where there is no Beinn Udlaidh Quartzite (Moore 2011).

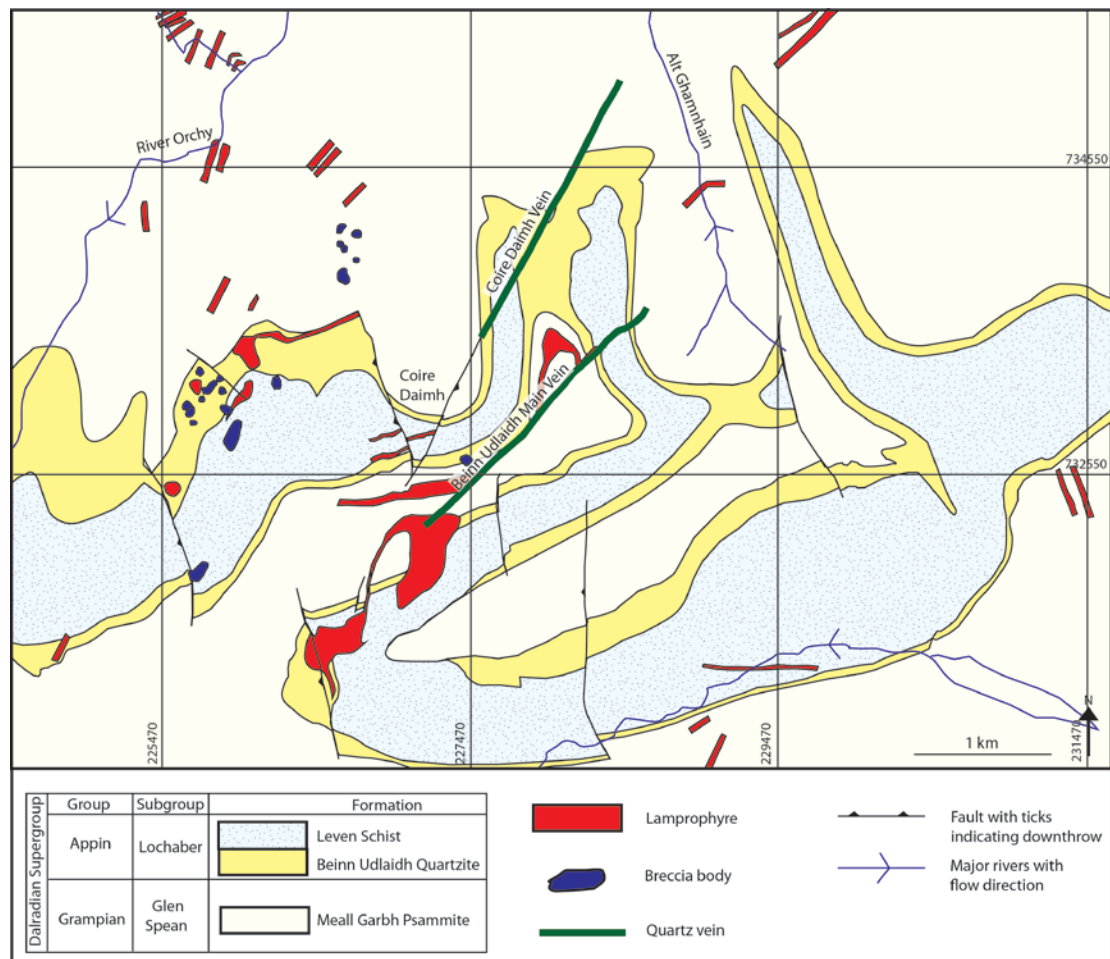


Figure 4.6: Detailed geology of the Beinn Udlaidh area showing location of key veins and breccia bodies. Geology adapted from the British Geological Survey 1:50,000 scale Bedrock Geology Crianlarich sheet with additional detail from this study and Tanner & Thomas (2009).

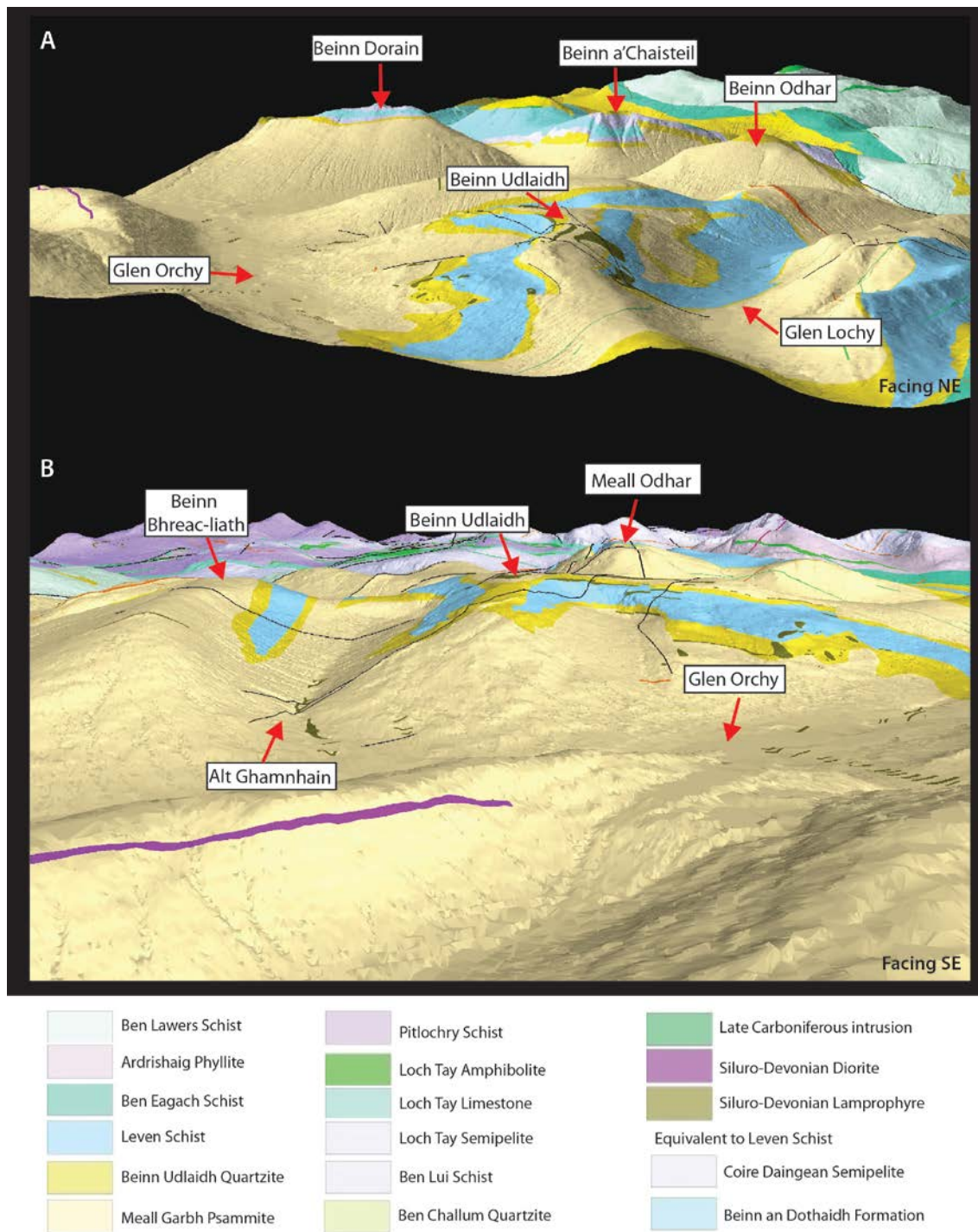


Figure 4.7: 3D representation of the geology draped over the topographic variation in the Beinn Udlaidh and Glen Orchy areas. A is viewed from Beinn na Sroine, B is viewed from behind Ben Inverveigh. Topographic surface was created in ArcScene by the author and the geology was draped over the surface. Geology (Crainlarich sheet) and topographic contours (British National Grid squares NN 22, 23, 32, 33) from EDINA.

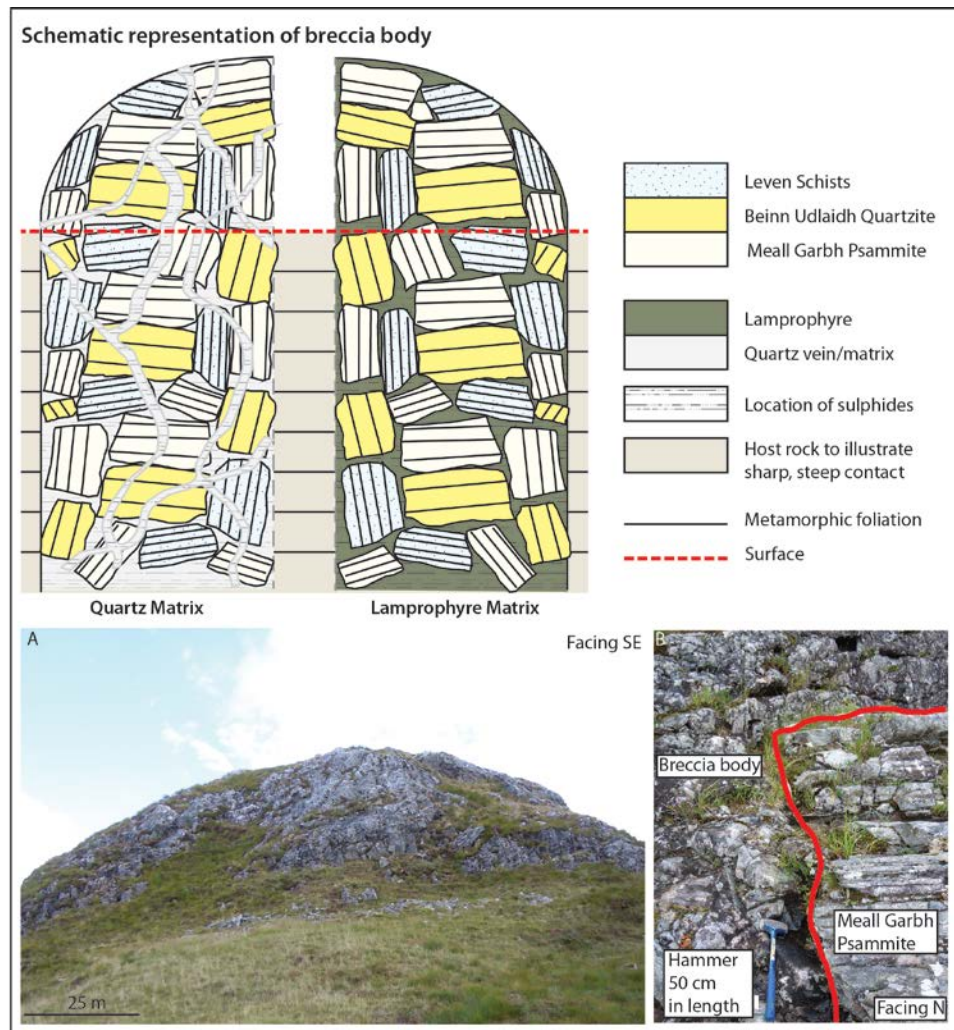


Figure 4.8: Schematic representation of the quartz- and lamprophyre-dominated matrix end-members within the breccia bodies at Beinn Udlaidh. A. Field photograph of surface exposure of breccia pipe 11 at Beinn Udlaidh. B. Sharp, steep contact between breccia and host rock.

The breccia bodies are tightly-packed clast-supported but where matrix occurs it is either quartz or lamprophyre. The presence of lamprophyre matrix indicates emplacement of the breccia bodies occurred pre- to syn-emplacement of the lamprophyre sills (Moore 2011). Three quartz stages are defined by Moore (2011):

1. Early quartz veinlets characterised by chlorite, sericite and minor K-feldspar
2. Main stage quartz forming the matrix and vein quartz and is host to the sulphide
3. Late quartz forms small, <1 cm veins cross-cutting main stage quartz

In breccia bodies with main stage quartz, the veins cross-cut clasts of host rock. The veining is visible between clasts and within clasts of all types. A decrease in the amount of quartz veining with increasing height within the breccia pipes is noted (Moore 2011). In breccia bodies with a lamprophyre matrix, the lamprophyre does not cross-cut the host rock clasts (Moore 2011).

Sulphide, dominantly pyrite, within the breccia bodies is known to carry gold (up to 0.26 g/t Au and 1.49 g/t Ag over 14 m; Scotgold Resources Ltd 2010). Gold, as Au-Ag-tellurides, occurs with Pb-tellurides in pyrite. Pyrite and tellurides are found within quartz veining/matrix and in altered host rock clasts, in particular the Meall Garbh Psammite Formation. The host rock does not affect the type or intensity of the mineralisation; the porosity and permeability are interpreted to control the distribution of mineralisation (Moore 2011).

Table 4.2 *Characteristics of clast and matrix in breccia pipes at Beinn Udlaidh from this study and Moore (2011)*

Clast characteristics	<i>Clast lithology ratio</i>	Pelite-Psammite	Pelite-Psammite-Quartzite
		Max 75:25	Max 45:40:15
		Min 15:85	Min 20:10:70
	<i>Clast shape</i> <i>Roundness</i>	Tabular blocks Angular to sub-angular	Tabular blocks Angular to sub-angular
Matrix characteristics	<i>Matrix lithology</i>	Vein quartz	Lamprophyre with minor quartz
	<i>Clast:matrix ratio</i>	Max 70:30	Max 90:10
		Min 55:45	Min 40:60
Mineralisation characteristics	<i>Sulphides</i>	Pyrite ± chalcopyrite, galena, arsenopyrite	
	<i>Location of sulphides</i>	Matrix quartz	
		Within altered lamprophyre	
	<i>Sulphide textures</i>	Disseminated	
Alteration characteristics	<i>Clasts</i>	Psammite - feldspathic	
		Pelite - chloritisation	
		Quartzite – some feldspathic	
	<i>Lamprophyre</i>	Extensive chlorite and sericite alteration	

4.4.2.2 Beinn Udlaidh Main Vein

The Beinn Udlaidh Main Vein, trending NE-SW, reaches up to 10 m in width at the top of Beinn Udlaidh (Fig. 4.6; 4.7; 4.9A & B). Previous work has been undertaken on the vein (Tanner & Thomas 2009; Plewes 2012; Chapter 2) and this section gives a brief overview of the observations made in this study and compares these with previous work.

The vein has multiple generations of quartz and while the overall trend of the vein is NE-SW the vein is segmented and there are zones of non-exposure. The vein has open-space filling quartz throughout (Fig. 4.9C & F). Some rust coloured discolouration of the largely clean white quartz is interpreted to be a late hematite alteration stage.

Plewes (2012) defined five quartz categories in the Beinn Udlaidh Main Vein:

1. Massive white quartz veins
2. Dark blue sulphide-rich quartz
3. Clear quartz
4. Late massive white quartz
5. Vuggy quartz

The five quartz vein types within the Beinn Udlaidh Main Vein show progressive anticlockwise rotation (Plewes 2012) consistent with regional structural extension and sinistral shearing (Treagus *et al.* 1999).

Brecciation of host rock occurred during vein emplacement with clasts of host metasedimentary rocks and lamprophyre in the vein (Fig. 4.9D & E). This places relative time constraints on the age of emplacement of the lamprophyre sills; the sills must have been emplaced prior to the quartz vein (Tanner & Thomas 2009). There is a decrease in the percentage of clasts towards the centre of the vein, with stockwork at the edges of the main vein structure.



Figure 4.9: Photo plate of Beinn Udlaidh Main Vein. A & B. Extent of Main Vein. C & D. Brecciated clasts of host rock within Main Vein. E & F. Euhedral quartz terminations in vein.

There is a low sulphide content in the vein; where present, pyrite dominates and cubic negative pseudomorphs are noted. Towards the northeastern extent of the vein, a zone of high sulphide content occurs with a characteristic blue discolouration to the quartz (Plewes 2012). This zone runs along the eastern edge of the main vein reaching 0.5 m in width and is only seen at the northeastern extent of the Main Vein. Diamond drilling was undertaken to try and establish the extent of the Beinn Udlaidh Main Vein at depth and the vein extends to >170 m beneath the topographic surface but decreases in total width to <4 m (true thickness) at 560 m (Fig. 4.10) with limited pyrite in drill core.

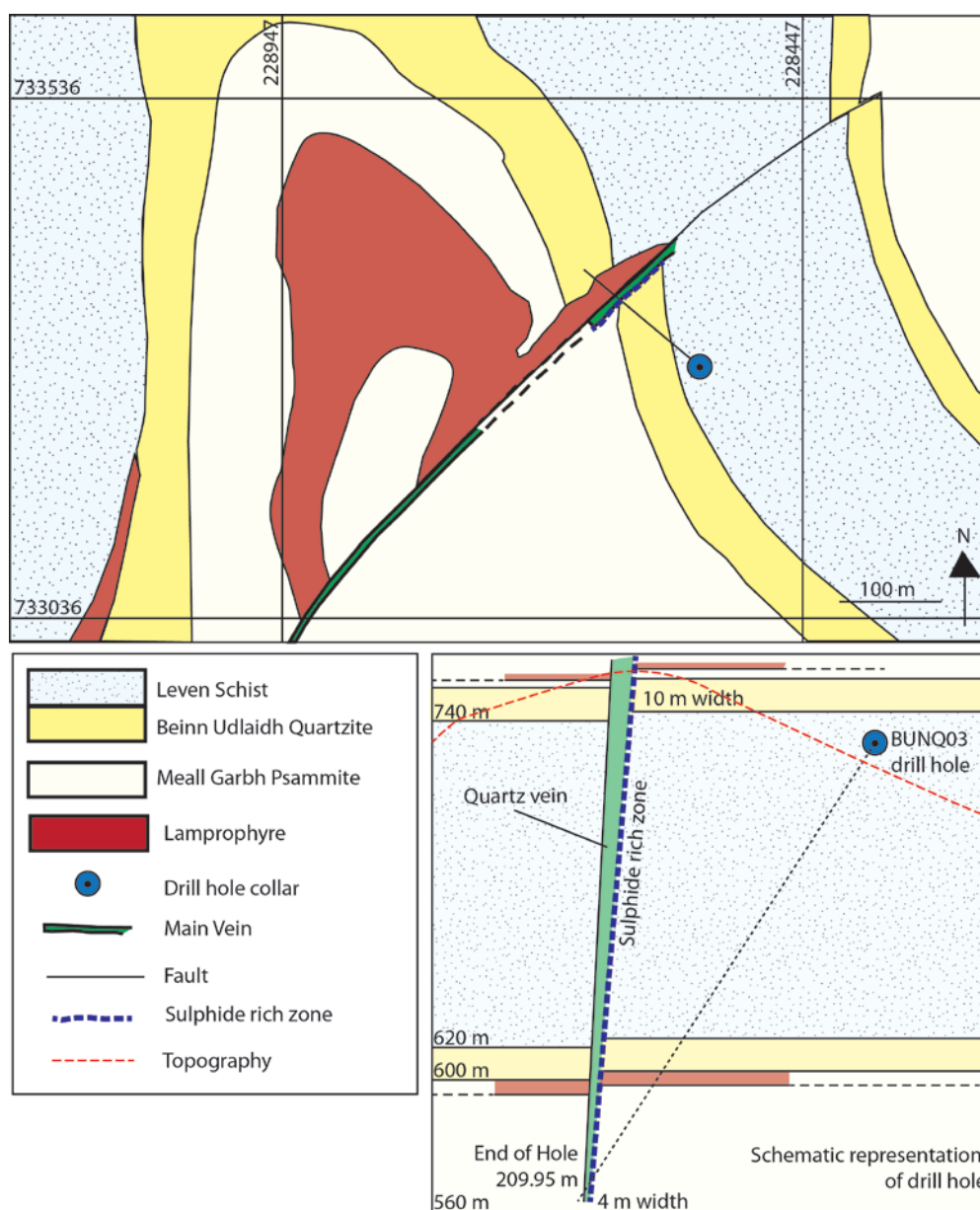


Figure 4.10: Map and cross-section showing variation in the Beinn Udlaidh Main Vein from drill core evidence.

4.4.2.3 Coire Daimh Vein

The Coire Daimh Vein, also known as the Beinn Udlaidh Barren Vein, is hosted in a NNE-trending fault structure with downthrow to the SE (Tanner 2012). The steeply-dipping quartz-only vein reaches up to 10 m in width and extends from Alt Ghamnhain to Beinn Udlaidh (Fig. 4.6; 4.11A & B). The vein has been traced to the edge of Coire Daimh and is tentatively inferred to occur in the cliff on the SW edge of the coire (Fig. 4.11D). The vein cross-cuts the Meall Garbh Psammities and folded units of the Beinn Udlaidh Quartzite and Leven Schists.

The vein has multiple quartz stages and has a complex series of cross-cutting relationships within the structure (Fig. 4.11C). Brecciation of earlier quartz is noted with the brecciated clasts largely remaining in place, cemented by later quartz (Fig. 4.11E). There is limited evidence of sulphide, some pyrite is identified in narrow veins within the stockwork. Cubic pyrite (<5 mm) is noted in 132°-trending veins at the edge of the vein; pyrite is not seen within the main structure of the vein. With increasing altitude, an increasing abundance of open-space filling quartz textures are interpreted to be due to space developing on the top of Beinn Udlaidh, related to the development of the Glen Orchy dome (Tanner 2012).

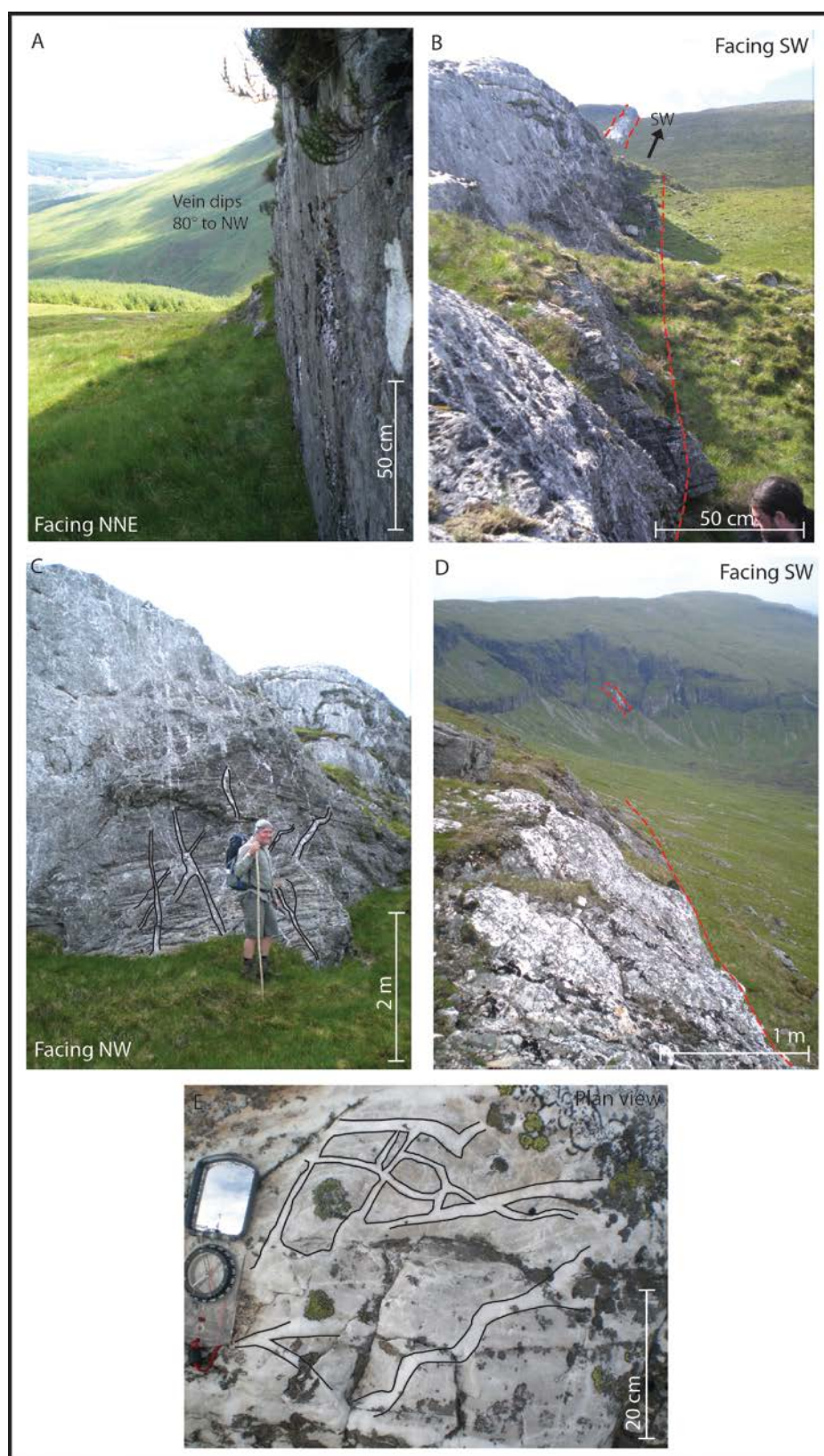


Figure 4.11: Photo plate of Coire Daimh Vein. A. Illustration of steep orientation of vein. B. Tracing of vein across the hill side. C. Extensive and multiple generation of veining visible within main vein. D. Potential extension of vein in cliff across Coire Daimh. E. Brecciated early quartz cemented by later generation.

4.4.3 Glen Orchy

The Glen Orchy River (~7 km NW of Cononish adit entrance; River Orchy henceforth) exhibits poly-metallic gold-bearing quartz veins and separate molybdenite-bearing fractures that are unique to the study area at current understanding (Fig. 4.1; 4.7). Detailed field mapping has been undertaken along the river from Invergaunien to the weir at Eas a'Chathaidh (Fig. 4.12; 4.13; 4.14).

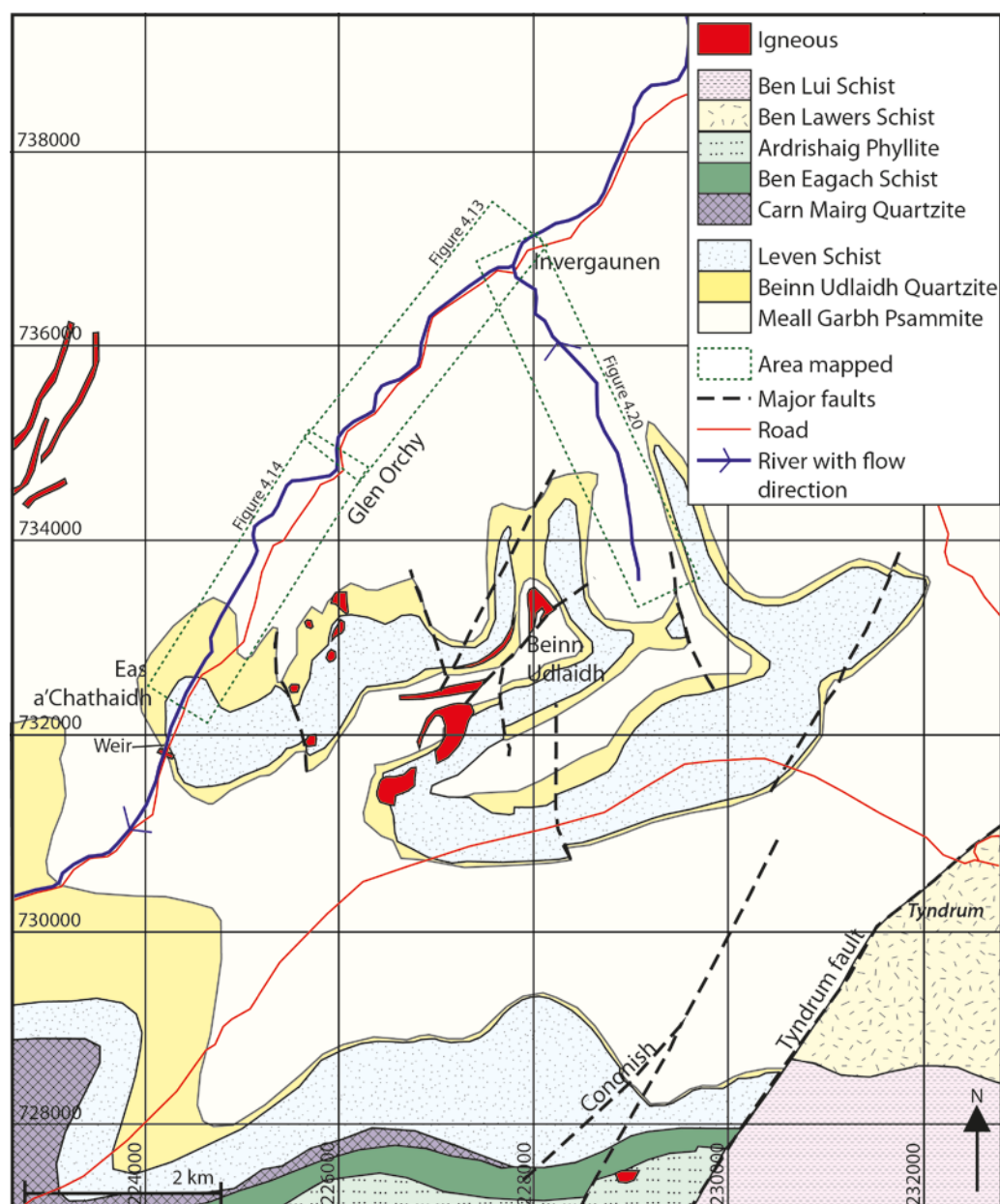


Figure 4.12: Glen Orchy area geology showing extent of detailed re-mapping of the area. Geology adapted from the British Geological Survey 1:50,000 scale Bedrock Geology Crianlarich and Dalmally sheets with additional detail from this study and Tanner & Thomas (2009).

Exposure beyond the river banks is limited and within the river there are significant zones of gravel cover. Host rocks are dominated by the variable mica- to quartz-dominated Meall Garbh Psammite Formation, which transitions into the Beinn Udlaidh Quartzite and Leven Schist Formations downstream towards the SW and with increasing altitude. The isoclinal D2 folds recorded at Beinn Udlaidh (Tanner & Thomas 2009) can be seen in repeating units of Beinn Udlaidh Quartzite and Leven Schists downstream towards Eas a'Chathaidh. Quartz veining is widespread in River Orchy with the majority of quartz veins being quartz-only.

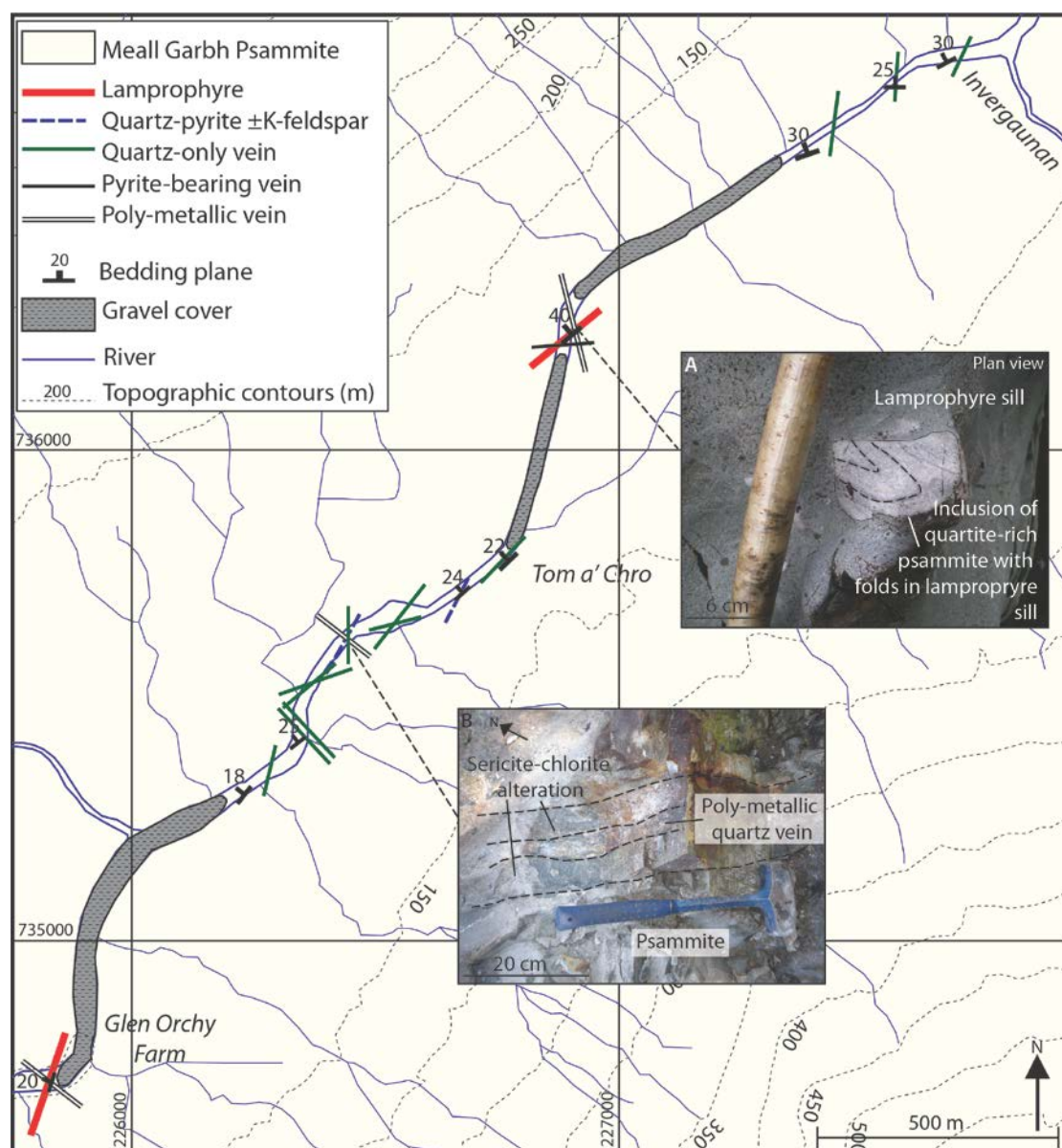


Figure 4.13: Detailed map of the NE-extent of mapping in Glen Orchy. A. Inclusion of folded host psammite in lamprophyre sill. B. Alteration selvage at edge of poly-metallic vein.

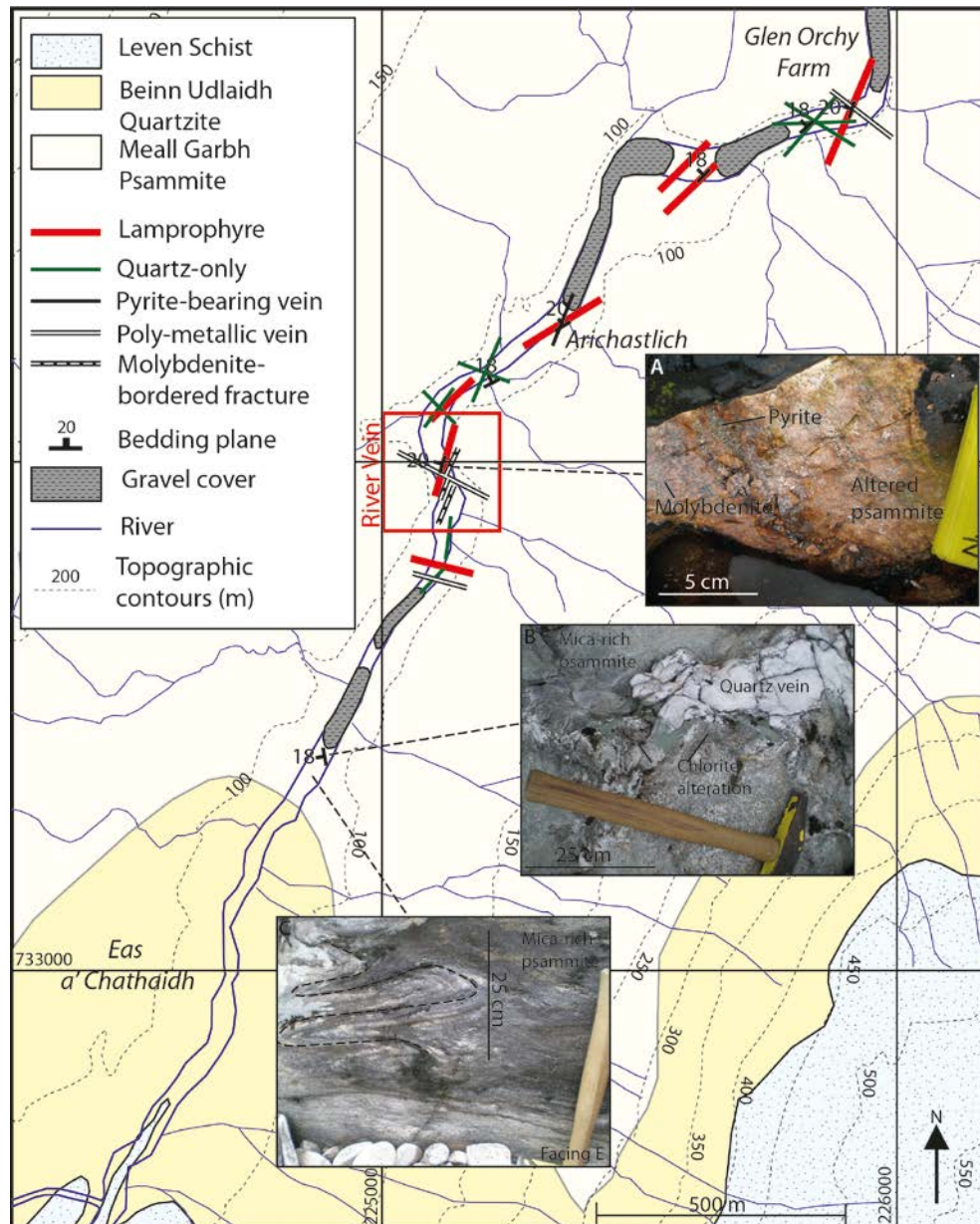


Figure 4.14: Detailed map of the SW-extent of mapping in Glen Orchy. River Vein is within the red box and is shown in more detail in Figure 4.15. A. Molybdenite and pyrite in altered fracture selvage in psammite. B. Large chlorite alteration zones at edge of quartz vein. C. Tight isoclinal folding in Meall Garbh Psammite Formation.

4.4.3.1 Molybdenite-bordered fracture

Molybdenite mineralisation is hosted in the alteration selvages of steeply-dipping 010° to 025°-trending fractures (Fig. 4.15; 4.16A, B, D). The fractures are usually narrow (mm scale) with alteration selvages reaching 20 cm in width. Fractures can reach 10 cm in width when late quartz infill is present. The selvages are a distinctive salmon pink colour and bedding and metamorphic foliation is destroyed in the alteration halo (Fig. 4.16C & D; 4.17C & D).

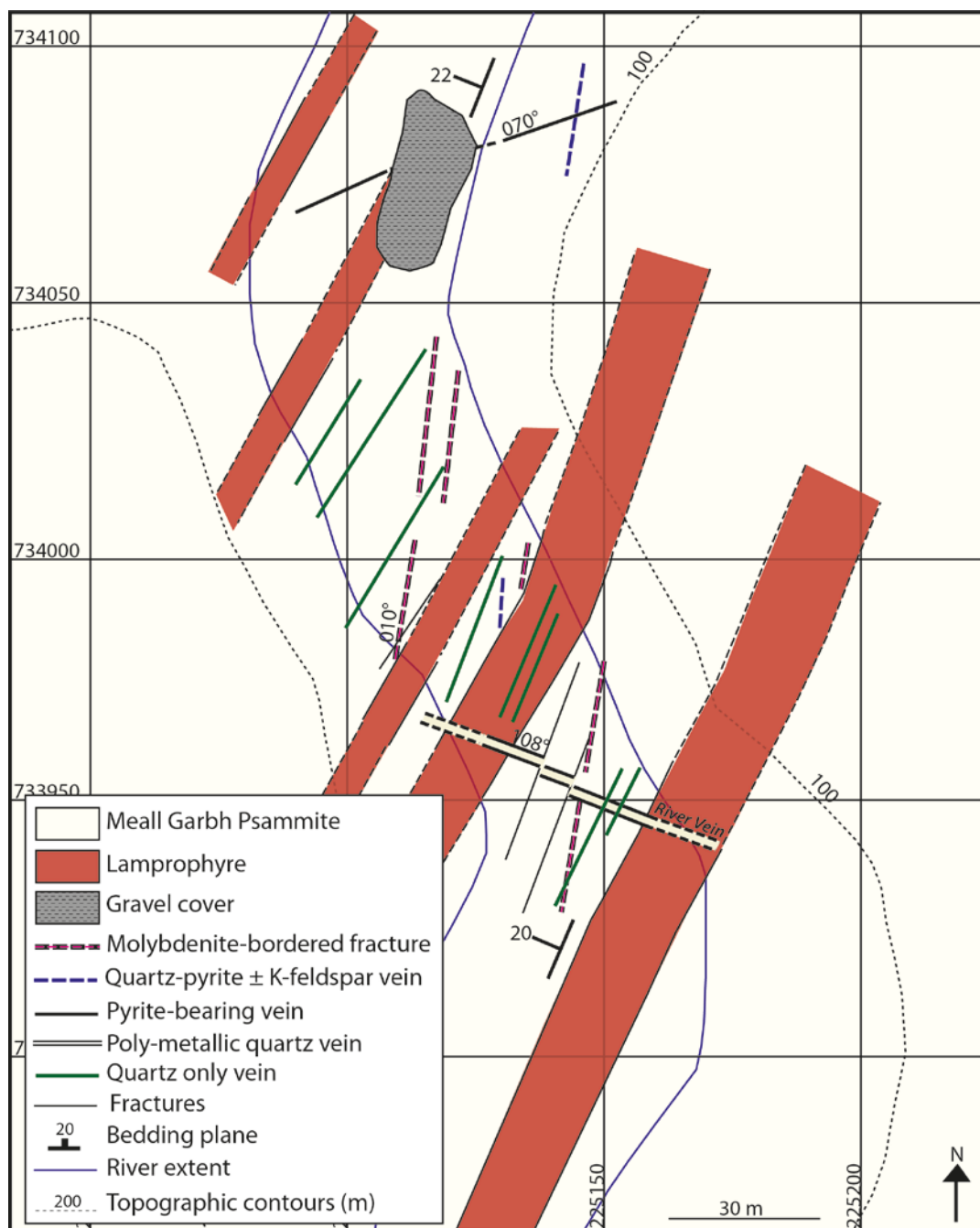


Figure 4.15: Detailed map of the River Vein area of Glen Orchy showing key cross cutting relationships.

4.4.3.2 Quartz-pyrite \pm K-feldspar veins

The earliest quartz veins (quartz-pyrite \pm K-feldspar veins; Table 4.1) in Glen Orchy trend N-032° and exhibit K-feldspar alteration comparable to molybdenite-bearing fractures, but have no molybdenite in the K-feldspar altered selvage (Fig. 4.16C). The quartz appears to be later infill of the pre-existing fractures with two generations of pyrite, one in the vein and the other in the alteration selvage (Fig. 4.16C; 4.17C & D).

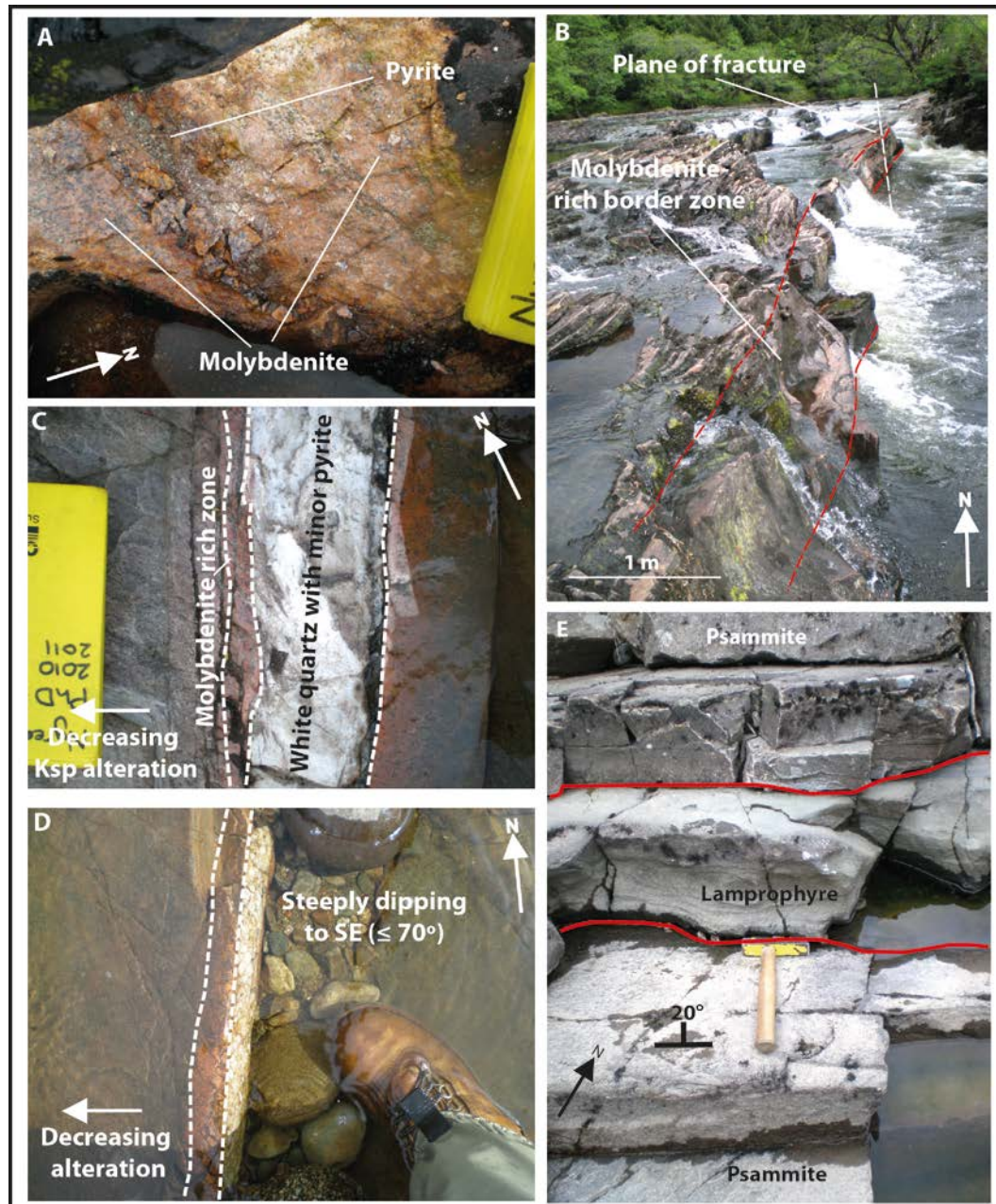


Figure 4.16: Photo plate of Glen Orchy area. A. Surface exposure of molybdenite-bordered fracture showing clean surface with molybdenite and pyrite B. Extent of molybdenite-rich zone on edge of fracture in River Vein area of Glen Orchy C. Molybdenite-bordered K-feldspar altered host rock with later quartz vein infilling pre-existing fracture (Quartz \pm K-feldspar & pyrite vein). D. Evidence of steeply-dipping nature of molybdenite-bordered veins. E. Lamprophyre sill within Meall Garbh Psammite host rock.

This vein set is interpreted to be equivalent to the molybdenite-bordered fractures but exhibits additional late quartz in the centre of the fracture.

4.4.3.3 Lamprophyre sills

Lamprophyre sills are found throughout River Orchy, increasing in abundance downstream. The sills vary in thickness between 0.5 and 2 m (Fig. 4.16E). The presence of biotite phenocrysts is variable with weathered phenocrysts visible in some sills but absent in others. Where biotite phenocrysts occur the host Meall Garbh Psammite or Leven Schist host rock has an increased mica content suggesting potassic alteration around the sills. Pyrite occurs as sporadic stringers (<1 mm wide) in the sills.

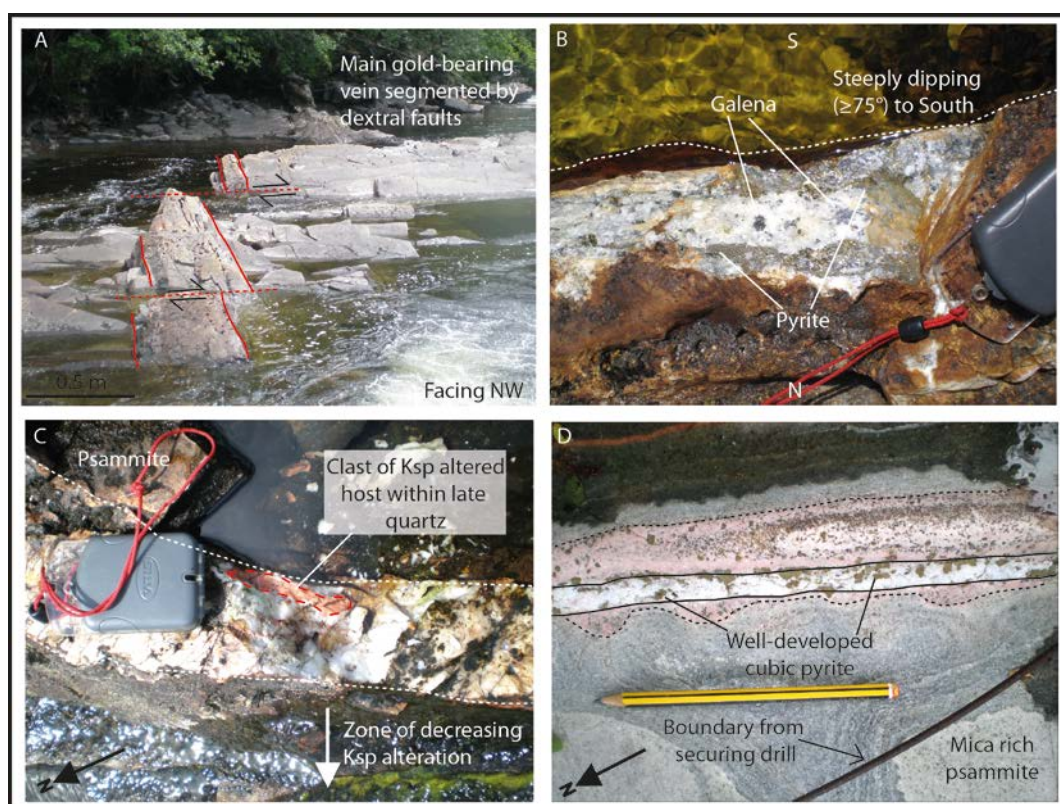


Figure 4.17: Photo plate of Glen Orchy area. A. River Vein poly-metallic vein offset by faulting across River Orchy. B. In situ mineralogy of River Vein poly-metallic vein. C. Clasts of K-feldspar altered host rock within pyrite-bearing quartz vein. D. Decreasing K-feldspar alteration away from pyrite-bearing quartz vein.

4.4.3.4 Pyrite-bearing veins

Pyrite-bearing veins, trending $065-070^\circ$, are mapped in Glen Orchy. The most significant of these is a 5 cm wide pyrite-bearing vein mapped upstream of the main River Vein gold vein. The vein has a single generation of quartz and is pyrite-rich with angular clasts of K-feldspar altered psammite.

4.4.3.5 Poly-metallic quartz veins

Poly-metallic quartz veins trend $108\text{--}138^\circ$ and dip steeply to the SW. The veins have multiple generations of quartz with pyrite and some galena. The River Vein, a significant sub-vertical 1 m wide gold-bearing quartz vein, trends 108° (Fig. 4.15). The sulphides are dominantly pyrite with a late galena phase. Brecciated clasts of K-feldspar- and chlorite-altered host rock are visible in the vein (Fig. 4.17B). Pyrite is disseminated into the host rock within 2 m of the cross-cutting poly-metallic quartz veins. The vein is offset by $020\text{--}030^\circ$ -trending fractures, with 2 m dextral offset visible at low water; any component of vertical movement is not constrained (Fig. 4.17A).

4.4.3.6 Quartz-only veins

A large number of quartz-only veins have been mapped with a variety of orientations; white quartz veins trending 050° are cross-cut and sinistrally offset by 100° -trending quartz veins which are in turn cross-cut by $020\text{--}030^\circ$ -trending fractures with dextral offset (Fig. 4.18).

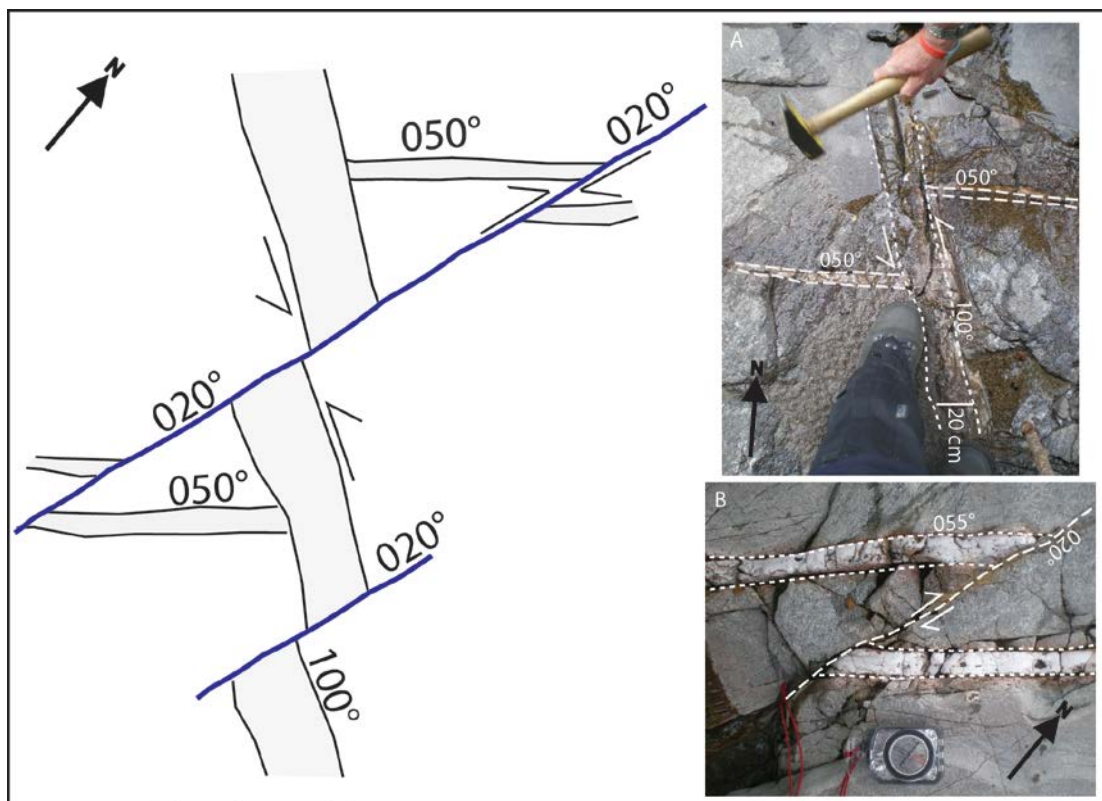


Figure 4.18: Cross-cutting relationships of quartz-only veins in the Glen Orchy River.

4.4.3.7 Carboniferous dykes

Dykes assumed to be from the Permo-Carboniferous Tholeiitic dyke swarm are mapped in River Orchy, particularly SW of the River Vein area (Fig. 4.13; 4.14). Dykes are defined as Permo-Carboniferous based on the prominent E-W trend and information from the BGS 1:50,000 Crianlarich bedrock geology sheet. Dykes are up to 2 m wide, dark grey in colour and coarse textured, with an absence of phenocrysts. Small 0.5 m wide 025°-trending dykes have been mapped along the river and late quartz-only veins are exploiting the same 025°-trending structures. The largest dyke trends 120° and is found downstream in the folded Beinn Udlaigh Quartzite and Leven Schists. The relationship between 025°-trending and 120°-trending dykes is unconstrained.

4.4.3.8 Constraints on timing relationships

All vein types in the Glen Orchy area cross-cut the metamorphic foliation and therefore are interpreted to be emplaced after ductile deformation and peak metamorphism (Fig. 4.19).

1. Molybdenite-bordered fractures

These represent the earliest vein set recorded in the study area and the molybdenite-bordered fractures cross-cut bedding parallel D2 schistosity.

2. Quartz-pyrite \pm K-feldspar veins.

No cross-cutting relationship has been observed between molybdenite-bearing fractures and quartz-pyrite \pm K-feldspar veins but the presence of K-feldspar clasts in the quartz veins is interpreted to indicate veins were emplaced syn- molybdenite-bordered fractures. This study interprets the two vein sets to be equivalent and these veins are described as molybdenite-bordered fractures henceforth.

3. Siluro-Devonian lamprophyre sills.

Clasts of bleached, well-rounded host psammite (up to 5 cm across) occur sporadically in the Siluro-Devonian lamprophyre sills indicating deformation of the Meall Garbh Psammite occurred pre-emplacment of the sills (Fig. 4.13A). The age of the Siluro-Devonian lamprophyre sills is based on information within the BGS Crianlarich bedrock geology sheet. The presence of a pervasive green discolouration, confirmed to be chlorite-sericite alteration by subsequent petrographic work is related to the emplacement of the gold-bearing quartz veins. This suggests lamprophyre sills have been altered by later fluid flow, related to the gold-bearing quartz veins.

4. Pyrite-bearing veins

The pyrite-bearing vein cross-cuts quartz-pyrite \pm K-feldspar veins and is interpreted to be later than molybdenite-bordered fractures. The relationship between the pyrite-bearing vein and lamprophyre sills is unconstrained, due to gravel cover. In addition, the relationship between poly-metallic quartz veins and the pyrite-bearing vein is not constrained due to no exposure at the extrapolated point of cross-cutting

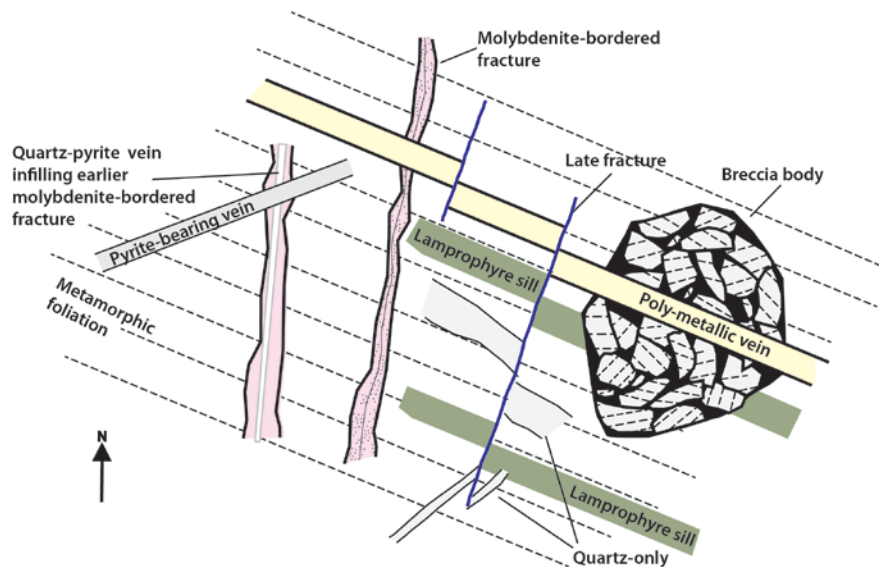


Figure 4.19: Schematic representation of the cross cutting relationships in the Glen Orchy area.

5. Poly-metallic quartz veins

Poly-metallic quartz veins cross-cut and alter lamprophyre sills and the veins contain brecciated clasts of altered host rock and lamprophyre (Figs. 4.17B; 4.19). The River Vein cross-cuts the molybdenite-bordered fractures (Fig. 4.15; 4.17A; 4.20).

6. Quartz-only veins

Quartz-only veins are complex with a number of different orientations recorded. Quartz-only veins trending 050° are cross-cut by 100° -trending quartz-only veins. Both of these vein sets are cross-cut by 020 - 030° -trending fractures, the latest event recorded in the Glen Orchy area.

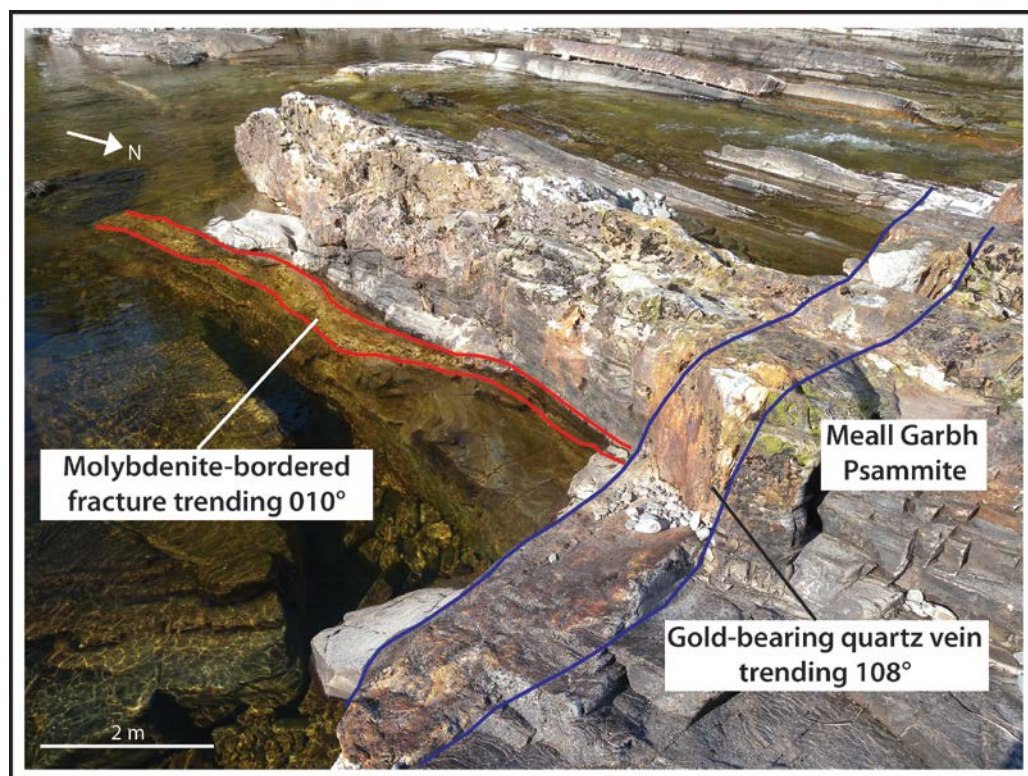


Figure 4.20: Cross-cutting relationship between molybdenite-bearing and gold-bearing quartz veins in the Glen Orchy area.

4.4.4 Alt Ghamnhain

Detailed mapping in the Alt Ghamnhain valley aimed to establish if the Beinn Udlaidh Main Vein could be traced into the valley, and to extend the mapping in Glen Orchy (Fig. 4.7; 4.21). As in Glen Orchy, exposure in Alt Ghamnhain is largely restricted to the river with areas of gravel cover throughout the river, particularly towards the south. Host rock is dominated by the Meall Garbh Psammite Formation which shows significant variation between pelite- and quartzite-dominated end members, with quartz veins abundant in pelite-dominated lithologies. Lamprophyre sills are mapped along the valley base increasing in abundance downstream towards River Orchy; sills are cross-cut by all veining directions. Mapping has identified a number of vein types, quartz-pyrite, poly-metallic and quartz-only veins. The relationship between the earliest white quartz-only veins trending $050\text{--}060^\circ$ and quartz-pyrite veins, trending $010\text{--}032^\circ$, is unconstrained. Quartz-pyrite veins have salmon pink alteration selvages with sporadic pyrite, similar to pyrite-bearing veins in River Orchy. The veins pinch and swell reaching 10 cm in width. Cross-cutting relationships between veins are constrained as:

1. $020\text{--}040^\circ$ -trending quartz-pyrite veins are host to clasts of K-feldspar altered psammite.

2. White quartz veins trending 140° are comparable to $010-020^{\circ}$ -trending veins and have K-feldspar alteration developed at the edge of the vein.
3. Late clean white quartz veins trend $100-160^{\circ}$

Constraining the relationship between veins in Alt Ghamnhain and Glen Orchy is challenging. Quartz-pyrite veins could be interpreted to be equivalent to be quartz-pyrite \pm K-feldspar veins in Glen Orchy. However, this means the quartz-pyrite veins with K-feldspar selvages are difficult to place into the vein paragenesis for Glen Orchy given all the veins cross-cut the lamprophyre sills in Alt Ghamnhain. Late quartz-only veins are interpreted to be equivalent to the late quartz-only veins in Glen Orchy.

At the point the Beinn Udlaidh Main Vein is projected to cross-cut the Alt Ghamnhain River there is an outcrop of massive white quartz which could be interpreted to be a continuation of the Main Vein structure (Plewes 2012). There is no continuity between the top of Beinn Udlaidh and the base of the river in Alt Ghamnhain to confirm this. Mapping by D. Catterall (pers. comm.) has traced the main vein down the cliff face in Coire Ghamnhain but not to the Alt Ghamnhain River and an eroded gully is visible, interpreted to represent the eroded sulphide-rich portion of the Beinn Udlaidh Main Vein (Plewes 2012).

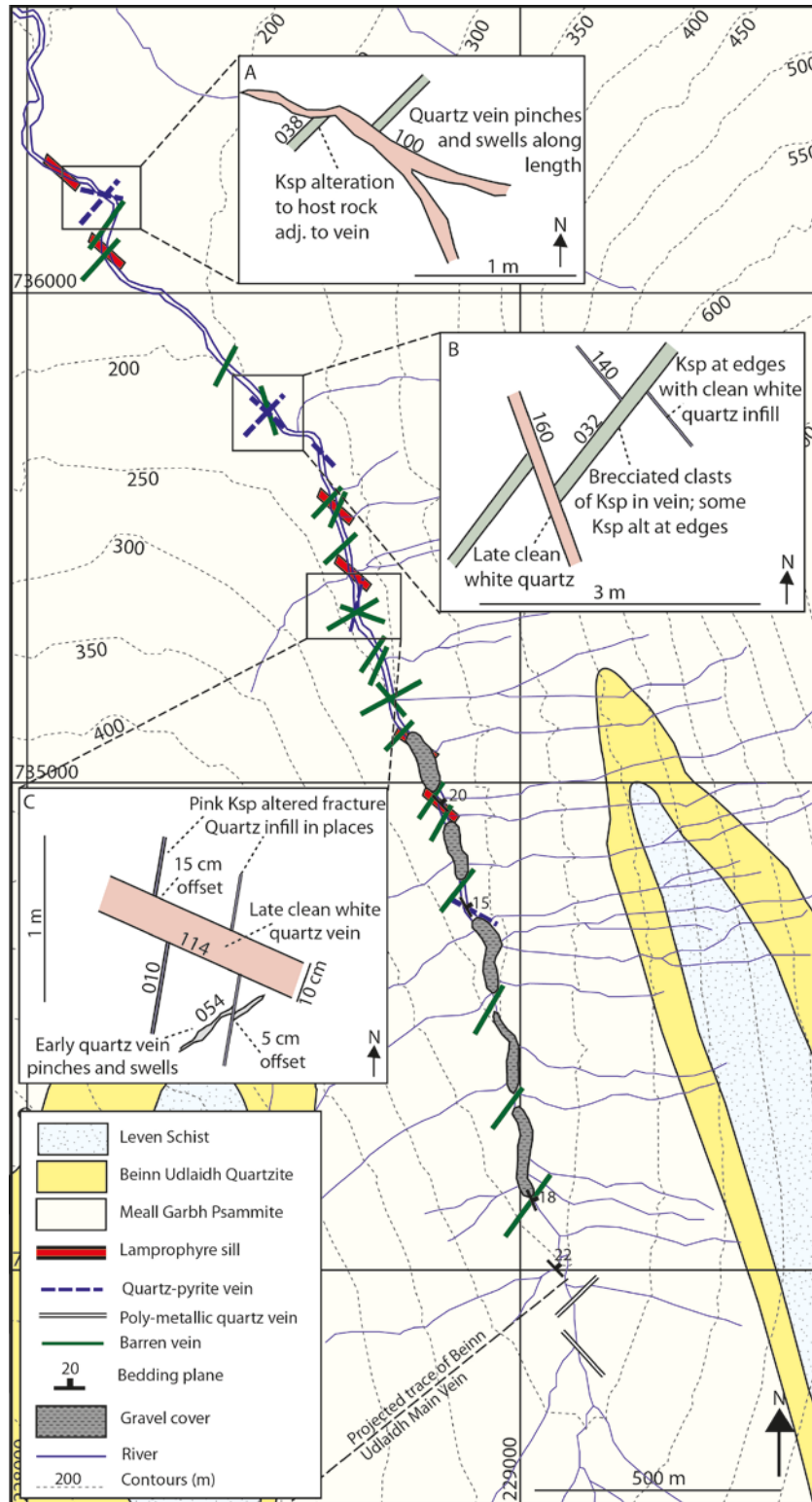


Figure 4.21: Map of Alt Ghamhnain. Insets show cross cutting relationships between veins within the river.

4.4.5 Auch Estate

The Auch Estate is cut by the Tyndrum Fault (Fig. 4.22; 4.23) and a small mapping study on the NW side of the fault aimed to find evidence of gold occurrences in the area. SE of the Tyndrum Fault, mapping aimed to re-examine known mineralised stratiform horizons (Willan & Coleman 1983) and to find new gold-bearing occurrences.

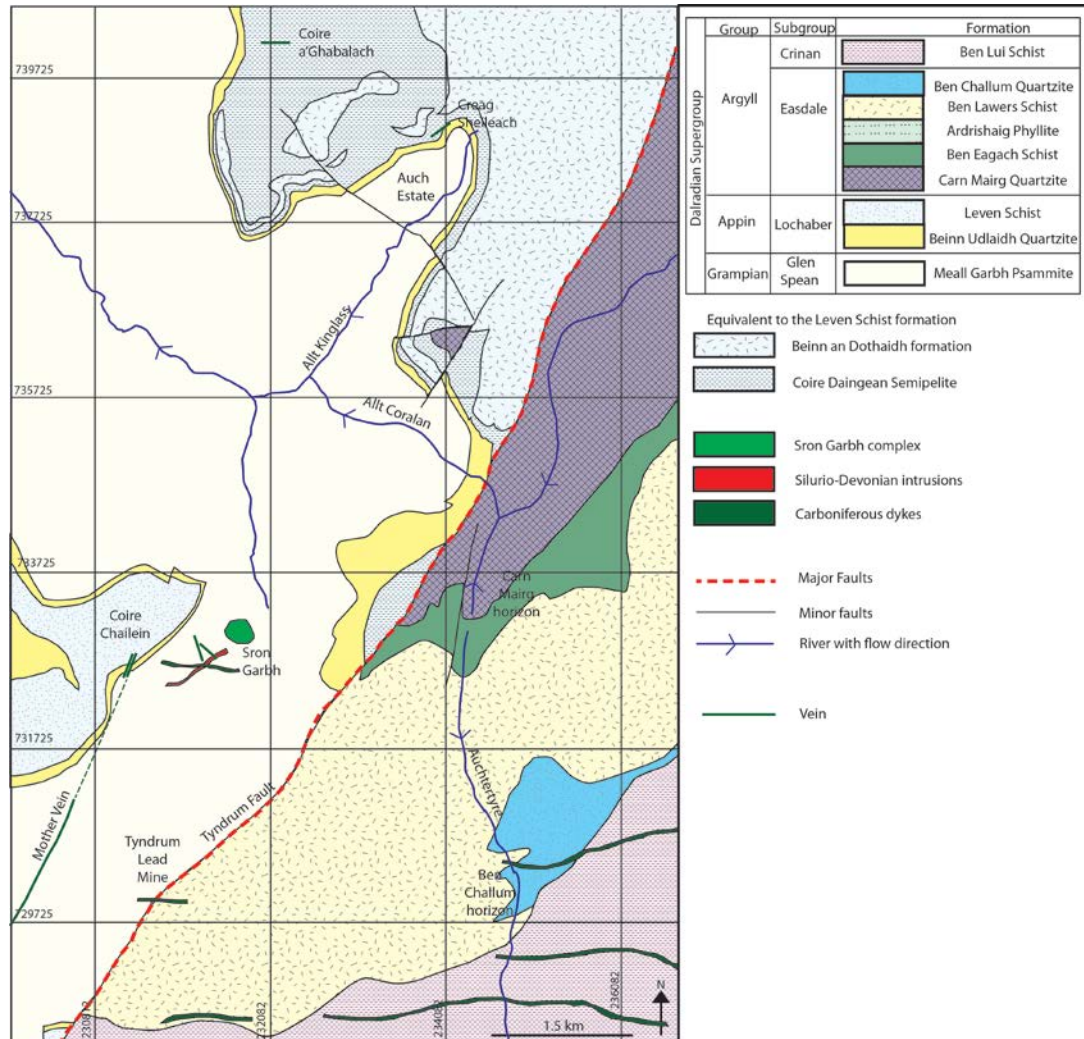


Figure 4.22: Detailed geology of Sron Garbh, Auch Estate and Auchtertyre showing locations of key intrusions and veins. Geology adapted from the British Geological Survey 1:50,000 scale Bedrock Geology Crianlarich sheet with additional detail from this study and Tanner & Thomas (2009).

To the NW of the Tyndrum Fault, two significant poly-metallic quartz veins have been identified as well as a number of quartz-only or pyrite-bearing veins (Fig. 4.24A). At Creag Sheileach, a brecciated vein with a simple sulphide assemblage was identified (Fig. 4.22). The 055°-trending vein is narrow (<25 cm) and has two quartz stages, with only the latter carrying gold-bearing pyrite with chalcopyrite and galena (Fig. 4.24B). The vein is comparable to the Cononish deposit. At Coire a'Ghabalach, a narrow (<30 cm), 090°-

trending, complex vein with multiple brecciation stages is mapped (Fig. 4.24C). The central zone of the vein shows extensive brecciation compared to the edges of vein suggesting repeated quartz input into the host structure with alteration of host rock clasts to K-feldspar and chlorite-sericite assemblages. The sulphide assemblage is dominated by pyrite and galena with folding of early quartz veining visible in clasts.

4.4.6 Auchtertyre

At Auchtertyre, the Ben Challum pyrite-bearing stratiform horizon was located (Willan & Coleman 1983), along with a newly identified horizon in the Carn Mairg Quartzite Formation at Alt Cumbang (Fig. 4.22). The Ben Challum horizon, as noted by Willan & Coleman (1983), is dominated by pyrite and can be identified by extensive rust coloured alteration on the surface of the quartzite (Fig. 4.24D). The horizon is cut by a 040°-trending quartz-only vein (Fig. 4.24E); no mineralised veins were identified at Auchtertyre. The Carn Mairg horizon is 1.5 m thick and hosted in well-silicified units, at the boundary between the ‘pebbly’ quartzite and quartzite proper with pyrite dominated by small (<3 mm) cubes. A number of tholeiite dykes were mapped (Fig. 4.24F) and have been defined as Permo-Carboniferous in age by the British Geological Survey (Crianlarich Bedrock Geology sheet information).

4.4.7 Sron Garbh

Sron Garbh is unique within the Tyndrum area with a large area of intrusive rocks exposed at surface (Fig. 4.22). The area is geologically complex with multiple igneous phases and a series of quartz veins (Graham 2013). Exposure is variable with significant exposure of igneous rocks but more limited exposure of veins.

4.4.7.1 Igneous intrusions

The igneous phases at Sron Garbh are complex and are currently not fully understood. The main igneous intrusion at Sron Garbh is a multi-phase intrusive body (Fig. 4.25A) with central diorite and marginal appinite (Fig. 4.25D); the timing relationships between the diorite and appinite are unconstrained with work on going in this area (Graham 2013). The top of the hill is cut by two dykes; the early altered lamprophyre dyke is cut by the late E-W-trending Permo-Carboniferous tholeiite dyke. A mineralised lamprophyre (at least 1 m thick), adjacent to the poly-metallic quartz veins, is mapped in a cliff face in Coire Chailein with small (<3 mm wide) cubic pyrite in the grey lamprophyre.

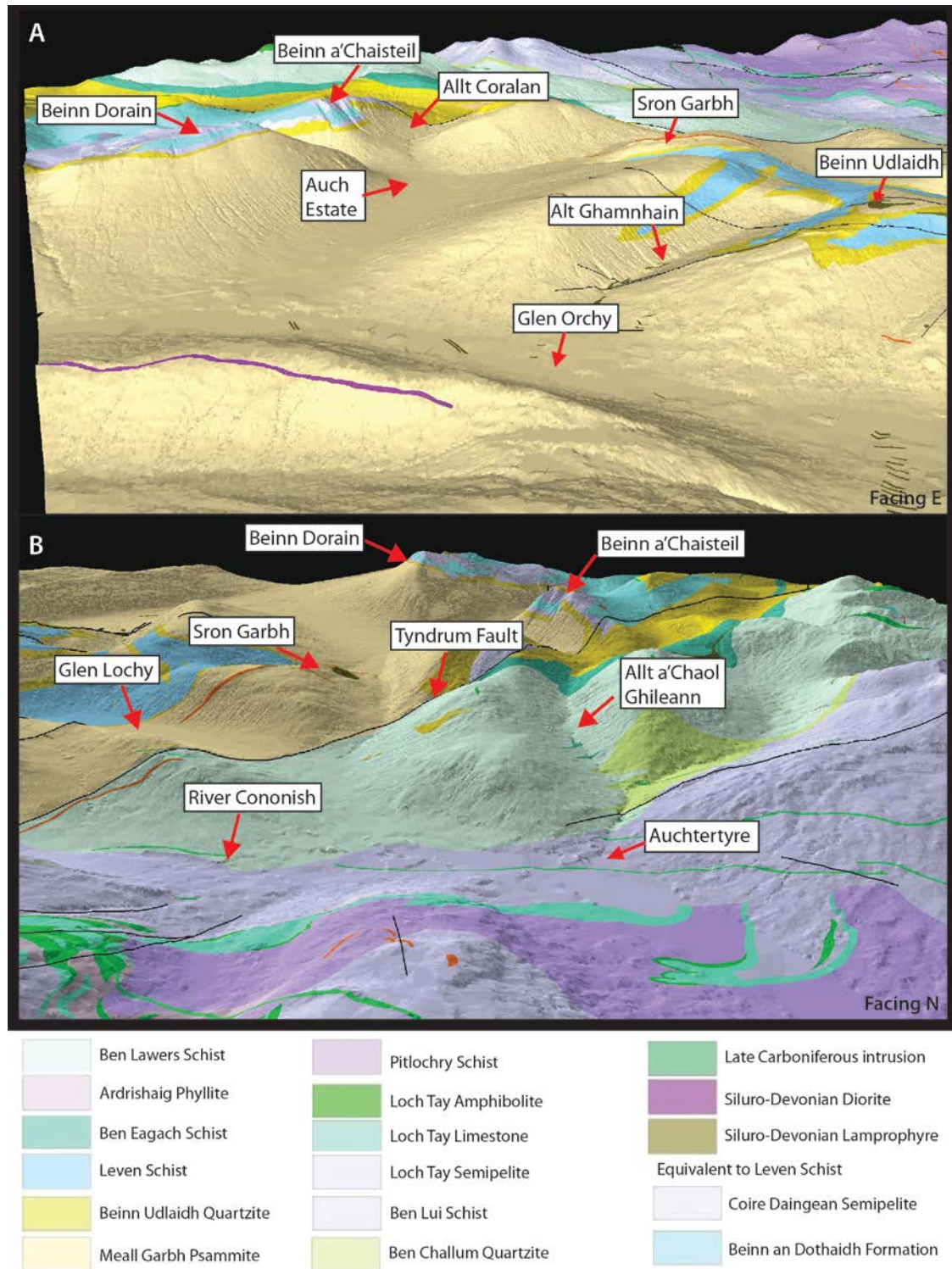


Figure 4.23: 3D representation of the geology draped over the topography in the Auch, Auchtertyre and Sron Garbh areas. A viewed from Meall an Laoigh, B viewed from Fierach. Topographic surface was created in ArcScene by the author and the geology was draped over the surface. Geology (Crainlarich sheet) and topographic contours (British National Grid squares NN 22, 23, 32, 33) from EDINA.

4.4.7.2 Quartz veins

Exposure of quartz veins is limited to rivers, with the exception of a large quartz-only vein trending-168°, exposed along a topographic high (Fig. 4.25F). Quartz veins can be traced for up to 20 m between river sections and through sub-cropping exposure. The veins exhibit some evidence of shearing (Fig. 4.25D) and are truncated by faulting in places (Fig. 4.25E). Poly-metallic veins, trending 020-040°, have extensive pyrite and galena, with K-feldspar alteration of the adjacent host rock (Fig. 4.25C).

A quartz-only vein at the top of Coire Chailein is inferred to be a continuation of the Mother Vein in Glen Cononish, based on the trend of the vein. Poly-metallic quartz veins have also been identified in Coire Chailein and can be mapped along the length of the valley until exposure is lost in the cliff face. Veins in Coire Chailein exhibit cataclasis and shearing with no evidence of open-space filling quartz.

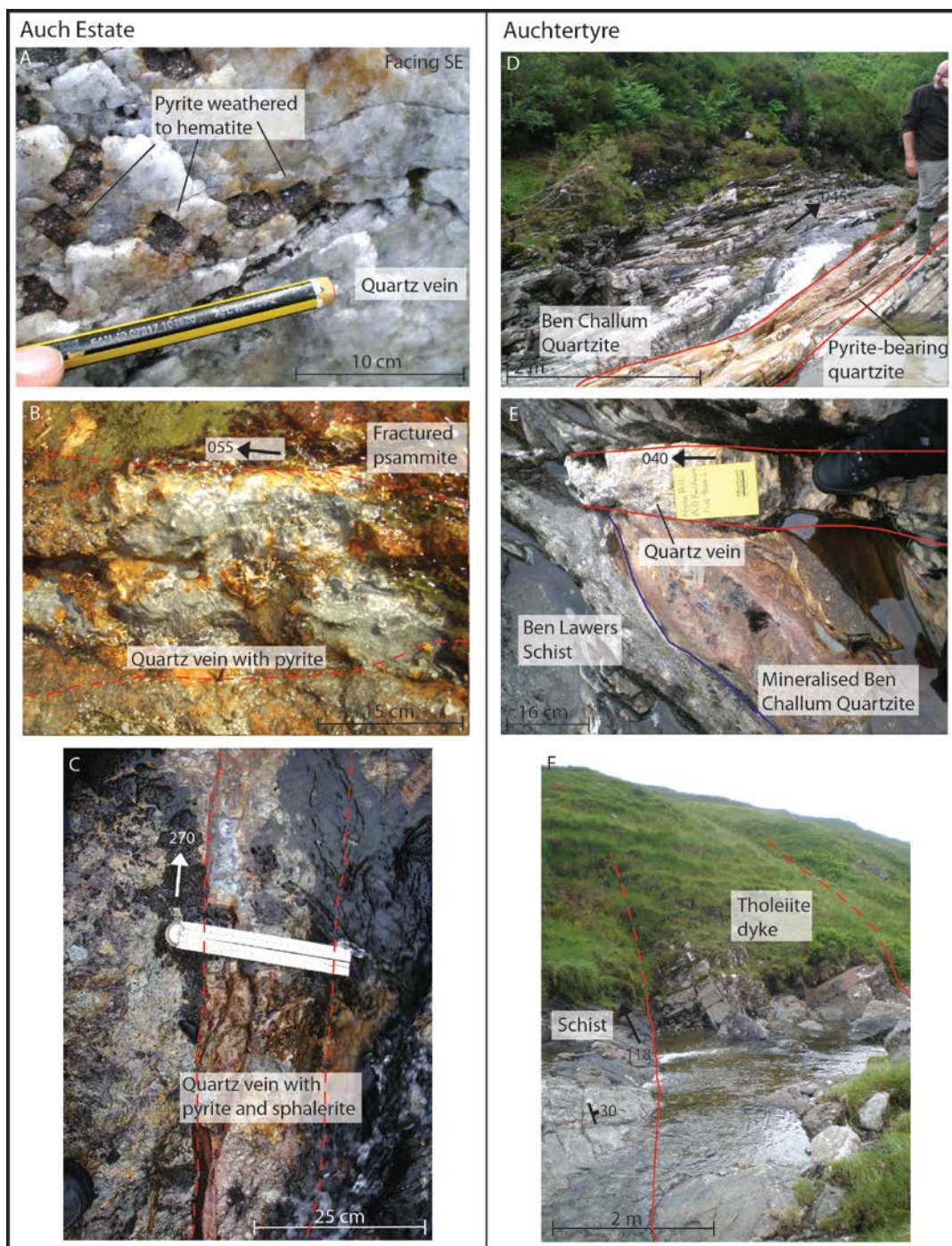


Figure 4.24: Photo plate of Auch Estate and Auchtertyre area. A. Pyrite cubes weathered to hematite in Allt Kinglass. B. Sheared vein at Creag Sheileach. C. Mineralised vein at Coire a’Ghabalach. D. Mineralised horizon in Ben Challum Quartzite. E. Mineralised horizon in Ben Challum Quartzite cut by quartz vein. F. Tholeiite dyke.



Figure 4.25: Photo plate of Sron Garbh area. A. Sron Garbh intrusion. B. Pyrite-chalcopyrite mineralised apinitite. C. Pyrite and galena in poly-metallic quartz vein. D. Quartz vein with sheared edge to vein. E. Quartz vein offset by truncated fault. F. Extent of main quartz vein at Sron Garbh.

4.5 Petrography

The various hydrothermal occurrences in the Tyndrum area have been classified based on field relations (Table 4.1). This section characterises the petrography of these different vein types. Veins with no sulphide are classified as quartz-only and petrographic characterisation has not been completed on these samples. Poly-metallic quartz veins are further categorised based on additional characteristics from petrography, in addition to variation in vein trend (Table 4.1). Basic characterisation was also undertaken on representative samples from both igneous intrusions and metasedimentary rocks in the study area.

4.5.1 Host metasedimentary rocks

4.5.1.1 Meall Garbh Psammite Formation

The Meall Garbh Psammite is a dominantly quartz-muscovite (\pm biotite) unit with varying proportions of muscovite and quartz throughout the sequence. Minor plagioclase, apatite and monazite occur in less altered samples. Large well developed detrital zircons occur and survive K-feldspar alteration.

Two different alteration assemblages are noted; K-feldspar dominated and chlorite-sericite dominated. Clasts of host rock are clearly identified in veins by orientated biotite and muscovite (Fig. 4.26B). The development of K-feldspar, as microcline, causes the loss of original structure and mineralogy, decreasing with distance away from the cross-cutting fracture. K-feldspar replaces some original quartz and plagioclase within the host rock.

The sericite-chlorite alteration assemblage is later than K-feldspar alteration and is caused by the poly-metallic gold vein precipitating fluids. The alteration is fine grained, with some calcite (Fig. 4.26C) and pyrite in the altered psammites (Fig. 4.26E). Rutile also occurs in the alteration halo of the molybdenite-bordered fractures and some poly-metallic veins, extending no more than 2 m away from the vein (Fig. 4.26G & H).

4.5.1.2 Other metasedimentary units

The Beinn Udlaigh, Carn Mairg and Ben Challum Quartzite Formations are dominated by quartz with minor muscovite (Fig. 4.27C, D & G; 4.28C) and detrital zircons (Fig. 4.27H). The Ben Challum Quartzite Formation has extensive pyrite at the base of the unit, as well-developed cubes (Fig. 4.28D).

The Leven, Ben Lawers, Ben Lui Schists and Ardrishaig Phyllite Formations are fine grained schists, dominated by quartz with significant muscovite and biotite (Fig. 4.27E &

F). The Ben Lawers and Ben Lui Schist Formations have a higher biotite-muscovite content than the Leven Schist Formation and are garnet-bearing (Fig. 4.28A, B, E & F). The Ben Eagach Schist Formation, whilst having a generally comparable paragenesis to the other schists, exhibits pyrite mineralisation, visible in bands, in the unit (Fig. 4.27A & B) and graphite.

The Ardrishaig Phyllite and Ben Lui Schist Formations are hydrothermally altered with the Ardrishaig Phyllite Formation characterised by intense calcite and alteration of metamorphic muscovite (Fig. 4.28G & H). The Ben Lui Schist Formation garnets are hydrothermally altered to a carbonate and chlorite with minor rutile (Fig. 4.28A & B).

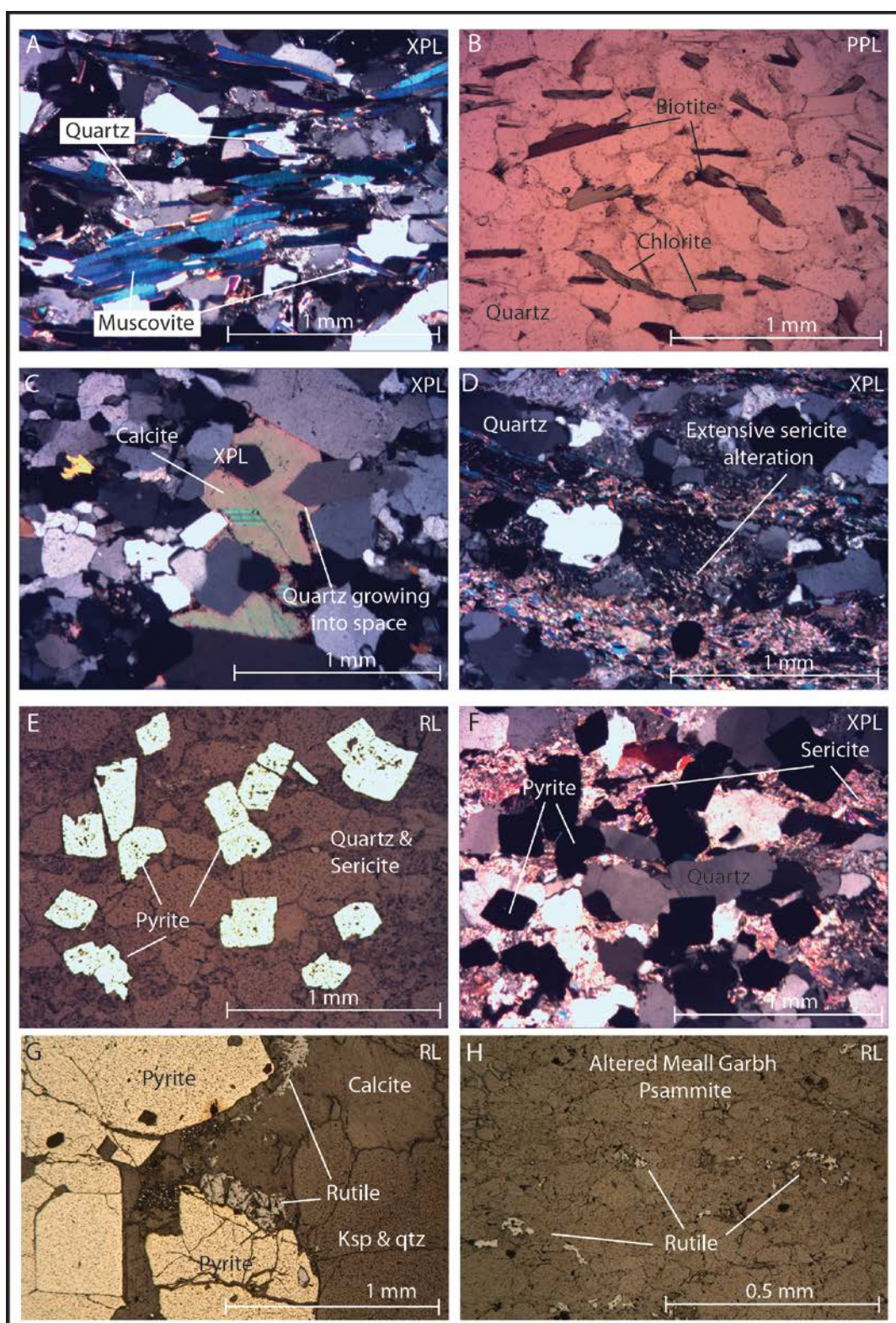


Figure 4.26: Photo plate of Meall Garbh Psammite Formation. A. Main texture of unaltered psammite (GO1202). B. Biotite and chlorite alteration of psammite (GO1202). C. Late carbonate alteration of psammite (GO1216). D. Extensive sericite alteration to psammite (GO1218). E & F. Secondary pyrite in alteration halo of cross-cutting mineralised quartz vein (GO1218). F. Rutile around pyrite in K-feldspar altered zone at edge of vein (RV16). G. Rutile around pyrite in K-feldspar altered Meall Garbh Psammite (RV10). H. Rutile in K-feldspar altered Meall Garbh Psammite (RV10). A-B are unaltered, C-H are hydrothermally altered.

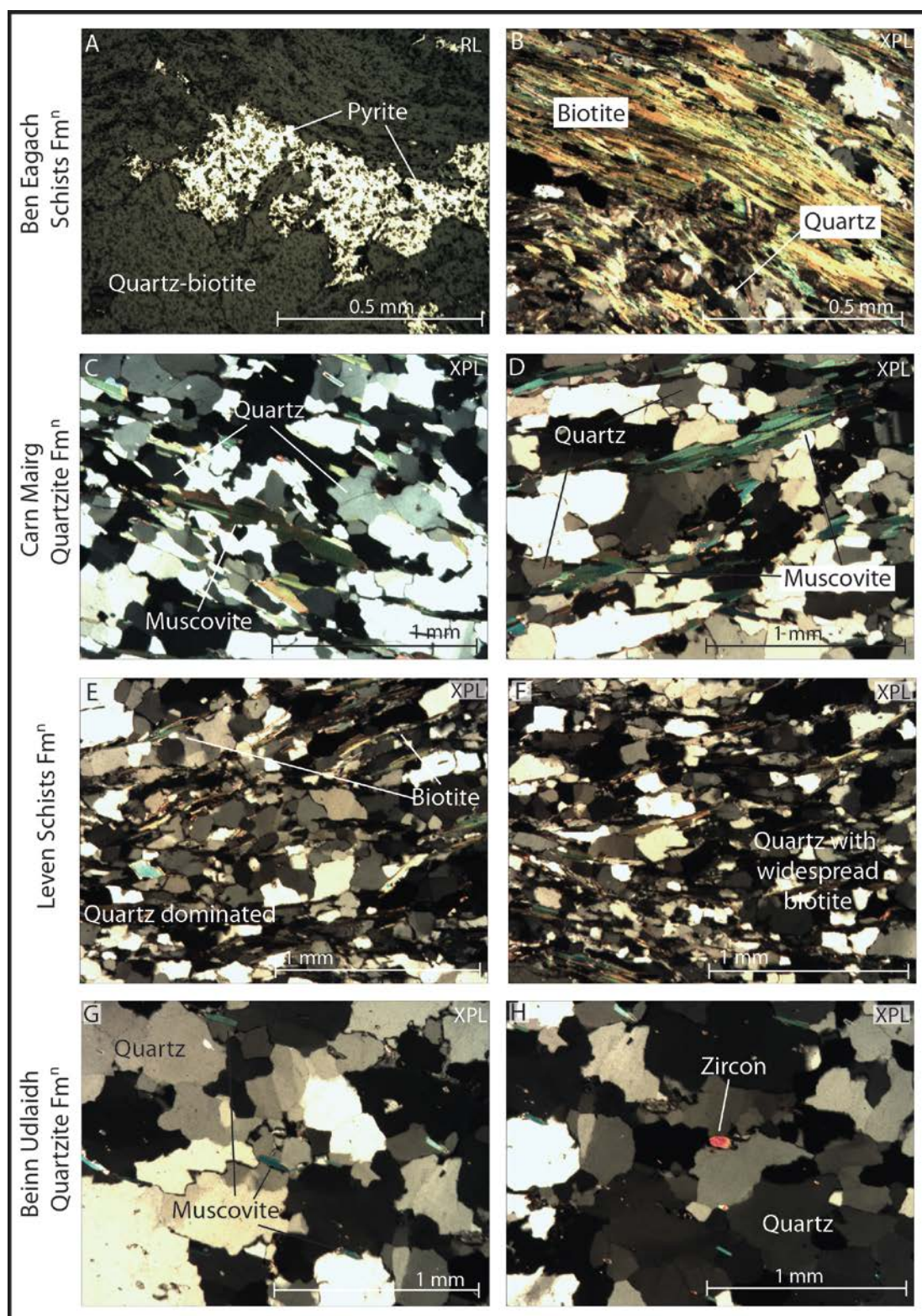


Figure 4.27: Photo plate of Dalradian metasediments in the Tyndrum area. A. Pyrite in the Ben Eagach Schist (ConBG06). B. Extensive biotite in the Ben Eagach Schist (ConBG06). C & D. Quartz dominated texture to Carn Maing Quartzite with minor muscovite (ConBG02). E & F. Fine grained quartz with minor biotite in the Leven Schists (ConBG03). G. Coarse grained quartz with small muscovite in Beinn Udlaidh Quartzite (GO1220). H. Detrital zircon present in Beinn Udlaidh Quartzite (GO1220). A-H metamorphic texture.

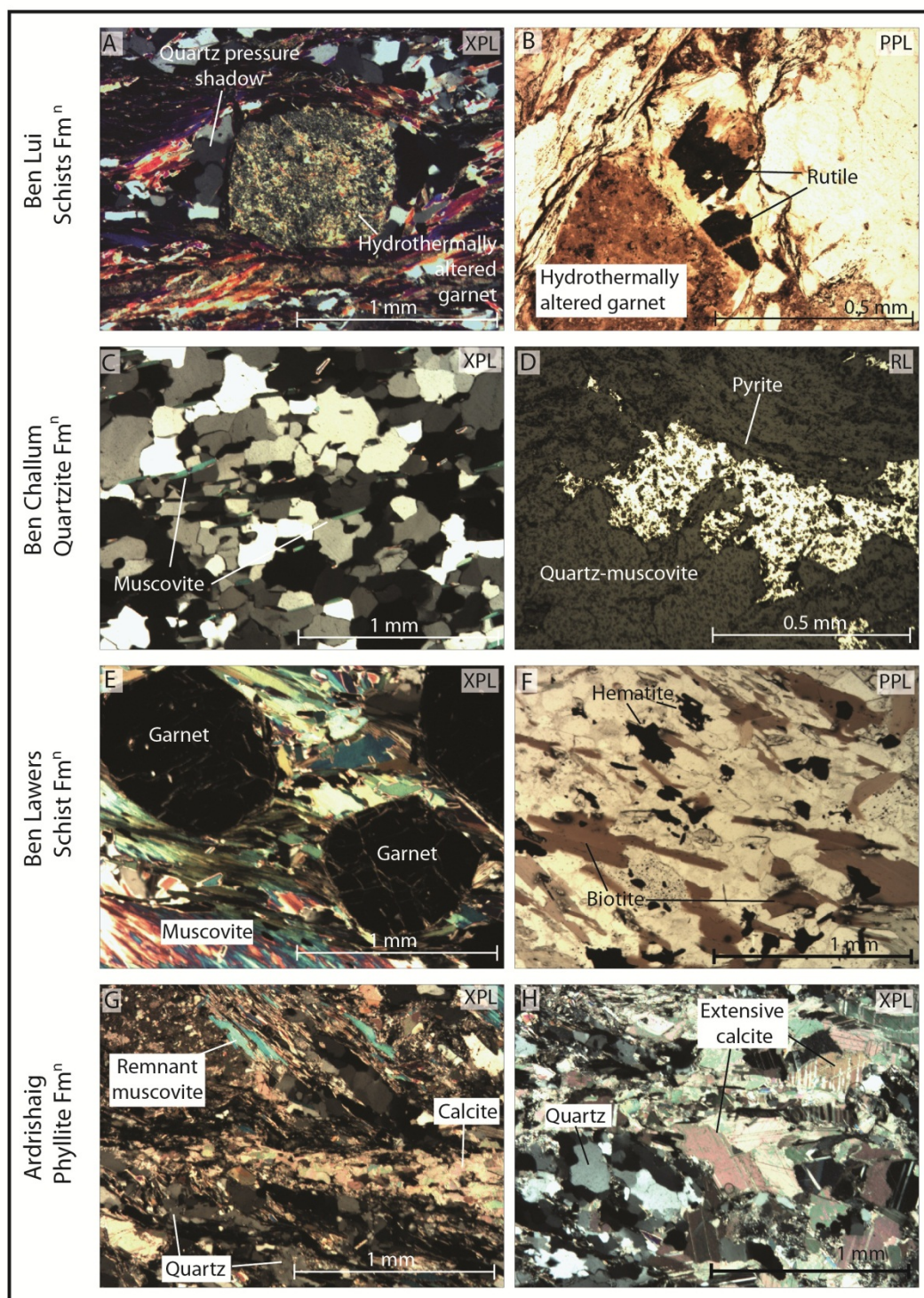


Figure 4.28: Photo plate of Dalradian metasediments in the Tyndrum area. A. Hydrothermally-altered (sericite-calcite-chlorite) garnet in Ben Lui Schists (ATT04). B. Rutile at edge of hydrothermally altered garnet in Ben Lui Schists (ATT04). C. Texture of Ben Challum Quartzite (ATT06). D. Pyrite within the Ben Challum Quartzite (ATT06). E. Garnet within Ben Lawers Schist (ConBG10). F. Biotite and hematite in Ben Lawers Schist (ConBG10). G & H. Texture of Ardrishaig Phyllite with extensive carbonate (ConBG11). A, B, E-H hydrothermally altered, C-D metamorphic texture.

4.5.2 Igneous intrusions

Two suites of igneous rocks have been identified in this study and have been classified in conjunction with information from the British Geological Survey 1:50,000 scale Bedrock Geology Crianlarich and Dalmally sheets (further details in Chapter 3).

4.5.2.1 Siluro-Devonian intrusions

Large lamprophyre sills mapped throughout the study area (Fig. 4.1) have been altered with little of the original mineralogy preserved (Fig. 4.29A). The lamprophyres are extensively altered to a sericite-chlorite assemblage (Fig. 4.29B) and phenocrysts have been altered to fine grained carbonate (Fig. 4.29C). Pyrite occurs in vein alteration haloes and is closely related to the development of chlorite (Fig. 4.29D).

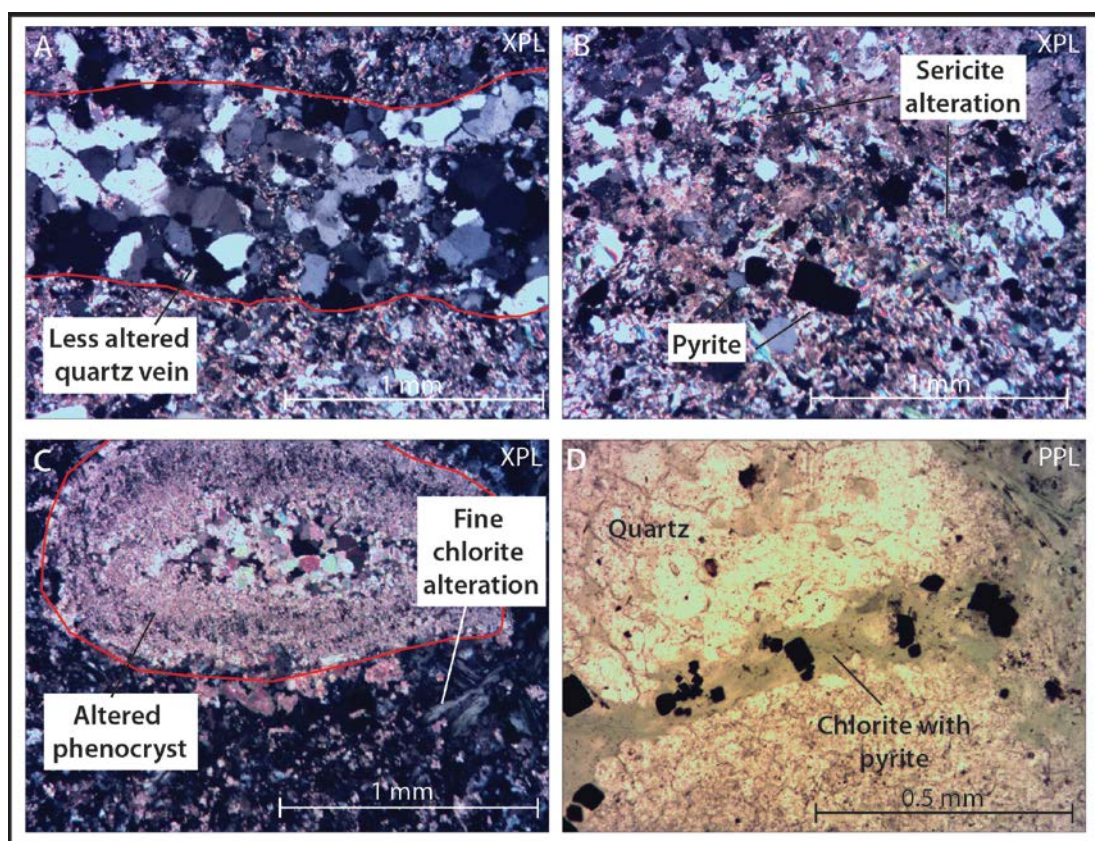


Figure 4.29: Photo plate of Siluro-Devonian dyke-sill swarm. A. Highly altered lamprophyre cross-cut by late quartz vein (GO1213). B. Texture of altered lamprophyre with some pyrite (GO1213). C. Carbonate altered phenocryst in fine grain chlorite altered lamprophyre (BUNQ02). D. Chlorite alteration with minor pyrite cross cutting main lamprophyre texture (LA55). A-D are hydrothermally altered

4.5.2.2 Permo-Carboniferous intrusions

E-W-trending dykes are found across the study area and cross-cut the Tyndrum Fault (Treagus *et al.* 1999). The dykes are defined as Permo-Carboniferous in age (*c.* 290-270 Ma; Francis 1991; BGS Crianlarich Bedrock Geology sheet; Chapter 3). The intrusions are fresher than the Siluro-Devonian intrusions and the original mineralogy remains (Fig. 4.30A, B, E & F). The intrusions are dominated by pyroxene and plagioclase with a phaneritic texture. There is no pyrite in the Permo-Carboniferous intrusions (Fig. 4.30D) but some minor sericite alteration (Fig. 4.30C). The dyke, crossing the Eas Anie vein, has chilled margins and comparable mineralogy to the other Permo-Carboniferous dykes in the area but exhibits minor calcite in cross-cutting veins, which is absent in other dykes.

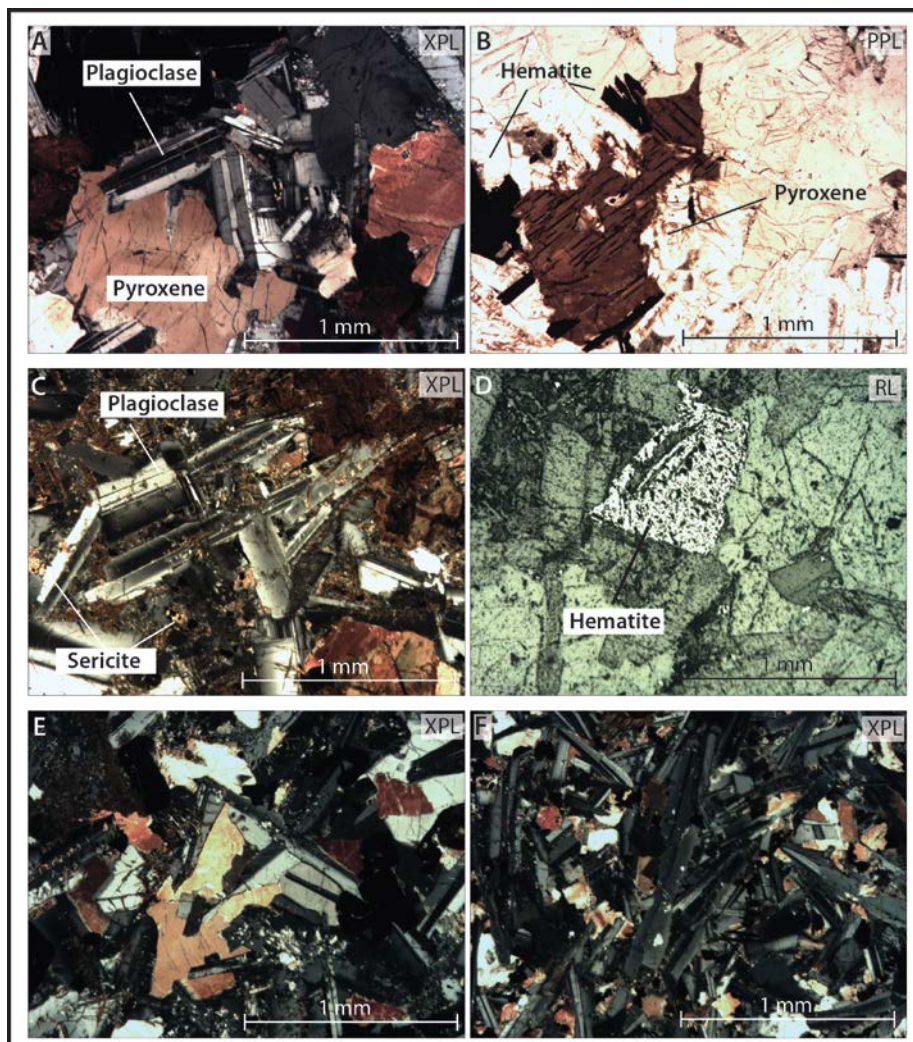


Figure 4.30: Photo plate of Carboniferous dyke swarm. A & B. Fresh groundmass of dyke from Auchtertyre (ATT05). C. Sericite alteration to parts of groundmass visible (ATT05). D. Late hematite in groundmass (ATT05). E. Groundmass of dyke from Glen Orchy comparable to Auchtertyre sample (GO1221). F. Finer grained dyke from Glen Cononish comparable to Auchtertyre sample (ConBG09).

4.5.3 Molybdenite-bordered fractures

Molybdenite-bordered fractures are characterised by the development of K-feldspar selvages (Fig. 4.31; 4.32A & B) in the host Meall Garbh Psammite Formation. Molybdenite overgrows K-feldspar and is in the altered host rock (Fig. 4.32C & D). The sulphide assemblage is dominated by molybdenite and pyrite (Fig. 4.32).

Quartz-pyrite \pm K-feldspar veins are comparable to the molybdenite-bordered fractures but with late quartz-pyrite fill with clasts of K-feldspar altered host rock in the quartz vein (Fig. 4.31; 4.32). Pyrite occurs within the vein and may be disseminated into the alteration halo.

Molybdenite occurs as small rosettes with well-developed twins (Fig. 4.32C). Pyrite has a range of inclusions including host rock fragments, quartz and plagioclase; no electrum or galena inclusions occur in pyrite in either the quartz vein or selvage. Rutile occurs in and around pyrite in the alteration halo and is disseminated into altered psammite (Fig. 4.32D). Calcite is found in the alteration halo but not in later quartz in fill. Both molybdenite-bordered fractures and quartz-pyrite \pm K-feldspar veins exhibit late hematite alteration.

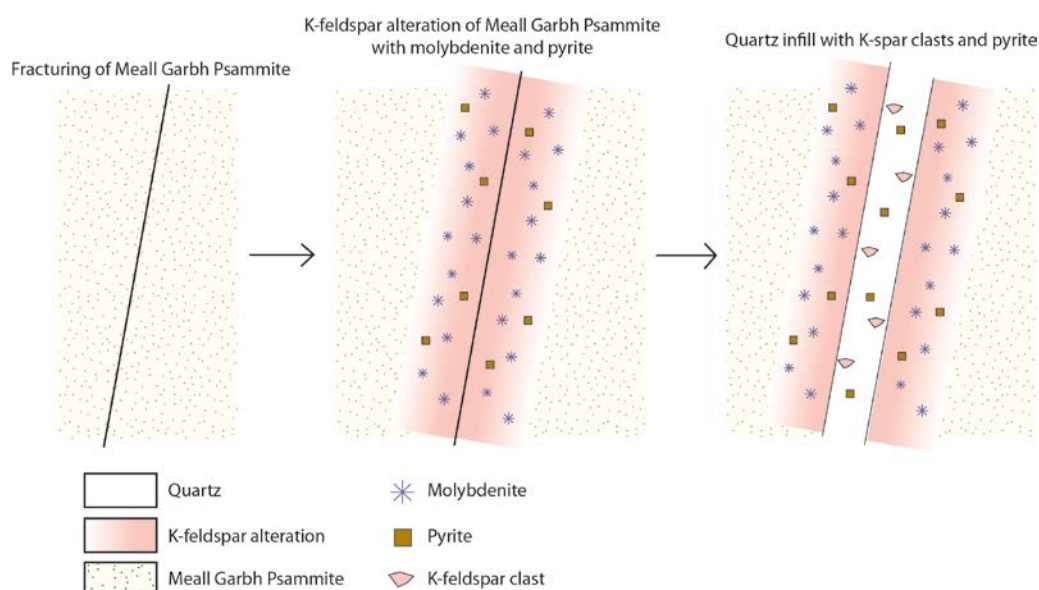


Figure 4.31: Schematic representation of molybdenite-bordered fracture development with subsequent quartz-pyrite \pm K-feldspar vein emplacement.

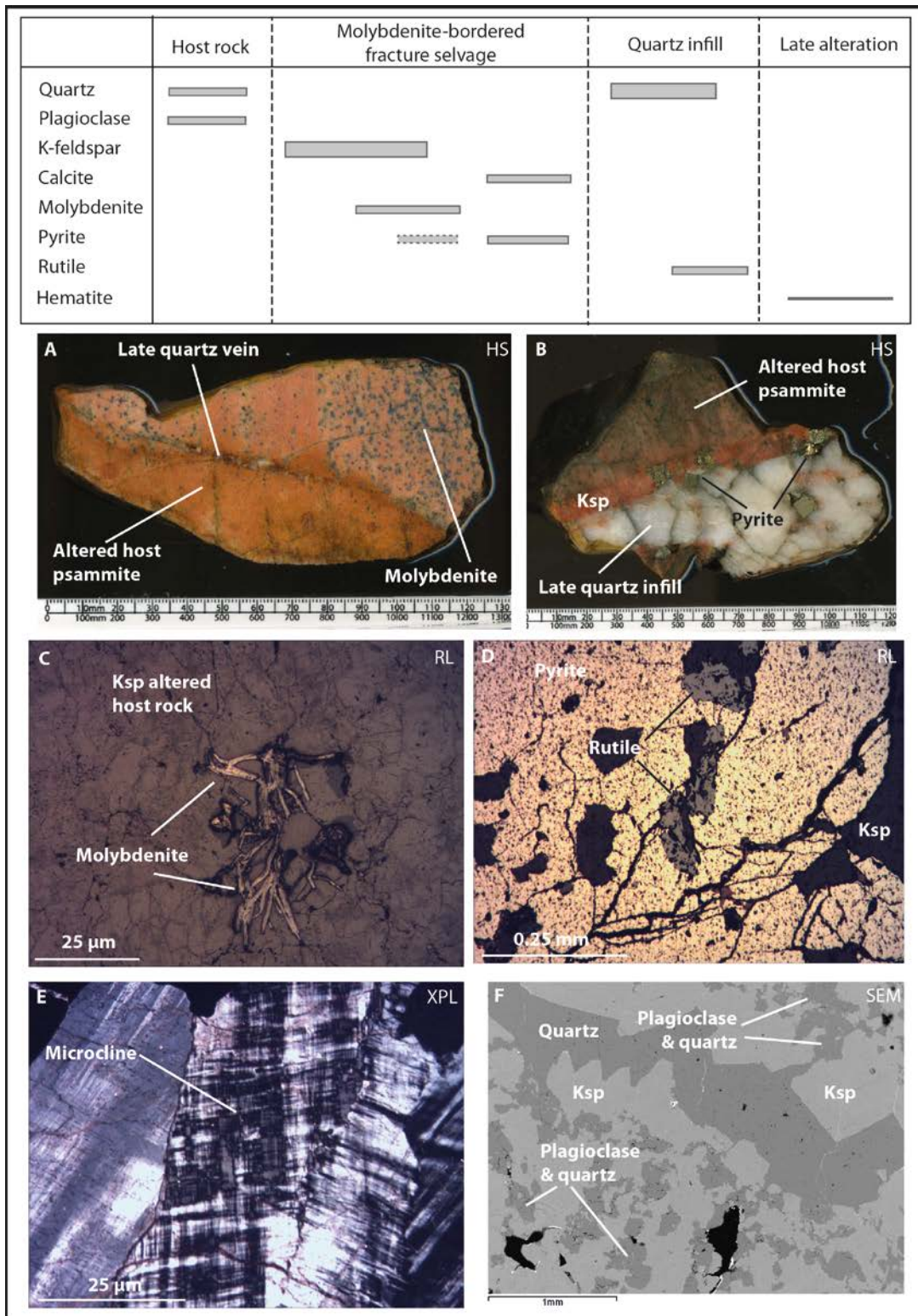


Figure 4.32: Paragenesis and photo plate of molybdenite-bordered fractures. A. Molybdenite in altered psammite at hand specimen scale (RV109). B. K-feldspar selvage, host to molybdenite, with pyrite at hand specimen scale (RV16). C. Molybdenite in K-feldspar altered host rock (RV109). D. Pyrite with minor rutile alteration in K-feldspar selvage at contact between vein and host rock (RV16). E. Extensive development of microcline in K-feldspar selvage (RV16). F. Cross-cutting quartz in K-feldspar alteration halo (RV109). Paragenesis developed from sample set n = 10. All photomicrographs from molybdenite-bordered fractures

4.5.4 Pyrite-bearing veins

The pyrite-bearing veins are characterised by a simpler paragenesis than other sulphide-bearing veins (Fig. 4.33). The veins have a single generation of clean white quartz with brecciated clasts of host rock in the vein. Host rock clasts in the vein (Fig. 4.33A) and wall rock adjacent to the pyrite-bearing vein are altered to K-feldspar. Where sulphide occurs, angular and highly fractured pyrite (Fig. 4.33B) dominates, overgrowing host rock clasts (Fig. 4.33C & D), with minor galena and chalcopyrite. Anhydrite inclusions are seen as inclusions within pyrite and are interpreted to have been preserved due to enclosure in the pyrite crystals.

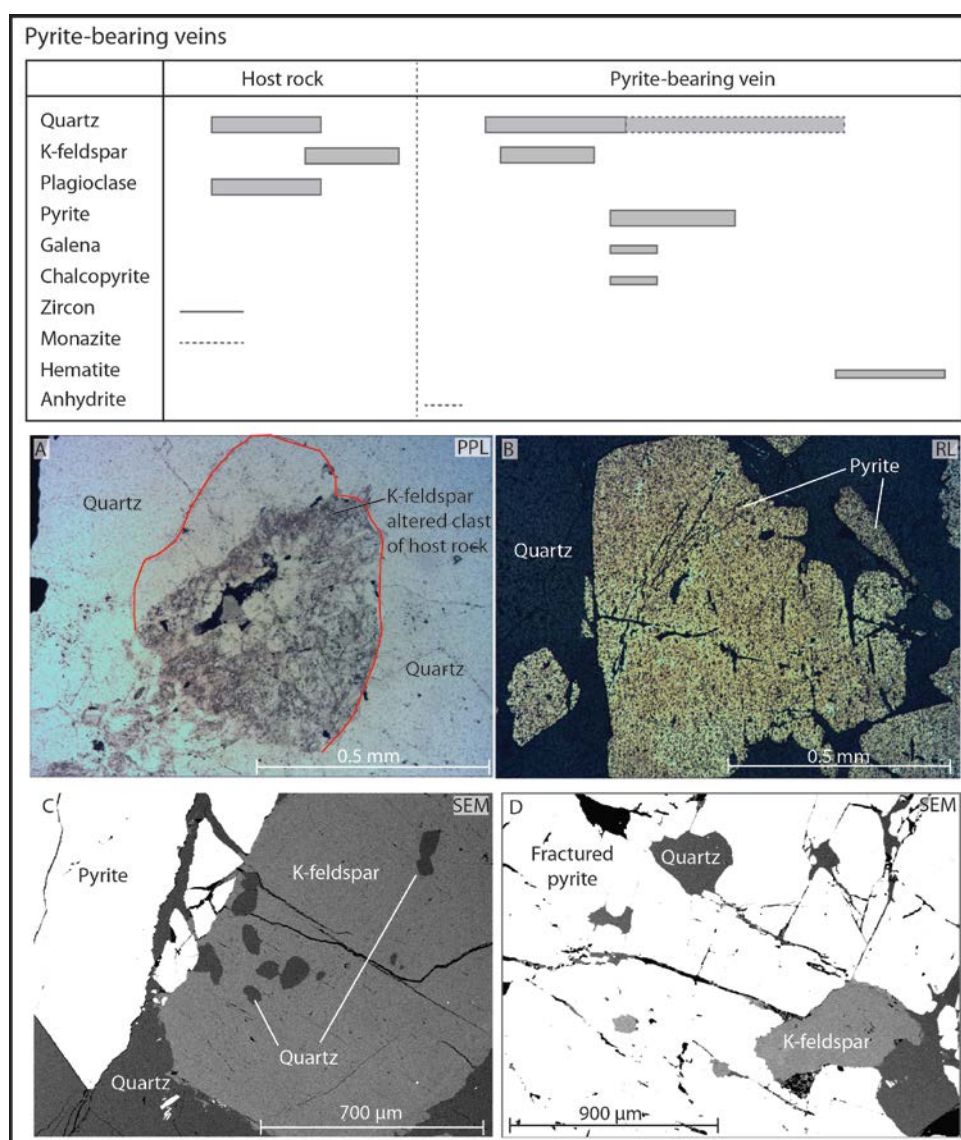


Figure 4.33: Paragenesis and photo plate of pyrite-bearing veins. A. Clast of K-feldspar altered psammite in quartz vein. B. Massive pyrite in main quartz vein. C. Pyrite growth over quartz and K-feldspar altered psammite clast. D. Highly fractured nature of pyrite showing growth over quartz and K-feldspar altered rock. All from sample RV14. Paragenesis developed from sample set $n = 4$

4.5.5 Poly-metallic quartz veins

Poly-metallic quartz veins are known to be gold-bearing (Chapter 5) and share a similar overall paragenesis which varies with location and orientation of the vein. Gold-bearing poly-metallic quartz veins are sub-divided by orientation and mineralogy with three subsets identified; the Cononish, River Vein and Kilbridge sets (Fig. 4.34; Table 4.1).

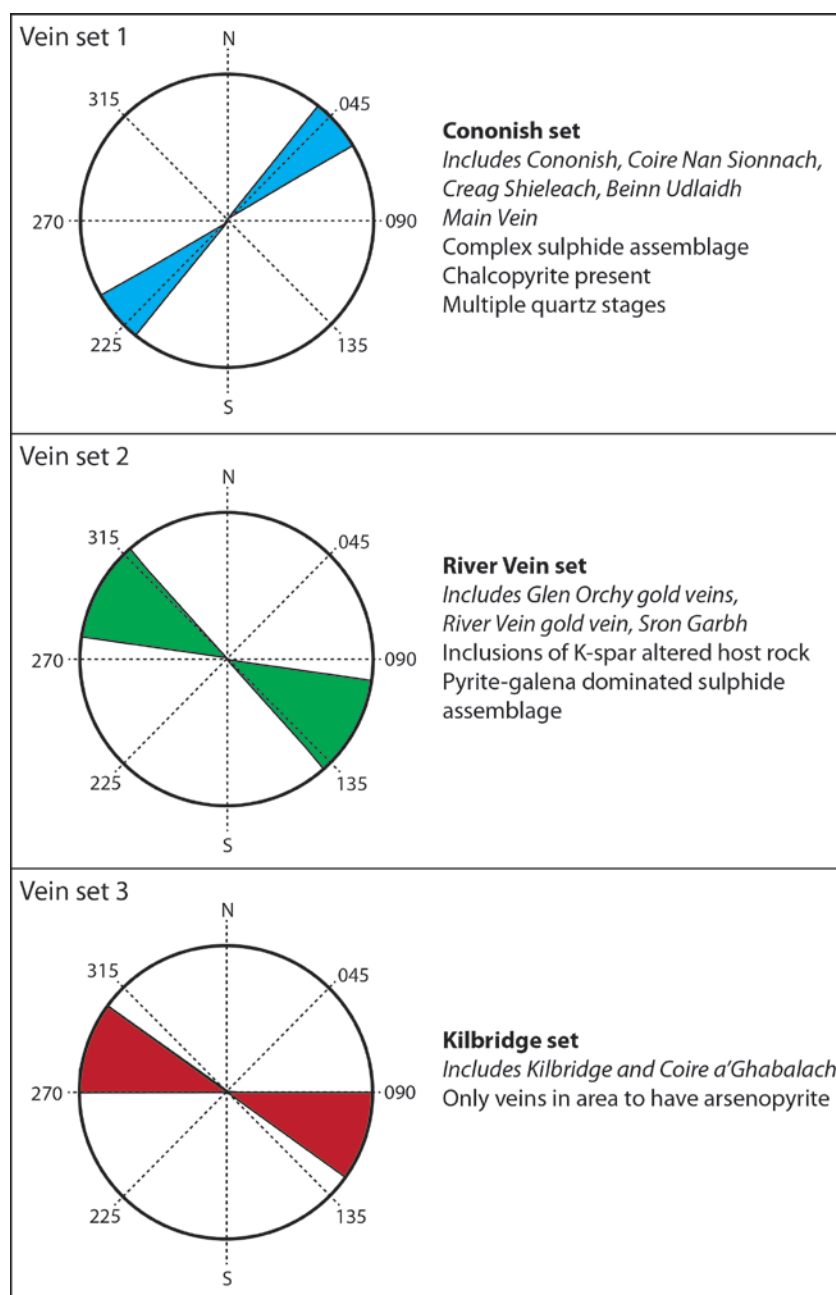


Figure 4.34: Sub-sets of poly-metallic veins defined in this study based on orientation and mineralogy.

4.5.5.1 Cononish set

The Cononish set is defined by a trend between 040° and 060° and the presence of a complex sulphide assemblage in the vein (Fig. 4.34). Cononish set veins have chalcopyrite within the assemblage, which is less well developed in other veins across the study area.

The general paragenesis is dominated by early barren white quartz which is brecciated by a sericite-chlorite altered assemblage with small (<1 mm) cubic pyrite but no gold (Fig. 4.35). The chlorite-sericite altered assemblage is then brecciated by white quartz with large gold-bearing pyrite crystals (up to 5 mm). Monazite occurs along the cleavage of altered biotite and muscovite, with rutile also developed in biotite, due to fluid alteration. Late veins, cross-cutting the main body of the Cononish vein, have formed in open space and have well developed euhedral crystal shapes (Fig. 4.35D); in places late chlorite, carbonate and hematite is filling remaining open space.

Large pyrite crystals contain inclusions of early galena and electrum with sporadic tetrahedrite. Sphalerite, with minor cadmium, occurs with late void-filling galena and chalcopyrite (Fig. 4.35A & B). In highly brecciated sections, pyrite crystals have pressure shadows of quartz and carbonate suggesting the vein has been sheared; fractured pyrite occurs throughout the vein (Fig. 4.35C). Late alteration of pyrite has occurred with the edges of crystals altered to hematite.

Hessite (Ag_2Te) occurs with Au-rich electrum and galena as stringers and at the edges of fractured early pyrite (Spence-Jones 2013). The hessite is a diagnostic feature of early electrum mineralisation and decreases in abundance through the paragenesis (Spence-Jones 2013). Chalcopyrite is sporadic in the assemblage; where seen it occurs syn- to post-pyrite with Ag-rich electrum late in the paragenesis (Fig. 4.35A & B; Spence-Jones 2013). The chalcopyrite is a minor but distinguishing component due to the relationship with Ag-rich electrum.

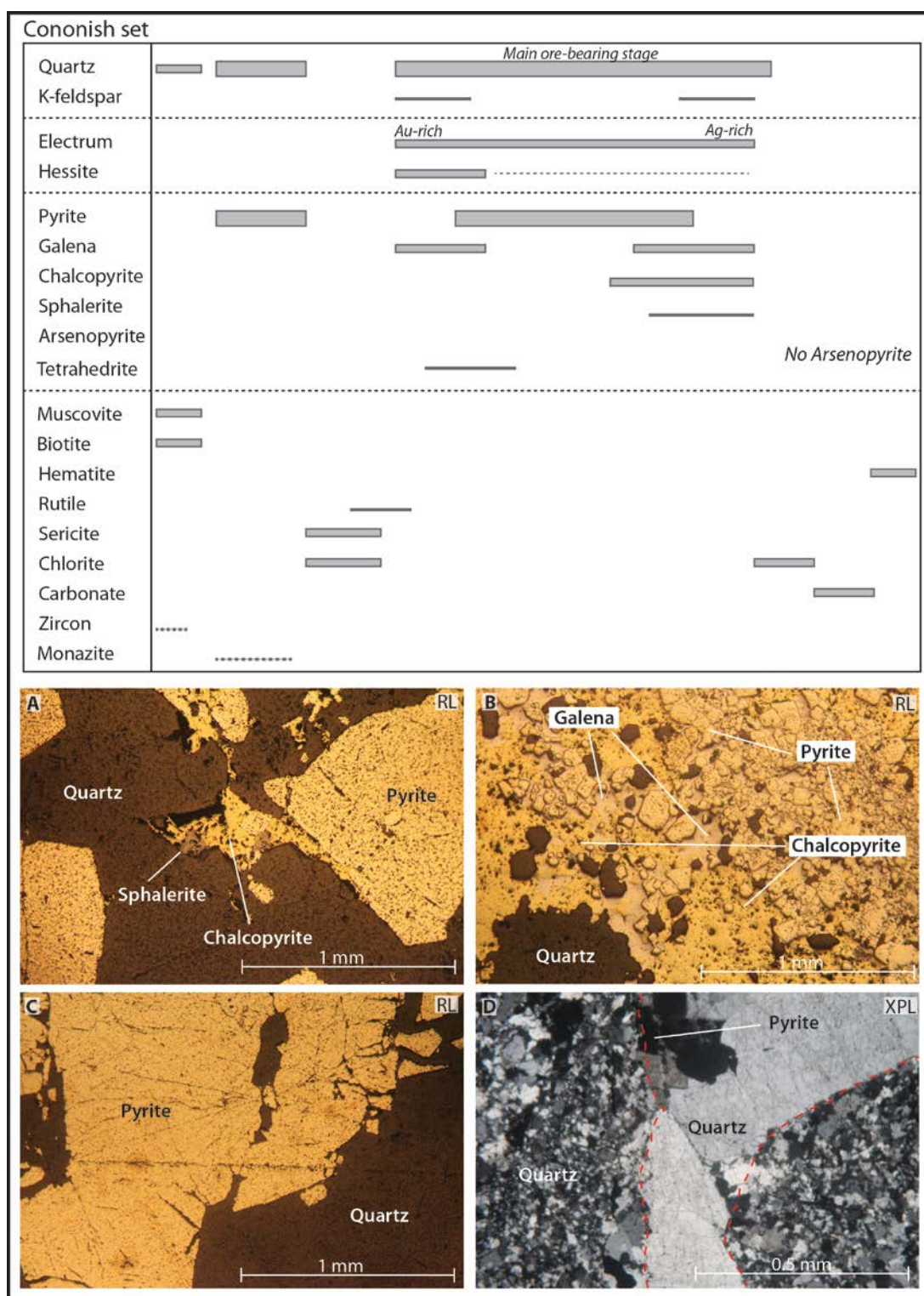


Figure 4.35: Paragenesis and photomicrographs for the Cononish vein set. Paragenesis after Cononish paragenesis from Spence-Jones (2013) with additional details from Coire Nan Sionnach and Creag Sheileach added from this study. A. Early pyrite with late void-filling chalcopyrite and sphalerite (CO05). B. Fractured early pyrite with later chalcopyrite and galena (CO03). C. Large well-developed pyrite in quartz vein. (CO05). D. Early brecciated quartz with later quartz with pyrite (CO03). Paragenesis developed from sample set n = 20. Dashed boxes in paragenesis indicate minerals present in some samples but absent in others.

4.5.5.2 River Vein set

The River Vein set, defined by a trend between 108° and 138°, occurs in Glen Orchy and at Sron Garbh (Fig. 4.34). Gold-bearing veins of this trend are absent elsewhere in the region, but quartz-only veins with this orientation do occur. The veins are characterised by abundant K-feldspar altered clasts and an absence of hessite and arsenopyrite. Clasts of chlorite-sericite altered host rock also occur in the veins (Fig. 4.36B). The River Vein gold-bearing vein is the most significant gold-bearing structure in the Glen Orchy area (Fig. 4.15) and exhibits the most complex petrographic relationships (Fig. 4.36A & C). Sulphide mineralogy at River Vein is comparable to other veins in Glen Orchy; large pyrite crystals have electrum, galena, sphalerite and chalcopyrite inclusions. Late-void filling galena with sphalerite is well developed; the sphalerite exhibits extensive chalcopyrite disease (Fig. 4.36A). Electrum is found with galena in fractures in large pyrite crystals (Fig. 4.36D).

4.5.5.3 Kilbridge set

The Kilbridge vein set, trends between 090° and 125° and is only seen at Kilbridge and Coire a'Ghabalach (Fig. 4.34). This vein set is defined by the presence of arsenopyrite (Fig. 4.37A) that is absent in other veins in the study area. Sericite-chlorite altered host rock clasts with pyrite occur within the veins (Fig. 4.37B & C). The veins exhibit significant cataclasis textures and a lack of open space-filling quartz textures (Fig. 4.37D).

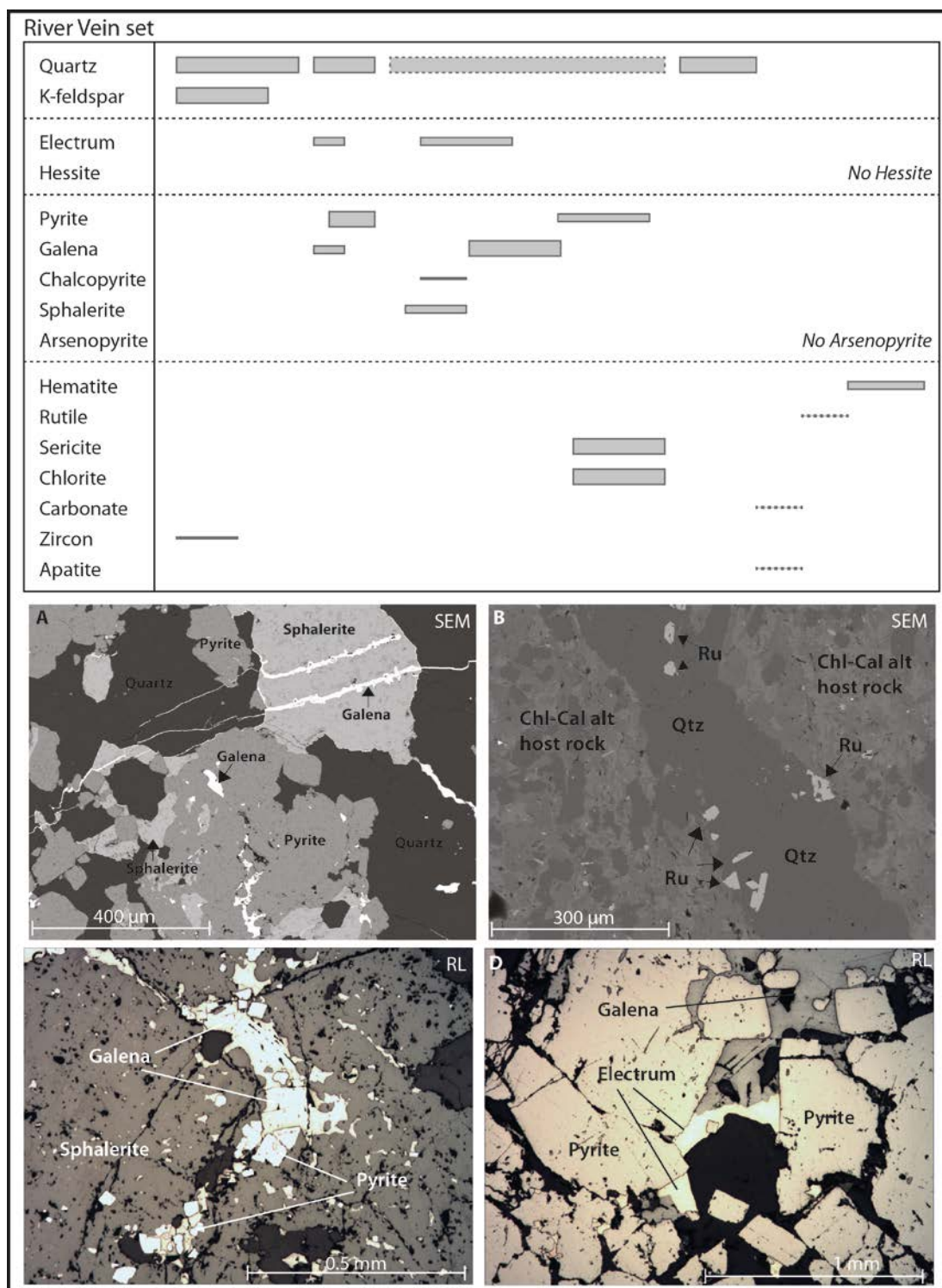


Figure 4.36: Paragenesis and photo plate for the River Vein set. A. Sulphide assemblage in main quartz vein (RV18). B. Late quartz with rutile (RV18). C. Early pyrite with late sphalerite and galena (RV18). D. Electrum with late galena (RV18). Paragenesis developed from sample set $n = 10$. Dashed boxes in paragenesis indicate minerals present in some samples but absent in others.

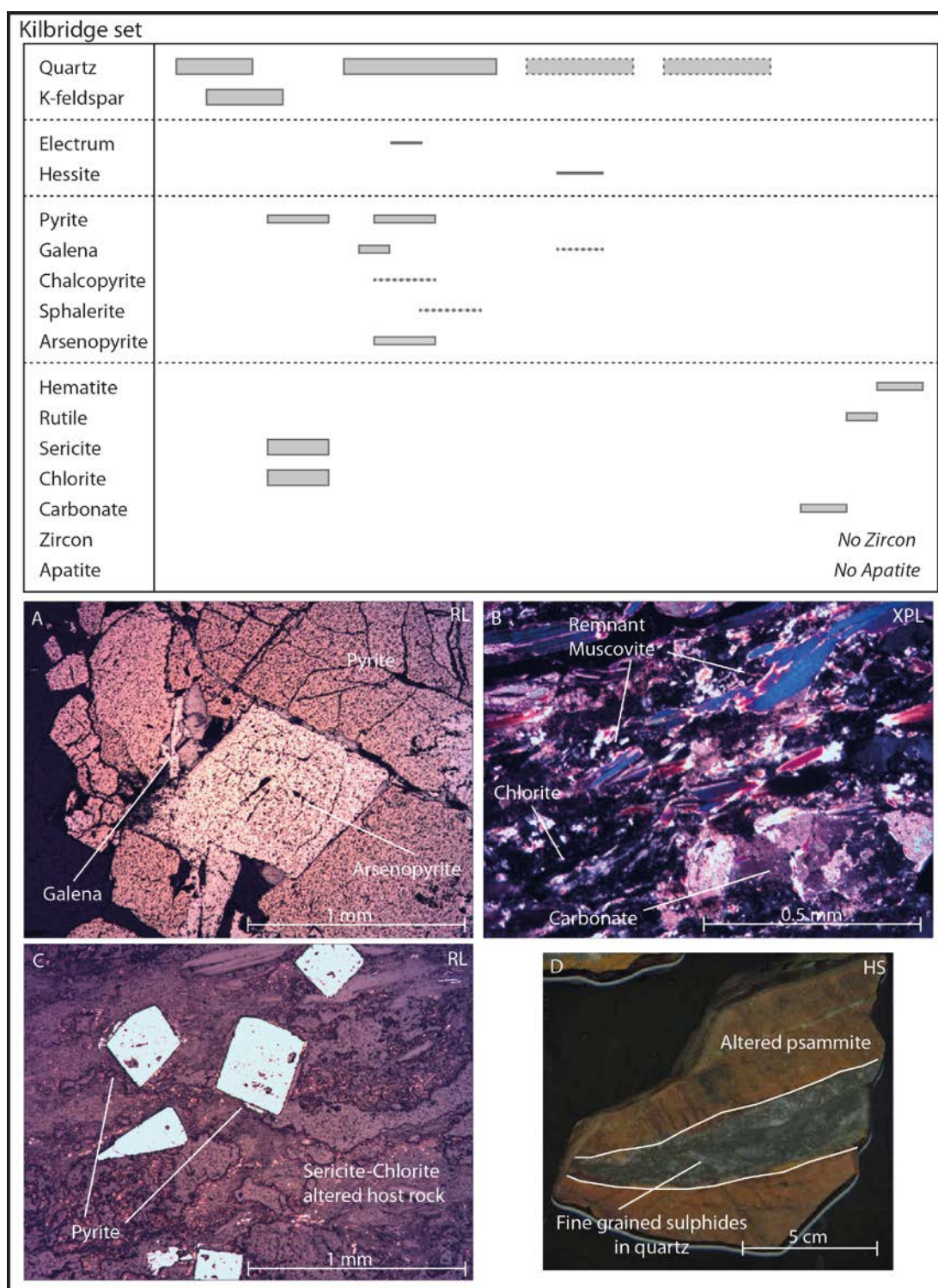


Figure 4.37: Paragenesis and photo plate for the Kilbridge set. A. Arsenopyrite with pyrite and late galena (CG01). B. Wall rock fragment with remnant metamorphic muscovite with chlorite and carbonate alteration (CG01). C. Early pyrite in altered host rock clast (KIL02b). D. Hand specimen of catalastic textures (KIL02b). Paragenesis developed from sample set $n = 5$. Dashed boxes in paragenesis indicate minerals present in some samples but absent in others.

4.6 Discussion

This work provides evidence that the extent, abundance and diversity of hydrothermal occurrences in the Tyndrum-Glen Orchy license area is much greater than previously noted. The field and petrographic timing constraints placed on hydrothermal events by this work are summarised below (Fig. 4.38; Table 4.1).

4.6.1 Constraints on relative timing of hydrothermal activity

All hydrothermal occurrences in the study area cross-cut the metamorphic D2 bedding parallel foliation and are interpreted to have formed after ductile deformation ceased, interpreted to be peak metamorphism (*c.* 475-470 Ma; Chew & Strachan 2014).

1. Molybdenite-bordered fractures are younger than peak metamorphism (Fig. 4.38). Quartz-pyrite \pm K-feldspar veins are interpreted to be equivalent to molybdenite-bordered fractures based on comparable mineralogy and vein trends in Glen Orchy (Fig. 4.38). The veins cross-cut the poly-metallic veins and are therefore older than 410 ± 14 Ma (Treagus *et al.* 1999). The relationship between the molybdenite-bordered fractures and the Siluro-Devonian lamprophyre sills (*c.* 430-415 Ma; Rogers & Dunning 1991; Neilson *et al.* 2009) is unconstrained.
2. Breccia bodies are emplaced pre- to syn- Siluro-Devonian lamprophyre sills (*c.* 430-415 Ma; Rogers & Dunning 1991; Neilson *et al.* 2009) and pre-date poly-metallic quartz veins based on the cross-cutting relationships (Fig. 4.38). The relationship between the breccia bodies and molybdenite-bordered fractures is unconstrained.
3. The Siluro-Devonian lamprophyre sills are interpreted to be equivalent to appinite intrusions elsewhere in the Dalradian Supergroup emplaced at *c.* 430-415 Ma (e.g. Garabal-Hill appinite; Rogers & Dunning 1991; Neilson *et al.* 2009). The Sron Garbh diorite-appinite is interpreted to be the same age as lamprophyre sills and regional appinite intrusions (Tanner 2012).
4. Pyrite-bearing veins cross-cut molybdenite-bordered fractures and are interpreted to be equivalent to poly-metallic quartz veins based on the comparable trend and relative timing relationships (Fig. 4.38).
5. Poly-metallic veins cross-cut molybdenite-bordered fractures and Siluro-Devonian lamprophyre sills and therefore emplacement of the breccia bodies. The veins are cross-cut by the Tyndrum Lead Mine-style veins (*c.* 360 Ma; Pattick 1981) and the Permo-Carboniferous dykes (Fig. 4.38; *c.* 290-270 Ma; Francis 1991).

6. Quartz-only veins occur throughout the paragenesis of the area. The largest quartz-only veins, Coire Daimh Vein and Mother Vein (Fig. 4.2; 4.6), are interpreted to post-date emplacement of the poly-metallic quartz veins based on structural analysis by Tanner (2012), in addition to cross cutting relationships between small (<0.5 m) quartz-only veins with poly-metallic veins.
7. Tyndrum Lead Mine-style veins at the Cononish deposit are interpreted to be equivalent to mineralisation at the Tyndrum Lead Mine emplaced at *c.* 360 Ma (Patrick *et al.* 1981); emplacement must post-date poly-metallic veins (410 ± 14 Ma; Treagus *et al.* 1999).
8. This study interprets the Permo-Carboniferous dykes to cross-cut the Tyndrum Lead Mine style veins supported by dating work (Fig. 4.38; Patrick 1981; Francis 1991). The Permo-Carboniferous dykes cross-cut the Tyndrum Fault suggesting major movement on this fault had ceased by this time (Fig. 4.38; Treagus *et al.* 1999).

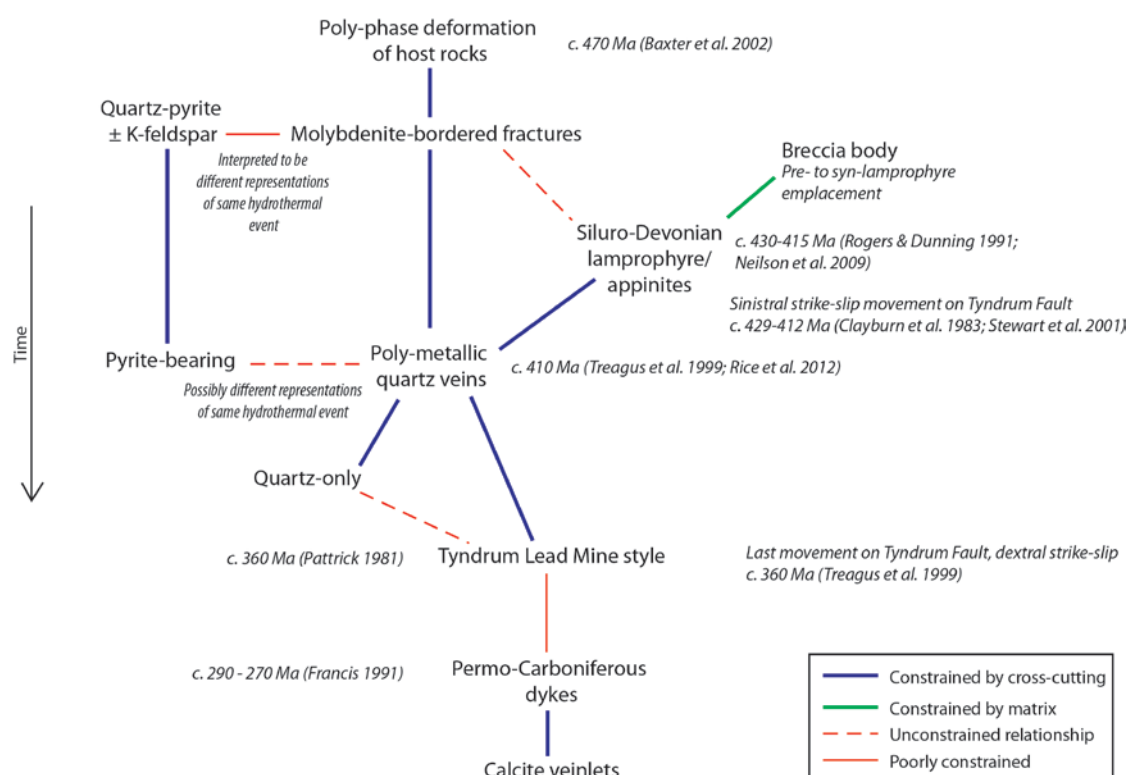


Figure 4.38: Simplified schematic constraints on the timing of hydrothermal events in the Tyndrum area.

4.6.2 Implications

There are a number of very different types of mineralisation found within the study area and correlating between different areas without precise geochronological constraints is challenging. The molybdenite-bordered fractures in Glen Orchy are difficult to relate to other areas as there is no evidence of molybdenite elsewhere in the study area. While there are differences in structural trend and mineralogy, the poly-metallic quartz veins have overall comparable paragenesis and field relations and are therefore interpreted to be equivalent; this is examined further in Chapters 5 (geochemistry), 6 (sulphur isotopes) and 7 (geochronology).

The relationship between mineralisation events and emplacement of magmatic bodies is constrained by the cross-cutting relationship between Siluro-Devonian lamprophyre sills and gold-bearing poly-metallic quartz veins. The relationship between earlier molybdenite-bordered fractures and lamprophyre sills is not constrained but the poly-metallic veins cross-cut both molybdenite-bordered fractures and lamprophyre sills.

From the field relations, it is suggested that the different mineralisation types were not all formed at the same time. It is unclear whether the mineralisation types represent a single evolving event or distinct separate events; however, given the significant variation in structural trends seen in the study area it is suggested the mineralisation types are unlikely to represent a single evolving event. This is investigated further in Chapters 5, 6, and 7.

Two possible origins are postulated for the origin of molybdenite in molybdenite-bordered fractures; either molybdenite is sourced from the sedimentary host rocks during peak metamorphism or there is a magmatic source rock at depth. It is difficult to constrain which of these is the most likely source and this is discussed in Chapters 5 and 7.

4.7 Conclusions

This chapter concludes there are multiple hydrothermal events identified in the Tyndrum area; the relationship between these events is poorly constrained. The early molybdenite-bordered fractures are newly identified by this work. Gold-bearing breccia bodies at Beinn Udlaidh are emplaced pre- to syn-Siluro-Devonian lamprophyre sills and are cross-cut by the gold-bearing poly-metallic quartz veins. Poly-metallic quartz veins are characterised by complex veins with poly-phase quartz and multiple sulphides. Three subgroups are defined; the Cononish, Kilbridge and River Vein sets. Late quartz-only veins occur throughout the Tyndrum area in a variety of orientations. In places, they are in the same orientation as the

poly-metallic and pyrite-bearing veins but do not exhibit mineralisation. This work suggests there is a change from an early molybdenum-dominated and gold-poor system to a gold-rich hydrothermal system. In the following chapters this work aims to establish whether the hydrothermal events are linked and represent the evolution of a single hydrothermal system or are independent of each other.

Chapter 5

Geochemical characterisation of gold and associated mineralisation in the Tyndrum area

Abstract: The genesis of gold- and molybdenite-bearing mineralisation in the Tyndrum area is poorly constrained. Field mapping and petrographic characterisation has defined vein sets based on variation in mineralogy and vein trend. In this chapter, the geochemistry of the sub-divisions is assessed to establish if clear geochemical divisions occur among the vein sets. This is used to determine whether vein sets represent different hydrothermal events or are differing representations of the same hydrothermal event. Geochemical trends in the vein sets were assessed through variation in gold pathfinder elements, including Ag, As, Sb, Te and W. This variation is compared to stream sediment data across the Tyndrum area to establish if gold-bearing quartz vein distribution can be traced in the stream sediment data. This study shows gold- and molybdenite-bearing mineralisation represents two distinct hydrothermal events. Molybdenum enrichment occurs with Sb depletion whereas gold enrichment is associated with high Ag, Te and moderate As. Overall, the poly-metallic quartz vein sets have comparable trends in key gold pathfinder elements but the Cononish deposit is anomalous with high tellurium with high grade gold. The Kilbridge and River Vein sets have different Au/Ag ratios, higher As and lower Te at high gold grade compared to the Cononish deposit. Areas with high tellurium in stream sediment data are proposed to be the most prospective for gold mineralisation, with areas with high arsenic enriched in gold, but at lower grades. This work suggests high tellurium is key to high gold grade and exploration should focus on areas with high Au, Ag, Te, where As is low, and high As, where Te is low, in stream sediment data.

5.1. Introduction

Field mapping and petrographic characterisation (Chapter 4) developed a classification scheme for the hydrothermal occurrences in the Tyndrum area. The classification scheme is interpreted to represent a series of hydrothermal systems through time. This chapter examines if there are geochemical distinctions between the different sets of poly-metallic quartz veins (and molybdenite-bordered fractures) to help constrain whether they formed from different hydrothermal events. In addition, this chapter will establish the implications of vein lithogeochemical data for the interpretation of stream sediment geochemistry data. The lithogeochemical data for the Cononish deposit are compared to data for typical orogenic, epithermal and reduced intrusion-related gold deposits to attempt to classify the deposit.

The relationship between the gold-bearing poly-metallic quartz veins and molybdenite-bordered fractures is poorly constrained. This work aims to establish if poly-metallic veins and molybdenite-bordered fractures represent two discrete hydrothermal occurrences. This is crucial to understanding the geometry of the hydrothermal system in the Tyndrum area. At current understanding, the poly-metallic quartz veins are grouped together, based on broadly similar mineralogy and a lack of cross-cutting relationships between veins. However, within the poly-metallic veins there is variation in trend and some variation in mineralogy. Therefore, it is possible the three vein sets, Cononish, Kilbridge and River Vein, represent different hydrothermal events. The understanding of the relationship between the poly-metallic quartz veins is furthered by assessing variation in the geochemical trends and Au/Ag ratios. Enrichment in gold pathfinder elements is compared to stream sediment anomalies to establish if the anomalies reflect the location of high grade gold veins.

This chapter builds on the grouping of veins from field relations and petrographic classification in Chapter 4 and aims to establish the potential use of geochemical anomalies in stream sediments as pathfinders for gold across the Tyndrum and regional area. This chapter also aims to establish if all poly-metallic quartz veins are potentially coeval and to constrain the size of the hydrothermal system in the Tyndrum area.

5.2. Analytical methods

5.2.1. Sampling methods

Samples were collected during three field seasons, between July 2010 and August 2012, in conjunction with Scotgold Resources' on-going exploration program. All samples used for geochemical analysis were whole rock samples and consist of a combination of *in situ* outcrop and samples from drill core. Outcrop samples were at least 2 kg in weight with half sent for assay and the other retained for further work. Samples were chosen to ensure they were representative of the sample site. Drill core was sampled after being logged and photographed. Drill core was of two sizes NQ and AQ; NQ core is 48 mm in diameter. AQ core at Scotgold Resources is slightly larger (~34 mm) than the standard 27 mm diameter as the AQ drill rig has been adapted to meet the company's needs. Where sampling was undertaken from NQ core, a quarter of the core was retained for reference, for AQ the whole core was sent for assay.

5.2.2. Whole rock geochemistry

All whole rock geochemistry was carried out at ALS Laboratories (formally OMAC Laboratories), Ireland. Samples were submitted as 1 kg representative samples before splitting, crushing (<2 mm grain size) and pulverising (<75 μm grain size) in a low-chrome steel grinding mill at ALS Laboratories (PREP-31; ALS Minerals 2012; ALS Geochemistry 2014).

All gold analyses are reported in ppm and were analysed using the preferred method for gold recovery - Fire Assay Fusion with Atomic Absorption Spectroscopy (Au-AA26; ALS Minerals 2006). This involves fusing 30 g of sample with lead oxide, sodium carbonate, borax and silica, mixed with 6 mg of gold-free silver. The fused sample is collected at the base of the fusion crucible. The excess lead is then removed through high temperature oxidation (cupellation) leaving the precious metals. The precious metal bead is dissolved in aqua regia (hydrochloric and nitric acid) and analysed by atomic absorption spectroscopy against standards. The lower detection limit for gold is 0.01 ppm throughout the assay database.

Multi-element analyses reported here were analysed by a four acid digestion method (ME-ICP61; ALS Minerals 2009a). This involves sample digestion in perchloric, nitric, hydrofluoric and hydrochloric acids, before analysis by ICP-MS. Four-acid digestion quantitatively dissolves nearly all minerals commonly present in geological samples, but may not fully digest barite, rare earth oxides, tin and tungsten minerals (ALS Geochemistry 2014). Detection limits for elements using the four-acid digestion method are detailed in Appendix 5.1. Accuracy and precision for the elements discussed in this chapter are shown in Figures 5.1 and 5.2. Accuracy is calculated by the average variation in analytical results compared to the Certified Reference Material (CRM). Precision is reported as relative standard deviation to the average analytical results for the CRM. Accuracy is reported as a percentage and precision is reported as a percentage representing 1σ standard deviation. Good accuracy and precision is <5%, reasonable 5- 10% and poor >10%.

There is some difficulty in using the entirety of the Scotgold Resources Ltd assay database without considering the variation in the lower detection limits of some elements. Lithogeochemical assay data from between 2007 and 2010 uses higher detection limits than data after 2010. For example, early analyses for tellurium had a lower detection limit of 5 ppm, at least a thousand times crustal abundance (Rudnick & Gao 2002). As a result, for a tellurium anomaly to be noted it must be enriched a thousand times background

continental crust. The detection limit for tellurium has since been reduced to 0.005 ppm (equal to crustal abundance, Rudnick & Gao 2002). Where possible later data are used and early data with high detection limits are not used. Where newer data are not available for an area, higher detection limits are shown.

Four-acid digestion may result in some elements, such as As, Se and Te, being volatilised and lost. As a result, a small test set of samples was run using an alternative geochemical method - aqua regia digestion. Aqua regia readily dissolves sulphides, oxides and carbonates but may leave the silicates and resistive oxides undissolved (ALS Geochemistry 2014). A set of stored pulp samples (n=10) were re-analysed using aqua regia digestion with analysis by ICP-AES (ME-ICP41; ALS Minerals 2009b). This involves sample digestion in aqua regia (nitro-hydrochloric acid) in a heated graphite block. The sample is then cooled and diluted with deionised water before analysis by ICP-AES. This sample set allows for direct comparison between four-acid and aqua regia digestion methods to establish if there is systematic variation in the abundance of elements reported between the two methods.

Samples were additionally run on a LECO sulphur analyser to confirm the total sulphur present in the ten samples (S-IR08; ALS Minerals 2009c) and to allow for comparison of reported sulphur % from four acid and aqua regia digestion methods to the preferred analysis method (LECO). LECO is used due to the difficulty in dissolving sulphides into solution meaning ICP spectroscopy is challenging and digestion methods may underestimate sulphur within the sample. Analysis involved heating of the sample to ~1350°C in a furnace under a stream of oxygen (ALS Minerals 2009c). Sulphur dioxide released from the sample was measured by infrared spectroscopy and provides total sulphur abundance.

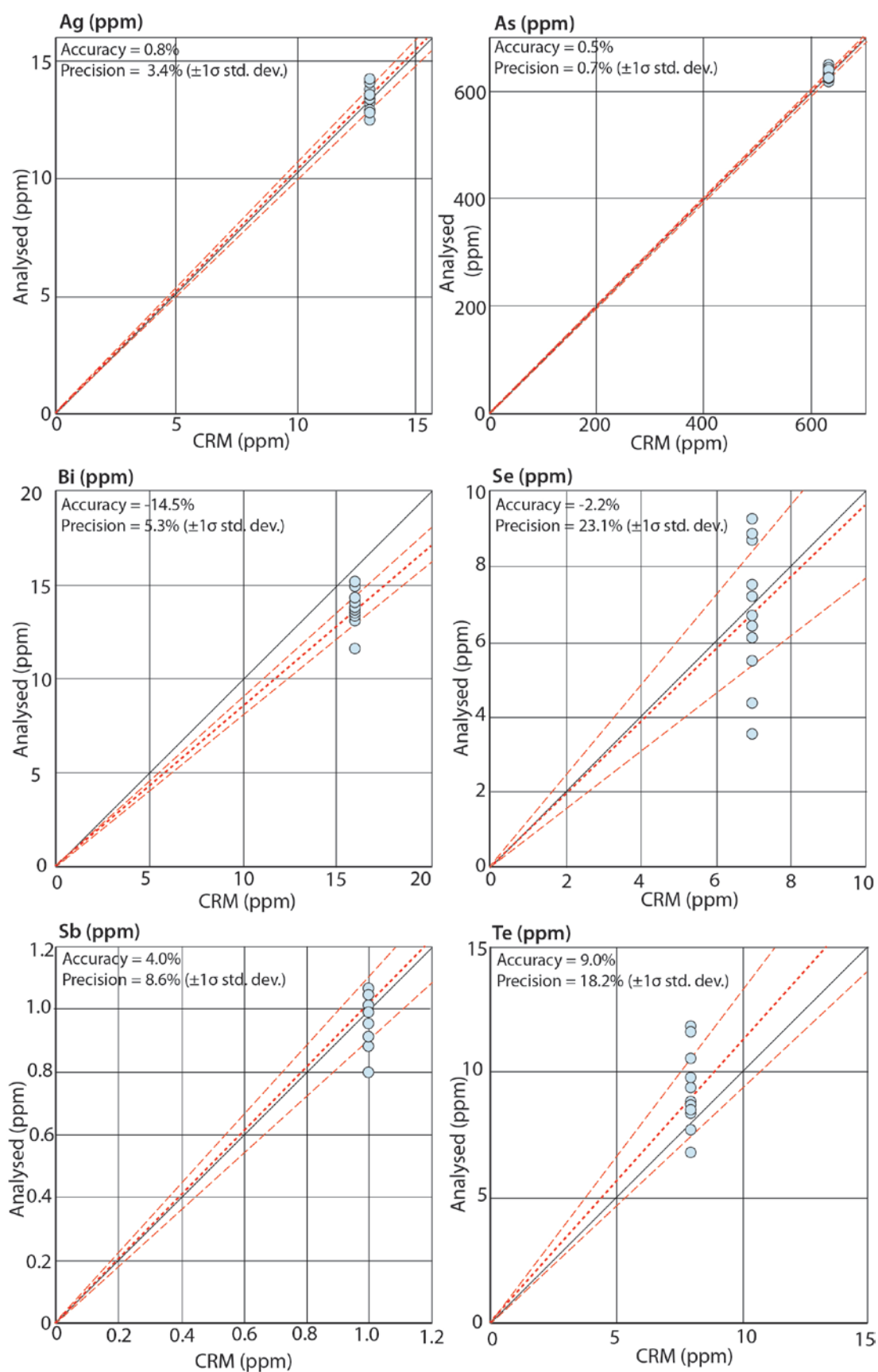


Figure 5.1: Accuracy and precision of gold pathfinder elements by four acid digestion methods. Accuracy is shown by red dotted line and precision by dashed lines around the accuracy line. CRM = Certified Reference Material. Good precision and accuracy are defined as <5%, reasonable 5-10% and poor >10%.

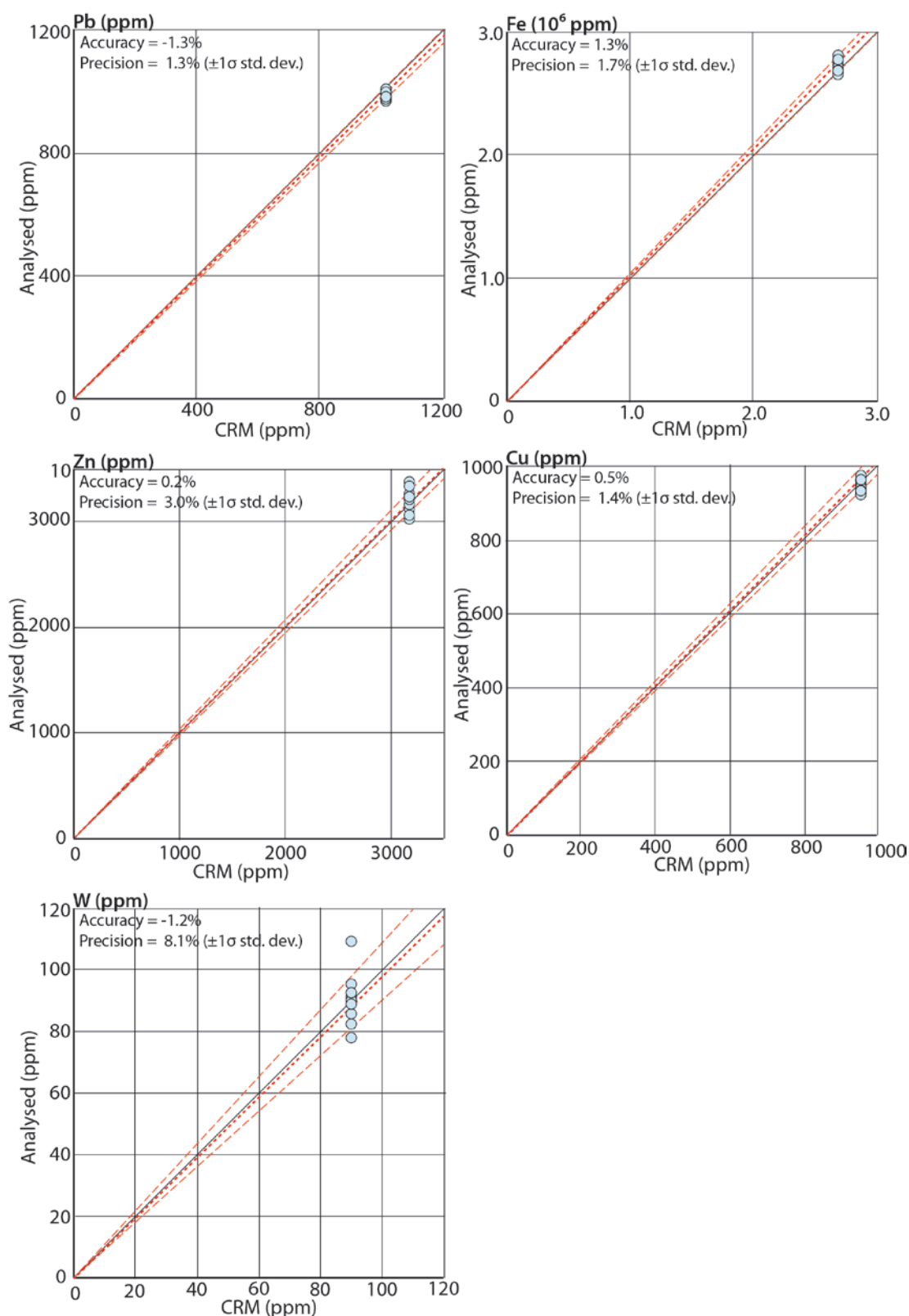


Figure 5.2: Accuracy and precision of elements of importance in the Tyndrum area mineralisation by four acid digestion methods. Accuracy is shown by red dotted line and precision by dashed lines around the accuracy line. CRM = Certified Reference Material. Good precision and accuracy are defined as <5%, reasonable 5-10% and poor >10%.

5.2.3. Microprobe analysis

A pilot set of microprobe analyses of electrum was undertaken at Leeds University on well-characterised thin sections. The microprobe was a JEOL 8230 with a LaB₆ electron source and a fully integrated Jeol SDD EDS system. A 30nA current, 15 kV accelerating voltage and a 10 µm beam were used for all analysis. The following element set was analysed; Au, Ag, As, Bi, Cd, Cu, Fe, Pb, S, Sb, Se, Te, Zn. Analyses with low totals (<98% for electrum) were discarded.

5.2.4. Stream sediment sampling

As part of Scotgold Resources' exploration program extensive stream sediment sampling was carried out in the Tyndrum-Glen Orchy license area. A silt-rich 500-125 µm fraction was taken from the stream to ensure a representative sample of the heavy minerals was collected. Samples were shovelled from the river bed and sieved to achieve the required fraction. As the sample was wet when collected, it was dried before submission for geochemical analysis at ALS Laboratories. A minimum sample size of 100 g of dry sample is required for geochemical analysis using four acid digestion methods (5.2.2).

5.3. Comparison between whole rock geochemical methods

Here, variations in the elemental abundances of key elements between different analytical methods are compared (Table 5.1). The range of elements considered are used in the following sections to describe the lithogeochemistry and stream sediment data and to make comparisons between different datasets. Gold, Ag, As, Bi, Se, Sb and Te, are considered due to their importance as gold pathfinder elements. The variation in Pb, Zn, Cu and Fe is also considered because of the relevance of these within the paragenesis at the Cononish deposit and in Tyndrum area mineralisation. Accuracy for auqa regia digestion is reported as a percentage using the same method of calculation as four-acid digestion (5.2.2).

The variation in reported sulphur abundance between four-acid digestion, auqa regia digestion and LECO analysis is compared. There is little variation across the three methods although the data suggests that both four-acid and auqa regia digestion methods over-estimate the amount of sulphur relative to the preferred LECO method (Fig. 5.3; 12% four-acid, 5% auqa regia).

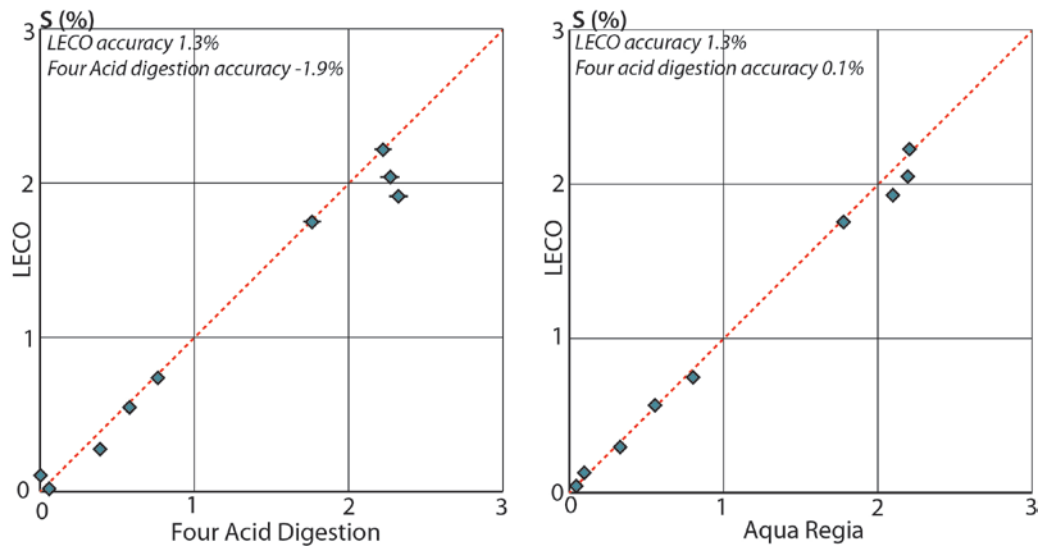


Figure 5.3: Variation in data obtained for sulphur from four acid digestion, aqua regia and LECO analytical methods. Both four acid digestion and aqua regia over estimate sulphur (%) compared to LECO.

A number of the gold pathfinders are considered volatile in four-acid digestion and may be under-estimated by this method (ALS Geochemistry 2014). For the gold pathfinders (Bi, As, Se, Sb, and Te), while aqua regia digestion is interpreted to be the more accurate digestion method, there is variation in the elemental abundances reported for the two digestion methods (Fig. 5.4).

Silver abundance using four-acid and aqua regia digestion is consistently within 30% of the other digestion method (Fig. 5.4; with the exception of samples RV11 and RV14 discussed below). Four-acid digestion under-estimates the abundance of selenium in samples, relative to aqua regia digestion (50 to 5000% > aqua regia). For bismuth, with the exception of one sample, four-acid digestion appears to under-estimate the total Bi in the sample compared to aqua regia digestion (average four-acid 25% < aqua regia) and four-acid digestion has lower accuracy than aqua regia.

The relationship is less clear for the other pathfinders (As, Sb and Te), in part, due to the limited size of the dataset and the lack of samples highly enriched in these elements. Arsenic and antimony have complicated profiles, for arsenic half of the samples, when digested by four-acids, under-estimate the amount of arsenic by up to 20% compared to aqua regia (Fig. 5.4). However, aqua regia has a lower accuracy than four acid digestion. The other five samples over-estimate by up to 300% for four-acid digestion compared to aqua regia digestion. Antimony has a comparable pattern with half samples under-estimating by up to 35% and half over-estimating by up to 300% (average 75%), when digested in four-acid compared to aqua regia (Fig. 5.4). The variation seen in arsenic and

antimony is interpreted to reflect four-acid digestion dissolving quartz or similar, host to arsenic and antimony, possibly as sulphide, not digested by aqua regia. For tellurium, the poor accuracy of aqua regia compared to four-acid digestion suggests while there is potential for high volatility of tellurium during four-acid digestion, this is likely to be the better digestion method (Fig. 5.4).

Sample RV14 has much higher As, Bi, Se and Te in four-acid digestion (475 to 4700% > aqua regia) interpreted to suggest elements are hosted in minerals undissolved by aqua regia digestion. Sample RV11 exhibits preferential digestion by aqua regia with Bi and Te 15% higher than reported for four-acid digestion, however, as As and Se are lower for aqua regia than four-acid digestion (As 23%, Se 72% greater in four-acid), Bi and Te are interpreted to have been lost as volatiles during four-acid digestion.

The base metals show a simpler pattern, iron and lead generally follow the 1:1 ratio with a slight under-estimation of abundance towards aqua regia digestion methods (Fig. 5.5). Both zinc and copper show a more scattered picture with the majority of samples being under-estimated by aqua regia digestion (Fig. 5.5).

Table 5.1 Four acid digestion and aqua regia digestion methods comparison for ten sample pilot set. 4AD – Four acid digestion, AR – Aqua Regia

Sample	GO1213		GO1216		GO1218		ConBG03		ConBG05	
Type	Lamp		MGp		MGp		Ls		BEs	
Mineralogy	Qtz, Ser, Chl, Py		Qtz, Musc Carb		Qtz, Musc Ser, Py		Qtz, Bio, Musc		Qtz, Bio, Musc, Py,	
Au (ppm) by Fire Assay	0.8		<0.01		0.04		<0.01		<0.01	
Method	4AD	AR	4AD	AR	4AD	AR	4AD	AR	4AD	AR
S (%)	2.26	2.19	0.05	0.04	0.76	0.80	0.01	0.09	0.39	0.33
S Leco (%)		[2.05]		[0.04]		[0.74]		[0.11]		[0.29]
Cu (ppm)	5.70	5.50	5.40	5.10	39.20	32.90	5.30	14.90	15.60	15.50
Fe (ppm)	57x10 ³	55x10 ³	54x10 ³	51x10 ³	392 x10 ³	329 x10 ³	53 x10 ³	149 x10 ³	156 x10 ³	155 x10 ³
Pb (ppm)	15.40	14.20	19.30	7.20	38.90	29.10	16.20	45.00	23.10	12.60
Zn (ppm)	106.00	93.00	13.00	12.00	52.00	45.00	56.00	68.00	80.00	70.00
Ag (ppm)	0.42	0.60	<0.01	0.01	0.24	0.23	0.02	0.24	0.08	0.08
As (ppm)	52.70	60.90	1.00	0.60	9.30	10.00	4.10	100.50	2.40	2.60
Bi (ppm)	0.01	0.04	0.02	0.03	0.11	0.13	<0.01	0.10	0.06	0.06
Sb (ppm)	0.65	0.19	0.08	0.07	0.48	0.13	0.06	0.76	0.11	0.11
Se (ppm)	1.00	0.30	1.00	0.20	1.00	0.40	1.00	<0.2	1.00	0.20
Sn (ppm)	1.80	0.20	1.00	0.50	2.20	0.20	1.40	0.30	1.00	0.20
Te (ppm)	0.08	0.10	<0.05	0.01	0.08	0.05	<0.05	<0.01	<0.05	0.01

Sample	ATT07		RV11		RV13		RV14		RV16	
Type	BCq		Poly-Met		Py-bearing		Py-bearing		Mo-bordered	
Mineralogy	Qtz, Musc, Py		Qtz, Ksp, Py, Ga, Musc		Qtz, Ksp, Py, Musc		Qtz, Py, Ksp		Qtz, Ksp, Py, Moly	
Au (ppm) by Fire Assay	0.02		0.33		0.13		0.08		0.02	
Method	4AD	AR	4AD	AR	4AD	AR	4AD	AR	4AD	AR
S (%)	2.32	2.10	1.76	1.78	0.59	0.55	15.60	0.02	2.21	2.20
S Leco (%)		[1.93]		[1.75]		[0.55]		[0.04]		[2.22]
Cu (ppm)	234.00	291.00	5.66	5.00	11.32	9.70	34.80	4.00	4.02	2.90
Fe (ppm)	2340 x10 ³	2910 x10 ³	56 x10 ³	50 x10 ³	113 x10 ³	97 x10 ³	347 x10 ³	40 x10 ³	402 x10 ³	29 x10 ³
Pb (ppm)	16.30	7.10	2973.79	2790.00	838.86	780.00	162.33	9.40	48.33	17.70
Zn (ppm)	3520.00	3800.00	12.09	5.00	11.77	6.00	5.61	17.00	17.92	13.00
Ag (ppm)	0.38	0.30	53.15	51.60	13.29	13.10	3.87	0.10	<0.5	0.39
As (ppm)	74.70	68.20	2.83	2.30	2.84	0.90	3.80	0.80	3.00	1.80
Bi (ppm)	0.57	0.58	89.13	104.00	21.42	26.20	9.93	0.21	0.71	0.67
Sb (ppm)	0.52	0.30	0.08	0.10	0.06	0.10	0.10	0.09	0.09	0.11
Se (ppm)	1.00	0.60	6.19	3.60	1.73	0.60	4.94	<0.2	<0.5	0.50
Sn (ppm)	<0.2	<0.2	<0.2	<0.2	0.24	<0.2	0.43	0.20	0.39	0.20
Te (ppm)	0.09	0.03	6.74	7.88	1.59	2.08	0.66	0.01	0.24	0.19

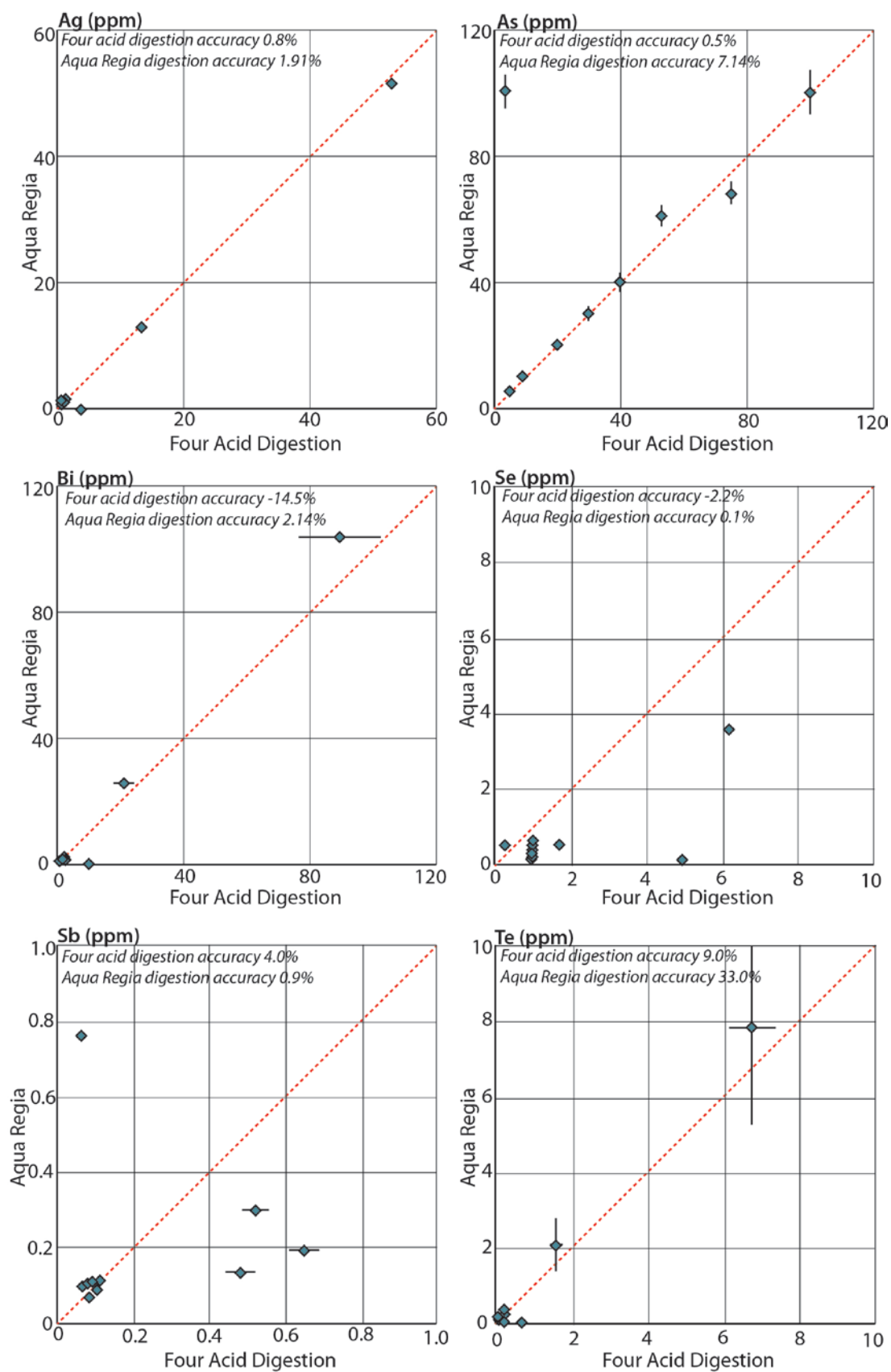


Figure 5.4: Comparison of four-acid and aqua regia digestion geochemical methods for key gold pathfinder elements. Error bars showing accuracy, where absent the error bars are within the extent of the symbol.

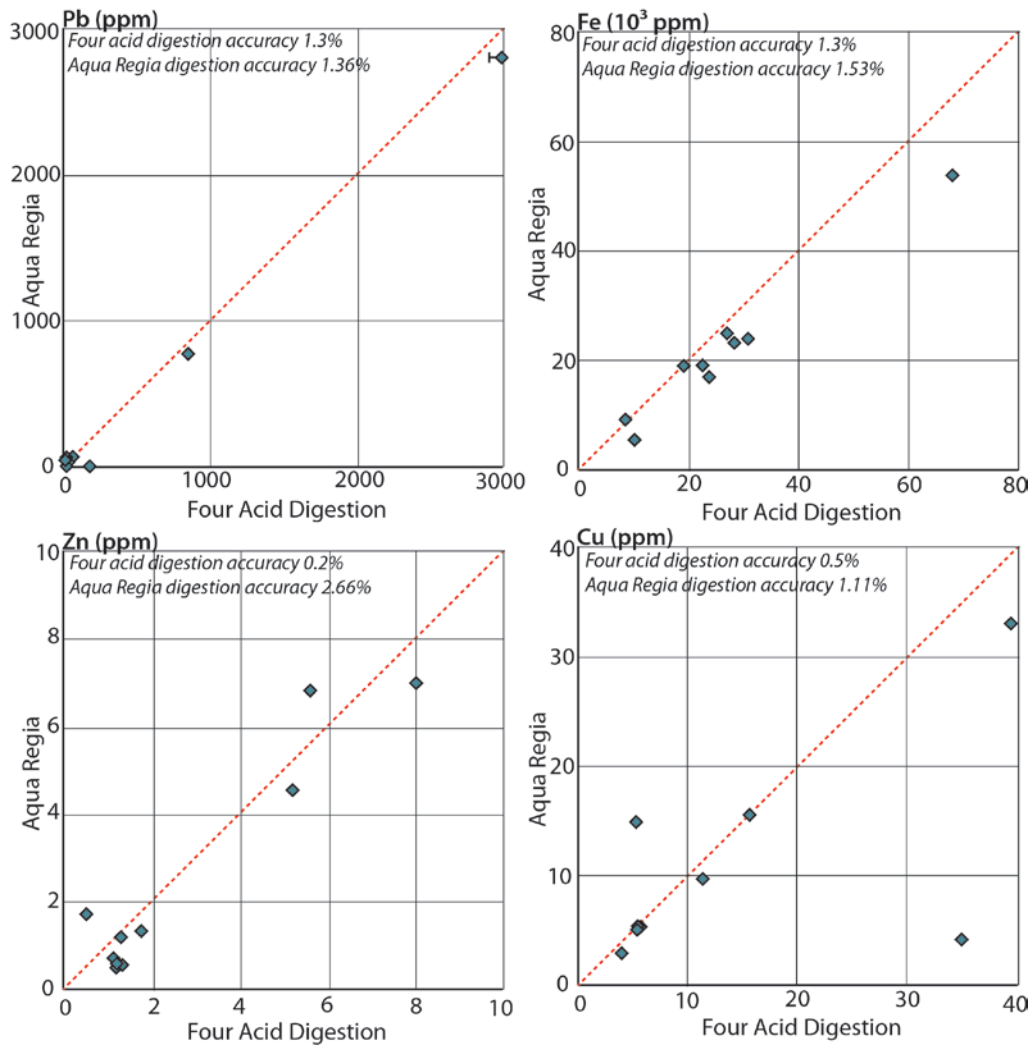


Figure 5.5: Comparison of geochemical methods for base metals. Error bars showing accuracy, where absent the error bars are within the extent of the symbol.

5.3.1. Implications for geochemical trends of vein sets

Overall, the variation across the two digestion methods suggests the four-acid digestion data are robust for sulphur and the base metals (Cu, Fe, Pb, Zn). For the gold pathfinder elements it is more complicated, due to the highly volatile nature of the elements in four-acid digestion (Table 5.1). Aqua regia digestion has good accuracy for most gold pathfinders with reasonable accuracy for arsenic (7.14%), and poor accuracy for tellurium (33.0%). Four-acid digestion has very good accuracy for all elements discussed in this chapter except reasonable accuracy for tellurium (9.0%), and poor accuracy for bismuth (14.5%). The errors on tellurium analyses for both digestion methods suggests four-acid is the better digestion method as accuracy is reasonable (9.0%), compared to the poor accuracy of aqua regia (33.0%).

5.4. Geochemical variation by location in gold-bearing quartz veins

5.4.1. Field and petrographic classifications

Based on the field relations, in combination with the dominant ore and gangue mineralogy, seven vein sets were defined in Chapter 4 (Table 5.2). The geochemical signature of these vein sets is examined using whole rock four-acid digestion ICP-MS data with the aim to establish if vein sets show geochemical distinctions or whether all gold mineralisation in the Tyndrum area shares the same geochemical characteristics and might therefore be formed broadly synchronously in the same hydrothermal event.

The most important mineralised veins are the poly-metallic quartz veins, as these are the dominant gold-bearing mineralisation in the region and have the greatest potential for future development into a resource or reserve. In this study, veins considered gold-bearing contain >0.1 ppm Au and samples considered to be molybdenite-bearing have >100 ppm Mo. Quartz-only veins are defined as having <0.1 ppm Au and <100 ppm Mo and an absence of sulphides in the main vein structure (Table 5.2). Here, the whole rock geochemical trends of molybdenite-bordered fractures, poly-metallic, pyrite-bearing, Tyndrum-Lead Mine style and quartz-only veins are discussed.

Table 5.2 *Classification of veins based on field criteria and mineralogy from this study*

Vein type	Field classification	Subset	Trend	Key characteristics	Average Au (ppm)	Average Mo (ppm)
Molybdenite-bordered fracture (n=20)	Molybdenite in K-feldspar altered host rock		N-030°	Extensive K-feldspar alteration of host rock, molybdenite in alteration halo, >100 ppm Mo	0.05	3830
Pyrite-bearing (n=5)	Pyrite-bearing quartz vein		065-070°	Pyrite only sulphide in quartz vein, brecciated host rock clasts in vein	<0.1	<100
Poly-metallic (n=37)	Complex veins with multiple sulphide phases dominantly pyrite and galena. Multiple quartz generations with brecciated host rock	Cononish set (n=15)	040-060°	Gold-bearing, pyrite and galena with chalcopyrite, multiple quartz generations, >0.1 ppm Au	8.6	44
		River Vein set (n=17)	108-138°	Inclusions of K-feldspar altered host rock, gold-bearing, pyrite-galena dominated assemblage, >0.1 ppm Au	63.1	5.2
		Kilbridge set (n=5)	090-125°	Pyrite with arsenopyrite, gold-bearing, >0.1 ppm Au	14.1	3
Tyndrum Lead Mine-style (n=4)	Galena and sphalerite bearing quartz vein		035-045°	Friable quartz, absence of pyrite, abundant galena and pale brown sphalerite	<0.01	<10
Quartz-only (n=53)	Quartz-only		Various	Quartz brecciation by later quartz. Absence of sulphides	<0.1	<100

5.4.2. Whole rock geochemistry

5.4.2.1. Molybdenite-bordered fractures

There is not a close association between molybdenum and any other element in the assay database (Appendix 5.2). The highest molybdenite grades (0.1-1%) have low tellurium (<2 ppm) and arsenic (<10 ppm). There is no correlation between gold and molybdenum within the geochemical dataset for the Tyndrum area (Fig. 5.6B & D). Gold is only associated with molybdenum where late poly-metallic veins have cross-cut earlier molybdenite-bordered fractures. There is a notable lack of silver (<12 ppm) associated with the highest molybdenum grades (0.1-1%; Fig. 5.6A). The lowest antimony values (<0.6 ppm) within the study area are associated with molybdenite mineralisation suggesting depletion in antimony may occur with molybdenum enrichment (Fig. 5.7). High molybdenum (>100 ppm Mo) at Cononish and Sron Garbh is recorded in the geochemical dataset (Fig. 5.6E & F) but no molybdenite mineralisation or cross-cutting relationships with poly-metallic veins are observed.

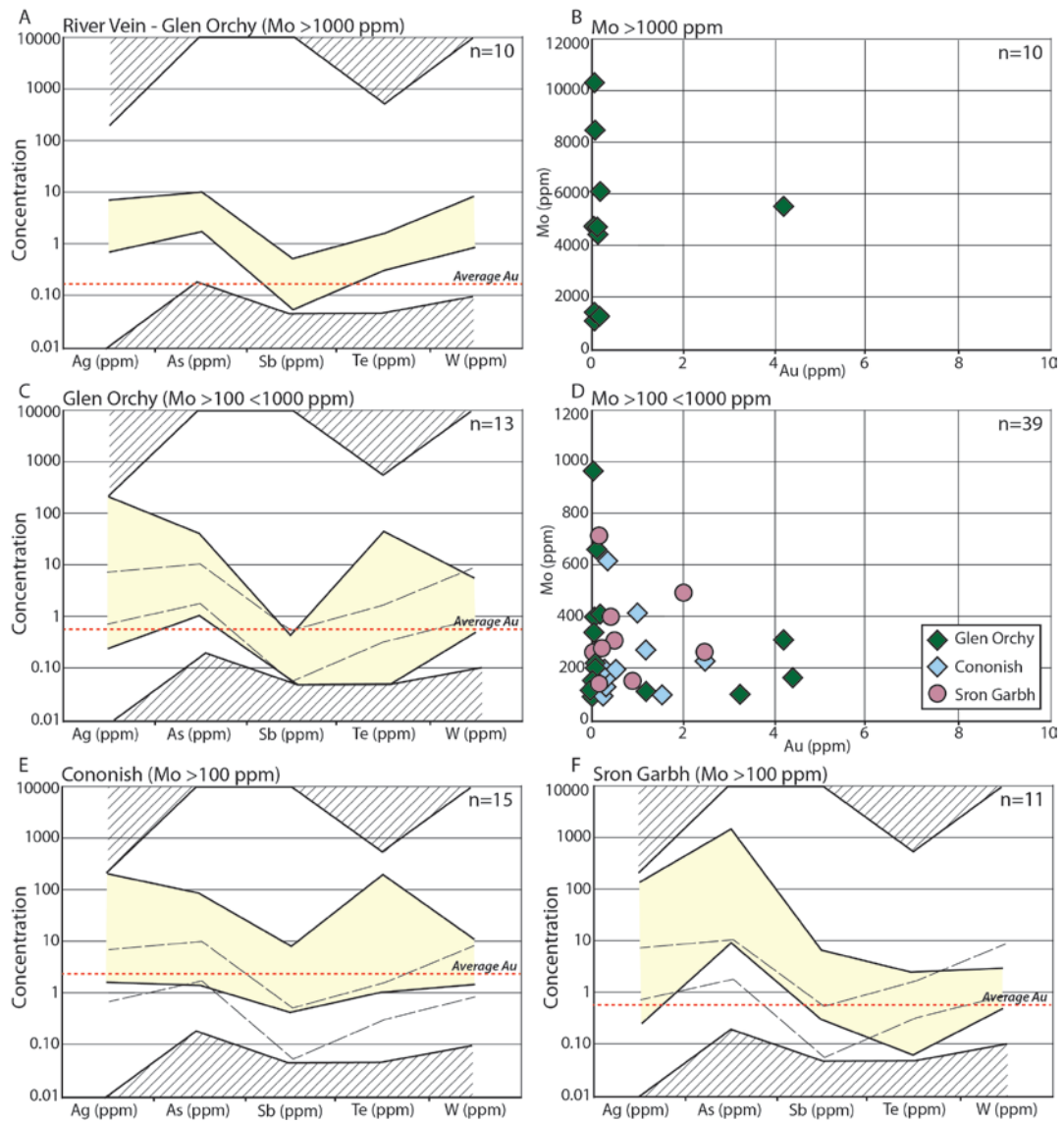


Figure 5.6: Geochemical trends for key gold pathfinder elements in molybdenite-bearing veins in the study area. The lack of any relationship between gold and molybdenum grade is also illustrated in B & D. Average Au in ppm is shown by the red dashed line. Black dashed line represents high grade (>1000 ppm) molybdenum at River Vein. Detection limits shown by hashed out area.

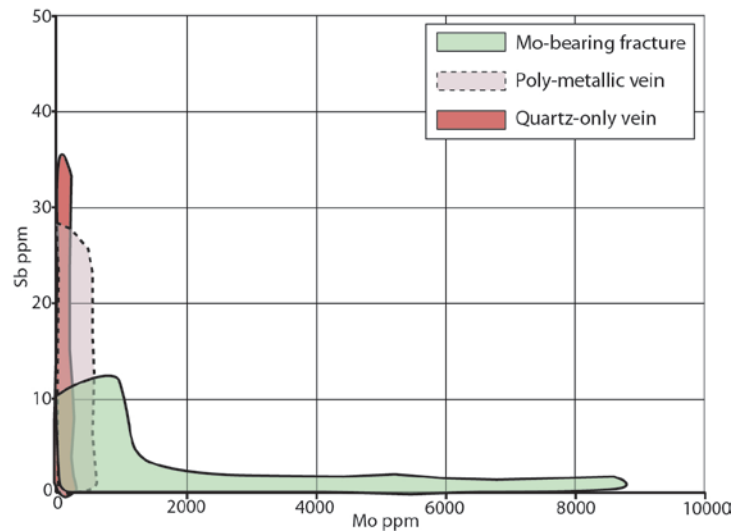


Figure 5.7: Mo vs. Sb for selected vein sets to illustrate the depletion of Sb seen in molybdenite-bearing fractures compared to the poly-metallic and quartz-only vein sets.

5.4.2.2. Pyrite-bearing and quartz-only veins

Quartz-only veins are defined by an abundance of quartz, absence of sulphide and are barren (<0.1 ppm Au, <100 ppm Mo). The quartz-only veins have low silver (<5 ppm), arsenic (<10 ppm), tellurium (<0.75 ppm) and antimony (<5 ppm) with moderate enrichment in tungsten (<12 ppm).

Pyrite-bearing veins, defined by the visually assessed presence of pyrite in the assemblage ($>0.5\%$ pyrite and absence of other sulphides), show a comparable trend in pathfinder elements to the quartz-only veins (Fig. 5.8; Table 5.1). The pyrite-bearing veins show a minor increase in tellurium enrichment compared to the barren veins but exhibit lower antimony enrichment (<5 ppm).

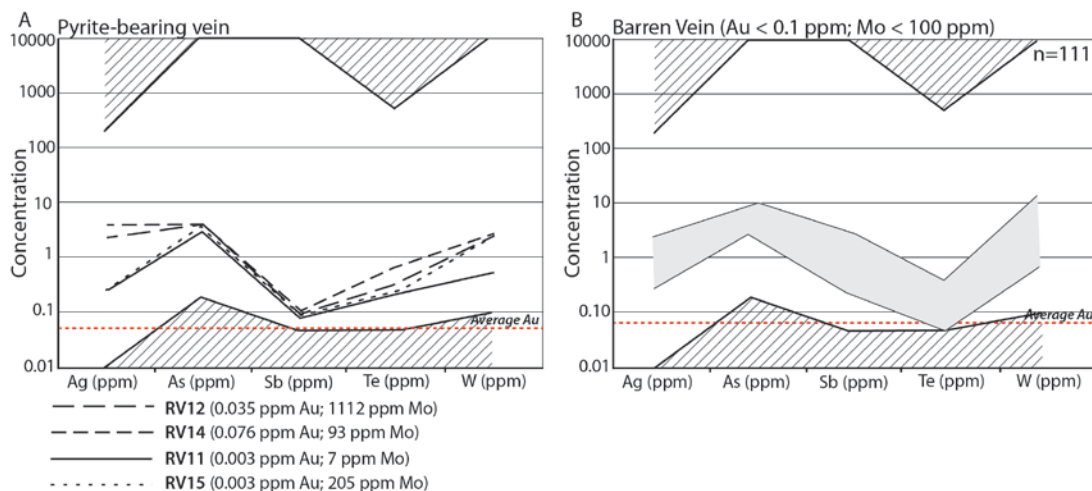


Figure 5.8: General trend in pyrite-bearing and barren veins in the Tyndrum area. Upper cut off limits for barren veins are defined as Au <0.1 ppm and Mo <100 (ppm). Detection limits shown by hashed out area. Average Au in ppm is shown by the red dashed line.

5.4.2.3. Poly-metallic veins

If the three vein sets (Cononish, Kilbridge and River Vein) are considered together, there is an overall comparable trend in the relative abundance of the pathfinder elements (Ag, As, Sb, Te and W; Figs. 5.9; 5.10). There is some difficulty associated with assessing the geochemical trends at Kilbridge and Beinn Udlaidh due to a lack of sampling in these areas since lower detection limits were high across the assay database (Figs. 5.9; 5.10).

Due to the large amount of data available for the Cononish deposit it is possible to split the dataset by gold grade to establish finer detail in geochemical trends within the vein (Fig. 5.9). With increasing gold grade (>1 to >10 ppm), tellurium (7 to 102 ppm) and silver (11 to 120 ppm) increase in abundance, coupled with a decrease in arsenic (21 to 12 ppm; Fig. 5.9). There is a slight increase in antimony (1 to 2 ppm) with increasing gold grade. Tungsten appears to be unrelated to gold enrichment with little variation in the abundance with gold grade variation.

Throughout the Cononish vein set arsenic decreases with increasing gold and tellurium grade (Fig. 5.11). Veins at Kilbridge have higher arsenic (average 125 ppm) and lower tellurium (<5 ppm, all results below lower detection limit) at low gold grades (<10 ppm) compared to the Cononish deposit. Veins from across the rest of the study area, Beinn Udlaidh (average 160 ppm As, 5.5 ppm Te), Creag Sheileach (average 227 ppm As; 0.4 ppm Te) and River Vein (average 143 ppm As; 7.6 ppm Te), are comparable to each other but have higher arsenic and lower tellurium than the Cononish deposit (<25 ppm As). Coire a'Ghabalach (average 4200 ppm As; 0.1 ppm Te), Sron Garbh (average 3800 ppm As; 1.6 ppm Te) and Glen Orchy (average 550 ppm As; 0.97 ppm Te) veins exhibit much higher arsenic enrichment than other veins in the study area.

High tellurium and low arsenic appear to be the optimum conditions for significant gold endowment in the veins, as seen in the high grade Cononish deposit (average 13.1 ppm; Scotgold Resources Ltd 2012a). This is demonstrated by the association of veins with the highest arsenic enrichment being commonly associated with a low abundance of tellurides and lower gold grades (Figs. 5.9; 5.10).

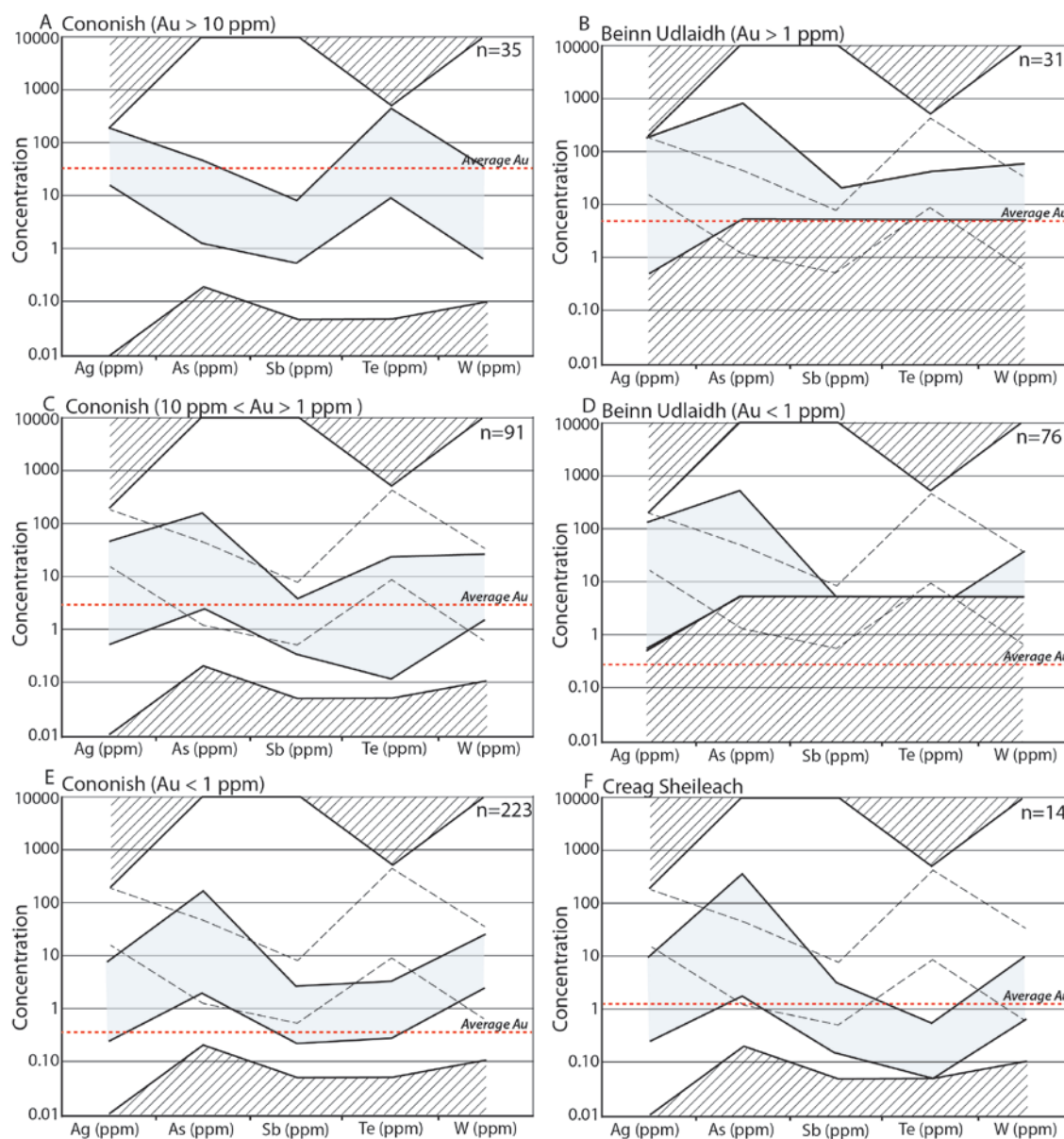


Figure 5.9: Geochemical trends for Cononish set poly-metallic quartz veins. Average Au in ppm is shown by the red dashed line. Black dashed line represents high grade (>10 ppm) gold mineralisation at Cononish. Key gold pathfinder elements are plotted to illustrate variation. Detection limits shown by hashed out area.

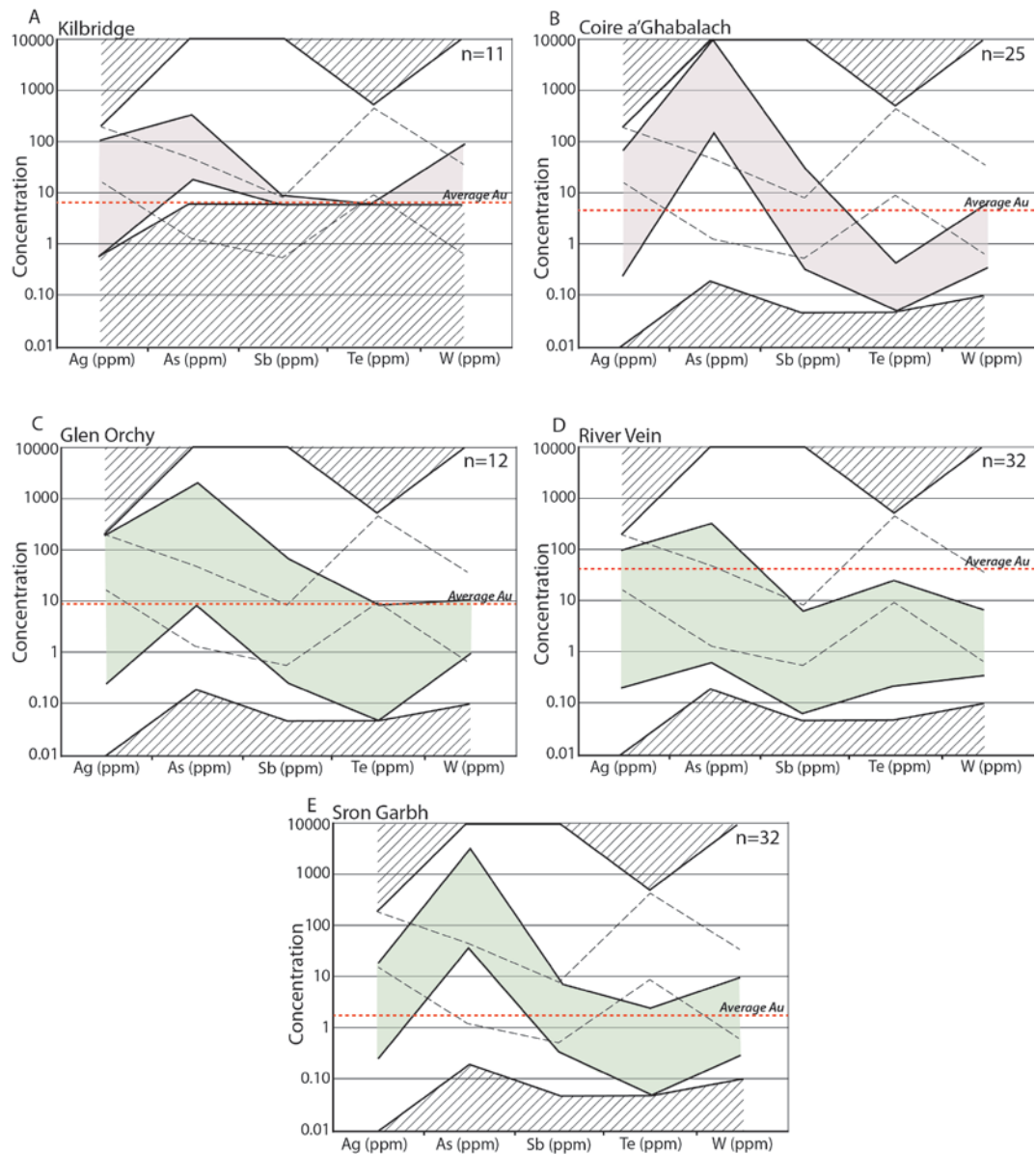


Figure 5.10: Geochemical trends for River Vein (green) and Kilbridge (red) poly-metallic vein sets. Average Au in ppm is shown by the red dashed line. Black dashed line represents high grade (>10 ppm) gold mineralisation at Cononish Key gold. Pathfinder elements are plotted to illustrate variation. Detection limits shown by hashed out area.

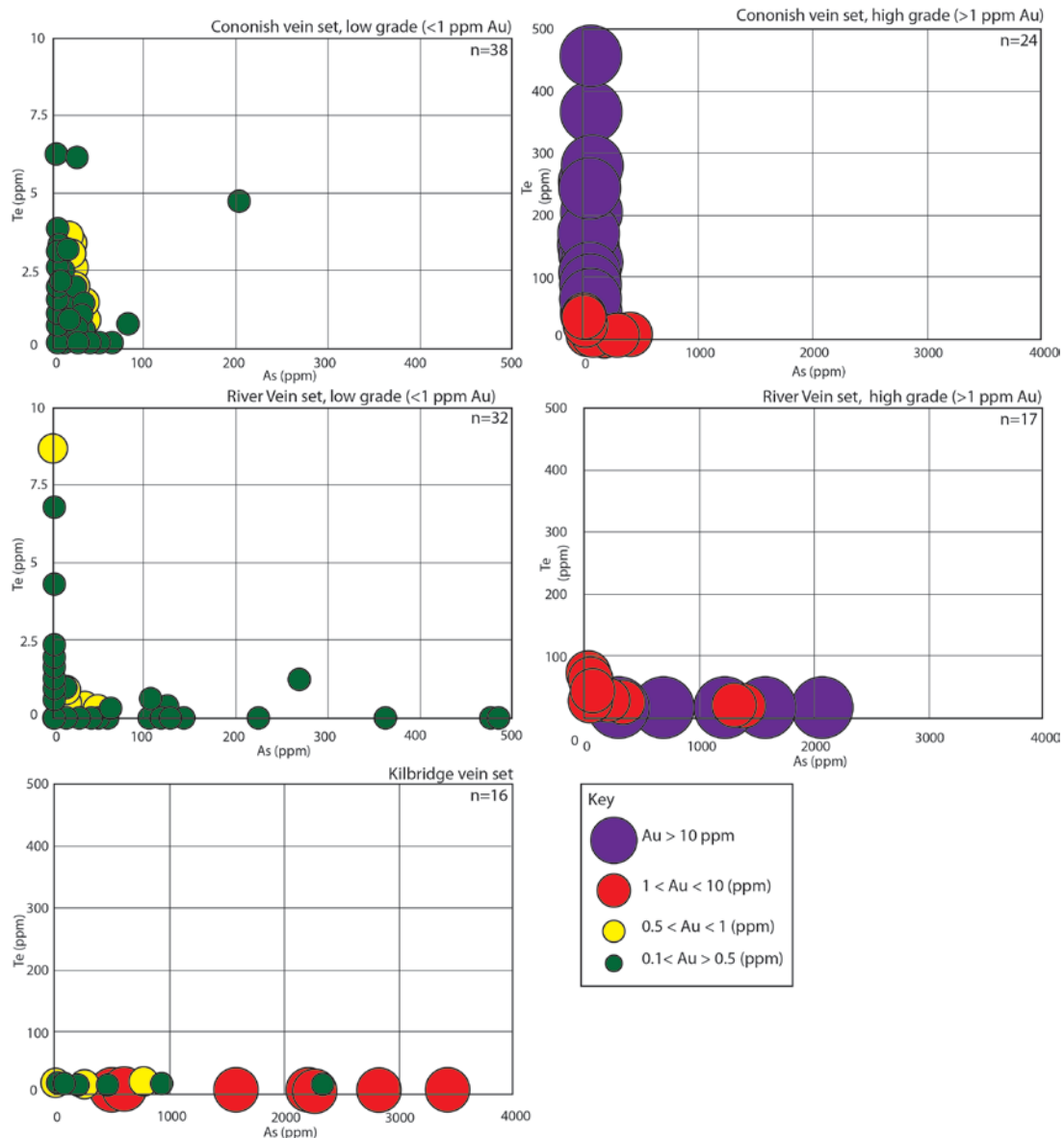


Figure 5.11: As vs. Te plot to show de-coupled nature of arsenic and tellurium at high and low grade within each poly-metallic vein set. Gold grade (ppm) shown by size and colour of the bubbles.

5.4.2.4. Tyndrum Lead Mine-style

There are limited data for the Tyndrum Lead Mine-style mineralisation within the assay database and all of the data have high detection limits (Fig. 5.12). Tyndrum Lead Mine-style mineralisation at Cononish has comparable silver and antimony enrichment to the Tyndrum Lead Mine mineralisation with tellurium and tungsten largely below detection limit (Appendix 5.1). The Tyndrum Lead Mine has much higher arsenic than the Tyndrum Lead Mine-style mineralisation (Fig. 5.12). Tyndrum Lead Mine samples are highly enriched in Pb (up to 2%) and Zn (>1000 ppm) with significant Cu (3000 ppm). Tyndrum Lead Mine style veins at Cononish have comparable Pb and Cu but lower Zn (20 ppm).

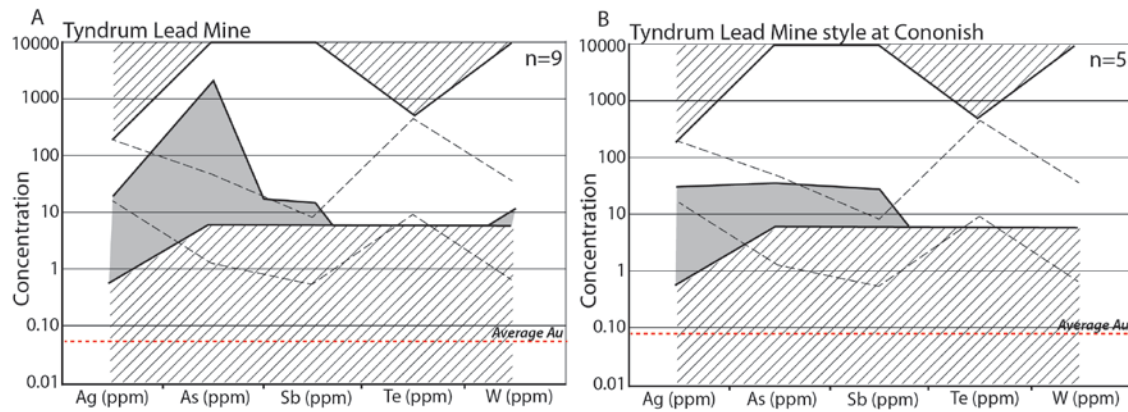


Figure 5.12: Geochemical trends for the Tyndrum Lead Mine and Tyndrum Lead mine style mineralisation at Cononish. Average Au in ppm is shown by the red dashed line. Black dashed line represents high grade (>10 ppm) gold mineralisation at Cononish. Key gold pathfinder elements are plotted to illustrate variation. Detection limits shown by hashed out area.

5.4.3. Whole rock gold/silver ratios

Whole rock Au/Ag ratios for each poly-metallic vein set (Table 5.2) are compared to establish whether there is variation between the vein sets (Fig. 5.13). Gold/silver ratios are calculated from wt. % ratios. Whole rock Au/Ag ratio is considered on veins with >1 ppm gold, a lower cut off value is not given for silver as the silver values in veins with >1 ppm gold are all >0.5 ppm (the lower detection limit; Appendix 5.1).

For the Cononish vein set, the Au/Ag ratio from whole rock geochemistry is generally 0.5-0.25 (Fig. 5.13). The Cononish vein has a range in Au/Ag ratio and the Beinn Udlaidh Main Vein has very little gold with very low Au/Ag ratios (Fig. 5.13). Gold/silver ratios at Beinn Udlaidh may be <0.25 but the upper detection limit of Ag (200 ppm) prevents this being accurately measured.

There is a more limited dataset, at lower grades than the Cononish set, available for the Kilbridge set. Overall the Au/Ag ratio is comparable to the Cononish set, with some variation across the vein set (Fig. 5.13). Kilbridge veins have a Au/Ag ratio close to 0.5 whereas, at the Coire a'Ghabalach vein the Au/Ag ratio is lower (0.25).

The River Vein set exhibits very different Au/Ag ratios to both the Cononish and Kilbridge vein sets (Fig. 5.13). There is greater variation in Au/Ag ratio within the River Vein set than other vein sets and the ratio ranges from 0.25 to 4 (average 1.3).

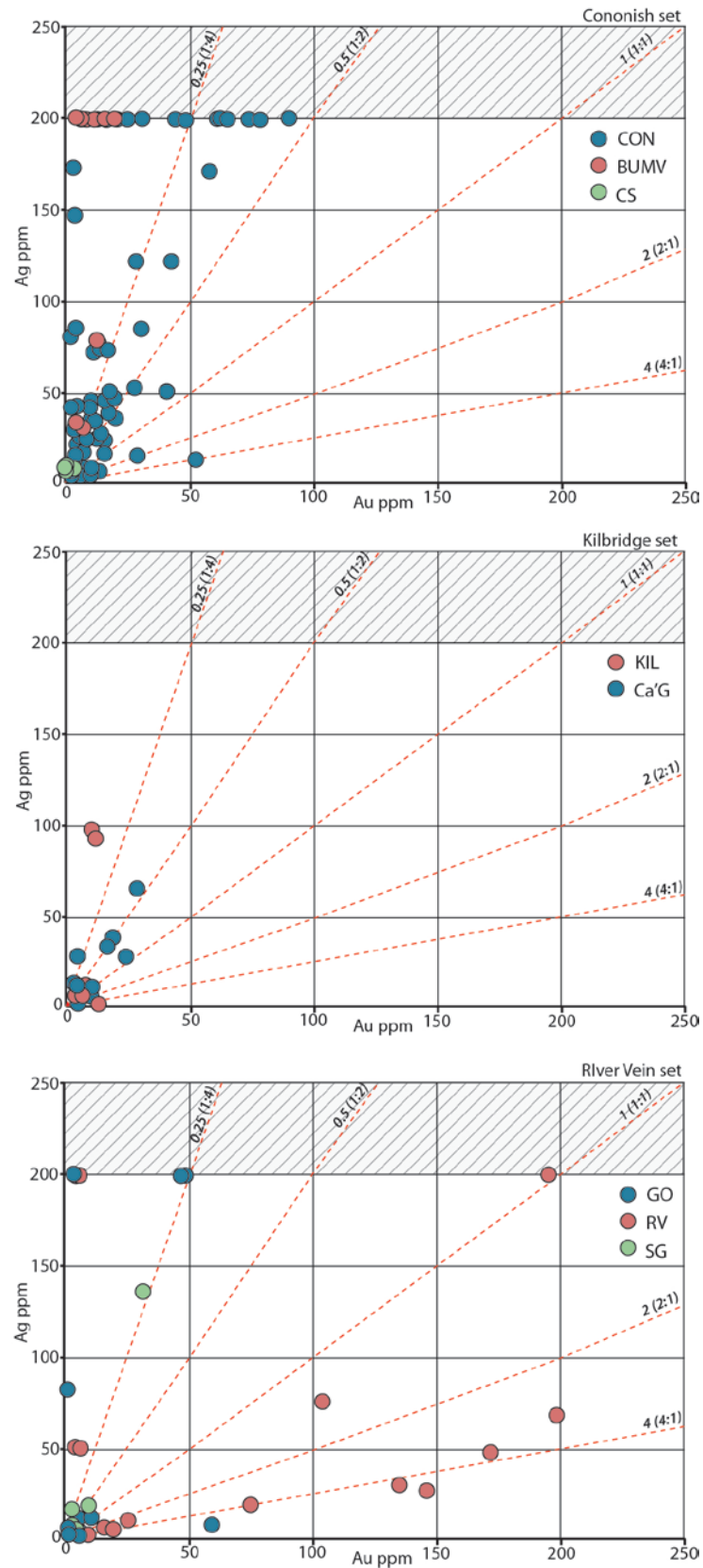


Figure 5.13: Whole rock gold/silver ratios for each vein set as defined by the field and petrographic constraints in Chapter 4. Data from Cononish and Kilbridge sets are comparable but ratios from Glen Orchy show significant variation.

5.4.3.1. Gold/silver ratios in electrum

The relationship between gold and silver in electrum was considered on a small pilot microprobe dataset from gold-bearing poly-metallic quartz vein samples in the Glen Orchy, River Vein and Kilbridge areas (Fig. 5.14; Table 5.3). The range in the Au/Ag ratio in electrum at Glen Orchy is 10-3.4 (9-22.5 wt. % Ag), with electrum in the River Vein area falling into this range (Au/Ag ratio 3.5-5.2; 16.5-22 wt. % Ag; Fig. 5.14). This ratio is comparable to the whole rock Au/Ag ratio (average River Vein set whole-rock Au/Ag ratio = 4; Fig. 5.13). Electrum Au/Ag ratios form a continuous profile and given there is no break in the range of data this suggests there are not two or more chemically different gold mineralisation events. The small dataset at Kilbridge suggests the electrum is more silver-rich than at Glen Orchy with 23-28 wt. % Ag (Au/Ag ratio 3.3-2.8; Fig. 5.14).

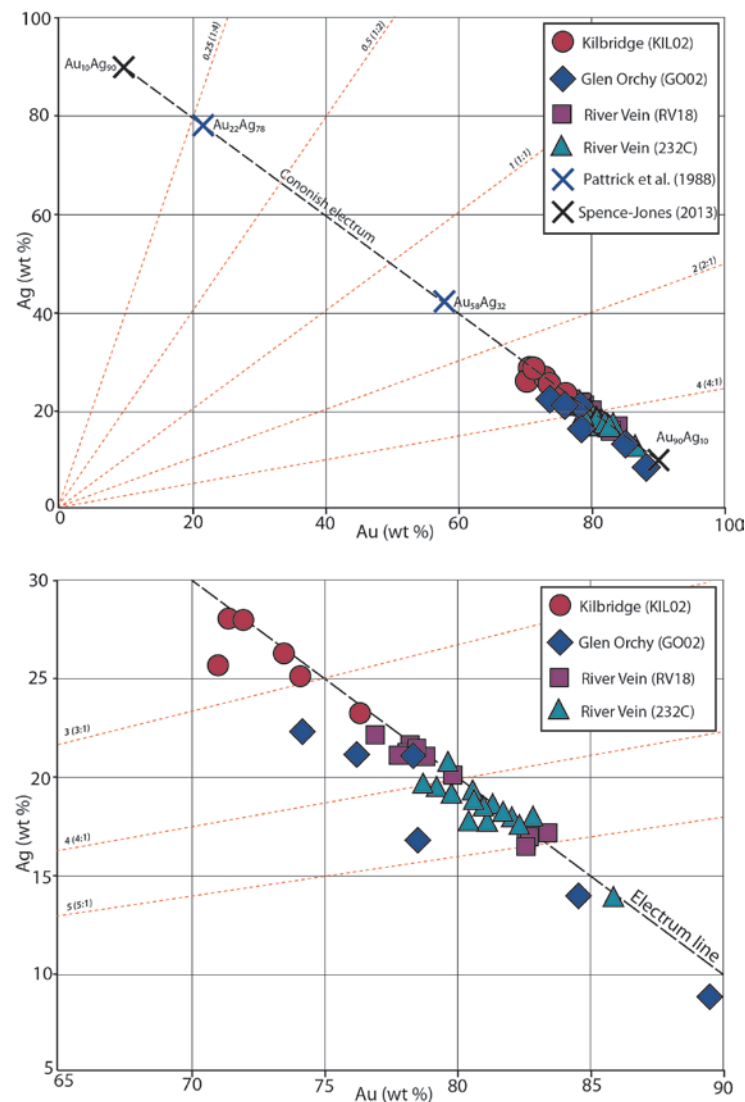


Figure 5.14: Gold/silver ratios for electrum at Glen Orchy, River Vein and Kilbridge. Gold/silver ratios for electrum from Cononish are given; quantitative data from Patrick *et al.* (1988) and semi-quantitative data from Spence-Jones (2013) are given for reference.

Whilst there are no probe data available for the Cononish vein set from this study, existing literature data indicate a different range in electrum Au/Ag ratios at the Cononish deposit than at Glen Orchy (Patrick *et al.* 1988; Spence-Jones 2013). Microprobe data for electrum from Cononish records Ag wt. % of 42-88 wt. % (Au/Ag ratio 1.4-0.1; Patrick *et al.* 1988), semi-quantitative work by Spence-Jones (2013) suggests the range may be as large as 10-90 wt. % Ag in electrum (Au/Ag ratio 9-0.1).

5.4.4. Summary

Whole rock geochemistry demonstrates distinct trends in molybdenite-bordered fractures and gold-bearing poly-metallic quartz veins. The de-coupled nature of Au and Mo within veins is highlighted in Figures 5.6B & D, with a greater correlation seen at lower Mo grade. This could be interpreted to be due to samples likely representing molybdenite-bordered fractures, potentially at depth at Cononish and Sron Garbh, with dilution of the molybdenum grade by the poly-metallic quartz veins. Alternatively the gold-bearing poly-metallic mineralising fluid may carry some molybdenum in the same event.

The molybdenite-bordered fractures are depleted in the gold pathfinders (Ag, As, Sb, Te and W), in particular Sb (Fig. 5.7), compared to the poly-metallic quartz veins. High As (>400 ppm) at Sron Garbh and Te (>10 ppm) in lower grade Mo samples (>1 ppm) at Glen Orchy is interpreted to be related to contamination by cross-cutting poly-metallic quartz veins.

The poly-metallic quartz veins exhibit variation across the three sets (Chapter 4). Cononish high-grade gold veins (>10 ppm Au) have low arsenic (average 12 ppm) and high silver (average 119 ppm) and tellurium (average 102 ppm; Fig. 5.9), no other veins within the Cononish, Kilbridge or River Vein sets have comparable geochemical trends (Fig. 5.9, 5.10). Arsenic and tellurium are decoupled across the study area (Fig. 5.11). At the Kilbridge vein set, high grade gold is enriched in arsenic. The River Vein set, in addition to trending a different direction, has high gold grades (up to 194.6 g/t Au and >200 g/t Ag from >1 kg grab samples; Scotgold Resources Ltd 2011a) with high arsenic (10 to 1000 ppm As) and low tellurium (<50 ppm Te). This could indicate the River Vein set represents a different hydrothermal episode.

Table 5.3 *Electrum data from microprobe analysis from this study*

Location	Sample		Au (wt%)	Ag (wt%)	Total (wt%)	Other elements present (not included in total)
River Vein	232C	1-1	82.9	17.9	100.8	
		1-2	80.8	18.4	99.2	
		2-1	81.2	18.1	99.3	
		2-2	79.3	19.5	98.8	
		3-1	80.8	19.2	100	
		3-2	82.4	17.6	100	
		4-1	80.6	19.4	100	
		4-2	81.2	17.7	98.9	
		5-1	82.3	17.6	99.9	
		5-2	78.9	19.6	98.5	
		6-1	81.7	18.5	100.2	
		6-2	79.9	19.1	99	
		7-1	85.9	13.7	99.6	
		8-1	81.1	18.4	99.5	
		8-2	81.4	18.7	100.1	
		8-3	81.2	18	99.2	
		9-1	80.4	17.7	98.1	
		10-1	82	17.9	99.9	
		11-1	79.7	20.6	100.3	
		12-1	80.7	18.8	99.5	
River Vein	RV18	1-1	78.3	21.6	99.9	
		1-2	78.2	21.3	99.5	
		2-1	78.6	21.5	100.1	
		2-2	78.9	21.2	100.1	
		3-1	82.6	16.5	99.1	
		3-2	82.6	16.8	99.4	
		3-3	83.4	17.2	100.6	
		4-1	77.8	21.2	99	
		4-2	78.2	21.2	99.4	
		5-1	76.9	22.2	99.1	
		6-1	79.9	20.1	100	
Glen Orchy	GO02a	17	89.53	9	98.53	0.4% Cd; 0.5% Fe
		20	74.28	22.52	96.8	0.4% S; 0.3% Cd; 3.4% Fe
		27	76.28	21.38	97.66	0.3% Cd; 1.6% Fe
		28	78.41	21.38	99.79	
		34	84.66	14.12	98.78	
		36	78.4	16.89	95.29	0.3% S; 0.3% Cd; 2.6% Fe
Kilbridge	KIL02a	11	73.58	26.31	99.89	
		12	76.52	23.34	99.86	
		13	74.18	25.19	99.37	
		18	71.94	28.1	100.04	
		19	71.13	25.71	96.84	0.13% S; 0.3% Cd; 1% Fe
		20	71.47	28.15	99.62	

Pyrite-bearing veins have low antimony (<5 ppm), comparable to the molybdenite-bordered fractures, but otherwise fit the quartz-only vein geochemical trend (Fig. 5.8). The Tyndrum Lead Mine has higher arsenic (>200 ppm) than Tyndrum Lead Mine-style mineralisation at Cononish (<50 ppm; Fig. 5.12).

The whole rock Au/Ag ratios suggest mineralisation at Kilbridge and Cononish may be comparable. However, this is not reflected in the quantitative data for electrum, with Kilbridge exhibiting higher Au wt. % in electrum than Cononish. Electrum from Glen Orchy has a higher Au wt. % than quantitatively recorded at Cononish (Patrick *et al.* 1988). This is comparable to whole rock Au/Ag ratios, where the River Vein set is gold-dominated compared to the silver-dominated Cononish and Kilbridge vein sets.

At Cononish, a large amount of silver is within hessite and other tellurides, reflected by the potential for the average whole rock Au/Ag ratio (0.52) to be lower than most of the range of microprobe Au/Ag ratio (0.3-1.8; Fig. 5.15). At Kilbridge, the whole rock and microprobe Au/Ag ratios are almost identical (Fig. 5.15; whole rock 2.9; microprobe 2.8). This suggests there is little tellurium, taking up silver, in the system and most silver is with gold, as electrum. Within the River Vein set, GO02 with low Te (0.18 ppm) sits closer to the 1:1 line than RV18 (Te = 8.7 ppm; Fig. 5.15).

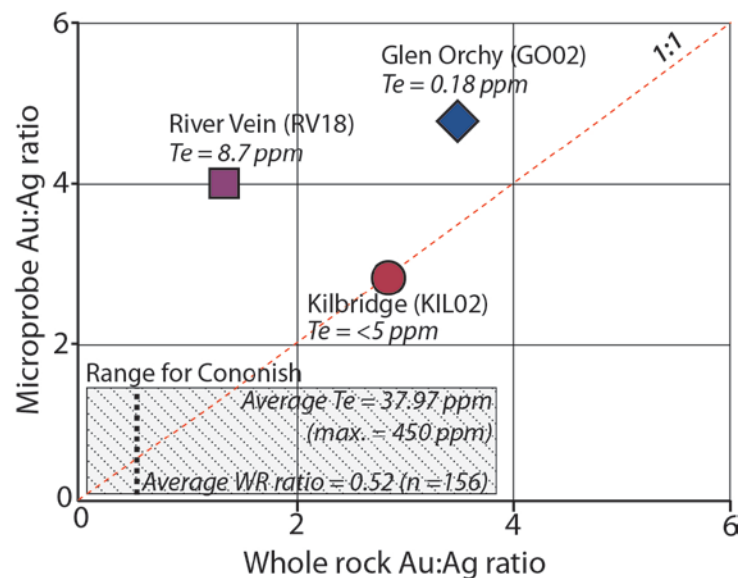


Figure 5.15: Whole rock vs. Microprobe Au/Ag ratios for key samples from each vein set with Cononish set samples showing microprobe data from Patrick *et al.* (1988) and whole rock data from this study.

5.5. Discussion

5.5.1. Regional geochemical anomalies

5.5.1.1. Literature data

The key gold pathfinder elements considered in this study (Ag, As, Bi, Sb, Te & W) have been variably examined by previous workers to determine gold distribution in the Scottish Dalradian Supergroup. In the Tyndrum area, Plant *et al.* (1989) determined the arsenic, antimony and bismuth anomalies in rock samples from the metasedimentary sequence and stream sediment data for the area is reported in Plant *et al.* (1997). It is noted, that while the potential for glacial displacement of geochemical anomalies in soil and stream sediment is high in the Grampian Highlands, there is a good correlation between stream sediment and rock samples and the displacement of geochemical anomalies is generally <2 km (Plant *et al.* 1997).

A stream sediment bismuth anomaly is recorded to the east of the Tyndrum Fault, interpreted to be due to the presence of bismuth-bearing minerals (Corkhill *et al.* 2010), which serve as a pathfinder for geochemical exploration (Plant *et al.* 1990, 1997). The anomaly surrounds the Tombuie and Calliachar-Urlar Burn gold occurrences, which are distinguished by bismuth-bearing minerals in the veins. The bismuth stream sediment anomaly appears to truncate at the Tyndrum Fault and only minor enrichment occurs to the west of the Fault, reflected in the lack of bismuth-bearing minerals in veins in this study. Antimony is not enriched in stream sediment data in the Tyndrum area except as minor anomalies (Plant *et al.* 1997), but there is an anomaly associated with Tyndrum Lead Mine mineralisation. Arsenic stream sediment anomalies have a footprint comparable to bismuth, with some spatial association with minor antimony anomalies (Plant *et al.* 1997; Corkhill *et al.* 2010).

5.5.1.2. This study – stream sediment data

In the Tyndrum area, new data from stream sediment exploration are mapped to establish if geochemical anomalies in the Tyndrum area are comparable with anomalies noted by previous workers (Plant *et al.* 1989, 1990, 1997; Corkhill *et al.* 2010), to establish whether additional anomalies can be identified and how anomalies compare to the distribution of mineralised vein occurrences.

Gold shows higher enrichment in stream sediment data than any other element in the study area (Fig. 5.16). The gold enrichment is generally 100-1000 times background crustal

enrichment (0.0013 ppm; Rudnick & Gao 2002); rare samples with >1000 times background are recorded. There is little structural control on the distribution of gold in stream sediments, with neither the Tyndrum Fault nor Cruachan Lineament placing strong controls on the distribution. Silver shows consistent distribution across the area with 1-10 times background crustal abundance (0.056 ppm; Rudnick & Gao 2002; Fig. 5.16). As with gold, the major structures in the area do not appear to control the distribution of silver. Gold/silver ratios in stream sediment data generally follow the electrum Au/Ag ratio with highest values in Glen Orchy and low ratios near Cononish.

Arsenic follows a similar pattern to silver with 1-10 times crustal abundance (Fig. 5.16; 2.5 ppm; Rudnick & Gao 2002). Samples with >25 ppm arsenic occur in the vicinity of the Tyndrum Fault, particularly to the south of the fault, suggesting the fault places some control on the distribution of arsenic. This is supported by observations in Plant *et al.* (1989) who noted greater arsenic enrichment in Argyll Group lithologies found to the south of the Tyndrum Fault. The correlation between lower grade gold and arsenic, seen in the Kilbridge and River Vein sets compared to Cononish (Figs. 5.9; 5.10), is not reflected in the distribution of arsenic in stream sediment data (Fig. 5.16).

There are no bismuth anomalies recorded in the Tyndrum area, all enrichment is <10 times crustal abundance (Fig. 5.16; 0.18 ppm; Rudnick & Gao 2002). The area is largely depleted in bismuth compared to the crustal average and enrichment is restricted to rivers in the Auchtertyre and Cononish areas. There is no bismuth enrichment to the north of the Tyndrum Fault; this supports Corkhill *et al.* (2010) who report the bismuth anomaly to be truncated at the Tyndrum Fault. There is bismuth enrichment within the Ardrishaig Phyllite Formation (lateral equivalent of the Ben Lawers Schist), which could be invoked to account for the bismuth anomaly seen in Auchtertyre (Plant *et al.* 1989).

Antimony is sporadic, most samples have 1-10 times crustal abundance (Fig. 5.17; 0.2 ppm; Rudnick & Gao 2002). There is depletion of antimony in the Glen Orchy area with lower antimony here than elsewhere in the study area (Fig. 5.17), comparable to the antimony depletion in molybdenite-bordered fractures (Fig. 5.7). This suggests that while there is no clear correlation between either lithology or faults and antimony enrichment, areas of antimony depletion may be prospective for molybdenite mineralisation but not gold.

Selenium is enriched throughout the study area, samples with >10 times crustal abundance (0.13 ppm; Rudnick & Gao 2002) are sporadic to the north of the Tyndrum Fault but to

the south of the fault, selenium enrichment is dominated by values >1.3 ppm (100 times crustal abundance; Fig. 5.17).

Tellurium is highly enriched across the study area (Fig. 5.17; >0.05 ppm; Wedepohl 1995). The distribution of tellurium cannot easily be tied to the poly-metallic vein geochemical trends, Cononish has higher tellurium than other veins in the area, but distribution across the study area is consistent. There does not appear to be a strong lithological or structural control on the distribution of tellurium in the study area.

Tungsten is limited in the study area, much of the area is depleted compared to background levels (1 ppm; Rudnick & Gao 2002) and there does not appear to be structural or lithological control on the distribution. This fits with the trends seen across the defined vein sets (Section 5.4.2) with all vein sets generally have <10 ppm W. Higher W (<100 ppm W) is only seen at Cononish, Kilbridge and Beinn Udlaidh (Figs. 5.9; 5.10). The stream sediment data reflects this with greatest enrichment near Cononish and at the base of Beinn Udlaidh; enrichment in Auchtertyre is unexplained.

Lead is enriched 1-10 times crustal abundance (11 ppm; Rudnick & Gao 2002) throughout the Tyndrum area (Fig. 5.18). Zinc has a more limited enrichment than lead with most samples >72 ppm Zn (crustal abundance; Rudnick & Gao 2002). The distribution of zinc is interpreted to be controlled by streams draining areas with veins containing sphalerite (Fig. 5.18). This is demonstrated by 100 times crustal abundance at the base of the Tyndrum Lead Mine, which is the greatest volume of sphalerite mineralisation in the study area.

Molybdenum in the study area is limited in stream sediment anomalies, 98% of the data has <10 times crustal abundance (0.8 ppm Mo; Rudnick & Gao 2002) with 77% at <1 time crustal abundance.

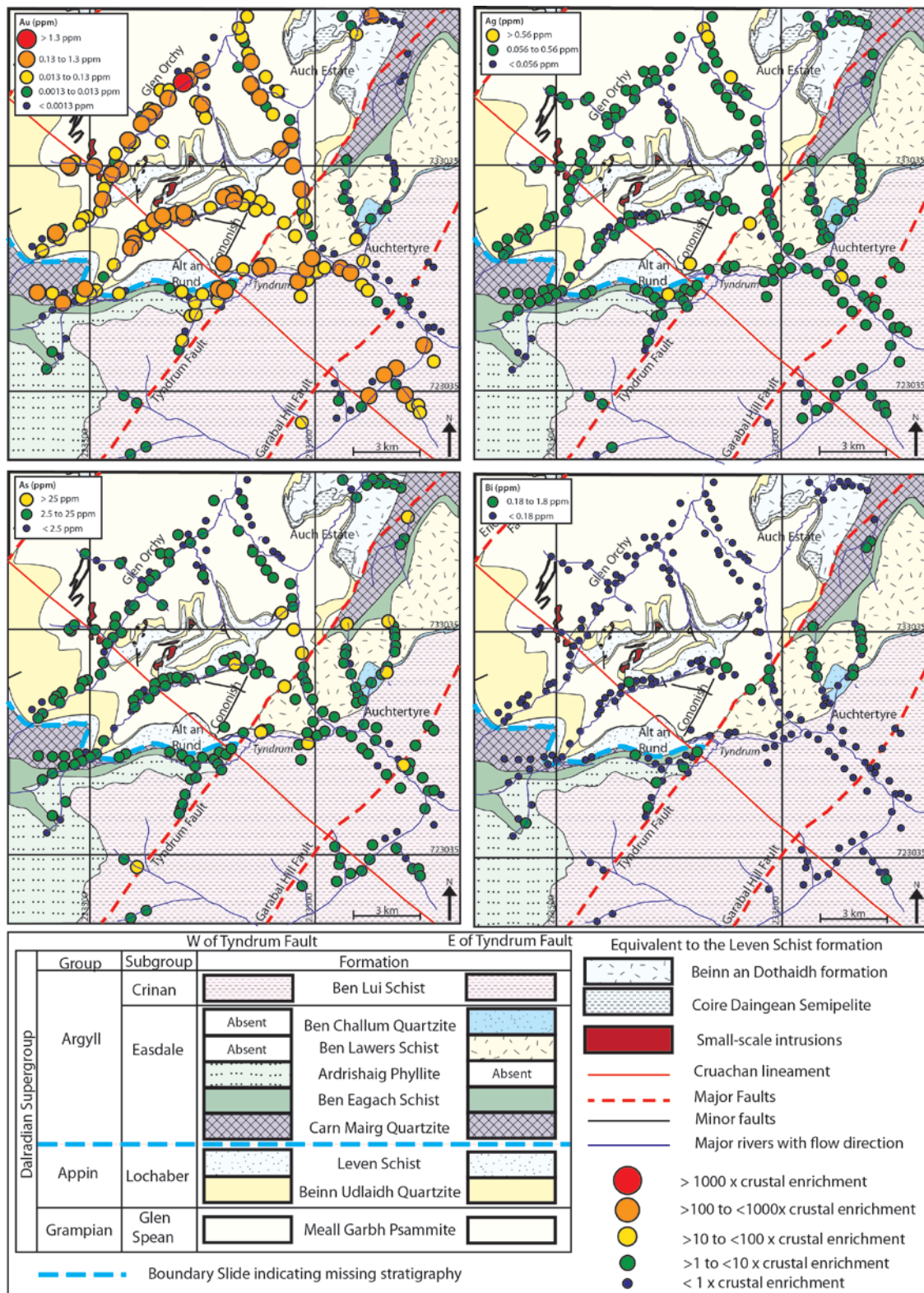


Figure 5.16: Au, Ag, As and Bi stream sediment results for the Tyndrum area. Data from Scotgold Resources Ltd's stream sediment sampling program. Elements were chosen due to their importance as gold pathfinder elements as illustrated by Plant *et al.* (1997). Samples are taken in tributaries running into the main rivers.

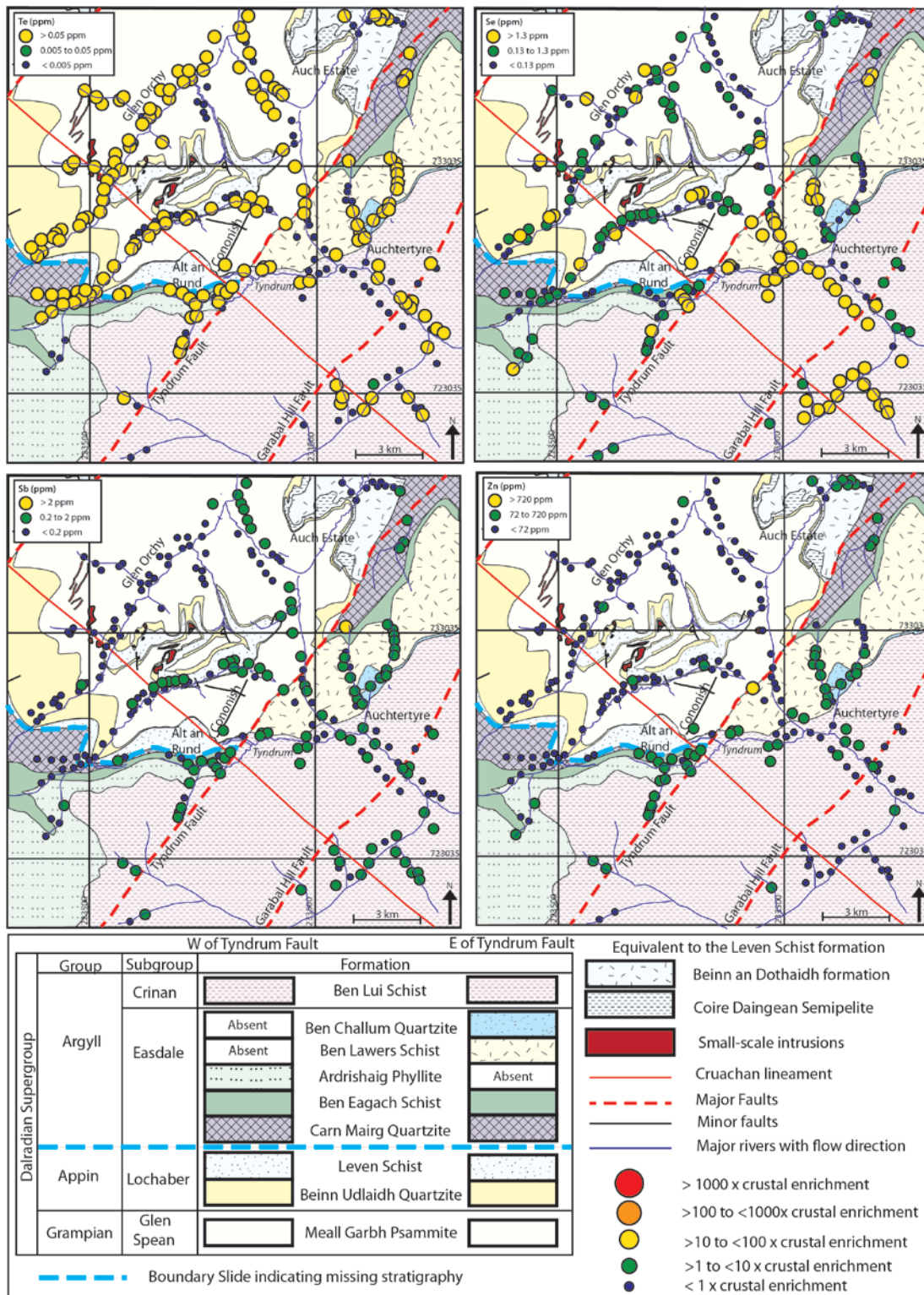


Figure 5.17: Te, Se, Sb and Zn stream sediment results for the Tyndrum area. Data from Scotgold Resources Ltd's stream sediment sampling program. Elements were chosen due to their importance as gold pathfinder elements as illustrated by Plant *et al.* (1997).

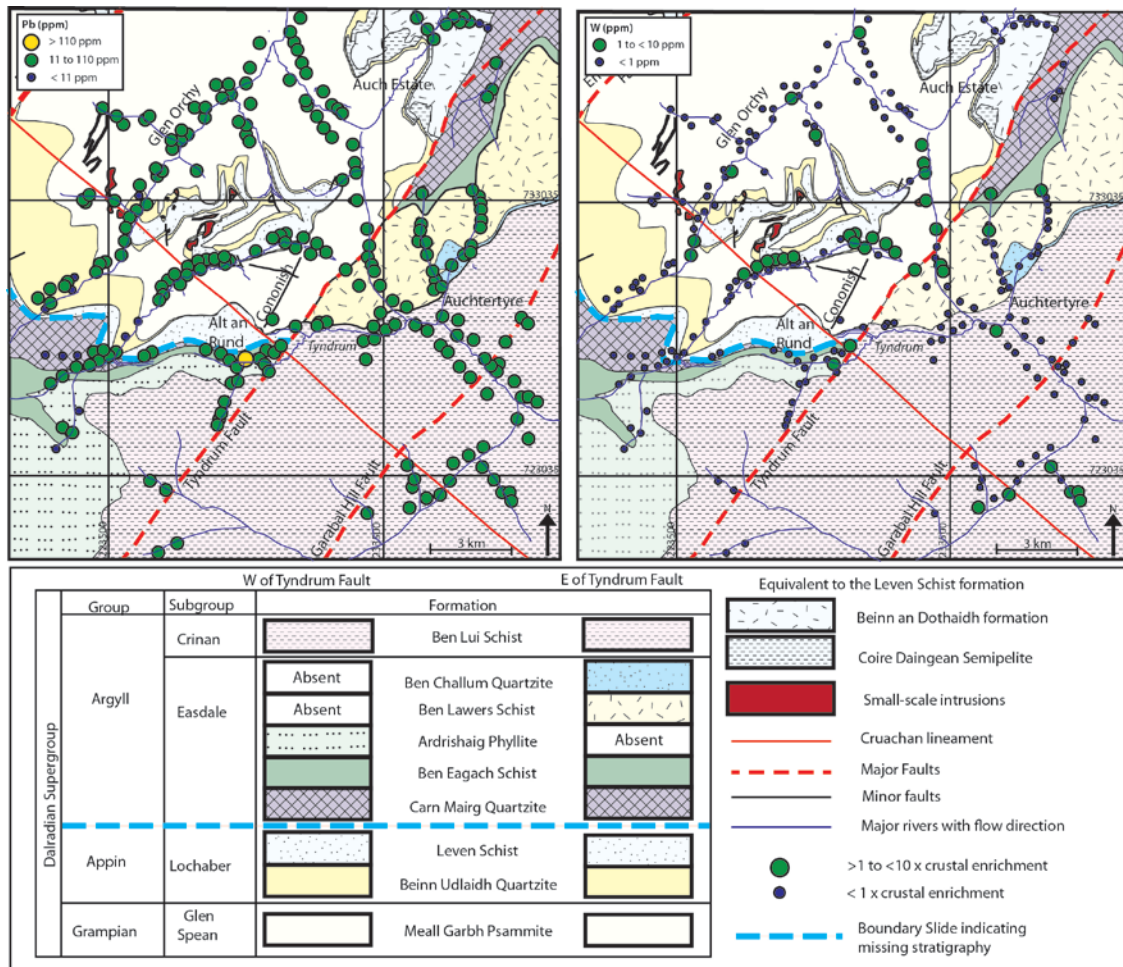


Figure 5.18: Pb and W stream sediment results for the Tyndrum area. Data from Scotgold Resources Ltd's stream sediment sampling program. Elements were chosen due to their importance in the mineralisation in the Tyndrum area.

5.5.1.3. Implications of results

High gold, silver and tellurium are important for mapping the distribution of the highest grade samples but high arsenic may also be an important pathfinder for lower grade gold. This study suggests when looking for large high grade gold-bearing poly-metallic veins it may be useful to discriminate based on high tellurium (>5 ppm) and low arsenic (<25 ppm).

The low enrichment of gold, to the south of the Tyndrum Fault, suggests the Auchtertyre area has limited prospectivity for gold mineralisation and while gold-bearing veins are found in the Auch Estate more sampling is required to establish prospectivity. Since silver shows greatest enrichment near Cononish, it is suggested that high silver in stream sediments reflects high silver in veins. This suggests Alt Ghamhain has potential to be host to gold-bearing poly-metallic quartz veins, with a high silver content in electrum, comparable to the Beinn Udlaidh Main Vein mineralisation.

Selenium and arsenic are closely related to lithology suggesting a lithological control on the distribution of these elements. The distribution of bismuth is comparable to known anomalies and appears largely unrelated to the distribution of gold mineralisation in the Tyndrum area suggesting it is controlled by lithology. To the south of the fault, the stratigraphy is dominated by Argyll and Southern Highland Group lithologies which are characterised by increased shales and turbidites (Stephenson *et al.* 2013) with higher bismuth and arsenic (Plant *et al.* 1989). Selenium also appears to be controlled by lithology; high selenium to the south of the Tyndrum Fault is coincident with a change to Argyll Group lithology. The amount of selenium in Argyll Group lithology is unconstrained by this study or previous workers.

While zinc in stream sediments is a useful pathfinder for sphalerite hosted within the poly-metallic quartz veins (high zinc in stream sediments is closely linked to veins with sphalerite in the paragenesis), the Tyndrum Lead Mine-style mineralisation also has abundant sphalerite. Therefore zinc anomalies cannot be used in isolation as a pathfinder for poly-metallic quartz veins. Antimony depletion in stream sediment data is a potential pathfinder for molybdenite-bordered fractures, the lowest antimony in the area is coincident with molybdenite-bordered fractures in Glen Orchy.

5.5.2. Gold/silver ratios in poly-metallic veins

While whole rock geochemical trends across the three vein sets suggest there is variation between vein sets, with the Cononish deposit highly enriched in tellurium compared to the Kilbridge and River Vein sets. The electrum Au/Ag ratios are highly variable between vein sets (Fig. 5.14). The Kilbridge vein set has a comparable whole rock Au/Ag ratio to the Cononish set whereas, the River Vein set shows atypical Au/Ag ratios (Fig. 5.13; 5.14). Whole rock Au/Ag ratios vary across the poly-metallic vein sets; the whole rock ratios are interpreted to be representative of the full range of ratios within each vein but may not reflect the Au/Ag ratio within electrum. The discrepancy between the two values is interpreted to be due to silver within hessite and other silver-bearing tellurides in some veins (Fig. 5.15). There are not multiple distinct populations in the microprobe electrum Au/Ag ratios within any of the veins. This is interpreted to suggest there are not multiple gold mineralisation events; within each poly-metallic vein set a continuum of a single gold-bearing hydrothermal event is represented. It is possible however, that the poly-metallic vein sets represent different hydrothermal events, supported by the variation in Au/Ag

ratios, differences in arsenic and tellurium enrichment and in the vein trend and mineralogy between the Cononish, Kilbridge and River Vein sets.

5.5.2.1. Gold/silver ratios of other gold deposit types

The range in whole rock Au/Ag ratios at the Cononish deposit is not typical of any classic gold deposit type. Given the 4 km proposed depth of formation for the deposit (Curtis *et al.* 1993), orogenic, reduced intrusion-related or porphyry deposit types are possible genetic models (Fig. 5.19), but as discussed in Chapter 2, the Cononish deposit has characteristics of orogenic, reduced intrusion-related and epithermal deposit types. The whole-rock ratios at the silver-dominated Cononish deposit are atypical of orogenic gold deposits; in orogenic gold deposits average Au/Ag ratios are 1-10 (Fig. 5.19; Groves *et al.* 1998). The Au/Ag ratio at Cononish suggests the deposit has anomalously high silver, compared to orogenic, reduced intrusion-related and epithermal deposit types. This demonstrates the distinct nature of the Cononish deposit and therefore argues a new model is required for the deposit (Chapter 2).

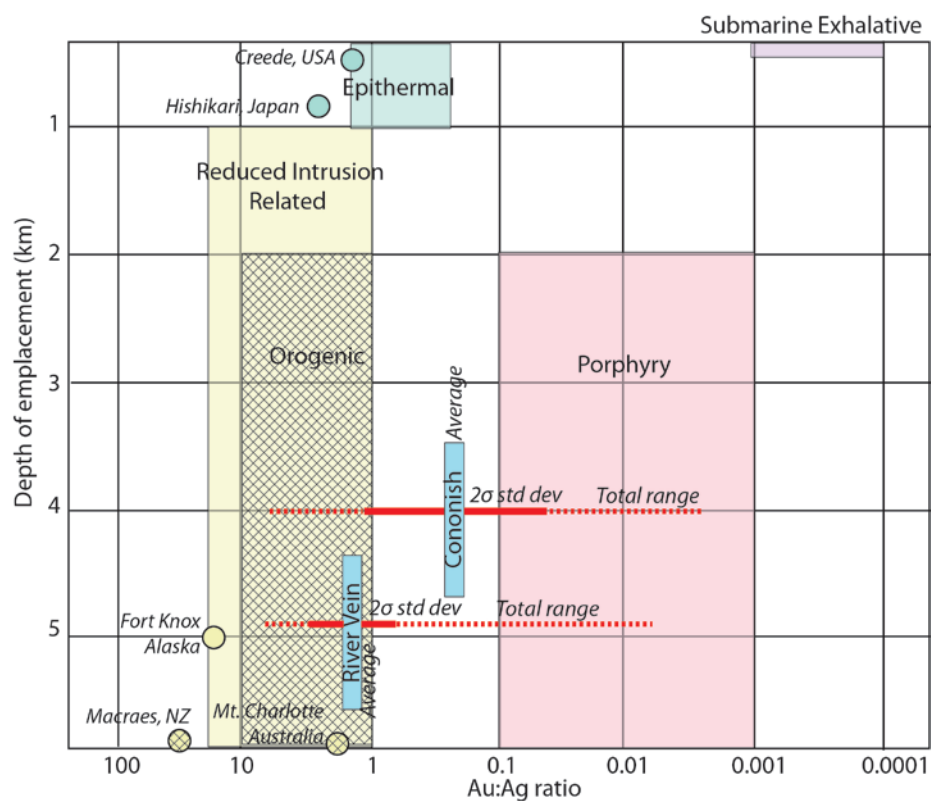


Figure 5.19: Whole rock Gold/silver ratios vs. depth of formation for major gold deposit types compared to data from the Cononish deposit and River Vein set. The River Vein set depth of emplacement is not constrained and is shown deeper than the Cononish deposit for clarity on the diagram. All deposit gold/silver ratios and depths (except reduced intrusion-related) from Groves *et al.* (1998). Data for reduced intrusion related deposit type from Hart & Goldfarb (2005). Individual deposit data from the Centre for Exploration Targeting, Australia's Ore Samples Normalised to Average Crustal Abundance project.

Variation between the poly-metallic quartz veins could be interpreted to represent differences in the source of metals and mineralising fluids. Two distinct groups are defined by the Au/Ag ratios and whole rock geochemical trends.

1. Cononish style – High grade gold veins (>10 ppm Au) with low Au/Ag ratios (0.25), high tellurium (102 ppm) and low arsenic (12 ppm).
2. River Vein style – Including Kilbridge set veins, have variable gold grade (>10 ppm to <1 ppm Au) with high Au/Ag ratios (1.3), low tellurium (3 ppm) and high arsenic (1500 ppm).

The River Vein style mineralisation could be interpreted to represent gold sourced during metamorphism of the sedimentary pile. Diagenetic pyrite is enriched in gold and arsenic (up to 1000 x background; Large *et al.* 2012) with variable enrichment in silver, molybdenum and tellurium. Sediments enriched in diagenetic pyrite have been proposed as sources of gold and other metals for orogenic gold deposits, with metals released during metamorphism (Pitcairn *et al.* 2010; Gaboury 2013). This study suggests gold and other metals, in particular arsenic, in the River Vein-style mineralisation could be sourced from the sedimentary pile, potentially during Grampian Event metamorphism. Molybdenum enrichment in the River Vein area may represent the presence of sediments at depth enriched in molybdenum prior to Grampian metamorphism. The low tellurium in River Vein-style mineralisation could be interpreted to suggest the sedimentary pile was not enriched in tellurium before metamorphism.

The Cononish-style mineralisation has higher silver and tellurium within the veins and cannot easily be accounted for with a metamorphogenic model. Following the model of Large *et al.* (2012) the release of metals from diagenetic pyrite under metamorphic conditions, tellurium is dispersed into the metamorphosed sediments and not concentrated into veins. Given the proximity of the Cononish deposit to the Tyndrum Fault, it could be proposed the fault is tapping fluids from depth, potentially from a concealed intrusion enriched in tellurium \pm silver.

These models can account for the discrepancy between the age of peak metamorphism (*c.* 475-470 Ma; Chew & Strachan 2014) and the current age of mineralisation for the Cononish deposit (410 \pm 14 Ma; $^{40}\text{Ar}/^{39}\text{Ar}$ K-feldspar; Treagus *et al.* 1999). If the Cononish deposit has a magmatic source, it is expected to be the same age as the post-orogenic granite suite (433 \pm 1.8 Ma to 408 \pm 1.8 Ma; Neilson *et al.* 2009; Conliffe *et al.* 2010; Chapter

3); geochronology of the hydrothermal events in the Tyndrum area is addressed in Chapter 7.

5.5.3. Comparison to gold deposit models

As discussed in Chapter 2, the Cononish deposit cannot be easily attributed to any of the traditional gold deposit types; orogenic, epithermal or reduced intrusion-related gold. The geochemical trends in the key pathfinder elements (Au, Ag, As, Te and W) and other elements of interest (Bi, Sb, Mo, Pb and Zn) at the Cononish deposit are compared to trends in orogenic, epithermal and reduced-intrusion related deposit types (Fig. 5.20).

Despite having similar Au/Ag ratios to some epithermal deposits the Cononish deposit has a different geochemical trend to all types of epithermal deposit (low, intermediate and high; Hedenquist *et al.* 2000). The Cononish deposit has significantly higher Mo, Te, Au and Bi than any of the epithermal deposit types (Fig. 5.20) and lower As. River Vein-style mineralisation has a comparable trend to the Hishikari low sulphidation epithermal deposit but exhibits higher Te and Au (Fig. 5.20).

The Cononish deposit also exhibits different geochemical trends to reduced intrusion-related deposits. The Cononish deposit has anomalously high Ag, Mo, Te and slightly higher Au compared to the Fort Knox deposit, Alaska (Fig. 5.20). The River Vein-style mineralisation has anomalously high As, Ag and Au compared to the reduced-intrusion related deposit type (Fig. 5.20).

Geochemical trends at both the Cononish deposit and in River Vein-style mineralisation are most comparable to the orogenic gold deposits (Fig. 5.20). River Vein-style gold mineralisation falls into the range of values for all elements except Pb (Fig. 5.20). The Cononish deposit has anomalously low As and high Te, Mo and Bi compared to the typical trend for orogenic gold deposits (Fig. 5.20). High molybdenum at the Cononish deposit could be interpreted to be related to the potential presence of early molybdenite-bordered fractures at depth. However, given River Vein-style mineralisation has comparable molybdenum to orogenic gold deposits this suggests Cononish-style mineralisation has a molybdenum-bearing mineralising component to the gold-bearing fluids. Bismuth, \pm Sb, W, Pb, Zn, Te, As and Ag, are commonly enriched in gold-bearing magmatic-hydrothermal deposits (porphyry and epithermal style), interpreted to form from fluids released from felsic to intermediate magmas (Richards 2009; Tomkins 2013). The high tellurium and silver in Cononish-style mineralisation compared to orogenic gold deposits could be interpreted to indicate a magmatic component to mineralising fluids, supported by stable

isotope evidence (Curtis *et al.* 1993). This study suggests metals in the Cononish deposit are sourced, in part, from fluids released from a felsic intrusion, potentially the Lochaber Batholith, at depth in the Tyndrum area (Patrick *et al.* 1988; Neilson *et al.* 2009) but the Cononish deposit is not a reduced intrusion-related gold deposit (Fig. 5.20).

5.5.4. Potential geochemical criteria for exploration

Molybdenite-bordered fractures are shown to be a structurally and chemically distinct hydrothermal event in the Tyndrum area (Fig. 5.6B & D). Geochemical analysis of polymetallic vein sets, in conjunction with stream sediment mapping, indicates high tellurium and silver are important for high-grade gold mineralisation in the Tyndrum area. There is correlation between arsenic and gold in the Kilbridge and River Vein sets. In the Kilbridge and River Vein sets, high grade gold with high arsenic is associated with electrum with a high Au/Ag ratio, whereas, high-grade gold in the Cononish set has low Au/Ag ratios with high tellurium and low arsenic. This suggests there are two gold-bearing hydrothermal events, Cononish- and River Vein-style mineralisation. River Vein-style mineralisation can be more easily classified as an orogenic gold deposit driven by fluids released during metamorphism. The Cononish-style mineralisation suggests a magmatic origin may be likely, supported by stable isotope and fluid inclusion microthermometry (Curtis *et al.* 1993). The Tyndrum Fault has the potential to act as a fluid pathway and the proximity of the Cononish deposit to the fault is interpreted to suggest a high fluid flux, potentially carrying fluids from further afield or from greater depth than seen in the River Vein-style mineralisation.

The stream sediment profiles suggest all of the Tyndrum area is prospective for gold but the structural control of the Tyndrum Fault and associated splays is likely to be important for high grade gold mineralisation. The use of stream sediment sampling to map areas of high prospectivity is potentially a very powerful tool in the Tyndrum and regional area by tracing tellurium. Exploration should be focussed in areas with high gold and silver with tellurium for deposits similar to Cononish. High arsenic anomalies in the stream sediment data may have potential as a tracer for gold mineralisation as seen at Kilbridge and River Vein.

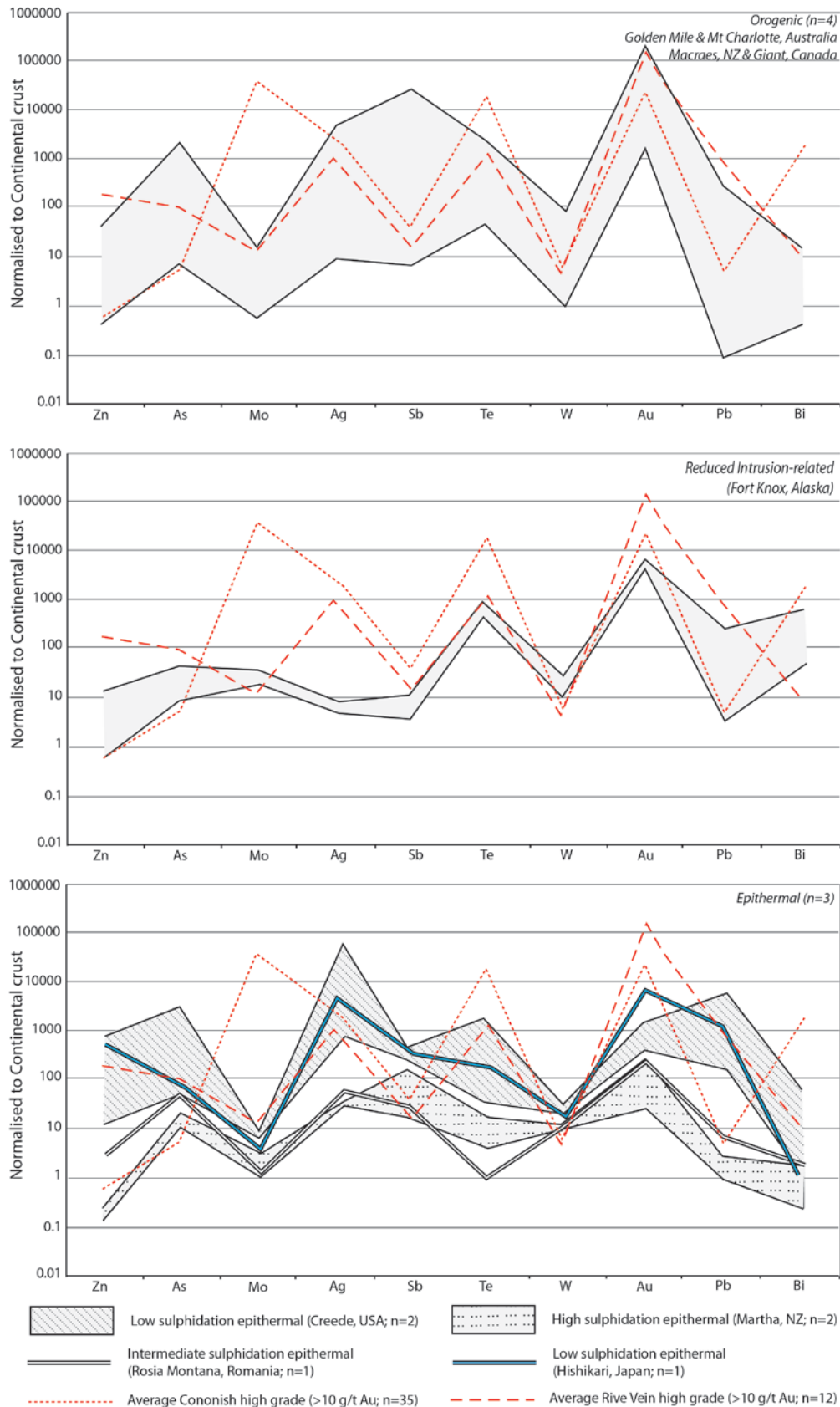


Figure 5.20: Geochemical trends for the three major deposit types considered potentially comparable to the Cononish deposit (see Chapter 2 for further details). Data downloaded from the Centre for Exploration Targeting, Australia's Ore Samples Normalised to Average Crustal Abundance project.

5.6. Conclusions

This chapter work provides evidence that multiple hydrothermal events are recorded in the Tyndrum area, supporting field and petrographic constraints (Chapter 4). The identification of high tellurium and low arsenic in Cononish-style mineralisation gives potential criteria for gold exploration in the Tyndrum and wider regional area. Key conclusions from this chapter can be summarised as:

1. The poly-metallic gold-bearing quartz veins and molybdenite-bordered fractures represent at least two distinct hydrothermal events. Molybdenum enrichment in the whole-rock geochemical dataset at Cononish and Sron Garbh may suggest there are molybdenite-bordered fractures at depth but a molybdenum-bearing component to the gold mineralising fluids cannot be excluded. Molybdenum mineralisation is related to antimony depletion, recognised in the stream sediment data, and this has potential as exploration criteria for molybdenum in the Tyndrum area.
2. The gold-bearing poly-metallic veins may not all represent the same hydrothermal event. The Cononish set has higher tellurium and silver and lower whole-rock and electrum Au/Ag ratios than the Kilbridge and River Vein sets. Two gold mineralisation styles are proposed for the poly-metallic quartz veins; Cononish-style, characterised by high tellurium, low arsenic and Au/Ag ratios, and River Vein-style (including the Kilbridge vein set) characterised by high arsenic, Au/Ag ratios, and low tellurium.
3. Whole rock Au/Ag ratios in Cononish-style mineralisation do not match the Au/Ag ratios of any of the classic gold deposit models (orogenic, reduced-intrusion related and epithermal). This is supported by comparison of the geochemical trends at Cononish to the classic gold deposit models. The Cononish deposit has anomalously high tellurium and low arsenic compared to the orogenic gold deposit type and cannot be easily classified as orogenic.
4. River vein-style mineralisation has Au/Ag ratios within the range for orogenic and reduced intrusion-related gold deposits but has distinct variation in the geochemical trend compared to the reduced intrusion-related deposits. The River Vein-style mineralisation has comparable geochemical trends to the orogenic gold deposit type.
5. While epithermal and reduced-intrusion-related models are excluded as potential models for the genesis of gold mineralization in the Tyndrum area, the orogenic gold

deposit type cannot be excluded. The Cononish deposit does not fit the orogenic gold model however; River Vein-style mineralisation is more comparable to the orogenic gold geochemistry trends and Au/Ag ratios. Therefore, an orogenic model cannot be excluded for all gold mineralisation in the area.

6. This study proposes there are multiple mineralisation events recorded in the Tyndrum area, early molybdenite- and later gold-mineralisation of two styles, Cononish- and River Vein-style. This study suggests molybdenite- and River Vein-style gold mineralisation may be metamorphogenic in origin with metals in the mineralisation sourced from the metamorphic succession. The Cononish-style mineralisation has high tellurium and more characteristics in common with their being a magmatic component to the mineralisation and here it is suggested Cononish-style mineralisation is related to post-orogenic intrusions in the Dalradian Supergroup.

Chapter 6

How the Neoproterozoic S-isotope record illuminates the genesis of vein gold systems: an example from the Dalradian Supergroup in Scotland

This chapter is published as a paper in *Ore deposits in an Evolving Earth*, a Geological Society of London Special Publication

Abstract: The genesis of quartz vein-hosted gold mineralisation in the Neoproterozoic–early Palaeozoic Dalradian Supergroup of Scotland remains controversial. An extensive new dataset of S-isotope analyses from the Tyndrum area, together with correlation of the global Neoproterozoic sedimentary S-isotope dataset to the Dalradian stratigraphy, demonstrates a mixed sedimentary and magmatic sulphur source for the mineralisation. $\delta^{34}\text{S}$ values for early molybdenite-, and later gold-bearing mineralisation range from -2 to $+12\text{‰}$, but show distinct populations related to mineralisation type. Modelling of the relative input of magmatic and sedimentary sulphur into gold-bearing quartz veins with $\delta^{34}\text{S}$ values of $+12\text{‰}$, indicates a maximum of 68% magmatic sulphur, and that S-rich, SEDEX-bearing, Easdale Subgroup metasedimentary rocks lying stratigraphically above the host rocks represent the only viable source of sedimentary sulphur in the Dalradian Supergroup. Consequently, the immediate host rocks were not a major source of sulphur to the mineralisation, consistent with their low bulk sulphur and lack of metal enrichment. Recent structural models of the Tyndrum area suggest Easdale Subgroup metasedimentary rocks, enriched in ^{34}S , sulphur, and metals, are repeated at depth due to folding, and it is suggested that these are most likely source of sedimentary sulphur, and possibly metals, for the ore fluids.

6.1. Introduction

The Dalradian rocks of Scotland and Ireland have been extensively studied since the mid-19th century (Murchison & Geikie 1861; Bailey & Macgregor 1912; Tilley 1925). The sequence is generally considered to be mid-Neoproterozoic (Cryogenian) to at least mid-Cambrian in age (Tanner & Sutherland 2007; Stephenson *et al.* 2013). However, there are only limited horizons where precise chronostratigraphy is available (Dempster *et al.* 2002; Rooney *et al.* 2011). Furthermore, correlation with other Neoproterozoic sequences is challenging, given that the Dalradian rocks have undergone polyphase deformation and regional metamorphism, locally reaching upper amphibolite grade during the Grampian Event of the Caledonian Orogeny (Oliver 2001; Stephenson *et al.* 2013). The Neoproterozoic Era is recognised as a crucial time in Earth history, incorporating two snowball Earth events (Hoffman *et al.* 1998) coupled with large fluctuations in seawater C-, O-, Sr- and S-isotope ratios (Halverson *et al.* 2010). The increasing understanding of Neoproterozoic events and global isotope variations (Halverson *et al.* 2010; Halverson & Shields-Zhou 2011) within the evolving Earth has impacted on the understanding of the Dalradian sequence and is beginning to refine the possible chronostratigraphies,

particularly through the use of stable isotope stratigraphy (Thomas *et al.* 2004; Prave *et al.* 2009; Moles *et al.* 2014).

The Dalradian sequence also hosts the UK's largest resource of gold in Northern Ireland at Curraghinalt, and its only active metal (gold) mine at Cavanacaw (Fig. 6.1), with resources of 2,700,000 oz Au and 438,300 oz Au respectively (Dalradian Resources Inc. 2012; Galantas Gold Corporation 2013). In Scotland, the Cononish deposit, near Tyndrum, hosts a JORC compliant resource of 169,000 oz Au and 631,000 oz Ag in the combined Measured, Indicated and Inferred categories (Scotgold Resources Ltd 2012a). More widely, the Tyndrum area contains a number of gold prospects and many mineralised occurrences within a 10 km radius of Cononish (Hill *et al.* 2011; Tanner 2012). The origin and timing of mineralisation in the Tyndrum area are subject to on-going debate (e.g. Curtis *et al.* 1993; Goldfarb *et al.* 2005).

The massive quartz veins which host the gold ores and other associated mineralisation at Tyndrum are dominated by sulphides. Early limited work on the isotopic composition of the sulphides was interpreted to suggest a mixed sedimentary/magmatic sulphur source (Patrick *et al.* 1983, 1988; Curtis *et al.* 1993). This paper presents an extensive new S-isotope dataset for sulphides from Cononish and for newly identified occurrences of a range of mineralisation styles in the area, together with a suite of local host metasedimentary rocks. The global Neoproterozoic sedimentary sulphide S-isotope dataset is correlated with recent data for the S-isotope stratigraphy of the Dalradian Supergroup to constrain the S-isotope composition of the local sequence where data are absent. The potential input of sedimentary and igneous sulphur is modelled to investigate the sources of sulphur in the Tyndrum area mineralisation. From this it is shown that the majority of the sulphur in the mineralisation must be derived from the Dalradian sequence and the proportion of magmatic sulphur is likely to be low, but nevertheless genetically significant. Furthermore, it is demonstrated that the local host metasedimentary rocks are unlikely to have been the dominant source of sulphur for the gold vein mineralisation; instead it was stratigraphically younger, but structurally underlying, Dalradian rocks which were the most likely source. This constrains a model for the source of metals and the fluid pathways for the development of mineralisation.

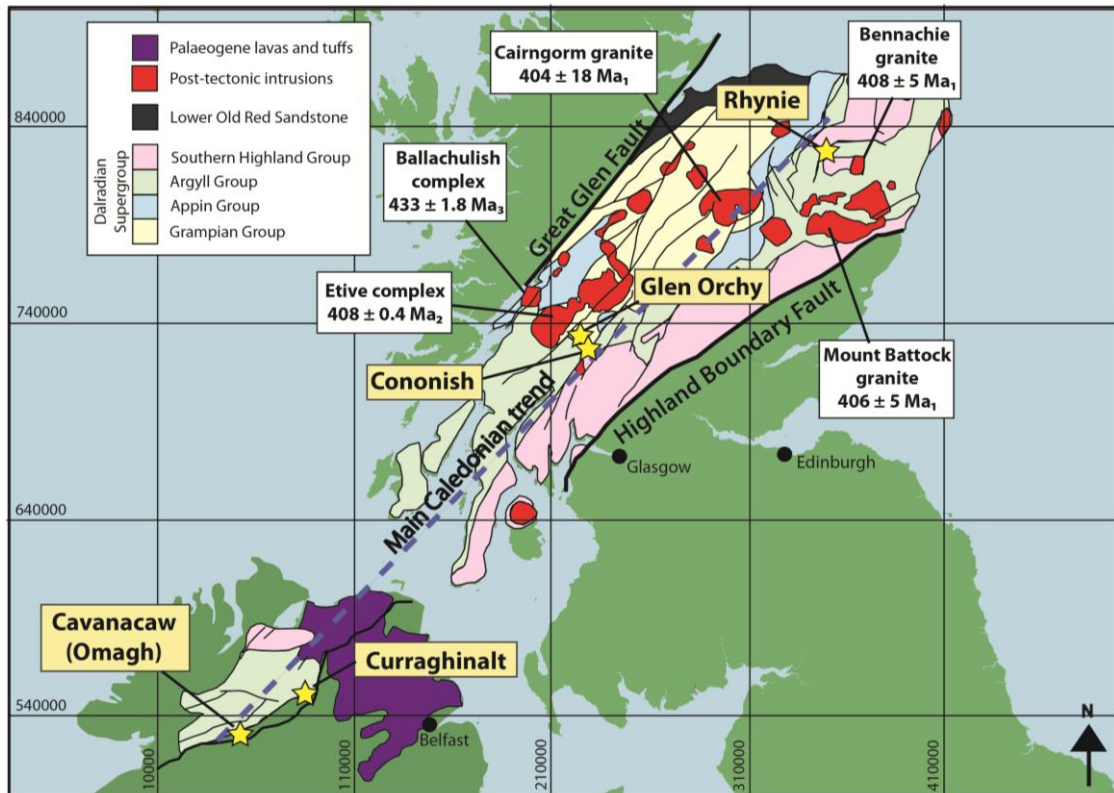


Figure 6.1: Simplified geological map of the Dalradian Supergroup in Scotland and Northern Ireland showing post-tectonic intrusions and major gold occurrences (stars). Representative dates for post-tectonic granites are provided; ¹Oliver *et al.* (2008); ²Neilson *et al.* (2009); ³Conliffe *et al.* (2010). Geology adapted from the British Geological Survey 1:625 000 scale Bedrock Geology map.

6.2. Geological setting of the Scottish Dalradian sequence

6.2.1 Global context

The formation of the Rodinia supercontinent (1100 to 1000 Ma; Kennedy *et al.* 2006) and its subsequent rifting provides the setting for the early Neoproterozoic Era. Wide-scale orogenic activity was accompanied by the drawdown of biolimiting elements, such as P, Fe and C, during weathering reactions (Lenton & Watson 2004) and an associated increase in atmospheric O₂. The onset of these conditions ultimately produced changes within the biosphere that led to the development of oceanic metazoans and a primitive land biota (Knauth & Kennedy 2009; Parnell *et al.* 2010). By the mid-Neoproterozoic Era the drawdown of CO₂ and oxidising atmospheric conditions caused the onset of global episodic glaciations extending to low latitudes (Hambrey & Harland 1981; Hoffman *et al.* 1998) with significant associated climate fluctuations (Knauth & Kennedy 2009). The Sturtian glacial episodes are variably constrained from 746 to 663 Ma (Condon & Bowring 2011) and the Marinoan glacial episode to a period of <10 Ma with global termination of glaciation by *c.* 653 Ma (Condon & Bowring 2011). The northwards drift of Laurentia

relative to Gondwana at *c.* 570 Ma began to open the Iapetus Ocean (Cawood *et al.* 2001). The subsequent closure of the Iapetus Ocean caused the Grampian Orogenic Event during the mid-Palaeozoic (Soper & Hutton 1984; Pickering *et al.* 1988; Soper *et al.* 1992).

6.2.2 Deposition and tectonic setting

The Dalradian sequence is bounded in Scotland by the Great Glen Fault to the north and Highland Boundary Fault to the south; both crustal-scale structures (Fig. 6.1). The sequence was deposited along the developing east Laurentian passive margin during a period of ocean widening (Anderton 1985). The Dalradian Supergroup has a depositional history spanning the Neoproterozoic (Cryogenian) to mid-Cambrian (Tanner & Sutherland 2007; Stephenson *et al.* 2013) and comprises marine-clastic sedimentary rocks with occasional carbonate beds and minor volcanic rocks (Stephenson *et al.* 2013). The oldest rocks are psammites and semi-pelitic schists deposited in an extensional basin, collectively called the Grampian Group (Figs. 6.1, 6.2). The overlying Appin Group is characterised by a limestone-pelite-quartzite assemblage deposited in a relatively stable shelf environment (Wright 1988). The Argyll and Southern Highland Groups, overlying the Appin Group, contain significant black slates and graphitic schists, and an increased incidence of mafic lavas and sills, grading upwards into coarse turbidite sequences (Harris *et al.* 1978; Anderton 1985), with the Argyll Group host to locally-developed stratabound exhalative mineralisation (Stephenson *et al.* 2013). The upper-Appin and lower-Argyll Group stratigraphy is absent in the Tyndrum area (Fig. 6.2) the missing stratigraphy is represented by the Boundary Slide (formerly termed the Iltay Boundary Slide; Bailey 1922; Hutton 1979; Roberts & Treagus 1979; Tanner 2012).

6.2.3 Chronostratigraphic and biostratigraphic constraints

The age of deposition is poorly constrained, a number of workers have advocated correlations within the existing age constraints (Fig. 6.2; Thomas *et al.* 2004; Prave *et al.* 2009; Rooney *et al.* 2011). The base of the Dalradian sequence is dated at a maximum age of *c.* 800 Ma by the presence of Knoydartian deformation in the basement rocks, combined with no evidence of pre-Caledonian mineral ages in the Dalradian Supergroup (Noble *et al.* 1996). The Leny Limestone within the Southern Highland Group is dated at 510 to 515 Ma (Cowie *et al.* 1972) based on the presence of the rare Mid-Cambrian trilobite *Pagetides* (Pringle 1940, Cowie *et al.* 1972). There are two radiometric dates for sedimentation within the Dalradian; U–Pb zircon has constrained the Tayvallich Volcanics, which represent the top of the Argyll Group, to 601 ± 4 Ma (Dempster *et al.* 2002), and a Re–Os whole rock

date on the Ballachulish Slate at 659 ± 9.6 Ma is interpreted to represent deposition (Rooney *et al.* 2011).

6.2.4 Deformation and metamorphism

The Dalradian package underwent polyphase deformation, the Grampian Event, as a result of the collision of Laurentia with an oceanic arc and the subsequent closure of the Iapetus ocean *c.* 480 to 465 Ma (Oliver 2001; Baxter *et al.* 2002; Stephenson *et al.* 2013). D1 is characterised by greenschist facies metamorphism and dominantly NE–SW–trending folds and ductile shears (Strachan *et al.* 2002). Peak metamorphism and maximum deformation occurred during continued over-thrusting recorded by D2 (Krabbendam *et al.* 1997; Crane *et al.* 2002), characterised by rotation and stacking of close to isoclinal, asymmetrical fold nappes (Strachan *et al.* 2002). Upright to SE–steeply dipping NE–trending structures dominate D3, reflecting decreasing intensity of deformation (Strachan *et al.* 2002). D4 deformation is associated with gently plunging, NE–SW–trending upright folds, late crenulation and brittle structures recording weak deformation in the final stages of the Grampian Event. Numerous faults occur sub-parallel to the NE–SW structural trend of the Dalradian, and have undergone largely left-lateral strike-slip movement with a component of normal movement during transtension (Stephenson & Gould 1995). The change to a transpressional regime is recorded by D4 and features a component of right-lateral strike-slip movement on the major Caledonian faults (Strachan *et al.* 2002). Peak metamorphism in the Dalradian Supergroup exhibits significant along-strike variation with a general increase from greenschist facies in the SW Highlands to upper amphibolite in the NE of the central Highlands (Fettes *et al.* 1985; Harte 1988). In the Tyndrum area garnet-grade amphibolite-facies metamorphism was reached (Harte 1988). Peak metamorphism is constrained to 473 to 465 Ma (garnet and whole rock isochron Sm–Nd; Baxter *et al.* 2002; Lu–Hf and Sm–Nd garnet and whole rock isochron; Bird *et al.* 2013) supported by the age range of broadly syn-metamorphic intrusions (Auchlee granite 475 ± 12 Ma U–Pb zircon; Inch gabbro 470 ± 8 Ma U–Pb zircon; Dempster *et al.* 2002; Oliver *et al.* 2008).

6.2.5 Post-tectonic magmatic activity

The Dalradian Supergroup hosts widespread post-tectonic granitic intrusions (Fig. 6.1) emplaced over a period of *c.* 25 Ma (Neilson *et al.* 2009; Conliffe *et al.* 2010). The intrusions are large granodiorite–granite multi-phase complexes and range in age from the Ballachulish Complex at 433 ± 1.8 Ma (Re–Os molybdenite; Conliffe *et al.* 2010) to the Etive Complex at 408 ± 0.4 Ma (U–Pb zircon; Neilson *et al.* 2009), both of which host

mineralisation (Neilson *et al.* 2009; Conliffe *et al.* 2010; Porter & Selby 2010). Although no outcrop of granite is observed within 10 km of the Tyndrum area mineralisation, a gravity low extending from the Etive Complex into the Tyndrum area has been interpreted to represent the extent of a concealed granite body (Fig. 6.3; Patrick *et al.* 1988). The Dalradian Supergroup also hosts intrusive bodies characterised by a significant diorite component with minor appinite/peridotite/pyroxenite (Stephenson & Gould 1995). The Garabal Hill-Glen Fyne, Arrochar and Rubha Mor appinites, 40 km south of Tyndrum, have been dated at between 426 ± 4.2 and 428 ± 9.8 Ma (U–Pb titanite and zircon; Rogers & Dunning 1991, Tanner 2012) and are interpreted by Tanner (2012) to be equivalent to the Sron Garbh diorite-appinite body near Tyndrum and widespread lamprophyre dykes and sills observed in the Beinn Udlaidh and Glen Orchy areas (Fig. 6.3).

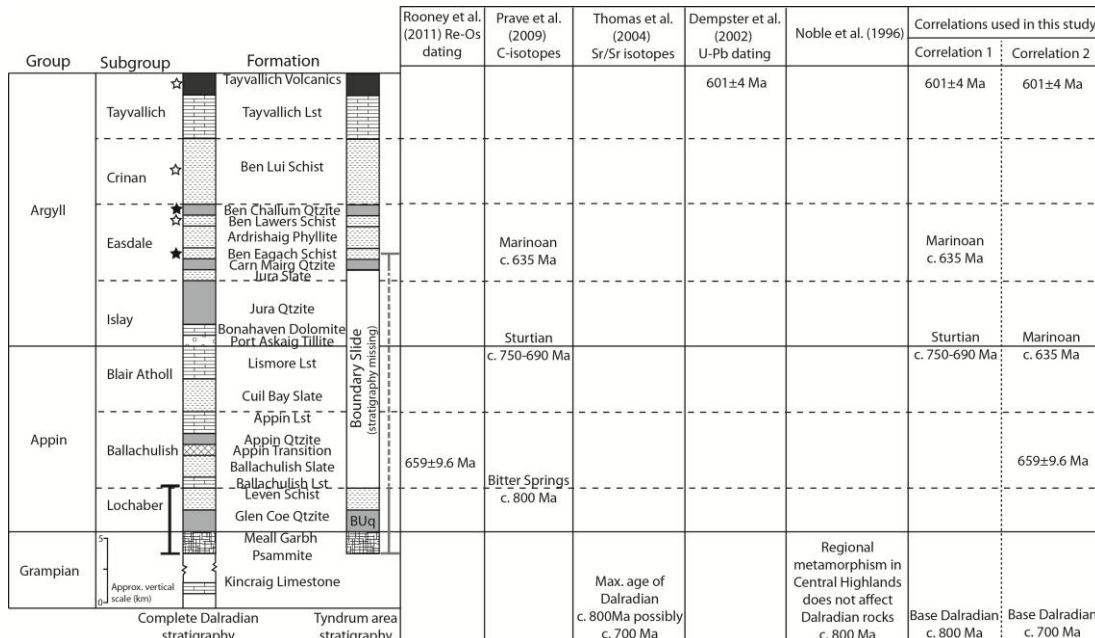


Figure 6.2: Simplified composite stratigraphic column of the lower three Groups of the Dalradian Supergroup showing missing stratigraphy in the Tyndrum area due to the Boundary Slide. The range of host rocks for vein samples from this study is shown by the black bar with the range of host rocks for the Eas Anie structure at Cononish shown by the grey bar. The age of the Dalradian Supergroup is highly debated with limited radiometric dating available; the two age correlations used for this study are shown. Unfilled stars indicate volcanogenic sulphide horizons; black stars indicate syn-sedimentary stratabound SEDEX horizons. BUq = Beinn Udlaidh Quartzite (equivalent to the Glen Coe Quartzite and present in the Tyndrum area).

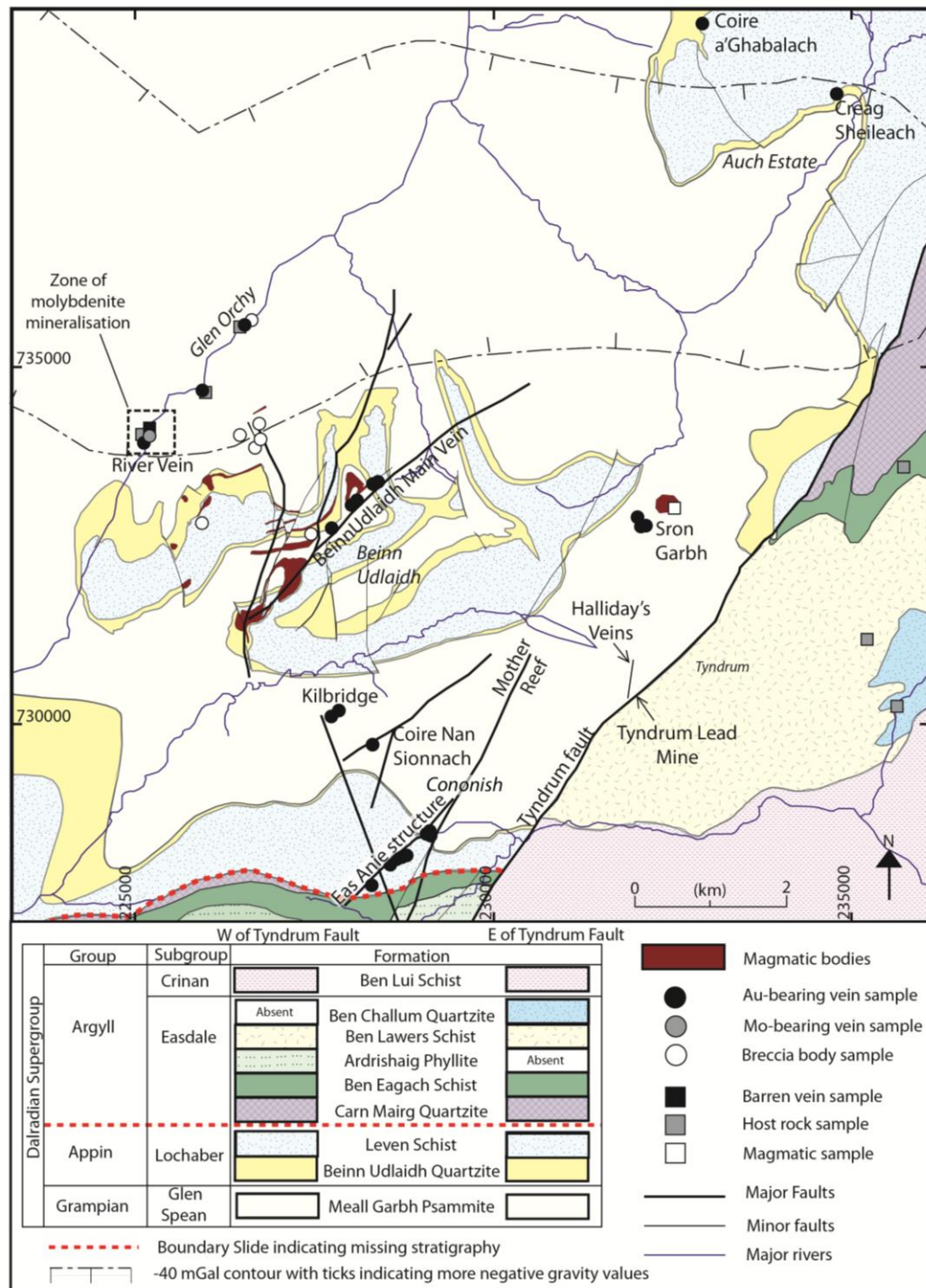


Figure 6.3: Simplified geology of the study area. Key structural features and sample localities are shown. Magmatic bodies shown include lamprophyre sills and dykes, appinite bodies and diorite dykes. Geology adapted from the British Geological Survey 1:50 000 scale Bedrock Geology Crianlarich and Dalmally sheets with additional detail from Tanner & Thomas (2009) and mapping in conjunction with Scotgold Resources Ltd. Gravity anomaly after Hussein & Hipkin (1981) and interpretation in Patrick *et al.* (1988).

6.3. Isotope stratigraphy of the Dalradian Supergroup

6.3.1 Global Context

Isotope stratigraphy has been extensively applied to Neoproterozoic sequences, in particular the correlation of glacial deposits (Halverson & Shields-Zhou 2011). Carbon-isotope stratigraphy is a powerful tool for correlating glacial deposits between Neoproterozoic sequences where there are limited biostratigraphic constraints but significant limestone deposition. Neoproterozoic carbonate sediments are characterised by high average $\delta^{13}\text{C}_{\text{carb}}$ values and large fluctuations to extremely low values, some of which correlate with glacial episodes (Halverson *et al.* 2010). Strontium isotopes are a useful measure of tectonic evolution and long-term climatic change and are valuable in Neoproterozoic carbonate sequences due to the consistent increase in $^{87}\text{Sr}/^{86}\text{Sr}$ values of seawater (Halverson *et al.* 2007a). Since both C- and Sr-isotopes are measured in carbonate rocks the two records can be tied together (Halverson & Shields-Zhou 2011). Neoproterozoic sedimentary rocks are also characterised by large fluctuations in both $\delta^{34}\text{S}_{\text{pyrite}}$ and $\delta^{34}\text{S}_{\text{sulphate}}$, which appear to be closely related to glacial episodes (Gorjan *et al.* 2000; Hurtgen *et al.* 2002; Halverson & Hurtgen 2007), although the record is not as well constrained as for C- and Sr-isotope variations. In this paper, existing data on the variation of C- and Sr-isotopes within the Dalradian Supergroup are utilised, in addition to existing radiometric dating, to establish potential age correlations for the Dalradian Supergroup. This study uses the global Neoproterozoic S-isotope record in conjunction with these age correlations to estimate $\delta^{34}\text{S}$ values in sulphur-poor stratigraphy.

6.3.2 Carbon isotopes

Prave *et al.* (2009) compared the trend in carbonate $\delta^{13}\text{C}$ in the Dalradian Supergroup with the global composite $\delta^{13}\text{C}$ curve (Halverson *et al.* 2005, 2007a) and correlated observed excursions with key Neoproterozoic events. The metamorphic fluids affecting Dalradian carbonates during Grampian Event orogenesis are known to be carbon-poor, therefore the isotopic composition of carbonate units is buffered (Holness & Graham 1995; Graham *et al.* 1997; Thomas 2000) and carbonate $\delta^{13}\text{C}$ values are interpreted to represent primary values. Prave *et al.* (2009) tentatively correlated the Ballachulish Limestone with the *c.* 800 Ma Bitter Springs anomaly (Hill & Walter 2000; Halverson *et al.* 2007b) and the Port Askaig Tillite at the base of the Argyll Group is interpreted to represent the Sturtian glacial episodes (Fig. 6.2). However, it should be noted that correlation of the Ballachulish

Limestone with the Bitter Springs anomaly would make the formations below too old if it is accepted that the base of the Dalradian is <800 Ma. Prave *et al.* (2009) interpret the negative $\delta^{13}\text{C}$ excursion in the Bonahaven Dolomite ($\delta^{13}\text{C} = -8$ to -4‰ ; Prave *et al.* 2009) to record a global depositional signal rather than local depositional variation and correlate the unit with the Tayshir anomaly within the Tsagaan Oloom Formation, Mongolia, which lies between Sturtian and Marinoan glacials (carbonate $\delta^{13}\text{C}$ as low as -7.5‰ ; MacDonald *et al.* 2009). Prave *et al.* (2009) use carbonate $\delta^{13}\text{C}$ excursions to correlate Mid-Easdale Group units (Fig. 6.2) with the Marinoan glacial episode; this is supported by $^{87}\text{Sr}/^{86}\text{Sr}$ and the presence of the Stralinchy Diamictite and overlying Cranford Limestone in the Dalradian stratigraphic sequence in NW Ireland (Thomas *et al.* 2004; McCay *et al.* 2006).

6.3.3 Strontium isotopes

Thomas *et al.* (2004) used $^{87}\text{Sr}/^{86}\text{Sr}$ values from limestones within the Dalradian Supergroup to constrain depositional age through comparison with the global $^{87}\text{Sr}/^{86}\text{Sr}$ trend (Kuznetsov 1998, given in Melezhik *et al.* 2001; Shields 1999; Walter *et al.* 2000). $^{87}\text{Sr}/^{86}\text{Sr}$ values for Grampian and Appin limestones are interpreted to be well preserved and therefore to represent primary values close to contemporaneous seawater. The level of preservation in the Argyll Group is less than observed in the Grampian and Appin Group and $^{87}\text{Sr}/^{86}\text{Sr}$ values are inferred to be less reliable. Thomas *et al.* (2004) conclude that $^{87}\text{Sr}/^{86}\text{Sr}$ values observed in the lower Dalradian Supergroup (Kincraig Limestone, Grampian Group; $^{87}\text{Sr}/^{86}\text{Sr} = 0.7069$ to 0.7074) suggest it is not older than *c.* 800 Ma and may be as young as 700 Ma using Kuznetsov's (1998) Neoproterozoic seawater $^{87}\text{Sr}/^{86}\text{Sr}$ curve. Comparison of the Thomas *et al.* (2004) data with the more recent Halverson *et al.* (2010) global $^{87}\text{Sr}/^{86}\text{Sr}$ curve of high-quality Sr-isotope data supports this interpretation for the age of the Dalradian; global $^{87}\text{Sr}/^{86}\text{Sr}$ does not increase to 0.7069 until 775 Ma when it decreases again before consistently increasing after 700 Ma. This suggests that the Dalradian Supergroup is not older than *c.* 775 Ma and may be as young as 700 Ma, in line with the geochronometric constraints that the base is <800 Ma (Noble *et al.* 1996).

6.4. Mineralisation in the Tyndrum area

The Cononish gold mineralisation is hosted in the <6 m wide Eas Anie structure, a complex of steeply-dipping quartz veins, which crosscuts Grampian and lower-Appin Group stratigraphic units (Fig. 6.3; Treagus *et al.* 1999; Tanner 2012). The sulphide assemblage is dominated by pyrite, chalcopyrite and galena; gold, as electrum, is associated with galena in fractured pyrite (Earls *et al.* 1992). Previous Ar–Ar and K–Ar dating suggests

mineralisation occurred at 410 ± 14 Ma (Treagus *et al.* 1999), significantly after peak metamorphism and overlapping with granite magmatism, but with very large uncertainties. Recent geochronological work also suggests the age of mineralisation is close to 410 Ma (Rice *et al.* 2012).

The Beinn Udlaidh Main Vein (Fig. 6.3) is hosted in Meall Garbh Psammite, Beinn Udlaidh Quartzite (regionally equivalent to the Glen Coe Quartzite) and Leven Schists, trends NE, dips sub-vertically and averages 4 m in width (Fig. 6.3; Tanner 2012). The Main Vein contains gold, as electrum, hosted within pyrite; galena and sphalerite are present (Plewes 2012).

Previous work in the Tyndrum area noted a number of gold-bearing veins in addition to the Cononish and Beinn Udlaidh veins (Fig. 6.3). Halliday's Veins were first reported by Halliday (1962), with further work by Patrick *et al.* (1988). The veins, hosted in N-trending structures, contain electrum, hessite (Ag_2Te) with minor sylvanite ($[\text{AuAg}]\text{Te}_4$) and petzite (Au_3AgTe_2) (Patrick *et al.* 1988). Electrum is the most common Au-Ag phase and is found as inclusions in galena and within fractures in pyrite (Patrick *et al.* 1988). Mineralised veins at Coire Nan Sionnach were noted by Earls *et al.* (1992) with additional veins observed at Kilbridge by Scotgold Resources. The Mother Reef, sub-parallel to the Tyndrum Fault, can be traced for 2 km and is interpreted to represent a series of segments at an oblique trend to the main structure and is largely barren except where the projected line of Eas Anie meets the Mother Reef (Tanner 2012). The Tyndrum Lead Mine mineralisation is hosted in NE-trending structures within the Tyndrum Fault zone as veins and vein breccias. The sulphide assemblage is dominated by galena and sphalerite with a notable absence of pyrite (Patrick *et al.* 1983). Mineralisation with a comparable assemblage is observed to cross-cut the gold-bearing Eas Anie structure (Earls *et al.* 1992).

6.4.1 Previous S-isotope data

A number of S-isotope studies have previously been undertaken on veins and other mineralisation styles across the Tyndrum area, and are summarised in Figure 6.4. Curtis *et al.* (1993) undertook initial S-isotope work at Cononish producing a limited dataset (pyrite $\delta^{34}\text{S} = +6.0$ to $+8.4\text{‰}$; $n = 9$) interpreted to reflect a mixture of magmatic and sedimentary sources, although the dataset did not examine variation among the different sulphide generations observed in the vein. In addition, Patrick *et al.* (1983, 1988) and Curtis *et al.* (1993) measured values on a limited number of samples (Figs. 6.3, 6.4) from the gold-bearing Halliday's Veins (pyrite $\delta^{34}\text{S} = -0.6$ to $+8.8\text{‰}$; galena $\delta^{34}\text{S} = +1.5$ to $+2.0\text{‰}$; $n =$

6) and the largely-barren Mother Reef (pyrite $\delta^{34}\text{S} = +8.0$ to $+9.8\text{‰}$; galena $\delta^{34}\text{S} = +7.2$ to $+11.2\text{‰}$; $n = 7$). Patrick *et al.* (1983) and Curtis *et al.* (1993) measured S-isotopes of galena ($\delta^{34}\text{S} = +3.5$ to $+6.6\text{‰}$; $n = 10$) and sphalerite ($\delta^{34}\text{S} = +6.6$ to $+10.0\text{‰}$; $n = 3$) from the Tyndrum Lead Mine (Figs. 6.3, 6.4). Molybdenite $\delta^{34}\text{S}$ data from mineralisation at Ballachulish and Etive ranges from 0 to $+4\text{‰}$ (Conliffe *et al.* 2009) and pyrite $\delta^{34}\text{S}$ values from Blackmount molybdenite veins (Etive Complex; $n = 2$; Fig. 6.1) are close to zero (Curtis *et al.* 1993).

The range of data for the different mineralisation styles as displayed in Figure 6.4 shows that different mineralisation types have distinct S-isotope signatures. Sulphide $\delta^{34}\text{S}$ data from all mineralisation types is generally positive with only rare values below 0‰ . Gold mineralisation is associated with $\delta^{34}\text{S}$ ratios in the range -0.6 to $+9.8\text{‰}$ with an average of 6.3‰ ($\pm 2.8\text{‰}$ σ_{n-1}) for pyrite. Molybdenite mineralisation has $\delta^{34}\text{S}$ values close to zero suggesting it is magmatic in origin and is comparable with $\delta^{34}\text{S}$ data from deep-seated plutonic intrusions across the area (average $\delta^{34}\text{S} +2.6 \pm 1.8\text{‰}$; Lowry *et al.* 1995; Fig. 6.4).

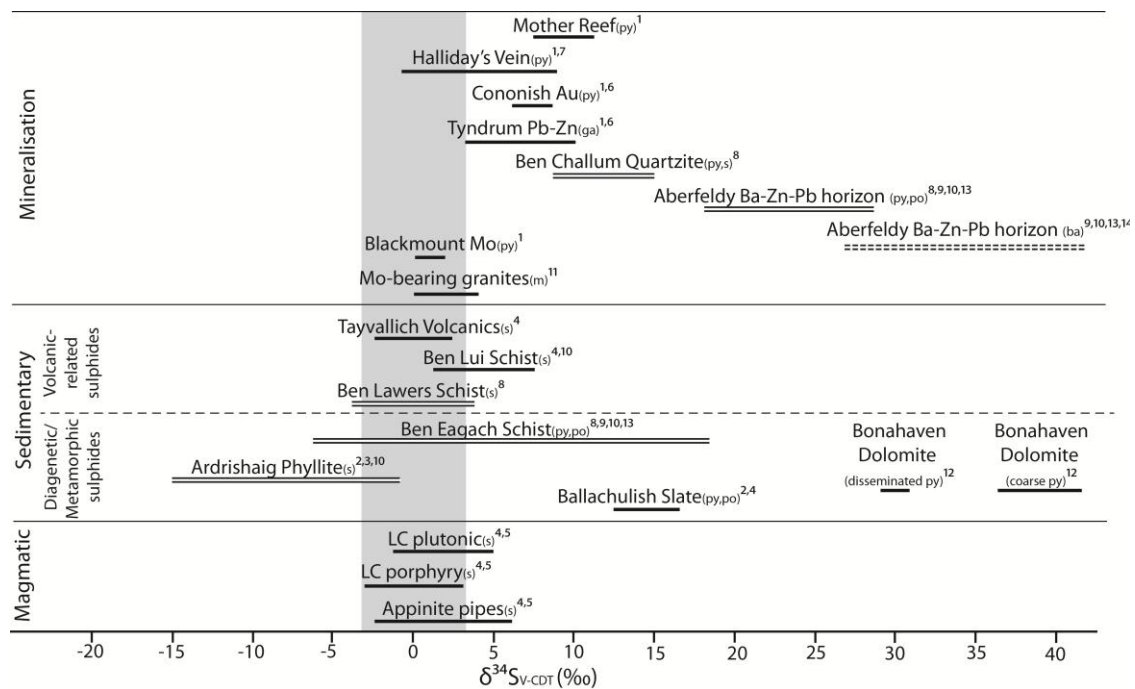


Figure 6.4: Previous sulphide and sulphate $\delta^{34}\text{S}$ data for sedimentary, magmatic bodies and mineralisation in the Dalradian Supergroup. Grey bar represents $\delta^{34}\text{S}$ range for uncontaminated mantle-derived magmatic melts ($\delta^{34}\text{S} = 0 \pm 3\text{‰}$; Ohmoto 1986). Dashed line represents sulphate $\delta^{34}\text{S}$ data. Double lines represent Easdale Subgroup stratigraphy. ¹Curtis *et al.* (1993); ²Hall *et al.* (1988); ³Hall *et al.* (1994a); ⁴Lowry (1991); ⁵Lowry *et al.* (1995); ⁶Patrick *et al.* (1983); ⁷Patrick *et al.* (1988); ⁸Scott *et al.* (1987); ⁹Scott *et al.* (1991); ¹⁰Willan and Coleman (1983); ¹¹Conliffe *et al.* (2009); ¹²Hall *et al.* (1994b); ¹³Moles *et al.* (2014); ¹⁴Hall *et al.* (1987). LC – Late Caledonian; ba – barite; ga – galena; m – molybdenite; py – pyrite; po – pyrrhotite; s – sulphides.

6.5. Analytical methods

Samples were obtained from surface and underground outcrop and quarter drill core from Scotgold Resources Ltd's on-going exploration program. Detailed mineralogical analysis was undertaken at the University of Leicester using a Hitachi S-3600N Environmental Scanning Electron Microscope, with an Oxford Instruments INCA 350 energy dispersive X-ray analysis system. Whole rock geochemistry was undertaken at ALS laboratories, Ireland, as part of Scotgold's assay program; only sulphur and gold concentrations are reported here. For sulphur, samples were dissolved in concentrated perchloric, nitric, hydrofluoric and hydrochloric acids. Sulphur was analysed by ICP-MS; lower detection limit is 0.01%. Gold was measured by fire assay, fusing the sample with lead oxide, sodium carbonate, borax and silica then digesting the bead in dilute nitric and hydrochloric acid. The digested solution is analysed by atomic absorption; lower detection limit is 0.01 ppm.

Sulphide minerals for S-isotope analysis were separated using micro-drilling from characterised sections. SO₂ was produced from sulphides by combustion with cuprous oxide for mass spectrometric analysis following the procedure of Robinson & Kusakabe (1975). *In situ* laser combustion analyses were undertaken on polished slabs from the Auch Estate, prepared using a method as described in Kelley & Fallick (1990) and Wagner *et al.* (2002). For both sulphur isotope methods mass spectrometric analysis was undertaken in a VG SIRA II gas mass spectrometer. Reproducibility, based on repeat analyses of internal and international lab standards (CP1, NBS 123 & IAEA S 3), was better than $\pm 0.3\%$. All data are reported as $\delta^{34}\text{S}$ per mil (‰) relative to the Canyon Diablo Troilite standard (V-CDT). Full standards run given in Appendix 6.1 and all sulphur isotope results are given in Appendix 6.2.

6.6. Field relations of newly identified mineralisation

Regional exploration by Scotgold since 2007 and work in this study have identified a number of additional occurrences of veins and clarified that mineralisation is of a number of distinct types:

1. Additional gold-bearing quartz veins have been identified in the Glen Orchy area, at Kilbridge and the Auch Estate (Fig. 6.3). Steeply-dipping gold-bearing quartz veins in the Glen Orchy area (up to 194.6 g/t Au and >200 g/t Ag from >1 kg grab samples; Scotgold Resources Ltd 2011a) trend east–west to SW–NE reaching up to 1 m in width. The veins are polyphase and exhibit brecciation with host rock clasts included

in the veins. Mineralised quartz veins at Kilbridge, trending 095–125 and reaching 20 cm in width, are characterised by fine grained pyrite concentrated in a zone, up to 3 cm wide, in the centre of the vein. Auch Estate gold-bearing quartz veins (up to 25.5 g/t Au and 14.3 g/t Ag over 1 m; Scotgold Resources Ltd 2011b) are up to 0.5 m in width and trend NE–SW to ENE–WSW. Coire a’Ghabalach veins (Fig. 6.3) exhibit significant brecciation with clasts of early white quartz and altered host rock in the vein. Veins at Creag Shieleach are characterised by a simple sulphide assemblage and exhibit a lack of brecciation compared to other veins in the Auch Estate (Fig. 6.3).

2. Largely barren quartz veins are observed throughout the study area (Fig. 6.3) and can be characterised into two sub-types; barren and pyrite-bearing. Barren veins are often massive and complex (e.g. Mother Vein at Cononish; Curtis *et al.* 1993; Treagus *et al.* 1999). Pyrite-bearing veins are characterised by a single quartz generation with some brecciation of altered host rock within the veins.
3. In Glen Orchy disseminated molybdenite mineralisation (up to 2.72% Mo from rock chip samples; Scotgold Resources Ltd 2012c) has been identified in alteration zones around steeply-dipping NNE–trending fractures. The alteration zones are up to 20 cm wide, but the fractures are narrow (mm scale), except where late quartz and pyrite infill has occurred (reaching up to 10 cm in width). Molybdenite occurs as small rosettes (1–2 mm across) with minor pyrite; there is no gold associated with the molybdenite mineralisation.
4. Gold-mineralised breccia bodies have been identified at Beinn Udlaidh (up to 0.26 g/t Au and 1.49 g/t Ag over 14 m; Scotgold Resources Ltd 2010). The breccia bodies have a sharp, near vertical, contact with the host rock where observed (Moore 2011) and are approximately circular in cross-section reaching 120 m in diameter (Tanner 2012). The breccia bodies are matrix poor due to the close fit of angular clasts of host quartzite, psammite, schist and lamprophyre; the matrix consists of either lamprophyre or quartz (Moore 2011). The breccia bodies exhibit strong similarities to explosion breccia bodies related to appinites (Wright & Bowes 1968) and Tanner (2012) has interpreted the emplacement of the breccia bodies to have occurred syn- to post-emplacement of the lamprophyres and appinites based on cross-cutting relationships.
5. A Platinum Group Element (PGE)-bearing appinite-diorite intrusive body has been identified at Sron Garbh (up to 0.22 g/t Au; 0.78 g/t Pd and 0.58 g/t Pt over 2 m;

Scotgold Resources Ltd 2012b; Fig. 6.3), PGEs are associated with the marginal appinite (Scotgold Resources Ltd 2012b).

In the Glen Orchy area all newly identified veins and breccia bodies cross-cut the metamorphic fabric and therefore post-date peak metamorphism. Cross-cutting relationships constrain gold-bearing quartz veins and pyrite-bearing veins to be younger than the molybdenite mineralisation (Fig. 6.5). In addition, gold-bearing quartz veins are observed to cross-cut the Sron Garbh appinite. There are currently no geochronological data for Glen Orchy to constrain age relationships and absolute timescale further and therefore this study assumes, in the absence of evidence otherwise, that all gold mineralisation is of the same age. However, based on structural relationships, Tanner (2012) has interpreted gold mineralisation at Cononish to be older than gold mineralisation at Glen Orchy.

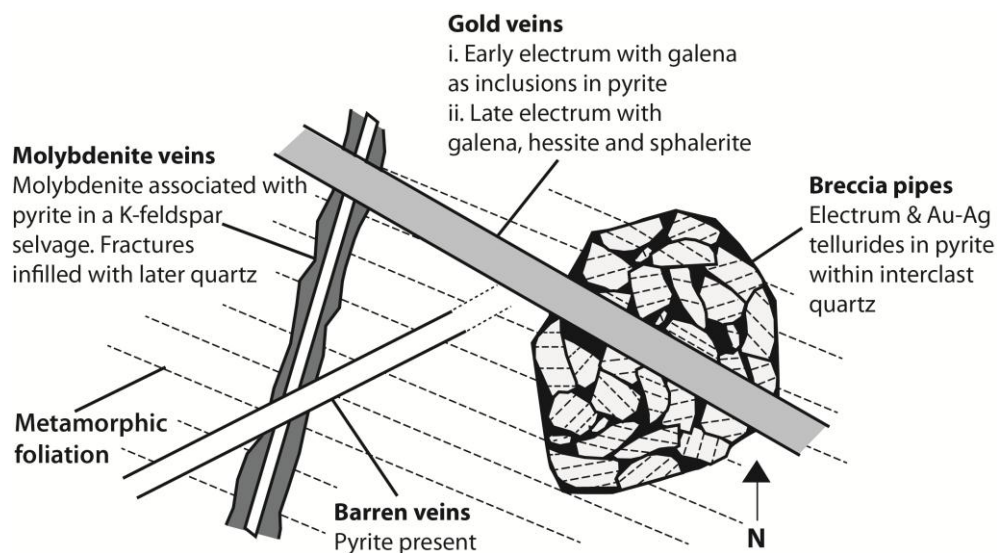


Figure 6.5: Schematic illustration of orientations and cross-cutting relationships of the veins and breccia pipes in Glen Orchy.

6.7. Ore petrography

Additional work at Cononish has clarified the paragenesis compared to previously published data (Pattrick *et al.* 1988; Earls *et al.* 1992; Curtis *et al.* 1993). Early gold (Au 1) is associated with hessite (Ag_2Te) and minor early galena found in fractures in pyrite. Late gold (Au 2) is associated with galena and chalcopryrite with minor sphalerite (Spence-Jones 2013); no telluride mineralisation is observed associated with late galena.

Gold-bearing quartz veins in Glen Orchy, Beinn Udlaidh, Sron Garbh, Kilbridge and Coire Nan Sionnach (Fig. 6.3) are characterised by a sulphide-assemblage dominated by pyrite and galena. Brecciation of adjacent host rock is observed with clasts altered to either K-feldspar or a chlorite-sericite assemblage. Early gold (Au 1) is associated with galena as inclusions in pyrite (Fig. 6.6A & B). A second phase of gold (Au 2) occurs with void-filling galena (Fig. 6.6D & E) often accompanied by sphalerite exhibiting chalcopyrite disease (Fig. 6.6C), and sporadic hessite. Gold-bearing veins in the Auch Estate (Fig. 6.3) have a comparable sulphide assemblage with the addition of arsenopyrite (Fig. 6.6H). Brecciation of the host rock and early white quartz is observed. Arsenopyrite forms syn-pyrite and electrum is hosted as inclusions within both arsenopyrite and pyrite and within fractures in pyrite. The veins at Coire a'Ghabalach (Fig. 6.3) have late void-filling galena with hessite, sphalerite (Fig. 6.6F & G) and occasional Au-Ag tellurides and altaite (PbTe); veins at Creag Sheileach (Fig. 6.3) have late galena, but no associated telluride mineralisation.

Mineralisation in breccia bodies is hosted in the quartz matrix and is associated with post-brecciation sericite-chlorite alteration of the clasts. Gold, in the form of Au-Ag tellurides, is found within pyrite with altaite (PbTe) and sporadic chalcopyrite and galena (Moore 2011).

Sulphides in lamprophyre sills are characterised by small (<5 mm wide) cubic pyrite; no other sulphides are observed. Mineralisation has been identified in the Sron Garbh appinite-diorite body; the assemblage is dominated by pyrite and chalcopyrite with platinum group minerals associated with the appinitic portion (Graham 2013).

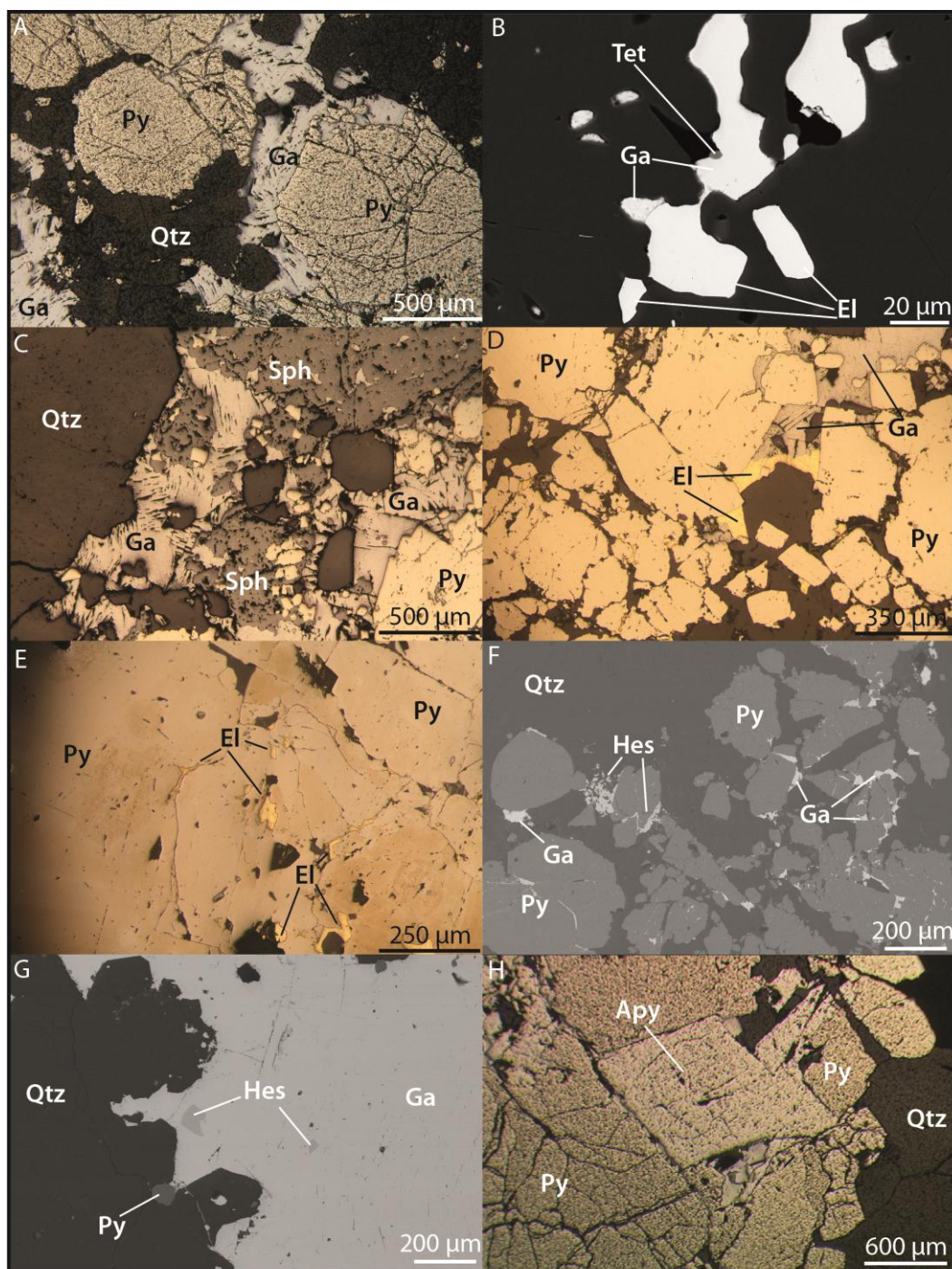


Figure 6.6: (A) Early well-developed pyrite cross-cut by late void-filling galena. (B) Gold 1 with early galena and tetrahedrite hosted within well-developed early pyrite. (C) Extensive sphalerite development with late void-filling galena. (D) Electrum (Au 2) observed on edges of pyrite with void-filling galena. (E) Gold 2 as electrum in fractures in early pyrite. (F & G) Hessite (Ag_2Te) associated with void filling galena forming on the edges of and within fractures in pyrite. (H) Well-developed diamond shaped crystals of arsenopyrite with pyrite.

Images A–E are from Glen Orchy; F–H are from the Auch Estate. Images A, C–E, H are reflected light photomicrographs; B, F–G are SEM images. El – electrum; Py – pyrite; Ga – galena; Qtz – quartz; Sph – sphalerite; Apy – arsenopyrite; Tet – tetrahedrite; Hes – hessite.

6.8. S-isotope results

Pyrite $\delta^{34}\text{S}$ values from gold-bearing quartz veins obtained for this study ($n = 46$) show wide variation from -2 to $+12\text{‰}$ (Fig. 6.7; Table 6.1) with an average value of $+6.9\text{‰}$ ($\pm 2.9\text{‰ } \sigma_{n-1}$), very similar to the $\delta^{34}\text{S}$ of sulphide float concentrate from crushed bulk ore at Cononish of $+6.7\text{‰}$. All pyrite $\delta^{34}\text{S}$ values at Cononish are pre-Au 1; galena, sphalerite and chalcopyrite $\delta^{34}\text{S}$ values are syn-Au 2 and overall follow the same distribution as pyrite $\delta^{34}\text{S}$ values. New data from veins at the Cononish deposit record a much wider range of values ($\delta^{34}\text{S} = -2$ to $+11\text{‰}$; Fig. 6.7A) than reported by Curtis *et al.* (1993). The majority of $\delta^{34}\text{S}$ data recorded for gold-bearing quartz veins at Glen Orchy, Sron Garbh and Beinn Udlaidh (Fig. 6.3) are within the range of previously published work from Cononish (Curtis *et al.* 1993; Fig. 6.4; 6.7A), $\delta^{34}\text{S}$ values below $+5\text{‰}$ are only observed at Cononish and in the Auch Estate veins. Kilbridge and Coire Nan Sionnach (Fig. 6.3) exhibit slightly higher $\delta^{34}\text{S}$ values between $+8$ and $+12\text{‰}$. Pyrite $\delta^{34}\text{S}$ values are generally syn- to post-Au 1 and arsenopyrite $\delta^{34}\text{S}$ values are post-Au 1; galena, sphalerite and chalcopyrite $\delta^{34}\text{S}$ values are syn-Au 2. Data obtained for Tyndrum Lead Mine-style mineralisation at Cononish (Table 6.1) are comparable to data from the Tyndrum Lead Mine (Pattrick *et al.* 1983; Curtis *et al.* 1993).

Beinn Udlaidh breccia bodies (Fig. 6.3) record $\delta^{34}\text{S}$ values of $+1$ to $+8\text{‰}$ ($n = 8$; Fig. 6.7B). Pyrite from molybdenite-bearing fractures has $\delta^{34}\text{S}$ values of between $+1.8$ and $+8.4\text{‰}$ ($n = 10$); higher than pyrite $\delta^{34}\text{S}$ values obtained at Blackmount (Curtis *et al.* 1993). Molybdenite $\delta^{34}\text{S}$ values measured ($\delta^{34}\text{S} = +6$ to 6.6‰ ; $n = 3$; Fig. 6.7B) are significantly higher than recorded for molybdenite elsewhere in the region.

Mineralised lamprophyre from Glen Orchy, taken at the contact with a cross-cutting gold-bearing quartz vein (GO1213, Table 6.1), has a $\delta^{34}\text{S}$ value of $+6.7\text{‰}$. Sron Garbh appinite-diorite body (Fig. 6.3) has $\delta^{34}\text{S}$ values of $+1$ to $+4.8\text{‰}$ (Fig. 6.7B; Graham 2013).

A limited S-isotope dataset has been developed for the host rocks in the study area ($n = 6$; Fig. 6.7B; Table 6.1). The metasedimentary rocks are generally sulphur poor and measured $\delta^{34}\text{S}$ values are from a range of sulphide types; stratabound sedimentary exhalative (SEDEX) mineralised horizons (Ben Challum Quartzite), volcanogenic sulphides (Ben Lawers Schist), a stratabound horizon of uncertain origin (Carn Mairg Quartzite) and alteration haloes around cross-cutting veins (Table 6.2). $\delta^{34}\text{S}$ values recorded for the Meall Garbh Psammite vary from $+4.7$ to $+6.9\text{‰}$ (Table 6.1), but are associated with mineralised veins and therefore may not represent the sedimentary values (see below). The Carn Mairg

Quartzite in the Auch Estate has a stratabound sulphide horizon with a $\delta^{34}\text{S}$ value of +8.0‰ and the Ben Challum mineralised SEDEX horizon at Auchtertyre, approximately 4 km east of Tyndrum, has a $\delta^{34}\text{S}$ value of +8.7‰. The Ben Lawers Schist volcanogenic-related sulphides record a lower $\delta^{34}\text{S}$ than seen in the other horizons of -3.2‰.

6.8.1 Relationship between veins and host rock alteration

Host rock alteration of metasedimentary rocks extends up to 1 m from cross-cutting veins and is characterised by addition of sulphides (Fig. 6.8A & B) and alteration to a K-feldspar or chlorite-sericite assemblage. Lamprophyres cross-cut by gold-mineralised quartz veins show strong chlorite-sericite alteration over comparable distances and are only observed to contain sulphides in the alteration zone (Fig. 6.8C). In all veins $\delta^{34}\text{S}$ values are higher than in the surrounding altered host rock (Fig. 6.8; Table 6.2) suggesting mixing in the alteration zone of high $\delta^{34}\text{S}$ sulphur from the veins with host rock sulphur that has a lower ($\leq +7\text{‰}$) $\delta^{34}\text{S}$ value. Host metasedimentary rocks and lamprophyre $\delta^{34}\text{S}$ values measured in alteration haloes of cross-cutting veins are therefore not representative of original sedimentary or magmatic values respectively, and instead are maximum values for these units. Vein fluids are thus indicated to be coming from a source with higher $\delta^{34}\text{S}$.

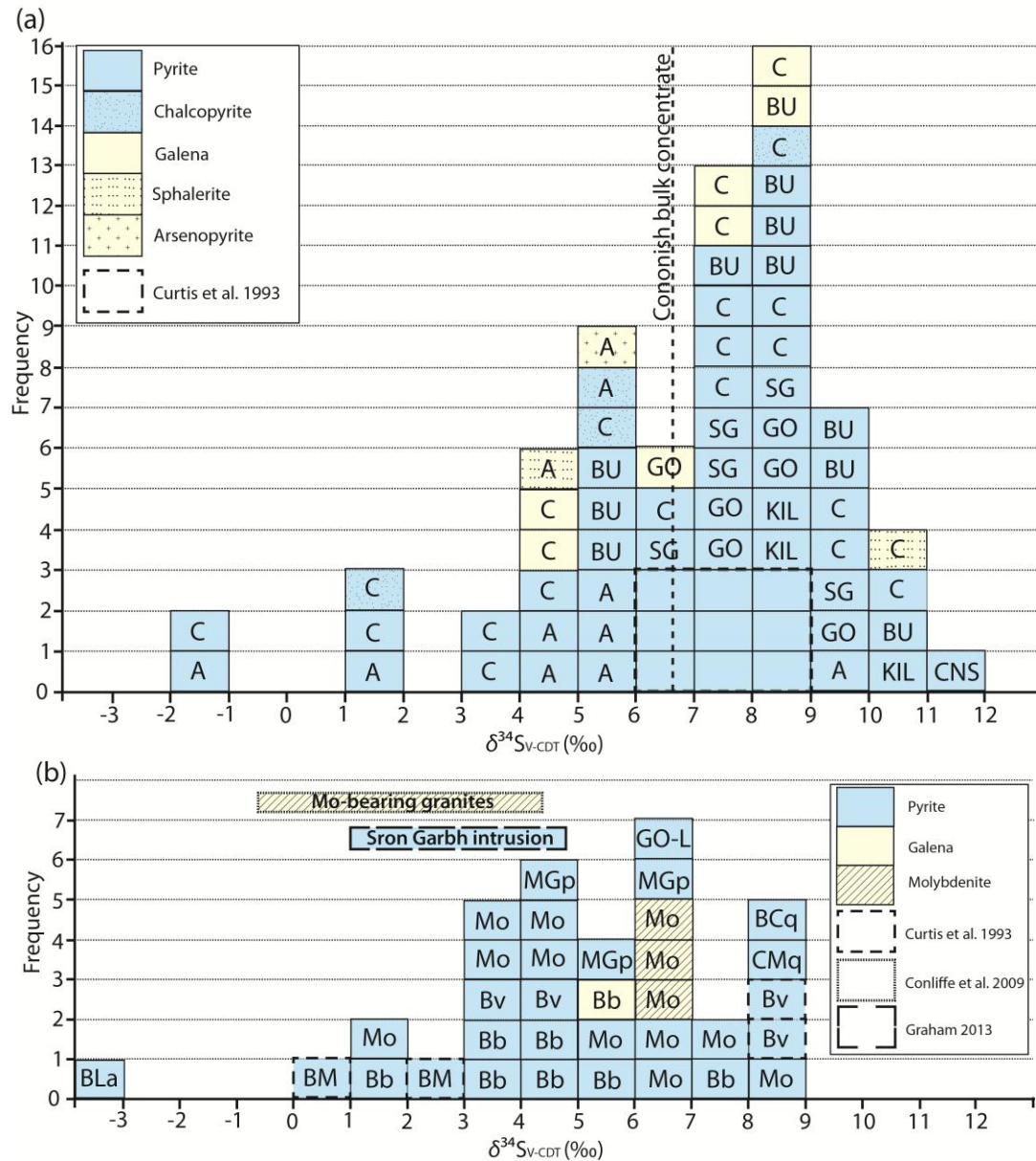


Figure 6.7: New S-isotope data for different mineralisation types, intrusions and host rocks in the Tyndrum area. **A.** S-isotope data for gold-bearing quartz veins in the Tyndrum area. Cononish bulk concentrate represents the $\delta^{34}\text{S}$ value measured for sulphide float concentrate from crushed bulk ore. **B.** S-isotope data for breccia bodies, barren veins, molybdenite mineralisation, magmatic bodies and host rocks. A – Auch Estate; BM – Blackmount; BU – Beinn Udlaidh; C – Cononish; CNS – Coire Nan Sionnach; KIL – Kilbride; GO – Glen Orchy (Au-bearing quartz veins); GO-L – Lamprophyre from Glen Orchy; SG – Sron Garbh; Bb – Breccia bodies at Beinn Udlaidh; Bv – Barren Veins; Mo – Molybdenite-related; MGp – Meall Garbh Psammite; CMq – Carn Maig Quartzite; BCq – Ben Challum Quartzite; BLa – Ben Lawers Schist.

Table 6.1 *S-isotope results from mineralisation, sedimentary and magmatic sulphide showings in the Tyndrum area*

	Location	Vein	ID number	Xco	Yco	Zco (m)	Sample type	Description	Species	Yield (%)	$\delta^{34}\text{S}$ (‰)
Gold-bearing veins	Auch Estate	Creag Sheileach	A01a	234779	738791	399	HS	Pyrite in brecciated quartz vein (Post Au1)	Py	87	9.56
Gold-bearing veins	Auch Estate	Creag Sheileach	A01b	234779	738791	399	HS	Massive pyrite between late quartz veins (Post Au1)	Py	73	5.56
Gold-bearing veins	Auch Estate	Coire a'Ghabalach	CG01B1	232890	739788	666	HS	Massive pyrite containing galena inclusions in brecciated	Py	60	1.40
Gold-bearing veins	Auch Estate	Coire a'Ghabalach	CG01B2	232890	739788	666	HS	Pyrite in brecciated zone (Post Au1)	Py	72	-2.00
Gold-bearing veins	Auch Estate	Coire a'Ghabalach	CG01N1	232890	739788	666	HS	Pyrite from main quartz vein (Post Au1/ Pre Au2)	Py	78	5.30
Gold-bearing veins	Auch Estate	Coire a'Ghabalach	CG01N2	232890	739788	666	HS	Pyrite within brecciated zone (Post Au1)	Py	80	5.00
Gold-bearing veins	Auch Estate	Coire a'Ghabalach	CG01N1	232890	739788	666	HS	Arsenopyrite with pyrite from main quartz vein (Post Au1/ Pre Au2)	Apy	Laser	5.40
Gold-bearing veins	Auch Estate	Coire a'Ghabalach	CG01S1	232890	739788	666	HS	Pyrite isolated in quartz (Post Au1)	Py	99	4.25
Gold-bearing veins	Auch Estate	Coire a'Ghabalach	CG01S2	232890	739788	666	HS	Pyrite next to sphalerite in main quartz vein (Post Au1)	Py	83	4.70
Gold-bearing veins	Auch Estate	Coire a'Ghabalach	CG01S1	232890	739788	666	HS	Chalcopyrite with pyrite in main quartz vein (Post Au1)	Cp	Laser	5.00
Gold-bearing veins	Auch Estate	Coire a'Ghabalach	CG01S1	232890	739788	666	HS	Sphalerite adjacent to pyrite in main quartz vein (Au2)	Sph	93	4.67
Gold-bearing veins	Beinn Udlaidh	Main vein	11/8 100 mark	228298	733354	740	HS	Galena in with pyrite in main quartz vein (Syn Au1)	Ga	57	8.90

	Location	Vein	ID number	Xco	Yco	Zco (m)	Sample type	Description	Species	Yield (%)	$\delta^{34}\text{S}$ (‰)
Gold-bearing veins	Beinn Udlaidh	Main vein	11/8 100 mark	228298	733354	740	HS	Pyrite with minor galena in main quartz vein (Post-Au1)	Py	35	8.40
Gold-bearing veins	Beinn Udlaidh	Main vein	27/7 'Transect	228293	733349	745	HS	Fine grained pyrite disseminated in brecciated zone (Post Au1)	Py	28	10.20
Gold-bearing veins	Beinn Udlaidh	Main vein	BU11	226733	733972	380	HS	Pyrite with minor galena from main quartz vein (Post Au1)	Py	45	9.70
Gold-bearing veins	Beinn Udlaidh	Main vein	BU12	228298	733354	748	HS	Cubic pyrite from main brecciated quartz vein (Post Au1)	Py	29	5.20
Gold-bearing veins	Beinn Udlaidh	Main vein	BU15	228069	733135	840	HS	Fine grained pyrite disseminated in brecciated zone (Post Au1)	Py	77	7.60
Gold-bearing veins	Beinn Udlaidh	Main vein	BU5	228375	733407	722	HS	Fine grained pyrite disseminated in brecciated zone (Post Au1)	Py	88	9.55
Gold-bearing veins	Beinn Udlaidh	Main vein	WP BU01A	228065	733121	830	HS	Disseminated pyrite from sulphide zone in massive quartz vein (Post Au1)	Py	76	8.16
Gold-bearing veins	Beinn Udlaidh	Main vein	WP BU02	227726	732746	813	HS	Disseminated pyrite from sulphide zone in massive quartz vein (Post Au1)	Py	93	5.74
Gold-bearing veins	Beinn Udlaidh	Main vein	WP BU05	228012	733069	838	HS	Disseminated pyrite from sulphide zone in massive quartz vein (Post Au1)	Py	75	5.83
Gold-bearing veins	Beinn Udlaidh	Main vein	WP BUNext	228346	733376	730	HS	Massive pyrite from NE extension sulphide rich zone (Post Au1)	Py	61	8.15
Gold-bearing veins	Cononish	Bulk concentrate	Con bulkcon					Bulk concentrate from Cononish		N/A	6.68
Gold-bearing veins	Cononish	Eas Anie	A-min 738m	228610	728079	400	UG	Massive pyrite in main brecciated quartz vein (Pre Au1)	Py	79	-1.95

	Location	Vein	ID number	Xco	Yco	Zco (m)	Sample type	Description	Species	Yield (%)	$\delta^{34}\text{S}$ (‰)
Gold-bearing veins	Cononish	Eas Anie	A-min end of adit	228284	727753	400	UG	Chalcopyrite with pyrite in main quartz vein (Au2)	Cp	70	1.80
Gold-bearing veins	Cononish	Eas Anie	A-min end of adit	228284	727753	400	UG	Pyrite with chalcopyrite in main quartz vein (Au2)	Py	53	3.05
Gold-bearing veins	Cononish	Eas Anie	CN666	228536	728020	400	UG	Highly brecciated zone within main vein (Au2)	Ga	92	7.50
Gold-bearing veins	Cononish	Eas Anie	CN666	228536	728020	400	UG	Highly brecciated zone within main vein (Au2)	Py	53	6.70
Gold-bearing veins	Cononish	Eas Anie	CO02	228632	728085	400	UG	Massive pyrite from gold-rich section within early quartz (Pre Au1)	Py	88	1.83
Gold-bearing veins	Cononish	Eas Anie	CO03a	228632	728085	400	UG	Closely related chalcopyrite and galena in narrow late sulphide rich shear in massive white quartz (Au2)	Cp	80	8.20
Gold-bearing veins	Cononish	Eas Anie	CO03b	228632	728085	400	UG	Closely related chalcopyrite and galena in narrow late sulphide rich shear in massive white quartz (Au2)	Ga	107	4.87
Gold-bearing veins	Cononish	Eas Anie	CO03c	228632	728085	400	UG	Cubic pyrite from massive white quartz by sulphide rich shear (Pre Au1)	Py	84	10.99
Gold-bearing veins	Cononish	Eas Anie	CO05	228770	728194	400	UG	Narrow late sulphide shear near cross-cutting Tyndrum Pb mine-style mineralisation (Pre Au1)	Py	90	8.88
Gold-bearing veins	Cononish	Eas Anie	CO12	228671	728114	400	UG	Sphalerite from carbonate vein in wall rock (Au2)	Sph	88	10.89
Gold-bearing veins	Cononish	Eas Anie	CO14a	229086	728542	400	UG	Vein with brecciated and altered clasts and central sulphide rich zone (Pre Au1)	Py	61	4.71
Gold-bearing veins	Cononish	Eas Anie	CO14b	229086	728542	400	UG	Vein with brecciated and altered clasts and central sulphide rich zone (Pre Au1)	Py	62	7.19

	Location	Vein	ID number	Xco	Yco	Zco (m)	Sample type	Description	Species	Yield (%)	$\delta^{34}\text{S}$ (‰)
Gold-bearing veins	Cononish	Eas Anie	Con 11B 248-249m	228613	728105	503	DC	Galena around fractured pyrite in brecciated vein (Au2)	Ga	226	7.80
Gold-bearing veins	Cononish	Eas Anie	Con 11B 248-249m	228613	728105	503	DC	Fractured pyrite from brecciated quartz vein (Pre Au1)	Py	76	8.20
Gold-bearing veins	Cononish	Eas Anie	Con 27 325-326m	228524	728093	496	DC	Pyrite in quartz vein (Pre Au1)	Py	63	9.00
Gold-bearing veins	Cononish	Eas Anie	EA01A	229060	728489	404	DC	High gold core sample, brecciated quartz vein with high sulfide content (Au2)	Ga	83	4.00
Gold-bearing veins	Cononish	Eas Anie	EA01B	229060	728489	404	DC	High gold core sample, brecciated quartz vein with high sulfide content (Au2)	Py	81	7.50
Gold-bearing veins	Cononish	Eas Anie	EA01C	229060	728489	404	DC	High gold core sample, brecciated quartz vein with high sulfide content (Au2)	Ga	73	8.40
Gold-bearing veins	Cononish	Eas Anie	EA01D	229060	728489	404	DC	High gold core sample, brecciated quartz vein with high sulfide content (Au2)	Cp	80	5.00
Gold-bearing veins	Cononish	Eas Anie	EA02 60.4m	229094	728454	405	DC	Pyrite in brecciated vein (Pre Au1)	Py	79	7.40
Gold-bearing veins	Cononish	Eas Anie	EA05 112.75m	229046	728485	405	DC	Pyrite in gold-bearing quartz vein which is cross-cut by Tyndrum Pb mine-style mineralisation	Py	81	9.10
Gold-bearing veins	Cononish	Eas Anie	EA06 75m	229087	728511	405	DC	Pyrite in small quartz veins cross-cutting K-feldspar altered psammite (Pre Au1)	Py	83	3.70
Gold-bearing veins	Cononish	Coire Nan Sionnach	CNS05	228302	729714	670	HS	Pyrite from silicified sulphide rich brecciated quartz vein (Pre Au1)	Py	77	11.10
Gold-bearing veins	Cononish	Kilbridge	Kil01	227819	730192	125	HS	Disseminated pyrite (Pre Au2) in brecciated quartz vein	Py	60	10.90

Location	Vein	ID number	Xco	Yco	Zco (m)	Sample type	Description	Species	Yield (%)	$\delta^{34}\text{S}$ (‰)
Gold-bearing veins	Cononish	Kil02a	227718	730108	95	HS	Pyrite from dark sulphide rich quartz vein (Pre Au2)	Py	65	8.50
Gold-bearing veins	Cononish	Kil02b	227718	730108	95	HS	Pyrite disseminated in altered host rock at contact with quartz vein (Pre Au2)	Py	57	8.90
Gold-bearing veins	Glen Orchy	GO02a	225922	734658	109	HS	Cubic pyrite from brecciated quartz vein (Syn Au1); Cross-cuts GO1213	Py	64	8.11
Gold-bearing veins	Glen Orchy	GO01	226467	735580	109	HS	Pyrite in contact with host rock at edge of vein (Syn Au1); Cross-cuts GO1206	Py	57	9.40
Gold-bearing veins	Glen Orchy	GO02b	225922	734658	109	HS	Gold-bearing cubic pyrite from brecciated quartz vein (Syn Au1); Cross-cuts GO1213	Py	90	8.20
Gold-bearing veins	Glen Orchy	RV18	225118	733967	99	HS	Large galena blebs from complex brecciated quartz vein (Syn Au2); Cross-cuts GO1218	Ga	114	6.31
Gold-bearing veins	Glen Orchy	RV18	225118	733967	99	HS	Cubic pyrite in vein from complex brecciated quartz vein (Syn Au1); Cross-cuts GO1213	Py	78	7.52
Gold-bearing veins	Glen Orchy	RVN/Q04 165m	225184	734025	108	DC	Large pyrite in 20 cm wide brecciated quartz vein in gold rich core (Syn Au1)	Py	93	7.77
Gold-bearing veins	Sron Garbh	SG04a	232065	732789	566	HS	Cubic pyrite from gold-bearing quartz vein (Syn Au1)	Py	100	6.77
Gold-bearing veins	Sron Garbh	SG04b	232065	732789	566	HS	Cubic pyrite from vein contact with altered Meall Garbh Psammite (Syn Au1)	Py	58	9.39
Gold-bearing veins	Sron Garbh	SG05	232005	732882	591	HS	Small pyrite from quartz vein (Syn Au1)	Py	84	7.78
Gold-bearing veins	Sron Garbh	SG07a	232039	732771	570	HS	Large cubic pyrite in brecciated quartz vein (Syn Au1)	Py	82	7.41

	Location	Vein	ID number	Xco	Yco	Zco (m)	Sample type	Description	Species	Yield (%)	$\delta^{34}\text{S}$ (‰)
Gold-bearing veins	Sron Garbh		SG07b	232039	732771	570	HS	Pyrite in fine stringers in brecciated quartz vein (Syn Au1)	Py	93	8.67
Tyndrum Pb mine-style	Cononish	Eas Anie	EA04 10.50m b-	229125	728471	404	DC	Chalcopyrite with galena from vein cross-cutting main Cononish structure	Cp	74	9.20
Tyndrum Pb mine-style	Cononish	Eas Anie	EA04 10.50m B-	229125	728471	404	DC	Galena with chalcopyrite from vein cross-cutting main Cononish structure	Ga	94	6.60
Barren veins	Glen Orchy		RV14	225145	734087	99	HS	Pyrite from barren central vein (Post Mo min)	Py	79	4.05
Barren veins	Glen Orchy		RV15	225098	734072	100	HS	Pyrite from alteration zone (Post Mo min)	Py	85	3.08
Breccia bodies	Beinn Udlaidh		BU 22	226708	734198	335	HS	Large single galena grain in lamprophyre.	Ga	84	5.20
Breccia bodies	Beinn Udlaidh		BU 01	226636	733870	400	HS	Small cubic pyrite disseminated in matrix (Post Au)	Py	41	1.30
Breccia bodies	Beinn Udlaidh		BU 12	227430	732664	765	HS	Small cubic pyrite disseminated in matrix (Post Au)	Py	46	3.65
Breccia bodies	Beinn Udlaidh		BU 22	226708	734198	335	HS	Small cluster of coarse euhedral pyrite grains in lamprophyre.	Py	69	3.80
Breccia bodies	Beinn Udlaidh		BU 11	225914	732806	480	HS	Small cubic pyrite disseminated in matrix (Post Au)	Py	66	4.70
Breccia bodies	Beinn Udlaidh		BU 21	226591	735659	105	HS	Small cluster of coarse euhedral pyrite grains in lamprophyre.	Py	64	4.90
Breccia bodies	Beinn Udlaidh		BU 15	226718	733975	380	HS	Small cluster of fine amorphous pyrite grains, next to breccia-host rock contact. (Post Au)	Py	62	5.15

	Location	Vein	ID number	Xco	Yco	Zco (m)	Sample type	Description	Species	Yield (%)	$\delta^{34}\text{S}$ (‰)
Breccia bodies	Beinn Udlaidh		BU 16	226448	734047	358	HS	Large single pyrite grain in lamprophyre.	Py	84	7.35
Molybdenite-bearing veins	Glen Orchy	River Vein	RV01	225150	733968	95	HS	Molybdenite from K-feldspar alteration zone (Syn-Mo)	Moly	64	6.00
Molybdenite-bearing veins	Glen Orchy	River Vein	RV109	225116	734032	97	HS	Molybdenite from K-feldspar alteration zone (Syn-Mo)	Moly	48	6.30
Molybdenite-bearing veins	Glen Orchy	River Vein	GO1217	225122	734033	114	HS	Molybdenite from K-feldspar alteration zone (Syn-Mo)	Moly	63	6.60
Molybdenite-bearing veins	Glen Orchy	River Vein	RV12	225138	733982	106	HS	Large cubic pyrite (Post-Mo)	Py	67	1.83
Molybdenite-bearing veins	Glen Orchy	River Vein	RV13b	225140	733998	104	HS	Pyrite in cross-cutting quartz vein (Post-Mo)	Py	61	3.74
Molybdenite-bearing veins	Glen Orchy	River Vein	RVNQ167	225184	734025	108	DC	Pyrite from molybdenite rich core (Post-Mo)	Py	75	3.99
Molybdenite-bearing veins	Glen Orchy	River Vein	RV13a	225140	733998	104	HS	Pyrite from K-feldspar alteration zone (Post-Mo)	Py	78	4.50
Molybdenite-bearing veins	Glen Orchy	River Vein	RV10	225136	733988	105	HS	Pyrite from K-feldspar alteration zone (Post-Mo)	Py	65	4.65
Molybdenite-bearing veins	Glen Orchy	River Vein	RV021	225150	733968	95	HS	Pyrite disseminated in host psammite (Post-Mo)	Py	73	5.00
Molybdenite-bearing veins	Glen Orchy	River Vein	RV16	225111	733992	95	HS	Large cubic pyrite in quartz at adjacent to alteration zone (Post-Mo)	Py	72	6.09
Molybdenite-bearing veins	Glen Orchy	River Vein	RV11	225136	733988	105	HS	Large cubic pyrite from late quartz vein (Post-Mo)	Py	58	6.24

	Location	Vein	ID number	Xco	Yco	Zco (m)	Sample type	Description	Species	Yield (%)	$\delta^{34}\text{S}$ (‰)
Molybdenite-bearing veins	Glen Orchy	River Vein	RV16b	225111	733992	95	HS	Pyrite in quartz vein with some K-feldspar alteration (Post-Mo)	Py	68	7.52
Molybdenite-bearing veins	Glen Orchy	River Vein	RV01	225150	733968	95	HS	Pyrite from alteration band within host rock (Post-Mo)	Py	50	8.40
Host rocks	Auchtertyre		ATT06	235614	730236	248	HS	Disseminated pyrite from Ben Challum Quartzite	Py	53	8.00
Host rocks	Auchtertyre		ATT01	235219	731141	321	HS	Disseminated pyrite from Ben Lawers Schist	Py	72	-3.20
Host rocks	Auch Estate		LT02	235714	733589	524	HS	Disseminated pyrite from Cam Mairg Quartzite	Py	54	8.71
Host rocks	Glen Orchy		GO1206	226467	735579	114	HS	Meall Garbh Psammite; Cross-cut by GO01 and sample taken at contact with vein	Py	62	4.78
Host rocks	Glen Orchy		GO1218	225131	733961	96	HS	Meall Garbh Psammite; Cross-cut by RV18 and sample taken at contact with vein	Py	64	6.95
Host rocks	Sron Garbh		17.04	232450	732991	490	DC	Meall Garbh Psammite	Py	Laser	5.3
Igneous	Glen Orchy		GO1213	225921	734658	104	HS	Lamprophyre; Cross-cut by GO02b and sample taken at contact with vein	Py	62	6.76

Table 6.2 *Geochemistry and S-isotope data of host lithology and key magmatic bodies and associated cross-cutting veins in the Tyndrum area.*

Sample ID	Location	Type	Xco	Yco	Zco (m)	Lithology	Origin of sulphides	S%	Species	This study $\delta^{34}\text{S}$ (‰)
ATT04	Auchtertyre	HS	235443	729154	200	Ben Lui Schist	Volcanogenic	0.02		
ATT06	Auchtertyre	HS	235614	730236	248	Ben Challum Quartzite	Syn-sedimentary mineralised SEDEX horizon	1.27	Pyrite	8.00
ATT07	Auchtertyre	HS	235602	730229	243	Ben Challum Quartzite	Syn-sedimentary mineralised SEDEX horizon	2.32		
ConBG10	Cononish	HS	231077	728647	254	Ben Lawers Schist	Volcanogenic	0.23		
ATT01	Auchtertyre	HS	235219	731141	321	Ben Lawers Schist	Volcanogenic	1.78	Pyrite	-3.20
ATT02	Auchtertyre	HS	235271	731056	317	Ben Lawers Schist	Volcanogenic	0.51		
ConBG11	Cononish	HS	228987	727238	305	Ardishaig Phyllite	Diagenetic sedimentary	0.02		
ConBG02	Cononish	HS	227080	727700	420	Carn Maing Quartzite	Unconstrained stratabound un-mineralised horizon	0.01		
ConBG03	Cononish	HS	227101	727751	413	Leven Schist	No sulphides present	0.01		
GO1219	Glen Orchy	HS	224998	733606	95	Beinn Udlaidh Quartzite	No sulphides present	0.02		
GO1220	Glen Orchy	HS	224624	732702	82	Beinn Udlaidh Quartzite	No sulphides present	0.01		
BGA06	Auch	HS	233561	736344	223	Meall Garbh Psammite	No sulphides present	0.09		
GO1202	Glen Orchy	HS	227536	736730	124	Meall Garbh Psammite 1 m from K-feldspar alteration	No sulphides present	0.19		
GO1203	Glen Orchy	HS	227345	736570	122	Meall Garbh Psammite near 0.5 m from K-feldspar alteration	No sulphides present	0.01		

SampleID	Location	Type	Xco	Yco	Zco (m)	Lithology	Origin of sulphides	S%	Species	This study $\delta^{34}\text{S}$ (‰)
GO1207	Glen Orchy	HS	226467	735579	114	Meall Garbh Psammite 5 m from vein GO01	No sulphides present	0.01		
GO1206	Glen Orchy	HS	226467	735579	114	Meall Garbh Psammite at contact with GO01	Vein cross-cutting	0.40	Pyrite	4.78
GO1216	Glen Orchy	HS	225106	734092	104	Meall Garbh Psammite 2 m from RV18	No sulphides present	0.05		
GO1218	Glen Orchy	HS	225131	733961	96	Meall Garbh Psammite at contact with RV18	Vein cross-cutting	0.76	Pyrite	6.95
RV18	Glen Orchy	HS	225118	733967	99	Au-bearing quartz vein, up to 1 m wide	Sulphides within vein	1.66	Pyrite	7.52
GO02b	Glen Orchy	HS	225922	734658	109	Au-bearing quartz vein, up to 30 cm wide	Sulphides within vein	7.13	Pyrite	8.2
GO1207	Glen Orchy	HS	226467	735579	114	Meall Garbh Psammite 5 m from vein GO01	No sulphides present	0.01		
GO1206	Glen Orchy	HS	226467	735579	114	Meall Garbh Psammite at contact with GO01	Vein cross-cutting	0.40	Pyrite	4.78
GO1216	Glen Orchy	HS	225106	734092	104	Meall Garbh Psammite 2 m from RV18	No sulphides present	0.05		
GO1218	Glen Orchy	HS	225131	733961	96	Meall Garbh Psammite at contact with RV18	Vein cross-cutting	0.76	Pyrite	6.95
GO1210	Glen Orchy	HS	225870	734653	108	Lamprophyre sill 40m away from veins	No sulphides present	0.20		
GO1213	Glen Orchy	HS	225921	734658	104	Mineralised lamprophyre sill cut by GO02b	Vein cross-cutting	2.26	Pyrite	6.76
GO01	Glen Orchy	HS	226467	735580	109	Au-bearing quartz vein, 10 cm wide	Sulphides within vein	7.12	Pyrite	9.40
RV18	Glen Orchy	HS	225118	733967	99	Au-bearing quartz vein, up to 1 m wide	Sulphides within vein	1.66	Pyrite	7.52
GO02b	Glen Orchy	HS	225922	734658	109	Au-bearing quartz vein, up to 30 cm wide	Sulphides within vein	7.13	Pyrite	8.2

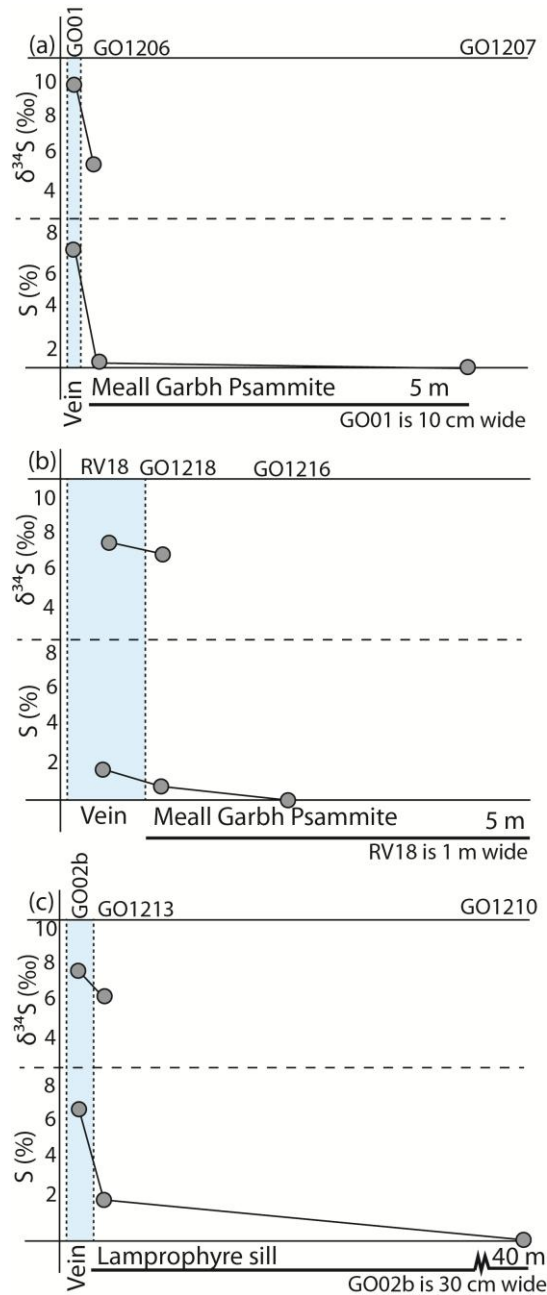


Figure 6.8: Variation in host rock $\delta^{34}\text{S}$ and S% with distance away from gold-bearing quartz veins: (A & B) psammite host rock. (C) Lamprophyre host rock.

6.8.2 S-isotope fractionations between mineral pairs

Pyrite and molybdenite pairs (Table 6.3) are not in sulphur isotope equilibrium when compared to experimental fractionation factors ($\Delta^{34}\text{S} = 0.31$ to -0.12 over 400 to 600 °C; Suvorova 1974), with the pyrite in equilibrium with a fluid ~ 2 ‰ higher if formed at similar temperatures. The fractionation between chalcopyrite and pyrite (Kajiwara & Krouse 1971) at Cononish indicates that for the low $\delta^{34}\text{S}$ values, chalcopyrite and pyrite are in equilibrium

at $326 \pm 89^{\circ}\text{C}$ (Table 6.3), within the suggested temperature range of precipitation (290 to 350°C ; Curtis *et al.* 1993). At higher $\delta^{34}\text{S}$ values fractionations between chalcopyrite and pyrite are large resulting in low apparent temperatures (Kajiwara & Krouse 1971); chalcopyrite is likely to be in equilibrium with a fluid ~ 1.2 to 1.5‰ lighter if pyrite and chalcopyrite formed at 290 to 350°C . Galena is consistently in disequilibrium (isotopic reversal with galena having higher values than the pyrite) over a temperature range of 250 to 500°C or gives low temperatures (Table 6.3) with chalcopyrite and pyrite (Li & Lui 2006; Kajiwara & Krouse 1971). The S-isotope fractionations between galena and chalcopyrite at Cononish give low temperatures that might reflect cooling during the development of the paragenesis. While the equilibrium fractionation of S-isotope between arsenopyrite and pyrite is not constrained, the similar $\delta^{34}\text{S}$ values observed at Coire a'Ghabalach (Table 6.3) suggests equilibrium was reached (Nesbitt 1988). Overall, the S-isotope fractionations are consistent with the petrographic evidence of early pyrite and later chalcopyrite and galena.

Table 6.3 *S*-isotope fractionation data and calculated apparent equilibrium temperatures for mineral pairs in the Tyndrum area.

Location	Vein	ID number	Species	Yield (%)	$\delta^{34}\text{S}$ (‰)	Species	$\Delta^{34}\text{S}$ (‰)	Temp range (°C)
Gold veins	Auch Estate	Coire a'Ghabalach	Py	83	4.70	Py-Sph	0.03	Dis-equilibrium over temperature range 250-500°C
Gold veins	Auch Estate	Coire a'Ghabalach	Sph	93	4.67			
Gold veins	Auch Estate	Coire a'Ghabalach	Py	78	5.30			
Gold veins	Auch Estate	Coire a'Ghabalach	Apy	Laser	5.40			
Gold veins	Beinn Udlaidh	Main vein	Ga	57	8.90	Py-Gal	-0.50	Dis-equilibrium over temperature range 250-500°C
Gold veins	Beinn Udlaidh	Main vein	Py	35	8.40			
Gold veins	Cononish	Eas Anie	Cp	70	1.80	Py-Cpy	1.25	Equilibrium - realistic temperature for Cononish
Gold veins	Cononish	Eas Anie	Py	53	3.05			
Gold veins	Cononish	Eas Anie	Ga	92	7.50	Py-Gal	-0.80	Dis-equilibrium over temperature range 250-500°C
Gold veins	Cononish	Eas Anie	Py	53	6.70			
Gold veins	Cononish	Eas Anie	Cp	80	8.20	Py-Cpy	2.79	Possibly in equilibrium but temperatures recorded are lower than previously noted at Cononish
Gold veins	Cononish	Eas Anie	Ga	107	4.87	Py-Gal	6.12	150±11
Gold veins	Cononish	Eas Anie	Py	84	10.99	Cpy-Gal	3.34	167±22
Gold veins	Cononish	Eas Anie	Ga	226	7.80	Py-Gal	0.40	1385±405
Gold veins	Cononish	Eas Anie	Py	76	8.20			Dis-equilibrium - un-realistic temperature

Location	Vein	ID number	Species	Yield (%)	$\delta^{34}\text{S}$ (‰)	Species	$\Delta^{34}\text{S}$ (‰)	Temp range (°C)
Gold veins	Cononish	Eas Anie	Ga A	83	4.00	Py-Gal a	3.50	287±26 Possibly in equilibrium
Gold veins	Cononish	Eas Anie	Py	81	7.50	Py-Gal b	-0.90	Dis-equilibrium over temperature range 250-500°C
Gold veins	Cononish	Eas Anie	Ga B	73	8.40	Py-Cpy	2.50	150±29 Possibly in equilibrium but temperatures recorded are lower than previously noted at Cononish
Gold veins	Cononish	Eas Anie	Cp	80	5.00	Cpy-Gal _a	1.00	523±167 Dis-equilibrium - un-realistic temperature
Gold veins	Cononish	Eas Anie				Cpy-Gal _b	-3.40	Dis-equilibrium over temperature range 250-500°C
Gold veins	Glen Orchy	River Vein	Ga	114	6.31	Py-Gal	1.22	676±144 Dis-equilibrium - un-realistic temperature
Gold veins	Glen Orchy	River Vein	Py	78	7.52			
Breccia bodies	Beinn Udlaidh		Ga	84	5.20	Py-Gal	-1.40	Dis-equilibrium over temperature range 250-500°C
Breccia bodies	Beinn Udlaidh		Py	69	3.80			
Molybdenite	Glen Orchy	River Vein	Moly	64	6.00	Moly-Py	-2.40	Dis-equilibrium over temperature range 400-650°C
Molybdenite	Glen Orchy	River Vein	Py	50	8.40			

6.9. Discussion

The wide range in S-isotope values from mineralisation in the Tyndrum area is inconsistent with a single source for the sulphur in these occurrences. Curtis *et al.* (1993) suggested that the sulphur in the Cononish gold-bearing quartz vein mineralisation had to have derived a significant proportion from the Dalradian sedimentary succession, the remainder being of magmatic origin. Results from this study confirm that sedimentary sulphur is a significant source in the gold mineralised veins, breccia bodies and molybdenite mineralisation in the Tyndrum area, and the enhanced dataset is used here to identify the likely sedimentary source rocks and their contribution to the veins; in particular whether the Grampian and lower-Appin host units could contribute to the sedimentary sulphur component. Following definition of the magmatic end-member and review of the existing data for the Dalradian metasedimentary pile, the likely sedimentary $\delta^{34}\text{S}$ values and how they vary through the Dalradian succession are further constrained by correlating the global $\delta^{34}\text{S}$ curve (Halverson *et al.* 2010) to the Dalradian stratigraphy. This provides probable $\delta^{34}\text{S}$ values for sulphur-poor metasedimentary rocks that have only limited existing data.

6.9.1 Magmatic S-sources

Sulphides in mineralisation associated with plutonic intrusions across the area average $\delta^{34}\text{S} +2.6 \pm 1.8\text{‰}$ (Fig. 6.4; Lowry *et al.* 1995) and, specifically, sulphides from the Etive granite (Fig. 6.1) have an average $\delta^{34}\text{S}$ of $+2.1\text{‰}$ suggesting that the granite may have derived some sulphur from crustal sources during emplacement (Lowry *et al.* 2005). $\delta^{34}\text{S}$ values from the Sron Garbh intrusion ($\delta^{34}\text{S} = +1.0$ to $+4.8\text{‰}$; Figs. 6.3; 6.7B) are comparable to appinite pipes elsewhere in the Dalradian ($\delta^{34}\text{S} = -2$ to $+6\text{‰}$; Lowry 1991; Lowry *et al.* 1995). Thus it appears that all potential magmatic sources have $\delta^{34}\text{S}$ values slightly higher than uncontaminated mantle-derived melts ($\delta^{34}\text{S} = 0 \pm 3\text{‰}$; Ohmoto 1986).

6.9.2 Sedimentary S-sources

The extensive dataset of $\delta^{34}\text{S}_{\text{sulphide}}$ for Dalradian metasedimentary rocks (Appin-Southern Highland Groups) records large variations through the sequence (Fig. 6.4 & 6.9; Willan & Coleman 1983; Scott *et al.* 1987, 1991; Hall *et al.* 1988, 1994a, b; Lowry 1991) ranging from as low as -15‰ in the Ardrishaig Phyllite to as high as $+42\text{‰}$ in Bonahaven Dolomite, consistent with the large variations in $\delta^{34}\text{S}_{\text{sulphide}}$ in the global Neoproterozoic record ($\delta^{34}\text{S}_{\text{sulphide}} = -30$ to $+50\text{‰}$; Halverson *et al.* 2010). Sulphates have a limited occurrence in

the Dalradian Supergroup and are mostly confined to the Aberfeldy deposits (Willan & Coleman 1983; Hall *et al.* 1991; Moles *et al.* 2014).

Most of the sulphide data comes from the Argyll Group, with only data from the Ballachulish Slate Formation deeper in the sequence. Stratabound sulphides in the Dalradian sequence are of three types: (a) sedimentary diagenetic sulphides which have usually undergone some recrystallisation during regional metamorphism; (b) sulphide rich but un-mineralised horizons thought to be of volcanogenic origin and (c) syn-sedimentary mineralised hydrothermal exhalative SEDEX horizons. All three types of sulphide could be potential sources for the sulphide in the Tyndrum mineralisation and all are referred to as 'sedimentary-sourced'. However, only sedimentary diagenetic sulphides that have been metamorphosed as a closed system are expected to correlate with the global sedimentary sulphide S-isotope record.

Sulphide $\delta^{34}\text{S}$ values within the un-mineralised Ballachulish Slate (Appin Group; Fig. 6.2), Bonahaven Dolomite, Ben Eagach Schist and Ardrishaig Phyllite ($\delta^{34}\text{S} = -15$ to $+42\text{‰}$; Willan & Coleman 1983; Hall *et al.* 1987, 1994a, 1994b; Lowry 1991; Moles *et al.* 2014) represent the background diagenetic sedimentary record. Diagenetic sedimentary sulphides in the Ben Eagach Schist have $\delta^{34}\text{S}$ values in the range -5.7 to $+18\text{‰}$ (Willan & Coleman 1983; Moles *et al.* 2014). The Ardrishaig Phyllite ($\delta^{34}\text{S} = -15$ to -1‰ ; Willan & Coleman 1983; Hall *et al.* 1994a) is sulphur poor in the Tyndrum area and Lowry *et al.* (1995) noted a lack of contamination by external sulphur in porphyries hosted in the Ardrishaig Phyllite, indicating that it is unlikely to represent a significant sulphur source. Sulphur isotopic signatures from sulphides in the Bonahaven Dolomite are not typical of diagenetic pyrite ($\delta^{34}\text{S} = +29$ to $+42\text{‰}$; Willan & Coleman 1983; Hall *et al.* 1994b; Moles *et al.* 2014) and are probably the result of closed-system reduction of evaporite sulphate (Hall *et al.* 1994b).

Sulphides within stratabound horizons of likely volcanogenic origin in the Ben Lawers and Ben Lui Schists, and in the Tayvallich Volcanics, have $\delta^{34}\text{S}$ sulphide values between -4 and $+8\text{‰}$ (Willan & Coleman 1983; Scott *et al.* 1987; Lowry 1991), with a single pyrite $\delta^{34}\text{S}$ value from this study from the Ben Lawers Schist (-3.2‰ ; Fig. 6.7B; Table 6.2) being comparable. These sulphides are interpreted to be related to the appearance of mafic lavas and sills (now amphibolites) in the Dalradian sequence (Scott *et al.* 1991; Stephenson & Gould 1995).

The Aberfeldy Ba-Zn-Pb SEDEX deposits, Perthshire, are hosted largely in the Ben Eagach Schist Formation (Willan & Coleman 1983; Moles 1985; Moles *et al.* 2014).

Sulphide $\delta^{34}\text{S}$ values of the mineralisation range from +18 to +28‰ (pyrite average +23.7‰) and barite $\delta^{34}\text{S}_{\text{sulphate}}$ values from +27 to +42‰ (average $36 \pm 1.5\text{‰}$; Willan & Coleman 1983; Hall *et al.* 1987; Scott *et al.* 1991; Moles *et al.* 2014). In addition, the Ben Challum Quartzite is host to SEDEX mineralisation (Fortey & Smith 1986) and a pyrite $\delta^{34}\text{S}$ value from this study ($\delta^{34}\text{S} = +8.0\text{‰}$; Fig. 6.7B; Table 6.1) is comparable to existing data ($\delta^{34}\text{S}_{\text{sulphide}} = +8$ to +15‰; Scott *et al.* 1987; Fig. 6.4).

All of the vein samples discussed in this paper are hosted in Grampian and lower-Appin Group units (Fig. 6.2), in particular the Meall Garbh Psammite, Beinn Udlaidh Quartzite and Leven Schists. The units are sulphur poor with bulk sulphur less than 0.2%, except where units are cross-cut by mineralised veins (Fig. 6.8; Table 6.2). Consistent with this, Laouar (1987) noted that no sulphide mineralisation is observed in granites hosted within Grampian Group units, suggesting that the host rocks of the mineralisation may not have been good sulphur sources. There are no published $\delta^{34}\text{S}_{\text{sulphide}}$ or $\delta^{34}\text{S}_{\text{sulphate}}$ data for these units.

To estimate the $\delta^{34}\text{S}$ values that might occur in trace sulphides in the Grampian and lower-Appin Group stratigraphic units the global composite sulphide S-isotope curve of Halverson *et al.* (2010) is superimposed onto the Dalradian stratigraphy using two age correlations suggested by previous workers (Figs. 6.2, 6.9). In both correlations the top of the Argyll Group (Tayvallich Volcanics) is fixed at 601 ± 4 Ma (Dempster *et al.* 2002). The potential correlations are:

1. The base of the Dalradian is *c.* 800 Ma (Noble *et al.* 1996) and, following Prave *et al.* (2009), the Port Askaig Tillite is correlated with the Sturtian glacial episodes and the mid-Easdale Subgroup is correlated to Marinoan glacial episodes.
2. The base of the Dalradian is *c.* 700 Ma based on $^{87}\text{Sr}/^{86}\text{Sr}$ variation (Thomas *et al.* 2004; Stephenson *et al.* 2013); this is consistent with the Re–Os date for the Ballachulish Slate (Rooney *et al.* 2011), which in turn suggests the Port Askaig Tillite represents the Marinoan glacial episodes.

Comparison of the measured $\delta^{34}\text{S}$ for the Dalradian sequence with the global curve show a good fit for correlation 1, the only outlying points being the mineralised horizons of the Ben Eagach Schist, but given that this is a SEDEX horizon with a hydrothermal component to the sulphides (Willan & Coleman 1983; Moles *et al.* 2014) it would not be expected to fit the global curve. The good fit of the Bonahaven Dolomite data to correlation 1 may be fortuitous as this is interpreted as being a local signature due to

closed-system reduction of evaporites, not a global signal. For correlation 2 the fit is rather poorer, but this correlation is still broadly consistent with the mostly positive $\delta^{34}\text{S}$ values measured through the Argyll Group. Further research is clearly required to refine correlations and distinguish local from global signals, nevertheless all existing data and both fits of the global curve indicate a significant amount of sedimentary and hydrothermal sulphide with positive $\delta^{34}\text{S}$ in the Easdale Subgroup stratigraphic units. Deeper in the stratigraphy, both correlations give good fits to the Ballachulish Slate data. Below this the correlations are used to provide predictions of $\delta^{34}\text{S}$ in the Grampian and lower-Appin host rocks. Using correlation 1 (Figs. 6.2 & 6.9) the pre-Sturtian $\delta^{34}\text{S}$ record is limited but suggests Grampian and lower-Appin Group host rocks may have an average $\delta^{34}\text{S}$ value less than 0‰, although some units could be enriched in ^{34}S by up to 10‰. Using correlation 2 (Figs. 6.2 & 6.9) the host rocks are expected to all have $\delta^{34}\text{S} \geq 0$ ‰, with values as high as +40‰ possible. This would not be consistent with observations of veins having higher $\delta^{34}\text{S}$ than their host rocks (Fig. 6.8). In either case, the lack of sulphur in the local Grampian and lower-Appin Group metasedimentary rocks (Table 6.2) suggests they are unlikely sources of sulphur, although they could still potentially contribute ^{34}S -enriched sulphur if correlation 2 was correct.

The Islay Subgroup is not present in the Tyndrum area due to the Boundary Slide and thus could not be the source of ^{34}S -enriched sulphide in the Tyndrum mineralisation. However, the Easdale Subgroup (Fig. 6.2) has varied $\delta^{34}\text{S}$ values ($\delta^{34}\text{S} = -15$ to $+28$ ‰; Figs. 6.4 & 6.9) but is largely enriched in ^{34}S , in particular within the Ben Challum Quartzite and Ben Eagach Schist SEDEX horizons. In addition, these units are sulphur-rich (bulk S = 0.39 to 2.32%; Table 6.2), suggesting that lithologies in this Subgroup have the potential to act as a significant source of sulphur. Thus, it is proposed that the only feasible source for the sedimentary sulphur component in the Tyndrum mineralisation is the Easdale Subgroup, stratigraphically above the mineralisation. Taken at face value this could be interpreted to suggest that fluids carrying sulphur, and possibly gold and other metals, are moving down through the stratigraphy.

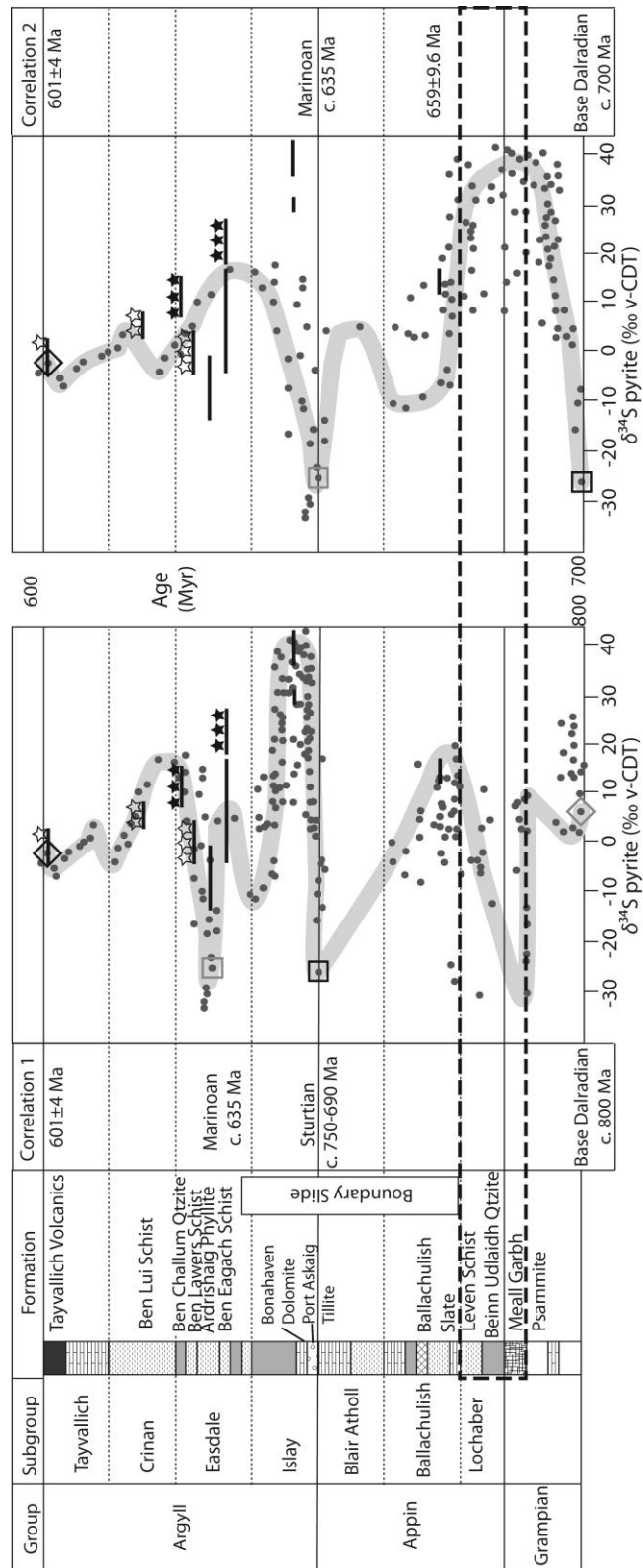


Figure 6.9: The global composite sulphide S-isotope curve of Halverson *et al.* (2010) superimposed onto the Dalradian stratigraphy using the two correlations detailed in Figure 6.2. The global data (grey dots; grey zone = line of best fit) are interpolated between tie points detailed in the text (black square and diamond; grey square and diamond) by simply scaling to stratigraphic thickness (Stephenson & Gould 1995; Stephenson *et al.* 2013). Solid black lines show the existing $\delta^{34}\text{S}_{\text{sulphide}}$ data for the Dalradian sedimentary succession (Fig. 6.4); unfilled stars = volcanogenic sulphide horizons; black stars = syn-sedimentary stratabound SEDEX horizons; black dashed box = host stratigraphy of mineralisation in the Tyndrum area.

6.9.3 Input of sedimentary vs. magmatic sulphur into mineralised veins and breccia bodies

It is possible to account for the total range of vein $\delta^{34}\text{S}$ values observed in this study ($\delta^{34}\text{S} = -2$ to $+12\text{‰}$; Fig. 6.7) with various mixtures of sulphides from the Easdale Subgroup units ($\delta^{34}\text{S} = -4$ to $+22\text{‰}$; Fig. 6.4 & 6.9) and there is no requirement to invoke an magmatic component, even for vein sulphide $\delta^{34}\text{S}$ values close to 0‰ (c.f. Craw *et al.* (1995) noted $\delta^{34}\text{S}_{\text{sulphide}}$ values of -3 to -1‰ for the metamorphogenic Macraes gold mineralisation). However, given the likely age and late tectonic setting, together with the wide range in $\delta^{34}\text{S}$ observed in the Tyndrum area mineralisation, variable mixing of magmatic and sedimentary sulphur is assumed here. The possible sedimentary rock-sourced end-members that would have been available, including both diagenetic and syn-sedimentary hydrothermal sources, are examined in Figure 6.10. Apart from five outliers out of 60 measurements, gold veins generally have $\delta^{34}\text{S}$ values in the range $+3$ to $+12\text{‰}$. Veins with $\delta^{34}\text{S}$ values of $+12\text{‰}$ can only be formed with 32 to 66% sulphur sourced from the SEDEX Ben Eagach horizon, 62 to 100% of the most ^{34}S rich diagenetic values from the Ben Eagach Schist, or 71 to 100% sedimentary sulphur sourced from the Ben Challum horizon (Fig. 6.10). It is not possible to generate a $\delta^{34}\text{S}$ of $+12\text{‰}$ by mixing involving sulphur from any other part of the stratigraphy in the area. Thus the highest $\delta^{34}\text{S}$ values measured in the veins place very strong constraints on the sources of sulphur and the hydrothermal pathways in the mineralising system, with a magmatic sulphur input constrained to a maximum of 68%. As vein $\delta^{34}\text{S}$ values decrease it becomes possible to invoke mixtures involving other sedimentary units and sulphides in gold-bearing quartz veins with $\delta^{34}\text{S}$ values of $+3\text{‰}$ could be 100% sourced from a magmatic component, or 100% from the Ben Lawers Schist or sedimentary diagenetic sulphides in the Ben Eagach Schist (Fig. 6.10). However, for vein values of $+3\text{‰}$, maximum proportions of sulphur from the syn-sedimentary SEDEX Ben Eagach Schist and Ben Challum Quartzite horizons are constrained to be $<14\%$ and $<32\%$ respectively.

The breccia bodies and molybdenite mineralisation have similar $\delta^{34}\text{S}$ ranges ($+1$ to $+8\text{‰}$; Fig. 6.10). The high $\delta^{34}\text{S}$ values for the molybdenite mineralisation compared to data from the regional magmatic complexes (Lowry *et al.* 1995; Conliffe *et al.* 2009) suggest a larger component of sedimentary-derived sulphur in the molybdenite mineralisation in the Glen Orchy area. Breccia bodies or molybdenite mineralisation with $\delta^{34}\text{S}$ values of $+8\text{‰}$ could have 18 to 43% sedimentary sulphur, sourced from the syn-sedimentary SEDEX Ben Eagach horizon or 37 to 100% sedimentary sulphur sourced from the Ben Challum

horizon. If it is assumed that the sulphur in all the mineralisation was derived from the same sedimentary-sourced end-member, sulphur isotope values indicate that the molybdenite mineralisation and gold-bearing mineralised breccia bodies have a larger magmatic component than gold-bearing quartz veins.

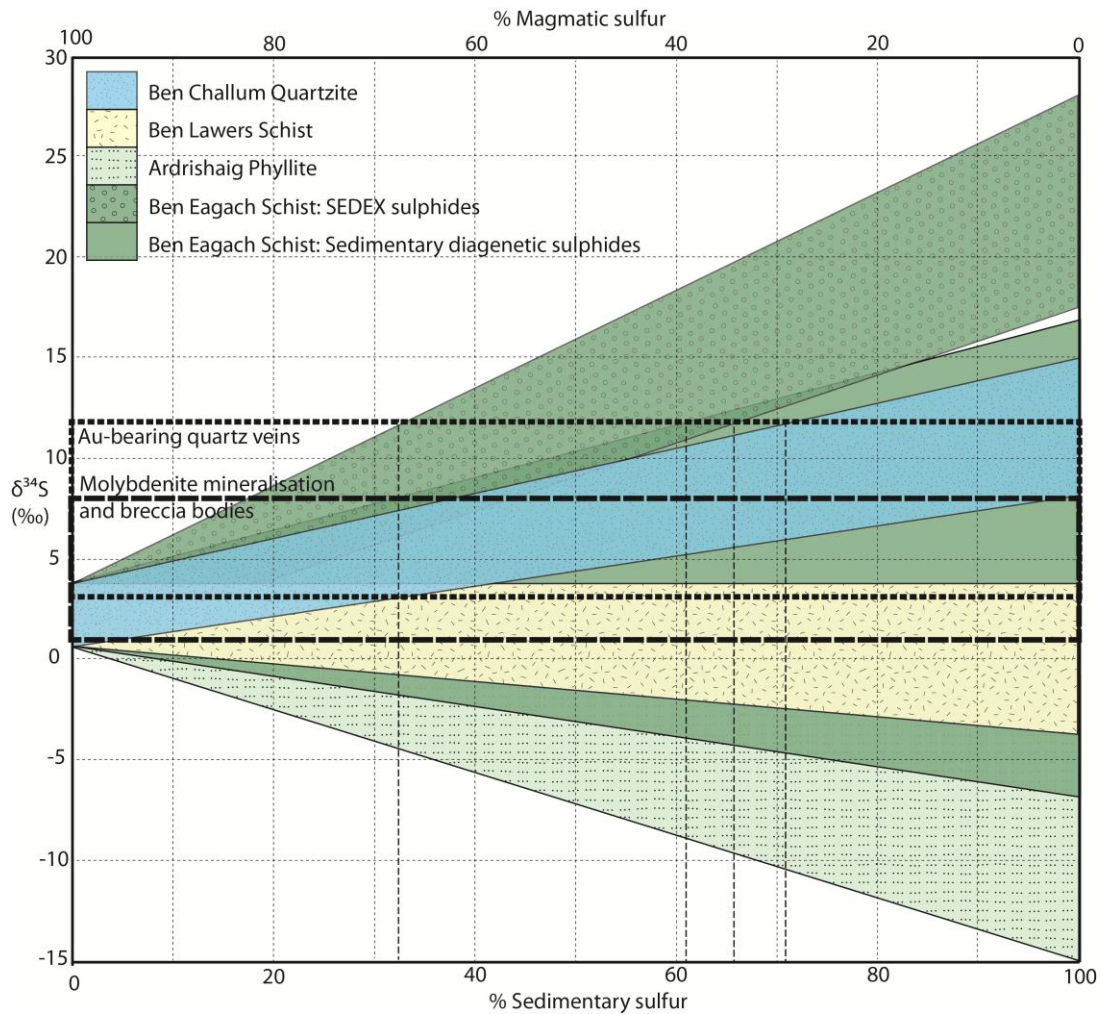


Figure 6.10: Mixing diagram showing percentage of sulphur from a magmatic and various possible sedimentary components required to account for the observed $\delta^{34}\text{S}$ mineral values. Vertical lines demonstrate the example of a mixture with $\delta^{34}\text{S} = +12\text{‰}$ that could be formed by mixing of magmatic sulphur with either 33 to 66% sedimentary sulphide from the Ben Eagach SEDEX horizon, 66 to 100% from diagenetic sulphides from the Ben Eagach Schist, or 71 to 100% from the Ben Challum horizon. References as given in Figure 6.4. Typical ranges of $\delta^{34}\text{S}$ mineral values are shown for gold-bearing quartz veins, and for molybdenite mineralisation and breccia bodies. Magmatic values are average $\delta^{34}\text{S}$ values from plutons in the Dalradian Supergroup ($\delta^{34}\text{S} = +2.6 \pm 1.8\text{‰}$; Lowry *et al.* 1995).

6.9.4 Implications of structure

The S-isotope data suggest that a significant component of the sulphur in the Tyndrum veins is sourced from the Easdale Subgroup, higher in the stratigraphy. The Eas Anie structure, host to Cononish gold mineralisation (Fig. 6.3), is not observed to cut the Boundary Slide at the current topography but is postulated to have extended across the Slide at emplacement, approximately 200 m above the mine portal (Tanner 2012). Thus here it might be possible that sulphides from the Easdale Subgroup could have been dissolved and re-precipitated in the mineralisation. However, at Glen Orchy and Beinn Udlaigh, the Easdale Subgroup and higher stratigraphic units are estimated to be approximately 4 km above at the time of mineralisation. If fluids were transported downwards from an enriched $\delta^{34}\text{S}$ source in Easdale Subgroup rocks it might be expected that the Cononish gold mineralisation would show a greater signature of this, but $\delta^{34}\text{S}$ values at Glen Orchy are comparable to Cononish (Fig. 6.7A; Table 6.1). In addition, the presence of hydraulic breccia bodies and quartz-breccia veins formed from supra-lithostatic fluids (Tanner 2012) suggest a fluid pressure gradient that would preclude fluids flowing downwards during breccia formation. Furthermore, it is difficult to envisage a thermochemical gradient that could transport sulphide 4 km downwards. These considerations suggest it was unlikely that the sulphur was derived from the overlying Easdale units.

However, consideration of the fold structures of the Tyndrum area (Tanner & Thomas 2009) has implications for possible fluid-flow pathways since all interpretations suggest that Easdale Subgroup units are likely to be repeated at depth due to the major recumbent fold of the Beinn Chuirn Anticline (Fig. 6.11). The details of the likely depth at which repetition might occur depend upon the interpretation of the Boundary Slide which represents a section of missing stratigraphy in the Tyndrum area (Figs. 6.2 & 6.3). Two interpretations are proposed (Fig. 6.11).

1. The Boundary Slide is a tectonic slide (Bailey 1922, Hutton 1979) that formed syn- to post-D2 (Roberts & Treagus 1979). The stratigraphy was folded around the Beinn Chuirn Anticline during D2 then removed by movement along the slide (Fig. 6.11A). The slide is inferred to continue to depth; the Ballachulish, Blair Atholl and Islay Subgroups and overlying stratigraphy (Fig. 6.2) are all interpreted to be represented on the inverted limb of the Beinn Chuirn anticline.

2. A more recent interpretation (Tanner & Thomas 2009) is that the Boundary Slide is a pre-tectonic disconformity and due to D2 folding stratigraphic units above the slide are expected to be represented at depth beneath the Glen Orchy dome (Fig. 6.11B; Tanner & Thomas 2009), with the Easdale Subgroup present, but at shallower depth than in Figure 6.11A.

Importantly, both interpretations imply the potential presence of the Easdale Subgroup, enriched in ^{34}S , at depth and would allow the sedimentary S-isotope signature associated with mineralisation to instead be sourced from the overturned limb of the Beinn Chuirn Anticline *beneath* the Grampian and lower-Appin Group rocks observed at surface. This seems a more realistic scenario and allows hotter fluids from depth (perhaps expelled by late-tectonic magmatism) to carry sulphur (and metals) upwards and along major structures into the current host rocks where precipitation is most likely driven by pressure reduction from lithostatic to hydrostatic and wall rock sulphidation. In this scenario gold-bearing quartz veins in Glen Orchy and Beinn Udlaidh would be closer to the postulated source rocks suggesting they should contain a greater component of sedimentary-sourced sulphur than Cononish. However, the similar $\delta^{34}\text{S}$ values in both areas do not support this. It is proposed, that the Tyndrum fault is a key fluid pathway in Glen Cononish allowing gold mineralisation in the Eas Anie structure to source significant sedimentary sulphur (as well as magmatic sulphur) from depth despite being further above the postulated sedimentary sulphur source rocks.

6.9.5 Metal source rocks

The S-isotope data cannot confirm, nor exclude, a magmatic input to the mineralisation, although the spread of data down to approximately 0‰ could be interpreted as supporting evidence and, together with the likely age that correlates with the intrusion of the granites, suggests it is probable. Thus a magmatic source for the gold and other metals is possible.

However, it is proposed that a significant proportion of the sulphur in the mineralisation must have originated from Easdale Subgroup lithologies at depth, in particular the SEDEX Ben Challum or Ben Eagach horizons. Whilst there is no requirement that metals and sulphur are derived from the same source, and this is frequently not the case in hydrothermal gold systems (Goldfarb *et al.* 1991; Goldfarb *et al.* 2001), the S-isotope data demonstrate that mineralising fluids originated from, or passed through, these units and hence it is reasonable to consider whether they could also be potential metal sources. This suggestion has some credence since, along with base metals, gold is known to be

concentrated in shale-hosted SEDEX mineralisation (e.g. Cooke *et al.* 2000; Alchin and Moore 2005). Furthermore, Willan (1996) demonstrated that the Ben Eagach Schist is regionally enriched by hydrothermal activity in Bi, Sb, As, Mo, Ni and Ba, whilst in the section between the Tyndrum Fault and Ericht-Laidon Fault to the NW, containing the study area, this unit has elevated Mo, Sb and Bi and isolated occurrences of strongly anomalous Cu, Zn and Pb. Unfortunately gold was not analysed in this study and no gold grains have been observed to date in the Aberfeldy deposits (N. Moles pers. comm.), but nevertheless it seems that SEDEX horizons in the Ben Eagach Schist represent feasible sources for at least some or all of the base metals in the veins, in particular lead, which is notably enriched as abundant galena.

Alternatively, gold and other metals could have been pre-concentrated from the sedimentary-volcanic pile during formation of volcanogenic exhalative horizons such as in the Ben Lawers Schist, which could subsequently produce gold-rich fluids (e.g. Hodgson *et al.* 1993; Mernagh & Bierli 2008). Some support for this comes from the observation by Moles (1985) of a gold inclusion within chalcocite-bornite in a sample of the Ben Lawers Schist.

A third option could be that the gold and other metals are sourced from carbonaceous pyritic metasedimentary rocks in the Dalradian Supergroup, such as parts of the Ben Eagach Schist, since these may also concentrate gold along with other metals including Ag, Zn, Mo and Cu (Large *et al.* 2011), as postulated for Dalradian rocks by Plant *et al.* (1997). Pitcairn *et al.* (2006) show that even quartzofeldspathic turbiditic metasedimentary rocks, which may not have anomalous metal contents, have the potential to release elements including Au, Ag, As, Sb, Hg, Mo, and W during metamorphism. Tomkins (2012) argues that pyritic organic-rich sedimentary rocks deposited after the second Great Oxidation Event (GOE2) (635 to 510 Ma) have the potential to be a better source of gold (and molybdenum) than sedimentary rocks deposited earlier, due to the increase in gold solubility in a more oxidised ocean. In both correlations (Fig. 6.9) sections of the Dalradian stratigraphy are deposited after 635 Ma (Marinoan) and therefore may have been enriched in gold and molybdenum at deposition.

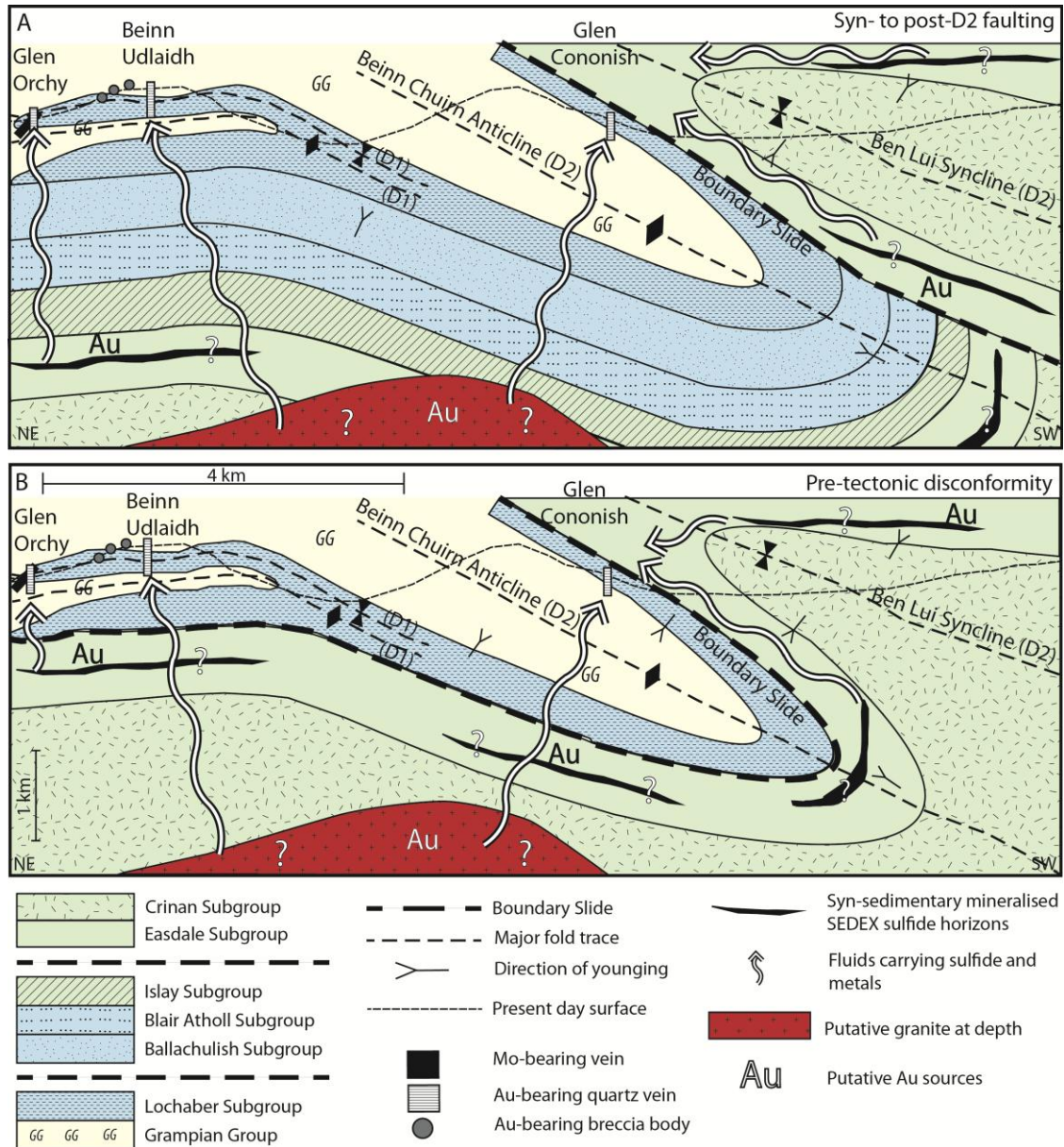


Figure 6.11: Cross-section through the Tyndrum area. Sulphur is interpreted to be sourced from stratigraphic units enriched in ^{34}S at depth, dependent upon the interpretation of the Boundary Slide: **(A)** - Interpretation after Roberts & Treagus (1979), the Boundary Slide is a tectonic slide formed syn- to post-D2. **(B)** - Interpretation after recent mapping at Cononish (Tanner & Thomas 2009). Diagram after Tanner & Thomas (2009). The Tyndrum Fault and many of the major structures in the area run sub-parallel to the strike of the section and much of the fluid flow is therefore likely to be parallel to the plane of the section. Vertical scale approximate only.

From the discussion above it is clear that carbonaceous pyritic metasedimentary rocks could have been a potential source for the molybdenum in the earliest veins in the area. Compared to the later gold-mineralisation, the generally lower $\delta^{34}\text{S}$ value of the molybdenite mineralisation either indicates a larger proportion of magmatic sulphur, or that the sulphur is from a distinct metasedimentary source. For example, average $\delta^{34}\text{S}$ for diagenetic sulphides in the Ben Eagach Schist is +5.6‰ (Willan & Coleman 1983; Moles *et al.* 2014), very close to the average value measured for the sulphides in the molybdenite mineralisation (Fig. 6.7B). Thus it is possible that both the sulphur and the molybdenite in the early molybdenum mineralisation could be wholly derived from parts of the Ben Eagach Schist. A potentially different source of sulphur and metals (and by inference fluid pathway) is conceivable for this mineralisation given the distinct timing and nature of this mineralisation compared with the later gold mineralisation.

Overall there are a number of reasons why the Easdale Subgroup rocks represent the likely source of sulphur and potentially gold and other associated metals in the gold veins and thus place important constraints on the fluid pathways to the mineralised systems. Further work is required to confirm the source of gold and other metals but the presence of Easdale Subgroup units at depth may be an important criterion determining the prospectivity of the Dalradian Supergroup as a whole.

6.10. Conclusions

This work provides clear evidence that gold and other metal mineralisation hosted in the Tyndrum area, Scotland, has a mixed magmatic and sedimentary source of sulphur. The identification of the individual units in the Dalradian Supergroup that have the potential to be the main source of sedimentary sulphur has been possible through thorough sampling of mineralisation and host rock Dalradian units, and correlation with the global Neoproterozoic S-isotope record for the units that are poorly exposed or there is a lack of data for. Key conclusions can be summarised as:

- The $\delta^{34}\text{S}$ values for quartz vein-hosted gold mineralisation in the Tyndrum area are variable ($\delta^{34}\text{S} = -2$ to $+12\text{‰}$) suggesting mixing between a contemporaneous magmatic sulphur component and sedimentary-sourced sulphur component derived from the Dalradian metasedimentary pile. However, a solely metasedimentary origin cannot be excluded by the data. This study concludes that the sedimentary sulphur component is not sourced from the S-poor Grampian and lower-Appin Group host

rocks and the only feasible source of sedimentary sulphur in mineralisation is the Easdale Subgroup, lying higher in the stratigraphy.

- The Ben Eagach Schist Formation is considered to be the dominant source of the sedimentary sulphur. Gold-bearing quartz veins with $\delta^{34}\text{S} = +12\text{‰}$ must have their sedimentary sulphur component sourced from 32 to 66% from lithologies similar to the Ben Eagach SEDEX horizon, 62 to 100% from the most ^{34}S enriched diagenetic sedimentary sulphides in the Ben Eagach Schist, or 71 to 100% from lithologies similar to the Ben Challum SEDEX horizon. It is *not* possible to generate a $\delta^{34}\text{S}$ of $+12\text{‰}$ by mixing involving sulphur from any other part of the stratigraphy.
- Gold-bearing breccia pipes and early molybdenite mineralisation have a lower range of $\delta^{34}\text{S}$ values ($+1$ to $+8\text{‰}$) than the later gold veins and this either reflects a larger magmatic component, or derivation of sedimentary sulphur from a different part of the stratigraphy.
- Easdale Subgroup units are interpreted to occur at depth beneath the lower Dalradian units observed at surface due to repetition on the overturned limb of the recumbent Beinn Chuirn Anticline; the likely depth is dependent upon interpretation of the Boundary Slide. This allows fluids carrying sedimentary sulphur enriched in ^{34}S to have been derived from depth.
- The Easdale Subgroup may be enriched in gold and other metals either in SEDEX or volcanogenic exhalative horizons, or in carbonaceous sedimentary units, and therefore could have been a significant source of sulphur, gold and other metals. Magmatic fluids may still be important for transporting sulphur, gold and other metals and variable proportions of a magmatic sulphur component can be invoked to account for the wide range in $\delta^{34}\text{S}$ observed.
- The presence of ^{34}S -enriched Easdale Subgroup lithologies containing metals and sulphur at depth may be important for forming mineralisation in areas of sulphur poor host rocks and should be potentially considered as an exploration criterion in the Dalradian Supergroup.

Chapter 7

**Geochronology of the River Vein prospect,
Tyndrum and its relationship to the
Cononish deposit**

Abstract: Vein-hosted gold mineralisation is found throughout the Dalradian Supergroup of Scotland and Ireland but there are currently limited age data available for these occurrences. Cross-cutting relationships in Glen Orchy demonstrate two distinct hydrothermal events; early molybdenum- and late gold-bearing mineralisation. New $^{40}\text{Ar}/^{39}\text{Ar}$ muscovite ages for gold-bearing poly-metallic quartz veins in the Glen Orchy area (407.7 ± 2.1 to 407.2 ± 1.1 Ma), together with existing data for other gold-bearing quartz vein occurrences in the Scottish Dalradian, indicates a regional-scale gold-bearing hydrothermal event at 407-408 Ma. Re-Os molybdenite and U-Pb rutile ages for molybdenite-bordered fractures range from 477.0 ± 2.4 to 439 ± 33 Ma suggesting a protracted molybdenum-bearing hydrothermal system. The low Re content in molybdenite (<52 ppm) and age relations within molybdenite-bordered fractures are interpreted to indicate a metamorphic origin, related to melting at depth during and after orogenesis. The 407-408 Ma regional hydrothermal gold event was a short-lived system, probably driven by heat from granite batholiths. Melting was induced by a change to a transtensional stress regime in the terrane between c. 420-400 Ma. Regional fluid flow was facilitated by movement along the trans-Caledonide faults that created a network of pathways and increased permeability in the Dalradian Supergroup.

7.1 Introduction

The origin of the Cononish deposit, Tyndrum, and other vein-hosted gold deposits in the Irish and Scottish Dalradian Supergroup is debated, with both orogenic and intrusion-related genesis advocated by previous workers (Curtis *et al.* 1993; Goldfarb *et al.* 2005). Existing age constraints for the Cononish deposit have large errors (410 ± 14 Ma; Treagus *et al.* 1999) but recent work by Rice *et al.* (2012) suggests the age of mineralisation is close to 407 Ma ($^{40}\text{Ar}/^{39}\text{Ar}$ K-feldspar; error not reported).

Recent field mapping, in conjunction with Scotgold Resources Ltd, has identified new mineralised occurrences across the Tyndrum area. Of particular note are the molybdenite-bordered fractures and gold-bearing poly-metallic quartz veins in Glen Orchy; the River Vein prospect is a high grade gold-bearing poly-metallic quartz vein (up to 194.6 g/t Au and >200 g/t Ag from >1 kg grab samples; Scotgold Resources Ltd 2011a). Field relations and petrographic constraints (Chapter 4) and geochemical distinctions between the Cononish deposit and gold-bearing poly-metallic quartz veins (Chapter 5) in Glen Orchy are recapped in this chapter.

Constraining the age of the River Vein gold prospect will allow comparison with age data for Cononish and establish if all gold mineralisation in the Tyndrum area is contemporaneous and therefore forms different parts of the same hydrothermal system. Field relations, petrography and geochemical trends show some differences between polymetallic quartz veins that could suggest they were formed in more than one event (Chapters 4 & 5).

This chapter aims to constrain the age of gold and associated mineralisation at the River Vein prospect (Fig. 7.1) through a combination of $^{40}\text{Ar}/^{39}\text{Ar}$, U-Pb and Re-Os techniques on vein and altered wall rock samples. The findings for the Tyndrum area are placed into the context of the tectonic evolution of the Dalradian Supergroup to help constrain whether the mineralisation is orogenic (after Groves *et al.* 1998), intrusion-related or of some other origin.

7.2 Regional setting

The Dalradian Supergroup was deposited on the passive Laurentian margin of the developing Iapetus Ocean and has a depositional history spanning the mid-Neoproterozoic (Cryogenian) to mid-Cambrian (Tanner & Sutherland 2007; Stephenson *et al.* 2013). In Scotland, the sequence is bounded by the Great Glen Fault to the north and Highland Boundary Fault to the south; both crustal-scale structures. The Supergroup comprises a marine-clastic sedimentary succession with occasional carbonate beds and minor volcanic rocks (Stephenson *et al.* 2013).

7.2.1 Caledonian Orogenesis

The Caledonian Orogeny consists of three collisional events, the Grampian, Scandian and Acadian events, as defined in Chew & Strachan (2014). The Dalradian sequence underwent polyphase deformation (D1-D4), the Grampian Event, as a result of the collision of Laurentia with a series of oceanic arcs from *c.* 490 Ma (Stephenson *et al.* 2013). During the Grampian Event, the Midland Valley Arc collided with the Scottish sector of the Dalradian Supergroup (Fig. 7.2). The final phase of deformation (D4) in the Grampian Event was completed by 455 Ma (Oliver *et al.* 2008); emplacement of granites related to erosion and decompression of the metamorphic pile occurred at this time (Oliver *et al.* 2008).

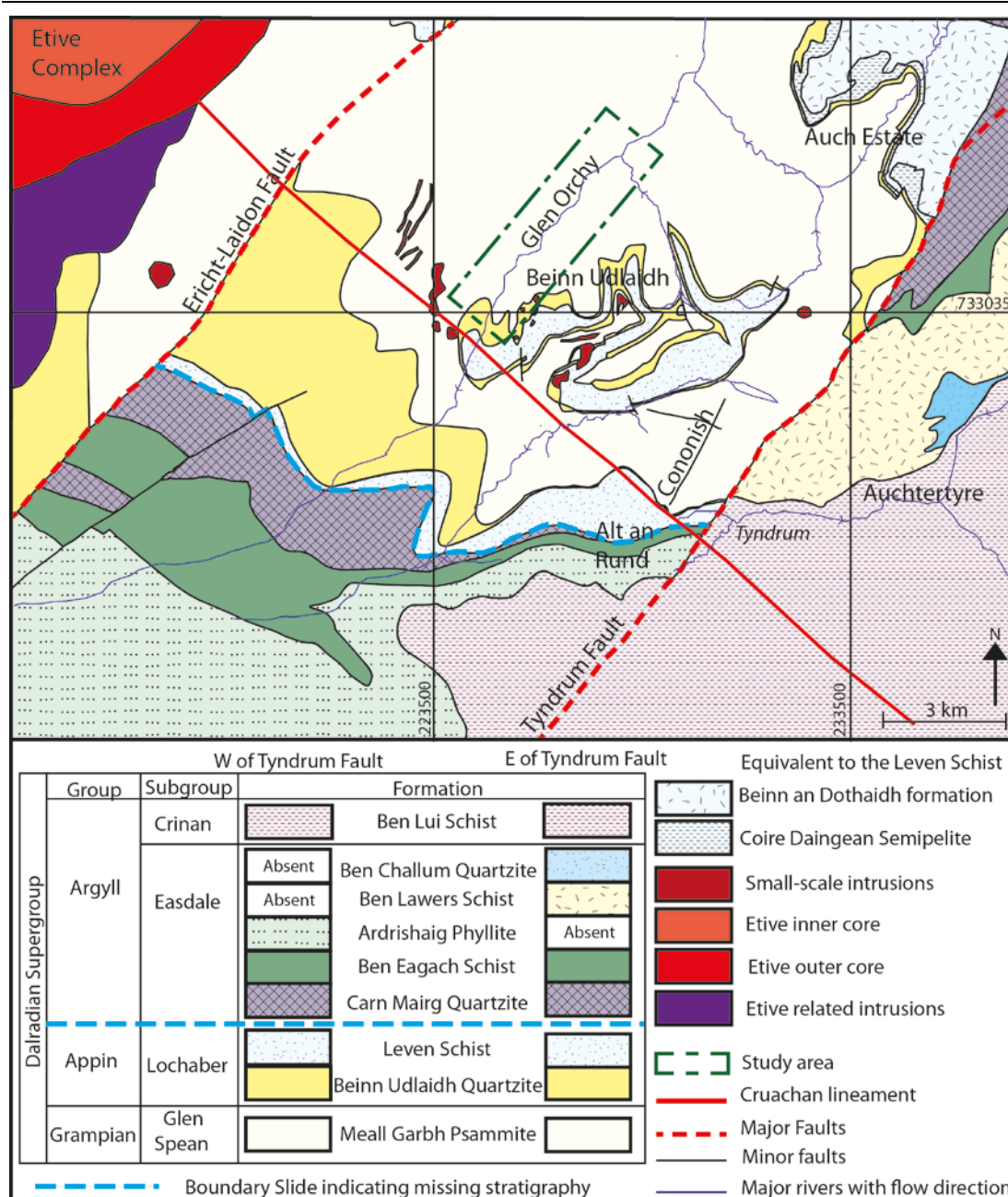


Figure 7.1: Map to show local geology and area mapped as part of this work. Geology adapted from British Geological Survey Crianlarich and Dalmally 1:25,000 bedrock geology sheets.

Grampian Event metamorphism in Scotland and Ireland is contemporaneous across the terrane (Table 3.1). The maximum age of Grampian Event orogenesis is younger than the youngest rocks affected, the top of the Trossachs Group, deposited at *c.* 477 Ma (Tanner & Sutherland 2007). Peak metamorphism is constrained to *c.* 475–470 Ma across the Dalradian Supergroup (Chew & Strachan 2014) supported by data from syn-orogenic intrusions (Table 3.1). Peak metamorphic conditions in the Tyndrum area were garnet-grade amphibolite-facies (Harte 1988; Tanner 2012). The Dalradian sequence underwent rapid cooling post-Grampian Event orogenesis and by 460 Ma erosion had exposed the metamorphic root (Oliver 2001). Dempster (1985) suggests the sequence cooled to 350°C

by 440 Ma (K-Ar amphibole, muscovite, Rb-Sr muscovite) with a further 50°C of cooling by 430 Ma (K-Ar & Rb-Sr biotite).

Folding and metamorphism during the Scandian (*c.* 435-425 Ma; Chew & Strachan 2014; Fig. 7.2) and Acadian (*c.* 400-390 Ma; Mendum & Noble 2010; Fig. 7.2) events of the Caledonian Orogenic cycle are not thought to be recorded in the Dalradian Supergroup. The Scandian Event was coincident with the beginning of I-type granite emplacement in the Grampian terrane (Oliver *et al.* 2008). The Acadian Event was coincident with a period of significant movement on the Great Glen Fault and subsidiary Caledonian trend faults (Chew & Strachan 2014).

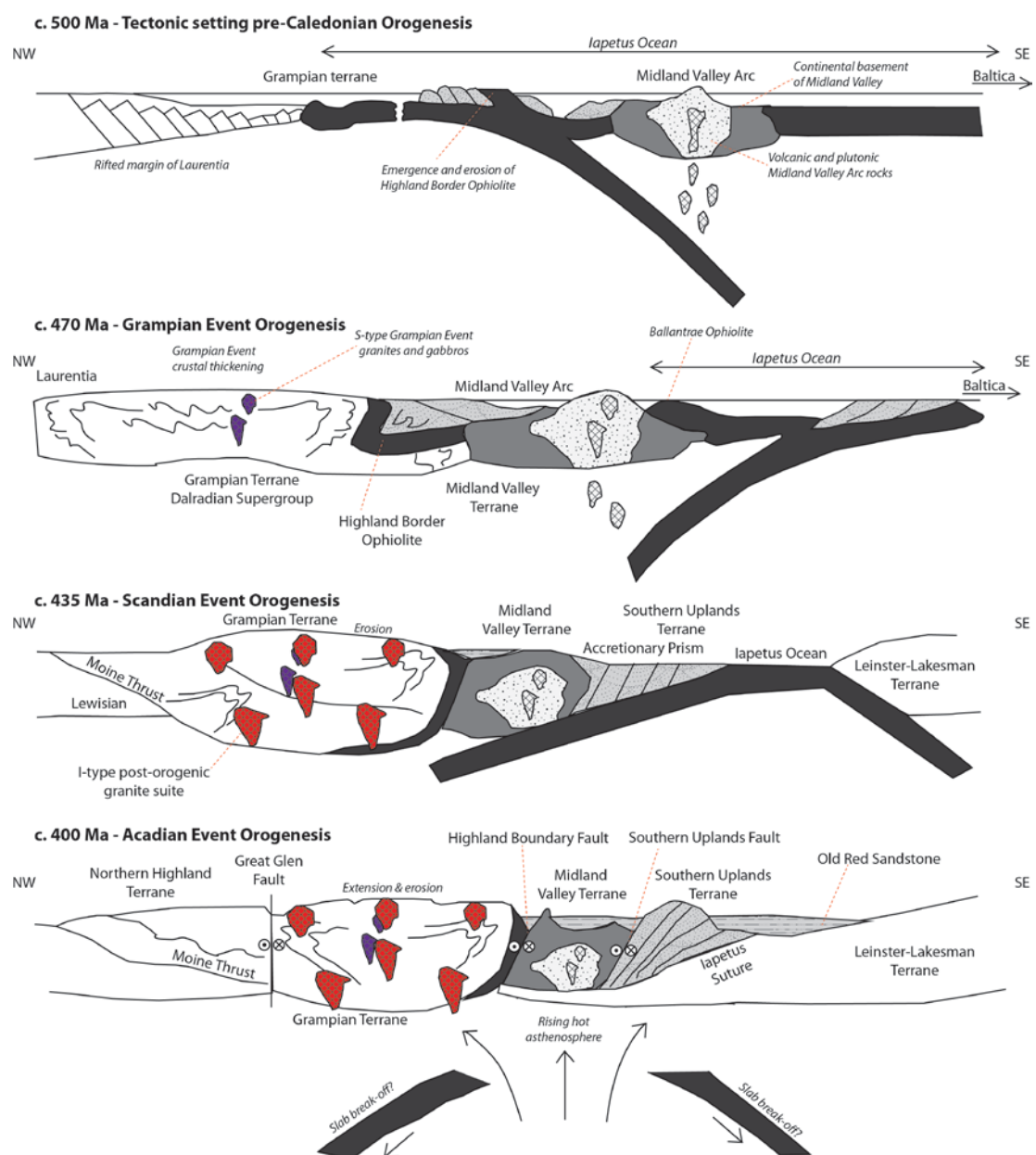


Figure 7.2: Tectonic evolution of the Dalradian Supergroup from pre-Caledonian Orogenesis through the orogenic cycle. Diagram after Dewey & Ryan (1990), Strachan (2000), Oliver *et al.* (2008) and Tanner (2013).

7.2.2 Fault movement

The Great Glen Fault underwent movement between 428 Ma and *c.* 390 Ma (Stewart *et al.* 2001). Microstructures in the Clunes Tonalite, dated at 428 ± 2 Ma (U-Pb zircon; Stewart *et al.* 2001), suggest it was emplaced during early sinistral movement on the Great Glen Fault (Stewart *et al.* 2001). The minimum age of movement on the fault is constrained by the Old Red Sandstone (*c.* 390 Ma), which unconformably overlies the sinistraly sheared rocks within the fault zone (Stewart *et al.* 2001). It is suggested there was hundreds of kilometres of movement on the Great Glen Fault, much larger than the observed movement on faults within the Dalradian Supergroup (Treagus *et al.* 1999; Stewart *et al.* 2001). Mendum & Noble (2010) report a change from sinistral transtension at *c.* 420 Ma to sinistral transpression at *c.* 400-390 Ma in response to Acadian Event deformation.

The subsidiary faults within the Grampian terrane, the Caledonian suite of faults, have variable movement constrained by work by Treagus (1991). Up to 8 km of left lateral strike slip and 2 km of dip slip movement is recorded on the Tyndrum Fault (Treagus 1991). The Glen Tilt granite was emplaced syn-sinistral movement on the Loch Tay Fault at 390 ± 5 Ma (Oliver *et al.* 2008).

7.2.3 Plutonic intrusions

The Dalradian Supergroup hosts a variety of intrusions emplaced throughout the tectonic evolution of the sequence. Oliver *et al.* (2008) classify these into four suites based on the timing of emplacement and the geochemical signatures of the intrusions. These are, in decreasing age;

1. Syn-depositional magmatism

Syn-depositional magmatism is characterised by emplacement of A-type granites and extensive contemporaneous basaltic lavas (Fig. 7.3).

2. Grampian Event intrusions

The foliated Grampian Event granite and gabbro intrusions were emplaced syn-metamorphism at *c.* 475-470 Ma (Fig. 7.3; Oliver *et al.* 2008; Chew & Strachan 2014).

3. Decompression granites

S-type granites were intruded at *c.* 460-455 Ma (Oliver *et al.* 2008) as a result of decompression melting during exhumation and erosion of the orogenic belt (Fig. 7.3).

4. Post-orogenic intrusions

The post-orogenic suite, dominantly I-type granites, was emplaced between *c.* 430 and 408 Ma after a 20 Ma hiatus in magmatic emplacement (Fig. 7.3; Oliver *et al.* 2008; Neilson *et al.* 2009). The intrusions are large granodiorite-granite multi-phase complexes with some intrusions containing molybdenite mineralisation (Conliffe *et al.* 2010; Porter & Selby 2010).

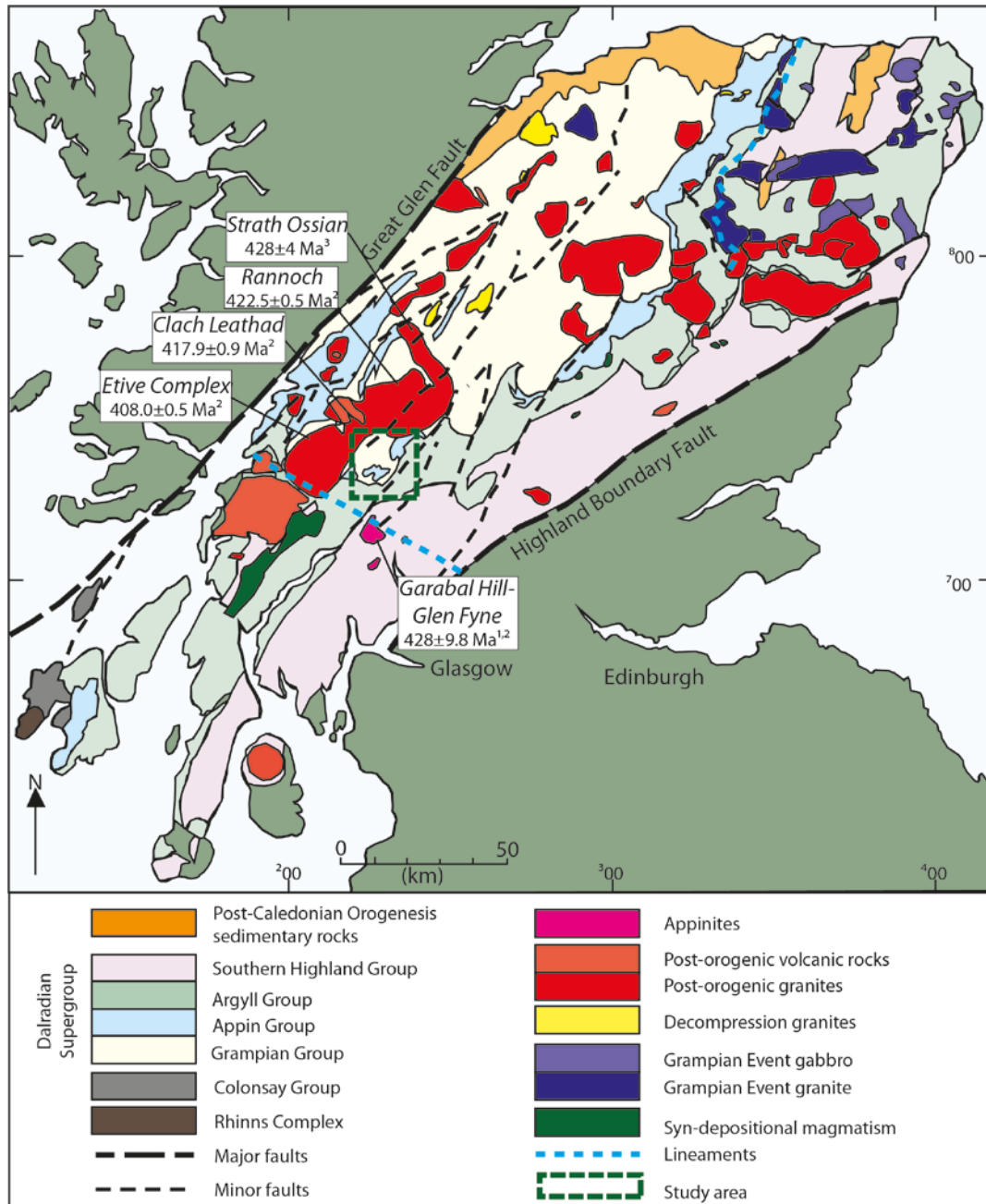


Figure 7.3: Late Caledonian granites and appinites with ages given for key intrusions; ¹Rogers & Dunning 1991; ²Neilson *et al.* 2009; ³Oliver *et al.* 2008.

The bulk of the volume of the I-type granites across Scotland was emplaced at *c.* 410 Ma (Oliver *et al.* 2008), which is interpreted to record continued melting in the lower crust under the Grampian terrane (Dewey 1971; Soper 1986; Thirlwall 1988; Oliver *et al.* 2002) as a result of either slab roll-back causing extension and mantle upwelling or possible slab break-off (Oliver *et al.* 2008; Neilson *et al.* 2009).

7.2.4 Existing age constraints on gold mineralisation

Initial radiometric dating at the Cononish deposit by Curtis (1990) was published in Treagus *et al.* (1999) who report an age of 410 ± 14 Ma ($^{40}\text{Ar}/^{39}\text{Ar}$ K-feldspar; Fig. 7.4). This age is from a sample from the spoil tip at Cononish and is therefore difficult to place within the complex paragenesis reported in Earls *et al.* (1992) and developed further by Spence-Jones (2013). In addition, the large error means it is challenging to fit the age into the extensive dataset now available for the timing of igneous intrusions and fault movement (e.g. Stewart *et al.* 2001; Oliver *et al.* 2008; Neilson *et al.* 2009) for the period 424–396 Ma (Fig. 7.4).

Detailed paragenetic work at Cononish has identified a K-feldspar stage that hosts small inclusions of electrum (Rice *et al.* 2012). The K-feldspar was dated by $^{40}\text{Ar}/^{39}\text{Ar}$ using both CO_2 step heating and UV laser *in situ* methods at SUERC, East Kilbride. The age of mineralisation is constrained to be 407–408 Ma (errors not reported; Rice *et al.* 2012).

Dating work at the gold-bearing Rhynie Chert, Aberdeenshire by Mark *et al.* (2011a) has constrained mineralisation to 407.6 ± 2.2 Ma (reported in Mark *et al.* 2013) by $^{40}\text{Ar}/^{39}\text{Ar}$ dating of adularia (K-feldspar) in the vein assemblage. A U-Pb zircon age by Parry *et al.* (2011) has dated the Milton of Noth andesite at 411.5 ± 1.1 Ma. While Parry *et al.* (2011) interpreted this age to represent the age of mineralisation at Rhynie, discussion by Mark *et al.* (2013) attributes this age to the emplacement of the stratigraphically underlying andesite.

In Ireland, work at the Curraghinalt deposit by Rice *et al.* (2012) brackets gold mineralisation to between 458 (Re-Os molybdenite) and 453 Ma ($^{40}\text{Ar}/^{39}\text{Ar}$ muscovite). Wall rock muscovite is dated at 459 Ma ($^{40}\text{Ar}/^{39}\text{Ar}$; errors not reported; Rice *et al.* 2012) and it is suggested this records metamorphic cooling, with the 453 Ma muscovite recording a hydrothermal event with fluid temperatures below 350°C (Rice *et al.* 2012).

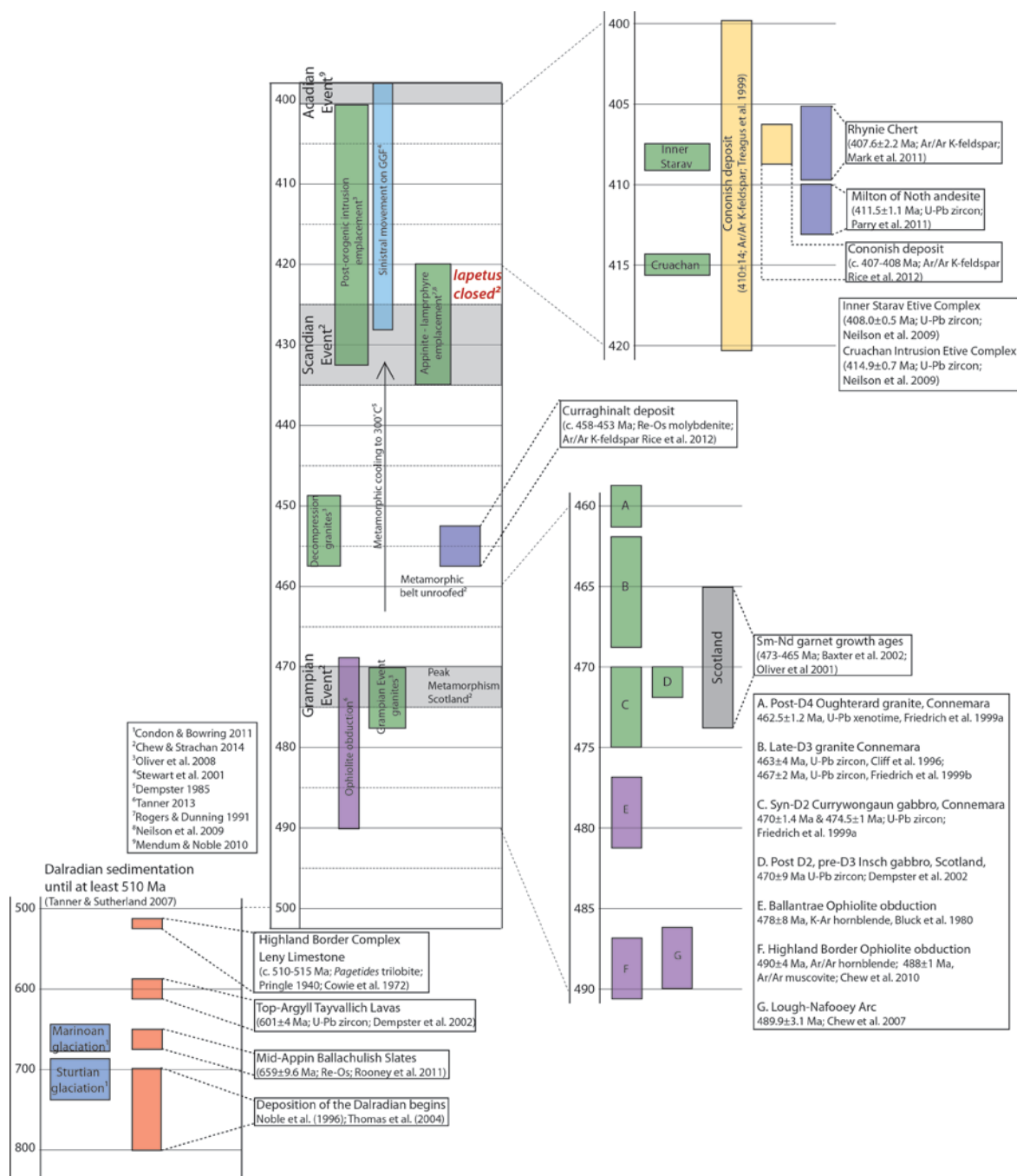


Figure 7.4: Existing age constraints from literature data for the Dalradian Supergroup and orogenic and magmatic processes affecting the sequence.

7.3 The Glen Orchy area

The Glen Orchy area is host to gold-bearing poly-metallic quartz veins which cross-cut lamprophyre sills and molybdenite-bordered fractures; the relationship between the lamprophyre sills and molybdenite-bordered fractures is unconstrained (Fig. 7.5; Chapter 4). The lamprophyre sills are interpreted by Tanner (2012) to be equivalent to the Sron

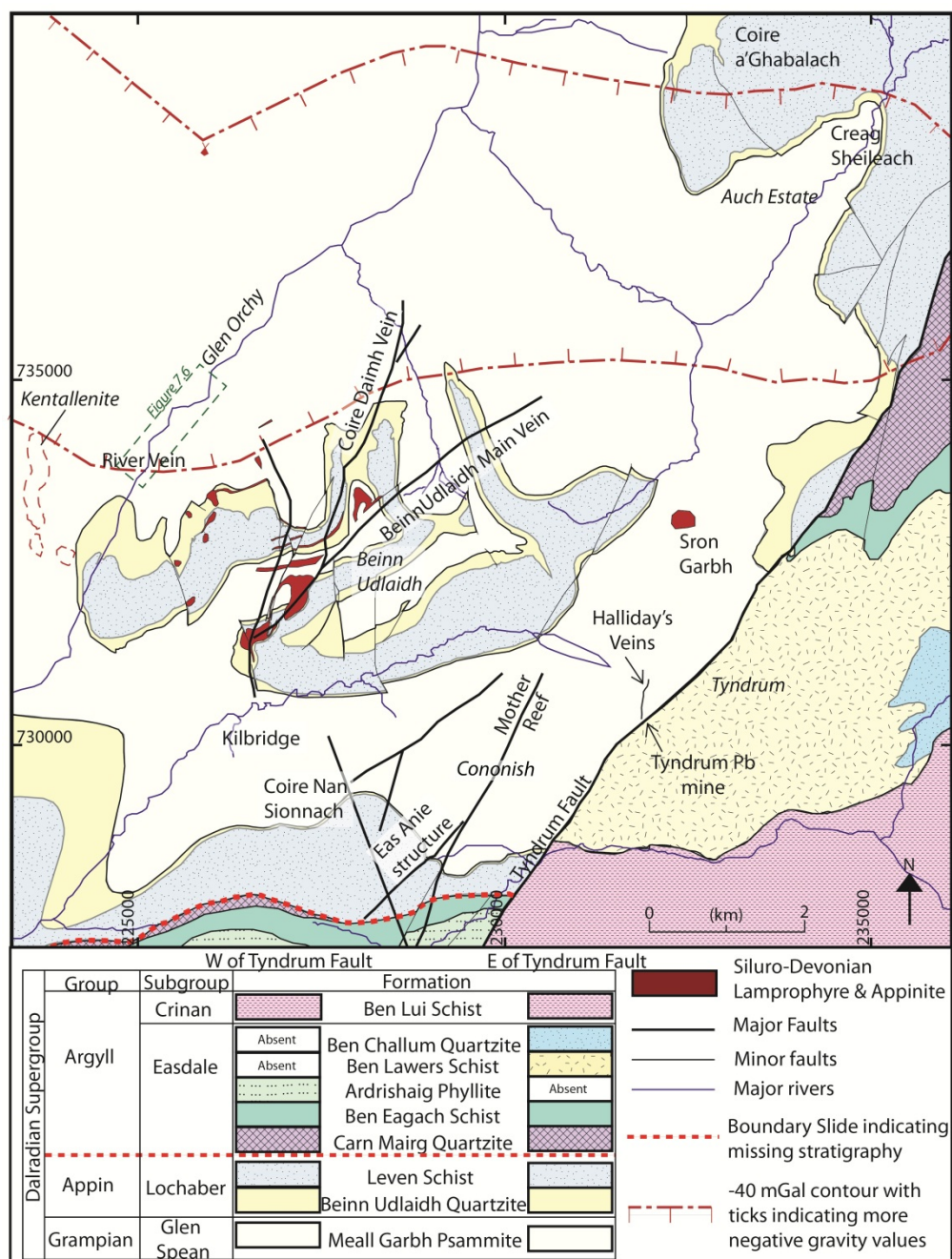


Figure 7.5: Simplified geology of the study area. Key structural features and sample localities are shown. Magmatic bodies shown include lamprophyre sills and dykes, appinite bodies and diorite dykes. Geology adapted from the British Geological Survey 1:50 000 scale Bedrock Geology Crianlarich and Dalmally sheets with additional detail from Tanner & Thomas (2009) and mapping in conjunction with Scotgold Resources Ltd. Gravity anomaly after Hussein & Hipkin (1981) and interpretation in Patrick *et al.* (1988).

Garbh diorite-appinite body near Tyndrum and the same age as appinite-lamprophyre intrusions throughout the SW Dalradian emplaced at 428 ± 9.8 Ma (Garabal Hill appinite; Rogers & Dunning 1991; Neilson *et al.* 2009).

Although no outcrop of granite is observed within 10 km of the Tyndrum area mineralisation, a gravity low extending from the Etive Complex into the Tyndrum area has been interpreted to represent the extent of a concealed granite body (Fig. 7.5; Pattick *et al.* 1988). Recent work by Neilson *et al.* (2009) and Tanner (2012) has re-introduced the idea of the Lochaber Batholith at depth in the Glen Orchy area (Kynaston & Hill 1908; Kokelaar & Moore 2006). There is no surface expression of the Lochaber Batholith in Glen Orchy apart from lamprophyre sills and dykes (Fig. 7.5). The Lochaber batholith is defined as the Strath Ossian, Rannoch, Clach Leathad and Etive plutons (Fig. 7.3; Neilson *et al.* 2009) and is interpreted to be more extensive at depth, decreasing in age to the SW (Kokelaar & Moore 2006; Neilson *et al.* 2009). This suggests there is potential for large volumes of fluid, heated by a batholith-scale granite at depth, to move through the Glen Orchy area. Kentallenite in Glen Orchy was emplaced at 387.5-411.8 Ma (K-Ar biotite; Westoll & Miller 1969, recalculated using Dalrymple 1979). Given that the Westoll & Miller (1969) data employed early instrumentation for K-Ar analytical methods, the ages may not be reliable even with recalculation. The kentallenite was not mapped in this study as it is under mature Forestry Commission planting, but the intrusion is recorded on the BGS Crianlarich & Dalmally 1:50,000 bedrock geology sheets (Fig. 7.5).

Faults in the area are controlled by movement on the Tyndrum and Ericht-Laidon faults, creating a shear couple, between 428 ± 9.8 Ma (Rogers & Dunning 1991; Neilson *et al.* 2009) and 412 ± 3 Ma (Clayburn *et al.* 1983), based on cross-cutting relationships with the Tyndrum Fault, Glen Fyne granite, and a microdiorite dyke (Treagus *et al.* 1999). The Coire Daimh barren quartz vein (Fig. 7.5) is hosted in a fault plane, with the plane visible on the edge of the vein (Chapter 4). This supports Tanner (2012)'s interpretation that the major faults in the area were acting as foci for fluid flow.

7.3.1 Cross-cutting relationships in the Glen Orchy area

Molybdenite-bordered fractures are newly identified in the River Vein area (Fig. 7.6; 7.7) and these are cross-cut by gold-bearing poly-metallic quartz veins. All mineralisation discussed cross-cuts the metamorphic D2 bedding-parallel foliation of the host metasedimentary rocks, and therefore is interpreted to have formed after peak metamorphism (*c.* 475-470 Ma; Chew & Strachan 2014).

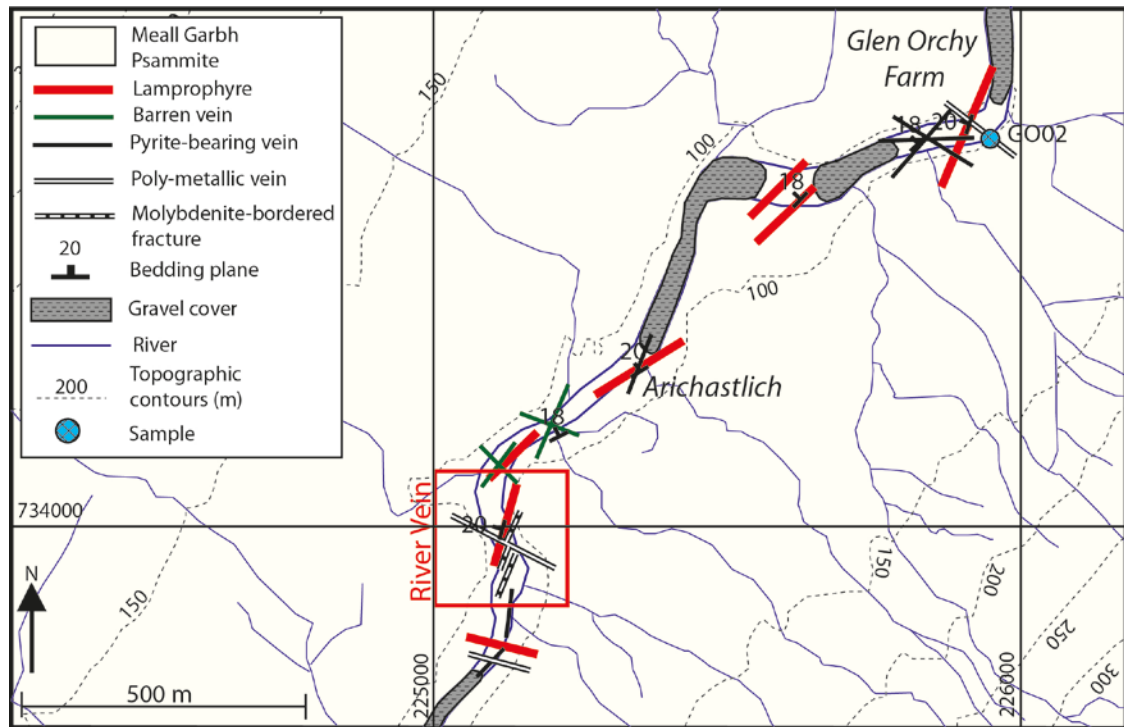


Figure 7.6: Detailed map of Glen Orchy showing River Vein area and location of sample GO02.

7.3.1.1 Molybdenite-bordered fractures

In the River Vein area, disseminated molybdenite mineralisation (up to 2.72% Mo from rock chip samples; Scotgold Resources Ltd 2012c) occurs in K-feldspar alteration around NNE-trending fractures (Figs. 7.8, 7.9A, B). The alteration zone reaches up to 20 cm in width, into the host Meall Garbh Psammite, but the fractures are narrow (mm scale).

Molybdenite occurs as small rosettes (1–2 mm across) with minor pyrite; there is no gold enrichment with molybdenite mineralisation. The alteration assemblage is dominated by K-feldspar replacing quartz and plagioclase. Minor pyrite is found with the K-feldspar alteration and in late quartz filling the fracture. Hydrothermal rutile is found around and in pyrite within the K-feldspar alteration selvage.

7.3.1.2 Poly-metallic quartz veins

Gold-bearing quartz veins cross-cut molybdenite-bordered fractures and trend 108–138°, reaching up to 1 m in width (Figs. 7.8, 7.9B, E). The veins are polyphase quartz and exhibit brecciation of early quartz and altered host rock. Host rock clasts are altered to either K-feldspar or chlorite-sericite. The sulphide assemblage is dominated by pyrite and galena (Fig. 7.9F), with minor sphalerite and chalcopyrite as inclusions in large pyrite crystals. There is a notable lack of arsenopyrite and only sporadic hessite, both of which are present in poly-metallic quartz veins elsewhere in the Tyndrum area (Chapter 4).

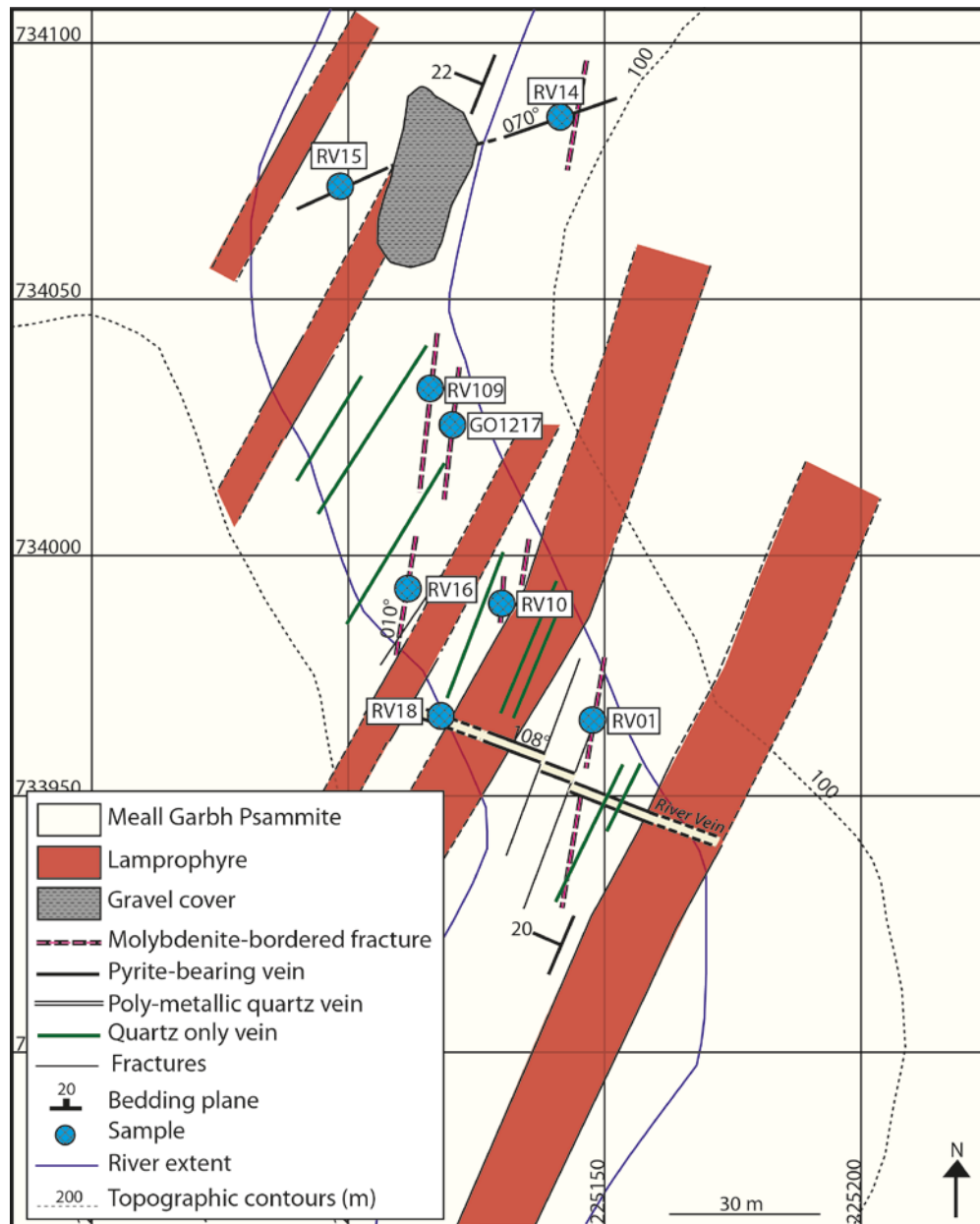


Figure 7.7: Detailed map of the River Vein area of Glen Orchy showing key cross-cutting relationships between molybdenite-bordered fractures and poly-metallic quartz veins.

Gold, as electrum, is interpreted to have two generations in the poly-metallic quartz veins. Early electrum (Au 1) occurs as small ($<50\ \mu\text{m}$) inclusions within large ($<0.5\ \text{mm}$) cubic pyrite. These inclusions range from well-rounded to sub-angular in shape. Galena inclusions occur in pyrite with electrum. Late electrum (Au 2) occurs with late void-filling galena, often accompanied by hessite, in fractures and around the edges of earlier pyrite. Microprobe analysis of the two generations of electrum from the River Vein and other gold-bearing poly-metallic quartz veins in the Glen Orchy area does not record distinct electrum compositions (Chapter 5) and thus could suggest the electrum formed in the same broad hydrothermal event.

7.3.2 Relationship to the Cononish deposit

The Cononish deposit is characterised by a sulphide assemblage dominated by pyrite with chalcopyrite, galena and minor sphalerite. The mineralogy varies between the Cononish deposit and gold-bearing poly-metallic quartz veins in Glen Orchy, with the absence of significant chalcopyrite and hessite in the Glen Orchy veins. Work by Spence-Jones (2013) clarified the paragenesis at Cononish showing that all gold was a single phase, with electrum becoming progressively Ag-rich through time. The change in the silver content is interpreted to reflect changes in the tellurium fugacity of the system and the availability of silver to complex with gold. The variation in the proportion of Ag in electrum at Cononish (42-88 wt. % Ag, Pattick *et al.* 1988; 10-90 wt. % Ag, Spence-Jones 2013) is not seen in gold-bearing poly-metallic quartz veins in Glen Orchy (16.5-22 wt. % Ag; Chapter 5).

The geochemical trends in gold-bearing quartz veins in the Glen Orchy area are largely comparable the Cononish deposit, with high gold, silver and minor enrichment in antimony, tin and bismuth (Chapter 5). Tellurium is highly enriched at the Cononish deposit reflecting increased hessite (Ag_2Te) compared to the Glen Orchy veins, which have a greater enrichment in arsenic (Chapter 5). Differences in the bulk Au/Ag ratio are also observed between the two areas, with $\text{Au} < \text{Ag}$ at Cononish and $\text{Au} > \text{Ag}$ in Glen Orchy veins (Chapter 5).

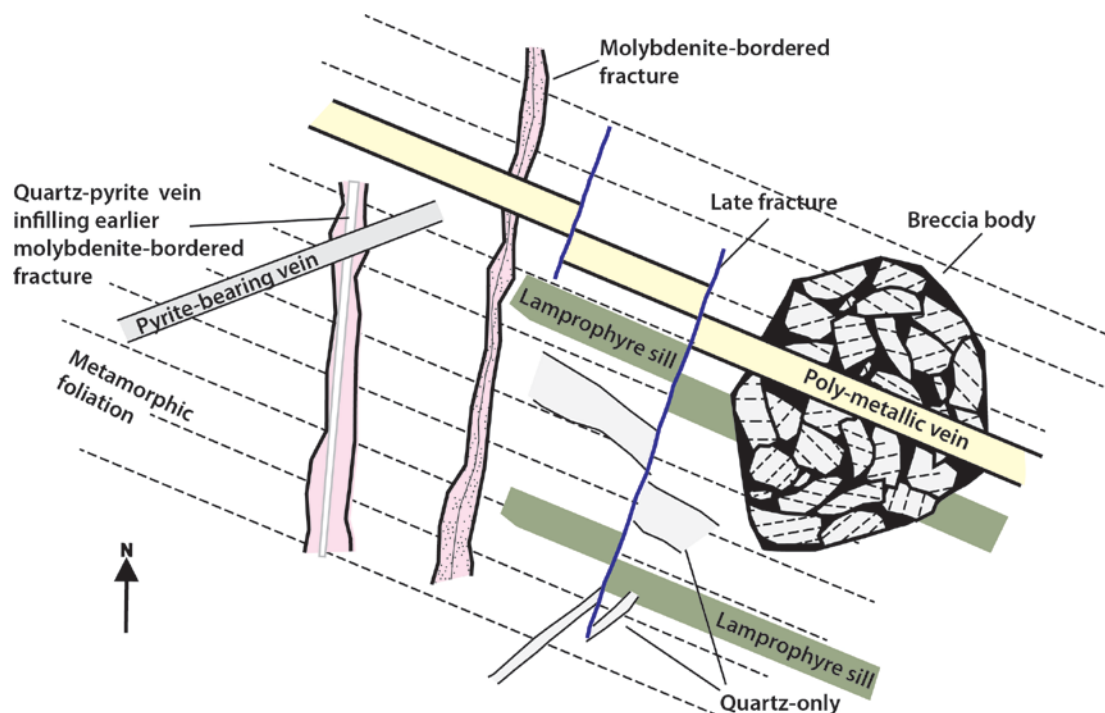


Figure 7.8: Schematic representation of cross-cutting relationships in the Glen Orchy area.



Figure 7.9: Key field relationships in the Glen Orchy and River Vein area. A. K-feldspar alteration at edge of white quartz vein with pyrite; B. Cross cutting relationship between molybdenite- and gold-bearing veins. Molybdenite-bordered fracture truncated by gold-bearing quartz vein. C & D. Molybdenite-bordered fracture selvage. E. Dextral off-set visible on gold-bearing quartz vein. F. Mineralogy of gold-bearing quartz vein.

7.4 Analytical methods

7.4.1 Sample preparation

Samples were collected as part of a mapping project in the Tyndrum area between June 2010 and August 2012, in conjunction with Scotgold Resources Ltd's on-going exploration program. Large samples (>2 kg) were taken, with half (~1 kg) sent for assay and the remainder kept for analysis. Polished thin sections were produced from key samples and detailed petrographic characterisation was carried out to establish a paragenetic sequence for the various hydrothermal occurrences in the Glen Orchy area. Vein samples were characterised by hand specimen and thin section analysis.

7.4.2 $^{40}\text{Ar}/^{39}\text{Ar}$ geochronology

Samples for step-heating CO_2 laser analysis were crushed and sieved to a 125-250 μm fraction. K-feldspar, muscovite and sericite were separated by magnetic separation and pristine crystals of each mineral were hand-picked under a binocular microscope. Samples for *in situ* laser analysis were cut from 3 mm thick slices of characterised samples.

Samples were loaded into high-purity Al discs for irradiation. International standard GA1550 biotite (98.79 ± 0.96 Ma), a primary standard against which the Fish Canyon sanidine age (FCs) (28.02 ± 0.16 Ma) of Renne *et al.* (1998) was calibrated, was loaded adjacent to the samples of unknown age. Crystals of MMhb-1 hornblende (523.1 ± 4.6 Ma; Renne *et al.* 1998) and FCs were also loaded adjacent to the samples to check J-parameter accuracy. Samples were irradiated for 35 hours in the Cd-lined RODEO facility of the McMaster reactor. GA1550 ($n = 50$) and FCs ($n = 15$) were analysed by total fusion with a focused CO_2 laser. MMhb-1 hornblende was step-heated by CO_2 laser. Using J-parameter measurements from GA1550, both FCs and MMhb-1 yield ages that overlap with those defined by Renne *et al.* (1998), indicating appropriate measurements of the J-parameter from GA1550 for the determination of unknown ages.

Small grain populations ($n=3$) for samples RV10, RV16 and RV18 were loaded into a Cu planchette in an ultra-high vacuum laser cell with a doubly pumped ZnSe window. Using a CO_2 laser the samples were step-heated. All gas fractions were subjected to 180 seconds of purification with two SAES GP50 getters (one at room temperature, the other at 450°C) and a cold finger maintained at -95.5°C , using a mixture of liquid nitrogen and acetone. Argon isotope ratios (i.e., ion beam intensities) were measured using a GV Instruments ARGUS V multi-collector noble gas mass spectrometer (e.g., Mark *et al.* 2009; 2011b). The

mass spectrometer has a measured sensitivity of 7×10^{-14} moles/volt. Both the extraction and clean-up processes were automated, as was the mass data acquisition. Backgrounds were measured after every two analyses of unknowns. Average backgrounds \pm standard deviation ($n = 41$: ^{40}Ar 1.01×10^{-15} moles, ^{39}Ar 3.03×10^{-17} moles, ^{38}Ar 1.50×10^{-17} moles, ^{37}Ar 7.11×10^{-17} moles, ^{36}Ar 1.01×10^{-17} moles) from the entire run sequence were used to correct raw isotope measurements of unknowns. Mass discrimination was monitored by analysis of air pipettes after every four analyses ($n = 23$, $^{40}\text{Ar}/^{36}\text{Ar} = 300.5 \pm 0.2$).

For *in situ* work a New Wave UP-213 nm laser was used (e.g., Moore *et al.* 2011) to ablate 50-100 μm spots in the sericite (sample GO02b). All gas fractions were subjected to the same procedures as for CO_2 step heating. Argon isotope ratios were measured using methods described for CO_2 step heating. Backgrounds were measured after every two analyses of unknowns. Average backgrounds \pm standard deviation ($n = 21$: ^{40}Ar 1.08×10^{-15} moles, ^{39}Ar 3.24×10^{-17} moles, ^{38}Ar 1.24×10^{-17} moles, ^{37}Ar 7.65×10^{-17} moles, ^{36}Ar 1.21×10^{-17} moles) from the entire run sequence were used to correct raw isotope measurements of unknowns. Mass discrimination was monitored by analysis of air pipettes after every four analyses ($n = 6$, $^{40}\text{Ar}/^{36}\text{Ar} = 300.3 \pm 0.2$).

The Ar isotope data were corrected for background, mass discrimination, and reactor-produced nuclides and processed using standard data reduction protocols. The decay constants of Steiger and Jäger (1977) and atmospheric argon ratios of Lee *et al.* (2006), the latter independently verified by Mark *et al.* (2011b), were employed.

The BGC software MassSpec was used for data regression. Data are displayed on ideograms and isotope correlation plots (inverse isochron plots). All raw $^{40}\text{Ar}/^{39}\text{Ar}$ data are presented in Appendix 7.1. Data are reported according to the recommendations of Renne *et al.* (2009). Plateau calculations are based on the acceptance criteria of $n = 3$ for a minimum of contiguous steps with no resolvable slope, $F = 0.60$ ($\geq 60\%$ of ^{39}Ar released) and $p = 0.05$ for the probability of fit.

The $^{40}\text{Ar}/^{39}\text{Ar}$ method is a relative dating technique with all ages referenced back to a standard of known age. Recently Renne *et al.* (2010, 2011) published an optimisation model that used constraints from ^{40}K activity, K-Ar isotopic data, and pairs of ^{238}U - ^{206}Pb and $^{40}\text{Ar}/^{39}\text{Ar}$ data as inputs for estimating the partial decay constants of ^{40}K and $^{40}\text{Ar}^*/^{40}\text{K}$ ratio of FCs. This calibration has reduced systematic uncertainties (i.e., accuracy) in the $^{40}\text{Ar}/^{39}\text{Ar}$ system from *c.* 2.5% to less than 0.25%. The optimisation model has also yielded an age for FCs that overlaps at the 2σ confidence level with the astronomically tuned FCs

age of Kuiper *et al.* (2008), but beyond the 2σ confidence level of Rivera *et al.* (2011). New $^{40}\text{Ar}/^{39}\text{Ar}$ data (Renne *et al.* 2013) for the Cretaceous-Palaeogene (K-Pg) boundary show that the calibration of Rivera *et al.* (2011) places the K-Pg boundary exactly intermediate between two possible choices of 405 ka orbital eccentricity cycles. The implication is that the astronomically tuned age for FCs (Rivera *et al.* 2011) is paradoxically inconsistent with any astronomically tuned age for the K-Pg boundary. It is the $^{40}\text{Ar}/^{39}\text{Ar}$ calibration of Renne *et al.* (2011) that is proven to be the most consistent with the astronomically tuned age (Kuiper *et al.* 2008) for the K-Pg boundary (Renne *et al.* 2013). Therefore, to present the most accurate $^{40}\text{Ar}/^{39}\text{Ar}$ age for the samples, the ages have been recalculated relative to the optimisation model of Renne *et al.* (2010, 2011) using the approach of Ellis *et al.* (2012) and Mark *et al.* (2014).

The ages ($\pm 1\sigma$) presented on the appropriate figures (step heating spectra, isotope correlation plots and relative probability plots) show the analytical uncertainty only relative to the decay constants and standard ages of Renne *et al.* (2010, 2011).

The uncertainties reported in Appendix 7.2 for all samples includes all sources of error ($\pm 2\sigma$), including decay constant uncertainty, and is hence directly comparable to all timescales as defined by other chronometers (e.g., U-Pb and Re-Os chronologies). These ages ($\pm 2\sigma$) are discussed throughout the remainder of this thesis. Note that the uncertainties were calculated by using the full optimization model spreadsheet that can be obtained directly from Prof. Paul Renne of the Berkeley Geochronology Centre.

7.4.3 U-Pb geochronology

U-Pb geochronology was primarily utilised to date rutile found with K-feldspar and molybdenite in molybdenite-bordered fractures. In addition, the technique was used to establish the age and therefore provenance of detrital zircons in the Meall Garbh Psammite Formation (sample RV10).

ICP-MS isotopic analysis was conducted on rutile and detrital zircon within polished thin sections from samples RV10 and RV16. The analyses were undertaken at the NERC Isotopic Geoscience Laboratory (NIGL) at BGS in Keyworth, UK, using a NU Instruments Attom single-collector ICP-MS coupled to a New Wave Research UP193ss laser ablation system. The full methods and instrument set up is described in Appendix 7.3 and Thomas *et al.* (2013), with rutile analyses using the same method as is described for titanite. A standard-sample bracketing routine was used to normalise Pb-Pb and Pb-U ratios, this involved the measurement of matrix-matched reference materials during the

analytical sessions. These were 91500, GJ-1 and Plešovice for zircon and Suglück and PCA for rutile. The ages quoted are $^{207}\text{Pb}/^{206}\text{Pb}$ ages for zircons, and $^{206}\text{Pb}/^{238}\text{U}$ ages for rutile, and use mean and two standard deviations for age and uncertainty. The precision and accuracy of the method is <3%, 2 σ for zircon and <4%, 2 σ for rutile. Uncertainties are reported as $\pm X(Y)$, where X is the internal or analytical uncertainty in the absence of systematic errors, and Y includes systematic errors (decay constants, reference material age uncertainty, long term analytical reproducibility). Data reduction used an in-house spreadsheet and Isoplot (Ludwig 2003) for age calculations and plotting.

7.4.4 Re-Os geochronology

Molybdenite is enriched in rhenium and typically contains no common osmium. Three samples were selected based on field relations and petrographic constraints.

Sample RV01 was crushed in agate and sieved to obtain a fraction of 37-125 μm before heavy liquid separation (sodium polytungstate) at the University of Leicester. Samples RV109 and GO1217 were crushed in agate, whilst wrapped in plastic, and sieved through nylon synthetic mesh to obtain a fraction of 37-125 μm with heavy liquid separation carried out at Durham University. Rhenium-osmium isotope analysis for all samples was carried out at Durham University's TOTAL Laboratory for Source Rock Geochronology and Geochemistry, a member of the Durham Geochemistry Centre.

The Re and Os abundances and isotopic compositions were measured by isotope dilution negative thermal ionization mass spectrometry (ID-NTIMS) following the methods of Selby & Creaser (2001). A measured amount of molybdenite was digested with a known amount of ^{185}Re and isotopically normal Os, spike-normal tracer solution. Samples were digested in reverse aqua regia in a Carius tube at 220°C for 24 hours. Os and Re were purified by solvent extraction, micro-distillation and anion chromatography.

The Re and Os isotope ratios were measured using ID-NTIMS with Faraday collectors; all Re-Os data are blank corrected. The uncertainties were calculated using uncertainties in weight of the sample and tracer solutions, calibration uncertainties, spike and standard Re and Os isotopic compositions, Re and Os mass spectrometer measurements and blank contributions. The ^{187}Re and ^{187}Os data with the ^{187}Re decay constant (1.666×10^{-11} ; Smoliar *et al.* 1996; 0.31% uncertainty; Stein *et al.* 2001) are used to calculate model Re-Os dates. Ages are reported to 2 σ which include analytical and decay constant uncertainty.

7.5 Petrographic constraints on dated phases

7.5.1 Zircon U-Pb

Detrital zircons occur in the Meall Garbh Psammite Formation, which hosts the molybdenite-bordered fractures and gold-bearing quartz veins. SEM examination showed the detrital zircons exhibit some zoning. The core of the zircon was analysed by U-Pb using LA-ICP-MS. The age of the youngest detrital zircon should constrain the maximum age of deposition of the Meall Garbh Psammite Formation.

7.5.2 Molybdenite Re-Os

Molybdenite, in molybdenite-bordered fractures in Glen Orchy, was dated using Re-Os techniques (samples RV01, RV109, GO1207; Fig. 7.10A; Table 7.1) because this should constrain the maximum age of gold-bearing quartz veins, which cross-cut the molybdenite-bordered fractures, in the Glen Orchy area. Molybdenite occurs as disseminated, small (<3 mm) rosettes within K-feldspar altered Meall Garbh Psammite Formation. The Re-Os chronometer is generally considered robust and not reset by later thermal events (Stein *et al.* 2001) and so the molybdenite ages are anticipated to record the primary age of molybdenite mineralisation.

7.5.3 K-feldspar $^{40}\text{Ar}/^{39}\text{Ar}$

Molybdenite is hosted in the K-feldspar altered selvage of molybdenite-bordered fractures. The K-feldspar was dated using $^{40}\text{Ar}/^{39}\text{Ar}$ techniques (samples RV10 & RV16; Table 7.1) and is expected to be pre- to syn- molybdenite in age based on the petrographic relationships.

7.5.4 Rutile U-Pb

Rutile is found around and in pyrite, associated with molybdenite mineralisation, and was dated using the U-Pb method (samples RV10 and RV16; Fig. 7.10D; Table 7.1). No rutile was observed in host metasedimentary rocks unaffected by hydrothermal fluids. On the basis of petrographic relations, rutile is expected to date syn- to post-molybdenite and associated K-feldspar but, as the rutile is hosted around the same structure it is not expected to post-date by a significant period of time.

Table 7.1 *Sample type and phases dated with methods*

Sample	Xco (m)	Yco (m)	Zco (m)	Description	Au (ppm)	Mo (ppm)	Phase	Method	Timing constraints from petrography
RV109	225116	734032	97	Molybdenite- bordered fracture	0.016	>10000	Moly	Re-Os	Syn- to post K- spar, pre-rutile, pre-Au veins
GO1217	251223	734032	114	Molybdenite- bordered fracture	No assay	No assay	Moly	Re-Os	Syn- to post K- spar & rutile, pre- Au veins
RV01	225150	733968	95	Molybdenite- bordered fracture	0.045	157	Moly	Re-Os	Syn- to post K- spar & rutile, pre- Au veins
RV16	225111	733992	95	Molybdenite- bordered fracture	0.021	205	Rut	U-Pb	Syn to post-Mo & K-spar and pre-Au veins
							Ksp	Ar/Ar Step-heating	Pre- to syn-Mo & rutile, pre-Au veins
RV10	225136	733988	105	Molybdenite- bordered fracture	0.091	4384	Musc	Ar/Ar Step-heating	Metamorphic muscovite
							Ksp	Ar/Ar Step-heating	Pre-Au veins and rutile
							Rut	U-Pb	Syn to post-Mo & K-spar and pre-Au
GO02b	225922	734658	109	Poly-metallic vein	171	5.6	Musc	Ar/Ar <i>In situ</i>	Maximum age of Au, within pyrite host to electrum
RV18	225118	733967	99	Poly-metallic vein	103	9.27	Musc	Ar/Ar Step-heating	Minimum age of Au, in veins host to Au-2

Xco & Yco co-ordinates relative to the British National Grid. Zco is the altitude above sea level in metres

7.5.5 Muscovite $^{40}\text{Ar}/^{39}\text{Ar}$

Metamorphic muscovite from the host metasedimentary Meall Garbh Psammite Formation was dated using $^{40}\text{Ar}/^{39}\text{Ar}$ techniques (RV10; Fig. 7.10B; Table 7.1). The muscovite occurs along the metamorphic foliation and, given its nominal closure temperature of $\approx 350^\circ\text{C}$ (Purdy & Jäger 1976; Hames & Bowring 1994), it is expected to date post-orogenic cooling associated with the Grampian Event, unless it is reset by later fluids $\geq 350^\circ\text{C}$.

Detailed characterisation of gold-bearing poly-metallic quartz vein samples from the Glen Orchy area, and in particular the River Vein area, has identified two white mica stages (Fig. 7.10C, E & F; Table 7.1). Early muscovite, hosted in pyrite (which also contains electrum

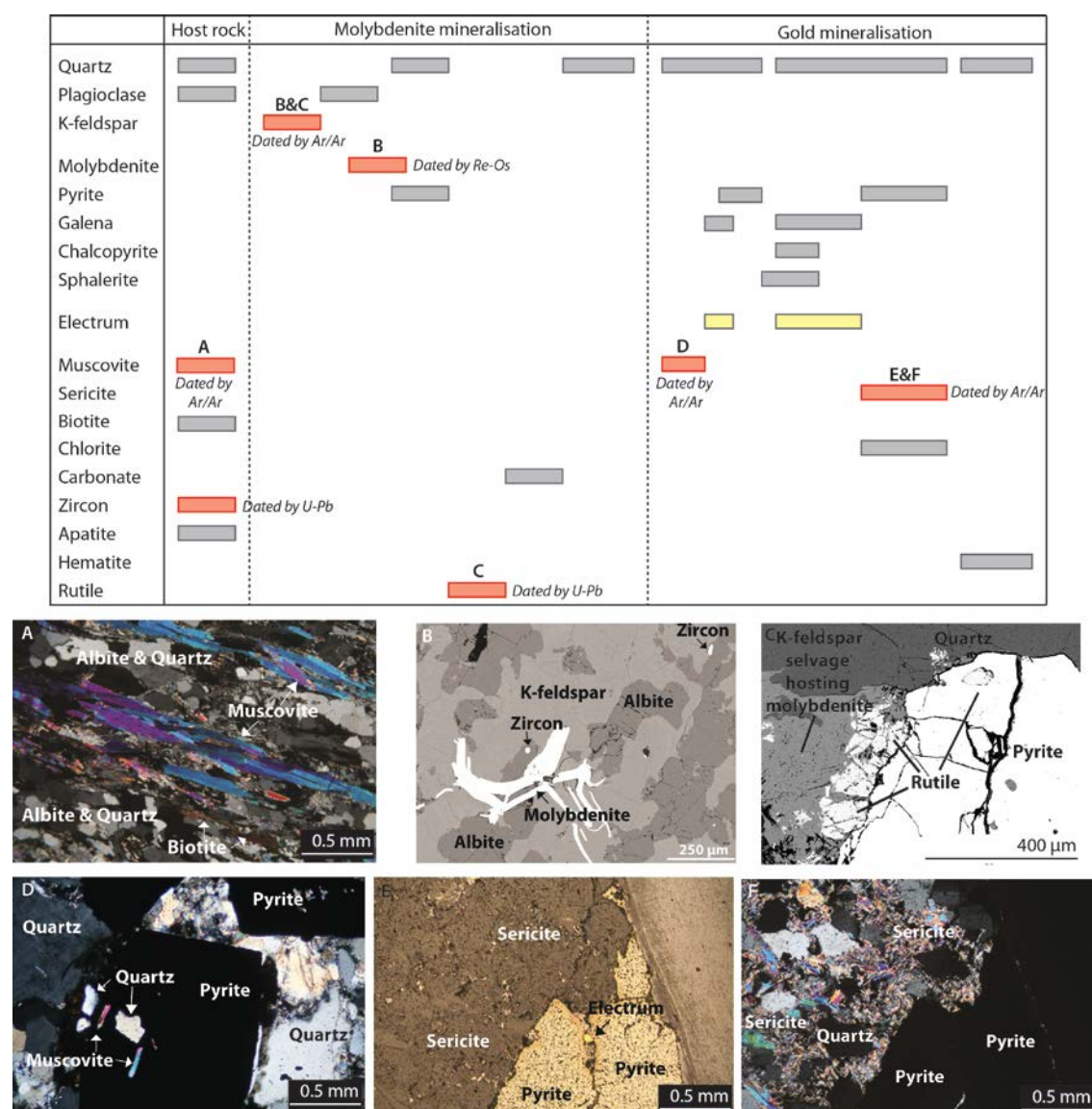


Figure 7.10: Paragenesis for mineralisation in the Glen Orchy area – letters link to photomicrographs. A. Metamorphic muscovite in Meall Garbh Psammite (RV10; XPL). B. Molybdenite and K-feldspar alteration (RV109; SEM image). C. Rutile halo around pyrite in K-feldspar altered selvage at contact between host rock and vein (RV16; SEM image). D. Muscovite within pyrite that also contains electrum inclusions (GO02b; XPL). E&F. Late sericite closing off fracture containing electrum (RV18; E – RL; F – XPL).

inclusions), was dated using $^{40}\text{Ar}/^{39}\text{Ar}$ techniques to give a maximum age for gold mineralisation in the Glen Orchy area (Fig. 7.10C). Late sericite (RV18), within sericite-chlorite alteration, occurs after late electrum (Au 2) allowing for the duration of gold mineralisation in the Glen Orchy area to be constrained (Fig. 7.10E & F).

7.6 Results

7.6.1 $^{40}\text{Ar}/^{39}\text{Ar}$ geochronology

7.6.1.1 *K-feldspar syn-molybdenite*

The age spectra for K-feldspar from RV10 and RV16 are similar with few large steps but the spectra are not smooth, with variation between every step (Figs. 7.11; 7.12; Table 7.2). These K-feldspar $^{40}\text{Ar}/^{39}\text{Ar}$ ages are dating the same geological event but the steps in the spectra suggest there has been resetting of the argon system by this event. Data predominantly occur towards the x-axis of the isochron plot and give an age within error of the $^{40}\text{Ar}/^{39}\text{Ar}$ age of the step-heating spectra for each sample. The $^{40}\text{Ar}/^{39}\text{Ar}$ age is thus considered to be robust and is reported to 2σ in Table 7.2. The low closure temperature of the $^{40}\text{Ar}/^{39}\text{Ar}$ system is noted (Table 7.3) and the potential for re-setting of the system by later fluids is acknowledged.

7.6.1.2 *Metamorphic muscovite*

The age spectrum for metamorphic muscovite from RV10 is smooth with little variation among the steps (Fig. 7.11; Table 7.2). The isochron plot shows data throughout the isochron but predominantly occurs towards the x-axis and gives an almost identical $^{40}\text{Ar}/^{39}\text{Ar}$ age to the step-heating spectrum (440.3 ± 0.2 Ma and 440.2 ± 0.9 Ma respectively). As the ages are both within uncertainty of each other, the step-heating $^{40}\text{Ar}/^{39}\text{Ar}$ age (440.3 ± 0.2 Ma) is considered to be robust and is reported to 2σ in Table 7.2. The higher closure temperature of the $^{40}\text{Ar}/^{39}\text{Ar}$ for muscovite than K-feldspar (Table 7.3) suggests it is less likely to have been reset by later fluids in the Tyndrum area.

Table 7.2 *Geochronology results for all samples from this study*

Sample	Description	Au grade	Mo grade	Phase	Method	To show	Results
GO02b	Poly-metallic vein	171	5.6	Muscovite Pre Au	Ar/Ar	Maximum age of gold	407.7 ± 2.1 (2σ)
RV18	Poly-metallic vein	103	9.27	Sericite Post Au	Ar/Ar	Minimum age of gold	407.2 ± 1.1 (2σ)
RV16	Molybdenite- bordered fracture	0.021	205	K-feldspar	Ar/Ar	Pre-Au and rutile, Pre- to syn-Mo	407.11 ± 0.7 (2σ)
RV10	Molybdenite- bordered fracture	0.091	4384	K-feldspar	Ar/Ar	Pre-Au and rutile	407.1 ± 0.6 (2σ)
RV10	Molybdenite- bordered fracture	0.091	4384	Rutile	U-Pb	Age of rutile, syn to post-Mo and pre-Au	439 ± 7 (33) (2σ)
RV10	Molybdenite- bordered fracture	0.091	4384	Muscovite	Ar/Ar	Metamorphic muscovite	440.3 ± 0.7 (2σ)
RV16	Molybdenite- bordered fracture	0.021	205	Rutile	U-Pb	Age of rutile, syn to post-Mo and pre-Au	455 ± 4 (28) (2σ)
GO1217	Molybdenite- bordered fracture	No assay	No assay	Molybdenite	Re-Os	Pre-Au and rutile, syn- to post K-spar	461.6 ± 2.4 (2σ)
RV109	Molybdenite- bordered fracture	0.016	>10000	Molybdenite	Re-Os	Pre-Au and rutile, syn- to post K-spar	468.1 ± 2.5 (2σ)
RV01	Molybdenite- bordered fracture	0.045	1570	Molybdenite	Re-Os	Pre-Au and rutile, syn- to post K-spar	476.8 ± 2.2 (2σ) 477.0 ± 2.4 (2σ)

See section 7.4.3 for dual rutile error explanation. 2σ Ar/Ar ages reported in Appendix 7.2, see 7.4.2 for full explanation

7.6.1.3 Sericite pre- and post-gold mineralisation

The age spectrum for sericite from RV18 is smooth with no variation in the steps for 95% of the ^{39}Ar release (Fig. 7.12; Table 7.3). Data occur throughout the isochron but predominantly towards the x-axis and give an age within error of the $^{40}\text{Ar}/^{39}\text{Ar}$ age of the step-heating spectrum (406.5 ± 1.6 Ma and 407.2 ± 0.5 Ma respectively). As the ages are both within uncertainty of each other the $^{40}\text{Ar}/^{39}\text{Ar}$ step-heating spectra age (407.2 ± 0.5 Ma) is considered to be robust and is reported to 2σ in Table 7.2.

Sample GO02b was analysed by *in situ* laser and the probability spectrum suggests the muscovite has an age of 407.7 ± 0.9 Ma (Fig. 7.13; Table 7.2). On the isochron plot the age (408.4 ± 1.7 Ma) is within the error of that of the probability spectrum, the *in situ* age is considered to be robust and is reported to 2σ in Table 7.2.

Table 7.3 Closure temperatures of minerals dated in this study

Mineral	Geochronometer	Closure temperature	Reference
Molybdenite	Re-Os	600-700°C	Stein <i>et al.</i> (1998a); Raith & Stein (2000)
Rutile	U-Pb	450±50°C	Mezger <i>et al.</i> (1989)
Muscovite	Ar/Ar	350±50°C	Purdy & Jäger (1976); Hames & Bowring (1994)
K-feldspar	Ar/Ar	150-300°C	Lovera <i>et al.</i> (1989)

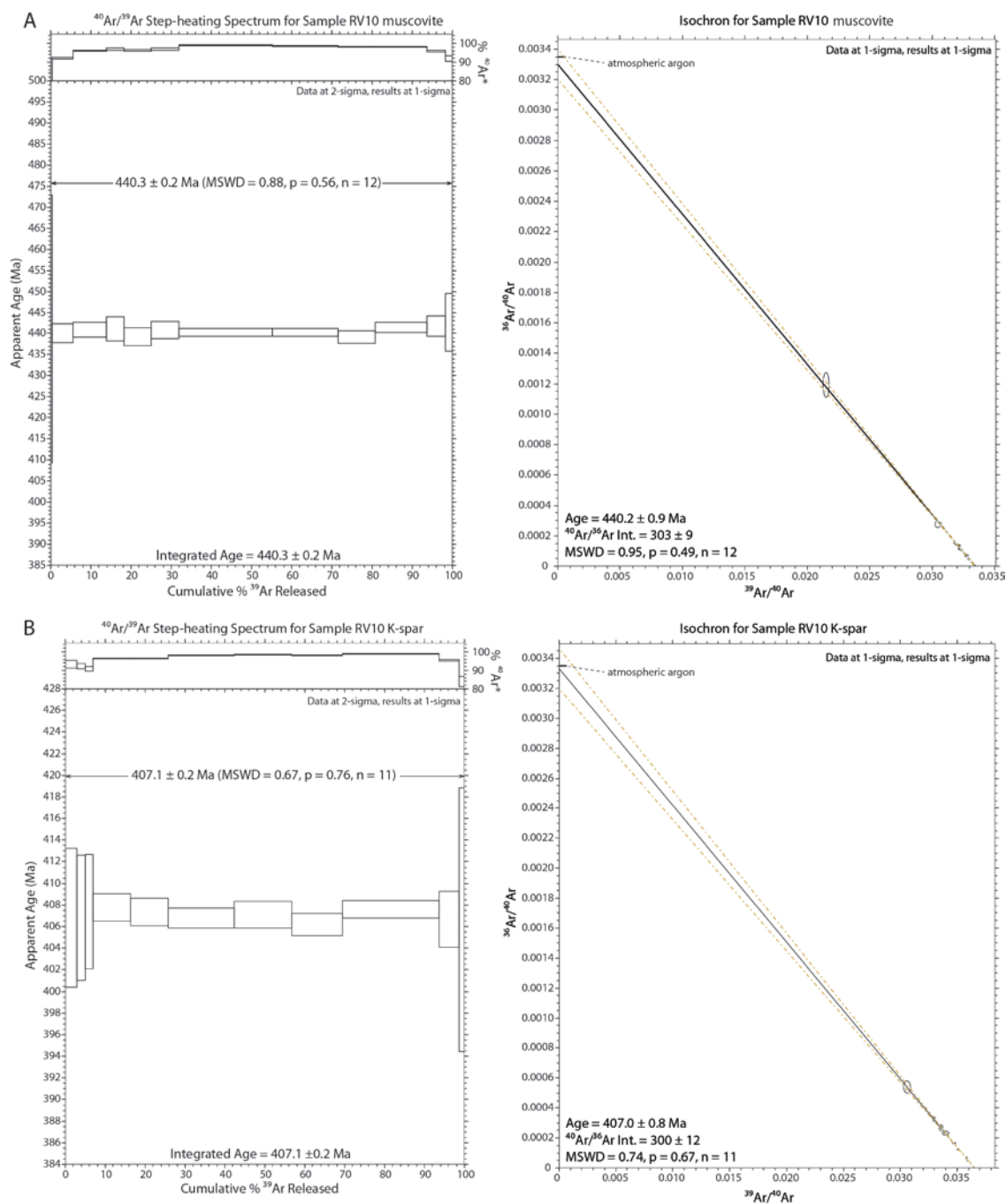


Figure 7.11: Step-heating spectra and isochron for $^{40}\text{Ar}/^{39}\text{Ar}$ on muscovite (A) and K-feldspar (B) from RV10. Plateau step criteria require steps to be indistinguishable at 2σ as a result data for step-heating are presented at 2σ and results at 1σ .

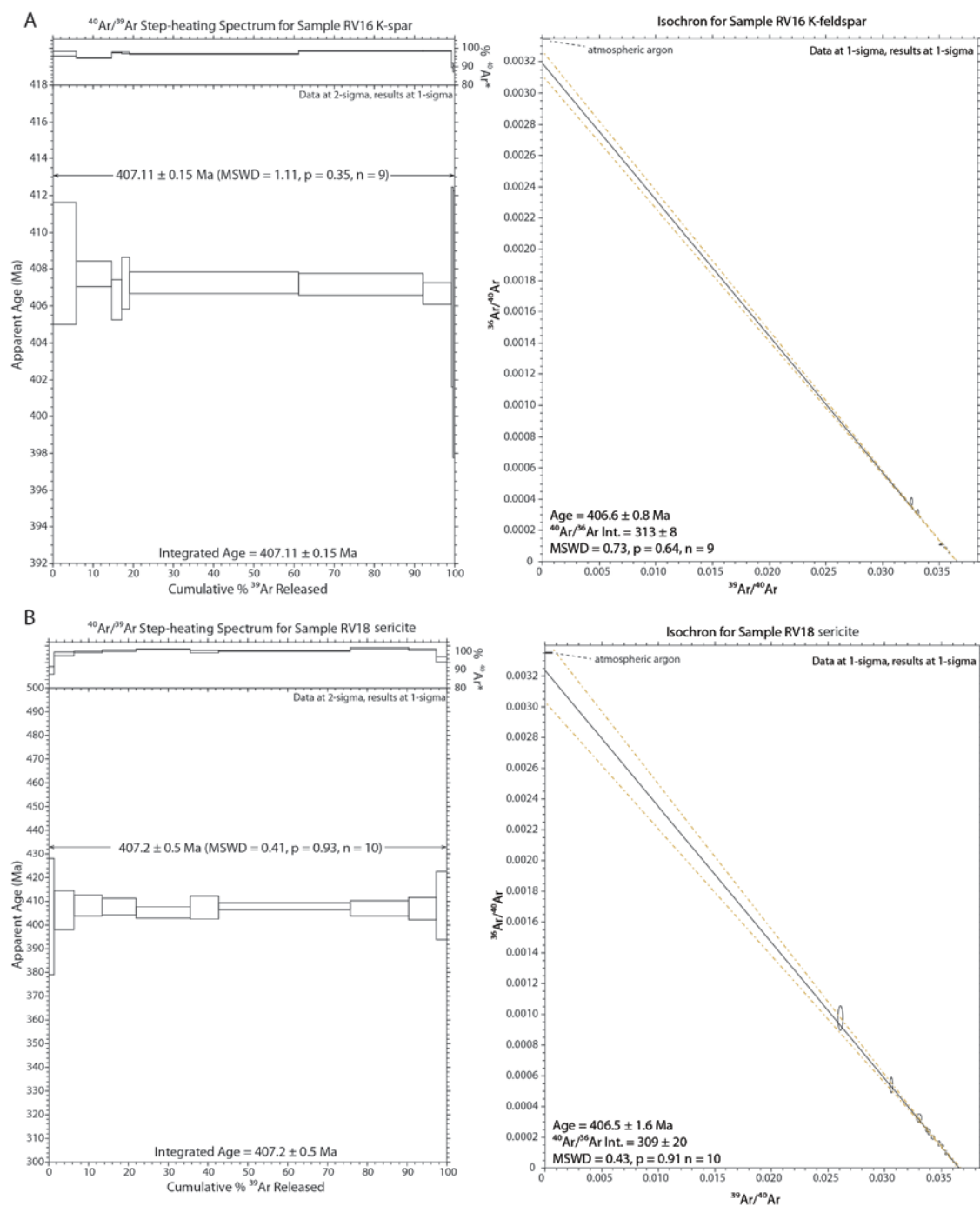


Figure 7.12: Step-heating spectra and isochron for $^{40}\text{Ar}/^{39}\text{Ar}$ on K-feldspar (A) from RV16 and sericite (B) from RV18. Plateau step criteria require steps to be indistinguishable at 2σ as a result data for step-heating are presented at 2σ and results at 1σ .

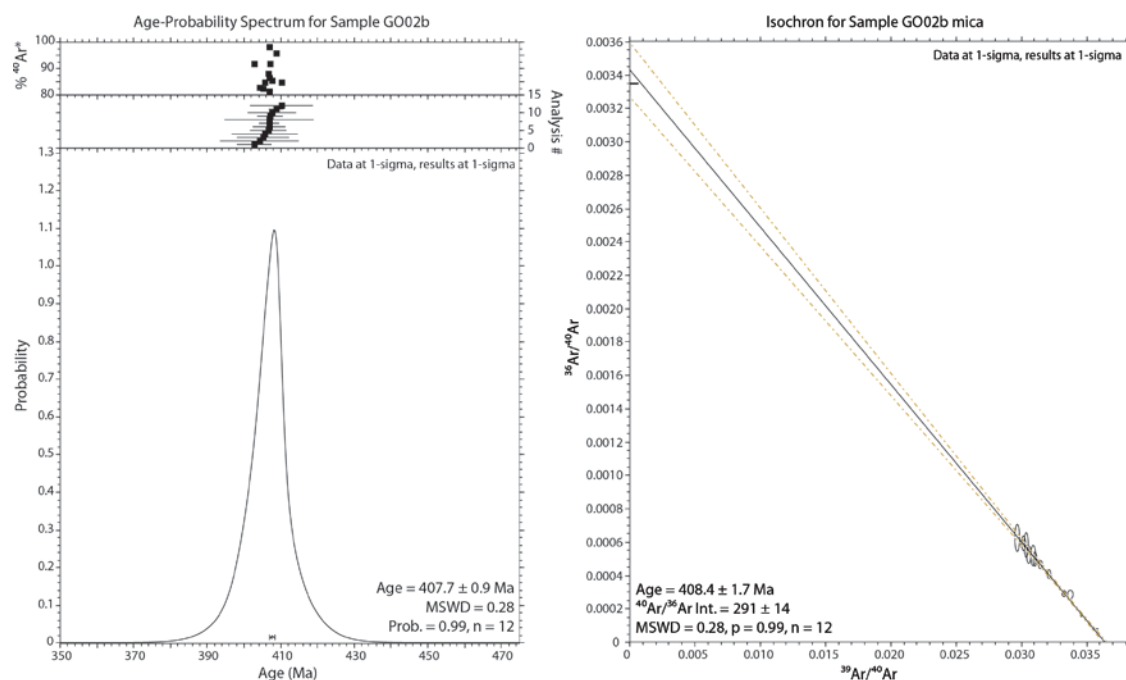


Figure 7.13: Age probability spectrum and isochron for $^{40}\text{Ar}/^{39}\text{Ar}$ on muscovite from GO02b using *in situ* laser analysis.

7.6.2 U-Pb geochronology

7.6.2.1 Detrital zircon

U-Pb ICP-MS ages from detrital zircons within the Meall Garbh Psammite (samples RV10 & RV16; Fig. 7.14) range from 706 to 2153 Ma ($n=75$). All data except two ($n=73$) are within the range 898 to 1800 Ma (average 1319 ± 247 Ma; 2σ standard deviation). Full data are reported in Appendix 7.4.

7.6.2.2 Rutile

U-Pb rutile results (Table 7.2) for RV10 and RV16 are detailed in Appendix 7.5. The rutile contains variable concentrations of common lead. Plotting the analyses on Tera-Wasserburg plots reveals that both samples fall on a mixing array between common lead and a radiogenic component. The analyses provide ages of $439 \pm 8(33)$ Ma for sample RV10 and $455 \pm 4(28)$ Ma for sample RV16 (2σ errors; Fig. 7.15). The uncertainties on the ages are large, and thus the ages overlap within uncertainty when using full errors.

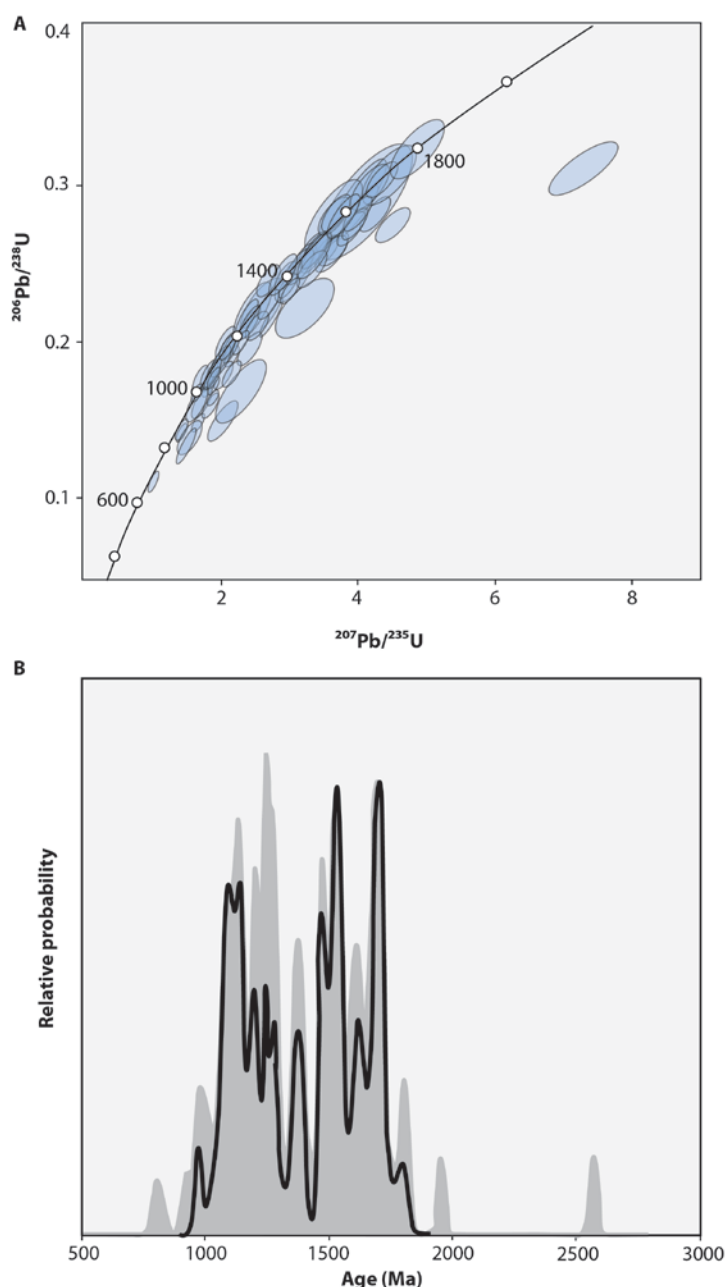


Figure 7.14: U-Pb LA-ICPMS detrital zircon results from RV10 and RV16 (both samples shown on same plot). A. Concordia showing 2σ errors on $n=75$ zircon samples. Data point ellipses are 2σ . B. Frequency distribution diagram for $n=75$ detrital zircons, filled grey curve incorporates all analyses whereas area under black line includes samples with $>90\%$ concordance.

It is probable that the ages are dating the same rutile-bearing event, with a combined weighted mean age of $447 \pm 8(43)$ Ma (MSWD = 1.5), but it remains a possibility that they represent an early phase at *c.* 455 Ma more closely associated with molybdenite mineralisation, and a later *c.* 439 Ma event. Given the high closure temperature of the U-Pb rutile geochronometer (Table 7.3) rutile is not expected to be reset by any later hydrothermal fluids.

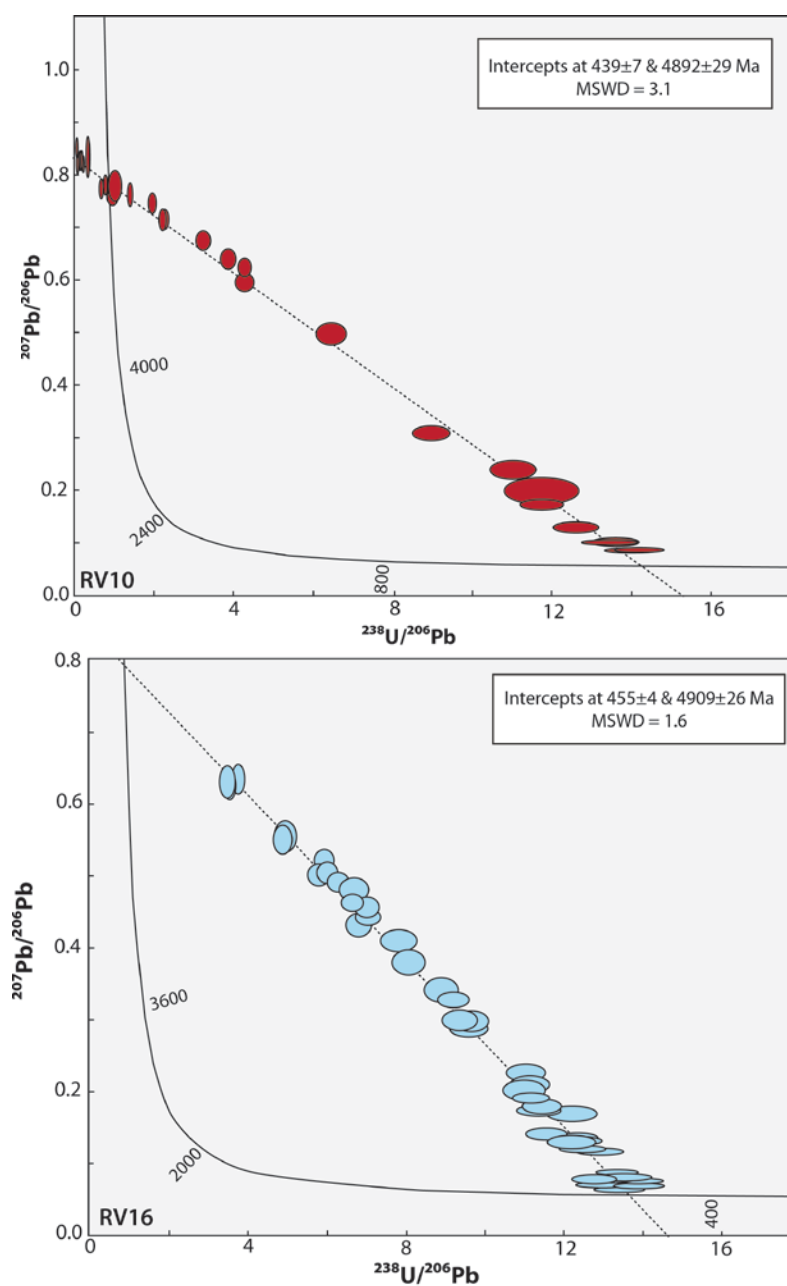


Figure 7.15: U-Pb LA-ICPMS hydrothermal rutile results for RV10 and RV16. Data point ellipses are 2σ .

7.6.3 Re-Os geochronology

The Re-Os molybdenite results for GO1217, RV109 and RV01 are detailed in Table 7.4. The Re-Os ages range from 477.0 ± 2.4 Ma (RV01) to 461.6 ± 2.4 Ma (GO1217; Table 7.4). All molybdenite contains low Re (<52 ppm; Table 7.4); RV109 contains a lower abundance of Re (19.3 ppm) than RV01 and GO1217 (Table 7.4)

Sample RV01 was analysed twice using two different spiking methods; normal Os doping (Selby & Creaser 2001) and double Os spike (190+188; Markey *et al.* 2007). The latter permits the evaluation of any common osmium in molybdenite, which determined 0.5 ppt common Os, and thus, negligible common ^{187}Os in comparison to the radiogenic ^{187}Os (257 ppb). Both analyses yield Re-Os ages that are indistinguishable within uncertainty (Table 7.4). The high closure temperature of the Re-Os geochronometer (Table 7.3) is likely to preclude resetting of the system by later hydrothermal events in the Tyndrum area.

Table 7.4 *Re-Os results*

Sample	Easting	Northing	Run No.	Re (ppm)	^{187}Re (ppm)	^{187}Os (ppb)	Osc (ppt)	Age (Ma)	\pm
RV01	225150	733968	1	45.6 ± 0.2	28.7 ± 0.1	228.8 ± 0.7		477.0	2.4
RV01	225150	733968	2	51.4 ± 0.2	32.3 ± 0.1	257.5 ± 0.4	0.5	476.8	2.2
RV109	225116	734032	1	19.3 ± 0.1	12.1 ± 0.1	95.0 ± 0.3		468.1	2.5
GO1217	225122	734033	1	41.8 ± 0.2	26.3 ± 0.1	203.0 ± 0.28		461.6	2.4

Osc is the common Osmium within the sample, calculated using the double spike method

7.7 Discussion

7.7.1 Constraints on the age of gold-bearing poly-metallic quartz veins

7.7.1.1 Glen Orchy

The $^{40}\text{Ar}/^{39}\text{Ar}$ ages for muscovite (pre-Au 407.7 ± 0.9 Ma) and sericite (post-Au 407.2 ± 0.5 Ma) bracket emplacement of electrum in gold-bearing poly-metallic veins (Fig. 7.16). The small age range of <0.5 Ma (± 1.0 Ma) suggests there is a single short-lived gold-bearing hydrothermal event. A single gold-bearing event is supported by the electrum geochemistry (Chapter 5) that records a continuum of gold content in electrum without distinct populations.

7.7.1.2 Tyndrum area

The new ages for gold mineralisation in the Glen Orchy area (407.2 ± 0.5 to 407.7 ± 0.9 Ma; $^{40}\text{Ar}/^{39}\text{Ar}$ muscovite) are within the age range of existing age data for the Cononish deposit, 410 ± 14 Ma ($^{40}\text{Ar}/^{39}\text{Ar}$ K-feldspar; Treagus *et al.* 1999; Fig. 7.16). Recent work at the Cononish deposit constrained K-feldspar, with inclusions of gold, to *c.* 408–407 Ma ($^{40}\text{Ar}/^{39}\text{Ar}$ K-feldspar; *in situ* laser and step-heating; Rice *et al.* 2012) concordant with the age of gold mineralisation at Glen Orchy.

The coeval ages are interpreted to suggest that, despite the variations in trend, mineralogy (Chapter 4) and geochemistry (Chapter 5) among gold-bearing poly-metallic veins, all gold-bearing poly-metallic veins in the Tyndrum area represent a single gold-bearing hydrothermal system. The previous age constraints for the Cononish deposit are $^{40}\text{Ar}/^{39}\text{Ar}$ K-feldspar ages (Treagus *et al.* 1999; Rice *et al.* 2012) and could be argued to have undergone low temperature resetting from an older age (e.g. Lee 1995; Parsons & Lee 2000). However, the highly concordant ages from this study and previous workers on both muscovite and K-feldspar (Treagus *et al.* 1999; Rice *et al.* 2012) are interpreted to suggest that the K-feldspar data are robust. Further evidence that the gold vein ages are not due to an overprinting hydrothermal/thermal event is the preservation of metamorphic cooling ages in muscovite in the surrounding host rocks (see below). It is concluded that all gold-bearing poly-metallic quartz-veins in the Tyndrum area are of the same age (407–408 Ma) and represent the same gold-bearing hydrothermal event.

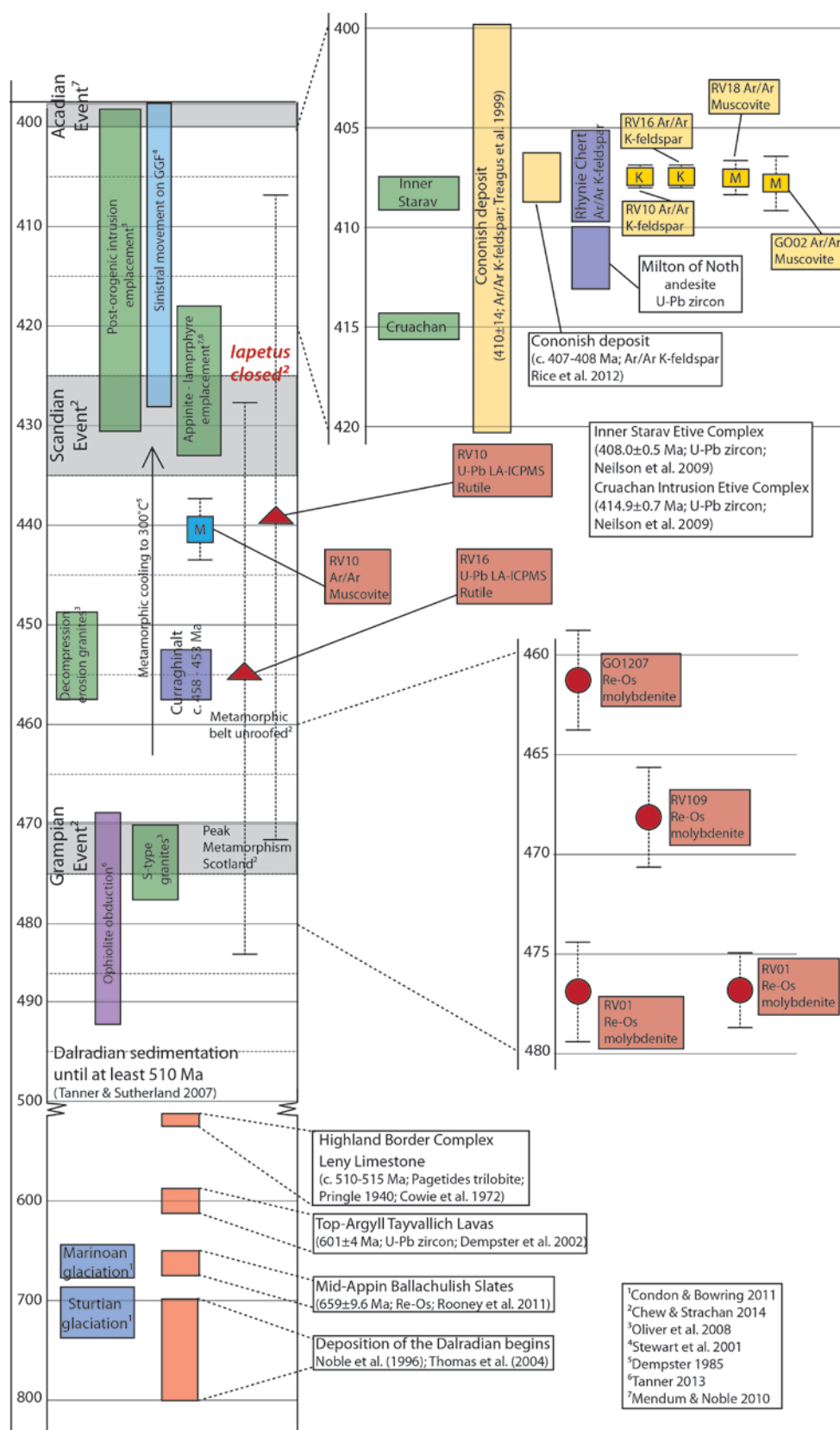


Figure 7.16: New data from this study for molybdenite-bordered fractures (red) and gold-bearing poly-metallic quartz veins (yellow) compared to existing constraints on the age of the Dalradian Supergroup and vein-hosted gold mineralisation. Note that the scale changes at 500 Ma. Rhynie Chert age from Mark *et al.* (2011), Milton of Noth age from Parry *et al.* (2011).

7.7.1.3 Implications of metamorphic muscovite age

The 440.5 ± 1 Ma age ($^{40}\text{Ar}/^{39}\text{Ar}$) for metamorphic muscovite within the Meall Garbh Psammite (RV10; Table 7.2) is close to the age the cooling Grampian orogen would have passed through $\sim 350^\circ\text{C}$, based on cooling models by Dempster (1985) for Perthshire (Fig. 7.17). The metamorphic muscovite age has a flat step-heating profile (Fig. 7.11) and has not been reset by fluids from the later gold-bearing quartz veins nearby including the River Vein (sample RV18), only *c.* 20 m away (Fig. 7.7). This suggests that it was neither recrystallised, nor heated above its closure temperature of *c.* 350°C (Table 7.3) for any significant period of time. This is in line with fluid inclusion data on gold veins from the area that suggest these veins formed at $290\text{--}350^\circ\text{C}$ (Curtis *et al.* 1993).

7.7.2 Constraints on the age of molybdenite-bordered fractures

To constrain the age of the pre-gold molybdenite-bordered fractures three mineral phases have been dated using different techniques (Table 7.2). Re-Os ages on molybdenite vary from 477.0 ± 2.4 to 461.6 ± 2.4 Ma, a range of 16 ± 3.4 Ma (2σ ; Table 7.4). U-Pb ages on rutile range from $455 \pm 4(28)$ to $439 \pm 7(33)$ Ma (2σ ; Table 7.2) and are indistinguishable within error. $^{40}\text{Ar}/^{39}\text{Ar}$ ages on K-feldspar range from 407.11 ± 0.6 to 407.7 ± 2.1 Ma (2σ ; Table 7.2) and are also indistinguishable within error.

The large 16 ± 3.4 Ma range in Re-Os molybdenite ages from molybdenite-bordered fractures in Glen Orchy is difficult to explain as a single hydrothermal pulse. The older (477.0 ± 2.4 Ma) or younger (461.6 ± 2.4 Ma) Re-Os molybdenite ages could be reset to account for the variation across the samples. Older Re-Os ages could be obtained by Re loss or ^{187}Os gain, with younger ages obtained by Re gain or ^{187}Os loss (Stein *et al.* 1998b). The mechanisms for Re loss or gain are unclear (Stein *et al.* 1998b) and the Re-Os geochronometer is not reset by later metamorphic deformation (Stein *et al.* 2001). Re and Os are not mobilised out of the individual molybdenite crystal by later solid-state recrystallisation (Stein *et al.* 2001) and loss of radiogenic ^{187}Os is very uncommon (Stein *et al.* 2001). Gain of ^{187}Os is interpreted to be unlikely given the low common Os in the samples (0.5 ppt Os; Table 7.4; Stein *et al.* 1998b). The small errors on Re-Os molybdenite dates suggest the data from all samples is robust and while metal contamination could be argued for the older ages from sample RV01, given the sample was prepared differently to RV109 and GO1217 (see section 7.4.4), there is no evidence of common Os metal contamination in the isotope data (Table 7.4). Given it seems unlikely the Re-Os geochronometer has been reset then the molybdenite ages are assumed to be correct and

therefore all ages from other geochronometers within the molybdenite-bordered fractures should fit with the Re-Os molybdenite ages.

The U-Pb rutile ages, at maximum errors, overlap with Re-Os molybdenite ages, or are just younger, and could be interpreted to indicate a longer overall event with multiple hydrothermal fluid pulses. The $^{40}\text{Ar}/^{39}\text{Ar}$ K-feldspar ages are a problem as they are much younger and are discordant with the Re-Os molybdenite and U-Pb rutile ages. The entire range of ages (477-407 Ma; Table 7.2) is not reasonable as the molybdenite-bordered fractures are cross-cut by the gold-bearing poly-metallic quartz veins (407.7 ± 2.1 to 407.2 ± 1.1 Ma; Table 7.2). It is notable that the $^{40}\text{Ar}/^{39}\text{Ar}$ K-feldspar ages are identical within error to the age of gold-bearing quartz veins in the Glen Orchy area strongly suggesting that the K-feldspar has been reset by the gold-bearing fluids at 407 Ma, as would be possible if those fluids had temperatures just over 300°C (Table 7.3).

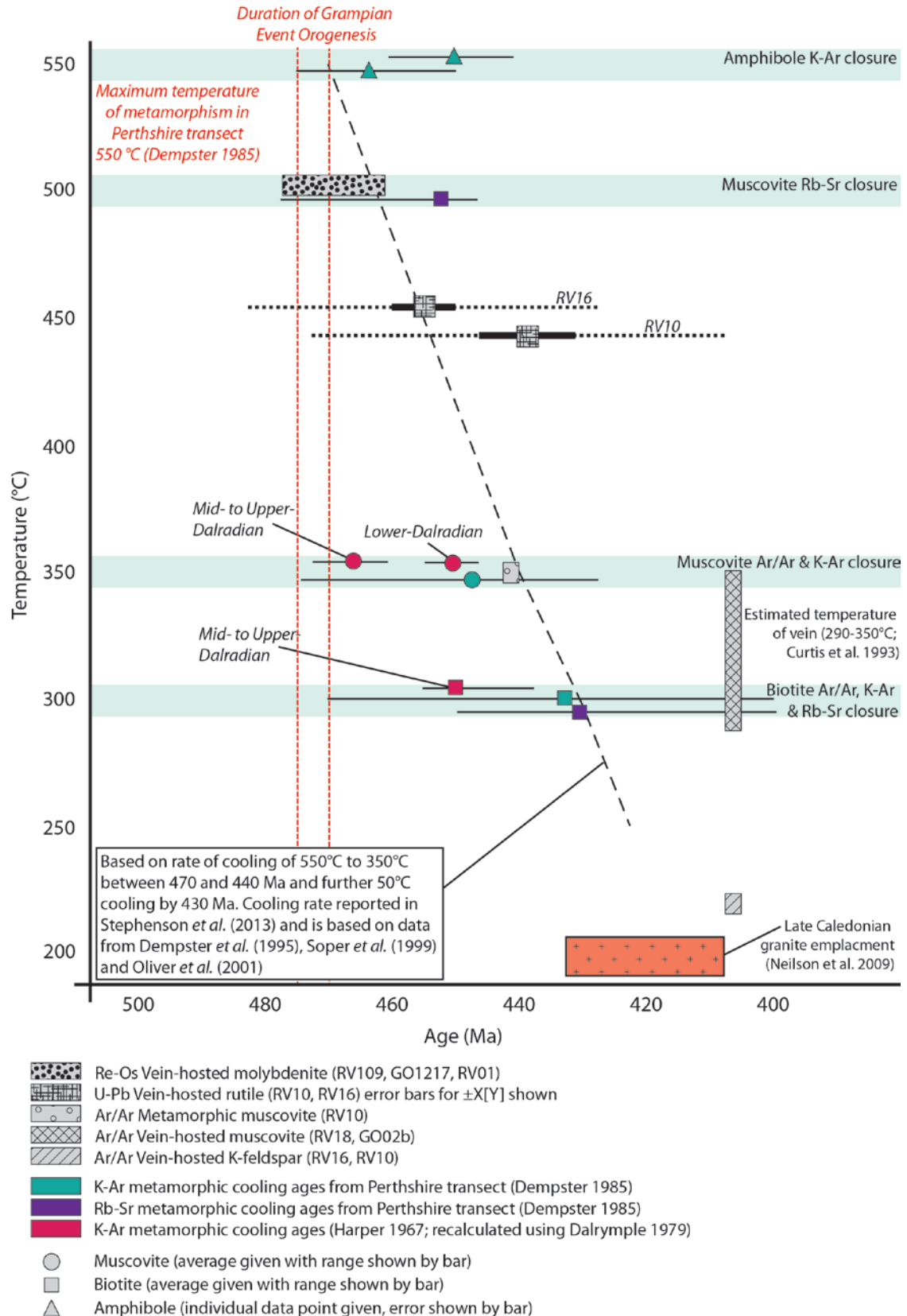


Figure 7.17: Cooling profile of the Grampian Orogen plotted from literature data for closure temperatures and showing ages obtained in this study. All data are vein-hosted except RV10 which is metamorphic muscovite. Data from Dempster (1985) is taken from the Perthshire transect (Highland Boundary Fault to Blair Atholl) and is ~60 km NE of the Cononish deposit. Harper (1967) ages are likely to be less reliable given the age and recalculation. Duration of Grampian Event Orogenesis is *c.* 475-470 Ma (Chew & Strachan 2014; Section 7.2.1).

7.8 Synthesis

7.8.1 Molybdenum-bearing hydrothermal event

All the constraints from geochronology, field relations, petrography (Chapter 4), geochemical trends (Chapter 5) and S-isotope ratios (Chapter 6) suggest that the molybdenite-bordered fractures represent a distinct hydrothermal event from the gold-bearing mineralisation. Two scenarios for the source of heat, fluids and the molybdenum for this hydrothermal system are considered:

1. Molybdenite- and rutile-mineralisation reflect multiple intrusion-driven mineralisation events

Hydrothermal activity related to a single intrusion is only likely to be sustained for 0.8 Ma (Cathles *et al.* 1997) so it is unreasonable for a single molybdenum-bearing hydrothermal event to span 16 Ma and potentially be sustained for up to 40 Ma. The range in ages (477-439 Ma; Table 7.2) in the molybdenite-bordered fractures could be interpreted to reflect multiple intrusion-related hydrothermal events utilising the same structures over a period of *c.* 40 Ma. For example, multiple intrusion-related hydrothermal episodes are invoked to account for the range in molybdenite ages, spanning 9 ± 0.85 Ma, seen at the Endako deposit, Canada (Selby & Creaser 2001), comparable to the 16 ± 3.4 Ma range at Glen Orchy. In addition, there is no variation in mineralogy or geochemistry between samples RV01, RV109 and GO1217 to suggest the samples would be expected to represent different hydrothermal events.

There are no intrusions of any type in the study area that were emplaced between 477-439 Ma, although intrusions of this age do occur elsewhere in the Grampian belt (NE Highlands; Chapter 3). Therefore it is possible, although implausible, that there are multiple intrusions at depth with no surface exposure of intrusions, to account for range in ages.

2. Molybdenite- and rutile-mineralisation reflect a single protracted metamorphic mineralisation event

It is proposed the range in ages (Table 7.2) within the molybdenite-bordered fractures reflect a single protracted metamorphic event consisting of a number of discrete fluid pulses. When considering the large errors on rutile (RV10 & RV16), the U-Pb data is within error of the younger Re-Os dates (Table 7.2) supporting a single protracted mineralisation event. In addition, the spatial relationship of the samples, collected within 50

m of each other (Fig. 7.7) suggests it is unlikely five completely independent events formed the veins but a series of discrete events within one overall process may be recorded.

The deeper crust will reach peak metamorphic conditions later than shallower levels (Stüwe *et al.* 1993) and therefore prograde metamorphism can be continuing at depth while brittle deformation is occurring nearer the surface (Yardley *et al.* 2000). Stüwe *et al.* (1993) suggest shallow levels may undergo prograde metamorphism up to 50 Ma before deeper levels, supported by the production of ore-bearing fluids for *c.* 20 Ma during prograde metamorphism in the European Alps (Pettke *et al.* 1999). In the Val d'Or district of Abitibi belt, Canada quartz-tourmaline-carbonate veins were precipitated in stages along the same fault system in response to crustal shortening, while at depth the crust was still undergoing prograde metamorphism (Robert *et al.* 1995). This supports a metamorphic model for the molybdenite-bordered fractures by suggesting the fractures represent a series of pulses of metamorphic fluids as parts of the underlying orogen cool at different rates. Variation in the timing of peak metamorphism with depth supports the 477.0 ± 2.4 Ma molybdenite age (RV01; Table 7.4) being slightly older than peak metamorphism (*c.* 475-470 Ma; Chew & Strachan 2014) if, at the depth of emplacement, brittle deformation is occurring while peak metamorphic conditions persist in the deeper crust.

The concentration of Re in molybdenite has been suggested to be indicative of the origin of the molybdenite, with high Re contents (100's-1000's ppm Re; Stein 2006) indicating a subduction-related porphyry source (e.g. Stein *et al.* 2004). Low Re (<20 ppm) and variable Re-Os ages are diagnostic of molybdenite sourced from dehydration of sediments during metamorphism (Stein 2006). The Glen Orchy molybdenite samples have 19-51 ppm Re (Table 7.4) which is more similar to the values suggested for metamorphic origin, supporting scenario 2.

Re-Os molybdenite ages from mineralisation in northern Sweden range from 1865 to 1750 Ma and reflect 12 individual events during Svecofennian metamorphism (Stein 2006). While this age range is much greater than the *c.* 40 Ma range in Glen Orchy, it demonstrates that protracted pulsed molybdenite mineralisation can occur during orogenic deformation and metamorphism. It is concluded a protracted pulsed metamorphic model for the molybdenum-bearing hydrothermal system is more likely given the geochronology and field constraints.

7.8.2 Gold-bearing hydrothermal event in Scottish Dalradian Supergroup

The ages of gold-bearing poly-metallic veins in Glen Orchy (407.2 ± 1.1 to 407.7 ± 2.1 Ma; $^{40}\text{Ar}/^{39}\text{Ar}$ muscovite), Rhynie Chert (407 ± 1 Ma; $^{40}\text{Ar}/^{39}\text{Ar}$ K-feldspar; Mark *et al.* 2011a) and the Cononish deposit (407-408 Ma; $^{40}\text{Ar}/^{39}\text{Ar}$ K-feldspar; Rice *et al.* 2012) are coeval. There is no evidence of significant ^{40}Ar loss as a result of later hydrothermal fluids or heating events on the dated K-feldspar phase at Rhynie. In addition, given the Rhynie Chert is at the surface and thus much less likely to be infiltrated with hot fluids in a second hydrothermal event, the age is considered robust (Mark *et al.* 2011a).

Hydrothermal and other fluids are known to be able to travel significant distances through terranes (Mark *et al.* 2007) suggesting there is potential for regional movement of fluids along shear structures and pre-existing lineaments. The concordance in dates from both K-feldspar and muscovite $^{40}\text{Ar}/^{39}\text{Ar}$ ages in gold-bearing occurrences, both locally to the Tyndrum area and regionally across the Scottish portion of the Dalradian Supergroup, suggests a regional gold-bearing hydrothermal event is recorded at 407-408 Ma.

The Curraghinalt deposit, Northern Ireland, is postulated to be an orogenic gold deposit, due to the timing of gold emplacement (458-453 Ma; Rice *et al.* 2012) relatively close to peak metamorphism (*c.* 475-470 Ma; Chew & Strachan 2014) and the occurrence of fluids with metamorphic characteristics in the fluid inclusions within the gold-bearing quartz veins (Parnell *et al.* 2000). The Bohau deposit is of unclear origin but is hosted in Silurian rocks of Llandovery to Wenlock age (*c.* 443-427 Ma; Lusty *et al.* 2011) suggesting gold mineralisation is not older than 427 Ma.

The limited geochronological data for gold occurrences in the Dalradian Supergroup suggests there are at least two distinct gold-bearing mineralisation events. In Ireland, an orogenic gold event is recorded at the Curraghinalt deposit (Rice *et al.* 2012); it is not clear if this event is recorded elsewhere in either the Irish or Scottish Dalradian Supergroup due to a lack of geochronological data. The second gold-bearing mineralisation event is recorded through the Scottish Dalradian Supergroup at 407-408 Ma, the limited data means it is currently unclear if this event is present in the Irish Dalradian Supergroup.

Results here suggest a regional-scale gold-bearing hydrothermal event occurs in the Scottish Dalradian Supergroup at 407-408 Ma. In the following sections, models are proposed and examined for the genesis of the hydrothermal system.

7.8.2.1 Comparison to the orogenic gold model

The Cononish deposit and other gold-bearing poly-metallic quartz veins in the Tyndrum area do not easily fit any of the deposit models for classic gold deposits (Chapters 2 & 5). Based on the geochemical characteristics (Chapter 5), the epithermal and reduced-intrusion related deposit types are discounted as possible models for mineralisation in the Tyndrum area. An orogenic model may be more relevant to the setting but the geochemistry of gold mineralisation at the Cononish deposit does not fit that of the orogenic gold model (Groves *et al.* 1998). The River Vein-style of gold mineralisation (seen in Glen Orchy) has more comparable geochemistry to the orogenic gold deposit model (Groves *et al.* 1998) and given the geochronology suggests gold mineralisation is all contemporaneous, the orogenic gold model is considered as a potential model for gold deposition in the Scottish Dalradian.

The orogenic gold model states emplacement of mineralisation occurs at or above the brittle-ductile transition (Bierlein *et al.* 2004) at syn- to post-peak metamorphic conditions (Groves *et al.* 1998). The age of the 407 Ma gold-bearing hydrothermal event is >63 Ma after peak metamorphism (*c.* 475-470 Ma; Chew & Strachan 2014). Therefore, the orogenic gold deposit type is discounted as a potential model for the emplacement of the 407-408 Ma gold-bearing hydrothermal event because it occurred >63 Ma after peak metamorphism and prograde metamorphism typically only continues for *c.* 50 Ma after peak metamorphic conditions (Stüwe *et al.* 1993).

7.8.2.2 Tectonic events at 407-408 Ma

Given the traditional gold deposit models (orogenic, epithermal, reduced-intrusion related models) have been discounted, an alternative model is required to explain the genesis of the 407-408 Ma gold-bearing hydrothermal event. Here, the tectonic setting at *c.* 407 Ma is examined to establish events within the Supergroup at this time that may be contributing sources of heat, fluids or metals to the gold-bearing hydrothermal system. Between 420 and 400 Ma two major events occur; emplacement of the post-orogenic granite suite and significant movement on the Great Glen and subsidiary faults.

Emplacement of the Late-Caledonian post-orogenic granite suite began at 433 ± 1.8 Ma and continued for 25 Ma (Neilson *et al.* 2009). There is no exposure of Late-Caledonian granite in the study area but a gravity anomaly extending from the Etive Complex (Fig. 7.5) has been postulated to represent a concealed granite (Pattrick *et al.* 1988). The gravity anomaly is coincident with the location of the postulated Lochaber Batholith (Kynaston & Hill 1908; Neilson *et al.* 2009; Tanner 2012).

Two models are proposed to produce the heat flow required to induce melting and emplacement of the large volume of post-orogenic granites at *c.* 430-408 Ma:

1. Slab break-off caused asthenosphere upwelling and emplacement of granite batholiths (Fig. 7.18; Oliver *et al.* 2008; Neilson *et al.* 2009).

Neilson *et al.* (2009) propose break-off of the subducted Iapetus Ocean slab beneath the Grampian Terrane allowed upwelling of the asthenosphere (Atherton & Ghani 2002), inducing melting and driving emplacement of granite batholiths with an I-type signature. The post-orogenic granite suite was emplaced over ≥ 25 Ma, comparable to the emplacement duration associated with Tertiary slab break-off in the European Alps (*c.* 17 Ma; Neilson *et al.* 2009).

The slab break-off model is supported by the volume of magma emplaced at *c.* 433-408 Ma, which is most easily explained by partial melting of the crust (Neilson *et al.* 2009). In addition, the variation in the incompatible trace-element patterns cannot be explained by fractional melting of the mantle (Neilson *et al.* 2009). However, the patterns could be explained by partial melting of the lower crust with variation caused by heterogeneity in the crust and different degrees of melting (Neilson *et al.* 2009).

Atherton & Ghani (2002) propose slab break-off is a progressive short-lived event supported by a progressive decrease in the age of granites ages towards the SW in the SW Highlands. However, lateral migration of slab break-off is rapid once initiated (Cooper *et al.* 2013) and the ≥ 25 Ma range in granite emplacement ages does not support this. Alternatively, Cooper *et al.* (2013) propose long lived heat flow from upwelling mantle associated with the slab break-off. Long-lived heat flow is supported by the duration of granite emplacement (≥ 25 Ma) and the volume of granites emplaced (Oliver *et al.* 2008; Neilson *et al.* 2009).

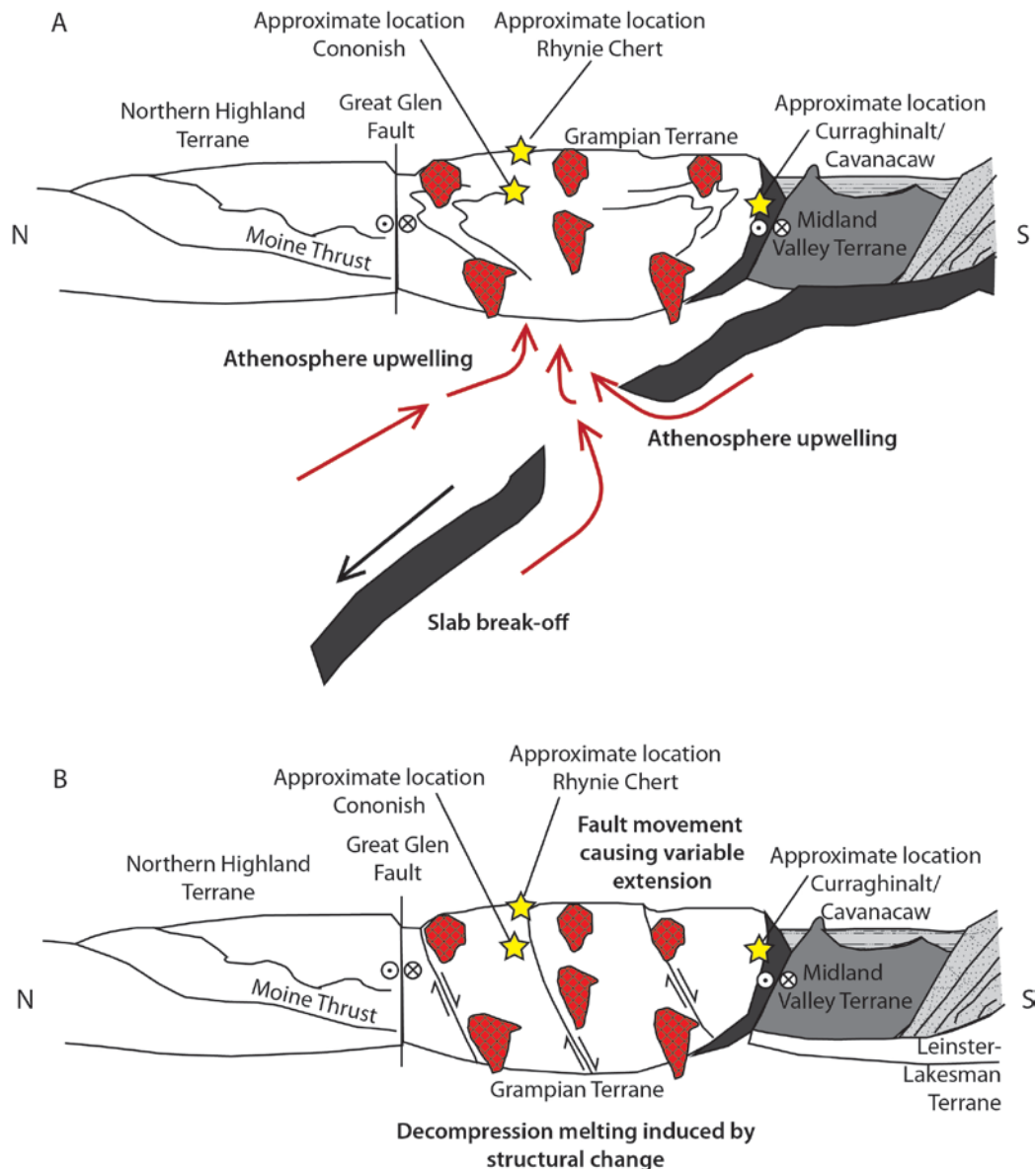


Figure 7.18: Two proposed models for heat and fluid fluxing event at *c.* 410 Ma. A. Slab break-off causing asthenosphere upwelling and emplacement of granite batholiths. B. Movement on Great Glen and subsidiary faults as structural regime changes causes decompression melting. Note that Curraghinalt and Cavanacaw are along strike on analogous terrane-bounding structures in Ireland.

2. Movement of regional faults during a transtensional stress regime (Fig. 7.18) induced passive melting which forms granite batholiths (Brown *et al.* 2008; Miles *et al.* 2014).

Miles *et al.* (2014) suggests emplacement of granites of the Trans-Suture suite (TSS) of the Southern Uplands terrane occurred during post-collisional transtension at *c.* 410–420 Ma. While the TSS granites are S-type (compared to Grampian terrane I-type) and span the Iapetus suture zone (Southern Uplands & Leinster-Lakesman terranes; Brown *et al.* 2008), geochronology suggests the granites are coeval with the post-orogenic granite suite (410 ± 6 to 416 ± 5 Ma; U-Pb zircon; Miles *et al.* 2014). This supports a decompression melting

model, as the location of TSS granites, across the Iapetus Suture Zone, precludes generation of the melt by N-dipping Iapetus Ocean subduction.

Between *c.* 428 and 390 Ma significant movement is recorded on the Great Glen and subsidiary faults (Stewart *et al.* 2001) in response to sinistral transtension (Mendum & Noble 2010) close to the age range of the Late-Caledonian post-orogenic granite suite (*c.* 433-408 Ma; Neilson *et al.* 2009). The Caledonian Faults are interpreted to focus fluids (Tanner 2013) and allow for regional fluid flow throughout the Dalradian Supergroup (Mark *et al.* 2007).

7.8.2.3 Model for gold mineralisation at 407-408 Ma

The concordancy of K-feldspar and muscovite $^{40}\text{Ar}/^{39}\text{Ar}$ ages from gold-bearing veins across the Scottish Dalradian Supergroup at 407-408 Ma is interpreted to reflect a regional tectonothermal event driving gold-bearing hydrothermal circulation. Late-Caledonian post-orogenic granites are invoked as the source of heat, fluids and possibly metals. While two models for emplacement of the granite intrusions are proposed, it is likely a combination of the two led to the development of gold-bearing hydrothermal systems across the region. The large volume of granite emplaced in the Grampian terrane at *c.* 430-408 Ma would be consistent with prolonged slab break-off and the timing of granite emplacement is also coincident with a transtensional stress regime (Mendum & Noble 2010; Miles *et al.* 2014). Movement on the Great Glen and subsidiary faults during transtension would have allowed for focussing of magmatic fluids, regional fluid flow and potential mixing with a meteoric water component. Fluid flow along regional fault structures is invoked to explain mixed sulphur and oxygen isotope signatures at the Cononish deposit (Curtis *et al.* 1993; Hill *et al.* 2013). It is suggested the impact of a transtensional structural regime in the Dalradian Supergroup may be greater than previously considered and may have implications for the timing of deposit formation.

7.9 Conclusions

Following application of $^{40}\text{Ar}/^{39}\text{Ar}$, U-Pb and Re-Os to vein material and altered wall rock in the Tyndrum area, key conclusions can be summarised as:

1. Mineralisation in the Glen Orchy area spans 70 Ma from 477 to 407 Ma - from post Grampian Event peak metamorphism to emplacement of the post-orogenic granite suite and movement on faults. The mineralisation is not continuous, with two distinct hydrothermal events identified; a molybdenum-bearing hydrothermal system at *c.* 477-439 Ma and a short-lived gold mineralisation event at 407-408 Ma.
2. The molybdenite-rutile mineralisation event is protracted and here, a metamorphic origin is proposed. Molybdenum is interpreted to have been released progressively over *c.* 40 Ma as the orogen undergoes post-orogenic cooling.
3. A single gold-bearing hydrothermal system is recorded in the Tyndrum area at 407-408 Ma. All gold-bearing poly-metallic quartz veins are of the same age and represent the same hydrothermal event despite different orientations and some variation in the geochemical features.
4. The gold-bearing hydrothermal system in Tyndrum area is significant in size spanning an area of at least 5 x 7 km. The hydrothermal system extends beyond the extent of the study as the 407-408 Ma age is recognised across the Scottish Dalradian Supergroup.
5. A 407 Ma tectonothermal event is postulated in the Scottish Dalradian, driving hydrothermal circulation and gold mineralisation. The heat, fluids and potentially metals for the gold mineralising hydrothermal system are caused by crustal melting as a result of the changing structural conditions and associated movement on the Great Glen and subsidiary Caledonian suite faults.

Chapter 8

Synthesis and Conclusions

8.1. Introduction

Globally, the size and grade of newly discovered gold deposits is decreasing (McKeith *et al.* 2010) and exploration companies are beginning to explore in areas not previously considered prospective for economic gold deposits. The Dalradian Supergroup metasedimentary sequence contains vein-hosted gold mineralisation, including the UK's largest gold resource at Curraghinalt (Dalradian Resources 2012), the only operating gold mine at Cavanacaw (Galantas Gold Corporation 2013), and the Cononish gold-silver deposit, the impetus for this study.

The vein-hosted gold mineralisation at the Cononish deposit shares many characteristics with the classic orogenic, epithermal and intrusion-related gold deposit types (Groves *et al.* 1998; Thompson *et al.* 1999; Hedenquist *et al.* 2000) but has many atypical features that preclude the deposit from being fully classified within any single model. Characterisation of the field relations, petrography, geochemistry, S-isotope ratios and geochronology of mineralised occurrences in the Tyndrum area has been carried out in order to improve the understanding of the genesis of the mineralised veins and to provide criteria to aid exploration for further deposits.

This study has demonstrated that the Cononish deposit and newly identified gold occurrences form a distinct deposit type, with a genesis closely related to the tectonic regime of the host terrane. This chapter will: 1. Examine possible analogues in light of the new data obtained in this study; 2. Integrate and synthesise the conclusions from Chapters 4-7 to develop a model for mineralisation in the Tyndrum area; and 3. Use the results to defined key criteria to maximise efficiency of further exploration for similar gold deposits in the region.

8.2. Possible analogues

Gold occurrences in the Tyndrum area have characteristics that preclude the mineralisation from being classified within any of the classic gold deposit types (Chapter 2; Groves *et al.* 1998; Thompson *et al.* 1999; Hedenquist *et al.* 2000). However, new data from this study suggests there are some gold deposits that may be potential analogues including the Jiaodong Peninsula gold deposits, China, and those within the Lachlan fold belt, Australia.

The origin of the Jiaodong Peninsula gold deposits of the South China Craton is controversial (Goldfarb *et al.* 2013). The Jiaodong deposits have been classified as orogenic

(Goldfarb *et al.* 2007) based on a comparable local structural setting (NE-trending in fault jogs), mineralisation style (sulphide-bearing veins) and ore fluid chemistry (6-14 wt. % NaCl equivalent at 250-350°C; Qiu *et al.* 2002) to classic orogenic gold deposits (e.g. Groves *et al.* 1998). However, there are significant differences in the tectonic environment and metamorphic setting that may preclude the deposits from being orogenic in origin (Goldfarb & Santosh 2014). Orogenic gold deposits (Groves *et al.* 1998) generally form within a few million years of peak metamorphism (<50 Ma; Stüwe *et al.* 1993); however, the Jiaodong gold deposits formed *c.* 2 billion years after high-grade metamorphism of the host Precambrian basement (Goldfarb & Santosh 2014) and have therefore been classified as ‘Jiaodong-type’, a unique deposit type (Zhai & Santosh 2013).

The Jiaodong gold deposits have many characteristics that are comparable with the non-standard features of the Tyndrum area gold deposits, these include:

- A close spatial association between gold mineralisation and lamprophyre dykes (Goldfarb & Santosh 2014) as seen in Glen Orchy (Section 4.4.3).
- Poly-metallic ores with pyrite, chalcopyrite, sphalerite, galena and pyrrhotite in the veins (Goldfarb & Santosh 2014) comparable to the Cononish deposit and variation in As, Te & Bi endowment between deposits (Li *et al.* 2006; Goldfarb & Santosh 2014) as seen in Cononish- and River Vein-style mineralisation (Section 5.5.2.1).
- A relatively high range of $\delta^{34}\text{S}_{\text{sulphides}}$ in the Jiaodong gold deposits (+3 to +14 ‰; Qui *et al.* 2002; Yao *et al.* 2002; Mai *et al.* 2008) is comparable to data for the Tyndrum area gold mineralisation (average $\delta^{34}\text{S}_{\text{pyrite}} = +6.7 \pm 2.8$ ‰; Fig. 6.7; Hill *et al.* 2013). The heavy sulphur isotope ratio is interpreted to suggest a non-mantle/magmatic source for sulphur in the mineralisation (Goldfarb & Santosh 2014).

In addition, the Jiaolai basin may be an analogue for the basin containing the gold-bearing Rhynie Chert. The basin contains clastic terrestrial sediments and andesite and has a probable transtensional origin (Rice & Ashcroft 2004). The Jiaolai basin, host to a *c.* 7 km thick sedimentary sequence, developed in response to transtensional movement on the Tu-Lan fault (Goldfarb & Santosh 2014). The Jiaolai basin also contains andesite, comparable to the Rhynie Chert basin (Rice *et al.* 1995; Mark *et al.* 2011a; Section 2.3.3.1).

Goldfarb & Santosh (2013) argue the Jiaodong gold deposits are not magmatic-related based on the following:

- While a large volume of granites was emplaced between *c.* 130-123 Ma, temporally coeval with gold mineralisation (126-120 Ma), there is no spatial relationship between gold ores and the intrusive bodies (Goldfarb & Santosh 2014).
- The form of the gold deposits, in linear belts along regional fault zones, is not typical of magmatic ore deposits (Goldfarb & Santosh 2014). Magmatic ore deposits are commonly found as stockwork and veinlet networks in porphyry systems and as sheeted vein networks in deeper systems (Goldfarb & Santosh 2014).

It is notable that the same arguments could be made regarding the Tyndrum gold-bearing quartz veins – there is no clear spatial relationship with intrusive bodies and the deposits are related overall to regional fault zones.

The structurally controlled post-metamorphic Jiaodong Peninsula gold mineralisation lacks a clear fluid source and Goldfarb *et al.* (2007) suggest a major change in the stress regime of the Tan-Lu fault system is the trigger for fluid production (Goldfarb & Santosh 2014). The stress regime of the Tu-Lan fault system changed from orthogonal subduction at *c.* 135 Ma to parallel subduction at *c.* 115 Ma (Engebretson *et al.* 1985; Maruyama *et al.* 1997). This change in the fault system regime temporally overlaps with emplacement of the gold ores (Goldfarb & Santosh 2014). The source of fluid and metals for the Jiaodong gold deposits is postulated to be related to either dehydration of the subducting paleo-Pacific plate or devolatilisation of an enriched mantle wedge (Goldfarb & Santosh 2014).

The Lachlan fold belt, Australia, exhibits characteristics broadly in common with the Cononish deposit (Table 2.4). In the Lachlan fold belt, the emplacement of granites has been interpreted to record a change in the tectonic setting from a transtensional to transpressional regime and reflect changing conditions in the local continental crust (Kemp *et al.* 2009). The Lachlan fold belt illustrates that a change in the structural regime could induce a change in the type and volume of intrusions emplaced and while the structural regime change in the Lachlan fold belt is in an active subduction setting, it provides a potential analogue for the Dalradian Supergroup. In addition, poly-metallic gold mineralisation in the Lachlan Orogenic belt, Australia, is temporally associated with granite intrusions emplaced *c.* 70 Ma after peak metamorphism (Table 2.4; Arne *et al.* 1998; Foster *et al.* 1998; Bierlein *et al.* 2001), comparable to the post-orogenic granite suite, emplaced *c.* 60 Ma after peak metamorphism in the Dalradian Supergroup.

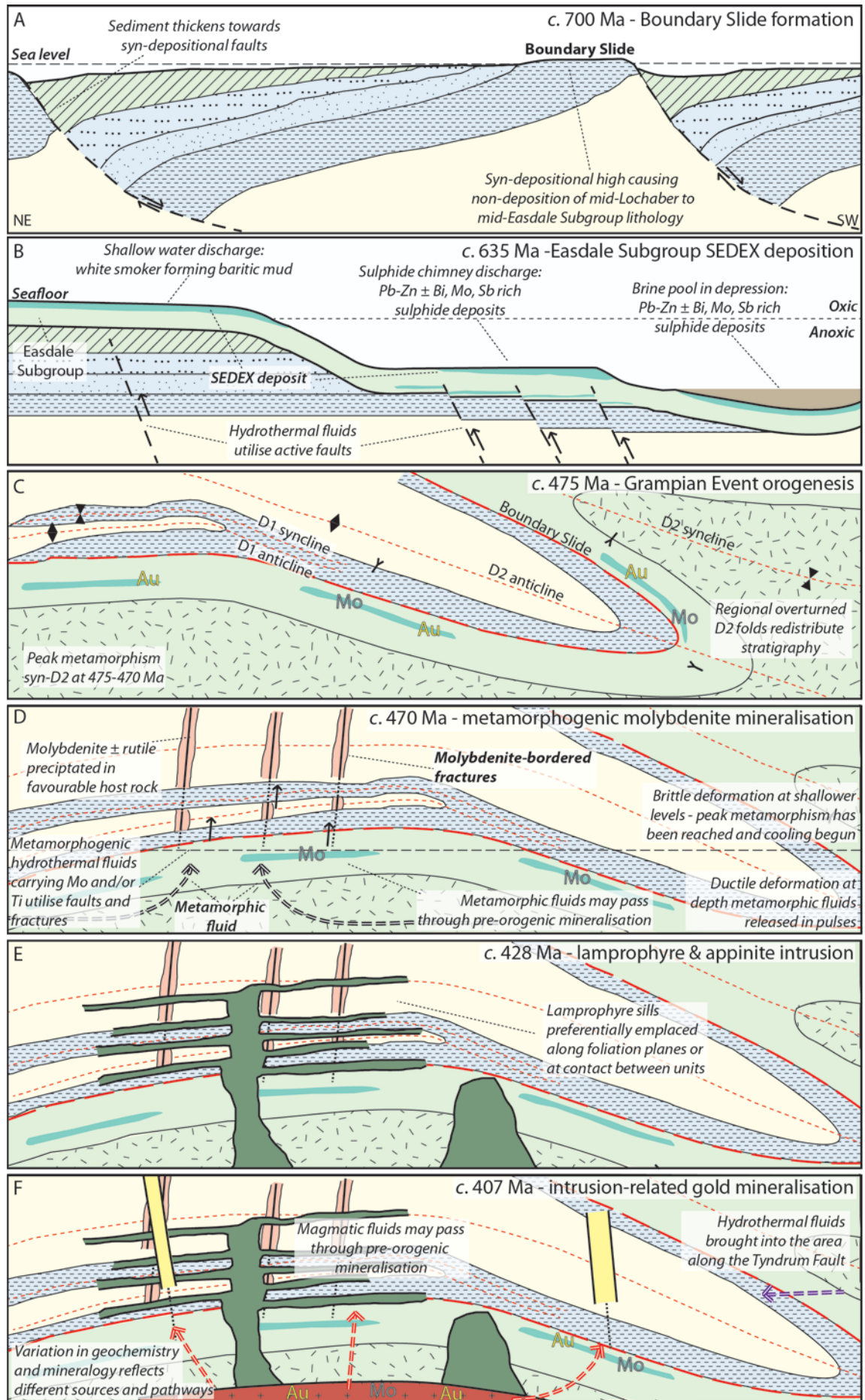
The emplacement of both the Jiaodong Peninsular and the Lachlan fold belt gold deposits was related to changes in the structural regime of the host terrane (Goldfarb *et al.* 2007; Kemp *et al.* 2009). This suggests that a change in structural regime may be significant for deposits where the classic orogenic gold model (Groves *et al.* 1998) is not sufficient to explain the genesis of gold mineralisation. Given the Tyndrum area mineralisation has characteristics in common with both deposit types, a change in structural regime could be invoked to account for the short-lived fluid migration event.

8.3. Synthesis and ore deposit formation

Here, ore deposit formation is placed into the framework of the depositional, tectonic and post-orogenic evolution of the Dalradian Supergroup (Chapter 3). Key events contributing to the development of gold- and molybdenum mineralisation are identified (Fig. 8.1).

The deposition of the Dalradian Supergroup has implications for hydrothermal vein formation (Fig. 8.1A). A section of mid-Appin to mid-Argyll Group stratigraphy is absent in the Tyndrum area, represented instead by the Boundary Slide. This is interpreted to be a pre-tectonic disconformity (Fig. 6.11; Sections 3.4.5.2 & 6.9.4; Tanner & Thomas 2009) formed due to a structural high, between subsiding basins, resulting in non-deposition of the missing stratigraphy (Fig. 3.7; Section 3.4.5.2; Anderton 1985). The Boundary Slide juxtaposes Easdale Subgroup lithologies against brittle Grampian Group and Lochaber Subgroup lithologies which may enable easier upwards fluid flow.

The Easdale Subgroup includes a series of stratabound sulphide horizons (Fig. 8.1B); of particular note are the syn-sedimentary mineralised hydrothermal exhalative SEDEX horizons (Willan & Coleman 1983; Moles 1985; Moles *et al.* 2014). As discussed in Chapter 6, shale-hosted SEDEX mineralisation is known to concentrate gold and base metals (e.g. Cooke *et al.* 2000; Alchin and Moore 2005). Willan (1996) demonstrated that the Ben Eagach Schist, which contains many of the SEDEX deposits, is regionally enriched in Bi, Sb, As, Mo, Ni and Ba. The syn-sedimentary mineralised horizons are inferred to contribute sulphur to the gold-bearing quartz veins and thus possibly could also contribute metals (Section 6.9.5). Isotope stratigraphy ($\delta^{13}\text{C}$, $^{87}\text{Sr}/^{86}\text{Sr}$) and correlation of potential glacial deposits in the Dalradian succession constrains deposition of the Easdale Subgroup to later than *c.* 635 Ma (Fig. 6.9; Section 6.3).



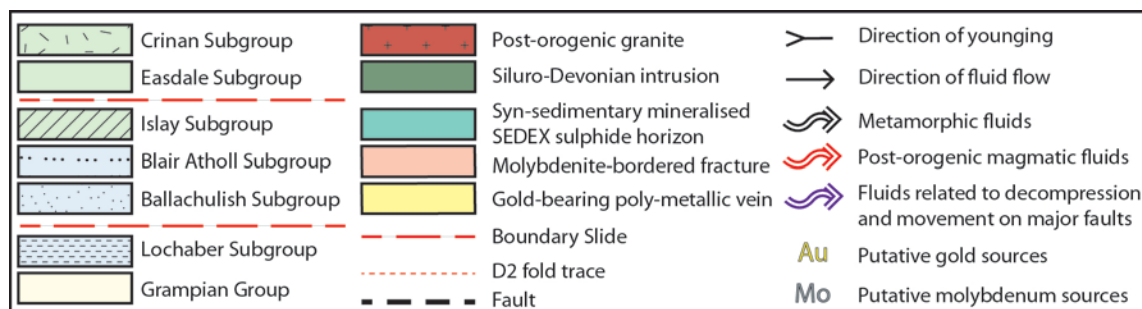


Figure 8.1: (Main diagram on previous page) Schematic cross-section synthesis model through time showing key depositional, tectonic and magmatic events and their relationship to the hydrothermal systems developed in the Tyndrum area. All panels orientated NE-SW as shown in A. A. Deposition of the lower- to mid-Dalradian with model for formation of the Boundary Slide. Modified from Anderton (1985). Panel shows approximately 35 x 16 km. B. Syn-sedimentary mineralised exhalative horizons deposited in the Easdale Subgroup at *c.* 635 Ma. Modified after (Moles 1985; Moles *et al.* 2014). Panel shows approximately 1 x 0.1 km. C. Grampian Event orogenesis showing D2 deformation at *c.* 475 Ma. Modified after Tanner (2012). Panel shows approximately 10 x 5 km. D. Metamorphogenic molybdenite mineralisation. Panel shows approximately 7 x 3 km. E. Lamprophyre and appinite intrusion at *c.* 430 Ma. The Tyndrum Fault is in the plane of the section and undergoing sinistral strike-slip movement from 429 ± 3 Ma (Rogers & Dunning 1991). Panel shows approximately 7 x 3 km. F. Emplacement of the post-orogenic granite suite and fault movement at *c.* 408 Ma leading to development of a gold-bearing hydrothermal system. The Tyndrum Fault undergoes continued sinistral strike-slip movement until 412 ± 3 Ma (Clayburn *et al.* 1983), 1 Ma within error of the gold mineralisation ages. Panel shows approximately 7 x 3 km. All scales are approximate.

The deposition age suggests pyritic organic-rich sedimentary units in the mid-Dalradian Supergroup have the potential to be a better source of gold (and molybdenum) than sedimentary rocks deposited before 635 Ma due to the increase in gold solubility in a more oxidised ocean (Tomkins 2012; Section 6.9.5).

Grampian Event metamorphism in Scotland and Ireland is contemporaneous across the terrane (Fig. 8.1C; Table 3.1) with peak metamorphism constrained to *c.* 475–470 Ma (Table 3.1; Chew & Strachan 2014). D2 folds are recumbent regional structures and place sulphur and metal enriched Easdale Subgroup at depth below the Tyndrum area (Section 6.9.4).

The earliest hydrothermal system recorded in the Tyndrum area is a molybdenum-depositing event (Fig. 8.1D). Molybdenite-bordered fractures are interpreted to reflect a single protracted metamorphic hydrothermal event between *c.* 477 and 439 Ma (Chapter 7), commencing close to peak metamorphism (*c.* 475–470 Ma; Chew & Strachan 2014). The molybdenite-bordered fractures have distinct $\delta^{34}\text{S}$ values ($\delta^{34}\text{S}_{\text{molybdenite}} +6.0$ to 6.6‰ ; $\delta^{34}\text{S}_{\text{pyrite}} +1.8$ to 8.4‰ ; Section 6.8; Hill *et al.* 2013). The sulphur isotope data suggests there is a large sedimentary-sourced sulphur component to the mineralisation with 18–43% sourced from the syn-sedimentary SEDEX Ben Eagach horizon or 37–100% from the Ben Challum horizon (Section 6.9.3), however, a magmatic component to sulphur cannot be excluded. At the depth of emplacement of molybdenite-bordered fractures, brittle deformation is

recorded while ductile conditions persist in the deeper crust (Stüwe *et al.* 1993; Yardley *et al.* 2000). The *c.* 40 Ma range in ages is interpreted to reflect pulses of metamorphic fluids, released as parts of the orogen cool at different rates.

Lamprophyre sills and appinite bodies are the earliest expression of the post-orogenic intrusion suite and the main igneous representation in the Tyndrum area (Fig. 8.1E). The lamprophyre and appinites are interpreted to be equivalent to the Garabal Hill-Glen Fyne appinites that are dated at 426 ± 4.2 to 428 ± 9.8 Ma (U–Pb titanite and zircon; Rogers & Dunning 1991; Tanner 2012).

A regional gold-bearing hydrothermal event at *c.* 408–407 Ma is interpreted to be driven by post-orogenic granite emplacement (Fig. 8.1F). Gold and other metals may be enriched in the post-orogenic granite suite, sourced from a subduction-modified lithosphere enriched in gold (Richards 2009). The gold-bearing poly-metallic veins have average $\delta^{34}\text{S}_{\text{pyrite}}$ values of $+6.9 \pm 2.9\text{‰}$. (Section 6.8; Hill *et al.* 2013) suggesting a mixed sulphur source. The highest $\delta^{34}\text{S}_{\text{pyrite}}$ values ($+12\text{‰}$) place very strong constraints on the sources of sulphur and the hydrothermal pathways in the mineralising system. The data constrains the magmatic sulphur input to $\leq 68\%$ with 32–100% of sulphur from a sedimentary source (Fig. 6.11; Section 6.9.3; Hill *et al.* 2013). Variation in the mineralogy and geochemistry of the gold-bearing vein-hosted occurrences is interpreted to reflect differences in the source of metals and fluids and fluid flow pathways.

A change in the structural regime from a collisional to transtensional setting is reflected in sinistral movement on the Great Glen Fault at *c.* 420 Ma (Brown *et al.* 2008; Mendum & Noble 2010; Miles *et al.* 2014). Granite emplacement is driven by melting invoked by the change to a transtensional setting at *c.* 420 Ma and continues until *c.* 408 Ma. It is proposed post-orogenic granites provide heat, fluid and potentially metals to the mineralising system, with sulphur isotopes indicating up to 68% of the sulphur in gold-bearing quartz veins is magmatic in origin (Fig. 6.11; Section 6.9.3; Hill *et al.* 2013). Hydrothermal fluids are focussed into the Caledonian fault suite (Tanner 2013) and travel extensive distances within the Supergroup (Mark *et al.* 2007). The regional fluid flow allows for mixing of magmatic fluids with meteoric fluids and allows for mixed sulphur isotope signatures (Chapter 6; Curtis *et al.* 1993; Hill *et al.* 2013).

8.4. Regional exploration implications

The results and conclusions presented in Chapters 4, 5, 6 and 7 have implications for exploration in the Scottish, and possibly Irish, Dalradian Supergroup. Here, key exploration criteria are discussed for the Tyndrum area and placed into the regional framework to highlight areas of potential.

- Poly-metallic quartz veins are most the prospective for gold mineralisation and veins with high tellurium are likely to have the highest gold grade.
- Enrichment in tellurium and silver is a key exploration criterion for the highest grade gold veins, as seen at Cononish, and Ag and Te enrichment can be traced in the stream sediment anomalies.
- High arsenic can be used as a secondary exploration criterion to tellurium. High arsenic should only be used as a tracer in areas where there is low tellurium. In gold-bearing poly-metallic veins with high tellurium, arsenic is commonly low. However, in some poly-metallic quartz veins the inverse relationship is observed.
- Gold veins with heavy $\delta^{34}\text{S}_{\text{pyrite}}$ (+12‰) can only be formed with 32-66% sedimentary sulphur sourced from the SEDEX Ben Eagach horizon with the remaining sedimentary sulphur from the diagenetic sulphide in the Ben Eagach Schist or the Ben Challum horizon (Sections 6.9.2 & 6.9.3). This demonstrates that for gold veins with comparable $\delta^{34}\text{S}_{\text{pyrite}}$ values to the Cononish deposit, sedimentary sulphur from the Ben Eagach Schist is likely to be an important criterion and the contribution of this unit can be potentially traced with sulphur isotopes, as demonstrated in Chapter 6.
- Areas where overturned D2 folds have placed mid- to upper-Dalradian Supergroup units at depth are prospective for gold mineralisation. The D2 folds place sulphur- and metal-rich Easdale Subgroup rocks or similar lithologies at depth, and therefore provide a source of sulphur, required for mineralisation, in areas with sulphur-poor host rocks.
- Localities near the regional Caledonian faults, such as the Tyndrum Fault, are important locations for exploration for gold deposits as hydrothermal fluids are utilising the faults for regional flow.

8.5. Unresolved problems and future work

This study has utilised a number of analytical techniques, highlighting the potential for these tools to be used to improve exploration efficiency and understanding of mineral deposits. The wide-ranging study has highlighted a number of areas with potential for further work, these are summarised below:

- An extensive geochronological study is required, on all gold occurrences across the Scottish and Irish Dalradian Supergroup, to determine the extent of the *c.* 408-407 Ma hydrothermal event (Chapter 7) and the earlier orogenic gold episode at Curraghinalt (Rice *et al.* 2012). Further geochronology on gold occurrences in Aberdeenshire is currently being undertaken by Clive Rice and Darren Mark to supplement their existing work at the Rhynie Chert and Cononish deposit.
- While the poly-metallic quartz veins cross-cut the Siluro-Devonian lamprophyre sills and the appinite-gabbro intrusion at Sron Garbh; no cross-cutting relationship between the molybdenite-bordered fractures and the lamprophyre sills or appinite-gabbro intrusion has been observed. The lamprophyre sills and appinite intrusion have been interpreted to be equivalent to the Garabal Hill-Glen Fyne appinites (426 ± 4.2 to 428 ± 9.8 Ma; Rogers & Dunning 1991; Tanner 2012) but the lack of accurate ages for the sills means the relationship with the molybdenite-bordered fractures is unclear. If the lamprophyre sills are older than expected, the sills may have contributed fluids and metals to molybdenite-bordered fractures. Age constraints on lamprophyre sills would improve the understanding of the genesis of molybdenite-bordered fractures and gold-bearing poly-metallic veins.
- Detailed geochemical analysis of the host metasedimentary sequence is suggested, with an aim to establish whether the metasedimentary succession has the potential to contribute metals to the poly-metallic quartz veins, as proposed in Chapter 6.
- A detailed fluid inclusion and oxygen isotope study to assess the different quartz stages from poly-metallic quartz veins, building on the existing data set from Curtis (1990), Curtis *et al.* (1993) and Patrick *et al.* (1988), and newly discovered molybdenite-bordered fractures is required. New data from both vein sets would be accurately tied to the paragenesis to link the data to the gold- or molybdenite-mineralising fluids. Work is on going to add to the existing dataset for the Cononish deposit to tie new data to the improved geochronology by Clive Rice and Darren Mark.

8.6. Conclusion

In conclusion, this integrated multi-aspect study suggests the Cononish deposit is likely to be an intrusion-related gold deposit, within a regional gold-bearing hydrothermal system, where the structural setting of the Supergroup places significant control on the system. The key conclusions can be summarised as:

- Mineralisation in the Tyndrum area spans 70 Ma from 477 to 407 Ma but is not continuous. Two distinct hydrothermal events are identified; molybdenum-bearing at *c.* 477-439 Ma and gold-bearing at *c.* 407-408 Ma.
 1. Molybdenite-rutile mineralisation is interpreted to be a protracted metamorphic event with molybdenum released progressively over *c.* 40 Ma, as the orogen undergoes post-orogenic cooling.
 2. A short-lived gold-bearing hydrothermal event at *c.* 407-408 Ma occurs throughout the Scottish Dalradian Supergroup. Variation in the mineralogy and geochemistry of the gold deposits is attributed to fluids sourcing metals from heterogeneous metasediments and variable mixing of magmatic and sedimentary sources.
- Pre-orogenic SEDEX horizons within the Dalradian Supergroup are interpreted to be a significant source of sulphur and metals for gold and possibly molybdenite mineralisation. Grampian Event deformation places SEDEX horizons at depth and regional and contact metamorphic release of metals from the lithostratigraphic succession is invoked as the possible source of molybdenum and gold.
- Regional gold mineralisation in the Scottish Dalradian Supergroup at *c.* 407-408 Ma is attributed to hydrothermal fluid movement along shear zones and lineaments driven by heat and fluids from post-orogenic granite intrusions. The Caledonian NE-SW-trending fault suite place significant control on the mineralisation by providing a network of fluid flow pathways and possibly inducing decompression melting to form granites during sinistral transtension.

Appendix 4.1

Large-scale topography, geology and sample maps

Figure A4.1: Map to show topography of the study area and location of places named in the main text. Map redrawn based on 1:25,000 OS map data from sheets NN22, 23, 32 and 33.

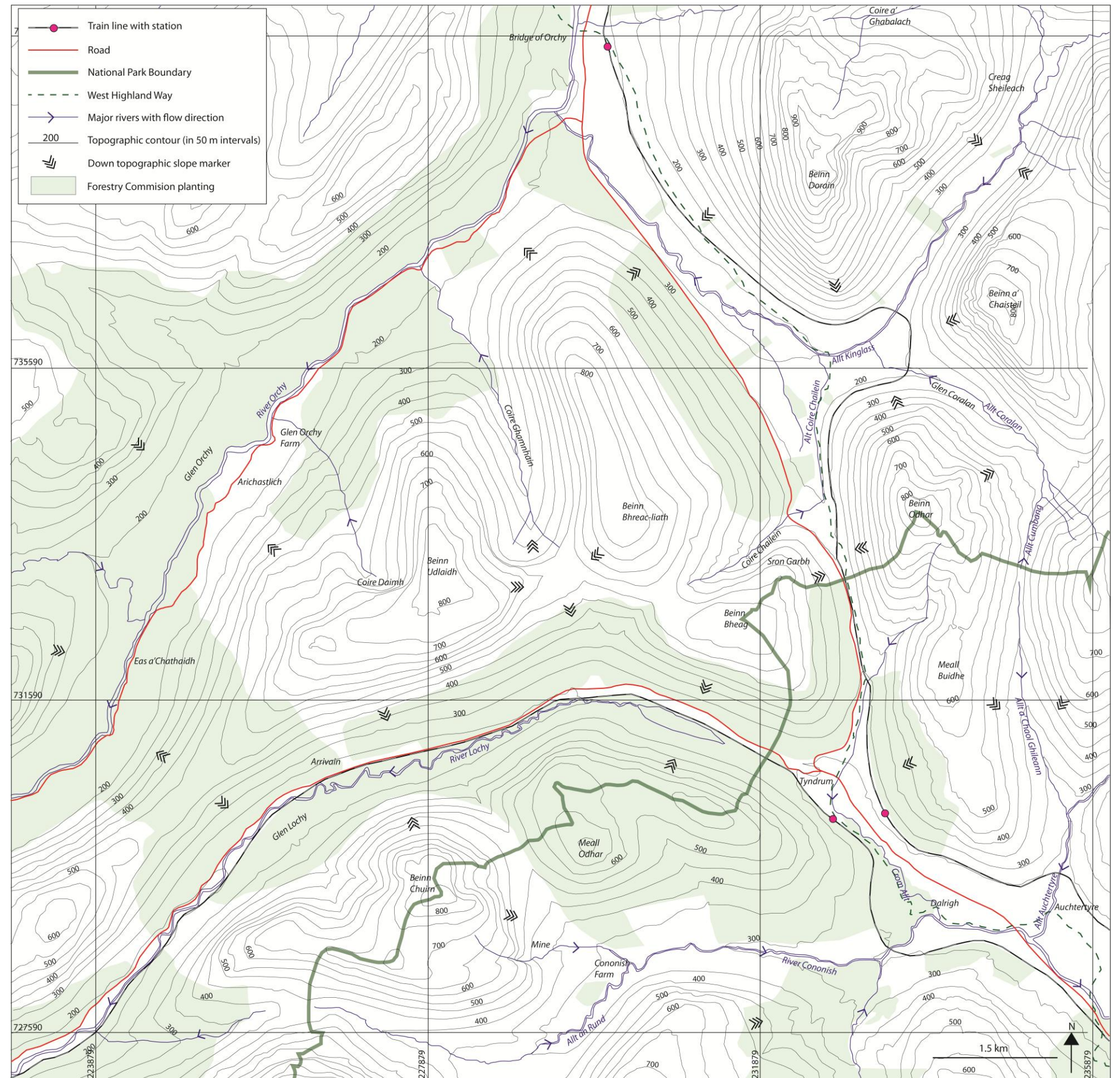
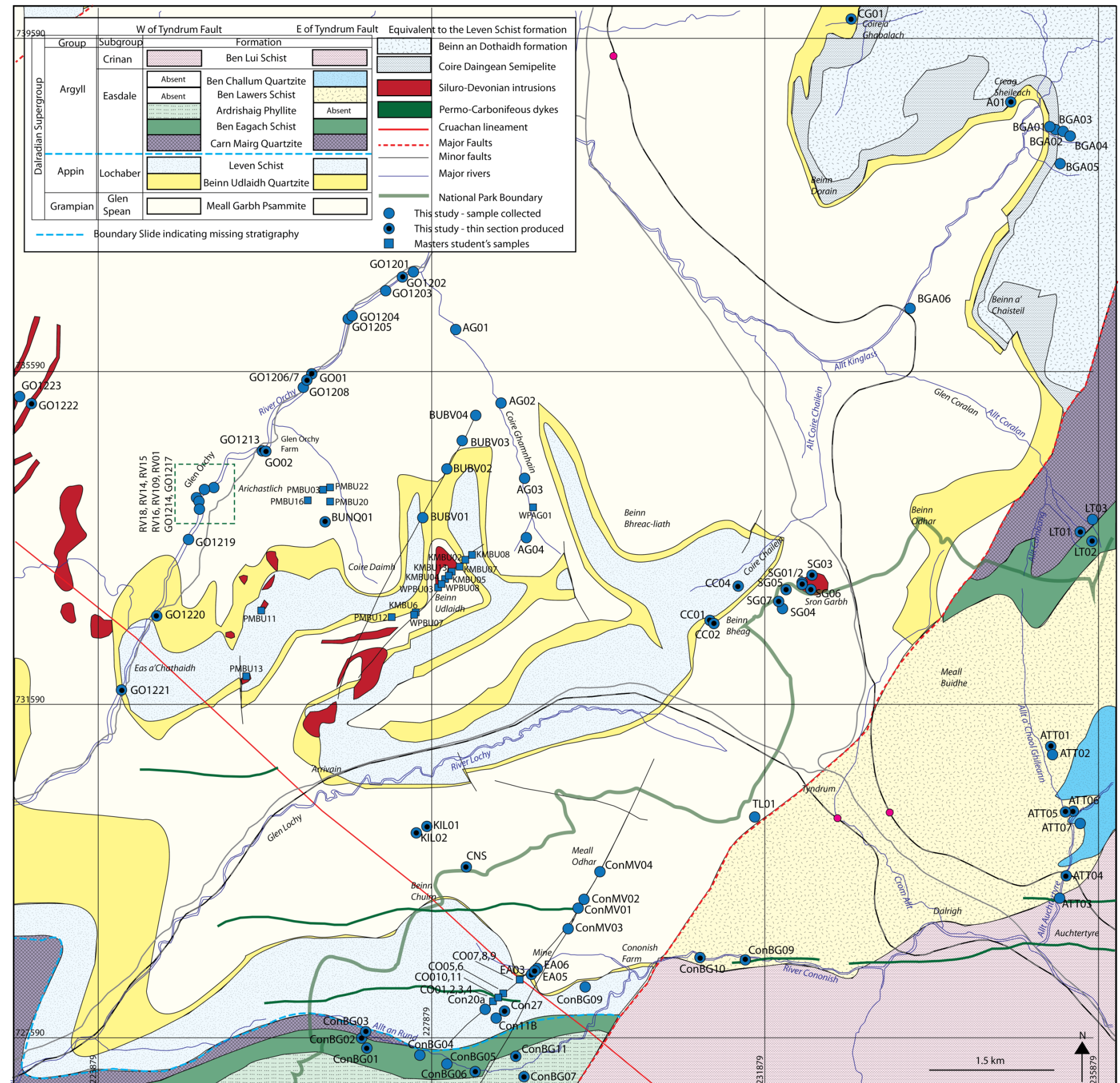


Figure A4.2: Sample map detailing location of all samples in the main text. Geology modified from Dalmally and Crianlarich 1:50,000 bedrock geology sheets



Appendix 7.3

U-Pb methodology

7.1. U-Pb geochronology

The full methods and instrument set up are described in Thomas *et al.* (2013) and summarised here. Detrital zircon and hydrothermal rutile were dated by Laser Ablation Inductively Coupled Plasma Mass Spectrometry (LA-ICP-MS) using a Nu Instruments Attom single-collector ICP-MS coupled to a New Wave Research UP193ss laser ablation system at the NERC Isotope Geosciences Laboratory (NIGL) at BGS in Keyworth, UK. Rutile analyses use the same method as is described for titanite in Thomas *et al.* (2013). Ablation parameters for zircon were a 25 μm laser spot size, 30 second ablation time, 15 second washout time and a 60 second background measurement every 20 analyses; for rutile, a 35 μm laser spot size was used.

Data processing used an in-house spreadsheet for data reduction and error propagation and Isoplot (Ludwig 2003) for data presentation. Data is tabulated in Appendix 7.4 (zircon) and 7.5 (rutile). All ages are quoted at 2 sigma as $^{207}\text{Pb}/^{206}\text{Pb}$ ages for zircons, and $^{206}\text{Pb}/^{238}\text{U}$ ages for rutile.

For zircon, a standard sample bracketing routine was used to normalise Pb/U and Pb/Pb ratios using the average drift-corrected normalisation values (measured/accepted) for three reference materials: 91500 (1062 Ma $^{206}\text{Pb}/^{238}\text{U}$; Wiedenbeck *et al.*, 1995; Fig. A7.1), GJ-1 (609 Ma for $^{207}\text{Pb}/^{206}\text{Pb}$ age, and $^{206}\text{Pb}/^{238}\text{U}$ age is *c.* 602-604 Ma due to its slight normal discordance; Jackson *et al.* 2004; Fig. A7.2) and Plešovice (337.13 Ma $^{206}\text{Pb}/^{238}\text{U}$ age; Sláma *et al.* 2008; Fig. A7.3). Appendix 7.4 records the accuracy and precision of the $^{207}\text{Pb}/^{206}\text{Pb}$ and $^{206}\text{Pb}/^{238}\text{U}$ measurements of the zircon reference materials. For rutile, Sugluk and PCA are used as reference materials, with Sugluk being used for normalisation. Sugluk results for the analytical sessions are 1726 ± 67 Ma (2σ); the accepted age is 1719 ± 14 Ma (Bracciali *et al.* 2013) and PCA results are 1859 ± 85 Ma (2σ); the accepted age is 1865 ± 7.5 Ma (Bracciali *et al.* 2013).

The precision and accuracy of the method is $<3\%$, 2σ for zircon and $<4\%$, 2σ for rutile. All final crystallisation ages on rutile are reported as $^{206}\text{Pb}/^{238}\text{U}$ ages and include uncertainties reported as $\pm X(Y)$, where X is the internal or analytical uncertainty in the absence of systematic errors, and Y includes systematic errors (decay constants, reference material age uncertainty, long term analytical reproducibility). Full analytical results are included in Appendix 7.4 (zircon) and 7.5 (rutile).

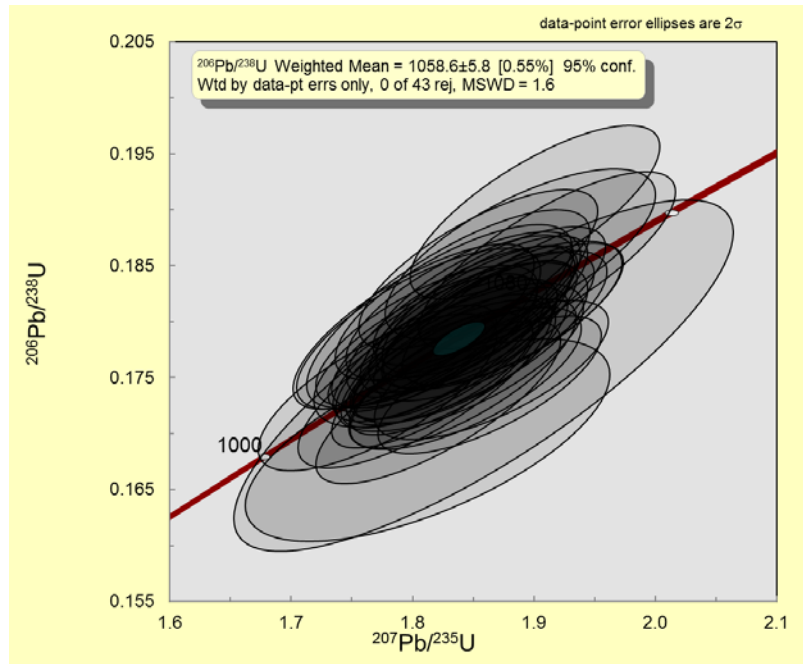


Figure A7.1: Concordia plot for all zircon reference material 91500 run.

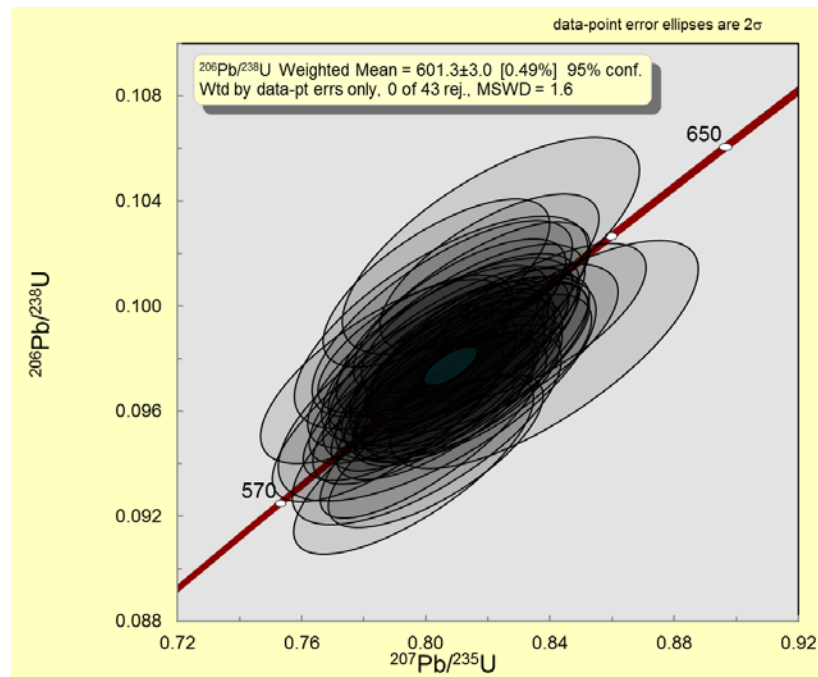


Figure A7.2: Concordia plot for all zircon reference material GJ-1 run.

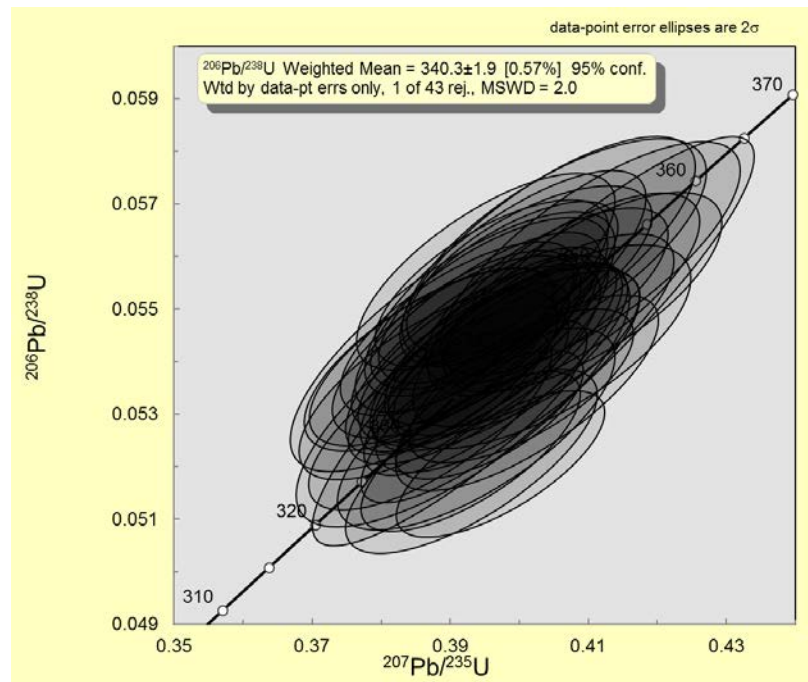


Figure A7.3: Concordia plot for all zircon reference material Plešovice run.

References

- ACA Howe International Limited. 2012. *Technical report on the Omagh gold project, Counties Tyrone and Fermanagh, Northern Ireland*. For: Galantas Gold Corporation.
- Alchin, D.J. & Moore, J.M. 2005. A review of the Pan-African, Neoproterozoic Rosh Pinah Zn-Pb deposit, southwestern Namibia. *South African Journal of Geology*, **108**, 71-86.
- Allan, D. 1928. The Geology of the Highland Border from Tayside to Noranside. *Transactions of the Royal Society of Edinburgh*, **56**, 57-88.
- Allan, D. 1940. The Geology of the Highland Border from Glen Almond to Glen Artney. *Transactions of the Royal Society of Edinburgh*, **60**, 171-193.
- ALS Geochemistry. 2014. *Service Schedule*. World Wide Web address: <http://www.alsglobal.com/Our-Services/Minerals/Geochemistry/Downloads>. Accessed on 15th March 2014.
- ALS Minerals. 2006a. *Au-AA25 Au-AA26 Fire Assay-Atomic Absorption Ore Grade Methods*. World Wide Web address: <http://www.alsglobal.com/Our-Services/Minerals/Geochemistry/Downloads>. Accessed on 15th March 2014.
- ALS Minerals. 2009a. *ME-ICP61 Four Acid Near Total-ICP Multi-element Method*. World Wide Web address: <http://www.alsglobal.com/Our-Services/Minerals/Geochemistry/Downloads>. Accessed on 16th March 2014.
- ALS Minerals. 2009b. *ME-ICP41 Aqua Regia-ICP Multi-element Method*. World Wide Web address: <http://www.alsglobal.com/Our-Services/Minerals/Geochemistry/Downloads>. Accessed on 20th March 2014.
- ALS Minerals. 2009c. *Sulphur Methods, Various Sulphur Methods including LECO Methods*. World Wide Web address: <http://www.alsglobal.com/Our-Services/Minerals/Geochemistry/Downloads>. Accessed on 7th March 2014.
- ALS Minerals. 2012. *Sample PREP-31 Standard Sample Preparation Package for Rock and Drill Samples*. World Wide Web address: <http://www.alsglobal.com/Our-Services/Minerals/Geochemistry/Downloads>. Accessed on 7th March 2014.
- Anderson, R., Graham, C.M., Boyce, A.J. & Fallick, A.E. 2004. Metamorphic and basin fluids in quartz-carbonate-sulphide veins in the SW Scottish Highlands: a stable isotope and fluid inclusion study. *Geofluids*, **4**, 169-185.
- Anderton, R. 1985. Sedimentation and Tectonics in the Scottish Dalradian. *Scottish Journal of Geology*, **21**, 407-436.
- Arne, D.C., Bierlein, F.P., McNaughton, N.J., Wilson, C.J.L. & Morand, V. 1998. Absolute timing of gold mineralisation in central Victoria: New constraints from SHRIMP II analysis of zircon grains from felsic intrusive rocks. *Ore Geology Reviews*, **13**, 251-273.
- Arthurs, J.W. 1976. The geology and metalliferous mineral potential of the Sperrin Mountains area. *Geological Survey of Northern Ireland Special Report*, **119**.
- Atherton, M.P. & Ghani, A.A. 2002. Slab breakoff: a model for Caledonian, late granite syn-collisional magmatism in the orthotectonic (metamorphic) zone of Scotland and Donegal, Ireland. *Lithos*, **62**, 65-85.
- Bailey, E.B. 1922. The structure of the South-West Highlands of Scotland. *Quarterly Journal of the Geological Society*, **78**, 82-131.
- Bailey, E.B. & MacGregor, M. 1912. The Glen Orchy Anticline (Argyllshire). *Quarterly Journal of the Geological Society*, **68**, 164-179.

- Bamford, D. 1979. Seismic constraints on the deep geology of the Caledonides of northern Britain. *In*: Harris, A., Holland, C.G. & Leake, B.E. *The Caledonides of the British Isles*. Geological Society, London, Special Publications, **8**, 93-96.
- Bamford, D., Nunn, K., Prodehl, C. & Jacob, B. 1977. LISPB-III. Upper crustal structure of northern Britain. *Journal of the Geological Society, London*, **133**, 481-488.
- Banks, C.J. 2005. *Neoproterozoic Basin Analysis: a combined sedimentological and provenance study in the Grampian Group, Central Highlands, Scotland*. Unpublished PhD Thesis. University of Keele.
- Baron, M., Hillier, S., Rice, C.M., Czapnik, K. & Parnell, J., 2005. Fluids and hydrothermal alteration assemblages in a Devonian gold-bearing hot-spring system, Rhynie, Scotland. *Transactions of the Royal Society of Edinburgh: Earth Sciences*, **94**, 309-324.
- Baxter, E.F., Ague, J.J. & DePaolo, D.J. 2002. Prograde temperature-time evolution in the Barrovian-type locality constrained by Sm/Nd garnet ages from Glen Clova, Scotland. *Journal of the Geological Society, London*, **159**, 71-82.
- Bentley, M.R., Maltman, A.J. & Fitches W.R. 1988. Colonsay & Islay – a suspect terrane within the Scottish Caledonides. *Geology*, **16**, 26-28.
- Bierlein, F.P. & Crowe, D.E. 2000. Phanerozoic orogenic lode gold deposits. *Reviews in Economic Geology*, **13**, 103-139.
- Bierlein, F.P., Arne, D.C., Foster, D.A. & Reynolds, P.R. 2001. A geochronological framework for orogenic gold mineralisation in central Victoria, Australia. *Mineralium Deposita*, **36**, 741-767.
- Bierlein, F.P., Gray, D.R. & Foster, D.A. 2002. Metallogenic relationships to tectonics evolution – the Lachlan orogen, Australia. *Earth and Planetary Science Letters*, **202**, 1-13.
- Bierlein, F.P., Christie, A.B. & Smith, P.K. 2004. A comparison of orogenic gold mineralisation in central Victoria (AUS), western South Island (NZ) and Nova Scotia (CAN): implications for variations in the endowment of Palaeozoic metamorphic terrains. *Ore Geology Reviews*, **25**, 125-168.
- Bird, A.F., Thirlwall, M.F., Strachan, R.A. & Manning, C.J. 2013. Lu-Hf and Sm-Nd dating of metamorphic garnet: evidence for multiple accretion events during the Caledonian Orogeny in Scotland. *Journal of the Geological Society, London*, **170**, 301-317.
- Bluck, B.J., Halliday, A.N., Aftalion, M. & MacIntyre, R.M. 1980. Age and origin of the Ballantrae ophiolite and its significance to the Caledonian orogeny and Ordovician time-scale. *Geology*, **8**, 492-495.
- Boyle, R.W. 1979. The geochemistry of gold and its deposits. *Canada Geological Survey Bulletin*, **280**, 584.
- Bracciali, L., Parrish, R.P., Hosrtwood, M.S.A., Condon, D.J. & Najman, Y. 2013. U-Pb LA-(MC)-ICP-MS dating of rutile: New reference materials and applications to sedimentary provenance. *Chemical Geology*, **347**, 82-101.
- Brasier, M.D. & Shields, G. 2000. Neoproterozoic chemostratigraphy and correlation of the Port Askaig glaciation, Dalradian Supergroup of Scotland. *Journal of the Geological Society, London*, **157**, 909-914.
- Brown, P.E., Ryan, P.D., Soper, N.J. & Woodcock, N.H. 2008. The Newer Granite problem revisited: a transtensional origin for the Early Devonian Trans-Suture suite. *Geological Magazine*, **145**, 235-256.
- Bruce S. 1996. *A petrographic and stable isotope study of the Cononish gold-silver deposit, near Tyndrum, Scotland*. Unpublished MRes Thesis. University of Edinburgh.
- Carty, J.P., Connelly, J.N., Hudson, N.F.C. & Gale, J.F.W. 2012. Constraints on the timing of deformation, magmatism and metamorphism in the Dalradian of NE Scotland. *Scottish Journal of Geology*, **48**, 103-117.

- Cathles, L.M., Erendi, A.H.J. & Barrie, T. 1997. How long can a hydrothermal system be sustained by a single intrusive event? *Economic Geology*, **92**, 766-771.
- Cawood, P.A., McCausland, P.J.A., Dunning, G.R. 2001. Opening Iapetus: constraints from the Laurentian margin in Newfoundland. *Geological Society of America Bulletin*, **113**, 443-453.
- Cawood, P.A., Nemchin, A.A., Smith, M., Loewry, S. 2003. Source of the Dalradian Supergroup constrained by U-Pb dating of detrital zircon and implications for the East Laurentian margin. *Journal of the Geological Society, London*, **160**, 231-246.
- Chew, D.M. & Strachan, R.A. 2014. The Laurentian Caledonides of Scotland and Ireland. In: Corfu, F., Gasser, D. & Chew, D.M. (Eds.) *New perspectives on the Caledonides of Scandinavia and related areas*. Geological Society, London, Special Publications, **390**, 45-91.
- Chew, D.M., Graham, J.R. & Whitehouse, M.J. 2007. U-Pb zircon geochronology of plagiogranites from the Lough Nafooe (= Midland Valley) arc in western Ireland: constraints on the onset of the Grampian orogeny. *Journal of the Geological Society, London*, **164**, 747-750.
- Chew, D.M., Daly, J.S., Magna, T., Page, L.M., Kirkland, C.L., Whitehouse, M.J. & Lam, R. 2010. Timing of ophiolite obduction in the Grampian orogen. *Geological Society of America Bulletin*, **122**, 1787-1799.
- Clayburn, J.A.P., Harmon, R.S., Pankhurst, R.J. & Brown, J.F. 1983. Sr, O and Pb isotope evidence for the origin and evolution of the Etive Igneous Complex, Scotland. *Nature*, **303**, 492-496.
- Cliff, R.A., Yardley, B.W.D. & Bussy, F.R. 1996. U-Pb and Rb-Sr geochronology of magmatism and metamorphism in the Dalradian of Connemara, western Ireland. *Journal of the Geological Society, London*, **153**, 109-120.
- Coats, J.S., Pease, S.F. & Gallagher, M.J. 1984. Exploration of the Scottish Dalradian. In: *Prospecting in areas of glaciated terrain*. Institute of Mining and Metallurgy, London, 21-34.
- Condon, D.J. & Prave, A.R. 2000. Two from Donegal: Neoproterozoic glacial episodes on the northeast margin of Laurentia. *Geology*, **28**, 951-954.
- Condon, D.J. & Bowring, S.A. 2011. Chapter 9 A user's guide to Neoproterozoic geochronology. In: Arnaud, E., Halverson, G.P. & Shields-Zhou, G. (Eds.) *The Geological record of Neoproterozoic glaciations*. Geological Society, London, Memoirs, **36**, 135-149.
- Conliffe, J., Wilton, D.H.C., Feely, M., Lynch, E.P. & Selby, D. 2009. S-isotope analyses of molybdenite in the Appalachian-Caledonian Orogen, Northeastern section - 44th annual meeting. *Geological Society of America, Abstracts with Programs*, **41**, 81.
- Conliffe, J., Selby, D., Porter, S.J. & Feely, M. 2010. Re-Os molybdenite dates from the Ballachulish and Kilmelford Igneous complexes (Scottish Highlands): age constraints for late Caledonian magmatism. *Journal of the Geological Society, London*, **167**, 297-302.
- Cooke, D.R., Bull, S.W., Large, R.R. & McGoldrick, P.J. 2000. The importance of oxidised brines for the formation of Australian Proterozoic stratiform sediment-hosted Pb-Zn (SEDEX) deposits. *Economic Geology*, **95**, 1-18.
- Cooper, M.R., Crowley, Q.G., Hollis, S.P., Noble, S.R. & Henney, P.J. 2013. A U-Pb age for the Late Caledonian Sperrin Mountains minor intrusions suite in the north of Ireland: timing of slab break-off in the Grampian terrane and the significance of deep-seated, crustal lineaments. *Journal of the Geological Society, London*, **170**, 603-614.
- Corkhill, C., Ixer, R.F., Mason, J.S., Irving, D. & Pattick, R.A.D. 2010. Polymetallic auriferous vein mineralisation near Loch Tay, Perthshire, Scotland. *Scottish Journal of Geology*, **46**, 23-30.

- Coward, M.P. 1983. The thrust and shear zones of the Moine Thrust Zone of NW Scotland. *Journal of the Geological Society, London*, **140**, 795-811.
- Cowie, J.W., Rushton, A.W.A. & Stubblefield, C.J. 1972. A correlation of the Cambrian rocks in the British Isles. *Special Report of the Geological Society of London*, **2**.
- Crane, A., Goodman, S., Krabbendam, M., Leslie, A.G., Paterson, I.B., Roberston, S. & Rollin, K.E. 2002. Geology of the Glen Shee District. *Memoir of the British Geological Survey, Sheet 56W with parts of sheets 55E, 65W and 64E, Scotland*.
- Craw, D. 1990. Regional fluid and metal mobility in the Dalradian metamorphic belt, southern Grampian Highlands. *Mineralium Deposita*, **25**, 281-288.
- Craw, D. & Chamberlain, C.P. 1996. Meteoric incursion and oxygen fronts in the Dalradian metamorphic belt, southwest Scotland: A new hypothesis for the regional gold mobility. *Mineralium Deposita*, **31**, 365-373.
- Craw, D., Hall, A.J., Fallick, A.E. & Boyce, A.J. 1995. Sulphur isotopes in a metamorphogenic gold deposit, Macraes mine, Otago Schist, New Zealand. *New Zealand Journal of Geology and Geophysics*, **38**, 131-136.
- Curtis, S.F. 1990. *Fault movement history, related mineralisation and age dating of the Tyndrum Fault, the Grampian Highlands of Scotland*. Unpublished PhD Thesis. University of Manchester.
- Curtis, S.F., Patrick, R.A.D., Jenkin, G.R.T., Fallick, A.E., Boyce, A.J. & Treagus, J.E. 1993. Fluid Inclusion and stable isotope study of fault related mineralisation in Tyndrum area, Scotland. *Transactions of the Institute of Mining and Metallurgy (Section B: Applied Earth Science)*, **102**, 39-47.
- Dalradian Resources Inc. 2012. *A preliminary economic assessment of the Curraghinalt gold deposit, Tyrone project, Northern Ireland*. Micon International Limited.
- Dalziel, I.W.D. 1997. Neoproterozoic-Paleozoic geography and tectonics: review, hypothesis, environmental speculation. *Geological Society of America Bulletin*, **109**, 16-42.
- Dalziel, I.W.D. & Soper, N.J. 2001. Neoproterozoic extension on the Scottish promontory of Laurentia: paleogeographic and tectonic implications. *Journal of the Geological Society, London*, **109**, 299-317.
- Dalrymple, G.B. 1979. Critical tables for conversion of K-Ar ages from old to new constants. *Geology*, **7**, 558-560.
- Dempster, T.J. 1985. Uplift patterns and orogenic evolution in the Scottish Dalradian. *Journal of the Geological Society, London*, **142**, 111-128.
- Dempster, T.J., Hudson, N.F. & Rogers, G. 1995. *Metamorphism and cooling of the NE Dalradian*. Special Publication of the Geological Society, London, **152**, 383-390.
- Dempster, T.J., Roger, G., Tanner, P.W.G., Bluck, B.J., Muir, R.J., Redwood, S.D., Ireland, T.R. & Paterson, B.A. 2002. Timing of deposition, orogenesis and glaciation within the Dalradian rocks of Scotland: constraints from U-Pb zircon ages. *Journal of the Geological Society, London*, **159**, 83-94.
- Dewey, J.F. 1971. A model for the Lower Paleozoic of the southern margin of the early Caledonides of Scotland and Ireland. *Scottish Journal of Geology*, **159**, 83-94.
- Dewey, J.F. & Ryan, P.D. 1990. The Ordovician evolution of the South Mayo Trough, western Ireland. *Tectonics*, **9**, 887-901.
- Dominy, S.C. & Platten, I. M. 2008. Scotgold Resources Limited: Cononish Gold Project, Scotland. Geological Review and Mineral Resource Estimate. Snowden Mining Industry Consultants Limited.

- Earls, G., Parker, R.T.G., Clifford, J.A. & Meldrum A.H. 1992. The geology of the Cononish gold-silver deposit, Grampian Highlands of Scotland. *In: Irish Minerals Industry 1980-1990*, Irish Association for Economic Geology, Dublin, 89-103.
- Earls, G., Hutton, D.W.H., Wilkinson, J., Moles, N., Parnell, J., Fallick, A. & Boyce, A. 1996. *The gold metallogeny of northwest Northern Ireland*. Geological Survey of Northern Ireland Technical Report 96/6, 107.
- Eby, G.N. 1992. Chemical subdivision of the A-type granitoids: petrogenetic and tectonic implications. *Geology*, **20**, 641-644.
- Elles, G.L. & Tilley, C.E. 1930. Metamorphism in relation to structure in the Scottish Highlands. *Transactions of the Royal Society of Edinburgh*, **56**, 621-646.
- Ellis, B.S., Wolff, J.A., Boroughs, S., Mark, D.F., Starkel, W.A. & Bonnicksen, B. 2013. Rhyolitic volcanism of the central Snake River Plain: A review. *Bulletin of Volcanology*, **75**, 1-19.
- Engebretson, D.C., Cox, A. & Gordon, E.G. 1985. Relative motions between the oceanic and continental plates in the Pacific basin. *Geological Society of America, Special Paper*, **206**, 56.
- Fairchild, I. 1980. Sedimentation and origin of a late Precambrian 'dolomite' from Scotland. *Journal of Sedimentary Petrology*, **50**, 432-446.
- Fettes, D.J., Long, C.B., Max, M.D. & Yardley, B.W.D. 1985. Grade and time of metamorphism in the Caledonide Orogen of Britain and Ireland. *In: Harris, A.L. (Ed.) The Nature and Timing of Orogenic activity in the Caledonian rocks of the British Isles*. Geological Society of London, Memoirs, **9**, 41-53.
- Fettes, D.J., Graham, C.M., Harte, B. & Plant, J.A. 1986a. Lineaments and basement domains: an alternative view of Dalradian evolution. *Journal of the Geological Society, London*, **143**, 453-464.
- Fettes, D.J., Harris, A.L. & Hall, L.M. 1986b. The Caledonian geology of the Scottish Highlands. *In: Fettes, D.J., Harris, A.L. (eds) Synthesis of the Caledonian rocks of Britain*. Proceedings of the NATO Advanced Study Institute, Reidel, Dordrecht, 303-334.
- Fettes, D.J., Macdonald, R., Fitton, J.G., Stephenson, D. & Cooper, M.R. 2011. Geochemical evolution of Dalradian metavolcanic rocks: implications for the break-up of the Rodinia Supercontinent. *Journal of the Geological Society, London*, **168**, 1133-1146.
- Fitches, W.R., Muir, R.J., Maltman, A.J. & Bentley, M.R. 1990. Is the Colonsay-west Islay block of SW Scotland an allochthonous terrane? Evidence from Dalradian Tillite clasts. *Journal of the Geological Society, London*, **147**, 417-420.
- Fortey, N.J. & Smith, C.G. 1986. Stratabound mineralisation in Dalradian rocks, near Tyndrum, Perthshire. *Scottish Journal of Geology*, **22**, 377-393.
- Foster, D.A., Gray, D.R., Kwak, T.A.P. & Bucher, M. 1998. Chronology and orogenic framework of turbidite hosted gold deposits in the western Lachlan fold belt: $^{40}\text{Ar}/^{39}\text{Ar}$ results. *Ore Geology Reviews*, **13**, 229-250.
- Francis, E.H. 1991. Carboniferous-Permian igneous rocks. *In: Craig, G.Y. (Ed.) The geology of Scotland (3rd edition)*. The Geological Society, London, 393-420.
- Fraser, G.L., Pattinson, D.R.M. & Heaman, L.M. 2004. Age of the Ballachulish and Glen Coe Igneous Complexes (Scottish Highlands) and paragenesis of zircon, monazite and baddeleyite in the Ballachulish Aureole. *Journal of the Geological Society, London*, **161**, 477-462.
- Friedrich, A.M., Bowring, S.A., Martin, M.W. & Hodges, K.V. 1999a. Short-lived continental magmatic arc at Connemara, western Ireland Caledonides: implications for the age of the Grampian orogeny. *Geology*, **27**, 27-30.

- Friedrich, A.M., Hodges, K.V., Bowring, S.A. & Martin, M.W. 1999b. Geochronological constraints on the magmatic, metamorphic and thermal evolution of the Connemara Caledonides, western Ireland. *Journal of the Geological Society, London*, **156**, 1217-1230.
- Gaboury, D. 2013. Does gold in orogenic deposits come from pyrite in deeply buried carbon-rich sediments?: Insight from volatiles in fluid inclusions. *Geology*, **41**, 1207-1210.
- Galantas Gold Corporation. 2013. *Technical report on the Omagh Gold Project, County Tyrone, Northern Ireland*. AIM announcement, 23rd July 2013.
- George, T.N. 1960. The stratigraphical evolution of the Midland Valley. *Transactions of the Geological Society of Glasgow*, **24**, 32-107.
- Glover, B.W., Key, R.M., May, F. Clark, G.C., Phillips, E.R. & Chacksfield, B.C. 1995. A Neoproterozoic multi-phase rift sequence: the Grampian and Appin groups of the southwestern Monadhliath Mountains of Scotland. *Journal of the Geological Society, London*, **152**, 391-406.
- Goldfarb, R.J. & Santosh, M. 2014. The dilemma of the Jiaodong gold deposits: Are they unique? *Geoscience Frontiers*, **5**, 139-153.
- Goldfarb, R.J., Newberry, R.J., Pickthorn, W.J. & Gent, C.A. 1991. Oxygen, Hydrogen and Sulphur isotope studies in the Juneau Gold Belt, Southeastern Alaska: Constraints on the origin of hydrothermal fluids. *Economic Geology*, **86**, 66-80.
- Goldfarb, R.J., Snee, L.W. & Pickthorn, W.J. 1993. Orogenesis, high-T thermal events and gold vein formation within metamorphic rocks of the Alaskan Cordillera. *Mineralogical Magazine*, **57**, 375-394.
- Goldfarb, R.J., Groves, D.I. & Gardoll, S. 2001. Orogenic gold and geologic time: a global synthesis. *Ore Geology Reviews*, **18**, 1-75.
- Goldfarb, R.J., Baker, T., Dube, B., Groves, D.I., Hart, C.J.R. & Gosselin, P. 2005. Distribution, character and genesis of Au deposits in metamorphic terranes. *In: Hedenquist, J.W., Thompson, J.F.H., Goldfarb, R.J. & Richards, J.P. (Eds.) Economic Geology 100th Anniversary volume 1905-2005*, **100**, 407-450.
- Goldfarb, R.J., Hart, C.J.R., Davis, G. & Groves, D.I. 2007. East Asian gold – Deciphering the anomaly of Phanerozoic gold in Precambrian cratons. *Economic Geology*, **102**, 341-346.
- Goldfarb, R.J., Santosh, M., Deng, J. & Yang, L.Q. 2013. The giant Jiaodong gold deposits, China: Orogenic gold in a unique tectonic setting or a unique gold deposits type? *Geological Society of America Abstracts with Programs*, 118.
- Gorjan, P., Veevers, J.J. & Walter, M.R. 2000. Neoproterozoic S-isotope variation in Australia and global implications. *Precambrian Research*, **100**, 151-179.
- Graham, C.M. 1983. High-pressure greenschist to epidote-amphibolite facies metamorphism of the Dalradian rocks of the SW Scottish Highlands. *Geological Society Newsletter*, **12**, 19.
- Graham, C.M. 1986. The role of the Cruachan Lineament during Dalradian evolution. *Scottish Journal of Geology*, **22**, 257-270.
- Graham, C.M., Skelton, A.D.L., Bickle, M. & Cole, C. 1997. Lithological, structural and deformational controls on fluid-flow during regional metamorphism. *In: Holness, M.B. (Ed.) Deformation-enhanced fluid transport in the Earth's crust and mantle*. Mineralogical Society Series, **8**, 196-226.
- Graham, S.D. 2013. *Characterisation of the newly discovered Cu-Ni-PGE mineralisation at Sron Garbh, Stirlingshire, Scotland*. Unpublished MGeol project. University of Leicester.

- Groves, D.I. & Foster, R.P. 1993. Archean lode gold deposits. *In*: Foster, R.P. (Eds.) *Gold metallogeny and exploration*. London, Blackie and Son Ltd, 63-103.
- Groves, D.I., Goldfarb, R.J., Gebre-Mariam, M., Hagemann, S.G. & Robert, F. 1998. Orogenic gold deposits: A proposed classification in the context of their crustal distribution and relationship to other gold deposit types. *Ore Geology Reviews*, **13**, 7-27.
- Groves, D.I., Goldfarb, R.J. & Hart, C.J.R. 2003. Gold deposits in metamorphic belts: Overview of current understanding, outstanding problems, future research and exploration significance. *Economic Geology*, **98**, 1-29.
- Hall, A.J., Boyce, A.J. & Fallick A.E. 1987. Iron sulphides in metasediments: isotopic support for a retrogressive pyrrhotite to pyrite reaction. *Chemical Geology (Isotope Geoscience Section)*, **65**, 305-310.
- Hall, A.J., Boyce, A.J. & Fallick A.E. 1988. A S-isotope study of iron sulfides in the Late Precambrian Dalradian Easdale Slate Formation, Argyll, Scotland. *Mineralogical Magazine*, **52**, 483-490.
- Hall, A.J., Boyce, A.J. & Fallick A.E. 1994a. A S-isotope study of iron sulfides in the Late Precambrian Dalradian Ardrishaig Phyllite Formation, Knapdale, Argyll. *Scottish Journal of Geology*, **30**, 63-71.
- Hall, A.J., McConville, P., Boyce, A.J. & Fallick A.E. 1994b. Sulfides with high $\delta^{34}\text{S}$ from the Late Precambrian Bonahaven Dolomite, Argyll, Scotland. *Mineralogical Magazine*, **58**, 486-490.
- Halliday, L.B. 1962. *Report of Surveys at Tyndrum*, British Geological Survey, Edinburgh.
- Halverson, G.P. & Hurtgen, M.T. 2007. Ediacaran growth of the marine sulfate reservoir. *Earth and Planetary Science Letters*, **263**, 32-44.
- Halverson, G.P. & Shields-Zhou, G. 2011. Chapter 4 Chemostratigraphy and the Neoproterozoic glaciations. *In*: Arnaud, E., Halverson, G.P. & Shields-Zhou, G (Eds.) *The Geological record of Neoproterozoic glaciations*. Geological Society, London, Memoirs, 36, 51-66.
- Halverson, G.P., Hoffman, P.F., Schrag, D.P., Maloof, A.C. & Rice, A.H. 2005. Towards a Neoproterozoic composite carbon-isotope record. *Geological Society of America Bulletin*, **117**, 1181-1207.
- Halverson, G.P., Dudas, F.O., Maloof, A.C. & Bowring, S.A. 2007a. Evolution of the $^{87}\text{Sr}/^{86}\text{Sr}$ composition of Neoproterozoic seawater. *Palaeogeography, Palaeoclimatology, Palaeoecology*, **256**, 103-129.
- Halverson, G.P., Maloof, A.C., Schrag, D.P., Dudas, F.O. & Hurtgen, M.T. 2007b. Stratigraphy and geochemistry of a c. 800 Ma negative isotope interval in northeastern Svalbard. *Chemical Geology*, **237**, 23-45.
- Halverson, G.P., Wade, B.P., Hurtgen, M.T. & Barovich, K.M. 2010. Neoproterozoic chemostratigraphy. *Precambrian Research*, **182**, 337-350.
- Hambrey, M.J. & Harland, W.B. (Eds.). 1981. *Earth's Pre-Pleistocene Glacial Record*. Cambridge Earth Science series. Cambridge University Press, Cambridge.
- Hames, W.E. & Bowring, S.A. 1994. An empirical study of the argon diffusion geometry in muscovite. *Earth and Planetary Science Letters*, **124**, 886-908.
- Harper, C.T. 1967. The geological interpretation of potassium-argon ages of metamorphic rocks of the Scottish Caledonides. *Scottish Journal of Geology*, **3**, 46-66.
- Harris, A.L., Baldwin, C.T., Bradbury, H.J., Johnson, H.D. & Smith, R.A. 1978. Enstatic basin sedimentation: the Dalradian Supergroup. *In*: Bowes, D.R. & Leake, B.L. (Eds.) *Crustal Evolution in Northwestern Britain and adjacent regions*. Seel House Press, Liverpool, 115-138.

- Harris, M., Key, E.A., Widnall, M.A., Jones, E.M. & Steele, G.B. 1988. Geology and mineralisation of the Lagaloachan intrusive complex, western Argyll, Scotland. *Transactions of the Institution of Mining and Metallurgy (Section B: Applied Earth Science)*, **97**, B15-21.
- Hart, C. & Goldfarb, R.J. 2005. Distinguishing intrusion-related from orogenic gold systems. *New Zealand Minerals Conference: Realising New Zealand's Mineral Potential, Proceedings, Australian Institute of Mining and Metallurgy* 125-133.
- Harte, B. 1988. Lower Palaeozoic metamorphism in the Moine-Dalradian belt of the British Isles. *In: Harris, A.L. & Fettes D.J. (Eds.) The Caledonian-Appalachian Orogen*. Geological Society, London, Special Publications, **38**, 123-134.
- Haselock, P.J. & Whittles, K.H. 1982. The stratigraphy and structure of the southern Monadhliath Mountains between Killin and upper Glen Roy. *Scottish Journal of Geology*, **18**, 275-290.
- Haslam, H.W., Cameron, D.G. & Miller, M.F. 1985. Disseminated molybdenum mineralisation in the Etive Plutonic Complex in the Western Highlands of Scotland. *British Geology Survey, Mineral Reconnaissance Program*, **76**
- Hedenquist, J.W., Arribas, A. Jr. & Gonzalez-Urien, E. 2000. Exploration for epithermal gold deposits. *Reviews in Economic Geology*, **13**, 245-277.
- Henley, R.W. 1990. Ore transport and deposition in epithermal ore environments. *In: Herbert, H.K & Ho, S.E. (Eds.) Stable isotopes and fluids processes in mineralisation*. University of Western Australia, Geology Department Publication, Perth, **23**, 51-69.
- Hickman, A.H. 1975. The stratigraphy of late Precambrian metasediments between Glen Roy and Lismore. *Scottish Journal of Geology*, **11**, 117-142.
- Highton, A.J., Hyslop, E.K. & Noble, S.R. 1999. U-Pb zircon geochronology of migmatization in the northern Central Highlands, evidence for pre-Caledonian (Neoproterozoic) tectonometamorphism in the Grampian block, Scotland. *Journal of the Geological Society, London*, **156**, 1195-1204.
- Hill, A.C. & Walter, M.R. 2000. Mid-Neoproterozoic (830-750 Ma) isotope stratigraphy of Australia and global correlation. *Precambrian Research*, **100**, 181-211.
- Hill, N.J., Jenkin, G.R.T., Holwell, D.A., Matthews, K.E., Moore, P., Catterall, D., Boyce, A.J., Mark, D.F., Gunn, G., Naden, J. & Rice, C.M. 2011. New gold occurrences in the Scottish Dalradian – nature and constraints on genesis. *In: Barra, F., Reich, M., Campos, E. & Tornos, F. (Eds.) Let's Talk Ore Deposits. Proceedings of the 11th Biennial Meeting, Antofagasta, Chile*, **2**, 577-579.
- Hill, N.J., Jenkin, G.R.T., Boyce, A.J., Sangster, C.J.S., Catterall, D.J., Holwell, D.A., Naden, J. & Rice, C.M. 2013. How the Neoproterozoic S-isotope record illuminates the genesis of vein gold systems: an example from the Dalradian Supergroup in Scotland. *In: Jenkin, G.R.T., Lusty, P.A.J., McDonald, I., Smith, M.P., Boyce, A.J. & Wilkinson, J.J. (Eds.) Ore Deposits in an Evolving Earth*. Geological Society, London, Special Publications, **393**, 9.
- Hodgson, C.J., Love, D.A. & Hamilton, J.V. 1993. Giant mesothermal gold deposits: descriptive characteristics, genetic model and exploration area selection criteria. *In: Whiting, B.H., Hodgson, C.J. & Mason, R. (Eds.) Giant Ore Deposits, Special Publication, Society of Economic Geologists*, **2**, 157-212.
- Hoffman, P.F., Kaufman, A.J., Halverson, G.P. & Schrag, D.P. 1998. A Neoproterozoic Snowball Earth. *Science*, **281**, 1342-1346.
- Holness, M.B. & Graham, C.M. 1995. *P-T-X* effects on equilibrium carbonate-H₂O-CO₂-NaCl dihedral angles: constraints on carbonate permeability and the role of deformation during fluid infiltration. *Contributions to Mineralogy and Petrology*, **119**, 301-313.

- Hurtgen, M.T., Arthur, M.A., Suits, N.S. & Kaufman, A.J. 2002. The S isotopic composition of Neoproterozoic seawater sulfate: implications for a snowball Earth? *Earth and Planetary Science Letters*, **203**, 413-429.
- Hussien, A. & Hipkin, R.E. 1981. *Bouguer anomaly map of the British Isles, northern sheet*. University of Edinburgh.
- Hutton, D.H.W. 1979. Tectonic slides: A review and reappraisal. *Earth Science Reviews*, **15**, 151-172.
- Ixer, R., Pattick, R. & Stanley, C. 1997. Geology, mineralogy and genesis of gold mineralisation at Calliachar-Urular Burn, Scotland. *Transaction of the Institute of Mining and Metallurgy (Section B Applied Earth Science)*, **106**, 99-108.
- Jackson, S.E., Pearson, N.J., Griffin, W.L. & Belousova, E.A. 2004. The application of laser ablation inductively coupled mass spectrometry to *in situ* U-Pb zircon geochronology. *Chemical Geology*, **211**, 47-69.
- Jacques, J.M. & Reavy, R.J. 1994. Caledonian plutonism and major lineaments in the SW Scottish Highlands. *Journal of the Geological Society, London*, **151**, 955-969.
- Kajiwar, Y. & Krouse, H.R. 1971. S-isotope partitioning in metallic sulfide systems. *Canadian Journal of Earth Science*, **8**, 1397-1408.
- Kelley, S.P. & Fallick, A.E. 1990. High precision spatially resolved analysis of $\delta^{34}\text{S}$ in sulfides using a laser extraction system. *Geochimica et Cosmochimica Acta*, **54**, 883-888.
- Kemp, A.I.S., Hawkesworth, C.J., Collins, W.J., Gray, C.M., Blevin, P.L. & EIMF. 2009. Isotopic evidence for rapid continental growth in an extensional accretionary orogen: the Tasmanides, eastern Australia. *Earth and Planetary Science Letters*, **284**, 455-466.
- Kennedy, M., Droser, M., Mayer, L.M., Pevear, D. & Mrofka, D. 2006. Late Precambrian oxygenation; inception of the clay mineral factory. *Science*, **311**, 1446-1449.
- Key, R.M., Clark, G.C., May, F., Phillips, E.R., Chacksfield, B.C. & Peacock, J.D. 1997. *Geology of the Glen Roy District. Memoir of the British Geological Survey, Sheet 63W, Scotland*.
- Kokelaar, B.P. & Moore, I.D. 2006. Classical areas of British Geology, Glencoe caldera volcano, Scotland. Keyworth, Nottingham, British Geological Survey.
- Koppers, A.A.P. 2002. ArArCALC-software for $^{40}\text{Ar}/^{39}\text{Ar}$ age calculations. *Computational Geoscience*, **28**, 605-619.
- Krabbendam, M., Leslie, A.G., Crane, A. & Goodman, S. 1997. Generation of the Tay Nappe, Scotland, by large-scale SE-directed shearing. *Journal of the Geological Society, London*, **154**, 15-24.
- Kuiper, K.F., Deino, A., Hilgen, F.J., Krijgsman, W., Renne, P.R. & Wijbrans, J.R. 2008. Synchronising rock clocks of Earth History. *Science*, **320**, 500-504.
- Kuznetsov, A.B. 1998. *Evolution of Sr composition in late Riphean seawater*. Unpublished PhD thesis, Institute of Precambrian Geology and Geochronology, Russian Academy of Science.
- Lang, J.R. & Baker, T. 2001. Intrusion-related gold systems: the present level of understanding. *Mineralium Deposita*, **36**, 477-489.
- Laouar, R. 1987. *A S-isotope study of the Caledonian granite of Britain and Ireland*. Unpublished MSc thesis, University of Glasgow.
- Large, R.R., Bull, S.W. & Maslennikov, V.V. 2011. A carbonaceous sedimentary source-rock model for Carlin-Type and Orogenic gold deposits. *Economic Geology*, **106**, 331-358.

- Large, R.R., Thomas, H., Craw, D., Henne, A. & Henderson, S. 2012. Diagenetic pyrite as a source for metals in orogenic gold deposits, Otago Schist, New Zealand. *New Zealand Journal of Geology and Geophysics*, **55**, 137-149.
- Lee, J.K.W. 1995. Multipath diffusion in geochronology. *Contributions to Mineralogy and Petrology*, **120**, 60-82.
- Lee, J.-L., Marti, K., Severinghaus, J.P., Kawamura, K., Yoo, H.-S., Lee, J.B. & Kim, J.S. 2006. A redetermination of the isotopic abundances of atmospheric Ar. *Geochimica et Cosmochimica Acta*, **70**, 4507-4512.
- Lenton, T.M. & Watson, A.J. 2004. Biotic enhancement of weathering, atmospheric oxygen and carbon dioxide in the Neoproterozoic. *Geophysical Research Letters*, **31**, L05202, doi:10.1029/2003GL018802.
- Leslie, A.G., Smith, M. & Soper, N.J. 2008. Laurentian margin evolution and the Caledonian orogeny – a template for Scotland and East Greenland. In: Higgins, A.K., Gilotti, J.A., Smith, M.P. (Eds.). *The Greenland Caledonides: Evolution of the Northeast margin of Laurentia*. Geological Society of America Memoir 202, 307-343.
- Leslie, A.G., Robertson, S., Smith, M., Banks, C.J., Mendum, J.R. & Stephenson, D. 2013. The Dalradian rocks of the northern Grampian Highlands. Proceedings of the Geologists' Association. <http://dx.doi.org/10.10016/j.pgeola.2012.07.010>.
- Li, Y. & Lui, J. 2006. Calculation of S-isotope fractionation in sulfides. *Geochimica et Cosmochimica Acta*, **70**, 1789-1795.
- Li, J.W., Vasconcelos, P.M., Zhou, M.F., Zhao, X.F. & Ma, C.Q. 2006. Geochronology of the Pangjiaikuang and Rushan gold deposits, Eastern Jiaodong gold province, Northeastern China: Implications for regional mineralisation and geodynamic setting. *Economic Geology*, **101**, 1023-1038.
- Loiselle, M.C. & Wones, D.R. 1979. Characteristics and origin of anorogenic granites. *Geological Society of America, Abstracts*, **11**, 468.
- Lovera, O.M., Richter, F.M. & Harrison, T.M. 1989. The $^{40}\text{Ar}/^{39}\text{Ar}$ thermochronometry for slowly cooled samples have a distribution of diffusion domain sizes. *Journal of Geophysical Research*, **94**, 17917-17935.
- Lowry, D. 1991. *The genesis of Late Caledonian granitoid-related mineralisation in Northern Britain*. Unpublished PhD thesis, University of St. Andrews.
- Lowry, D., Boyce, A.B., Fallick, A.E. & Stephens, W.E. 1995. Genesis of porphyry and plutonic mineralisation systems in metaluminous granitoids of the Grampian Terrane, Scotland. *Transactions of the Royal Society of Edinburgh: Earth Science*, **85**, 221-237.
- Lowry, D., Boyce, A.J., Fallick, A.E., Stephens, W.E. & Grassineau, N.V. 2005. Terrane and basement discrimination in northern Britain using S-isotopes and mineralogy of ore deposits. In: McDonald, I., Boyce, A.J., Butler, I.B., Herrington, R.J. & Polya, D.A. (Eds.) *Deposits and Earth Evolution*. Geological Society, London, Special Publications, **248**, 133-151.
- Ludwig, K.R. 2003. *Isoplot/Ex 3.00. A Geochronological Toolkit for Microsoft Excel*. Special Publication, **4**. Berkeley Geochronological Centre, Berkeley, CA.
- Lusty, P.A., Naden, J., Bouch, J.J., McKervey, J.A. & McFarlane, J.A. 2011. Atypical gold mineralisation in an Orogenic setting – The Bohaun deposit, Western Irish Caledonides. *Economic Geology*, **106**, 359-380.
- MacDonald, F.A., Jones, D.S. & Schrag, D.P. 2009. Stratigraphic and tectonic implications of newly discovered glacial diamictite-cap carbonate couplet in southwestern Mongolia. *Geology*, **37**, 123-126.

- Mair, J.L. 2004. *Tectonic setting, magmatism and magmatic-hydrothermal systems at Scheelite Dome, Tombstone Gold Belt, Yukon Territory, Canada*. Unpublished PhD thesis. University of Western Australia.
- Mao, J.W., Wang, Y.T., Li, H.M., Pirajno, F., Zhang, C.Q. & Wang, R.T. 2008. The relationship of mantle-derived fluids to fold metallogenesis in the Jiaodong Peninsula: evidence from D-O-C-S isotopic systematic. *Ore Geology Reviews*, **33**, 361-381.
- Marcantonio, F., Dickin, A.P., McNutt, R.H. & Heaman, L.M. 1988. A 1880-million year old Proterozoic gneiss terrane in Islay with implications for crustal evolution of Britain. *Nature*, **335**, 62-64.
- Mark, D.F., Parnell, J., Kelley, S.P. & Sherlock, S.C. 2007. Resolution of regional fluid flow related to successive orogenic events on the Laurentian margin. *Geology*, **35**, 547-550.
- Mark, D.F., Barfod, D., Stuart, F.M. & Imlach, J. 2009. The ARGUS multicollector noble gas mass spectrometer: Performance for $^{40}\text{Ar}/^{39}\text{Ar}$ geochronology. *Geochemistry, Geophysics, Geosystems*, **10**, Art. No. Q0AA02.
- Mark, D.F., Rive, C.M., Fallick, A.E., Trewin, N.H., Lee, M.R., Boyce, A. & Lee, J.K.W. 2011a. $^{40}\text{Ar}/^{39}\text{Ar}$ dating of hydrothermal activity, biota and gold mineralisation in the Rhynie hot-spring system, Aberdeenshire, Scotland. *Geochimica et Cosmochimica Acta*, **75**, 555-569.
- Mark, D.F., Stuart, F.M. & de Podesta, M. 2011b. New high-precision measurements of the isotopic composition of atmospheric argon. *Geochimica et Cosmochimica Acta*, **75**, 7494-7501.
- Mark, D.F., Rice, C.M. & Trewin, N.H. 2013. Discussion on 'A high-precision U-Pb age constraint on the Rhynie Chert Konservat-Lagerstätte: time scale and other implications'. *Journal of the Geological Society, London*, **170**, 701-703.
- Mark, D.F., Lindgren, P. & Fallick, A.E. 2014. A high-precision $^{40}\text{Ar}/^{39}\text{Ar}$ age for hydrated impact glass from the Dellen impact, Sweden. *In: Jourdan, F., Mark, D.F. & Verati, C. (Eds.) Advances in $^{40}\text{Ar}/^{39}\text{Ar}$ dating: from Archaeology to Planetary Sciences*, Geological Society, London, Special Publications, **378**, 349-366.
- Markey, R.J., Stein, H.J., Hannah, J.L., Zimmerman, A., Selby, D. & Creaser, R.A. 2007. Standardising Re-Os geochronology: A new molybdenite reference material Henderson, USA and the stoichiometry of Os salts. *Chemical Geology*, **244**, 74-87.
- Maruyama, S., Isozaki, Y., Kimura, G. & Terabayashi, M. 1997. Palaeogeographic maps of the Japanese Islands: Plate tectonic synthesis from 750 Ma to the present. *Island Arc*, **6**, 121-142.
- Mason, J., Patrick, R.A.D. & Gallagher, M.J. 1991. Auriferous vein mineralisation near Aberfeldy, Scotland. Exploration and the Environment, Institution of Mining and Metallurgy meeting, Edinburgh, program with extended abstracts, 50-52.
- Matthews, K.E. 2011. *Comparison of the Cononish deposit and Beinn Udlaidh Main Vein, Tyndrum, Scotland*. Unpublished MGeol project. University of Leicester.
- McCaffery, K.J.W. & Johnston, J.D. 1996. Fractal analysis of a mineralised vein deposit: Curraghinalt gold deposit, County Tyrone. *Mineralium Deposita*, **31**, 52-58.
- McCay, G.A., Prave, A.R., Alsop, G.I. & Fallick, A.E. 2006. Glacial trinity: Neoproterozoic earth history within the British-Irish Caledonides. *Geology*, **34**, 909-912.
- McCuaig, T.C., Kerrich, R., Groves, D.I. & Archer, N. 1993. The nature and dimensions of regional and local gold-related hydrothermal alteration in tholeiitic metabasalts in the Norseman goldfields: The missing link in a crustal continuum of gold deposits? *Mineralium Deposita*, **28**, 420-435.

- McKeith, T.D., Schodde, R.C. & Baltis, E.J. 2010. Gold discovery trends. *Society for Economic Geology Newsletter*, **81**, 1-20-26.
- Melezhik, V.A., Gorokhov, I.M., Kuznetsov, A.B. & Fallick, A.E. 2001. Chemostratigraphy of Neoproterozoic carbonates: implications for 'blind dating'. *Terra Nova*, **13**, 1-11.
- Mendum, J.R. & Noble, S.R. 2010. Mid-Devonian sinistral transpressional movements on the Great Glen Fault: the rise of the Rosemarkie Inlier and the Acadian Event in Scotland. *In*: Law, R.D., Butler, R.W.H., Holdsworth, R.E., Krabbendam, M. & Strachan, R.A. (Eds.) *Continental tectonics and mountain building: the legacy of Peach and Horne*. Geological Society, London, Special Publications, **335**, 161-187.
- Mernagh, T.P. & Bierlein, F.P. 2008. Transport and precipitation of gold in Phanerozoic metamorphic terranes from chemical modelling of fluid-rock interaction. *Economic Geology*, **103**, 1613-1640.
- Mezger, K., Hanson, G.N. & Bohlen, S.R. 1989. High-precision U-Pb ages of metamorphic rutile: application to the cooling history of high-grade terranes. *Earth and Planetary Science Letters*, **96**, 106-118.
- Miles, A., Graham, C., Hawkesworth, C., Gillespie, M., Dhuime, B. & Hinton, R. 2014. Using zircon isotope compositions to constrain crustal structure and pluton evolution: the Iapetus Suture Zone granites in northern Britain. *Journal of Petrology*, **55**, 181-207.
- Moles, N.R. 1985. Metamorphic conditions and uplift history in central Perthshire: evidence from mineral equilibria in the Foss celsian-barite-sulfide deposit, Aberfeldy. *Journal of the Geological Society, London*, **142**, 39-52.
- Moles, N.R., Boyce, A.J. & Fallick, A.E. 2014. Abundant sulfate in the Neoproterozoic ocean: implications of constant $\delta^{34}\text{S}$ of barite in the Aberfeldy SEDEX deposits, Scottish Dalradian. *In*: Jenkin, G.R.T., Lusty, P.A.J., McDonald, I., Smith, M.P., Boyce, A.J. & Wilkinson, J.J. (Eds.) *Ore Deposits in an Evolving Earth*. Geological Society of London, Special Publications, 393, <http://dx.doi.org/10.1144/SP393.7>.
- Moore, P. 2011. *Developing an exploration guide for the auriferous breccia pipes at Beinn Udlaidh, Scotland*. Unpublished MGeol project. University of Leicester.
- Moore, J.M., Kuhn, B.K., Mark, D.F. & Tsikos, H. 2011. A sugilite-bearing assemblage from the Wolhaarkop breccia, Bruce iron-ore mine, South Africa: Evidence for alkali metasomatism and $^{40}\text{Ar}/^{39}\text{Ar}$ dating. *European Journal of Mineralogy*, **23**, 661-673.
- Muir, R.J., Fitches, W.R. & Maltman, A.J. 1989. An early Proterozoic link between Greenland and Scandinavia in the Inner Hebrides of Scotland. *Terra Abstract* **1**, 5.
- Muir, R.J., Fitches, W.R., Maltman, A.J., Dickin, A.P. & Bowes, D.R. 1992. Discussion of isotopic evidence for the extent of early Proterozoic basement in Scotland and northwest Ireland. *Geological Magazine*, **129**, 501-504.
- Muir, R.J., Fitches, W.R. & Maltman, A.J. 1995. The Colonsay Group and basement cover relationships on the Rhinns of Islay, Inner Hebrides. *Scottish Journal of Geology*, **31**, 125-130.
- Neilson, J.C., Kokelaar, B.P. & Crowley, Q.G. 2009. Timing, relations and cause of plutonic and volcanic activity of the Siluro-Devonian post-collision magmatic episode in the Grampian Terrane, Scotland. *Journal of the Geological Society, London*, **166**, 545-561.
- Nesbitt, B.E. 1988. Reconnaissance study of $\delta^{34}\text{S}$ values of sulphides from mesothermal gold deposits of the Eastern Canadian Cordillera. *British Columbia Ministry of Energy, Mines and Petroleum Resources, Geological Fieldwork 1987*, **Paper 1988-1**.

- Noble, S.R., Hyslop, E.K. & Highton, A.J. 1996. High precision U-Pb monazite geochronology of the c. 806 Ma Grampian Shear Zone and the implications for the evolution for the Central Highlands of Scotland. *Journal of the Geological Society, London*, **153**, 511-514.
- Ohmoto, H. 1986. Stable isotope geochemistry of ore deposits. Chapter 14. *In*: Valley, J.W., Taylor, H.P. Jnr & O'Neil, J.R. (Eds.) *Stable isotopes in high temperature geological processes*. Mineralogical Society of America. Reviews in Mineralogy, **16**, 491-559.
- Oliver, G.J.H., 2001. Reconstruction of the Grampian episode in Scotland: its place in the Caledonian Orogeny. *Tectonophysics*, **332**, 23-49.
- Oliver, G.J.H., Chen, F., Buchwald, R., Hegner, E. 2000. Fast tectonometamorphism and exhumation in the type area of the Barrovian and Buchan zones. *Geology*, **28**, 459-462.
- Oliver, G.J.H., Stone, P. & Bluck, B.J. 2002. The Ballantrae Complex and the Southern Uplands terrane. *In*: Trewin, N.H. (Ed.) *The Geology of Scotland*. The Geological Society, London, 167-200.
- Oliver, G.J.H., Wilde, S.A. & Wan, Y. 2008. Geochronology and geodynamics of Scottish granitoids from the late Neoproterozoic break-up of Rodinia to Palaeozoic collision. *Journal of the Geological Society, London*, **165**, 661-674.
- Parker, R.T.G., Clifford, J.A. & Meldrum, A.H. 1989. The Cononish gold-silver deposit, Perthshire, Scotland. *Transactions of the Institution of Mining and Metallurgy (Section B: Applied Earth Science)*, **98**, B51-B54.
- Parnell, J., Earls, G., Wilkinson, J.J., Hutton, D.H.W., Boyce, A.J., Fallick, A.E., Ellam, R.E., Gleeson, S.A., Moles, N.R., Carey, P.F., Legg, I. 2000. Regional fluid flow and gold mineralization in the Dalradian of the Sperrin Mountains, Northern Ireland. *Economic Geology*, **95**, 1389-1416.
- Parnell, J., Boyce, A.J., Mark, D. Bowden, S. & Spinks, S. 2010. Early oxygenation of the terrestrial environment during the Mesoproterozoic. *Nature*, **468**, 290-293.
- Parry, S.F., Noble, S.R., Crowley, Q.G. & Wellman, C.H. 2011. A high-precision U-Pb age constraint on the Rhynie Chert Konservat-Lagerstätte: time scale and other implications. *Journal of the Geological Society, London*, **168**, 863-872.
- Parsons, I. & Lee, M.R. 2000. Alkali feldspars as microtextural markers of fluid flow. *In*: Stober, I. & Bucher, K. (Eds.). *Hydrogeology of crystalline rocks*. Kluwer Academic Publishers, Dordrecht, Netherlands.
- Patrick, R.A.D. 1981. *The vein mineralisation at Tyndrum, Scotland and a study of substitutions in tetrahedrites*. Unpublished PhD thesis. University of Strathclyde.
- Patrick, R.A.D., Coleman, M.L. & Russell, M.J. 1983. Sulphur isotopic investigation of vein lead-zinc mineralisation at Tyndrum, Scotland. *Mineralium Deposita*, **18**, 477-485.
- Patrick, R.A.D., Boyce, A. & MacIntyre, R.M. 1988. Au-Ag vein mineralisation at Tyndrum, Scotland. *Mineralogy and Petrology*, **38**, 61-76.
- Pettke, T., Diamond, L.W. & Villa, I.M. 1999. Mesothermal gold veins and metamorphic devolatilisation in the northwestern Alps: The temporal link. *Geology*, **27**, 641-644.
- Pickering, K.T., Bassett, M.G. & Siveter, D.J. 1988. Late Ordovician-Early Silurian destruction of the Iapetus Ocean; Newfoundland, British Isles and Scandinavia; a discussion. *Transactions of the Royal Society of Edinburgh: Earth Sciences*, **79**, 361-381.
- Pitcairn, I.K., Teagle, D.A.H., Craw, D., Oilvio, G.K., Kerrich, R. & Brewer, T.S. 2006. Sources of metals and fluids in orogenic gold deposits; Insights from the Otago and Alpine schists, New Zealand. *Economic Geology*, **101**, 1525-1546

- Pitcairn, I.K., Olivio, G.R., Teagle, D.A.H. & Craw, D. 2010. Sulfide evolution during prograde metamorphism of the Otago and Alpine Schists, New Zealand. *Canadian Mineralogist*, **48**, 1267-1295.
- Plant, J.A., Smith, R.t., Stevenson, A.G., Forrest M.D. & Hodgson, J.F. 1984. Regional geochemical mapping for mineral exploration in Northern Scotland. *In: Prospecting in areas of glaciated terrain*. Institute of Mining and Metallurgy, London, 103-120.
- Plant, J.A., Breward, N., Simpson, P.R. & Slater, D. 1990. Regional geochemistry and the identification of metallogenic provinces: examples from lead-zinc-barium, tin-uranium and gold deposits. *Journal of Geochemical Exploration*, **39**, 195-224.
- Plant, J.A., Stone, P., Flight, D.M.A., Green, P.M. & Simpson, P.R. 1997. Geochemistry of the British Caledonides: the setting for metallogeny. *Transactions of the Institute of Mining and Metallurgy: Section B Applied Earth Science*, **106**, B67-78.
- Plewes, W.T. 2012. *Comparison of the Main Vein and Northeast extension vein at Beinn Udlaidh and Coire Ghamhnain, for Scotgold's gold exploration project, Tyndrum, Scotland*. Unpublished MGeol project. University of Leicester.
- Porter, S.J. & Selby, D. 2010. Rhenium-Osmium (Re-Os) molybdenite systematics and geochronology of the Cruachan granite skarn mineralisation, Etive complex: implications for emplacement chronology. *Scottish Journal of Geology*, **46**, 17-21.
- Prave, A.R. 1999. The Neoproterozoic Dalradian Supergroup of Scotland: an alternative hypothesis. *Geological Magazine*, **136**, 609-617.
- Prave, A.R., Fallick, A.E., Thomas, C.W. & Graham, C.M. 2009. A composite C-isotope profile for the Neoproterozoic Dalradian Supergroup of Scotland and Ireland. *Journal of the Geological Society, London*, **166**, 845-857.
- Pricewaterhouse Coopers. 2013. *The direct economic impact of gold. Independent report from Pricewaterhouse Coopers commissioned by the World Gold Council*. Downloaded from <http://www.gold.org/gold-mining/economic-contribution>. 30th April 2014
- Pringle, J. 1940. The discovery of Cambrian Trilobites in the Highland Border rocks near Callendar, Perthshire (Scotland). *Advancement of Science*, **1**, 252.
- Purdy, J. & Jäger, E. 1976. K-Ar ages on rock-forming minerals from the Central Alps.
- Qui, Y.M., Groves, D.I., McNaughton, N.J., Wang, L.J. & Zhou, T. 2002. Nature, age and tectonic setting of granitoids-hosted orogenic gold deposits of the Jiaodong Peninsula, eastern North China craton, China. *Mineralium Deposita*, **37**, 283-305.
- Raith, J.G. & Stein, H.J. 2000. Re-Os dating and sulphur isotopic composition of molybdenite from tungsten deposits in western Namaqualand, South Africa: implications for ore genesis and the timing of metamorphism. *Mineralium Deposita*, **35**, 741-753.
- Ramsey, D.M. 1964. Deformation of pebbles in Lower Old Red Sandstone conglomerates adjacent to the Highland Boundary Fault. *Geological Magazine*, **101**, 228-248.
- Renne, P.R., Swisher, C.C., Deino, A.L., Karner, D.B., Owens, T.L. & DePaolo, D.L. 1998. Intercalibration of standards, absolute ages and uncertainties in $^{40}\text{Ar}/^{39}\text{Ar}$ dating. *Chemical Geology*, **145**, 117-152.
- Renne, P.R., Deino, A.L., Hames, W.E., Heizler, M.T., Hemming, S.R., Hodges, K.V., Koppers, A.A.P., Mark, D.F., Morgan, L.E., Phillips, D., Singer, B.S., Turrin, B.D., Villa, I.M., Vileneuve, M. & Wijbrans, J.R. 2009. Data reporting norms for $^{40}\text{Ar}/^{39}\text{Ar}$ Geochronology. *Quaternary Geochronology*, **4**, 346-352.

- Renne, P.R., Mundil, R., Balco, G., Min, K. & Ludwig, K.R. 2010. Joint determination of ^{40}K decay constraints and $^{40}\text{Ar}^*/^{40}\text{K}$ for the Fish Canyon sanidine standard, and improved accuracy for $^{40}\text{Ar}/^{39}\text{Ar}$ geochronology. *Geochimica et Cosmochimica Acta*, **74**, 5349-5367.
- Renne, P.R., Balco, G., Ludwig, K.R., Mundil, R. & Min, K. 2011. Joint determination of ^{40}K decay constraints and $^{40}\text{Ar}^*/^{40}\text{K}$ for the Fish Canyon sanidine standard, and improved accuracy for $^{40}\text{Ar}/^{39}\text{Ar}$ geochronology; reply. *Geochimica et Cosmochimica Acta*, **75**, 5097-5100.
- Renne, P.R., Deino, A.L., Hilgen, F.J., Kuiper, K.F., Mark, D.F., Mitchell III, W.S., Morgan, L.E., Mundil, R. & Smith, J. 2013. Time scales of critical events around the Cretaceous-Paleogene boundary. *Science*, **339**, 684-687.
- Rice, C.M. & Trewin, N.H. 1988. A Lower Devonian gold bearing hot-spring system, Rhynie, Scotland. *Transactions of the Institute of Mining and Metallurgy (Section B: Applied Earth Science)*, **97**, 141-144.
- Rice, C.M. & Ashcroft, W.A. 2004. Geology of the northern half of the Rhynie Basin, Aberdeenshire, Scotland. *Transactions of the Royal Society of Edinburgh: Earth Sciences*, **94**, 299-308.
- Rice, C.M., Ashcroft, W.A., Batten, D.J., Boyce, A.J., Caulfield, J.B.D., Fallick, A.E., Hole, M.J., Jones, E., Pearson, M.J., Rogers, G., Saxton, J.M., Stuart, F.M., Trewin, N.H. & Turner, G. 1995. A Devonian auriferous host spring system, Rhynie, Scotland. *Journal of the Geological Society, London*, **152**, 229-250.
- Rice, C.M., Mark, D.F., Selby, D. & Hill, N.J. 2012. Dating vein-hosted Au deposits in the Caledonides of N. Britain. Mineral Deposit Studies Groups meeting abstracts. *Transactions of the Institute of Mining and Metallurgy (Section B: Applied Earth Science)*, **121**, 199-200.
- Richards, J.P. 2009. Postsubduction porphyry Cu-Au and epithermal Au deposits: Products of remelting of subduction-modified lithosphere. *Geology*, **37**, 247-250.
- Rivera, T.A., Storey, M., Zeeden, C., Hilgen, F.J. & Kuiper, K. 2011. A refined astronomically calibrated $^{40}\text{Ar}/^{39}\text{Ar}$ age for Fish Canyon sanidine. *Earth and Planetary Science Letters*, **311**, 420-426.
- Robert, F., Boullier, A-M. & Firdaous, K. 1995. Gold-quartz veins in metamorphic terranes and their bearing on the role of fluids in faulting. *Journal of Geophysical Research*, **100**, 12861-12879.
- Roberts, A.M. & Treagus, J.E. 1979. Stratigraphical and structural correlation between the Dalradian rocks of the SW and Central Highlands of Scotland. In: Harris, A.L., Holland, C.H. & Leake, B.E. (Eds.) *The Caledonides of the British Isles*. Geological Society of London, Special Publication, **8**, 199-204.
- Robertson, S. & Smith, M. 1999. The significance of the Geal Charn-Ossian Steep Belt in basin development in the Central Scottish Highlands. *Journal of the Geological Society, London*, **156**, 1175-1182.
- Robinson, B.W. & Kasakabe, M. 1975. Quantitative preparation of SO_2 for $^{34}\text{S}/^{32}\text{S}$ analysis from sulfides by combustion with cuprous oxide. *Analytical Chemistry*, **47**, 1179-1181.
- Rock, N.M.S. & Groves, D.I. 1988. Can lamprophyres resolve the genetic controversy over mesothermal gold deposits? *Geology*, **16**, 538-541.
- Rogers, G. & Dunning, G.R. 1991. Geochronology of appinitic and related granitic magmatism in the W Highlands of Scotland: constraints on the timing of transcurrent fault movement. *Journal of the Geological Society, London*, **148**, 17-27.
- Rooney, A.D., Chew, D.M. & Selby, D. 2011. Re-Os geochronology of the Neoproterozoic-Cambrian Dalradian Supergroup of Scotland and Ireland: implications for Neoproterozoic stratigraphy, glaciations and Re-Os systematics. *Precambrian Research*, **185**, 202-214.

- Rudnick, R.L. & Gao, S. 2002. Composition of the Continental Crust. *In*: Rudnick R.L. (Ed.) *Treatise on Geochemistry, Volume 3*. Elsevier, 1-64.
- Rushton, A.W.A., Owen, A.W., Owens, R.M. & Prigmore, J.K. 1999. *British Cambrian and Ordovician stratigraphy, Geological Conservation Review Series, 18*. Joint Nature Conservation Committee, Peterborough.
- Ryan, P.D., Soper, N.J., Snyder, D.B., England, R.W. & Hutton, D.H.W. 1995. The Antrim-Galway line: a resolution of the Highland Border Fault enigma of the Caledonides of Britain and Ireland. *Geological Magazine*, **132**, 171-184.
- Scotgold Resources Limited. 2008. *Scotgold Resources Limited Annual Report 2008*.
- Scotgold Resources Limited. 2010. *Drilling confirms further anomalous gold mineralisation in breccia pipes at Beinn Udlaidh*. ASX announcement, 17th February 2010
- Scotgold Resources Limited. 2011a. *Exploration update: River Vein and Beinn Udlaidh areas*. ASX announcement, 8th February 2011
- Scotgold Resources Limited. 2011b. *Exploration update: Auch project area*. ASX announcement, 19th January 2011
- Scotgold Resources Limited. 2012a. *Cononish Resource Update*. ASX announcement, 14th November 2012
- Scotgold Resources Limited. 2012b. *Sron Garbh Mafic complex*. ASX announcement, 7th March 2012
- Scotgold Resources Limited. 2012c. *Exploration progress at River Vein*. ASX announcement, 27th January 2012
- Scott, R.A., Patrick, R.A.D. & Polya, D.A. 1987. *S isotopic and related studies on Dalradian stratabound mineralisation in the Tyndrum region, Scotland*. British Geological Survey Stable Isotope Report, **130**, 40.
- Scott, R.A., Patrick, R.A.D. & Polya, D.A. 1991. Origin of Sulphur in metamorphosed stratabound mineralisation from the Argyll Group, Dalradian of Scotland. *Transactions of the Royal Society of Edinburgh: Earth Science*, **82**, 91-98.
- Selby, D. & Creaser, R.A. 2001. Re-Os geochronology and systematics from the Endako porphyry molybdenum deposit, British Columbia, Canada. *Economic Geology*, **96**, 197-204.
- Shackleton, R.M. 1958. Downward-facing structures of the Highland Border. *Quarterly Journal of the Geological Society of London*, **113**, 361-392.
- Shields, G. 1999. Working towards a new stratigraphic calibration scheme for the Neoproterozoic-Cambrian. *Eclogae Geologicae Helveticae*, **92**, 221-233.
- Simmons, S.F. 1995. Magmatic contributions to low-sulphidation epithermal deposits. *Mineralogical Association of Canada Short Course Handbook*, **23**, 455-477.
- Simmons, S.F., White, N.C. & John, D.A. 2005. Geological characteristics of epithermal precious and base metal deposits. *100th Anniversary Volume of Economic Geology*, **100**, 485-522.
- Sláma, J., Košler, J., Condon, D.J., Crowley, J.L., Gerdes, A., Hanchar, J.M., Horstwood, M.S.A., Morris, G.A., Nasdala, L., Norberg, N., Schaltegger, U., Schoene, B., Tubrett, M.N. & Whitehouse, M.J. 2008. Plešovice zircon – A new reference material for U-Pb and Hf isotopic microanalysis. *Chemical Geology*, **249**, 1-35.
- Smith, C.G., Pitfield, P.E.J., Burley, A.J., Howard, S.H.D., Parker, M.E., Michie, U, McL. & Fortey, N.J. 1977. *Investigation of stratiform sulphide mineralisation in parts of central Perthshire*. Mineral Reconnaissance Program Report No. 8. British Geological Survey.

- Smoliar, M.I., Walker, R.J. & Morgan, J.W. 1996. Re-Os isotope constrains on the age of Group IIA, IIIA, IVA and IVB iron meteorites. *Science*, **271**, 1099-1102.
- Soper, N.J. 1986. The Newer Granite problem: a geotectonic view. *Geological Magazine*, **123**, 227-236.
- Soper, N.J. & Anderton, R. 1984. Did the Dalradian slides originate as extensional faults? *Nature*, **307**, 357-360.
- Soper, N.J. & Hutton, D.H.W. 1984. Late Caledonian sinistral displacements in Britain – Implications for a 3-plate collision model. *Tectonics*, **3**, 781-794.
- Soper, N.J. & Evans, J.A. 1997. Discussion on metamorphism and cooling of the NE Dalradian. *Journal of the Geological Society, London*, **154**, 357-360.
- Soper, N.J., Strachen, R.A., Holdsworth, R.E., Gayer, R.A. & Greiling, R.O. 1992. Sinistral transpression and the Silurian closure of Iapetus. *Journal of the Geological Society, London*, **146**, 871-880.
- Soper, N.J., Ryan, P.D. & Dewey, J.F. 1999. Age of the Grampian Orogeny in Scotland and Ireland. *Journal of the Geological Society, London*, **156**, 1231-1236.
- Spence-Jones, C.P. 2013. *Metallurgic investigation of the ore from the Cononish Gold Deposit, Scotland*. Unpublished MGeol project. University of Leicester.
- Spencer, A.M. 1971. Late Precambrian Glaciation in Scotland. *Memoir of the Geological Society, London*, **6**.
- Spencer, A.M. 1981. The late Precambrian Port Askaig Tillite in Scotland. *In: Hambrey, M.J. & Harland, W.B. (Eds.). Earth's Pre-Pleistocene Glacial Record*. Cambridge University Press, Cambridge, 632-636.
- Spencer, A.M. & Spencer, M.O. 1973. The late Precambrian/Lower Cambrian Bonahaven Dolomite of Islay and its stromatolites. *Scottish Journal of Geology*, **8**, 269-282.
- Steiger, R.H. & Jäger, E. 1977. Subcommittee on geochronology: convention on the use of decay constants in geo- and cosmochemistry. *Earth and Planetary Science Letters*, **6**, 359-362.
- Stein, H.J. 2006. Low-rhenium molybdenite by metamorphism in northern Sweden: Recognition, genesis and global implications. *Lithos*, **87**, 300-327.
- Stein, H.J., Morgan, J.W., Markey, R.J. & Hannah, L. 1998a. An introduction to Re-Os: What's in it for the mineral industry? *Society of Economic Geologists Newsletter*, **32**, 8-15.
- Stein, H.J., Sundblad, K., Markey, R.J., Morgan, J.W. & Motuza, G. 1998b. Re-Os ages for Archean molybdenite and pyrite, Kuittila-Kivisuo, Finland and Proterozoic molybdenite, Kabeliai, Lithuania: testing the chronometer in a metamorphic and metasomatic setting. *Mineralium Deposita*, **33**, 329-345.
- Stein, H.J., Markey, R.J., Morgan, J.W., Hannah, J.L., Scherstén, A. 2001. The remarkable Re-Os chronometer in molybdenite: how and why it works. *Terra Nova*, **13**, 479-486.
- Stein, H.J., Hannah, J.L., Zimmerman, A., Markey, R., Sarkar, S.C. & Pal, A.B. 2004. A 2.5 Ga porphyry Cu-Mo-Au deposit at Malanjkhand, central India: implications for Late Archean continental assembly. *Precambrian Research*, **134**, 189-226.
- Stephenson, D. & Gould, D. 1995. *British regional geology: The Grampian Highlands*. HMSO, London.
- Stephenson, D., Mendum, J.R., Fettes, D.J. & Leslie, A.G. 2013. The Dalradian rocks of Scotland: an introduction. *In: Stephenson, D., Leslie, A.G., Mendum, J.R., Tanner, P.W.G. & Treagus, J.E. (Eds.) The Dalradian Rocks of Scotland*. Proceedings of the Geologists' Association, **124**, 3-82.

- Stewart, A.D. & Hackman, B.D. 1973. Precambrian sediments of western Islay. *Scottish Journal of Geology*, **9**, 185-201.
- Stewart, M., Strachan, R.A., Martin, M.W. & Holdsworth, R.E. 2001. Constraints on early sinistral displacements along the Great Glen Fault Zone, Scotland: structural setting, U-Pb geochronology and the emplacement of the syn-tectonic Clunes tonalite. *Journal of the Geological Society, London*, **158**, 821-830.
- Strachan, R.A. 2000. The Grampian Orogeny: Mid-Ordovician arc-continent collision along the Laurentian margin of Iapetus. In: Woodcock, N. & Strachan, R.A. (Eds.) *Geological History of Britain and Ireland*. Blackwell Science, Oxford, 88-106.
- Strachan, R.A., Smith, M., Harris, A.L. & Fettes, D.J. 2002. The Northern Highland and Grampian terranes. In: Trewin, N.H. (Ed.) *The Geology of Scotland*. The Geological Society, London, 81-148.
- Stüwe, K. 1998. Tectonic constraints on the timing relationships of metamorphism, fluid production and gold-bearing quartz vein emplacement. *Ore Geology Reviews*, **13**, 219-228.
- Stüwe, K., Will, T.M. & Zhou, S. 1993. On the timing relationship between fluid production and metamorphism in metamorphic piles: some implications for the origin postmetamorphic gold mineralisation. *Earth and Planetary Science Letters*, **114**, 417-430.
- Suvorova, V.A. 1974. Temperature dependence of the distribution coefficient of S-isotopes between equilibrium sulfides. *National Symposium on Stable Isotope Geochemistry, 5th, Moscow, Program*, **1**, 128.
- Tanner, P.W.G. 1995. New evidence that the Lower Cambrian Leny Limestone at Callander, Perthshire, belongs to the Dalradian Supergroup, and a reassessment of the 'exotic' status of the Highland Border Complex. *Geological Magazine*, **134**, 565-570.
- Tanner, P.W.G. 2008. Tectonic significance of the Highland Boundary Fault. *Journal of the Geological Society, London*, **165**, 915-921.
- Tanner, P.W.G. 2012. The giant quartz-breccia veins of the Tyndrum-Dalmally area, Grampian Highland, Scotland: their geometry, origin and relationship to the Cononish Au-Ag deposit. *Transactions of the Royal Society of Edinburgh: Earth Science*, **103**, 1-26.
- Tanner, P.W.G. 2013. The giant quartz-breccia veins of the Tyndrum-Dalmally area, Grampian Highland, Scotland: their geometry, origin and relationship to the Cononish Au-Ag deposit. *Transactions of the Royal Society of Edinburgh: Earth Science*, **103**, 1-26.
- Tanner, P.W.G. & Sutherland, S. 2007. The Highland Border Complex, Scotland: a paradox resolved. *Journal of the Geological Society, London*, **164**, 111-116.
- Tanner, P.W.G. & Thomas, P.R. 2009. Major nappe-like D2 folds in the Dalradian rocks of the Beinn Udlaidh area, Central Highlands, Scotland. *Transactions of the Royal Society of Edinburgh: Earth Science*, **100**, 371-389.
- Tanner, P.W.G., Leslie, A.G. & Gillespie, M.R. 2006. Structural setting and petrogenesis of rift-related intrusion: the Ben Vuirich Granite of the Grampian Highlands, Scotland. *Scottish Journal of Geology*, **42**, 113-136.
- Thirlwall, M.F. 1988. Geochronology of Late Caledonian magmatism in northern Britain. *Journal of the Geological Society*, **145**, 951-967.
- Thomas, C.W. 2000. *The petrology and isotope geochemistry of Dalradian carbonate rocks*. PhD thesis, University of Edinburgh.

- Thomas, C.W., Graham, C.M., Ellam, R.M. & Fallick, A.E. 2004. $^{87}\text{Sr}/^{86}\text{Sr}$ chemostratigraphy of Neoproterozoic Dalradian limestones of Scotland and Ireland: constraints on depositional ages and time scales. *Journal of the Geological Society, London*, **161**, 229-242.
- Thomas, R., Roberts, N.M.W., Jacobs, J., Bushi, A.M., Horstwood, M.S.A. & Mruma, A. 2013. Structural and geochronological constraints on the evolution of the eastern margin of the Tanzania Craton in the Mpwapwa area, central Tanzania. *Precambrian Research*, **224**, 671-689.
- Thompson, S.J., Shine, C.H., Cooper, C., Halls, C. & Zhao, R. 1992. Shear-hosted gold mineralisation in Co. Mayo, Ireland. In: Bowden, A.A., Earls, G., O'Conner, P.G. & Pyne, J.F. (Eds.) *The Irish Minerals Industry 1980-1990: Dublin, Irish Association for Economic Geology*, 21-37.
- Thompson, A.J.B., Hauft, P.L. & Robitaille, A.J. 1999. Alteration mapping in exploration: Application of short-wave infrared (SWIR) spectroscopy. *Society of Economic Geologists Newsletter*, **39**, 16-27.
- Tilley, C.E. 1925. A preliminary study of the metamorphic zones in the Southern Highlands of Scotland. *Quarterly Journal of the Geological Society*, **81**, 100-112.
- Tomkins, A.G. 2012. A biochemical influence of the secular distribution of orogenic Au. *Economic Geology*, **108**, 193-197.
- Tomkins, A.G. & Grundy, C. 2009. Upper temperature limits of orogenic gold deposit formation: Constrains from the Granulite-hosted Griffin's Find deposit, Yilgarn Craton. *Economic Geology*, **104**, 669-685.
- Tosdal, R.M., Haxel, G.B. & Dillon, J.T. 1985. Lithological associations of gold deposits, southeastern California and southwest Arizona. *Geological Society of America, Abstracts with Programs*, **17**, 414.
- Treagus, J.E. 1987. The structural evolution of the Dalradian of the Central Highlands of Scotland. *Transactions of the Royal Society of Edinburgh: Earth Sciences*, 1-15.
- Treagus, J.E. 1991. Fault displacements in the Dalradian of the Central Highlands. *Scottish Journal of Geology*, **27**, 135-145.
- Treagus, J.E. 2000. *The solid geology of the Schiehallion District. Memoir of the British Geological Survey, Sheet 55W, Scotland*.
- Treagus, J.E. & King, G. 1978. A complete Lower Dalradian succession in the Schiehallion district, Central Perthshire. *Scottish Journal of Geology*, **14**, 157-166.
- Treagus, J.E., Patrick, R.A.D. & Curtis, S.F. 1999. Movement and mineralisation in the Tyndrum Fault Zone, Scotland and its regional significance. *Journal of the Geological Society, London*, **156**, 591-604.
- Trewin, N.H. 2002. *The Geology of Scotland*. 4th Edition, The Geological Society, London.
- Upton, P.S. 1986. A structural cross-section of the Moine and Dalradian rocks of the Braemar area. *Report of the British Geological Survey*, **17**, 9-19.
- USGS Gold. 2014. Mineral commodity summaries: Gold. Downloaded from <http://minerals.usgs.gov/minerals/pubs/commodity/gold>. April 30th 2014.
- Wagner, T., Boyce, A.J. & Fallick, A.E. 2002. Laser combustion analysis of $\delta^{34}\text{S}$ of sulfosalt minerals: determination of the fractionation systematics and some crystal-chemical considerations. *Geochimica et Cosmochimica Acta*, **66**, 2855-2863.
- Wedepohl, K.H. 1995. The composition of the continental crust. *Geochimica et Cosmochimica Acta*, **59**, 1217-1232.

- Westoll, N.D.S. & Miller, J.A. 1969. The ages of some Kentallenite intrusion in Argyll. *Scottish Journal of Geology*, **5**, 11-14.
- Wiedenbeck, M., Alle, P., Corfu, F., Griffin, W.L., Meier, M., Oberli, F., Von Quadt, A., Roddick, J.C. & Spiegel, W. 1995. Three natural zircon standards for the U-Th-Pb, Lu-Hf, trace element and REE analysis. *Geostandards Newsletter*, **19**, 1-23.
- Wilkinson, S.B. 1907. *The Geology of Islay. Memoirs of the Geological Survey of Scotland, Sheets 19 & 27 and parts of 20.*
- Wilkinson, J.J., Jenkin, G.R.T., Fallick, A.E. & Foster, R.P. 1995. Oxygen and hydrogen isotopic evolution of Variscan crustal fluids, south Cornwall, UK. *Chemical Geology*, **123**, 239-254.
- Wilkinson, J.J., Boyce, A.J., Earls, G. & Fallick, A.E. 1999. Gold remobilisation by low-temperature brines: Evidence from the Curraghinalt gold deposit, Northern Ireland. *Economic Geology*, **79**, 969-990.
- Willan, R.C.R. 1996. Geochemistry of the Ben Eagach Schist, Dalradian Supergroup: Dispersion haloes from Aberfeldy-type hydrothermal centres? *Mineralisation in the Caledonides, Mike Gallagher Meeting, Edinburgh, 27-28 June 1996. Abstract.*
- Willan, R.C.R. & Coleman, M.L. 1983. S-isotope study of the Aberfeldy barite, zinc, lead deposit and minor sulfide mineralisation in the Dalradian metamorphic terrain, Scotland. *Economic Geology*, **78**, 1619-1656.
- Willis, G.F. & Tosdal, R.M. 1992. Formation of gold veins and breccias during dextral strike-slip faulting in the Mesquite Mining District, Southeastern California. *Economic Geology*, **87**, 2002-2022.
- Wilson, J.S.G. & Flett, D.S. 1921. The lead, zinc, copper and nickel ores of Scotland. *Memoir of the Geological Survey of Scotland. Special Report on the Mineral Resources of Great Britain*, **17**.
- World Gold Council. 2014. *Gold demand trends: Full year 2013*. Downloaded from <http://www.gold.org/supply-and-demand/gold-demand-trends>. 30th April 2014.
- Woodcock, N.H. & Strachan R. 2000. (Eds.) *Geological History of Britain and Ireland*. Blackwell, Oxford.
- Wright, A.E. 1988. The Appin Group. In: Winchester, J.A. (Ed.) *Later Proterozoic stratigraphy of the Northern Atlantic regions*. Glasgow and London: Blackie.
- Wright, A.E. & Bowes, D.R. 1968. Formation of Explosion Breccias. *Bulletin Volcanologique*, **32**, 15-32.
- Yao, Y., Robb, L.J., Anhaeusser, C.R., Ying, H.L., Liu, B.G. & Tu, G.Z. 2002. Mesozoic gold deposits in the Eastern Shandong Peninsula, P.R. China – Preliminary geology, geochemistry and fluid inclusion investigations. In: *University of Witwatersrand, Economic Geology Research Institute Circular*, **361**, 11.
- Yardley, B.W.D., Banks, D.A. & Barnicoat, A.C. 2000. The chemistry of crustal brines: tracking their origins. In: Porter, T.M. (Ed.) *Hydrothermal iron oxide copper-gold and related deposits*, Australian Mineral Foundation, 61-70.
- Zhai, M. & Santosh, M. 2013. Metallogeny of the North China Craton: Link with secular changes in the evolving Earth. *Gondwana Research*, **24**, 275-297.